Electrospray Mass Spectrometric Analysis of Transition Metal Carbonyl Clusters

A thesis
completed in partial fulfilment
of the requirements for the Degree
of
Doctor in Philosophy
at the University of Waikato
by

Cameron Evans

University of Waikato
2002

Abstract

A key objective of this thesis was to develop Electrospray (Ionisation) Mass Spectrometry (ESMS) within organometallic chemistry, specifically as a technique for investigating transition metal carbonyl cluster chemistry.

An initial survey of air-sensitive high-nuclearity rhodium and nickel clusters, such as $[Rh_9As(CO)_{21}]^{2-}$ and $[H_2Ni_{12}(CO)_{21}]^{2-}$, demonstrated the usefulness of ESMS for characterisation.

ESMS was applied to monitoring the reactions of μ_4-E$[M_2(CO)_x]_2$ [E = Si, Ge, Sn; M = Co (x = 7), Fe (x = 8)] with anionic transition metal carbonyl reagents. Analysis of the reaction between μ_4-Ge$[Co_2(CO)_7]_2$ and $[Co(CO)_4]^-$ revealed the inter-conversion processes between previously isolated clusters, and was crucial in identifying the unheralded $[Co_{10}Ge_2(CO)_{24}]^{2-}$ product. Conditions for optimal yields of this anion were established and the cluster subsequently isolated and structurally characterised (below).

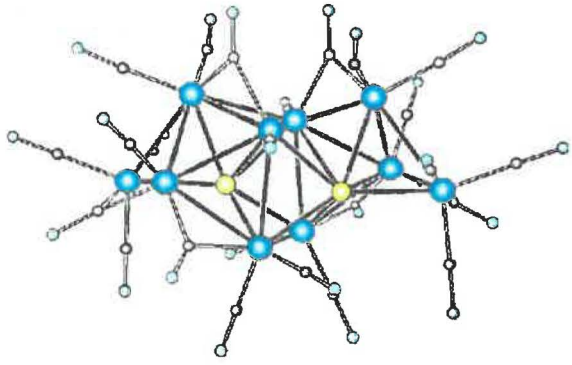

The core structure of $[Co_{10}Ge_2(CO)_{24}]^{2-}$ is unprecedented and is discussed in terms of electron-counting theories.

The analogous reaction with μ_4-Si$[Co_2(CO)_7]_2$ gave indication of novel cluster products. These included $[Co_5Si(CO)_{16}]^-$, $[Co_9Si(CO)_{22}]^-$ and $[Co_7Si(CO)_{21}]^-$, as well as the previously reported $[Co_9Si(CO)_{21}]^{2-}$. Reactions with $[Fe_2(CO)_8]^{2-}$, $[HFe(CO)_4]^-$, $[Fe(CO)_3(NO)]^-$, $[Mn(CO)_5]^-$ and $[Mo(CO)_3(\eta^5\text{-}C_5H_5)]^-$ were less straight-forward, but again led to the detection of new clusters.

ESMS analysis confirmed the unusual result that $[Co_{14}N_3(CO)_{26}]^{3-}$ is the only high-nuclearity thermolysis product of $[Co_6N(CO)_{15}]^-$. The specificity of the reaction can

only be established by ESMS since the technique precludes the existence of any other significant ionic products.

The reaction between PCl_5 and $[Co(CO)_4]^-$ gave the known $[Co_6P(CO)_{16}]^-$ and $[Co_9P(CO)_{21}]^{2-}$ clusters while the analogous reaction with $AsCl_3$ produced three novel cobalt arsenido species, $[Co_6As(CO)_{16}]^-$, $[Co_7As_2(CO)_{17}]^-$ and $[Co_9As_2(CO)_{21}]^-$. The previously reported $[Co_4Sb_2(CO)_{11}]^-$ and novel $[Co_5Sb_2(CO)_{14}]^-$ clusters were identified in the reaction between $SbCl_3$ and $[Co(CO)_4]^-$.

The synthesis and characterisation of a series of $Co_4(\mu_4\text{-}ER)_2(CO)_{11}$ clusters are described. The dimethylamino functionalised examples, $Co_4(\mu_4\text{-}EC_6H_4NMe_2)_2(CO)_{11}$ E = Si, Ge, were characterised by ESMS as their $[M+H]^+$ ions. The $Co_4(\mu_4\text{-}SiR)_2(CO)_{11}$ [R = Ph, C_6H_4OMe, $(CH_2)_3OMe$] clusters underwent facile substitution with isonitrile and phosphite reagents but equivalent phosphine-substituted products were not observed by ESMS. Isonitrile-substituted clusters (n > 2) gave clear M^+ ions in their ES mass spectra arising from *in situ* oxidation. The novel $Co_4(\mu_4\text{-}SiC_6H_4OMe)_2(CO)_7(XyNC)_4$ cluster was structurally characterised (below). Linked clusters of the form $[Co_4(\mu_4\text{-}SiC_6H_4R)(CO)_{11}Si]_2X$ [R = H, OMe; X = $(CH_2)_8$, C_6H_4] were isolated, albeit in very low yield. An oligomeric $-[XSiCo_4(CO)_{11}Si]-_n$ species was tentatively identified.

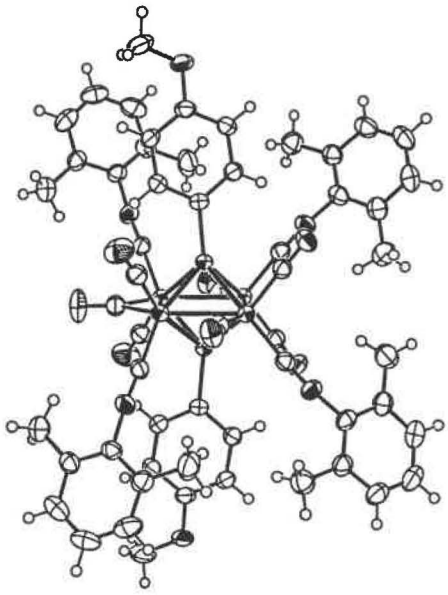

A new structural isomer of $[CoFe_3(CO)_{13}]^-$ was characterised. The ligand arrangement for $[NEt_4][CoFe_3(CO)_{13}]$ differs significantly from that of $[PPN][CoFe_3(CO)_{13}]$ and $[NEt_4][CoRu_3(CO)_{13}]$. A structure determination of $[PPN][Mo(CO)_3(\eta^5\text{-}C_5H_5)]$ is also reported.

Acknowledgments

First and foremost I wish to thank Professor Brian Nicholson for his support and enthusiasm throughout this project, and for introducing me to the fascination of crystallography. I am indebted to Brian for his advice and encouragement. The assistance and counsel offered by Associate Professor Bill Henderson and Professor Ken Mackay during this research was greatly appreciated, as was their depth of knowledge in ESMS and cluster chemistry.

I am grateful for the friendship and camaraderie of my co-workers (fellow lab rats), despite the trials and tribulations I put them through. The list of victims is endless but special mention is made of Corry Decker, Wade Mace, Victor Fester, Dr. Steven Alley, Gwion Harfoot, Rebecca Taylor, Nick Lloyd, Sam Whitley and Sally Gaw. The numerous discussions with Dr. Scott McIndoe, both relating to this research and chemistry in general are gratefully acknowledged.

All members of the Chemistry Department at the University of Waikato are thanked for their friendship and assistance over the last few years. Wendy Jackson and Pat Gread deserve special mention, both for the demands I put upon them with regards ESMS time and for tolerating the state in which I often left the equipment after use.

The X-ray crystallography departments at the University of Auckland and the University of Canterbury provided an exemplary service throughout this project, despite the poor quality of crystals often sent their way. Professor Brian Robinson, University of Otago, is thanked for performing the electrochemical analyses of the $Co_4(\mu_4\text{-}SiR)_2(CO)_{11}$ clusters.

Financial assistance throughout this project was provided by the Marsden Fund, administered by the Royal Society of New Zealand. Monetary grants from the New Zealand Institute of Chemistry and the Royal Society of New Zealand alleviated the expenses associated with conference travel and accommodation.

Finally, the support of friends and family has been constant throughout this research. The tension and stress that are associated with completing a Ph.D. thesis must find an outlet and all too often it is those closest to us that bear the cost. My apologies to all I have afflicted during this time.

Table of Contents

Chapter Two - Experimental Methods and Materials

Chapter Three - Development of Air-Sensitive ESMS

Chapter Four - Reactions of μ_4-E[$M_2(CO)_x]_2$ [E = Si, Ge, Sn; M = Co (x = 7), Fe (x = 8)] with $[Co(CO)_4]^-$

Chapter Five - Reactions of μ_4-E[$Co_2(CO)_7]_2$ (E = Si, Ge) with Transition Metal Carbonyl Anions

Chapter Six - Synthesis of Group 15/Transition Metal Clusters

Chapter Seven - Synthesis, Characterisation and Reactivity of $Co_4(\mu_4\text{-}ER)_2(CO)_{11}$ (E = Si, Ge) Clusters

Chapter Eight – Structure Solutions of Anionic Metal Carbonyls

List of Figures

List of Schemes and Tables

List of Abbreviations

M	Transition Metal Atom, Parent Cluster (ESMS)		
E	Main Group Atom	L	Ligand
R	Organic Substituent	X	Halogen
Me	Methyl	Et	Ethyl
Bu	Butyl	Ph	Phenyl (C_6H_5)
Cp	Cyclopentadienyl (η^5-C_5H_5)	Xy	Xylyl (C_8H_9)
Ad	Adamantyl ($C_{10}H_{15}$)	Bz	Benzyl (CH_2Ph)
PPN	Bis(triphenylphosphine)iminium	py	Pyridine (C_5H_5N)
thf	tetrahydrofuran	DMSO	Dimethylsulfoxide
acac	acetylacetanato		

s	strong (IR), singlet (NMR)	sh	shoulder (IR)
d	doublet (NMR)	t	triplet (NMR)
m	medium (IR), multiplet (NMR)	vs	very strong (IR)
br	broad (IR and NMR)	w	weak (IR)
cV	cone voltage	*m/z*	mass to charge ratio
ppm	chemical shift (NMR)	J	coupling constant
b.p.	boiling point	m.p.	melting point
Lit.	literature	av	average

ES(MS)	Electrospray (Mass Spectrometry)
IR	Infra-red
NMR	Nuclear Magnetic Resonance
EI	Electron Impact
FAB	Fast Atom Bombardment
(MA)LDI	(Matrix Assisted) Laser Desorption Ionisation
SEP	Skeletal Electron Pairs
MO	Molecular Orbital
AO	Atomic Orbital
PSEPT	Polyhedral Skeletal Electron Pair Theory
EAN	Effective Atomic Number
TLC	Thin Layer Chromatography
LPM	Ligand Polyhedral Model
PEPE	Parallel Expanded Phenyl Embrace
OEPE	Orthogonal Expanded Phenyl Embrace
SPE	Sextuple Phenyl Embrace

Chapter One – Transition Metal Carbonyl Clusters/Electrospray Mass Spectrometry

1.1 Introduction

The objective of the research reported within this thesis was to develop Electrospray Mass Spectrometry (ESMS) for the characterisation of transition metal carbonyl cluster compounds. As an introduction to this research, a brief review of the literature concerning both cluster compounds and ESMS is provided.

1.2 Transition Metal Carbonyl Clusters

The accepted definition of a transition metal cluster is 'a finite group of metal atoms held together mainly, or to a significant degree, by bonds directly between the metal atoms'[1]. Unless otherwise stated, use of the term 'cluster' in this thesis implies a compound containing at least three transition metal atoms, with a minimum of one direct metal-metal (M-M) bond. Various classes of cluster materials have been reported and reviewed including metal halides[2,3], chalcogenides[3] and 'naked' clusters composed solely of post-transition main group elements (e.g. Zintl clusters[4]).

The research presented in this thesis concerns the synthesis and reactions of low-valent transition metal carbonyl clusters and discussion is restricted to these compounds. These clusters are either neutral or anionic, with the metal atom formally in zero or negative oxidation states (hence low-valent). Examples range from trinuclear $M_3(CO)_n$ [e.g. $Ru_3(CO)_{12}$ [5]] to high-nuclearity species {e.g. $[Os_{20}(CO)_{40}]^{2-}$ [6]} and are typically sensitive to oxygen, with the degree of sensitivity dependent upon the metallic element, the nuclearity and the cluster charge.

[1] F.A. Cotton, *Inorg. Chem.*, 1964, **3**, 1217.
[2] N. Prokopuk and D.F. Shriver, *Adv. Inorg. Chem.*, 1999, **46**, 1.
[3] S.C. Lee and R.H. Holm, *Angew. Chem. Int. Ed. Engl.*, 1990, **29**, 840.
[4] J.D. Corbett, *Chem. Rev.*, 1985, **85**, 383.
[5] B.F.G. Johnson and J. Lewis, *Inorg. Syn.*, 1972, **13**, 92 and references therein.
[6] L.H. Gade, B.F.G. Johnson, J. Lewis, M. McPartlin, H.R. Powell, P.R. Raithby and W-T. Wong, *J. Chem. Soc., Dalton Trans.*, 1994, 521.

One aspect of the chemistry of transition metal carbonyl clusters is the incorporation of main group elements into the metal framework in encapsulated or semi-encapsulated positions (also referred to as interstitial and semi-interstitial). The presence of the main group element gives rise to unusual geometric arrangements [e.g. the bridged-butterfly structure commonly displayed by EM_5 clusters such as $Os_5C(CO)_{16}$ [7] – Figure 1.1] and stabilises higher-nuclearity clusters by providing an internal source of electrons (effectively acting as internal ligands, reducing the number of external ligands required for stability[8]). The research presented within this thesis employs group 14 and 15 elements with coordination numbers > 3 and lacking organic substituents (occasionally described as 'bare' or 'naked' main group atoms).

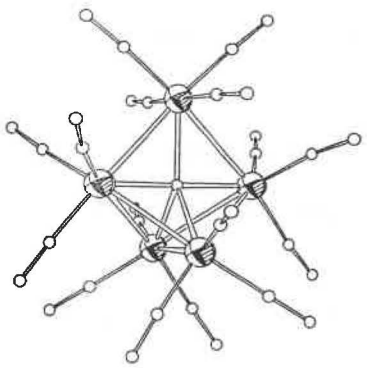

Figure 1.1 – The structure of $Os_5C(CO)_{16}$ [7].

1.2.1 Synthesis

Numerous synthetic routes to mixed main group/transition metal clusters have been reported and reference to several excellent reviews of this field is recommended[9]. The commonly employed methods are briefly outlined below with examples relevant to this research.

[7] B.F.G. Johnson, J. Lewis, W.J.H. Nelson, J.N. Nicholls, J. Puga, P.R. Raithby, M.J. Rosales, M. Schröder and M.D. Vargas, *J. Chem. Soc., Dalton Trans.*, 1983, 2447.

[8] B.F.G. Johnson and C.M. Martin, *The role of interstitial elements in transition metal carbonyl clusters*, Metal Clusters in Chemistry, Ed. P. Braunstein, L.A. Oro and P.R. Raithby, Wiley-VCH (Weinheim, Germany), 1999, 877.

[9] P.J. Dyson and J.S. McIndoe, Transition Metal Carbonyl Cluster Chemistry, Gordon and Breach Science Publishers (Amsterdam, Netherlands), 2000; K.H. Whitmire, *Adv. Organomet. Chem.*, 1998, **42**, 1; K.H. Whitmire, *J. Coord. Chem.*, 1988, **17**, 95; P. Chini, *J. Organomet. Chem.*, 1980, **200**, 37.

1.2.1.1 Thermolysis and Pyrolysis

The most common route to metal carbonyl clusters is thermal treatment of a lower-nuclearity metal carbonyl precursor, whether in an appropriate solvent (thermolysis) or in the solid state (pyrolysis). The resulting decarbonylation induces cluster formation, though the synthesis is seldom systematic, with various cluster products formed along with a metallic deposit. Carbido clusters are often produced during thermal reactions, with the carbon sourced from either carbonyl ligands[10] or the solvent[11]. The clusters produced and relative yields are dependent upon the reaction conditions with regards to temperature, solvent, and reaction time. The pyrolysis of $Os_3(CO)_{12}$ [10] and thermolysis of $Ru_3(CO)_{12}$ [12] are indicated in Scheme 1.1.

$$Os_3(CO)_{12} \xrightarrow{250^\circ C} Os_5(CO)_{16} + Os_5C(CO)_{15} + Os_6(CO)_{18} + Os_7(CO)_{21} + Os_8(CO)_{23} + Os_8C(CO)_{21}$$

$$Ru_3(CO)_{12} \xrightarrow[Bu_2O]{142^\circ C} Ru_6C(CO)_{17}$$

Scheme 1.1 – Examples of cluster synthesis through pyrolysis and thermolysis.

1.2.1.2 Redox Condensation

Redox condensation between two metallic reagents in different oxidation states is commonly employed as a route to mixed metal (heteronuclear) clusters. Redox condensation usually provides a more systematic route to specific clusters, as the reaction conditions are significantly milder than standard thermolytic or pyrolytic methods. Main group elements are usually incorporated into either reagent prior to reaction and the mild conditions prevent loss or scrambling of the element. Two examples are the syntheses of $[CoRh_6N(CO)_{15}]^{2-}$ [13] and $[Fe_6C(CO)_{16}]^{2-}$ [14] displayed in Scheme 1.2.

[10] C.R. Eady, B.F.G. Johnson and J. Lewis, *J. Organomet. Chem.*, 1972, **37**, C39; C.R. Eady, B.F.G. Johnson and J. Lewis, *J. Chem. Soc., Dalton Trans.*, 1975, 2606.
[11] V.G. Albano, P. Chini, S. Martinengo, D.J.A. McCaffrey, D. Strumolo and B.T. Heaton, *J. Am. Chem. Soc.*, 1974, **96**, 8106.
[12] B.F.G. Johnson, R.D. Johnston and J. Lewis, *J. Chem. Soc. A*, 1968, 2865; B.F.G. Johnson, J. Lewis and I.G. Williams, *J. Chem. Soc. A*, 1970, 901.
[13] S. Martinengo, G. Ciani and A. Sironi, *J. Chem. Soc., Chem. Commun.*, 1984, 1577.
[14] M. Tachikawa, A.C. Sievert, E.L. Muetterties, M.R. Thompson, C.S. Day and V.W. Day, *J. Am. Chem. Soc.*, 1980, **102**, 1725.

$$[Rh_6N(CO)_{15}]^- + [Co(CO)_4]^- \longrightarrow [CoRh_6N(CO)_{15}]^{2-}$$

$$[Fe_5C(CO)_{14}]^{2-} + Fe_2(CO)_9 \longrightarrow [Fe_6C(CO)_{16}]^{2-}$$

Scheme 1.2 – Examples of cluster synthesis *via* redox condensation.

1.2.1.3 Oxidation and Reduction

The use of alkali metals (Li, Na, K) as reducing agents has been reported in synthesis of anionic cluster species. An example is the generation of $[M_6(CO)_{15}]^{2-}$ from $M_4(CO)_{12}$ (M = Co[15], Ir[16]) in the presence of sodium (Scheme 1.3). The use of hard bases {$[OH]^-$, $[OR]^-$} as reducing agents has also been reported (discussed in the following section).

$$M_4(CO)_{12} \xrightarrow[thf]{Na} [M_6(CO)_{15}]^{2-}$$

Scheme 1.3 – The reductive synthesis of $[M_6(CO)_{15}]^{2-}$ (M = Co, Ir).

Oxidation as a method of cluster formation is less prevalent. The use of Fe^{3+} salts have been reported in the synthesis of $Rh_8C(CO)_{19}$ and $[Rh_{15}C_2(CO)_{28}]^-$ from $[Rh_6C(CO)_{15}]^{2-}$ [17] (Scheme 1.4), whereas acids have proved effective oxidising agents in the synthesis of $[Rh_{12}C_2(CO)_{24}]^{2-}$ from $[Rh_6C(CO)_{15}]^{2-}$ [18].

$$[Rh_{15}C_2(CO)_{28}]^- \xleftarrow[N_2]{Fe^{3+}} [Rh_6C(CO)_{15}]^{2-} \xrightarrow[CO]{Fe^{3+}} Rh_8C(CO)_{19}$$

$$2\,[Rh_6C(CO)_{15}]^{2-} + 2H^+ \longrightarrow [Rh_{12}C_2(CO)_{24}]^{2-} + H_2$$

Scheme 1.4 – Examples of oxidative cluster synthesis.

1.2.1.4 Treatment with Ionic Reagents

An extensively employed route to anionic cluster compounds is treatment of a neutral metal carbonyl with MOH (M = Na, K), also referred to as base-assisted

[15] P. Chini, V.G. Albano and S. Martinengo, *J. Organomet. Chem.*, 1968, **16**, 471.
[16] M. Angoletta, L. Malatesta and G. Caglio, *J. Organomet. Chem.*, 1975, **94**, 99.
[17] V.G. Albano, P. Chini, S. Martinengo, M. Sansoni and D. Strumolo, *J. Chem. Soc., Chem. Commun.*, 1974, 299.
[18] V.G. Albano, D. Braga, P. Chini, D. Strumolo and S. Martinengo, *J. Chem. Soc., Dalton Trans.*, 1983, 249.

decarbonylation. Treatment with hydroxide often produces hydrido clusters (*via* CO_2 release) as identified in the synthesis of $[H_3Rh_{13}(CO)_{24}]^{2-}$ (Scheme 1.5[19]).

$$Rh_4(CO)_{12} + NaOH \xrightarrow[{}^{i}PrOH,\ H_2]{80^{o}C} [H_3Rh_{13}(CO)_{24}]^{2-}$$

Scheme 1.5 – The synthesis of $[H_3Rh_{13}(CO)_{24}]^{2-}$.

Ionic reagents may also serve as a source of main group elements. Examples include the synthesis of $[M_6N(CO)_{15}]^-$ (M = Co, Rh) through reaction of $M_4(CO)_{12}$ with $[NO_2]^-$ [20], and formation of $HOs_4N(CO)_{12}$ from $[H_3Os_4(CO)_{12}]^-$ and $[NO]^+$ [21] (Scheme 1.6). More unusual is the decomposition of $[PPN]^+$ providing a phosphorus source in formation of $[Rh_{10}P(CO)_{22}]^{3-}$ [22].

$$M_4(CO)_{12} + [PPN][NO_2] \xrightarrow{thf} [PPN][M_6N(CO)_{15}] \quad M = Co, Rh$$

$$[H_3Os_4(CO)_{12}]^- + [NO][BF_4] \xrightarrow{CH_2Cl_2} HOs_4N(CO)_{12}$$

Scheme 1.6 – The use of $[NO_2]^-$ and $[NO]^+$ as nitrido sources.

1.2.1.5 Salt Elimination

An alternative method of incorporating a main group element into a transition metal cluster is through salt elimination. The reaction between main group halides and anionic transition metal reagents (mononuclear or preformed anionic clusters) occurs readily and provides a source of 'naked' main group elements. Two examples are displayed in Scheme 1.7 with incorporation of antimony[23] (interstitial position) or phosphorus[24] (semi-interstitial) into the metal framework.

[19] C. Allevi, B.T. Heaton, C. Seregni, L. Strona, R.J. Goodfellow, P. Chini and S. Martinengo, *J. Chem. Soc., Dalton Trans.*, 1986, 1375.
[20] R.E. Stevens, P.C.C. Liu and W.L. Gladfelter, *J. Organomet. Chem.*, 1985, **287**, 133.
[21] M.A. Collins, B.F.G. Johnson, J. Lewis, J.M. Mace, J. Morris, M. McPartlin, W.J.H. Nelson, J. Puga and P.R. Raithby, *J. Chem. Soc., Chem. Commun.*, 1983, 689.
[22] F. Ragaini, A. Sironi and A. Fumagalli, *Chem. Commun.*, 2000, 2117.
[23] V.G. Albano, F. Demartin, C. Femoni, M.C. Iapalucci, G. Longoni, M. Monari and P. Zanello, *J. Organomet. Chem.*, 2000, **593-594**, 325.
[24] P. Chini, G. Ciani, S. Martinengo and A. Sironi, *J. Chem. Soc., Chem. Commun.*, 1979, 188; G. Ciani and A. Sironi, *J. Organomet. Chem.*, 1983, **241**, 385.

$$[NEt_4]_2[Ni_6(CO)_{12}] + SbCl_3 \longrightarrow [NEt_4]_2[Ni_{15}Sb(CO)_{24}] + [NEt_4]Cl$$

$$Na[Co(CO)_4] + PCl_3/PCl_5 \longrightarrow Na[Co_6P(CO)_{16}] + NaCl$$

Scheme 1.7 – Examples of cluster synthesis through salt elimination.

1.2.2 Structures

A wide variety of structural arrangements have been identified for cluster compounds. A general discussion is provided below and specific examples incorporating group 14 and 15 elements are provided in the relevant chapters.

The majority of transition metal clusters (especially those incorporating first row main group elements) are based around a deltahedral arrangement of metal atoms enclosed within a shell of carbonyl ligands. Deltahedra are polyhedra comprised solely of triangular faces (alternatively referred to as platonic polyhedra). The deltahedral arrangement minimises inter-atom and inter-ligand repulsions, and often provides a suitable cavity for the encapsulation of main group elements. Various theoretical models have been reported to rationalise the structures expressed, generally grouped under the title 'electron-counting procedures'.

1.2.3 Electron-Counting Procedures

An overview of the different models available is outlined below. These models rationalise the cluster arrangements based on the nature and number of both the metal atoms and ligands involved. A common concept through these models is the number of valence-electrons associated with a cluster. This number is the sum of the d-electrons provided by the metal atoms, the electrons provided by the ligands (dependent both upon ligand type and bonding mode) and the cluster charge. For example, $Os_5C(CO)_{16}$ (refer to Figure 1.1) is a 76 valence-electron cluster – (5 x 8) electrons from the osmium atoms, (16 x 2) electrons from the carbonyl ligands and 4 electrons from the encapsulated carbon atom.

Clusters containing the late transition metals (groups 10-12) fail to conform to the models outlined below and alternative procedures (beyond the scope of this discussion) are used to account for the cluster arrangements of these elements. The use of heavier

main group elements (of larger atomic size) often precludes encapsulation and the models are less effective at predicting the cluster shape.

1.2.3.1 Effective Atomic Number (EAN)

The EAN rule (a cluster extension of the 18 electron rule) states that metal atoms require full valence orbitals for stability, achieved through formation of M-M and M-L bonds. This model accounts for the atomic arrangements of simple metal carbonyls but is generally of little use in predicting cluster geometries. From the EAN rule, the number of M-M edges within a cluster can be predicted (Equation 1.1) but the model often over-estimates the electron-counts of higher-nuclearity clusters. The model is employed in localised electron-counting to justify the number of substituents (metal atoms and ligands) attached to a single metal centre but is otherwise seldom utilised.

$$n = \frac{18N - NVE}{2}$$

n = number of M – M edges
N = number of metal vertices
NVE = number of valence electrons

Equation 1.1

1.2.3.2 Polyhedral Skeletal Electron Pair Theory (PSEPT)

The most commonly employed method is the PSEPT model initially developed by Wade[25] and Mingos[26] (often referred to as Wade's Rules). The model was initially applied to rationalising the polyhedra displayed by boranes and was extended to transition metal clusters through the isolobal analogy. Effectively, the similarity between the orbital configurations of borane and metallic fragments results in similar polyhedral cluster arrangements for the different species.

The polyhedral arrangement adopted is a factor of the number of electrons available for cluster bonding. Six atomic orbitals (AO's) on each transition metal atom are involved in metal-ligand bonding (or associated with non-bonding electrons), with the 3 remaining AO's allocated to cluster bonding. The orbitals associated with ligand

[25] K. Wade, *Inorg. Chem. Nucl. Lett.*, 1972, **8**, 559; K. Wade, *Adv. Inorg. Chem. and Radiochem.*, 1976, **18**, 1.
[26] D.M.P. Mingos, *Nature*, 1972, **236**, 99; D.M.P. Mingos, *Acc. Chem. Res.*, 1984, **17**, 311.

bonding are given priority and the number of electron pairs available for cluster bonding (skeletal electron pairs, SEP) is determined using Equation 1.2.

$$SEP = \frac{(NVE - 12N)}{2}$$

NVE = number of valence electrons
N = number of metal vertices

Equation 1.2

The polyhedral structure predicted is determined from the number of SEP (n) compared to the number of metal vertices (N). For n = N + 1, a full-N vertex deltahedron (referred to as a *closo*-structure) is predicted, while higher numbers of SEP cause more open arrangements (n = N + 2, *nido*-structure and n = N + 3, *arachno*-structure, related to the appropriate *closo*-form by removal of one and two vertices respectively). This sequence is displayed by the $[Fe_6C(CO)_{16}]^{2-}$ [27], $[Fe_5C(CO)_{14}]^{2-}$ [28] and $[Fe_4C(CO)_{12}]^{2-}$ [29] clusters, all of which possess 7 SEP and are thus based around a parent octahedron (Figures 1.2a, b and c). The 6 vertex $[Fe_6C(CO)_{16}]^{2-}$ cluster displays the *closo*-octahedral arrangement while $[Fe_5C(CO)_{14}]^{2-}$ and $[Fe_4C(CO)_{12}]^{2-}$ adopt the *nido*- (square pyramid) and *arachno*- (butterfly) structures respectively. An alternative *arachno*-octahedron is displayed by $Fe_4(\mu_4\text{-}PC_6H_4CH_3)_2(CO)_{11}$ (again 7 SEP – Figure 1.2d), where the iron atoms are arranged in a square plane[30].

Nido- and *arachno*-structures are common for boranes and carboranes but transition metal clusters more commonly display capping of the parent deltahedron. PSEPT accounts for the presence of additional vertices by stipulating that capped clusters contain the same number of SEP as the parent deltahedron (referred to as the capping principle). An example is $Os_8(CO)_{20}(C_6H_6)$ (Figure 1.3) which possesses 7 SEP (110 valence electrons), identical to the parent octahedron[31]. Although PSEPT correctly predicts the structure to be a bi-capped octahedron, the locations of the two capping atoms cannot be determined from electron-counting procedures.

[27] M.R. Churchill and J. Wormald, *J. Chem. Soc., Dalton Trans.*, 1974, 2410.
[28] A. Gourdon and Y. Jeannin, *J. Organomet. Chem.*, 1985, **290**, 199.
[29] R.F. Boehme and P. Coppens, *Acta Cryst. Sect. B.*, 1981, **37**, 1914.
[30] H. Vahrenkamp and D. Wolters, *J. Organomet. Chem.*, 1982, **224**, C17.
[31] A.J. Amoroso, B.F.G. Johnson, J. Lewis, C-K. Li, C.A. Morewood, P.R. Raithby, M.D. Vargas and W-T. Wong, *J. Cluster Sci.*, 1995, **6**, 163.

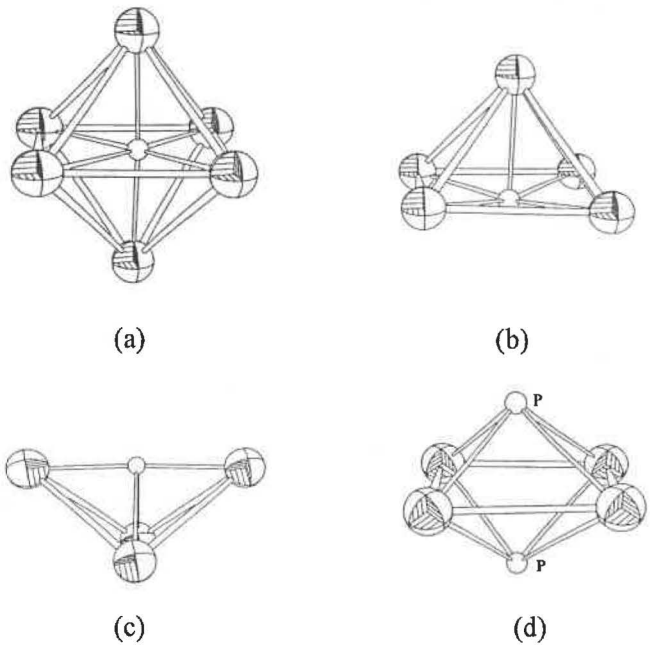

Figure 1.2 – The core structures of $[Fe_6C(CO)_{16}]^{2-}$ [27] (a), $[Fe_5C(CO)_{14}]^{2-}$ [28] (b), $[Fe_4C(CO)_{12}]^{2-}$ [29] (c) and $Fe_4(\mu_4\text{-}PC_6H_4CH_3)_2(CO)_{11}$ [30] (d).

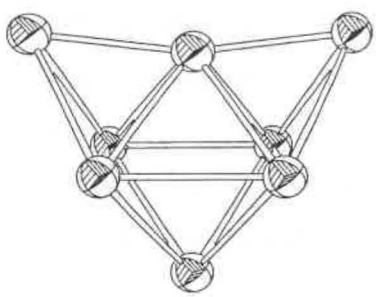

Figure 1.3 – The core structure of $Os_8(CO)_{20}(C_6H_6)$ [31].

In general, PSEPT is successful in rationalising the structures of moderate-nuclearity transition metal clusters. For higher-nuclearity examples, the method is less effective because several atomic arrangements are possible, all of similar energy. Another weakness is that all PSEPT predictions are based on parent deltahedra, though alternative stable polyhedral arrangements are known {e.g. $[Rh_6C(CO)_{15}]^{2-}$ is based on a trigonal-prism rather than the six vertex deltahedron, an octahedron[32]}.

[32] V.G. Albano, M. Sansoni, P. Chini and S. Martinengo, *J. Chem. Soc., Dalton Trans.*, 1973, 651.

1.2.3.3 Cluster Valence Molecular Orbitals (CVMO's)

Lauher[33,34] has provided an alternative approach to the rationalisation of cluster polyhedra through use of molecular orbital theory. The molecular orbitals associated with transition metal clusters (composed from the atomic orbitals of the metal atoms) are divided into high-energy (high-lying) anti-bonding orbitals (HLAO's) and cluster valence molecular orbitals (CVMO's). The geometry expressed by the cluster is dependent upon the number of CVMO's available and the values determined for a wide variety of cluster shapes have been reported[33]. As with PSEPT theory, the procedure fails for high-nuclearity clusters as various atomic arrangements have the same number of CVMO's available.

1.2.4 Characterisation Methods

1.2.4.1 Infra-red (IR) Spectroscopy

Infra-red spectroscopy is the most widely applied technique for the characterisation of transition metal clusters, allowing rapid analysis in either solution or solid media. In particular, the carbonyl stretching frequency range (2200-1600 cm^{-1}) is useful for cluster characterisation, with the frequency dependent upon the metal atom to which the ligand is attached, the charge on the cluster, and the bonding mode of carbonyl ligand (terminal, edge-bridging or face-bridging). One of the more useful applications of IR in cluster chemistry has been in monitoring reactions. The extent of reaction can be gauged by shifts in the carbonyl stretching frequencies from signals characteristic of the reactant to those of the product.

Despite its widespread application, IR characterisation of cluster compounds is hampered by a number of factors. Although the number of IR signals for simple carbonyl compounds can be predicted from symmetry rules, higher-nuclearity clusters display significantly fewer signals than expected[35,36]. The simplicity of IR spectra for cluster species is attributed to similarity in carbonyl stretching frequencies causing extensive signal overlap. In particular, as a cluster increases in size, the carbonyl ligands

[33] J.W. Lauher, *J. Am. Chem. Soc.*, 1978, **100**, 5305.
[34] J.W. Lauher, *J. Am. Chem. Soc.*, 1979, **101**, 2604.
[35] S.F.A. Kettle, E. Diana, R. Rossetti and P.L. Stanghellini, *Inorg. Chem.*, 1998, **37**, 6502; S.F.A. Kettle, E. Diana, E. Boccaleri and P.L. Stanghellini, *Eur. J. Inorg. Chem.*, 1999, 1957.

approach a spherical arrangement, which provides a single IR signal[36]. The simplicity and poor resolution of spectra also hamper distinguishing between similar cluster species (containing similar metallic elements and charge).

1.2.4.2 Nuclear Magnetic Resonance (NMR) Spectroscopy

Nuclear magnetic resonance is an extremely powerful technique for determining the structures of organic molecules in solution. With regards to characterisation of transition metal cluster compounds, the lack of suitable nuclei detracts from its utility. One of the few NMR 'handles' available in many cluster compounds is the ^{13}C signal associated with the carbonyl ligands. The ^{13}C signal is notoriously weak (a factor both of a limited natural abundance and low gyromagnetic ratio) and samples are often enriched for analysis. Signals associated with the carbonyl ligands occur at high frequency (typically > 200 ppm) and spectra are often simple owing to ligand fluxionality[37]. Fluxionality is caused by the interchange between different atomic arrangements (of similar energy) in solution, with the NMR spectra observed corresponding to an average of the signals expected. The interchange between the different atomic arrangements can be minimised by analysis at low temperature, sometimes allowing resolution of the different ligand environments.

Although most inorganic nuclei are unsuitable for NMR analysis, an exception is ^{103}Rh which has 100% natural abundance in the I = ½ spin active state. Cluster analysis by ^{103}Rh NMR is widely reported and has been reviewed in detail[38]. ^{103}Rh NMR analysis has been reported for clusters encompassing a range of nuclearities, ligand environments and interstitial elements. The analysis allows determination of the cluster configuration in solution, and formulation of mechanisms for metal and ligand migrations. Aside from rhodium clusters, NMR analysis of transition metal carbonyl clusters has been limited.

---

[36] S.F.A. Kettle, E. Diana, R. Rossetti and P.L. Stanghellini, *J. Am. Chem. Soc.*, 1997, **119**, 8228.

[37] Refer to relevant chapters in standard texts e.g. D.M.P. Mingos and D.J. Wales, Introduction to Cluster Chemistry, Prentice Hall (New Jersey, USA), 1990 or The Chemistry of Metal Cluster Complexes, Ed. D.F. Shriver, H.D. Kaesz and R.D. Adams, VCH (New York, USA), 1990.

[38] Refer to B.T. Heaton, J.A. Iggo, I.S. Podkorytov, D.J. Smawfield and S.P. Tunik, *Multinuclear NMR studies on homo- and heterometallic rhodium clusters containing 6 or more metal atoms*, Metal Clusters in Chemistry, Ed. P. Braunstein, L.A. Oro and P.R. Raithby, Wiley-VCH (Weinheim, Germany), 1999, 960 and references therein.

1.2.4.3 Electron Spin Resonance (ESR) Spectroscopy

Electron spin resonance spectroscopy [also referred to as electron paramagnetic resonance (EPR) spectroscopy] is complementary to NMR spectroscopy. ESR involves analysis of unpaired electrons rather than nuclei, allowing the distribution of the electron over the cluster to be examined. As paramagnetic clusters are relatively rare, the technique has found limited application.

1.2.4.4 X-Ray Crystallography

The only unambiguous method for characterising cluster compounds in the solid state is crystallography (whether by X-ray or neutron diffraction methods). The structural information provided by crystallography with regard to the arrangement of metal atoms and ligands is of key importance in any discussion of these materials. Recent advances in both detection methods and computer processing allow routine crystallographic analysis of these materials.

One difficulty noted in structural characterisation of transition metal clusters is disorder. In a number of cluster species, some atoms are distributed over two or more different sites within the crystal lattice, with the remaining atoms in fixed positions. The final structure solution contains partial atoms, often related to one another through rotation or inversion of the metal framework. The most widely reported example of disorder for transition metal carbonyl clusters is the 'Star of David' motif found for $Fe_3(CO)_{12}$ and derivatives, where the locations of the ligands are unambiguous but two orientations of the Fe_3 triangle are present, related by a 2-fold rotation (Figure 1.4)[39].

A limitation of crystallographic analysis of cluster species is the requirement for single crystals. Unsystematic syntheses often produce several different cluster species, which hampers crystallisation of any single cluster compound. Also, space filling models of cluster compounds indicate a roughly spherical shape for higher-nuclearity clusters, not an ideal geometry for the formation of the macroscopic ordered array of molecules required for crystal formation. Despite these limitations, crystallographic characterisation is essential for determining the structures of cluster species.

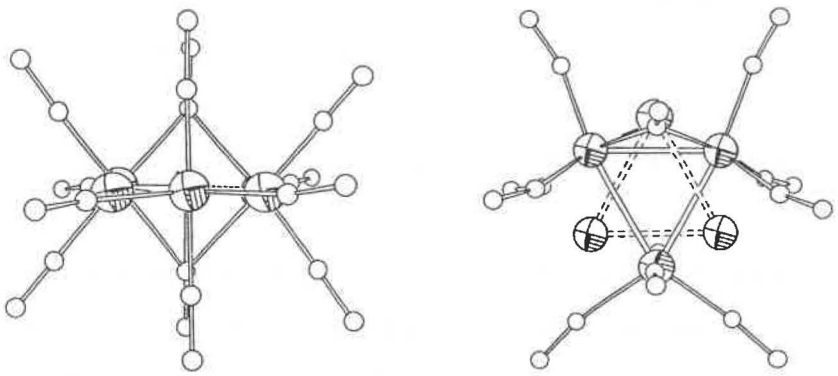

Figure 1.4 – The 'Star of David' motif in the structure of $Fe_3(CO)_{12}$ (views parallel and perpendicular to the Fe_3 plane)[39].

1.2.4.5 Mass Spectrometry

Mass spectrometric methods have been available for the characterisation of isolated compounds for decades. Brief mention of the techniques available is provided below, with emphasis on the analysis of transition metal clusters. Reference to reviews of this area is recommended[40]. Numerous MS detectors are available, all of which determine the mass to charge ratio of gas phase ions. Various methods of ion detection have been reviewed previously[41] and are beyond the scope of this discussion, which focuses on the methods available for generating ions for analysis.

1.2.4.5A Electron Impact (EI)

The most common method for generating gas phase ions involves the emission of electrons from a heated filament, with subsequent acceleration enabling them to dislodge an electron from a neutral gas phase analyte. This produces molecular ions that tend to fragment prior to detection. The fragmentation pattern observed is characteristic of the analyte involved but is sometimes so extensive that parent ions are not detected.

EI requires prior generation of the gas phase analyte, usually through heating under high vacuum. This is effective for volatile, thermally-stable samples (particularly organic compounds) but precludes analysis of many cluster materials. Analysis of clusters by

[39] C.H. Wei and L.F. Dahl, *J. Am. Chem. Soc.*, 1969, **91**, 1351; L.J. Farrugia, A.L. Gillon, D. Braga and F. Grepioni, *Organometallics*, 1999, **18**, 5022.
[40] B.F.G. Johnson and J.S. McIndoe, *Coord. Chem. Reviews*, 2000, **200-202**, 901.

EIMS has been mainly limited to smaller neutral clusters [e.g. $M_4(CO)_{12}$, M = Co, Rh, Ir[42]] though some high-nuclearity examples are reported [e.g. $Os_8C(CO)_{21}$ [43]].

1.2.4.5B Fast Atom Bombardment (FAB)

The development of Fast Atom Bombardment (FAB) mass spectrometry extended the application of spectrometric methods. In FABMS, the analyte is transferred into the gas phase from an involatile matrix through collision with accelerated argon or xenon atoms. A closely related method is liquid secondary ion mass spectrometry (LSIMS), which involves the use of accelerated ions (e.g. Ar^+, Xe^+) and these two methods (FABMS and LSIMS) are not distinguished in this discussion.

The application of FABMS to organometallic compounds (including transition metal carbonyl clusters) has been reviewed[44] and only examples of direct relevance are provided here. One report deserving discussion is the systematic examination of a series of anionic ruthenium clusters[45]. FABMS spectra of mono-anions were dominated by parent ions across a range of nuclearities {from $[H_3Ru_4(CO)_{12}]^-$ to $[HRu_{10}C(CO)_{24}]^-$} but equivalent spectra of di-anionic clusters were dominated by $[M+H]^-$ adducts. Extensive fragmentation was also apparent, with signals observed for $[M]^-$ to $[M-14CO]^-$.

1.2.4.5C Matrix Assisted Laser Desorption Ionisation (MALDI)

A variety of mass spectrometric techniques involve the rapid heating of a sample to generate gas phase ions. The most recent example is MALDI, where a UV laser is employed to produce a mixture of gaseous ions from the sample. The technique has found significant application for biological analytes with the sample mixed within a solid matrix (often an organic compound which efficiently absorbs UV radiation e.g. nicotinic acid) while equivalent analysis of cluster samples often forgo the use of a matrix.

---

[41] Refer to relevant chapters in standard texts e.g. Instrumental Analysis, G.D. Christian and J.E. O'Reilly, Allyn and Bacon (Boston, USA), 1986.
[42] J. Lewis and B.F.G. Johnson, *J. Chem. Soc. A*, 1968, 245.
[43] C.R. Eady, B.F.G. Johnson and J. Lewis, *J. Chem. Soc., Dalton Trans.*, 1975, 2606.
[44] M.I. Bruce and M.J. Liddell, *Appl. Organomet. Chem.*, 1987, **1**, 191.
[45] T. Chihara, L. Yang, Y. Esumi and Y. Wakatsuki, *J. Mass Spectrom.*, 1995, **30**, 684.

The analysis of neutral clusters by LDI often provides insight into aggregation processes. Although fragmentation (through carbonyl loss) is observed, intact parent ions are usually detected along with higher-nuclearity signals corresponding to aggregation of sample ions prior to detection. For example, LDI-TOF spectra of $Ru_3(CO)_{12}$ [46] and phosphine derivatives[47] indicate a range of nuclearities (Ru_3 to Ru_9) are present, attributed to aggregation of cluster fragments. The aggregates reported in LDI-TOF analysis of $Ru_6C(CO)_{17}$ [48] and $Os_6(CO)_{18}$ [49] correspond to multiples of the metal core, indicating that the core remains intact during desorption and aggregation.

In contrast, LDI-TOF analysis of anionic transition metal clusters seldom displays aggregate formation. An example is analysis of $[Os_{10}C(CO)_{24}]^{2-}$, where carbonyl loss was apparent (up to 19 CO ligands) without indication of higher mass aggregates[50]. The simplicity of the spectra assists characterisation of these cluster materials.

1.3 Electrospray (Ionisation) Mass Spectrometry (ESMS/ESI-MS)

1.3.1 Background

As discussed above, the analysis of neutral and thermally stable compounds is relatively routine. The conditions required for generation of gas phase ions are often harsh but the fragmentation patterns observed are usually characteristic of the analyte. Despite the wide applications of traditional mass spectrometry, there exist a number of situations where these techniques are unsuitable. Examples include mass determination for biological samples (e.g. peptides, proteins and oligonucleotides) and for inorganic and/or organometallic compounds. In each case, the sample is either involatile, or too fragile to be transferred to the gas phase intact through EI mass spectrometric techniques, though other methods (e.g. FAB and MALDI) have addressed these limitations to a degree. Another key flaw with traditional mass spectrometric techniques is that they are only applicable to solid or gaseous samples, with the techniques

[46] G. Critchley, P.J. Dyson, B.F.G. Johnson, J.S. McIndoe, R.K. O'Reilly and P.R.R. Langridge-Smith, *Organometallics*, 1999, **18**, 4090.
[47] P.J. Dyson, A.K. Hearley, B.F.G. Johnson, J.S. McIndoe and P.R.R. Langridge-Smith, *Inorg. Chem. Commun. 2*, 1999, 590.
[48] M.J. Dale, P.J. Dyson, B.F.G. Johnson, P.R.R. Langridge-Smith and H.T. Yates, *J. Chem. Soc., Dalton Trans.*, 1996, 771.
[49] W.J. Dollard, P.J. Dyson, T. Jackson, B.F.G. Johnson, J.S. McIndoe and P.R.R. Langridge-Smith, *Inorg. Chem. Commun. 2*, 1999, 587.
[50] P.J. Dyson, B.F.G. Johnson, J.S. McIndoe and P.R.R. Langridge-Smith, *Inorg. Chem.* 2000, **39**, 2430.

unsuitable for solution (especially aqueous) state chemistry. Solution state chemistry is often of key importance especially for biological samples.

The recent technique of Electrospray (Ionisation) Mass Spectrometry (ESMS or ESIMS) addresses these limitations by allowing the transfer of ions within a solution (often aqueous or of similar polarity to water) directly to the gas phase through a 'soft' method, allowing fragile samples to remain intact. This technique has been exploited in the study of biological systems[51] but its application to inorganic samples has only recently been explored.

1.3.2 Process of ESMS

A detailed account of the mechanistic background to the ESMS technique is beyond the scope of this review. An overview of the procedure is provided but for extended mechanistic detail the reader is referred to reviews of this area[52].

Dole *et al* initially developed ESMS (shown schematically in Figure 1.5) in the late 1960's[53,54] but its potential in mass spectrometry was unrealised until Fenn and colleagues[55] applied the technique to the detection and characterisation of biological samples. These samples are unsuitable for traditional mass spectrometric analysis because of their fragile nature and intimate association with water. In contrast, the ESMS technique has proven 'soft' enough to transfer the sample intact into the gas phase and allow spectrometric characterisation of these materials.

The ESMS technique (Figure 1.6) involves elution of a solution containing both sample and solvent from a highly-charged stainless-steel capillary. The surface of the solution at the capillary tip is drawn into a 'Taylor Cone' (attributed to competing electric field and surface tension forces[56]), from which charged droplets of the solution are discharged. These droplets are accelerated towards the sample and skimmer cones, with

[51] J.A. Loo, *Mass Spectrom. Reviews*, 1997, **16**, 1.
[52] Electrospray Ionisation Mass Spectrometry, Ed. R.B. Cole, John Wiley and Sons (New York, USA), 1997 and references therein; P. Kebarle and L. Tang, *Anal. Chem.*, 1993, **65**, 972; P. Kebarle, *J. Mass Spectrom.*, 2000, **35**, 804; D.S. Ashton, C.R. Beddell, D.J. Cooper, B.N. Green and R.W.A. Oliver, *Organic Mass Spectrometry*, 1993, **28**, 721; M. Mann, *Organic Mass Spectrometry*, 1990, **25**, 575; I.I. Stewart and G. Horlick, *Trends in Anal. Chem.*, 1996, **15**, 80; I.I. Stewart, *Spectrochimica Acta B*, 1999, **54**, 1649.
[53] M. Dole, L.L. Mach, R.L. Hines, R.C. Mobley, L.P. Ferguson and M.B. Alice, *J. Chem. Phys.*, 1968, **49**, 2240.
[54] L.L. Mack, P. Kralik, A. Rheude and M. Dole, *J. Chem. Phys.*, 1970, **52**, 4977.
[55] J.B. Fenn, M. Mann, C.K. Meng, S.K. Wong and C.M. Whitehouse, *Science*, 1989, **246**, 64.

solvent evaporated from the droplets *en route* through contact with the drying gas (also referred to as the bath gas).

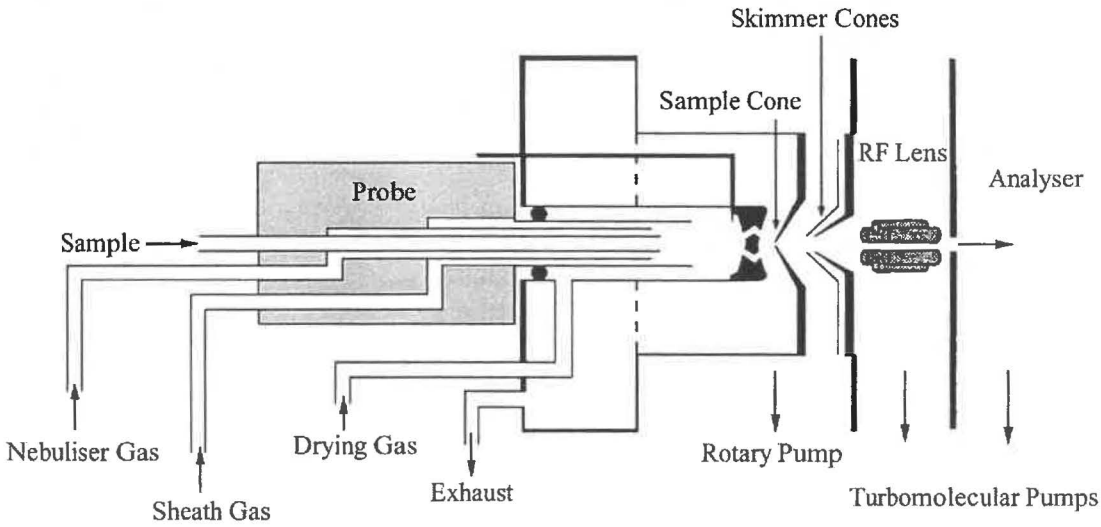

Figure 1.5 – A schematic diagram of the ESMS [57].

The next step in the process is still uncertain. One proposal (referred to as the charged residue model[53]) is that solvent evaporation from the droplets continues, increasing surface charge-density until the Rayleigh Limit is reached (where electrostatic repulsion and surface tension forces approach equality[58]). At this point, the instability of the droplet causes a 'Columbic Explosion', producing a raft of smaller droplets of lower-charge density. This process of droplet evaporation and explosion continues until the droplets contain very little charge or solvent (effectively consisting solely of the ionised analyte) with subsequent detection. An alternative mechanism proposed for generation of gas phase ions (referred to as the ion evaporation model[59]) involves the ionised analyte being directly desorbed into the gas phase from a small highly-charged droplet near the Rayleigh limit.

[56] G.I. Taylor, *Proc. R. Soc. London A,* 1969, **313**, 453.
[57] VG Platform II User Manual, Issue 3, Fisons Instruments, 1994.
[58] J.W.S. Rayleigh, *Philos. Mag,* 1882, **14**, 184.
[59] J.V. Iribane and B.A. Thomson, *J. Chem. Phys.*, 1976, **64**, 2287; B.A. Thomson and J.V. Iribane, *J. Chem. Phys.*, 1979, **71**, 4451.

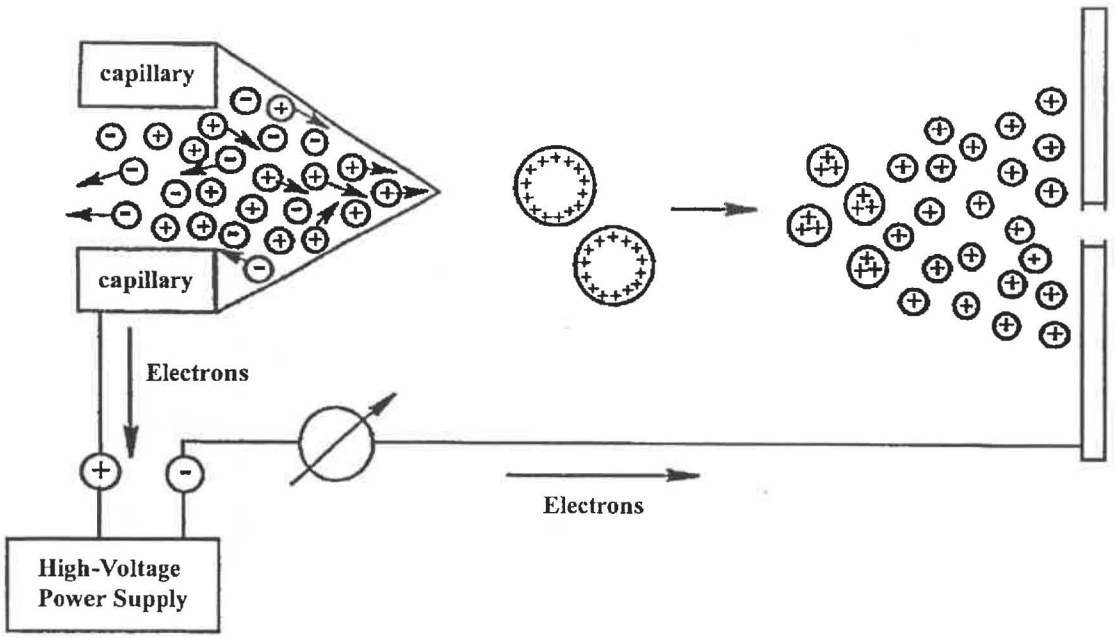

Figure 1.6 – The generation of gas phase ions from charged droplets[60,61].

Ultimately, regardless of the mechanism of formation the analyte is detected with little or no solvent attached. The process also leaves the analyte intact throughout, providing a 'soft' method of transferring the analyte from solution to the gas phase and thus allowing analysis of samples previously unsuitable for mass spectrometric characterisation.

A significant advantage ESMS has over other mass spectrometric methods is the ability to control fragmentation. As discussed above, ESMS is considered a 'soft' ionisation method since the analyte remains intact during analysis. However, fragmentation can be induced if required, providing a measure of sample fragility and the stability of ionised fragments. The sample cone and a series of skimmer cones (also referred to as the skimmer lens) are positioned between the analyser and the sample injector (refer to Figure 1.5), and the potential difference between these cones controls the degree of collisional energy imparted on to the analyte prior to detection. The collisions between ions and neutral molecules (solvent and drying gas) are often minimised to allow detection of intact parent ions but the potential difference applied across the cones can be systematically increased, imparting a higher degree of collisional energy to the ions and allowing fragmentation of the sample in a controlled manner [referred to as collision-induced dissociation (CID)].

[60] C.V. Depree, M.Sc. Thesis, University of Waikato, 1995.

1.3.3 Ionisation Methods

The solution nature of ESMS is of key importance to its effectiveness. In solution, neutral samples often associate with ions from the mobile phase (e.g. H^+ or Na^+) and these adducts are maintained through transfer to the gas phase, allowing detection of the neutral analyte. Providing the sample has a sufficiently acidic or basic functional site, formation of ion adducts in solution is likely, if only to a limited degree. The sensitivity of the mass spectrometric method provides intense spectra for even a small degree of ion association. Specific adduct formation can be induced by 'dosing' the sample with the appropriate ion {e.g. addition of KCl assists formation of $[M+K]^+$ adducts} which assists analyte detection and simplifies the spectra by removing competitive adducts {e.g. $[M+H]^+$, $[M+Na]^+$}.

Electrochemical ionisation of neutral analytes has also been identified by ESMS. The exact ionisation mechanism is still debated in the current literature but detection of oxidised or reduced analytes is well reported. Electrochemical ionisation is proposed to occur within the spectrometer at the interface of the solution and the charged capillary. The discharge of ions from the capillary tip causes a build-up of charge within the solution (refer to Figure 1.6), which is dissipated through electrochemical processes acting upon the analyte, solvent or capillary[61]. Electrochemical processes are not often observed under ESMS conditions since it is easier to oxidise (or reduce) the solvent or capillary than the analyte (e.g. the generation of Fe^{2+} ions has been reported, attributed to loss of iron from the capillary followed by oxidation[61]). However, if an easily oxidised analyte is present in the sample, the transfer of electrons from these species generates $[M]^+$ ions unlikely to have been present in the solution prior to injection. There are a numerous reports of *in situ* oxidation processes occurring, including the analysis of fullerenes[62,63], metallocenes[64] and polyaromatic hydrocarbons[65]. Various factors that influence the electrochemical process have been identified, including the redox properties of the analyte, the flow rate at which the solution is delivered to the ES source and the presence of electrolytes[66]. Although reports have mainly focussed on *in*

[61] A.T. Blades, M.G. Ikonomou and P. Kebarle, *Anal. Chem.*, 1991, **63**, 2109.
[62] A. Dupont, J-P. Gisselbrecht, E. Leize, L. Wagner and A. Van Dorsselaer, *Tet. Letters*, 1994, **35**, 6083.
[63] T-Y. Liu, L-L. Shiu, T-Y. Luh and G-R. Her, *Rapid Commun. Mass Spectrom.*, 1995, **9**, 604.
[64] X. Xu, S.P. Nolan and R.B. Cole, *Anal. Chem.*, 1994, **66**, 119.
[65] G.J. Van Berkel, S.A. McLuckey and G.L. Glish, *Anal. Chem.*, 1992, **64**, 1586.
[66] G.J. Van Berkel and F. Zhou, *Anal. Chem.*, 1995, **67**, 3958.

situ oxidation, equivalent reduction has been noted for appropriate analytes e.g. fullerenes[63] and quinones[62].

1.3.4 Inorganic Applications of ESMS

The application of ESMS to the analysis of biological samples has been extensively reported. The analysis of inorganic and organometallic compounds is less common, though publications in this field are increasing each year (150 in 2001 compared to 148, 125, 106 and 89 in the four preceding years[67]). The application of ESMS to the analysis of organometallic samples has been reviewed previously[68], especially in regards to the methods available for analyte ionisation[69].

A useful aspect of mass spectrometric analysis of organometallic compounds is the isotopic variation present in these materials. A number of commonly employed inorganic and metallic elements possess a characteristic isotope distribution, and the elemental composition of an ESMS signal can often be determined from high-resolution spectra. In contrast, the majority of organic elements display limited isotopic variation and the elemental composition cannot readily be inferred from mass spectrometric data.

1.3.5 ESMS Analysis of Transition Metal Clusters

Transition metal clusters are uniquely suited to ESMS analysis. Their involatility and fragility hampers traditional mass spectrometric analysis, and the only unambiguous characterisation method available is X-ray crystallography. There is also no guarantee that the compounds characterised crystallographically are the major products present in solution or that the solid-state structure mimics that of the compound in solution. For these reasons, the electrospray analysis of transition metal clusters has attracted interest.

1.3.5.1 Neutral Transition Metal Clusters

The majority of mass spectrometric studies of transition metal carbonyl clusters have been restricted to neutral compounds. These materials are typically more stable and easier to handle but require ionisation for detection.

[67] SciFinder Scholar database search for the keywords 'electrospray' and 'metal'.
[68] W. Henderson, B.K. Nicholson and L.J. McCaffrey, *Polyhedron*, 1998, **17**, 4291.

1.3.5.1A Methods of Ionisation

An impediment to the ESMS analysis of neutral transition metal carbonyl compounds or clusters is ionisation. The carbonyl ligands lack sufficient basicity to form adducts with H^+ or other common cations, hampering sample detection. However, a number of methods have recently been reported for ESMS identification of these materials. These methods involve chemical ionisation of the sample in solution immediately prior to injection and a few of the approaches available are outlined below.

1.3.5.1B Reaction with Alkoxide Ions

One of the more general methods employed in ionisation of transition metal carbonyls is the reaction with alkoxide ions[70,71]. The nucleophile attacks a coordinated carbonyl ligand, generating a $[M+OR]^-$ anion which is readily identifiable in negative ion ESMS. The method is remarkably general, equally applicable to mono-nuclear compounds and multinuclear clusters [the hexa-nuclear $Ru_6C(CO)_{17}$ species being one of the higher-nuclearity clusters analysed through this method]. The method is finding widespread use as a systematic method for ESMS characterisation of cluster materials [as reported for analysis of $Ru_3(CO)_{12-n}(PMe_3)_n$, n = 1, 2[72]].

1.3.5.1C Reaction with Azide Ions

Another ionisation process acting upon coordinated carbonyl ligands is the reaction with azide ions[73]. The conversion of a neutral carbonyl ligand into an anionic isocyanate (NCO) group has been reported[74] (*via* N_3^- coordination and subsequent N_2 loss). The method works equally well in ionising neutral metal carbonyls to allow ESMS analysis, with parent ions corresponding to either $[M-CO+NCO]^-$ or, more interestingly, $[M+N_3]^-$. Some ambiguity is associated with ion assignment using this method since the masses of N_2 and CO are identical but previous studies have shown that N_2 loss is facile from these compounds. Also, the action of the azide ion appears less specific than the

[69] J.C. Traeger and R. Colton, *Adv. Mass Spectrom.*, 1998, **14**, 637; R. Colton, A. D'Agostino and J.C. Traeger, *Mass Spectrometry Reviews*, 1995, **14**, 79.
[70] W. Henderson, J.S. McIndoe, B.K. Nicholson and P.J. Dyson, *J. Chem. Soc., Dalton Trans.*, 1998, 519.
[71] W. Henderson, J.S. McIndoe, B.K. Nicholson and P.J. Dyson, *Chem. Commun.*, 1996, 1183.
[72] M.I. Bruce, B.W. Skelton, A.H. White and N.N. Zaitseva, *Aust. J. Chem.*, 1997, **50**, 163.
[73] J.S. McIndoe and B.K. Nicholson, *J. Organomet. Chem.*, 1999, **573**, 232.
[74] W. Beck, *J. Organomet. Chem.*, 1990, **383**, 143.

alkoxide, with signals detected corresponding to $[M+N_3]^-$, $[M-CO+NCO]^-$, $[M-H]^-$, and in one case $[M-CO+CN]^-$ [73].

1.3.5.1D Metal Ion Adducts

The addition of metal ions provides an alternative method of ionising transition metal carbonyl clusters. The formation of adducts with H^+ ions has been reported for many neutral mono-nuclear species, and equivalent adducts with Na^+ [70] and Ag^+ [75] have been identified in ESMS analysis of transition metal clusters. The sodium ion presumably associates with the carbonyl ligand within solution whereas silver ions are effective for analytes containing M-M bonds. The ability of silver ions to bridge two metal atoms has been reported[76] and a similarly structured adduct is presumably formed in solution.

1.3.5.1E 'Electrospray-Friendly' Ligands

An alternative approach is the development of 'electrospray-friendly' ligands[77]. These neutral ligands are designed to mimic traditional ligands in terms of steric and electronic properties but they also possess a basic site, allowing generation of $[M+H]^+$ ions in solution. An example is $Ph_xP(C_6H_4OMe\text{-}p)_{3-x}$ (x = 0, 1, 2), which mimics PPh_3, yet contains a basic methoxide functionality that assists ESMS detection. The functionalised clusters can be characterised by ESMS {e.g. $Ru_3(CO)_9[P(Ph)_2C_6H_4OMe\text{-}p]_3$ - Figure 1.7} whereas the unfunctionalised analogues provide no ESMS signal. A series of functionalised ligands are currently being developed [e.g. $HSC_6H_4OMe\text{-}p$, $Ph_xP(C_6H_4NMe_2\text{-}p)_{3-x}$ and $CNC_6H_4OMe\text{-}p$] to extend the range of clusters examinable[78].

[75] W. Henderson and B.K. Nicholson, *J. Chem. Soc., Dalton Trans.*, 1995, 2531.
[76] A.J. Carty, G.N. Mott and N.J. Taylor, *J. Am. Chem. Soc.*, 1979, **101**, 3131; G.N. Mott, N.J. Taylor and A.J. Carty, *Organometallics*, 1983, **2**, 447.
[77] C. Decker, W. Henderson and B.K. Nicholson, *J. Chem. Soc., Dalton Trans.*, 1999, 3507.
[78] C. Decker, unpublished results.

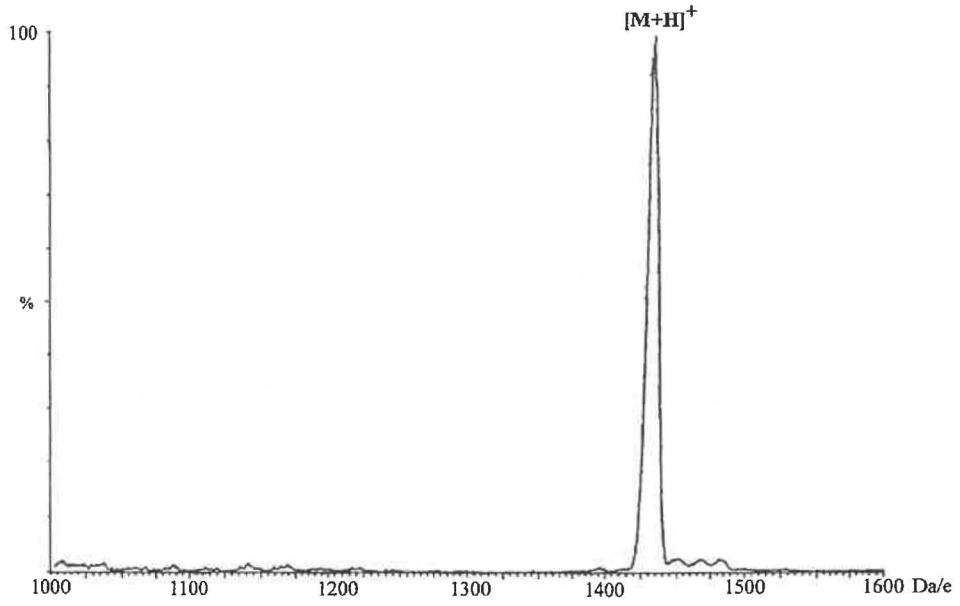

Figure 1.7 – The ES mass spectrum (+ve ion, 20 cV) of $Ru_3(CO)_9[P(Ph)_2C_6H_4OMe]_3$ [79].

The use of $P(C_6H_4SO_3Na\text{-}m)_3$ as an alternative 'electrospray-friendly' phosphine has also been reported[80]. Rather than the protonation observed for the methoxy- and dimethylamino-functionalised ligands, $P(C_6H_4SO_3Na\text{-}m)_3$ loses Na^+ in solution to provide $[M\text{-}nNa]^{n-}$ ions. The phosphine is commonly employed to provide water-soluble products, with the 'electrospray-friendly' character incidental. The use of $P(C_6H_4SO_3Na\text{-}m)_3$ allowed detection of the series of derived clusters: $Ru_3(CO)_{12-x}P_x$ (x = 1-3), $H_4Ru_4(CO)_{12-x}P_x$ (x = 1, 2, 4), $Ru_6C(CO)_{16}P$ and $H_2Os_3(CO)_9P$ [where P corresponds to $P(C_6H_4SO_3Na\text{-}m)_3$].

1.3.5.2 ESMS of Ionic Clusters

The discussion above has been restricted to neutral cluster compounds, with ionisation required prior to detection. An advantage of analysing ionic cluster species is that only the transfer of solution ions to the gas phase is required. There have been a number of isolated examples of ESMS analysis of ionic cluster species (discussed below) but no systematic examination of ionic cluster materials has been reported.

One of the earliest reported examples was the characterisation of $[PtRh_5(CO)_{15}]^-$, formed from the reduction of Na_2PtCl_6 and $RhCl_3.nH_2O$ under a CO atmosphere on the surface of a MgO support[81]. The dominant signal corresponded to the intact parent

[79] Provided by C. Decker, University of Waikato.
[80] D.J.F. Bryce, P.J. Dyson, B.K. Nicholson and D.G. Parker, *Polyhedron*, 1998, **17**, 2899.
[81] Z. Xu, S. Kawi, A.L. Rheingold and B.C. Gates, *Inorg. Chem.*, 1994, **33**, 4415.

cluster with less intense signals observed for the $[M\text{-}CO]^-$ and $[M\text{-}2CO]^-$ fragmented ions.

A higher-nuclearity example was the analysis of $[Pt_{12}(CO)_{24}]^{2-}$ (structure shown in Figure 1.8 [82]), with intense signals detected for an adduct of the parent ion, $[M+PPh_4]^-$, and a $[M\text{-}13CO]^{2-}$ fragment[83]. A less intense signal was identified for $[M\text{-}Pt_3(CO)_6+PPh_4]^-$, corresponding to loss of a Pt_3 triangle from the parent cluster. Another isolated example was the ESMS characterisation of $[Ru_6C(CO)_{16}(SnCl_3)]^-$ [84].

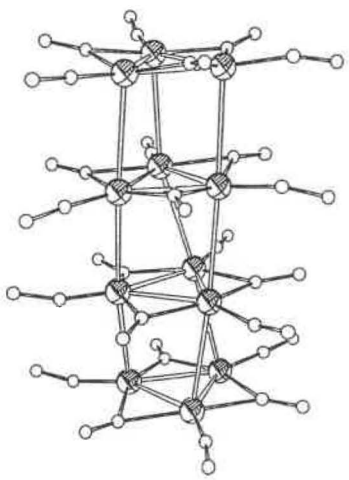

Figure 1.8 – The structure of $[Pt_{12}(CO)_{24}]^{2-}$ [82].

ESMS characterisation of transition metal carbonyl clusters has often been reported with little understanding of the controlled fragmentation available. The ESMS data reported for $[Ni_{10}(Sb^iPr)_2(CO)_{18}]^{2-}$ (with a $Ni_{10}Sb_2$ icosahedral cage arrangement) are an example where fragmentation ions dominate over the intact parent cluster[85]. Signals corresponding to loss of both carbonyl and propyl ligands were reported, though the extent of fragmentation could have been reduced considerably by application of a lower accelerating voltage and the intensity of the parent ion, $[M]^{2-}$, increased (from the 0.7% reported). Similar ESMS analysis of $[Ni_{10}(BiMe)_2(CO)_{18}]^{2-}$ has been reported without identification of the intact parent cluster because of a high applied voltage[86].

The characterisation of $[Fe_3(\mu_2\text{-}HgML)(CO)_{11}]^-$ [ML = $Co(CO)_4$, $Mo(CO)_3(\eta^5\text{-}C_5H_5)$, $W(CO)_3(\eta^5\text{-}C_5H_5)$, $Fe(CO)_2(\eta^5\text{-}C_5H_5)$, $Mn(CO)_5$] compounds have also been reported at

[82] J.C. Calabrese, L.F. Dahl, P. Chini, G. Longoni and S. Martinengo, *J. Am. Chem. Soc.*, 1974, **96**, 2614.
[83] C.E.C.A. Hop and R. Bakhtiar, *J. Chem. Ed*, 1996, **73**, A160.
[84] S. Hermans and B.F.G. Johnson, *Chem. Commun.*, 2000, 1955.
[85] P.D. Mlynek and L.F. Dahl, *Organometallics*, 1997, **16**, 1641.
[86] P.D. Mlynek and L.F. Dahl, *Organometallics*, 1997, **16**, 1655.

high applied voltage[87]. Spectra were acquired across a wide voltage range (50-100 V), with dominant signals corresponding to fragmentation ions rather than the intact parent clusters. A comparison of FABMS and ESMS analyses of $[Fe_6C(CO)_{16}(AuPPh_3)]^-$ was also provided[87], with ES mass spectra displaying a lesser degree of fragmentation.

The recently reported ESMS characterisation of $[Pd_{16}Ni_4(CO)_{22}(PPh_3)_4]^{2-}$ was also examined at high applied voltage (60 V), with detection of fragmentation ions {$[M\text{-}xCO]^{2-}$, x = 6-11} but lacking a signal from the intact parent cluster[88]. Attempted characterisation of the cluster by FABMS was unsuccessful. The larger $[Pd_{33}Ni_9(CO)_{41}(PPh_3)_6]^{4-}$ cluster was unable to be characterised by ESMS, presumably because of instability in dilute solution though de-oxygenated conditions were applied. ESMS was also inappropriately applied to the attempted characterisation of the large $[Cu_xNi_{35-x}(CO)_{40}]^{5-}$ (x = 3 or 5) cluster[89]. Using a high applied voltage (60 V), no signals attributable to the parent cluster were detected and the composition of the cluster was unable to be established. Equivalent analysis at lower voltage (*ca.* 5 V) may well have provided an intact parent ion.

Ignorance relating to the ESMS technique was also indicated in characterisation of $[Mo_4\{\mu_3\text{-}AsMo(CO)_5\}(CO)_{12}(OMe)_3]^{2-}$, produced from $NaAsO_2$ and $Mo(CO)_6$ [90]. The method was described as "FABMS (electrospray)" though the two are completely separate techniques and spectra were acquired only in positive-ion mode, with identification of the parent cluster as the $[NEt_4]_3[M]^+$ adduct. A comparison of observed and calculated isotope profiles was provided, with serious discrepancies between the two, no doubt a factor of the low intensity of the $[NEt_4]_3[M]^+$ signal. A negative-ion spectrum of this sample would almost certainly have been more informative.

ESMS has recently been applied to the analysis of samples containing a mixture of cluster species[91]. After reaction between $Ru_6C(CO)_{17}$ and $[Co(CO)_4]^-$ in thf, examination of the solution by ESMS (using the technique of EDESI-MS, discussed in Section 1.3.5.3) detected the presence of $[Co_3Ru(CO)_{12}]^-$, $[CoRu_3(CO)_{13}]^-$,

[87] M. Ferrer, R. Reina, O. Rossell, M. Seco and G. Segalés, *J. Organomet. Chem.*, 1996, **515**, 205.
[88] M. Kawano, J.W. Bacon, C.F. Campana, B.E. Winger, J.D. Dudek, S.A. Sirchio, S.L. Scruggs, U. Geiser and L.F. Dahl, *Inorg. Chem.*, 2001, **40**, 2554.
[89] P.D. Mlynek, M. Kawano, M.A. Kozee and L.F. Dahl, *J. Cluster Sci.*, 2001, **12**, 313.
[90] J.W. Van Hal, K.H. Whitmire, B. Zouchoune, J-F. Halet and J-Y. Saillard, *Inorg. Chem.*, 1995, **34**, 5455.
[91] P.J. Dyson, A.K. Hearly, B.F.G. Johnson, T. Khimyak, J.S. McIndoe and P.R.R. Langridge-Smith, *Organometallics*, 2001, **20**, 3970.

$[HCo_2Ru_4C(CO)_{15}]^-$ and $[CoRu_5C(CO)_{16}]^-$. Analysis of the equivalent reaction with $[Ir(CO)_4]^-$ identified $[Ir_3Ru(CO)_{12}]^-$, $[IrRu_3(CO)_{13}]^-$ and $[IrRu_5C(CO)_{16}]^-$. The ability to monitor cluster reactions using ESMS was also reported, allowing reaction conditions to be tuned to produce the desired products.

Direct comparison between ESMS and other spectrometric techniques has been reported for cluster samples. An example was the analysis of a series of rhenium, ruthenium and osmium clusters by both ESMS and LDI[92]. The LDI spectra usually contained the intact parent ion but also displayed significant carbonyl loss, while ES mass spectra were composed of a single signal corresponding to the intact parent cluster. The ability to induce carbonyl loss from the parent signal was also reported.

1.3.5.3 Energy-Dependent Electrospray Ionisation Mass Spectrometry (EDESI-MS)

A recently reported extension to ESMS is the technique of energy-dependent electrospray (ionisation) mass spectrometry (EDESI-MS)[93]. The ability to induce fragmentation through manipulation of the potential difference between the sample and skimmer cones was discussed earlier, and EDESI-MS effectively provides a 2D representation of induced fragmentation through a contour plot of cone voltage against *m/z*. The 2D spectra are usually capped by a 1D spectrum comprising a sum of all spectra across the cone voltage range. A negative-ion EDESI mass spectrum of $[NEt_4][CoRu_3(CO)_{13}]$ is displayed in Figure 1.9.

[92] P.J. Dyson, A.K. Hearley, B.F.G. Johnson, J.S. McIndoe and P.R.R. Langridge-Smith, *J. Cluster Sci.*, 2001, **12**, 273.
[93] P.J. Dyson, B.F.G. Johnson, J.S. McIndoe and P.R.R. Langridge-Smith, *Rapid Commun. Mass Spectrom.*, 2000, **14**, 311.

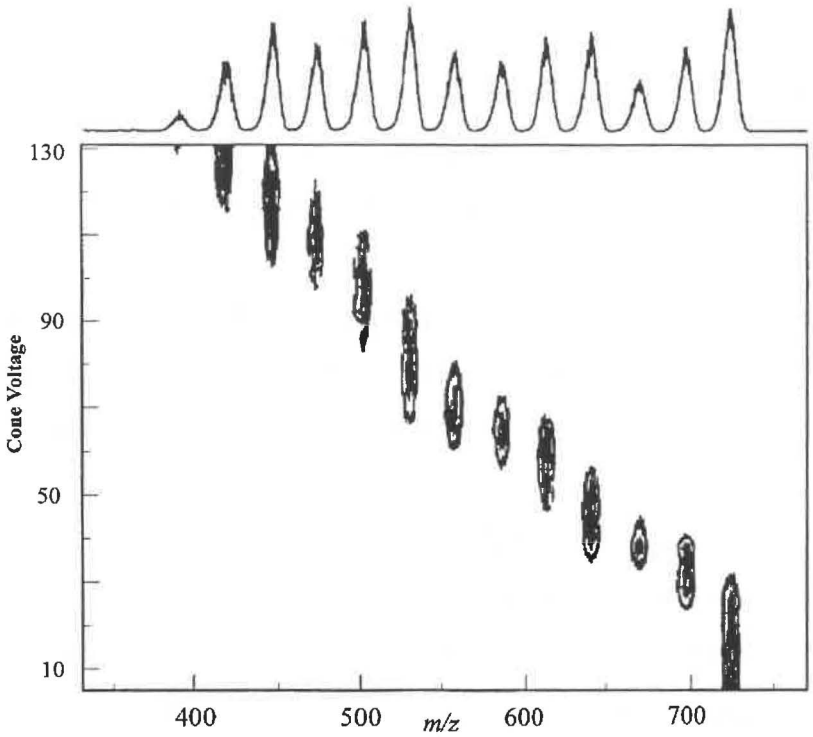

Figure 1.9 – The EDESI mass spectrum (-ve ion) of $[NEt_4][CoRu_3(CO)_{13}]$ using a MeOH carrier solvent, with voltage increments of 1V/10 seconds. The data was normalised and plotted using the AXUM program.

EDESI-MS provides information regarding the fragmentation of parent clusters, with the observed fragmentation occasionally providing key mechanistic information. An example was the elimination of HCHO from $[Ru_6C(CO)_{16}(CO_2Me)]^-$ (after initial loss of 2 CO ligands), generating the $[HRu_6C(CO)_{15}]^-$ cluster[94]. Equivalent HCHO loss from $[Rh_6(CO)_{15}(CO_2Me)]^-$ was noted but only after initial loss of 7 CO ligands[94]. Analogous loss of MeCHO was observed in the EDESI mass spectrum of $[Ru_6C(CO)_{16}(CO_2Et)]^-$.

[94] P.J. Dyson, N. Feeder, B.F.G. Johnson, J.S. McIndoe and P.R.R. Langridge-Smith, *J. Chem. Soc., Dalton Trans.*, 2000, 1813.

1.4 Prelibation[95]

The research presented within this thesis involves the application of ESMS to the analysis of transition metal carbonyl clusters. The thesis has been divided into eight chapters, six of which represent independent sections of research (Chapters 1 and 2 provide a literature review of the field and reference to experimental procedures).

The systematic ESMS analysis of a series of rhodium and nickel clusters is presented in Chapter 3. These clusters were used to establish the effectiveness of the ESMS technique and as a trialing system for the analysis of air-sensitive samples.

The reactions between μ_4-E[$M_2(CO)_x$]$_2$ [E = Si, Ge, Sn; M = Co (x = 7), Fe (x = 8)] and various anionic transition metal carbonyl reagents are reported in Chapters 4 and 5. The reactions between μ_4-E[$M_2(CO)_x$]$_2$ and $[Co(CO)_4]^-$ are discussed in greater detail since several high-nuclearity cluster products have previously been identified in these systems. Equivalent reactions with other mono-, di- and tri-nuclear anionic transition metal carbonyl reagents are presented in Chapter 5.

The synthesis and reactions of clusters incorporating group 15 elements are described in Chapter 6. The research documents thermolysis and salt elimination reactions involving the full series of group 15 elements (N, P, As, Sb, Bi). In particular, ESMS analysis of the reactions between $M_3(CO)_{12}$ (M = Ru, Os) and $[PPN]N_3$ are documented.

Research detailed in Chapter 7 involves the synthesis, characterisation and reactions of a series of neutral $Co_4(\mu_4\text{-}ER)_2(CO)_{11}$ (E = Si, Ge) clusters. The examination of ligand substitution reactions of these clusters using isonitriles, phosphites, and phosphines are reported. The synthesis and characterisation of a series of linked $Co_4(\mu_4\text{-}ER)_2(CO)_{11}$ clusters are also described.

The final chapter reports the crystallographic structure determinations of a series of anionic transition metal carbonyl species. A new structural isomer of $[CoFe_3(CO)_{13}]^-$ is presented and discussed with respect to the Ligand Polyhedral Model. The structure of

[95] Prelibation – 'a tasting beforehand or by anticipation; a foretaste', Oxford English Dictionary, Second Edition , Clarendon Press (Oxford, England), 1989.

$[PPN][Mo(CO)_3(\eta^5\text{-}C_5H_5)]$ is also described, with the $[PPN]^+$ cations displaying an 'extended phenyl embrace' supramolecular motif.

Chapter Two – Experimental Methods and Materials

2.1 Methods

2.1.1 Electrospray Mass Spectrometry (ESMS)

All ES mass spectra were acquired on a VG Platform II (Fisons/Micromass) electrospray mass spectrometer using a quadrupole detector. Data were processed using the Mass Lynx™ software package with assignment of signals aided by simulation using the Isotope program[1]. Nitrogen was employed as both the nebulising and drying gas (15 L hr^{-1} and 250 L hr^{-1} respectively). The carrier solvent was delivered to the ES interface at a flow rate of 0.02 mL min^{-1} with the source maintained at 60°C.

The carrier solvent employed varied depending upon the nature of the sample. ESMS analysis of reaction mixtures was typically carried out using a carrier solvent with similar chemical properties to the reaction solvent while being more suited to ESMS (with respect to boiling point, density etc). For reactions involving group 14/transition metal clusters, 1,2-dichloroethane was used exclusively (the selection of the most suitable solvent for these studies is outlined in Chapter 4). The system was purged with distilled CH_2Cl_2 for approximately 30 minutes to 1 hour before connection to the dichloroethane in order to remove traces of acetonitrile and methanol from the capillaries, and to prevent contamination of the dichloroethane. Using these practices, traces of water or methanol were not detected in the solvent for periods up to a month after distillation.

Samples were prepared and analysed under inert conditions using standard Schlenk apparatus, allowing samples to be alternated between vacuum and an argon atmosphere. Samples were injected *via* a Rheodyne Model 7125 injector fitted with a 10 μL sample loop. Spectra were acquired in either positive- or negative-ion mode depending upon the nature of the sample. Initial spectra were acquired at low resolution (*ca.* 1 amu) over a large mass range with higher-resolution data (*ca.* 0.3 amu) acquired for specific peaks of interest. Spectra were acquired at very low applied cone voltage (5 cV) to minimise

[1] L.J. Arnold, *J. Chem. Ed.*, 1992, **69**, 811.

fragmentation of the parent ions, with systematic increase in the voltage inducing carbonyl loss. The *m/z* values listed correspond to the most intense peak in the isotope pattern.

2.1.2 Infra-red (IR) Spectroscopy

Infra-red spectra were acquired on a Digilab FTS-40 instrument using a ceramic source and mid-infrared DTGS detector. Unless otherwise stated, samples were acquired as solutions in a KBr window solution cell (0.1 mm pathlength) using 16 scans at a resolution of 2 cm^{-1}. IR analysis was limited to the carbonyl stretching region (1600-2200 cm^{-1}), and the data manipulated using the subtraction and smoothing functions of the software (BIO RAD Win-IR version 4.14).

2.1.3 Nuclear Magnetic Resonance (NMR) Spectroscopy

^{29}Si-{^{1}H} and ^{31}P-{^{1}H} NMR spectra were recorded on a Bruker AC300P FT-NMR spectrometer at 59.6 MHz and 121.5 MHz respectively in $CDCl_3$. ^{1}H and ^{13}C-{^{1}H} spectra were acquired on either this machine or a Bruker DRX 400 FT-NMR spectrometer. Assignment of signals was aided by the use of COSY (^{1}H-^{1}H correlation), HSQC (Heteronuclear single quantum ^{1}H-^{13}C correlation) and HMBC (Heteronuclear multiple bond ^{1}H-^{13}C correlation) experiments[2]. ^{1}H, ^{13}C and ^{29}Si spectra were referenced to tetramethylsilane (TMS) and ^{31}P spectra were referenced to 85% H_3PO_4.

NMR analysis was limited to $Co_4(\mu_4\text{-}ER)_2(CO)_{11}$ and related clusters reported in Chapter 7. The spectra were assigned according to the labelling scheme presented in Scheme 2.1.

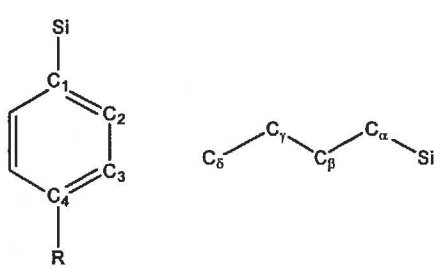

Scheme 2.1 – The NMR labelling scheme.

[2] All NMR experiments were performed using standard Bruker pulse sequences.

2.1.4 X-Ray Crystallography

Single crystals of suitable compounds were obtained through liquid/liquid diffusion. The diffusions were often performed in modified Schlenk flasks (Figure 2.1) by layering of the appropriate solvents under an inert atmosphere and storage at –20°C. The modified flasks had a small internal diameter (5 mm) to slow the diffusion process, assisting formation of single crystals[3]. A number of these modified flasks were produced and have been used successfully by various members of the inorganic group at Waikato.

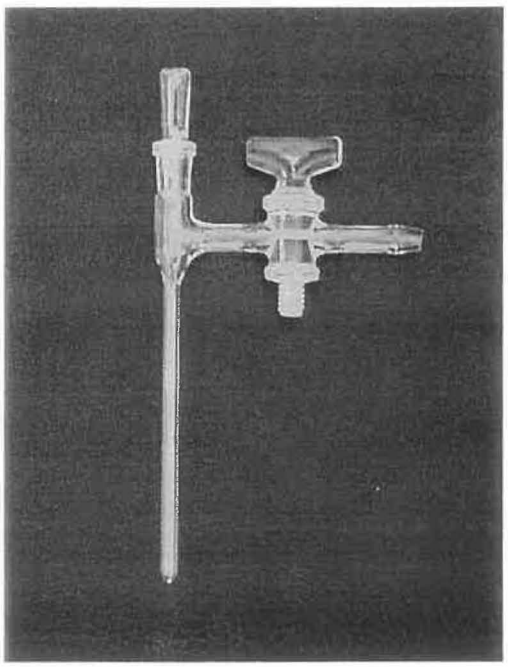

Figure 2.1 – The modified Schlenk flask to assist crystallisation.

X-ray crystal data were recorded at either the University of Auckland or the University of Canterbury with a Siemens SMART CCD diffractometer using Mo-K_α radiation[4]. The data reduction and cell refinement were performed using the SAINT[5] application, and the absorption correction calculated using SADABS[6].

[3] Experience showed that the ideal environment for crystallisation was within NMR tubes. The modified flasks have similar dimensions to NMR tubes while allowing storage under an inert atmosphere.

[4] Siemens SMART, 1994, Siemens Analytical Instruments Inc., Madison, Wisconsin, USA.

[5] Siemens SAINT, 1994, Siemens Analytical Instruments Inc., Madison, Wisconsin, USA.

[6] R.H. Blessing, *Acta. Cryst. Sect. A*, 1995, **51**, 33.

The structures were solved and refined using the SHELX-97[7] suite of programs, manipulated through the use of the WinGX package[8]. The structures were solved using direct methods and developed from subsequent difference maps. Hydrogen atoms were placed in calculated positions (U_{iso} 1.2 times that of the atom to which they were attached) using a riding model. In cases of disorder, hydrogen atoms were omitted.

Diagrams were prepared using ORTEP-3 for Windows[9], CAMERON[10] and PLUTON[11]. Tables of relevant bond parameters and structure solution data are provided in appropriate chapters while full tables of crystallographic data are supplied in the Appendices. Crystallographic Information Files (CIF's) are provided on a supplied 3.5" disc.

2.1.5 Elemental Analysis

All elemental analyses were performed by the University of Otago Microanalytical Laboratory.

2.1.6 Chromatography

Isolation of cluster products through chromatography was only applicable to the $Co_4(\mu_4\text{-}ER)_2(CO)_{11}$ clusters reported in Chapter 7. Thin Layer Chromatography (TLC) was used in the first instance to determine the extent of reaction and to ascertain an appropriate solvent composition for larger scale separation. The separation was performed on aluminium backed silica TLC plates (0.2 mm thickness) and visualised under white light.

Column chromatography was used to separate the reaction products on a preparative scale. A slurry of pre-weighed silica (Merck Kieselgel 60, 70-230 mesh) or Florisil

---

[7] G.M. Sheldrick, SHELX-97: Programs for the solution and refinement of crystal structures, University of Göttingen, Germany, 1997.

[8] L.J. Farrugia, *J. Appl. Cryst.*, 1999, **32**, 837.

[9] L.J. Farrugia, *J. Appl. Cryst.*, 1997, **30**, 565.

[10] D.M. Watkin, L. Pearce and C.K.A. Prout, Molecular Graphics Package, 1993, Chemical Crystallography Laboratory, University of Oxford, England.

[11] A.L. Spek, *Acta Cryst. Sect. A.*, 1990, **46**, C34.

(activated magnesium silicate, 60-100 mesh) was suspended in the appropriate solvent, transferred into a column (20 mm diameter) plugged with cotton wool and allowed to settle for 2-24 hours. Mixtures were loaded onto the column as solutions and collected as separate fractions on the basis of colour. Column chromatography was also performed under a positive pressure of nitrogen in an attempt to minimise contact with oxygen though little difference was noted.

The use of alumina (BDH, Brockman Grade II) rather than silica was unsuccessful, with decomposition of the clusters noted within minutes of sample loading. Similarly, separation using the Chromatotron® (Model 79247T) was trialed and found ineffective. The ability to perform separation under a nitrogen atmosphere is an advantage of this apparatus but the limited scale tolerated by the technique and poor resolution detracted from its application. Preparative Layer Chromatography (PLC) was trialed on various occasions but was found to be inappropriate to the scale required and samples tended to adhere to the silica, preventing recovery in acceptable yield.

2.2 Materials

2.2.1 Solvents

All solvents (with the exception of 1,2-dichloroethane) were distilled and stored under a nitrogen atmosphere until use. 1,2-dichloroethane was purified in a similar manner though under an argon atmosphere. Solvents were transferred *via* a nitrogen flushed syringe to the reaction vessel without exposure to atmospheric oxygen.

Dichloromethane, petroleum spirits (60-80°C), 1,2-dichloroethane, acetonitrile and *n*-heptane were distilled over calcium hydride; tetrahydrofuran (thf), diethylether and bis-2-methoxyethylether (diglyme) were distilled over sodium/benzophenone ketyl, and toluene was distilled over molten sodium. Throughout the course of this thesis, reference to petroleum spirits implies the fraction collected between 60-80°C.

2.2.2 μ_4-E[$M_2(CO)_x$]$_2$ Compounds

μ_4-Ge[$Co_2(CO)_7$]$_2$ [12], μ_4-Si[$Co_2(CO)_7$]$_2$ [13] and μ_4-Si[$Fe_2(CO)_8$]$_2$ [14] were provided by previous research students. The compounds were produced from the reaction of EH_4 with the appropriate metal carbonyl.

2.2.2.1 Synthesis of μ_4-Sn[$Fe_2(CO)_8$]$_2$ [14]

A thf solution (20 mL) of $Fe(CO)_5$ (1.3 mL, 1.94 g, 10 mmol) was reduced over a 1% sodium amalgam for 3 hours and added slowly to a thf solution (5 mL) of distilled $SnCl_4$ (0.3 mL, 0.668 g, 2.6 mmol). The solution was stirred for 3 hours, solvent removed under vacuum and products extracted into CH_2Cl_2 (10 mL). Ionic impurities were removed through chromatography to yield μ_4-Sn[$Fe_2(CO)_8$]$_2$ (1.07 g, 1.3 mmol, 52%)

μ_4-Sn[$Fe_2(CO)_8$]$_2$

M_r – 790.2

IR – (ν_{CO}, CH_2Cl_2) 2073 (s), 2045 (s), 2029 (ms), 2010 (ms) cm^{-1} [Lit. 2072 (m), 2044 (s), 2027 (ms), 2010 (s) cm^{-1} [15]]

ESMS – ($C_2H_4Cl_2$, -ve ion, 5 cV) *m/z* 837 (100% - $[M+CO_2H]^-$) after addition of Na[CO_2H]

2.2.3 Transition Metal Carbonyl Precursors

$Co_2(CO)_8$, $Fe(CO)_5$, $Fe_2(CO)_9$, $Mn_2(CO)_{10}$, [$Mo(CO)_3(\eta^5$-$C_5H_5)$]$_2$, [$Fe(CO)_2(\eta^5$-$C_5H_5)$]$_2$, $Co(\eta^5$-$C_5H_5)_2$, $Ir_4(CO)_{12}$, $Os_3(CO)_{12}$ and $Ru_3(CO)_{12}$ were used as supplied by Strem Chemicals Ltd.

$Fe_3(CO)_{12}$ (Strem) was purified through Soxhlet extraction with petroleum spirits prior to use.

---

[12] R.F. Gerlach, K.M. Mackay and B.K. Nicholson, *J. Organomet. Chem.*, 1979, **178**, C30.

[13] K.M. Mackay and C.C. Tan, *J. Chem. Research*, 1982, 229.

[14] S.G. Anema, G.C. Barris, K.M. Mackay and B.K. Nicholson, *J. Organomet. Chem.*, 1988, **350**, 207.

[15] J.D. Cotton, S.A.R. Knox, I. Paul and F.G.A. Stone, *J. Chem. Soc. A*, 1967, 264.

2.2.3.1 Synthesis of $Co_4(CO)_{12}$ [16]

A 20 mL solution (heptane, benzene or toluene) of $Co_2(CO)_8$ (1.0 g, 2.9 mmol) was heated under an inert atmosphere (argon or nitrogen) to 50°C until IR spectra indicated complete conversion to $Co_4(CO)_{12}$. The time required varied between 24-48 hours (benzene and toluene) and *ca.* 120 hours (heptane). Solvent was removed under vacuum and recrystallisation from CH_2Cl_2/petroleum spirits at –20°C yielded black cubes of $Co_4(CO)_{12}$ (0.62 g, 1.1 mmol, 74 %).

$Co_4(CO)_{12}$
M_r – 571.9
IR – (ν_{CO}, pet. spirits) 2063 (s), 2055 (s), 2028 (m), 1867 (s) cm^{-1}

2.2.4 Anionic Transition Metal Carbonyl Reagents

2.2.4.1 Synthesis of [Cat.][$Co(CO)_4$] (Cat. = NEt_4, PPN, $PhCH_2NMe_3$, PPh_4, $AsPh_4$)

Various salts of $[Co(CO)_4]^-$ were used in the course of this research. All were prepared from the reduction of a thf solution of $Co_2(CO)_8$ over a *ca.* 1% sodium amalgam. After 1-2 hours, the appropriate cation was added (usually as the chloride salt) and the mixture stirred for an additional 10 minutes. The clear, pale yellow solution was transferred *via* syringe to a separate Schlenk flask, solvent removed under vacuum and the product recrystallised from CH_2Cl_2/Et_2O.

In the case of Na[$Co(CO)_4$], the thf solution was transferred from the amalgam and solvent removed under vacuum. Recrystallisation of Na[$Co(CO)_4$] was not attempted and the compound was diluted in CH_2Cl_2 to known concentration from which a stoichiometric volume was added to the reaction flask. For example, a 0.129 mol L^{-1} solution of Na[$Co(CO)_4$] was prepared from reduction of $Co_2(CO)_8$ (0.88 g, 2.6 mmol) in thf (40 mL), with ¾ of the solution transferred to a separate Schlenk flask, solvent removed under vacuum and the oily solid redissolved in CH_2Cl_2 (30 mL).

The ES mass spectra of these compounds indicated the purity of the samples. Negative-ion spectra displayed signals corresponding to $[Co(CO)_4]^-$ (*m/z* 171), $[Cat.][Co(CO)_4]_2^-$

[16] M.F. Mirbach, A. Saus, A-M. Krings and M.J. Mirbach, *J. Organomet. Chem.*, 1981, **205**, 229.

(where Cat. is the appropriate cation) and $[Hg\{Co(CO)_4\}_3]^-$ (*m/z* 715). The mercury salt was a by-product of the reduction process and was only present at low intensity after recrystallisation. A typical negative-ion ES mass spectrum of $[NEt_4][Co(CO)_4]$ is shown in Figure 2.2.

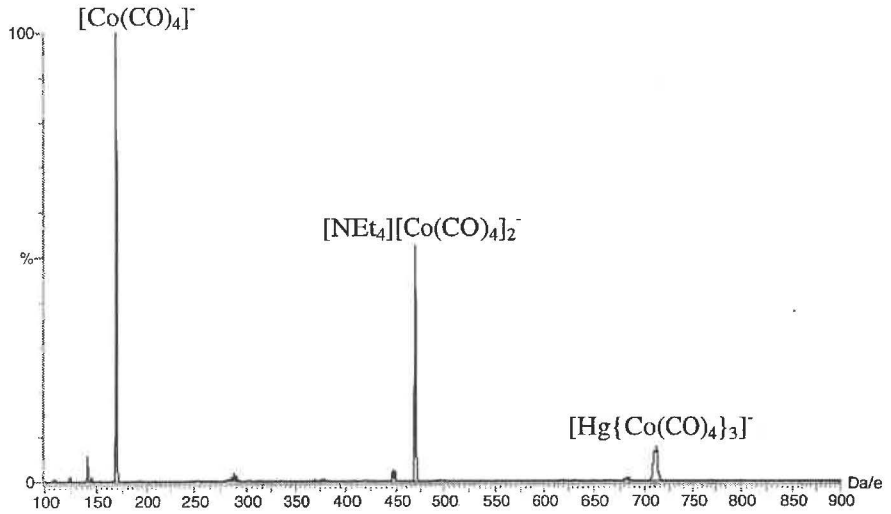

Figure 2.2 – The ES mass spectrum (-ve ion, 10 cV) of $[NEt_4][Co(CO)_4]$.

$[NEt_4][Co(CO)_4]$

M_r – 301.2

IR – (ν_{CO}, CH_2Cl_2) 2004 (vw), 1887 (vs) cm^{-1} [Lit. 1890 (vs) cm^{-1} [17]]

ESMS – ($C_2H_4Cl_2$, -ve ion, 5 cV) *m/z* 171 (100% - $[Co(CO)_4]^-$), *m/z* 472 (55% - $[NEt_4][Co(CO)_4]_2^-$), *m/z* 715 (10% - $[Hg\{Co(CO)_4\}_3]^-$)

In a number of experiments involving $[Co(CO)_4]^-$, an additional signal corresponding to $[Ag\{Co(CO)_4\}_2]^-$ (*m/z* 449) was detected (Figure 2.3). The silver adduct was attributed to contamination in the ESMS capillaries since Ag^+ is commonly employed by other researchers as an ionisation aid and has tendency to linger in the system. The $[Ag\{Co(CO)_4\}_2]^-$ anion is unusual but not unprecedented, with the analogous $[PPN][Au\{Co(CO)_4\}_2]$ salt[18] and the neutral $[AgCo(CO)_4]_4$ compound[19] known. The anion was synthesised directly by mixing stoichiometric quantities of $Ag[BF_4]$ and various salts of $[Co(CO)_4]^-$. Similarly, addition of $Ag[BF_4]$ to a thf solution of

[17] J.K. Ruff and W.J. Schlientz, *Inorg. Syn.*, 1974, **15**, 84.

[18] R. Usón, A. Laguna, M. Laguna, P.G. Jones and G.M. Sheldrick, *J. Chem. Soc., Dalton Trans.*, 1981, 366.

[19] R.D. Ernst and T.J. Marks, *Inorg. Chem.*, 1978, **17**, 1477.

$Na[Co(CO)_4]$ followed by treatment with $[PPN][BF_4]$[20] produced $[PPN][Ag\{Co(CO)_4\}_2]$. Attempts to crystallise the anion with various cationic species were unsuccessful.

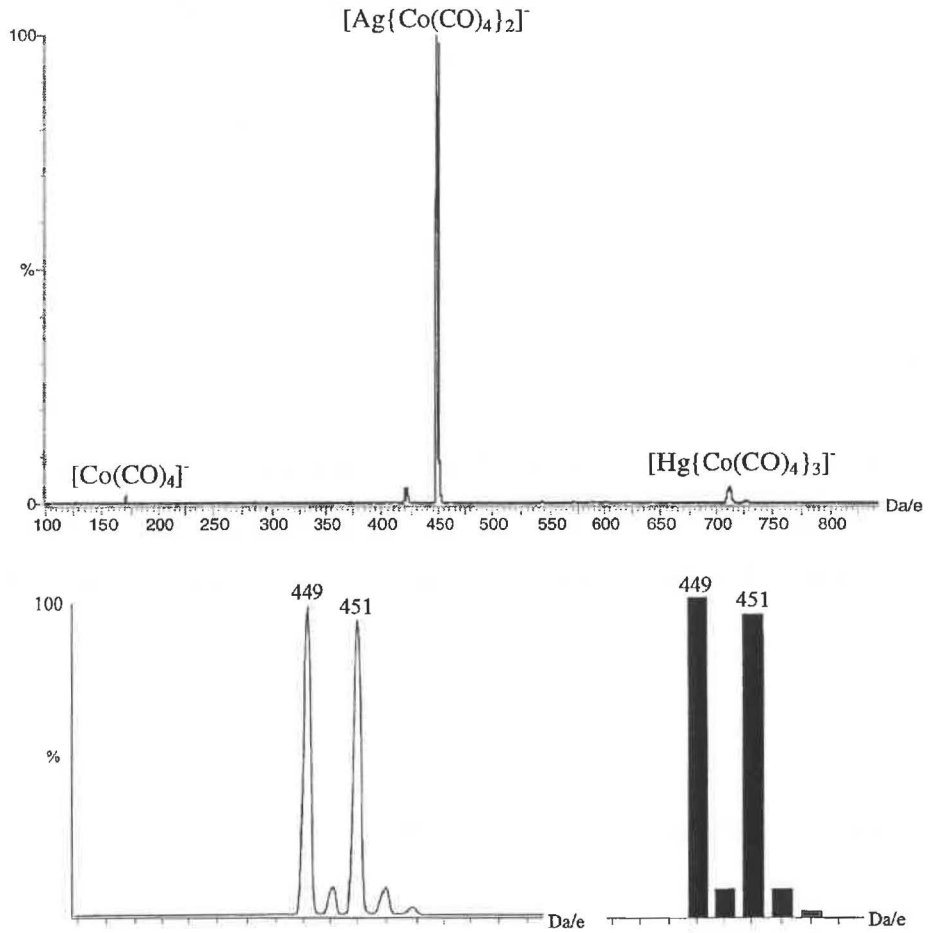

Figure 2.3 – The ES mass spectrum (-ve ion, 10 cV) of $Na[Ag\{Co(CO)_4\}_2]$ with observed and calculated isotope patterns for $[Ag\{Co(CO)_4\}_2]^-$.

$[PPN][Ag\{Co(CO)_4\}_2]$

M_r – 988.4

IR – (ν_{CO}, CH_2Cl_2) 2072 (w), 2027 (s), 1940 (br,vs) cm^{-1}

ESMS – ($C_2H_4Cl_2$, -ve ion, 5 cV) *m/z* 449 (100% - $[Ag\{Co(CO)_4\}_2]^-$)

[20] Prepared from equimolar amounts of $Ag[BF_4]$ and [PPN]Cl.

2.2.4.2 Synthesis of $[NEt_4]_2[Fe_2(CO)_8]$[21]

$Fe_2(CO)_9$ was reduced in a 1 mol L^{-1} KOH methanolic solution over 1-2 hours with a colour change from golden yellow to deep red. The solution was filtered and an aqueous solution of $[NEt_4]Cl$ added slowly, yielding a deep red precipitate of $[NEt_4]_2[Fe_2(CO)_8]$ which was subsequently washed with petroleum spirits and dried under vacuum.

$[NEt_4]_2[Fe_2(CO)_8]$
M_r – 597.7
IR – (ν_{CO}, Nujol mull) 1922 (s), 1846 (s,br) cm^{-1} [Lit. 1920 (s,br), 1852 (s,br) cm^{-1} [21]]

2.2.4.3 Synthesis of $[PPN][HFe(CO)_4]$[22]

$Fe(CO)_5$ was reduced in a methanolic KOH solution over a 2 hour period. A saturated methanolic solution of [PPN]Cl was added slowly, yielding a pale pink precipitate of $[PPN][HFe(CO)_4]$. The precipitate was filtered, washed with H_2O and dried under vacuum.

$[PPN][HFe(CO)_4]$
M_r – 706.9
IR – (ν_{CO}, Nujol mull) 1902 (sh), 1860 (s,br) cm^{-1} [Lit. 2008 (vw), 1910 (sh), 1848 (s,br) cm^{-1} [21]]

2.2.4.4 Synthesis of $[NEt_4][HFe_3(CO)_{11}]$

In one attempted synthesis of $[HFe(CO)_4]^-$, a deep red precipitate was produced rather than the pale pink material expected. Both IR and ESMS analysis indicated the precipitate was $[NEt_4][HFe_3(CO)_{11}]$ rather than $[NEt_4][HFe(CO)_4]$. The sample was retained for use in reactions involving a tri-nuclear iron reagent. Synthesis of $[HFe_3(CO)_{11}]^-$ from $Fe(CO)_5$ has been noted previously[23].

---

[21] K. Farmery, M. Kilner, R. Greatrex and N.N. Greenwood, *J. Chem. Soc. A*, 1969, 2339.

[22] M.Y. Darensbourg, D.J. Darensbourg and H.L.C. Barros, *Inorg. Chem.*, 1978, **17**, 297.

[23] G.P. Boldrini, A. Umani-Ronchi and M. Panunzio, *J. Organomet. Chem.*, 1979, **171**, 85.

$[NEt_4][HFe_3(CO)_{11}]$

M_r – 607.5

IR – (ν_{CO}, Nujol mull) 2003 (m), 1976 (s), 1955 (m) cm^{-1} [Lit. 2067 (w), 2001 (s), 1981 (s), 1953 (s), 1932 (w), 1741 (w) cm^{-1} [21]]

2.2.4.5 Synthesis of $[PPN][Mn(CO)_5]$

A thf solution of $Mn_2(CO)_{10}$ was reduced over a 1% sodium amalgam for 2 hours. A thf solution of [PPN]Cl was added, the solution stirred for 10 minutes then transferred *via* syringe to a separate Schlenk flask. Solvent was removed under vacuum and the compound recrystallised from CH_2Cl_2/Et_2O.

$[PPN][Mn(CO)_5]$

M_r – 732.9

IR – (ν_{CO}, thf) 1896 (s), 1866 (s) cm^{-1} [Lit. 1892 (s), 1854 (s) cm^{-1} [24]]

2.2.4.6 Synthesis of $[PPN][Mo(CO)_3(\eta^5\text{-}C_5H_5)]$

A thf solution of $[Mo(CO)_3(\eta^5\text{-}C_5H_5)]_2$ was stirred over a 1% sodium amalgam for 2 hours with a significant colour change from a deep purple to pale yellow. A thf solution of [PPN]Cl was added, the mixed solution transferred *via* syringe to a separate Schlenk flask, solvent removed under vacuum and the compound recrystallised from CH_2Cl_2/Et_2O. The structural characterisation of $[PPN][Mo(CO)_3(\eta^5\text{-}C_5H_5)]$ is reported in Chapter 8.

$[PPN][Mo(CO)_3(\eta^5\text{-}C_5H_5)]$

M_r – 783.0

IR – (ν_{CO}, thf) 1897 (s), 1782 (s,br), 1770 (s,br) cm^{-1} [Lit. 1896 (s), 1786 (br), 1764 (br) cm^{-1} [25]]

[24] D.N. Duffy and B.K. Nicholson, *J. Organomet. Chem.*, 1979, **164**, 227.

2.2.4.7 Synthesis of $[NEt_4][Fe(CO)_2(\eta^5\text{-}C_5H_5)]$

A thf solution of $[Fe(CO)_2(\eta^5\text{-}C_5H_5)]_2$ was reduced over a 1% sodium amalgam for 3 hours with a colour change from yellow to deep red. A thf solution of $[NEt_4]Cl$ was added, the solution transferred to a separate Schlenk flask, solvent removed under vacuum and the product recrystallised from CH_2Cl_2/Et_2O.

$[NEt_4][Fe(CO)_2(\eta^5\text{-}C_5H_5)]$
M_r – 307.9
IR – (ν_{CO}, thf) 1993 (s), 1947 (m), 1783 (m) cm^{-1}

2.2.4.8 Synthesis of $[NEt_4][Fe(CO)_3(NO)]$

$Fe(CO)_5$ was added to a methanolic solution of KNO_2 and stirred overnight at 40°C to generate $K[Fe(CO)_3(NO)]$. An aqueous solution of $HgCl_2$ was added slowly and the mixture stirred for 1 hour with precipitation of $Hg[Fe(CO)_3(NO)]_2$ [26]. The precipitate was filtered, extracted into CH_2Cl_2 and solvent removed under vacuum.

The Na^+ and $[NEt_4]^+$ salts of $[Fe(CO)_3(NO)]^-$ used in this research were prepared by reduction of a thf solution of $Hg[Fe(CO)_3(NO)]_2$ over a 1% sodium amalgam. The $[NEt_4]^+$ salt was produced by addition of a CH_2Cl_2 solution of $[NEt_4]Cl$ to a stirred solution of $Na[Fe(CO)_3(NO)]$, with subsequent recrystallisation from CH_2Cl_2/Et_2O. $Na[Fe(CO)_3(NO)]$ was used without recrystallisation.

$[NEt_4][Fe(CO)_3(NO)]$
M_r – 300.8
IR – (ν_{CO}, thf) 1985 (m), 1878 (s) cm^{-1} [Lit. 1982 (m), 1876 (s) cm^{-1} [27]]
ESMS – ($C_2H_4Cl_2$, -ve ion, 5 cV) *m/z* 170 (100% - $[Fe(CO)_3(NO)]^-$), *m/z* 713 (15% - $[Hg\{Fe(CO)_3(NO)\}_3]^-$)

[25] D.E. Crotty, E.R. Corey, T.J. Anderson, M.D. Glick and J.P. Oliver, *Inorg. Chem.*, 1977, **16**, 920.

[26] W. Hieber and H. Beutner, *Z. Anorg. Allgem. Chem.*, 1962, **320**, 101.

[27] R.E. Stevens, T.J. Yanta, W.L. Gladfelter, *Inorg. Syn.*, 1983, **22**, 163.

2.2.4.9 Synthesis of $[PPN][Ir(CO)_4]$ [28, 29]

$Ir_4(CO)_{12}$ was added to a 10% KOH/DMSO solution under a carbon monoxide atmosphere. The solution was stirred for 24 hours then added slowly to an aqueous ^{i}PrOH solution of [PPN]Cl, causing immediate precipitation of $[PPN][Ir(CO)_4]$. The ^{i}PrOH was removed under vacuum, the water decanted and the product recrystallised from thf/^{i}PrOH. The product was initially pale brown in colour (indicative of minor impurities in the sample) with the colour deepening during storage at –20°C.

$[PPN][Ir(CO)_4]$

M_r – 842.2

IR – (ν_{CO}, thf) 1898 (vs) cm^{-1} [Lit. 2000 (vw), 1895 (vs) cm^{-1} [29]]

ESMS – ($C_2H_4Cl_2$, -ve ion, 5 cV) *m/z* 305 (100% - $[Ir(CO)_4]^-$), *m/z* 1079 (25% - $[HIr_4(CO)_{11}]^-$), *m/z* 1325 (5% - $[Ir_5(CO)_{13}]^-$)

The reduction process was also monitored by ESMS. Aliquots of the DMSO solution were diluted and analysed using de-oxygenated methanol as the carrier solvent. Initial spectra were dominated by the $[Ir_4(CO)_{12}(OMe)]^-$ signal (*m/z* 1137) with detection of $[HIr_4(CO)_{11}]^-$ (*m/z* 1079) noted after 1 hour. Extended reduction led to complete conversion of $Ir_4(CO)_{12}$ to $[HIr_4(CO)_{11}]^-$, and finally to $[Ir(CO)_4]^-$ (*m/z* 305) as shown in Figure 2.4. An additional signal attributed to $[Ir_5(CO)_{13}]^-$ (*m/z* 1325) was detected but only at limited intensity. ESMS analysis of the isolated $[PPN][Ir(CO)_4]$ compound showed trace amounts of $[HIr_4(CO)_{11}]^-$ and $[Ir_5(CO)_{13}]^-$.

[28] L. Garlaschelli, P. Chini and S. Martinengo, *Gaz. Chim. Italiana*, 1982, **112**, 285.

[29] L. Garlaschelli, R.D. Pergola and S. Martinengo, *Inorg. Syn.*, 1991, **29**, 211.

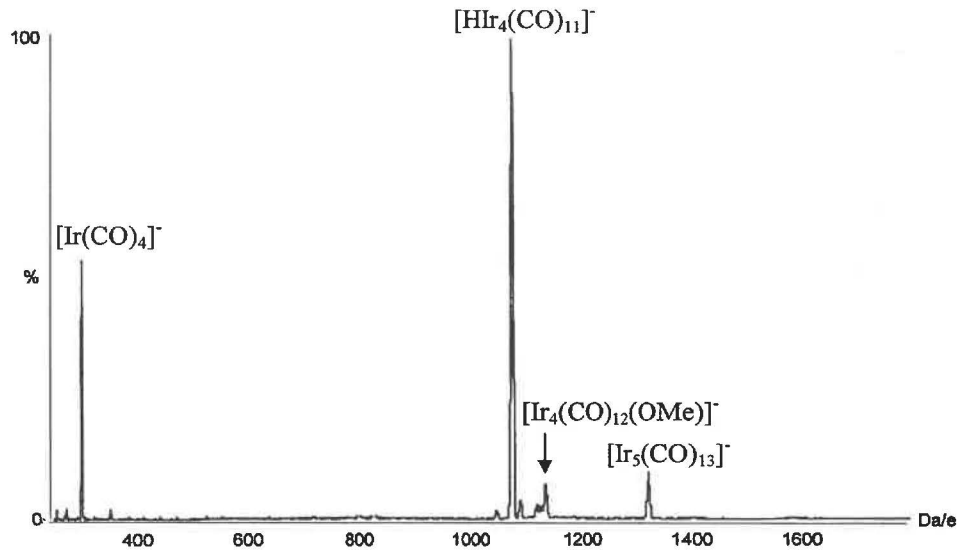

Figure 2.4 – The ES mass spectrum (-ve ion, 5 cV) of the reduction of $Ir_4(CO)_{12}$ after 8 hours.

2.2.4.10 Attempted Synthesis of [PPN][Rh(CO)$_4$]

The synthesis of $[Rh(CO)_4]^-$ was attempted on several occasions, both from $[Rh(CO)_2Cl]_2$ [30] and $RhCl_3.3H_2O$ [29]. $[Rh(CO)_2Cl]_2$ was produced from mild pyrolysis of $RhCl_3.3H_2O$ under a CO atmosphere (and isolated through sublimation)[31].

Reduction of $[Rh(CO)_2Cl]_2$ and $RhCl_3.3H_2O$ was performed in a similar manner to that reported for [PPN][Ir(CO)$_4$]. The reduction of $[Rh(CO)_2Cl]_2$ was monitored by ESMS, with signals attributable to $[Rh_5(CO)_{13}]^-$ (*m/z* 879), $[Rh_7(CO)_{17}]^-$ (*m/z* 1197) and $[Rh_9(CO)_{21}]^-$ (*m/z* 1515) detected (Figure 2.5) but not the intended anion, $[Rh(CO)_4]^-$ (expected *m/z* 215). The presence of oxygen is particularly harmful to this reaction and has been reported to stop the reduction process completely[28]. Although a positive carbon monoxide atmosphere was applied, oxygen may have been introduced when aliquots of the solution were removed for analysis. Attempts at synthesis of $[Rh(CO)_4]^-$ were unsuccessful and the mononuclear anion was never isolated.

[30] P. Chini and S. Martinengo, *Inorg. Chim. Acta*, 1969, **3**, 21.

[31] J.A. McCleverty and G. Wilkinson, *Inorg. Syn.*, 1966, **8**, 211.

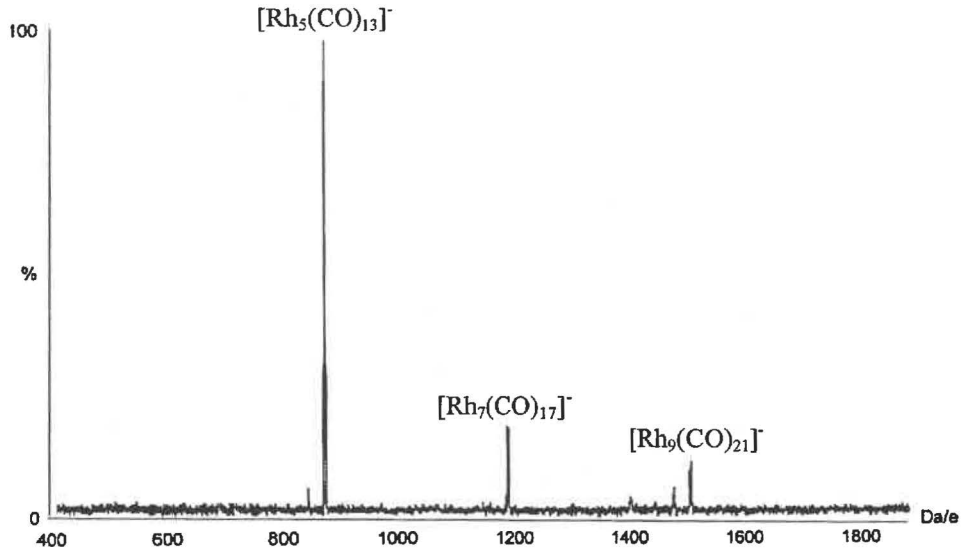

Figure 2.5 – The ES mass spectrum (-ve ion, 5 cV) of the reduction of $[Rh(CO)_2Cl]_2$ after 6 hours.

2.2.5 Preparation of mono-silanes/mono-germanes

Silicon starting materials were used as supplied (Petrarch or Gelest) unless otherwise stated. $SiCl_4$ and $PhSiCl_3$ were distilled prior to use to remove impurities and ubiquitous HCl. A sealed ampoule of $GeCl_4$ was provided by previous research students and used without purification. In the synthesis of primary silanes and germanes, an excess of $LiAlH_4$ was used to ensure full reduction of the precursor.

2.2.5.1 Synthesis of phenyl silane ($PhSiH_3$)[32]

A solution of $PhSiCl_3$ (17 mL, 23.0 g, 109 mmol) in Et_2O (20 mL) was added slowly to a suspension of $LiAlH_4$ (4.76 g, 126 mmol) in Et_2O (5 mL). The mixture was refluxed for 3 hours, cooled to room temperature and poured slowly into a saturated aqueous NH_4Cl solution at 0°C. The organic layer was separated, dried over anhydrous $MgSO_4$ and Et_2O removed under partial vacuum. The residue was fractionally distilled to afford $PhSiH_3$ (7.27 g, 67 mmol, 62%).

[32] W.H. Nebergall, *J. Am. Chem. Soc.*, 1950, **72**, 4702.

$PhSiH_3$

M_r – 108.2

NMR – ^1H – 7.63 (d, 2H, C_6H_4), 7.45-7.28 (m, 3H, C_6H_4), 4.25 (s, 3H, SiH_3, $^1J_{Si-H}$ 201 Hz) ppm

2.2.5.2 Synthesis of *p*-methoxyphenyl silane ($MeOC_6H_4SiH_3$) [33]

$MeOC_6H_4SiH_3$ was provided by J.S. McIndoe. The silane was produced through standard Grignard procedures from *p*-bromoanisole ($MeOC_6H_4Br$), with subsequent reaction with an excess of $SiCl_4$ yielding $MeOC_6H_4SiCl_3$. The trichlorosilane was reduced using $LiAlH_4$ to produce $MeOC_6H_4SiH_3$.

$MeOC_6H_4SiH_3$

M_r – 138.2

NMR – ^1H – 7.55 (d, 2H, C_6H_4), 6.96 (d, 2H, C_6H_4), 4.24 (s, 3H, SiH_3, $^1J_{Si-H}$ 200 Hz), 3.85 (s, 3H, OCH_3) ppm

2.2.5.3 Synthesis of *p*-dimethylaminophenyl silane ($Me_2NC_6H_4SiH_3$) [33]

An Et_2O solution (10 mL) of $Me_2NC_6H_4Br$ (10.0 g, 50 mmol) was added slowly to a suspension of magnesium turnings (2.2 g, 91 mmol) in Et_2O (5 mL), with a trace amount of iodine added to initiate reaction. The mixture was refluxed for 3 hours, cooled to room temperature and an ethereal solution of $Me_2NC_6H_4MgBr$ filtered from the unreacted Mg residue. The Grignard solution was added slowly to an Et_2O (10 mL) solution of $SiCl_4$ (15 mL, 22.2 g, 131 mmol) and refluxed for 3 hours. The solution was cooled to room temperature overnight (16 hours) before solvent and unreacted $SiCl_4$ were removed under vacuum. It is essential that $SiCl_4$ is removed prior to reduction since treatment with $LiAlH_4$ would generate pyrophoric SiH_4. The residue was redissolved in Et_2O (20 mL) and added slowly to a suspension of $LiAlH_4$ (2.7 g, 72 mmol) in Et_2O (10 mL). The mixture was refluxed for 4 hours, cooled to room temperature and poured slowly into a saturated aqueous solution of NH_4Cl at 0°C. Separation of the organic layer followed by solvent removal afforded a white crystalline solid of $Me_2NC_6H_4SiH_3$ (4.16 g, 28 mmol, 55%).

[33] Y. Nagai, M-A. Ohtsuki, T. Nakano and H. Watanabe, *J. Organomet. Chem.*, 1972, **35**, 81.

$Me_2NC_6H_4SiH_3$

M_r – 151.3

NMR – ^1H – 7.46 (d, 2H, C_6H_4), 6.77 (d, 2H, C_6H_4), 4.22 (s, 3H, SiH_3, $^1J_{Si-H}$ 197 Hz), 2.97 (s, 6H, CH_3) ppm

2.2.5.4 Synthesis of 3-methoxypropyl silane [$MeO(CH_2)_3SiH_3$] [34]

The preparation of this compound has been reported as set out in Scheme 2.2[34]. The availability of $MeO(CH_2)_3Si(OMe)_3$ allowed simple reduction of this compound to the desired silane.

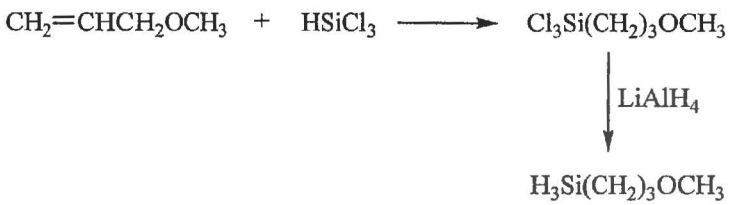

Scheme 2.2 – The reported synthetic route to $MeO(CH_2)_3SiH_3$.

An Et_2O solution (20 mL) of $MeO(CH_2)_3Si(OMe)_3$ (5 mL, 4.98 g, 25.6 mmol) was added slowly to a stirred suspension of $LiAlH_4$ (1.85 g, 50 mmol) in Et_2O (20 mL). The mixture was refluxed for 3 hours and cooled overnight (14 hours). The flask was transferred to a vacuum line, and the silane and solvent removed. The silane and approximately 20 mL of Et_2O were condensed in a chlorobenzene trap (-45°C), while the remainder of the Et_2O condensed in a liquid nitrogen trap (-196°C). After careful disposal of the solid $LiAlH_4$ residue, the silane/Et_2O mixture was transferred to a Schlenk flask and the majority of the Et_2O removed by fractional distillation, yielding a solution composed of the silane and Et_2O in a 1:2 ratio (determined from NMR analysis). Since the presence of Et_2O would not effect subsequent reactions, its removal was not attempted.

Attempts at isolation in the manner described for the aryl silanes (i.e. addition to a saturated aqueous NH_4Cl solution) resulted in the formation of cloud of a white vapour without recovery the silane. Alkyl silanes are not reported to be air- or moisture-

[34] J.M. Bellama and L.L. Gerchmann, *Inorg. Chem.*, 1975, **14**, 1618.

sensitive and the reason for the different synthetic procedure required for $MeO(CH_2)_3SiH_3$ is unknown.

$MeO(CH_2)_3SiH_3$

M_r – 104.2

NMR – ^1H – 3.49 (t, 3H, SiH_3, $^1J_{Si-H}$ 194 Hz, $^3J_{H-H}$ 3.87 Hz), 3.35 (m, 2H, CH_2O), 3.30 (s, 3H, CH_3), 1.68 (m, 2H, CH_2Si), 0.78 (m, 2H, $-CH_2-$) ppm

^{13}C – 74.4 (CH_2O), 58.4 (CH_3), 26.3 (CH_2Si), 2.62 ($-CH_2-$) ppm

2.2.5.5 Synthesis of *p*-dimethylaminophenyl germane ($Me_2NC_6H_4GeH_3$)

A thf (10 mL) solution of $Me_2NC_6H_4Br$ (3.0 g, 15 mmol) was added slowly to magnesium turnings (1.0 g, 41 mmol) suspended in thf (15 mL), with a trace of iodine added to initiate reaction. The solution was refluxed for 2 hours, cooled to room temperature and filtered from the unreacted Mg residue. The solution was added slowly to a thf solution (20 mL) of $GeCl_4$ (1.8 mL, 3.38 g, 15.8 mmol), refluxed for 4 hours and cooled to room temperature, with solvent and unreacted $GeCl_4$ removed *in vacuo*. The residue was re-dissolved in a mixture of thf (20 mL) and Et_2O (40 mL), and slowly added to a suspension of $LiAlH_4$ (0.75 g, 20 mmol) in Et_2O (40 mL). Following addition, the solution was refluxed for 2 hours, cooled overnight, then refluxed for a further 2 hours. ESMS analysis of the crude solution identified the primary germane {$[M+H]^+$, *m/z* 198} as the dominant product, though impurities of $(Me_2NC_6H_4)_2GeH_2$ {$[M+H]^+$, *m/z* 317} and $(Me_2NC_6H_4)_3GeH$ {$[M+H]^+$, *m/z* 436} were detected. The reaction mixture was added slowly to a saturated aqueous NH_4Cl solution at 0°C, the organic layer removed and dried over $MgSO_4$, with subsequent solvent removal producing a deep red oil. The colour was removed by extracting the germane products into petroleum spirits. Cooling to –20°C produced a waxy white solid that contained detectable amounts of the R_2GeH_2 and R_3GeH species (determined by ESMS and NMR analyses).

The presence of R_2GeH_2 and R_3GeH by-products in this reaction is attributed to the limited amount of $GeCl_4$ used. The synthesis of the analogous silane used a large excess of $SiCl_4$ to prevent formation of by-products but the prohibitive cost of $GeCl_4$ prevented a similar excess in this reaction. As the dominant component of the solution was the intended germane, no attempt was made to remove the impurities.

$Me_2NC_6H_4GeH_3$

M_r – 195.8

NMR – ^1H – 7.44 (d, 2H, C_6H_4), 6.80 (d, 2H, C_6H_4), 4.26 (s, 3H, GeH_3), 2.96 (s, 6H, CH_3) ppm

^{13}C – 151.0 (C_1), 136.4 (C_2), 127.5 (C_4), 113.1 (C_3), 35.1 (CH_3) ppm

2.2.6 Preparation of disilanes

2.2.6.1 Synthesis of 1,8-bis(silyl)octane [$H_3Si(CH_2)_8SiH_3$]

An Et_2O solution (40 mL) of $Cl_3Si(CH_2)_8SiCl_3$ (10 mL, 12.2 g, 32 mmol) was added slowly to a suspension of $LiAlH_4$ (3.6 g, 0.096 mol) in Et_2O (40 mL). The solution was refluxed for 2 hours before cooling to room temperature overnight (18 hours). The solution was refluxed for a further 2 hours, cooled and added slowly to a saturated aqueous NH_4Cl solution at 0°C. The mixture was stirred for 2 hours, the organic phase separated and solvent removed under vacuum producing a pale yellow oil. The oil was fractionally distilled under vacuum to afford $H_3Si(CH_2)_8SiH_3$ (4.166 g, 24 mmol, 75%).

$H_3Si(CH_2)_8SiH_3$

M_r – 174.4

b.p. – 33-37°C at 0.5 mmHg (corrected to 200-205°C at atmospheric pressure)

NMR – ^1H – 3.65 (t, 6H, SiH_3, $^1J_{Si-H}$ 192 Hz, $^3J_{H-H}$ 3.8 Hz), 1.58 (m, 4H, $C_\beta H_2$), 1.50 (m, 4H, $C_\gamma H_2$), 1.46 (m, 4H, $C_\delta H_2$), 0.88 (m, 4H, $C_\alpha H_2$) ppm

^{13}C – 33.1 (C_δ), 29.7 (C_γ), 27.0 (C_β), 6.5 (C_α) ppm

2.2.6.2 Preparation of *p*-disilylbenzene [*p*-$(H_3Si)_2C_6H_4$][35]

An Et_2O solution (10 mL) of *p*-$Br_2C_6H_4$ (12.0 g, 51 mmol) was added slowly to a suspension of magnesium turnings (3.0 g, 123 mmol) in Et_2O (5 mL), with a trace amount of iodine added to initiate reaction. The mixture was refluxed for 3 hours, cooled to room temperature, and an ethereal solution of *p*-$(BrMg)_2C_6H_4$ filtered from the unreacted Mg residue. The solution was added slowly to an Et_2O solution (20 mL) of $SiCl_4$ (20 mL, 29.6 g, 174 mmol), refluxed for 4 hours and cooled overnight (16 hours). Solvent and unreacted $SiCl_4$ were removed under vacuum, the residue

[35] F. Carre, C. Chuit, R.J.P. Corriu, A. Mehdi and C. Reyé, *Organometallics*, 1995, **14**, 2754; R.J.P. Corriu, J.J.E. Moreau, P. Thepot and M.W.C. Man, *Chem. Mater.*, 1992, **4**, 1217; D.R. Anderson and J.M. Holovka, *J. Chem. Soc.*, 1965, 2269.

redissolved in Et_2O (10 mL) and added slowly to a suspension of $LiAlH_4$ (6.0 g, 158 mmol) in Et_2O (10 mL). The mixture was refluxed for 4 hours, cooled and poured slowly into a saturated aqueous NH_4Cl solution. The organic layer was separated and Et_2O removed by fractional distillation to afford *p*-$(H_3Si)_2C_6H_4$ (0.62 g, 4.5 mmol, 9%). The silane was used for subsequent reactions without removal of traces of ether and other impurities.

$(H_3Si)_2C_6H_4$

M_r – 138.3

NMR – ^1H – 7.46 (s, 4H, C_6H_4), 4.25 (s, 6H, SiH_3, $^1J_{Si-H}$ 201 Hz) ppm

^{13}C – 135.4 (C_2), 130.3 (C_1) ppm

2.2.6.3 Synthesis of 1,1'-disilylferrocene [$Fe(\eta^5\text{-}C_5H_4SiH_3)_2$]

The synthesis of $Fe(\eta^5\text{-}C_5H_4SiH_3)_2$ has been reported[36] though the compound has never been fully characterised. Preparation involved synthesis of $Fe(\eta^5\text{-}C_5H_4Li)_2$, reaction with $ClSi(OR)_3$ (R = Me, Et) to yield $Fe[\eta^5\text{-}C_5H_4Si(OR)_3]_2$ and finally reduction (using $LiAlH_4$) to $Fe(\eta^5\text{-}C_5H_4SiH_3)_2$. It should be noted that the reaction of $Fe(\eta^5\text{-}C_5H_4Li)_2$ with $SiCl_4$ leads to the formation of a ferrocenophane species (Scheme 2.3), useful in the synthesis of ferrocenylsilicon polymers but not as a precursor to $Fe(\eta^5\text{-}C_5H_4SiH_3)_2$ [37]. Recent reports indicate that treatment of $Fe(\eta^5\text{-}C_5H_4)_2SiCl_2$ with a stoichiometric quantity of HCl produces $Fe(\eta^5\text{-}C_5H_5)(\eta^5\text{-}C_5H_4SiCl_3)$[38], though this was not attempted in this research. The most effective synthesis was *via* reaction between of $Fe(\eta^5\text{-}C_5H_4Li)_2$ and $Si(OEt)_4$ [39], with the $Fe[\eta^5\text{-}C_5H_4Si(OEt)_3]_2$ product reduced (using $LiAlH_4$) to $Fe(\eta^5\text{-}C_5H_4SiH_3)_2$.

[36] G. Cerveau, C. Chuit, E. Colomer, R.J.P. Corriu and C. Reyé, *Organometallics*, 1990, **9**, 2415.

[37] M.S. Wrighton, M.C. Palazzotto, A.B. Bocarsly, J.M. Bolts, A.B. Fischer and L. Nadjo, *J. Am. Chem. Soc.*, 1978, **100**, 7264.

[38] K. Pannell, Personal communication.

[39] M.J. Calhorda, P.E.M. Lopes, A. Schier and R. Herrmann, *J. Organomet. Chem.*, 1997, **543**, 93.

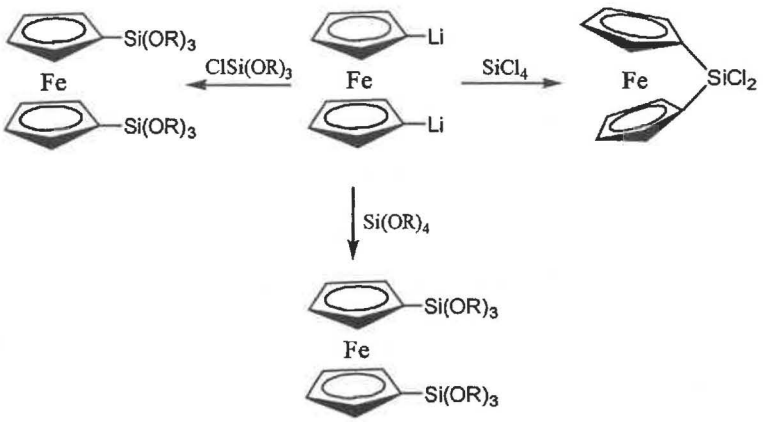

Scheme 2.3 – The reaction of $Fe(\eta^5\text{-}C_5H_4Li)_2$ with silicon reagents.

A solution of ^{n}BuLi (11.2 mmol, 7.0 mL of a 1.6 mol L^{-1} heptane solution) was added slowly to a cooled (0°C) petroleum spirits solution (20 mL) of $Fe(\eta^5\text{-}C_5H_5)_2$ (0.9 g, 4.8 mmol). Tetramethylethylenediamine (TMEDA - 0.9 mL, 0.7 g, 6 mmol) was added, the solution warmed to room temperature and stirred overnight (14 hours). The 'milky' orange solution of $Fe(\eta^5\text{-}C_5H_4Li)_2$ produced was added slowly to a cooled (0°C) petroleum spirits solution of $Si(OEt)_4$ (3 mL, 2.8 g, 13 mmol) and the solution was refluxed for 3 hours. Solvent and unreacted $Si(OEt)_4$ were removed under vacuum, the residue redissolved in Et_2O (10 mL) and added slowly to a suspension of $LiAlH_4$ (0.55 g, 14 mmol) in Et_2O (10 mL). After refluxing for 3 hours, the cooled solution was decanted carefully into a cooled (0°C) saturated aqueous NH_4Cl solution. The organic layer was removed and dried over anhydrous $MgSO_4$. Removal of the solvent yielded a viscous orange oil (0.45 g) that GC-EIMS analysis indicated was composed predominantly of $Fe(\eta^5\text{-}C_5H_4SiH_3)_2$, with *ca.* 25% unreacted $Fe(\eta^5\text{-}C_5H_5)_2$ and a trace amount (< 10%) of $Fe(\eta^5\text{-}C_5H_5)(\eta^5\text{-}C_5H_4SiH_3)$. The $Fe(\eta^5\text{-}C_5H_4SiH_3)_2$ was used without purification since the presence of unreacted $Fe(\eta^5\text{-}C_5H_5)_2$ was unlikely to impact upon the reactions involved.

$Fe(\eta^5\text{-}C_5H_4SiH_3)_2$

M_r – 246.3

NMR – ^{1}H – 4.28 (m, C_5H_4), 4.16 (m, SiH_3 and C_5H_4) ppm[40]

GC-EIMS – *m/z* 246 $[M]^+$, 215 $[M\text{-}SiH_3]^+$, 93 $[?]^+$

[40] Signal overlap and the presence of $Fe(\eta^5\text{-}C_5H_5)_2$ and $Fe(\eta^5\text{-}C_5H_5)(\eta^5\text{-}C_5H_4SiH_3)$ hampered NMR characterisation.

2.2.7 Miscellaneous Compounds

$(MeOC_6H_4)_3PAuCl$, $MeOC_6H_4(Ph)_2PAuCl$ (referred to as P***AuCl and P*AuCl respectively), 1,3,5-triaza-7-phosphaadamantane (PTA) and tris(2-carboxyethyl)phosphine (TCEP) were provided by Corry Decker. PPh_3 (Aldrich), [PPN]Cl, $[PPh_4]Br$, $[AsPh_4]Cl$, $[N(Me)_3CH_2Ph]Cl$, $Ag[BF_4]$ (Strem) and $Tl[PF_6]$ (BDH) were used as supplied. The sources of other chemicals used in this project are provided in the experimental section of the appropriate chapter.

Chapter Three – Development of Air-Sensitive Electrospray Mass Spectrometry

3.1 Introduction

The research reported in this thesis focuses upon the ESMS analysis of transition metal carbonyl clusters. These materials are often air-sensitive, with exposure to the atmosphere (specifically oxygen) causing sample decomposition. The degree of sensitivity is dependent upon a number of factors including the transition metals concerned, the nuclearity and the cluster charge.

Typical ESMS analysis involves sample dilution in a small amount (*ca.* 1 mL) of the mobile phase. The solution is injected into a silica capillary and pumped through a stainless steel capillary before being sprayed into the source. After injection, the sample has no further contact with the atmosphere as it is carried through the capillaries by the mobile phase (also referred to as the carrier solvent) and is sprayed into the source using nitrogen as a nebulising gas.

The conceptual basis for this project was that ESMS analysis of air-sensitive samples was possible provided a de-oxygenated carrier solvent was employed, with the mobile phase and sample solution transferred to the spectrometer under an inert atmosphere. By limiting or eliminating contact with oxygen, sample decomposition should not be a significant factor during analysis.

3.2 Method

A standard Schlenk line was installed in the ESMS room within reach of the carrier solvent inlet (Figure 3.1). Carrier solvents were degassed and stored in grease-less Schlenk flasks[1] under an argon atmosphere prior to use, and the solvent was transferred directly into the ESMS without contact to oxygen. In addition, the availability of a

[1] The use of grease may result in contamination of the solvent and subsequent blockage of the ESMS capillaries.

Schlenk line within the ESMS room allowed manipulation of air-sensitive samples prior to injection.

Figure 3.1 – The modified ESMS system.

3.3 Trialing System

To test the effectiveness of the modified ESMS procedure, a series of air-sensitive transition metal carbonyl cluster samples were analysed[2]. The samples consisted of a series of rhodium and nickel carbonyl clusters of various size and composition (listed in Table 3.1). The samples are considered moderately air-sensitive, with higher sensitivity as the ratio of charge to nuclearity increases[3].

[2] The samples were kindly provided by Prof. B.T. Heaton, University of Liverpool.

[3] B.T. Heaton, Personal communication.

Table 3.1 – List of clusters analysed

$[NMe_3Bz]_2[Rh_6C(CO)_{15}]$	$[NBu_4][Rh_6(CO)_{15}I]$	$[NEt_4]_4[Rh_{14}(CO)_{25}]$
$[NBu_4]_2[Rh_6C(CO)_{15}]$	$[NEt_3Bz]_2[Rh_9As(CO)_{21}]$	$[NEt_4]_2[Ni_8C(CO)_{16}]$
$[NMe_3Bz]_2[Rh_6{}^{13}C(CO)_{15}]$	$[NEt_3Bz]_3[Rh_{10}As(CO)_{22}]$	$[NEt_4]_2[Ni_9{}^{13}C(CO)_{17}]$
$[NEt_4]_2[Rh_6C(CO)_{13}]$	$[PPN]_2[Rh_{10}S(CO)_{22}]$	$[NEt_4]_3[HNi_{12}(CO)_{21}]$
$[NBu_4][Rh_6(CO)_{15}Br]$	$[NEt_4]_3[HRh_{14}(CO)_{25}]$	$[NEt_4]_2[H_2Ni_{12}(CO)_{21}]$

As discussed in Chapter 1, no systematic examination of anionic transition metal carbonyl clusters by ESMS has been reported. Although ESMS data is available for isolated examples, the examination of a series of related clusters had not been performed previously.

3.4 Anionic Rhodium Clusters

3.4.1 $[Rh_6C(CO)_{15}]^{2-}$

The $[Rh_6C(CO)_{15}]^{2-}$ cluster is well known[4] and commonly prepared from the reduction of $Rh_4(CO)_{12}$ by sodium hydroxide in the presence of chloroform (which acts as the carbon source[5]). The core of the anion displays the trigonal-prismatic geometry expected for a 90 valence-electron species, with the carbon atom adopting an interstitial position in the centre of the prism (Figure 3.2).

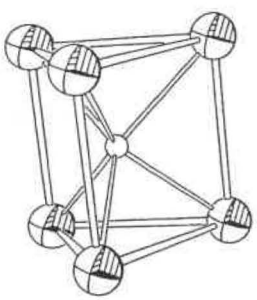

Figure 3.2 – The core structure of $[Rh_6C(CO)_{15}]^{2-}$[4].

[4] V.G. Albano, M. Sansoni, P. Chini and S. Martinengo, *J. Chem. Soc., Dalton Trans.*, 1973, 651.

[5] V.G. Albano, P. Chini, S. Martinengo, D.J.A. McCaffrey, D. Strumolo and B.T. Heaton, *J. Am. Chem. Soc.*, 1974, **96**, 8106.

Three samples of this cluster were supplied; $[NMe_3Bz]_2[Rh_6C(CO)_{15}]$, $[NBu_4]_2[Rh_6C(CO)_{15}]$ and $[NMe_3Bz]_2[Rh_6{}^{13}C(CO)_{15}]$. Spectra of the three compounds were essentially identical and are discussed as a group.

At low cone voltage (5 cV – Figure 3.3), the ES mass spectra were dominated by an intense peak corresponding to the intact parent di-anion, $[Rh_6C(CO)_{15}]^{2-}$ (*m/z* 525). Loss of the carbonyl ligands became apparent with increasing cone voltage, typical of transition metal carbonyl clusters. In the case of anionic clusters, the magnitude of the applied voltage did not have to be significantly large before carbonyl loss was noted (typically an applied voltage of 10 V or higher resulted in detectable fragmentation). For the $[Rh_6C(CO)_{15}]^{2-}$ clusters, initial loss of two carbonyl ligands was followed by stepwise loss of a number of the remaining ligands.

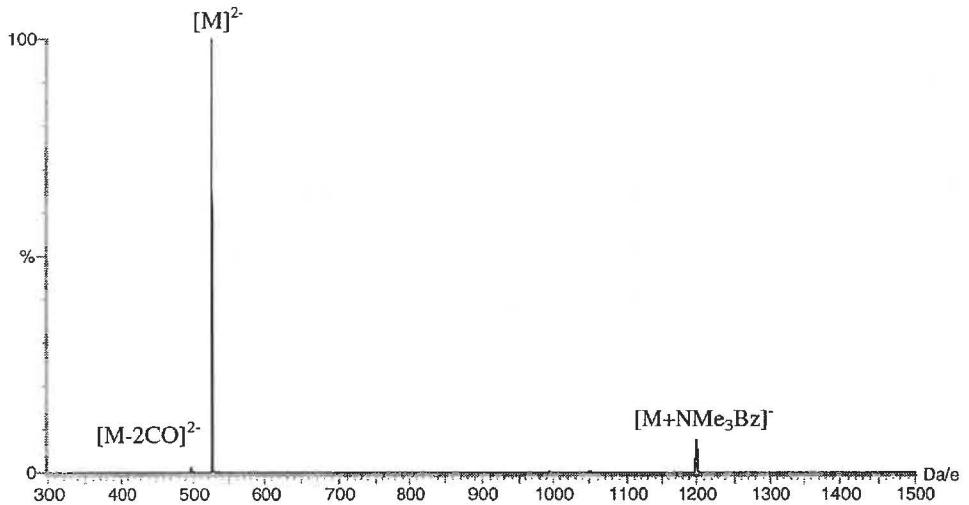

Figure 3.3 – The ES mass spectrum (-ve ion, 5 cV) of $[NMe_3Bz]_2[Rh_6C(CO)_{15}]$.

The initial loss of two carbonyl ligands may be caused by the stable nature of the $[Rh_6C(CO)_{13}]^{2-}$ anion in comparison to the unknown $[Rh_6C(CO)_{14}]^{2-}$ cluster (generated by loss of a single carbonyl ligand). The octahedral $[Rh_6C(CO)_{13}]^{2-}$ cluster is well known and prepared through thermolysis of $[Rh_6C(CO)_{15}]^{2-}$ [6]. ESMS detection of $[Rh_6C(CO)_{13}]^{2-}$ may reflect a similar structural rearrangement within the spectrometer to generate the octahedral species (Scheme 3.1).

[6] V.G. Albano, D. Braga and S. Martinengo, *J. Chem. Soc., Dalton Trans.*, 1981, 717; D. Braga and B.T. Heaton, *J. Chem. Soc., Chem. Commun.*, 1987, 608.

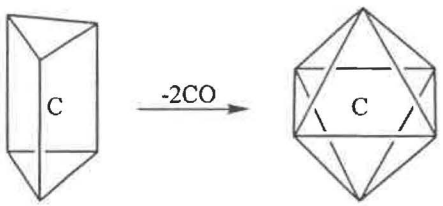

Scheme 3.1 – The conversion of $[Rh_6C(CO)_{15}]^{2-}$ to $[Rh_6C(CO)_{13}]^{2-}$.

A recently reported effect is the simultaneous loss of a carbonyl ligand and negative charge from highly-charged clusters[7], an effect apparent in the analysis of the $[Rh_6C(CO)_{15}]^{2-}$ clusters. For applied voltages < 35 cV, stepwise loss of seven ligands from the $[M]^{2-}$ parent ion was observed, with higher voltages generating signals attributable to $[M\text{-}xCO]^{-}$ (x = 4-12) ions (Figure 3.4). The mechanism for the loss of charge is not understood and further studies are required to establish the prevalence of this effect.

The formation of adducts between the parent anion and the appropriate cation {e.g. $[NMe_3Bz][Rh_6C(CO)_{15}]^{-}$ (*m/z* 1200) or $[NBu_4][Rh_6C(CO)_{15}]^{-}$ (*m/z* 1292)} was noted but at relatively low intensity (compared to the $[M]^{2-}$ signal). Adduct formation was not unexpected as it serves to reduce the charge-density associated with the cluster. Effectively, adduct formation provides an alternative charge-dissipation mechanism to the fragmentation reported above.

[7] J.S. McIndoe, Personal communication.

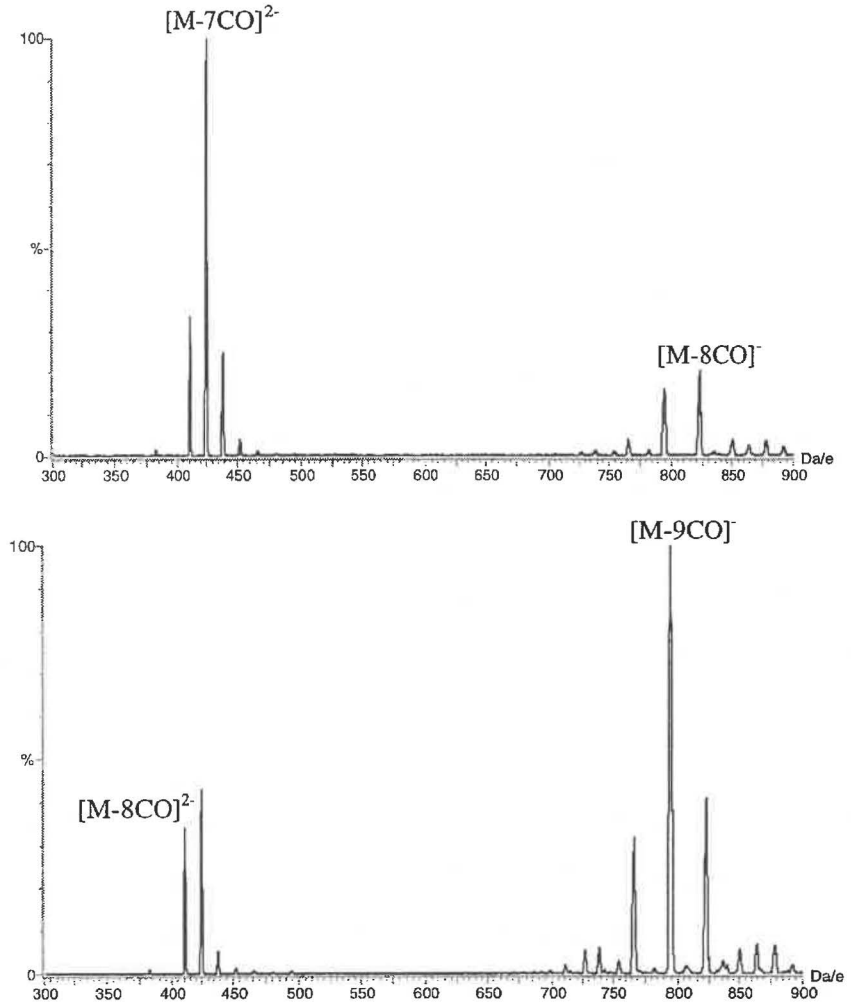

Figure 3.4 – The ES mass spectra (-ve ion) of $[NMe_3Bz]_2[Rh_6C(CO)_{15}]$ at 35 (upper) and 50 cV (lower).

The ^{13}C labelled sample behaved in a similar manner to the unlabelled samples with the only difference noted in the high-resolution spectra of the dominant ions. These spectra were more complex, a difference attributable to the presence of the ^{13}C label (a comparison between the high-resolution spectra of the labelled and unlabelled clusters is provided in Figure 3.5). The ability to detect the presence and extent of isotope labelling in a sample provides a novel application of ESMS. Isotopic labelling of samples assists NMR characterisation, and ESMS analysis provides a simple and effective method for determining the degree of labelling introduced.

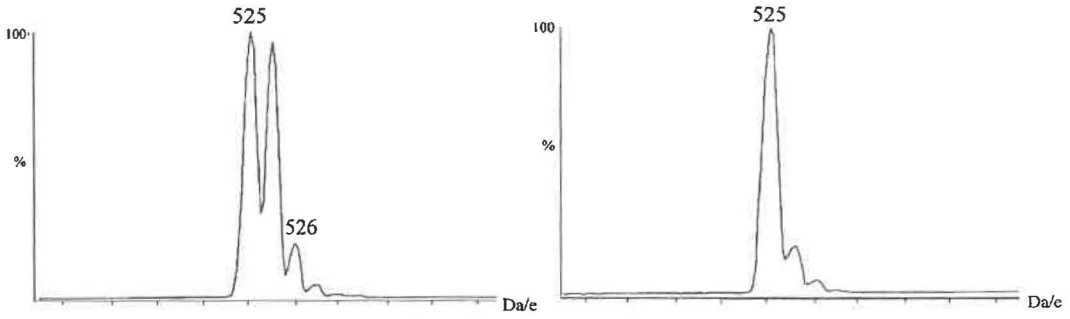

Figure 3.5 – The isotope patterns for the ^{13}C labelled (left) and unlabelled (right) $[Rh_6C(CO)_{15}]^{2-}$ clusters.

3.4.2 $[NEt_4]_2[Rh_6C(CO)_{13}]$

The loss of two carbonyl ligands from $[Rh_6C(CO)_{15}]^{2-}$ was achieved preparatively by thermolysis of the parent di-anion, generating the octahedral $[Rh_6C(CO)_{13}]^{2-}$ cluster[6]. The unique carbon atom is located within the central cavity of the octahedron (refer to Scheme 3.1).

ESMS analysis of this sample indicated the compound was $[NEt_4]_2[Rh_6C(CO)_{15}]$ rather than $[NEt_4]_2[Rh_6C(CO)_{13}]$. Spectra acquired at low voltage were dominated by a signal at *m/z* 525 rather than the *m/z* 497 signal expected for $[Rh_6C(CO)_{13}]^{2-}$. The *m/z* 497 signal was observed at increased voltage, though this was attributed to induced carbonyl loss from $[Rh_6C(CO)_{15}]^{2-}$ rather than the presence of $[Rh_6C(CO)_{13}]^{2-}$ in the sample initially. The detection of $[NEt_4][Rh_6C(CO)_{15}]^-$ (*m/z* 1180) confirmed the presence of $[NEt_4]^+$, indicating the discrepancy was not attributable to simple mislabelling. Analysis was repeated on several occasions with identical results, indicating that cross contamination between samples was not the cause.

As mentioned above, $[Rh_6C(CO)_{13}]^{2-}$ was prepared directly from $[Rh_6C(CO)_{15}]^{2-}$, providing an explanation for the presence of the larger cluster. The IR spectra of the two anions display certain similarities (Table 3.2) and distinguishing between the clusters spectroscopically may be difficult. In contrast, the two clusters were easily distinguished by ESMS.

Table 3.2 – IR data (thf solution) for $[Rh_6C(CO)_x]^{2-}$ (x = 13, 15)

$[Rh_6C(CO)_{13}]^{2-}$ [6]	$[Rh_6C(CO)_{15}]^{2-}$ [8]
	2040 (vw)
1968 (vs)	1990 (vs)
	1885 (vw)
	1845 (s)
1825 (m)	1830 (m,sh)
1800 (w,sh)	1815 (sh)
	1775 (vw)

3.4.3 $[NBu_4][Rh_6(CO)_{15}X]$ (X = Br, I)

The substitution of a carbonyl ligand on $Rh_6(CO)_{16}$ by a halide ion produces anionic clusters with identical core geometries to the parent octahedron. The chloro- [9] and iodo-substituted[10] clusters have been structurally characterised.

As with the carbido clusters reported above, intense ES mass spectra were acquired for these samples. Spectra at low cone voltage were dominated by signals from the intact parent ions (*m/z* 1119 and 1165 for the bromo- and iodo-clusters respectively – Figure 3.6), while an increase in the applied voltage resulted in initial loss of two carbonyl ligands followed by stepwise loss of the majority of the remaining ligands. Identification of the parent ion for $[Rh_6(CO)_{15}Br]^-$ was aided by the characteristic bromine isotope pattern.

The simultaneous loss of two carbonyls (rather than single CO loss) was unexpected. A rearrangement similar to that discussed above for $[Rh_6C(CO)_{15}]^{2-}$ is unlikely since $[Rh_6(CO)_{13}X]^-$ clusters have not been previously reported and would correspond to 6 vertex, 82 valence-electron species, none of which are known [the most condensed 6 vertex structure is the 84 electron bi-capped tetrahedron e.g. $Os_6(CO)_{18}$ [11]].

[8] S. Martinengo, D. Strumolo and P. Chini, *Inorg. Syn.*, 1980, **20**, 212.

[9] A.L. Rheingold, C.B. White, P.D. Macklin and G.L. Geoffroy, *Acta Cryst. Sect. C*, 1993, **49**, 80.

[10] V.G. Albano, P.L. Bellon and M. Sansoni, *J. Chem. Soc. A*, 1971, 678.

[11] A.J. Blake, B.F.G. Johnson and J.G.M. Nairn, *Acta Cryst. Sect. C*, 1994, **50**, 1052.

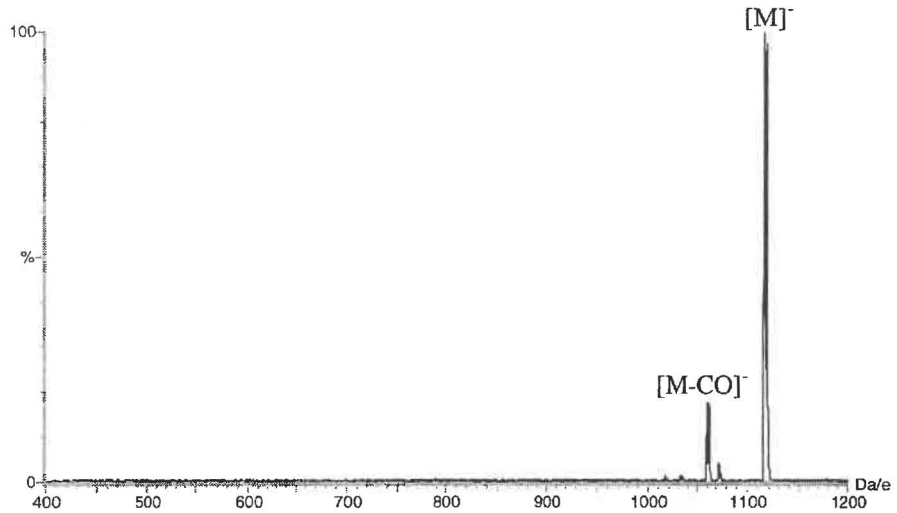

Figure 3.6 – The ES mass spectrum (-ve ion, 10 cV) of $[NBu_4][Rh_6(CO)_{15}Br]$.

3.4.4 $[NEt_3Bz]_2[Rh_9As(CO)_{21}]$

The reaction between $Rh(CO)_2(acac)$ and Ph_3As under a carbon monoxide atmosphere produced a pair of rhodium/arsenic clusters, $[Rh_9As(CO)_{21}]^{2-}$ and $[Rh_{10}As(CO)_{22}]^{3-}$ [12]. The latter cluster was structurally characterised[12], while the former is isoelectronic (and presumably isostructural) to $[Rh_9P(CO)_{21}]^{2-}$ [13] (Figure 3.7). The mono-capped and bi-capped square anti-prism structures identified for these clusters are those expected from electron-counting procedures (both clusters possess 11 SEP). In each case, the group 15 element is located in the central cavity of the anti-prism.

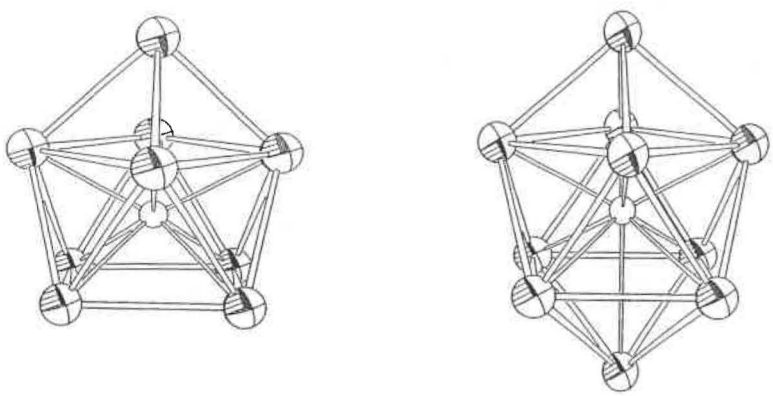

Figure 3.7 – The core structures of $[Rh_9P(CO)_{21}]^{2-}$ and $[Rh_{10}As(CO)_{22}]^{3-}$.

Analysis of the $[Rh_9As(CO)_{21}]^{2-}$ sample provided some differences from expectation. The parent ion observed at low cone voltage corresponded to $[Rh_9As(CO)_{21}]^{2-}$ (*m/z* 795)

[12] J.L. Vidal, *Inorg. Chem.*, 1981, **20**, 243.

[13] J.L. Vidal, W.E. Walker, R.L. Pruett and R.C. Schoening, *Inorg. Chem.*, 1979, **18**, 129.

and stepwise loss of carbonyl ligands from this ion was observed with increasing voltage. However, high-resolution spectra of the ions indicated the presence of an additional signal *m/z* 0.5 higher than that expected, causing overlap of the isotope patterns. This effect was attributed to the presence of ^{13}C labelling in the carbonyl ligands of the sample. The extent of labelling was calculated at *ca.* 5% through comparison of observed and simulated isotope patterns. Although details associated with the synthesis of this sample have not been provided, ^{13}CO labelling is likely since the laboratory involved specialises in ^{13}CO NMR analysis.

3.4.5 $[NEt_3Bz]_3[Rh_{10}As(CO)_{22}]$ *ca.* 50% ^{13}CO

The ES mass spectra of this sample also differed slightly from expectation. Highly-charged ions are often undetected by ESMS because of the charge-density and more typical is either oxidation (in the case of highly-charged anions) or adduct formation with counter ions. Both these effects were apparent in analysis of $[Rh_{10}As(CO)_{22}]^{3-}$, with the triply-charged parent ion (expected *m/z* 577.3) absent and signals observed at low cone voltage corresponding to $[Rh_{10}As(CO)_{22}]^{2-}$ (*m/z* 866) and $[NEt_3Bz][Rh_{10}As(CO)_{22}]^{2-}$ (*m/z* 962).

An important consideration in the assignment of ES mass spectra is distinguishing between oxidation and protonation. These two processes generate ions which differ by a single mass unit (which lowers to *m/z* 0.5 for a doubly-charged species) and careful examination of high-resolution spectra is required. Protonation requires the presence of H^+ ions in either the sample or mobile phase (possibly provided by traces of H_2O). The alternative explanation involves oxidation of the anion within the capillary prior to analysis, an effect noted previously (outlined in Section 1.3.3) and common with redox active analytes.

For $[Rh_{10}As(CO)_{22}]^{3-}$, the assignment of the *m/z* 866 anion as $[Rh_{10}As(CO)_{22}]^{2-}$ rather than $[HRh_{10}As(CO)_{22}]^{2-}$ was confirmed by high-resolution spectra of both the $[Rh_{10}As(CO)_{22}]^{2-}$ and $[NEt_3Bz][Rh_{10}As(CO)_{22}]^{2-}$ ions. The latter signal confirmed the calibration of the ESMS while the isotope pattern for the former was centred on *m/z* 866 rather than *m/z* 866.5 (expected for the protonated cluster). Assignment of the anion was also complicated by the presence of the ^{13}C label (producing a more complex isotope pattern than that predicted for the unlabelled form). As with the previous samples,

sequential loss of carbonyl ligands was observed with increasing cone voltage (Figure 3.8).

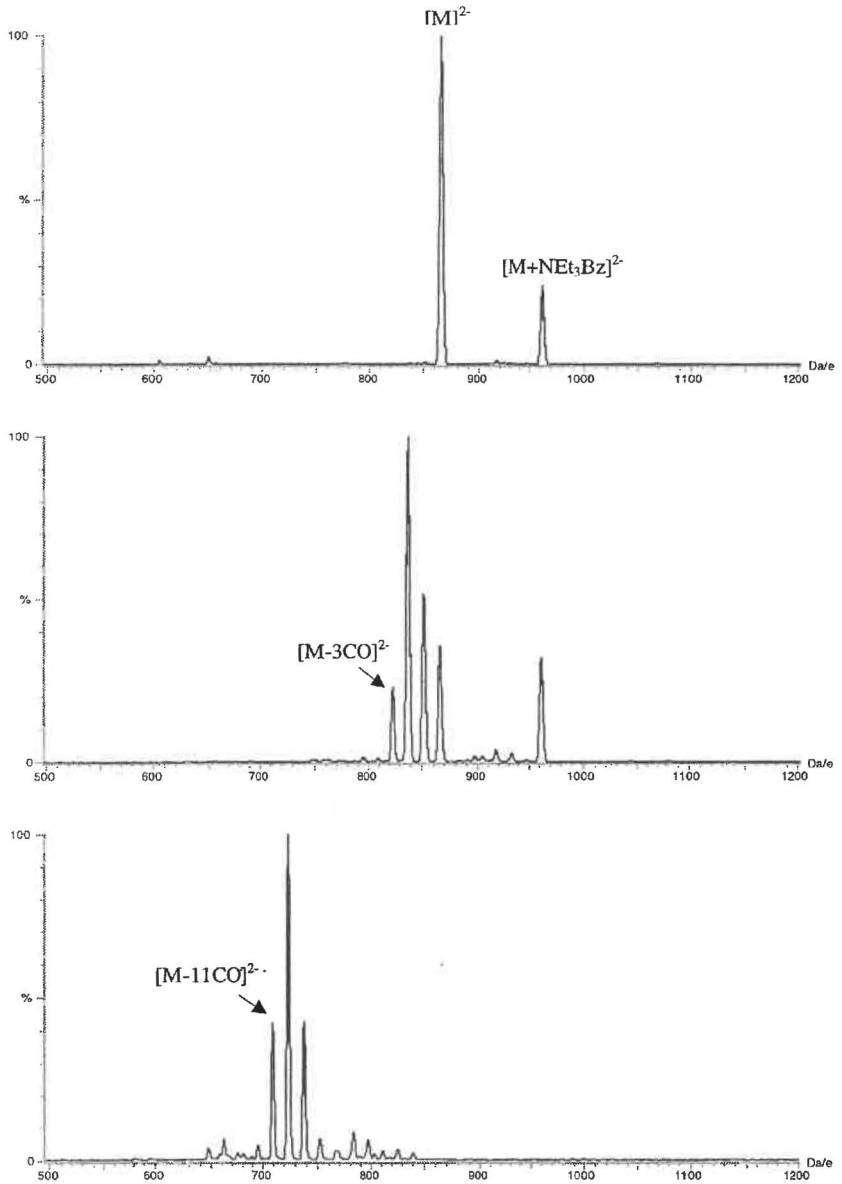

Figure 3.8 – The ES mass spectra (-ve ion) of $[NEt_3Bz]_3[Rh_{10}As(CO)_{22}]$ at 5, 15, and 40 cV. $[M]^{2-}$ corresponds to $[Rh_{10}As(CO)_{22}]^{2-}$.

3.4.6 $[PPN]_2[Rh_{10}S(CO)_{22}]$ *ca.* 40% ^{13}CO

$[Rh_{10}S(CO)_{22}]^{2-}$ [14] is isostructural and isoelectronic to the $[Rh_{10}As(CO)_{22}]^{3-}$ cluster discussed above. Although characterised crystallographically, the structure contains a

[14] G. Ciani, L. Garlaschelli, A. Sironi and S. Martinengo, *J. Chem. Soc., Chem. Commun.*, 1981, 563.

significant degree of disorder[14], with the arsenic and phosphorus analogues providing more conclusive evidence for the bi-capped square anti-prism geometry.

The ES mass spectra of this sample indicated it was not the assigned compound (expected *m/z* 839). At low cone voltage it was apparent that there were two clusters (both triply-charged) in the sample (Figure 3.9), one with *ca.* 40% ^{13}CO labelling (*m/z* 908) and the other unlabelled (*m/z* 903.5). The charge associated with the anions was determined from the peak separation in the isotope pattern (*m/z* 0.3) and from induced CO loss (generating signals *m/z* 9.3 apart). Neither of these signals corresponds to the title anion and from the *m/z* data the cluster was calculated to be $[Rh_{17}S_2(CO)_{32}]^{3-}$ (*m/z* 903.7).

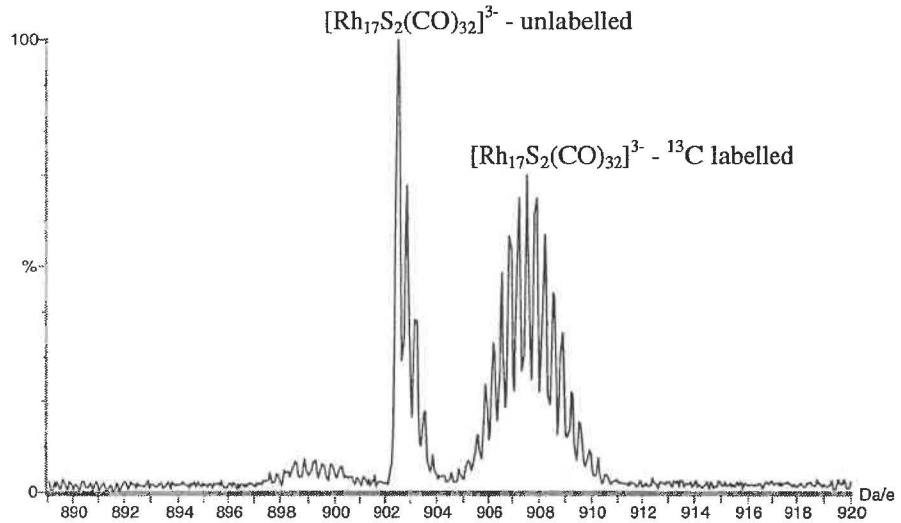

Figure 3.9 – The ES mass spectrum (-ve ion, 5 cV) of "$[Rh_{10}S(CO)_{22}]^{2-}$".

There was no ESMS evidence for label scrambling within the sample. The labelled and unlabelled ions were easily distinguished, and both clusters lost carbonyl ligands at a similar rate as the applied voltage was increased. There was also no evidence for ligand exchange between the two clusters during induced fragmentation. The detection of triply-charged ions is unusual. The ability to detect the highly-charged anions is presumably a factor of the large size of the $[Rh_{17}S_2(CO)_{32}]^{3-}$ cluster (core structure shown in Figure 3.10) reducing the charge-density. For smaller clusters {e.g. $[Rh_{10}As(CO)_{22}]^{3-}$ discussed above}, a higher charge-density caused the parent cluster to form adducts or undergo oxidation prior to detection.

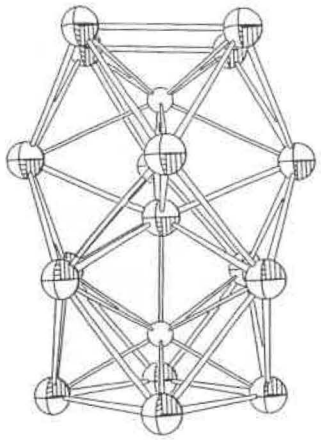

Figure 3.10 – The core structure of $[Rh_{17}S_2(CO)_{32}]^{3-}$ [16].

The discrepancy between the sample assignment provided and that established by ESMS requires explanation. The synthesis of $[Rh_{10}S(CO)_{22}]^{2-}$ involved reaction of $Rh_4(CO)_{12}$ with $[SCN]^-$ [15]. Although $[Rh_{17}S_2(CO)_{32}]^{3-}$ was initially prepared through a different route[16], it may be a by-product of the $[Rh_{10}S(CO)_{22}]^{2-}$ synthesis since generation of $[Rh_{17}S_2(CO)_{32}]^{3-}$ from thermolysis of $[Rh_{10}S(CO)_{22}]^{2-}$ has been reported[15]. Similarity in the IR spectra of the two clusters (presented in Table 3.3) has been noted and distinguishing between the clusters spectroscopically may be difficult, providing an explanation for the mistaken assignment of the sample.

Table 3.3 – IR data (thf solution) for $[Rh_{10}S(CO)_{22}]^{2-}$ and $[Rh_{17}S_2(CO)_{32}]^{3-}$ [15]

$[Rh_{10}S(CO)_{22}]^{2-}$	$[Rh_{17}S_2(CO)_{32}]^{3-}$
2002 (vs)	2002 (vs)
1831 (m)	1840 (m)
	1805 (m)

3.4.7 $[NEt_4]_4[Rh_{14}(CO)_{25}]$

Thermolysis of a mixture of $Rh_4(CO)_{12}$ and NaOH produced several anionic clusters, one being $[Rh_{15}(CO)_{27}]^{3-}$ which fragmented on reaction with bromine to generate

[15] L. Garlaschelli, A. Fumagalli, S. Martinengo, B.T. Heaton, D.O. Smith and L. Strona, *J. Chem. Soc., Dalton Trans.*, 1982, 2265.

[16] J.L. Vidal, R.A. Fiato, L.A. Cosby and R.L. Pruett, *Inorg. Chem.*, 1978, **17**, 2574.

$[Rh_{14}(CO)_{25}]^{4-}$ (core structure shown in Figure 3.11)[17]. Subsequent treatment of this cluster with acid or traces of H_2O produced the hydrido cluster, $[HRh_{14}(CO)_{25}]^{3-}$ [18].

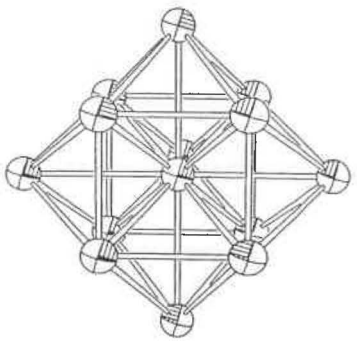

Figure 3.11 – The core structure of $[Rh_{14}(CO)_{25}]^{4-}$ [19].

ESMS analysis of the $[Rh_{14}(CO)_{25}]^{4-}$ sample differed from that anticipated. Rather than a $[M]^{4-}$ anion (expected *m/z* 535.5), spectra were dominated by a di-anion at *m/z* 1071. The charge of the ion was established from peak separation in high-resolution spectra and from induced carbonyl loss (generating signals *m/z* 14 apart). The *m/z* 1071 ion was identified as $[Rh_{14}(CO)_{25}]^{2-}$, resulting from oxidation of the parent cluster during analysis. Unfortunately, the electrochemical properties of $[Rh_{14}(CO)_{25}]^{4-}$ have not been reported so a propensity for oxidation cannot be confirmed. Protonation of the sample (to produce $[H_2Rh_{14}(CO)_{25}]^{2-}$, *m/z* 1072) was considered but high-resolution spectra indicated such assignment was inaccurate.

To confirm that the ion observed was not a result of sample protonation by traces of H_2O in the solvent or ESMS system, the analysis was repeated with dried acetonitrile (distilled over CaH_2 prior to use) with spectra identical to those previously acquired. The evidence provided by both the high-resolution spectra and the use of dry solvent indicated that the ion was attributable to oxidation rather than protonation.

[17] S. Martinengo, G. Ciani, A. Sironi and P. Chini, *J. Am. Chem. Soc.*, 1978, **100**, 7096.

[18] G. Ciani, A. Sironi and S. Martinengo, *J. Organomet. Chem.*, 1980, **192**, C42; G. Ciani, M. Moret, A. Sironi and S. Martinengo, *J. Organomet. Chem.*, 1989, **363**, 181.

[19] S. Martinengo, G. Ciani and A. Sironi, *J. Chem. Soc., Chem. Commun.*, 1980, 1140; G. Ciani, A. Sironi and S. Martinengo, *J. Chem. Soc., Dalton Trans.*, 1982, 1099.

3.4.8 $[NEt_4]_3[HRh_{14}(CO)_{25}]$

Analysis of $[NEt_4]_3[HRh_{14}(CO)_{25}]$ was performed in a similar manner to the clusters reported above. Spectra acquired at low cone voltage (5 cV - Figure 3.12) were dominated by a signal corresponding to the parent $[HRh_{14}(CO)_{25}]^{3-}$ cluster (*m/z* 714.3), with additional signals attributable to $[Rh_{14}(CO)_{25}]^{2-}$ (*m/z* 1071) and $[NEt_4][HRh_{14}(CO)_{25}]^{2-}$ (*m/z* 1136.5) observed. The triply-charged nature of the parent ion was confirmed from peak separation in high-resolution spectra (*m/z* 0.3 – Figure 3.13) and from induced carbonyl loss (generating signals *m/z* 9.3 apart). Adduct formation with $[NEt_4]^+$ was identical to that noted for earlier samples, while the $[Rh_{14}(CO)_{25}]^{2-}$ signal was attributed to the presence of $[Rh_{14}(CO)_{25}]^{4-}$ in the sample. High-resolution spectra of this ion indicated that alternative assignment as $[HRh_{14}(CO)_{25}]^{2-}$ (*m/z* 1071.5) or $[H_2Rh_{14}(CO)_{25}]^{2-}$ (*m/z* 1072) was incorrect.

The detection of the highly-charged parent ion was presumably a factor of the high-nuclearity reducing charge-density. This was verified to a degree by noting that the triply-charged ion was apparent only at low cone voltage, with increasing voltage (> 20 cV) yielding ions corresponding to carbonyl loss from $[Rh_{14}(CO)_{25}]^{2-}$. An alternative explanation is hydride loss at increased voltage.

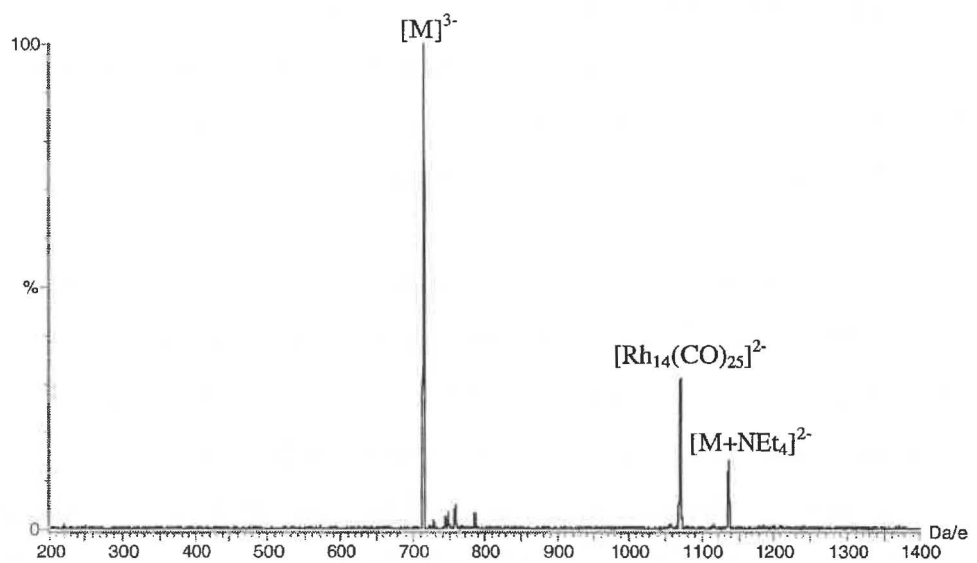

Figure 3.12 – The ES mass spectrum (-ve ion, 5 cV) of $[NEt_4]_3[HRh_{14}(CO)_{25}]$.

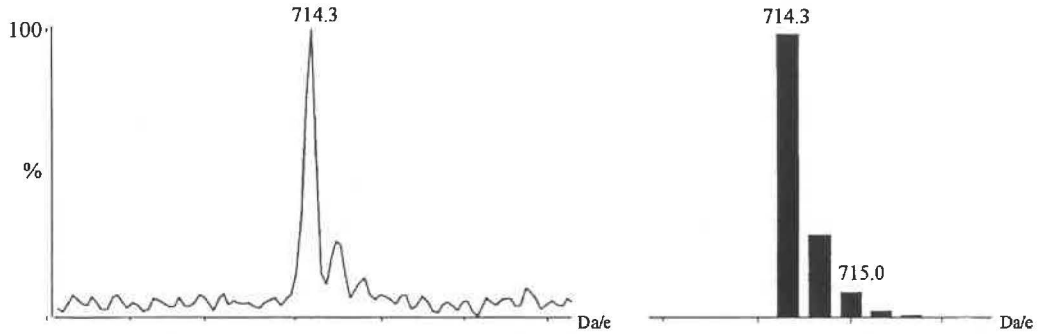

Figure 3.13 – The observed and calculated isotope patterns for $[HRh_{14}(CO)_{25}]^{3-}$.

3.5 Anionic Nickel Clusters

3.5.1 $[NEt_4]_2[Ni_8C(CO)_{16}]$

$[Ni_8C(CO)_{16}]^{2-}$ and $[Ni_9C(CO)_{17}]^{2-}$ adopt the square anti-prism and capped square anti-prism geometries expected for 118 and 130 valence-electron (11 SEP) species[20]. The unique carbon atom is located within the central cavity of the anti-prism in each case. The clusters were produced by treatment of $[Ni_6(CO)_{12}]^{2-}$ with CCl_4 [20].

ESMS analysis of the $[NEt_4]_2[Ni_8C(CO)_{16}]$ sample indicated that it was not the assigned cluster. Rather than the expected signal (*m/z* 464), a parent ion was detected at low applied voltage corresponding to $[Ni_9C(CO)_{17}]^{2-}$ (*m/z* 508). The ion appeared remarkably fragile under ESMS conditions, with loss of up to six ligands apparent at very low voltage (3 cV). This indicates that the cluster is remarkably prone to carbonyl loss, which may hamper the isolation and handling of this material.

The presence of $[Ni_9C(CO)_{17}]^{2-}$ in this sample requires explanation. The reported synthesis of $[Ni_8C(CO)_{16}]^{2-}$ involved stirring a solution of $[Ni_9C(CO)_{17}]^{2-}$ under a carbon monoxide atmosphere, generating $[Ni_8C(CO)_{16}]^{2-}$ and $Ni(CO)_4$ as a by-product[20]. The solvent and $Ni(CO)_4$ were subsequently removed under vacuum. It is possible that either the sample of $[Ni_8C(CO)_{16}]^{2-}$ provided had not been synthesised correctly {leaving unreacted $[Ni_9C(CO)_{17}]^{2-}$} or that $Ni(CO)_4$ had not been completely removed from the sample (allowing re-generation of the Ni_9C cluster prior to analysis). The similarity between the IR spectra of the two clusters (Table 3.4) hampers unambiguous

[20] A. Ceriotti, G. Longoni, M. Manassero, M. Perego and M. Sansoni, *Inorg. Chem.*, 1985, **24**, 117.

discrimination between the two clusters, providing an explanation for the mis-labelling. In comparison to IR, ESMS analysis established the composition of the sample without ambiguity.

Table 3.4 – IR data (thf solution) for $[Ni_8C(CO)_{16}]^{2-}$ and $[Ni_9C(CO)_{17}]^{2-}$ [20]

$[Ni_8C(CO)_{16}]^{2-}$	$[Ni_9C(CO)_{17}]^{2-}$
1995 (s)	2000 (s)
1850 (s)	1855 (ms)
	1800 (m)

3.5.2 $[NEt_4]_2[Ni_9{}^{13}C(CO)_{17}]$

The ES mass spectra acquired for this sample confirmed the previous assignment. The signals observed were equivalent to those reported above, with the detection of a parent ion (*m/z* 508.5) at low cone voltage. The only significant difference between the spectra of the two samples was a *m/z* 0.5 increase attributed to the ^{13}C label (compared to the unlabelled cluster discussed above). As noted for the previous sample, carbonyl loss occurred at very low cone voltage (Figure 3.14) indicating a significant degree of fragility for the sample.

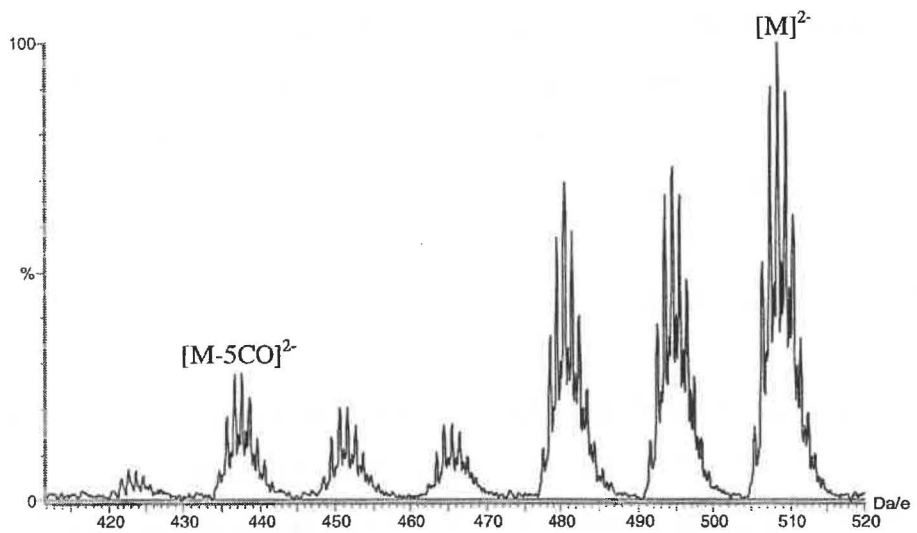

Figure 3.14 – The ES mass spectrum (-ve ion, 3 cV) of $[NEt_4]_2[Ni_9{}^{13}C(CO)_{17}]$.

3.5.3 $[NEt_4]_3[HNi_{12}(CO)_{21}]$

The structures of $[HNi_{12}(CO)_{21}]^{3-}$ and $[H_2Ni_{12}(CO)_{21}]^{2-}$ have attracted interest because of the hexagonal close-packed arrangement of the nickel atoms[21] (Figure 3.15), an arrangement that encourages analogies between high-nuclearity clusters and metal surfaces. The presence of the hydrogen atoms in interstitial environments has been confirmed by neutron diffraction studies.

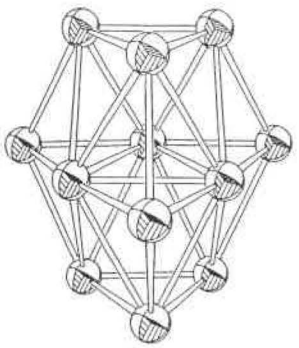

Figure 3.15 – The core structure of $[Ni_{12}(CO)_{21}]^{4-}$ [21].

Although ESMS analysis of this sample failed to detect the triply-charged parent cluster (expected *m/z* 431.3), the title compound was likely to be the major component of the sample. As noted with previous samples, the low cone voltage ES mass spectrum was dominated by signals associated with oxidation $\{[HNi_{12}(CO)_{21}]^{2-}$, *m/z* 646.5$\}$ and adducts $\{[NEt_4][HNi_{12}(CO)_{21}]^{2-}$, *m/z* 711.5$\}$ of the parent cluster. As discussed previously, distinguishing between oxidation and protonation requires high-resolution spectra. In this case, direct comparison was available between the oxidised ion, $[HNi_{12}(CO)_{21}]^{2-}$, and the parent ion of the $[H_2Ni_{12}(CO)_{21}]^{2-}$ cluster, with a *m/z* 0.5 difference between the signals evident.

3.5.4 $[NEt_4]_2[H_2Ni_{12}(CO)_{21}]$

Analysis of this sample indicated that the sample was predominantly that expected $\{[H_2Ni_{12}(CO)_{21}]^{2-}$ *m/z* 647$\}$, with the complexity of the isotope pattern (Figure 3.16) confirming the presence of a number of nickel atoms. However, there was also evidence

---

[21] A. Ceriotti, P. Chini, R.D. Pergola and G. Longoni, *Inorg. Chem.*, 1983, **22**, 1595; J.V. Barkley, T. Eguchi, R.A. Harding, B.T. Heaton, G. Longoni, L. Manzi, H. Nakayama, K. Miyagi, A.K. Smith and A. Steiner, *J. Organomet. Chem.*, 1999, **573**, 254.

for three smaller nickel clusters in the sample (*m/z* 516, 415 and 344). Spectra acquired at higher cone voltage indicated that these signals were di-anions (from induced CO loss generating signals *m/z* 14 apart), implying the clusters were $[Ni_9(CO)_{18}]^{2-}$, $[Ni_7(CO)_{15}]^{2-}$ and $[Ni_6(CO)_{12}]^{2-}$ respectively. Both $[Ni_6(CO)_{12}]^{2-}$ [22] and $[Ni_9(CO)_{18}]^{2-}$ [23] have been isolated previously, and all three clusters are known intermediate products *en route* to $[H_2Ni_{12}(CO)_{21}]^{2-}$ [24]. The assignment of these smaller clusters was uncertain as they were of insufficient intensity to allow the acquisition of high-resolution spectra.

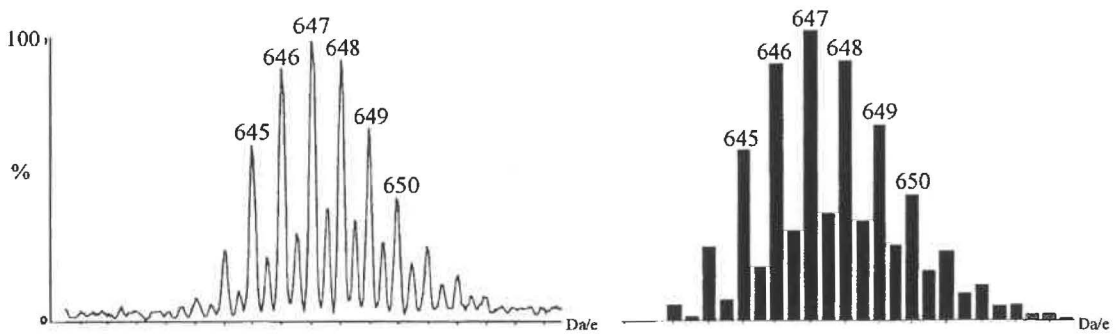

Figure 3.16 – The observed and calculated isotope patterns for $[H_2Ni_{12}(CO)_{21}]^{2-}$.

3.6 Summary

A summary of the ESMS results (-ve ion) discussed above is provided in Table 3.5. The $[M]^{n-}$ label corresponds to the intact parent ion.

Table 3.5 – Summarised ESMS data

Sample	Cone Voltage	Detected Ions - *m/z* (Intensity) - Assignment
$[NMe_3Bz]_2[Rh_6C(CO)_{15}]$	3	1200 (5) – $[M+NMe_3Bz]^-$
		525 (100) – $[M]^{2-}$
$[NBu_4]_2[Rh_6C(CO)_{15}]$	5	1292 (< 3) – $[M+NBu_4]^-$
		525 (100) – $[M]^{2-}$
		497 (5) – $[M-2CO]^{2-}$
$[NMe_3Bz]_2[Rh_6{}^{13}C(CO)_{15}]$	5	1200 (15) – $[M+NMe_3Bz]^-$
		525 (100) – $[M]^{2-}$

[22] J.C. Calabrese, L.F. Dahl, P. Chini, G. Longoni and S. Martinengo, *J. Am. Chem. Soc.*, 1974, **96**, 2616.

[23] D.A. Nagaki, L.D. Lower, G. Longoni, P. Chini and L.F. Dahl, *Organometallics*, 1986, **5**, 1764.

[24] G. Longoni, B.T. Heaton and P. Chini, *J. Chem. Soc., Dalton Trans.*, 1980, 1537.

"$[NEt_4]_2[Rh_6C(CO)_{13}]$"	5	1180 (5) – $[Rh_6C(CO)_{15}+NEt_4]^-$
		525 (100) – $[Rh_6C(CO)_{15}]^{2-}$
		497 (5) – $[Rh_6C(CO)_{15}-2CO]^{2-}$
$[NBu_4][Rh_6(CO)_{15}Br]$	5	1119 (100) – $[M]^-$
$[NBu_4][Rh_6(CO)_{15}I]$	5	1165 (100) – $[M]^-$
$[NEt_3Bz]_2[Rh_9As(CO)_{21}]$	10	795 (100) – $[M]^{2-}$
		781 (10) – $[M-CO]^{2-}$
$[NEt_3Bz]_3[Rh_{10}As(CO)_{22}]$	5	962 (25) – $[M+NEt_3Bz]^{2-}$
		866 (100) – $[M]^{2-}$
"$[PPN]_2[Rh_{10}S(CO)_{22}]$"	5	908 (70) – $[Rh_{17}S_2(CO)_{32}]^{3-}$ with ^{13}CO label
		903.5 (100) – $[Rh_{17}S_2(CO)_{32}]^{3-}$ unlabelled
		899 (2) – $[Rh_{17}S_2(CO)_{32}-CO]^{3-}$ with ^{13}CO label
$[NEt_4]_4[Rh_{14}(CO)_{25}]$	5	1071 (100) – $[M]^{2-}$
$[NEt_4]_3[HRh_{14}(CO)_{25}]$	5	1136.5 (20) – $[M+NEt_4]^{2-}$
		1071 (30) – $[Rh_{14}(CO)_{15}]^{2-}$
		714.3 (100) – $[M]^{3-}$
"$[NEt_4]_2[Ni_8C(CO)_{16}]$"	5	508 (100) – $[Ni_9C(CO)_{17}]^{2-}$
		494 (85) – $[Ni_9C(CO)_{17}-CO]^{2-}$
		480 (85) – $[Ni_9C(CO)_{17}-2CO]^{2-}$
		466 (10) – $[Ni_9C(CO)_{17}-3CO]^{2-}$
		452 (10) – $[Ni_9C(CO)_{17}-4CO]^{2-}$
		436 (30) – $[Ni_9C(CO)_{17}-5CO]^{2-}$
$[NEt_4]_2[Ni_9{}^{13}C(CO)_{17}]$	3	508.5 (100) – $[M]^{2-}$
		494.5 (80) – $[M-CO]^{2-}$
		480.5 (80) – $[M-2CO]^{2-}$
		466.5 (15) – $[M-3CO]^{2-}$
		452.5 (20) – $[M-4CO]^{2-}$
		436.5 (35) – $[M-5CO]^{2-}$
		422.5 (5) – $[M-6CO]^{2-}$
$[NEt_4]_3[HNi_{12}(CO)_{21}]$	5	711.5 (5) – $[M+NEt_4]^{2-}$
		646.5 (100) – $[M]^{2-}$
		632.5 (5) – $[M-CO]^{2-}$
$[NEt_4]_2[H_2Ni_{12}(CO)_{21}]$	5	647 (100) – $[M]^{2-}$
		633 (12) – $[M-CO]^{2-}$
		516 (20) – $[Ni_9(CO)_{18}]^{2-}$
		502 (10) – $[Ni_9(CO)_{18}-CO]^{2-}$
		488 (5) – $[Ni_9(CO)_{18}-2CO]^{2-}$
		415 (15) – $[Ni_7(CO)_{15}]^{2-}$
		344 (35) – $[Ni_6(CO)_{12}]^{2-}$

3.7 Conclusions

A number of conclusions can be drawn from the ESMS results reported in this chapter.

Firstly, it is evident that ESMS can be successfully applied to the analysis of air-sensitive transition metal carbonyl clusters. The spectra acquired were typically of high-intensity without evidence for sample decomposition. For the majority of the samples, spectra acquired at low cone voltage were composed almost exclusively of the intact parent ion, while for highly-charged clusters the dominant signals observed often corresponded to oxidation of the parent ion or adducts formed with counter ions. These processes are presumably favoured in order to reduce the charge-density associated with the ion. Initial speculation that the oxidised ions were instead caused by protonation was disproved from high-resolution spectra and the use of dried solvents.

A key outcome of this research was the evidence that ESMS is more reliable in sample characterisation than traditional spectroscopic methods (e.g. IR, NMR). ESMS analysis for the majority of samples confirmed the previous assignment and the simple spectra obtained (often composed of a single signal) were easily interpreted. For a few of the samples provided, ESMS analysis indicated the presence of clusters other than those expected. The presence of these clusters was explainable in each case, and the mis-labelling attributed to the inability of IR and NMR to distinguish between clusters of similar composition. An example was the "$[Rh_{10}S(CO)_{22}]^{2-}$" sample which ESMS analysis clearly indicated was a mixture of ^{13}C labelled and unlabelled samples of $[Rh_{17}S_2(CO)_{32}]^{3-}$. These results indicate that ESMS is a superior technique to IR or NMR for the characterisation of these materials.

A novel application of ESMS has been identified in the characterisation of isotopically labelled compounds. The presence of ^{13}C was easily detected, and the extent of labelling determined through comparison of observed and simulated isotope patterns. The use of ESMS in this role has not been previously reported (though traditional MS techniques have been extensively employed for determining isotope levels in samples).

ESMS analysis of these cluster samples indicated that low applied voltages are required for the identification of intact parent ions, though carbonyl loss can be induced if desired (to provide confirmation of cluster charge). For the most fragile cluster reported,

$[Ni_9C(CO)_{17}]^{2-}$, carbonyl loss was evident at the lowest voltage practical, though even for this sample a parent ion was clearly evident. The loss of key numbers of carbonyl ligands may reflect structural rearrangements {e.g. $[Rh_6C(CO)_{15}]^{2-} \longrightarrow [Rh_6C(CO)_{13}]^{2-}$} though equivalent loss was noted for clusters where more condensed structures are unlikely.

In general, the application of ESMS to air-sensitive transition metal carbonyl clusters has proven successful and the ability of the technique to characterise these materials is conclusive.

3.8 Experimental

Acetonitrile was employed both in sample dilution and as the mobile phase in the ESMS. The solvent was degassed prior to use (using freeze/thaw cycles, alternating between vacuum and an inert atmosphere) and stored under argon throughout the course of sample analysis. Oxygen was removed from the solvent lines of the ESMS by flushing the solvent through the system for an extended period of time (typically overnight).

The presence of H_2O was not considered to be a significant hindrance to analysis of the majority of the samples, confirmed by the lack of protonation observed in the ESMS analysis of these samples. However, for the larger hydrido clusters the presence of H_2O could lead to protonation of the sample, complicating the analysis. Analysis was repeated for these samples using acetonitrile that had been freshly distilled over CaH_2 under an inert atmosphere. Analyses using this dried and de-oxygenated solvent were identical to those using the unpurified solvent.

The samples were provided in small glass ampoules (*ca.* 2 mL volume) sealed under a nitrogen atmosphere. These vials were broken into a Schlenk flask against a positive pressure of argon, with a small amount of the sample removed and placed in a micro Schlenk flask. This sub-sample was diluted (to *ca.* 1 mg mL^{-1}) with degassed acetonitrile and the solution was drawn and injected into the ESMS through an argon flushed syringe. Spectra were acquired in negative-ion mode across over a wide cone voltage range (5 to 90 cV).

Chapter Four - Reactions of μ_4-E[$M_2(CO)_x$]$_2$ [E = Si, Ge, Sn; M = Co (x = 7), Fe (x = 8)] with [$Co(CO)_4$]$^-$

4.1 Introduction

4.1.1 Application of ESMS to Monitoring Cluster Reactions

A key objective of the research reported in this thesis was the application of ESMS to monitoring of cluster reactions. Analysis by ESMS allows the identification of all ionic cluster products throughout reaction and by monitoring changes in the clusters present, key intermediate species and the reaction pathway can be established. Infra-red spectroscopy has been used in this role previously, with changes in carbonyl stretching frequencies used to follow the reaction. The disadvantages of IR analysis are that different clusters are often indistinguishable (refer to Section 1.2.4.1) and only limited information about the cluster composition is provided from the spectra. The ability of ESMS to distinguish between cluster species on the basis of mass and charge make it a superior method for monitoring these reactions.

One of the main systems examined involved the reactions of μ_4-E[$M_2(CO)_x$]$_2$ [E = Si, Ge, Sn; M = Co (x = 7), Fe (x = 8)] compounds with various anionic transition metal reagents. Several cluster species have been isolated from these reactions previously, though the mechanisms by which these reactions proceed were poorly understood and the existence of a wider variety of cluster products than those isolated was always suspected. For these reasons, the reactions were re-examined using ESMS to monitor changes in the composition of the solution.

4.1.2 Structures of Group 14/Transition Metal Clusters

As an introduction to this research, a discussion of the synthesis and structures of transition metal clusters incorporating group 14 elements is provided. This discussion is not intended to be a complete review of the field but provides an overview of the clusters available, with focus on the heavier group 14 elements. The discussion is

restricted to clusters with a minimum of 4 E-M bonds and incorporating a 'naked' group 14 element (i.e. lacking any organic substituent).

Carbido clusters are largest class of group 14/transition metal clusters reported, with a noted preference for encapsulation of the carbon atom. The lowest-nuclearity carbido clusters known are the CM_4 examples which commonly adopt the 'butterfly' arrangement {e.g. $[Fe_4C(CO)_{12}]^{2-}$ [1], $[Fe_3MC(CO)_x]^-$ M = Rh (x = 12)[2], Mn, W, Cr[3] (x = 13) and various analogues}. The arrangement (Figure 4.1a), considered an *arachno*-octahedron, maximises M-M bonding, though an open geometry about the carbon atom is apparent. Addition of another metal vertex produces more encapsulated structures, noted for the bridged-butterfly and square-pyramid arrangements (Figures 4.1b and c respectively). The square-pyramid (or *nido*-octahedron) structure is displayed by $M_5C(CO)_{15}$ (M = Fe[4], Ru[5], Os[6]) clusters and isoelectronic analogues (with respect to ligands and charge). The carbon atom is located beneath the M_4 plane in each case and increasing the charge-density on the cluster (through loss of CO ligands or replacement by weaker π–acceptor ligands) increases the offset distance. The bridged-butterfly structure is often displayed by CM_5 clusters of the heavier transition metal elements [e.g. $Os_5C(CO)_{16}$[7]].

[1] M. Tachikawa and E.L. Muetterties, *J. Am. Chem. Soc.*, 1980, **102**, 4541; R.F. Boehme and P. Coppens, *Acta. Cryst. Sect. B.*, 1981, **37**, 1914.

[2] J.A. Hriljac, P.N. Swepston and D.F. Shriver, *Organometallics*, 1985, **4**, 158.

[3] J.A. Hriljac, E.M. Holt and D.F. Shriver, *Inorg. Chem.*, 1987, **26**, 2943.

[4] E.H. Braye, L.F. Dahl, W. Hübel and D.L. Wample, *J. Am. Chem. Soc.*, 1962, **84**, 4633; A. Gourdon and Y. Jeannin, *J. Organomet. Chem.*, 1985, **290**, 199.

[5] D.H. Farrar, P.F. Jackson, B.F.G. Johnson, J. Lewis, J.N. Nicholls and M. McPartlin, *J. Chem. Soc., Chem. Commun.*, 1981, 415.

[6] P.F. Jackson, B.F.G. Johnson, J. Lewis, J.N. Nicholls, M. McPartlin and W.J.H. Nelson, *J. Chem. Soc., Chem. Commun.*, 1980, 564.

[7] B.F.G. Johnson, J. Lewis, W.J.H. Nelson, J.N. Nicholls, J. Puga, P.R. Raithby, M.J. Rosales, M. Schröder and M.D. Vargas, *J. Chem. Soc., Dalton Trans.*, 1983, 2447.

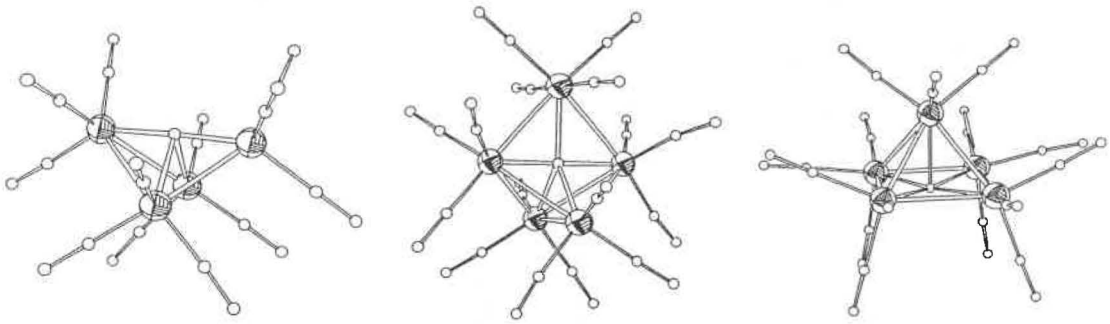

(a) (b) (c)

Figure 4.1 – The structures of $[Fe_4C(CO)_{12}]^{2-}$ [1] (a), $Os_5C(CO)_{16}$ [7] (b) and $Ru_5C(CO)_{15}$ [5] (c).

Encapsulation is more pronounced for CM_6 clusters, with the carbon located within a trigonal-prism or octahedron of metal atoms. The trigonal-prismatic structure {displayed by $[M_6C(CO)_{15}]^{2-}$ M = Co[8], Rh[9]} is less common than the octahedral arrangement {adopted by $[M_6C(CO)_{13}]^{2-}$ (M = Co[10], Rh[11] - Figure 4.2a) and $[Ru_6C(CO)_{16}]^{2-}$ [12]}, though the latter possesses a smaller internal cavity [with a radius ratio between the interstitial and metal atoms (r_I:r_M) of 0.414 compared to 0.528[13]]. The majority of higher-nuclearity carbido clusters are comprised of capped or condensed CM_6 polyhedra {e.g. $Os_8C(CO)_{22}$ [14] (Figure 4.2b), $[Os_{10}C(CO)_{24}]^{2-}$ [15] and $[Ru_{10}C_2(CO)_{24}]^{2-}$ [16]}.

Although coordination numbers greater than six are rare for carbon, eight coordinate examples have been reported {e.g. $[Co_8C(CO)_{18}]^{2-}$ [17], $[Ni_8C(CO)_{16}]^{2-}$ (Figure 4.2c) and

---

[8] S. Martinengo, D. Strumolo, P. Chini, V.G. Albano and D. Braga, *J. Chem. Soc., Dalton Trans.*, 1985, 35.

[9] V.G. Albano, M. Sansoni, P. Chini and S. Martinengo, *J. Chem. Soc., Dalton Trans.*, 1973, 651.

[10] V.G. Albano, D. Braga and S. Martinengo, *J. Chem. Soc., Dalton Trans.*, 1986, 981.

[11] V.G. Albano, D. Braga, and S. Martinengo, *J. Chem. Soc., Dalton Trans.*, 1981, 717.

[12] B.F.G. Johnson, J. Lewis, S.W. Sankey, K. Wong, M. McPartlin and W.J.H. Nelson, *J. Organomet. Chem.*, 1980, **191**, C3.

[13] G. Ciani and A. Sironi, *J. Organomet. Chem.*, 1983, **241**, 385.

[14] A.J. Amoroso, B.F.G. Johnson, J. Lewis, C-K. Li, P.R. Raithby and W–T. Wong, *J. Organomet. Chem.*, 1993, **444**, C55.

[15] P.F. Jackson, B.F.G. Johnson, J. Lewis, M. McPartlin and W.J.H. Nelson, *J. Chem. Soc., Chem Commun.*, 1980, 224.

[16] C-M.T. Hayward, J.R. Shapley, M.R. Churchill, C. Bueno and A.L. Rheingold, *J. Am. Chem. Soc.*, 1982, **104**, 7347; M.R. Churchill, C. Bueno and A.L. Rheingold, *J. Organomet. Chem.*, 1990, **395**, 85.

[17] V.G. Albano, P. Chini, G. Ciani, S. Martinengo and M. Sansoni, *J. Chem Soc., Dalton Trans.*, 1978, 463.

$[Ni_9C(CO)_{17}]^{2-}$ [18] - the ESMS analysis of which were reported in Chapter 3}. In each case, the carbon atom resides within a square anti-prism of metal atoms, though this arrangement may be slightly distorted.

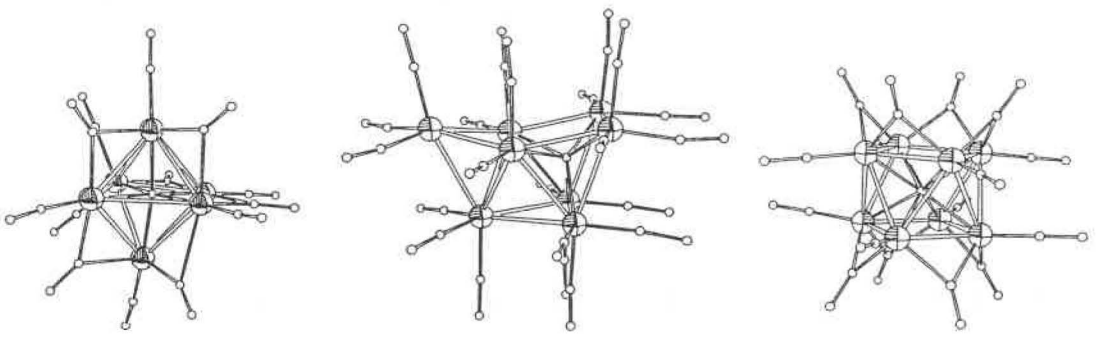

(a) (b) (c)

Figure 4.2 – The structures of $[Rh_6C(CO)_{13}]^{2-}$ [13] (a), $Os_8C(CO)_{22}$ [14] (b) and $[Ni_8C(CO)_{16}]^{2-}$ [18] (c).

Clusters containing the heavier group 14 elements bear little structural resemblance to the carbido clusters discussed above. The larger size of these elements often precludes encapsulation, leading to the adoption of more open arrangements.

The structures displayed by the heavier EM_4 compounds fall into three main categories (indicated in Figure 4.3). The fully-open arrangement is known for M = Co, E = Ge[19], Sn[20], Pb[21]; M = Mn, Re, E = Si[22], though only the tin and lead compounds have been structurally characterised. A similar semi-open structure (intermediate between the 'spiro' and open arrangements) was reported for M = Fe, E = Sn[23], Pb[24] but is unknown for the earlier elements.

[18] A. Ceriotti, G. Longoni, M. Manassero, M. Perego and M. Sansoni, *Inorg. Chem.*, 1985, **24**, 117.

[19] R.F. Gerlach, B.W.L. Graham and K.M. Mackay, *J. Organomet. Chem.*, 1979, **182**, 285.

[20] A. Cabrera, H. Samain, A. Mortreux, F. Petit and A.J. Welch, *Organometallics*, 1990, **9**, 959.

[21] J.S. Leigh and K.H. Whitmire, *Acta Cryst. Sect. C.*, 1990, **46**, 732.

[22] B.J. Aylett and M.T. Taghipour, *J. Organomet. Chem.*, 1983, **249**, 55.

[23] J.M. Cassidy, K.H. Whitmire and A.M. Kook, *J. Organomet. Chem.*, 1993, **456**, 61.

[24] C.B. Lagrone, K.H. Whitmire, M.R. Churchill and J.C. Fettinger, *Inorg. Chem.*, 1986, **25**, 2080.

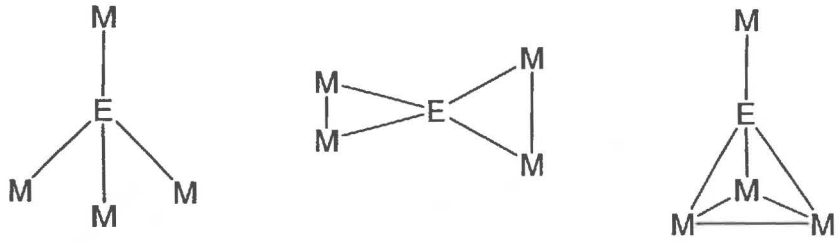

Open 'Spiro' 'Spiked'-tetrahedron

Figure 4.3 – The common EM_4 structures displayed by the heavier group 14 elements.

The dominant EM_4 structures adopted by germanium and silicon are based around the 'spiro' and 'spiked'-tetrahedral configurations. The 'spiro' structures consist of two mutually perpendicular EM_2 triangles linked through a common vertex (Figure 4.4a) as expressed by μ_4-E[$M_2(CO)_x$]$_2$ [M = Co (x = 7), E = Si[25], Ge[26]; M = Fe (x = 8), E = Si[27], Ge[28], Sn[29], Pb[30]]. The reactions of the germanium and silicon cobalt compounds form the majority of the research reported in this and the following chapter. These compounds were prepared most conveniently from reaction between EH_4 and $Co_2(CO)_8$, though an alternative synthesis of μ_4-Ge[$Co_2(CO)_7$]$_2$ using GeI_4 and Na[$Co(CO)_4$] has been reported[26]. Extended 'spiro' structures in which EM_2 triangles are linked through shared M-M bonds are also known [e.g. $Ge_2Co_6(CO)_{20}$[31] and $Ge_3Co_8(CO)_{26}$[32] - Figure 4.4b].

[25] K.M. Mackay and C.C. Tan, *J. Chem. Research*, 1982, 229; K.M. Mackay, B.K. Nicholson, A.W. Sims and C.C. Tan, *Acta Cryst. Sect. C,* 1987, **43**, 633.

[26] R.F. Gerlach, K.M. Mackay and B.K. Nicholson, *J. Organomet. Chem.*, 1979, **178**, C30; R.F. Gerlach, K.M. Mackay, B.K. Nicholson and W.T. Robinson, *J. Chem. Soc., Dalton Trans.*, 1981, 80.

[27] S.G. Anema, G.C. Barris, K.M. Mackay and B.K. Nicholson, *J. Organomet. Chem.*, 1988, **350**, 207.

[28] J.D. Cotton and R.M. Peachey, *Inorg. Nucl. Chem. Lett.*, 1970, **6**, 727.

[29] J.D. Cotton, S.A.R. Knox, I. Paul and F.G.A. Stone, *J. Chem. Soc. A*, 1967, 264.

[30] K.H. Whitmire, C.B. Lagrone, M.R. Churchill, J.C. Fettinger and B.H. Robinson, *Inorg. Chem.*, 1987, **26**, 3491.

[31] S.P. Foster and K.M. Mackay, *J. Organomet. Chem.*, 1982, **238**, C46.

[32] S.G. Anema, K.M. Mackay, L.C. McLeod, B.K. Nicholson and J.M. Whittaker, *Angew. Chem. Int. Ed. Engl.*, 1986, **25**, 759.

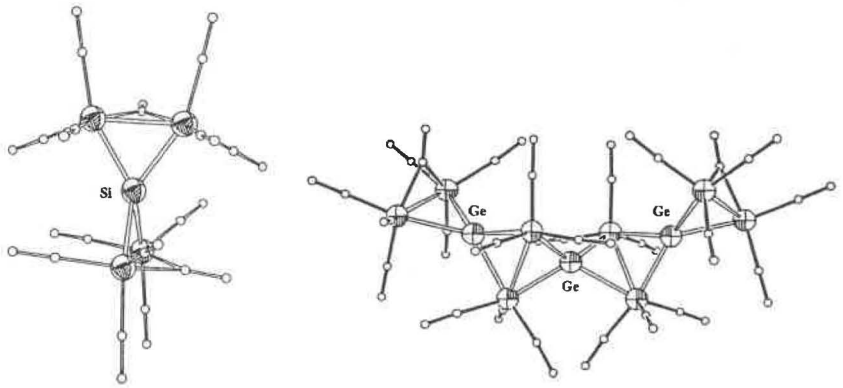

(a) (b)

Figure 4.4 – The structures of μ_4-Si[$Co_2(CO)_7$]$_2$ [25] (a) and $Ge_3Co_8(CO)_{26}$ [32] (b).

The final commonly observed EM_4 structure is the 'spiked'-tetrahedral MEM_3 arrangement. This geometry is expressed by various $LMECo_3(CO)_9$ clusters [e.g. E = Si, ML = $Co(CO)_4$ [33], $Fe(CO)_2(\eta^5\text{-}C_5H_5)$ [34]; E = Ge, ML = $Co(CO)_4$ [35], $Fe(CO)_2(\eta^5\text{-}C_5H_5)$, $Ni(CO)(\eta^5\text{-}C_5H_5)$[36]] though the analogous iron compounds are less well known {one of the few examples being $[(CO)_4FeGeFe_3(CO)_{10}]^{2-}$ [30]}. The $(CO)_4CoECo_3(CO)_9$ (E = Si[33], Ge[35]) clusters were produced from reaction between EI_4 and $Na[Co(CO)_4]$ or from decarbonylation of the equivalent 'spiro' cluster. Extension of the MEM_3 arrangement is reported through either the apical metal atom {as observed in $[Co_7Ge(CO)_{20}]^-$ and $[Co_7Ge_2(CO)_{21}]^-$ [37] - Figures 4.5a and b} or through capping of the M_3 triangle {e.g. $Fe_3[\mu_3\text{-}SnM(CO)_5]_2(CO)_9$, M = Mn, Re[38] - Figure 4.5c}.

The most common arrangement for EM_5 clusters incorporating heavier main group elements is based around a 'spiked'-square-pyramid. This motif is noted in the structures of $Co_4[\mu_4\text{-}ECo(CO)_4]_2(CO)_{11}$ (E = Si[39], Ge[40] - Figure 4.6a) and various analogues of these clusters, the synthesis and structures of which are discussed in

---

[33] G. Schmid, V. Balzel and G. Etzrodt, *J. Organomet. Chem.*, 1976, **112**, 345.

[34] W. Malisch, H.U. Wekel, I. Grob, F.H. Kohler and M. Baudler, *Z. Naturforch B*, 1982, **37**, 601.

[35] R. Boese and G. Schmid, *J. Chem. Soc., Chem. Commun.*, 1979, 349; G. Schmid and G. Etzrodt, *J. Organomet. Chem.*, 1977, **137**, 367.

[36] P. Gusbeth and H. Vahrenkamp, *Chem. Ber.*, 1985, **118**, 1746.

[37] D.N. Duffy, K.M. Mackay, B.K. Nicholson and R.A. Thomson, *J. Chem. Soc., Dalton Trans.*, 1982, 1029.

[38] H-J. Haupt, A. Goetze and U. Florke, *Z. Anorg. Allg. Chem.*, 1988, **557**, 82.

[39] M. Van Tiel, K.M. Mackay and B.K. Nicholson, *J. Organomet. Chem.*, 1987, **326**, C101.

Chapter 7. An alternative EM_5 arrangement is displayed by $[Co_5Ge(CO)_{16}]^-$ (Figure 4.6b), where a $GeCo_3$ tetrahedron and a $GeCo_2$ triangle share a common vertex[41]. Unlike the majority of EM_3 containing clusters, the $GeCo_3$ unit in $[Co_5Ge(CO)_{16}]^-$ contains 3 μ_2-CO ligands, an arrangement well known for $LMCo_3(CO)_9$ clusters (M = Rh, Ru, Os) but not for main group analogues[42].

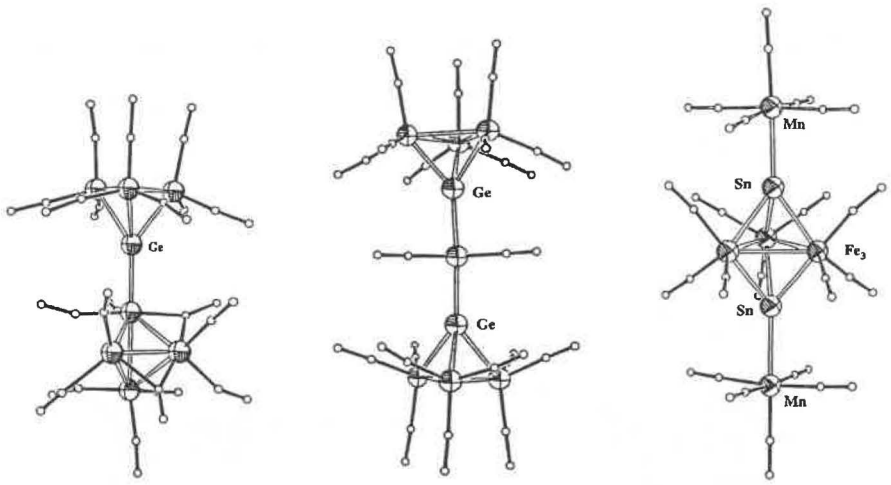

(a) (b) (c)

Figure 4.5 – The structures of $[Co_7Ge(CO)_{20}]^-$ [37] (a), $[Co_7Ge_2(CO)_{21}]^-$ [37] (b) and $Fe_3[\mu_3\text{-}SnMn(CO)_5]_2(CO)_9$ [38] (c).

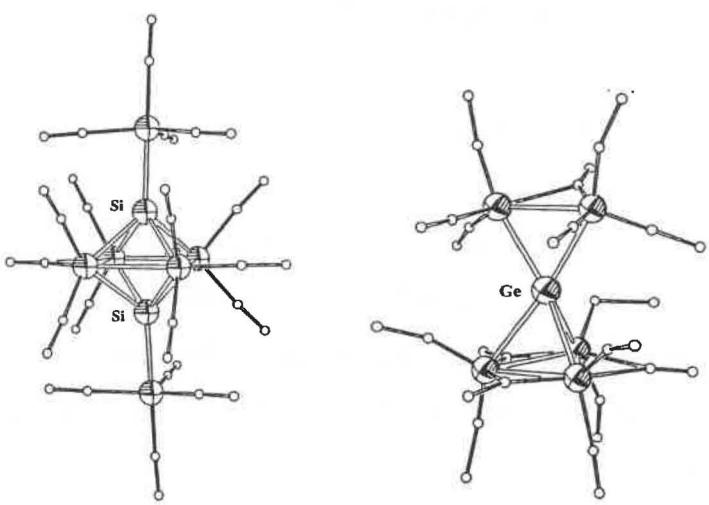

(a) (b)

Figure 4.6 – The structures of $Co_4[\mu_4\text{-}SiCo(CO)_4]_2(CO)_{11}$ [39] (a) and $[Co_5Ge(CO)_{16}]^-$ [41] (b).

[40] S.P. Foster, K.M. Mackay and B.K. Nicholson, *Inorg. Chem.*, 1985, **24**, 909.

[41] R.A. Croft, D.N. Duffy and B.K. Nicholson, *J. Chem. Soc., Dalton Trans.*, 1982, 1023.

[42] G. Schmid, *Angew. Chem. Int. Ed. Engl.*, 1978, **17**, 392 and references therein.

Encapsulation of the heavier group 14 elements is rare but not unprecedented. The only cluster containing an encapsulated silicon atom is $[Co_9Si(CO)_{21}]^{2-}$ (Figure 4.7a), formed from reaction between μ_4-Si[$Co_2(CO)_7$]$_2$ and $[Co(CO)_4]^-$ [43]. The silicon resides within a square anti-prism of cobalt atoms and the cluster is formally electron-deficient (possessing 129 valence-electrons, 10.5 SEP). Encapsulated germanium and tin atoms are known for the $[Ni_{10}Ge(CO)_{20}]^{2-}$ (Figure 4.7b) and $[Ni_{12}E(CO)_{22}]^{2-}$ (E = Ge, Sn) clusters, with the nickel atoms defining a pentagonal anti-prism and icosahedron respectively. These clusters were produced from reaction between $[Ni_6(CO)_{12}]^{2-}$ and $GeCl_4$ or $SnCl_2.2H_2O$ [44].

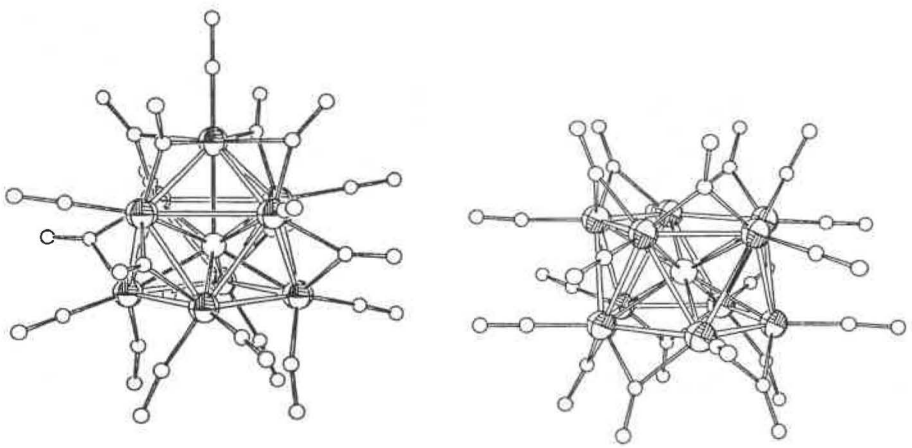

(a) (b)

Figure 4.7 – The structures of $[Co_9Si(CO)_{21}]^{2-}$ [43] (a) and $[Ni_{10}Ge(CO)_{20}]^{2-}$ [44] (b).

4.1.3 Reactions of μ_4-E[$M_2(CO)_x$]$_2$ with [$Co(CO)_4$]$^-$

The reactions of μ_4-E[$M_2(CO)_x$]$_2$ compounds with anionic transition metal reagents, specifically $[Co(CO)_4]^-$, were targeted in this research because several cluster species have been previously isolated from these reactions. In particular, the reaction between μ_4-Ge[$Co_2(CO)_7$]$_2$ and $[Co(CO)_4]^-$ was considered to be relatively well understood prior to this investigation.

The first reported product of this reaction was $[Co_5Ge(CO)_{16}]^-$ (refer to Figure 4.6b), in which the germanium atom bridges both a Co-Co bond and a Co_3 triangle, a unique

[43] K.M. Mackay, B.K. Nicholson, W.T. Robinson and A.W. Sims, *J. Chem. Soc., Chem. Commun.*, 1984, 1276.

geometry amongst the group 14 elements[41]. Recrystallisation of $[Co_5Ge(CO)_{16}]^-$ was found to yield crystals of $[Co_7Ge(CO)_{20}]^-$ (refer to Figure 4.5a), where a four coordinate germanium atom caps a Co_3 triangle and replaces a carbonyl ligand on $Co_4(CO)_{12}$ [37]. Reaction of $[Co_5Ge(CO)_{16}]^-$ with $Co_2(CO)_8$ resulted in formation of the highly symmetric $[Co_7Ge_2(CO)_{21}]^-$ cluster (Figure 4.5b), where two $GeCo_3$ fragments are linked through a common $Co(CO)_3$ unit[37]. As with $[Co_7Ge(CO)_{20}]^-$, the germanium atom is only four coordinate, in contrast with the starting cluster. $[Co_7Ge_2(CO)_{21}]^-$ is the only cluster in this series lacking bridging carbonyl ligands. Although a number of clusters species were isolated from this reaction, the mechanism by which these clusters were interrelated was unknown.

In contrast to the germanium system, the only isolated product from the reaction between μ_4-Si[$Co_2(CO)_7$]$_2$ and $[Co(CO)_4]^-$ was the unusual $[Co_9Si(CO)_{21}]^{2-}$ cluster (refer to Figure 4.7a), the only reported example of an encapsulated silicon atom (or of silicon with a coordination number > 5)[43]. The cluster is paramagnetic and electron-deficient from an electron-counting perspective (with 129 valence electrons rather than the 130 predicted for a capped square anti-prism). The mechanism by which this cluster was produced from the 'spiro' starting material was unknown, as was the identity of any intermediate products *en route* to $[Co_9Si(CO)_{21}]^{2-}$.

The reactions of μ_4-Si[$Fe_2(CO)_8$]$_2$ and μ_4-Sn[$Fe_2(CO)_8$]$_2$ with $[Co(CO)_4]^-$ have not been reported.

For the reasons outlined above, the reactions of various 'spiro' μ_4-E[$M_2(CO)_x$]$_2$ compounds with $[Co(CO)_4]^-$ were considered a useful system for examination by ESMS. It was anticipated that ESMS would provide information complementary to that already reported for the germanium system while allowing the identification of novel cluster products for the silicon and tin systems.

[44] A. Ceriotti, F. Demartin, B.T. Heaton, P. Ingallina, G. Longoni, M. Manassero, M. Marchionna and N. Masciocchi, *J. Chem. Soc., Chem. Commun.*, 1989, 786.

4.2 Selection of an Appropriate ESMS Solvent

An initial difficulty with ESMS monitoring of these reactions was selection of an appropriate carrier solvent with which to acquire spectra. Traditional ESMS solvents are based around aqueous mixtures of methanol or acetonitrile. Distilled water provides lesser quality spectra, presumably caused by the surface-tension preventing effective spray of the solvent into the ESMS source. The lower surface-tension of methanol and acetonitrile based solvents assists spray formation while the higher volatility of these solvents allow the ESMS to be run at lower temperatures (60°C typically). Both methanol and acetonitrile were trialed as potential solvents but were found inappropriate since solutions of the μ_4-E[$M_2(CO)_x$]$_2$ compounds decomposed within minutes at room temperature.

Initial attempts using CH_2Cl_2 as a carrier solvent were unsuccessful. Although the reactions were often carried out in CH_2Cl_2, the spectra acquired with this solvent were typically of low intensity. Similarly, Et_2O is a suitable solvent for performing cluster reactions but its properties (especially high volatility) preclude its use as an electrospray solvent.

The ESMS properties of various ethereal solvents were examined including di-butylether, di-propylether and monoglyme (ethyleneglycol-dimethylether), though none of these solvents provided clean, reproducible spectra under standard ESMS conditions. Various chlorinated solvents including chloroform and tetrachloro-ethane were trialed with limited success. After extensive trial and error, 1,2-dichloroethane was found to be an ideal ESMS solvent for examination of cluster reactions. The solvent is cheap, easily purified and provided reproducible ES mass spectra across a range of cluster reactions.

To remove traces of acetonitrile, methanol and water from the ESMS capillaries, the system was routinely purged with dichloroethane for a period of hours prior to sample analysis. The solvent was stored under an argon atmosphere at all times (a positive pressure during times of use and a static atmosphere at all other times).

4.3 Identification of μ_4-E[$M_2(CO)_x$]$_2$ Compounds

An initial unexpected result from ESMS analysis of these reactions was detection of the starting 'spiro' reagents. These compounds are neutral and thus expected to be 'electrospray-invisible', however the parent compounds were identified on numerous occasions as $[M+A]^-$ ions (A = OH, OMe, CO_2H) when traces of water, methanol or formic acid (often used to clean the ESMS system) were present. In the absence of these ions, $[M+X]^-$ (X = Cl, Br) signals were observed.

The association of μ_4-E[$M_2(CO)_x$]$_2$ compounds with methoxide ions was not completely unexpected. The use of sodium methoxide as an ionisation aid in the ESMS analysis of metal carbonyl compounds was discussed in the introductory Chapter (Section 1.3.5) and nucleophilic attack of alkoxide ions upon carbonyl ligands is well known[45]. The evidence that hydroxide and formate ions act in a similar manner is more interesting, especially hydroxide because of its implications in the water-gas shift process (where H_2 and CO_2 are produced from H_2O and CO). The assignment of the methoxide and formate ions were confirmed by 'dosing' the sample with a small amount of Na[A], resulting in a significant increase in the intensity of the appropriate signal. Similar confirmation of the hydroxide ions {e.g. $[Co_4Ge(CO)_{14}OH]^-$ - Figure 4.8} was unavailable as the addition of sodium hydroxide caused sample decomposition.

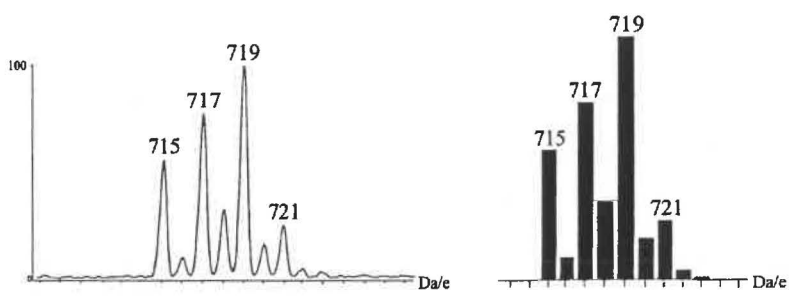

Figure 4.8 – The observed and calculated isotope patterns for $[Co_4Ge(CO)_{14}OH]^-$.

When hydroxide, methoxide and formate ions were absent, association with halide ions (usually chloride) was detected {shown for μ_4-Ge[$Co_2(CO)_7$]$_2$ - Figure 4.9}, with the halide ions presumably a trace contaminant in the ESMS system. As before, assignment

[45] F.A. Cotton and G. Wilkinson, *Advanced Inorganic Chemistry, 5th Edition*, John Wiley and Sons, (New York, USA), 1988.

of the ions was confirmed by 'dosing' the sample with the appropriate halide, preferably a CH_2Cl_2 soluble salt such as [PPN]Cl or [PPh_4]Br.

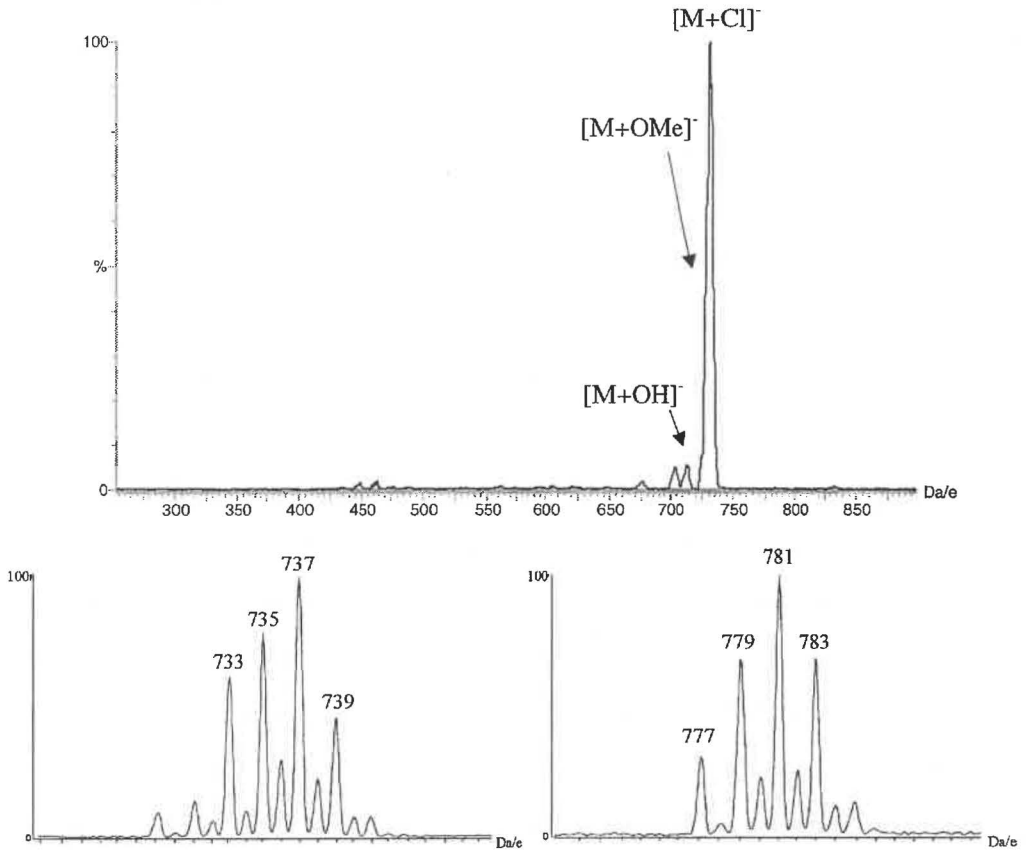

Figure 4.9 – The ES mass spectrum (-ve ion, 5 cV) of μ_4-Ge[$Co_2(CO)_7$]$_2$ in the presence of Cl^-. Isotope patterns for [M+Cl]$^-$ {with a trace of [M+OMe]$^-$ - left} and [M+Br]$^-$ (right) are presented.

The association of the 'spiro' compounds with halides is more interesting than that of the other nucleophiles. Nucleophilic attack of halides on carbonyl ligands has been proposed for $M_3(CO)_{12}$ (M = Fe, Ru, Os[46]) compounds but the products rapidly evolve CO, producing [$M_3(CO)_{10}X$]$^-$ clusters where the halide bridges two metal atoms[47]. Another possibility is that halide addition occurs at a transition metal or the group 14 atom rather than the carbonyl ligand. The ability of halides, especially chloride, to bridge M-M bonds is well known[48] and the ionisation of 'spiro' compounds through

[46] G. Lavigne and H.D. Kaesz, *Metal Clusters in Catalysis,* Ed. B.C. Gates *et al*, Elsevier Science Publishers (Amsterdam, Netherlands), 1986.

[47] G. Lavigne and H.D. Kaesz, *J. Am. Chem. Soc.*, 1984, **106**, 4647.

[48] Examples include M.R. Churchill and R.H. Lashewycz, *Inorg. Chem.*, 1979, **18**, 1926 and N.C. Leadbeater, J. Lewis, P.R. Raithby and M.A. Rennie, *Polyhedron*, 1998, **17**, 1755.

bridging agents has been reported {e.g. Ag^+ addition allowed ESMS detection of μ_4-Si[$Fe_2(CO)_8$]$_2$ [49]}. Halide addition might instead be occurring at the group 14 element, generating a structure similar that found for $Co_4(\mu_4\text{-}ER)_2(CO)_{11}$ compounds (Figure 4.10). The absence of equivalent halide adducts for the 'spiked'-tetrahedral $(CO)_4CoECo_3(CO)_9$ clusters (E = Ge, Si – detected through IR analysis) provides indirect evidence for such a structure.

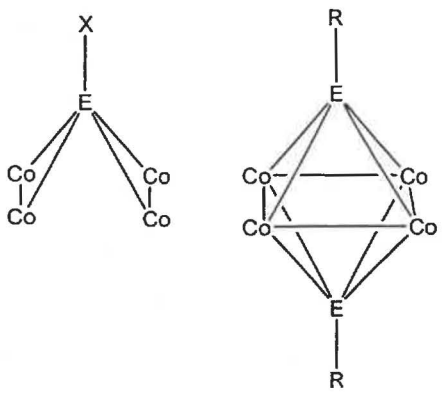

Figure 4.10 – The comparison of a suggested arrangement for [$Co_4E(CO)_{14}X$]$^-$ and $Co_4(\mu_4\text{-}ER)_2(CO)_{11}$.

Following the detection of [M+X]$^-$ species by ESMS, a larger scale synthesis of a halide cluster was attempted. Treatment of a CH_2Cl_2 solution of μ_4-Ge[$Co_2(CO)_7$]$_2$ with a stoichiometric amount of [PPh_4]Br caused an immediate colour change from orange to deep red. ESMS analysis indicated the formation of the [$Co_4Ge(CO)_{14}Br$]$^-$ anion (*m/z* 781), while IR spectra displayed a shift in the carbonyl stretching frequencies from those characteristic of the starting 'spiro' compound [2082 (s), 2062 (s), 2033 (m,br), 1839 (w,br) cm^{-1}] to broader signals at lower wavenumber [2052 (s), 2049 (m,sh), 2002 (m,br), 1970 (m), 1890 (m,br), 1822 (w,br) cm^{-1}]. The shift to lower wavenumber is characteristic of the formation of an anionic cluster. Within 15-20 minutes at room temperature the solution faded to pale yellow and analysis (both IR and ESMS) indicated [$Co(CO)_4$]$^-$ was the only significant component of the sample. In general, analysis indicated that halide adducts form readily but were unstable at room temperature which prevented their isolation.

[49] W. Henderson and B.K. Nicholson, *J. Chem. Soc., Chem. Commun.*, 1995, 2531.

4.4 Reaction of μ_4-Ge[$Co_2(CO)_7$]$_2$ with [$Co(CO)_4$]$^-$

4.4.1 ESMS Analysis

The reaction between μ_4-Ge[$Co_2(CO)_7$]$_2$ and [$Co(CO)_4$]$^-$ was carried out in both Et_2O and CH_2Cl_2, using various reactant ratios and employing a range of cations. The reaction was found to be solvent dependent, though relatively immune to changes in the cation or reactant ratios.

When the two reagents were refluxed in Et_2O, a rapid reaction ensued generating the previously characterised [$Co_5Ge(CO)_{16}$]$^-$ anion (*m/z* 817 – Figure 4.11) within 5-15 minutes. The intensity of this signal decreased as reaction progressed (30-60 minutes) and two higher-nuclearity anions, [$Co_7Ge(CO)_{20}$]$^-$ (*m/z* 1047) and [$Co_7Ge_2(CO)_{21}$]$^-$ (*m/z* 1147), were detected. Both of these clusters have been previously isolated through different synthetic procedures (discussed in Section 4.1.3)[37]. The reaction was maintained at reflux for several hours with no further products detected.

In contrast, when the reaction was performed in CH_2Cl_2, the [$Co_5Ge(CO)_{16}$]$^-$ cluster was not apparent at any stage. This indicates that either the cluster was not produced under these conditions or that it reacted further at a rate preventing detection (the latter of these explanations appears more plausible). The published synthetic route to [$Co_5Ge(CO)_{16}$]$^-$ required refluxing in CH_2Cl_2 for 2 hours[41] but under these conditions the cluster was not detected by ESMS. It is possible that the initial preparation of this cluster was performed in Et_2O and misreported. The IR spectra of [$Co_5Ge(CO)_{16}$]$^-$ and [$Co_7Ge(CO)_{20}$]$^-$ are very similar (discussed in Section 4.4.2) and distinguishing between the two clusters spectroscopically would be difficult.

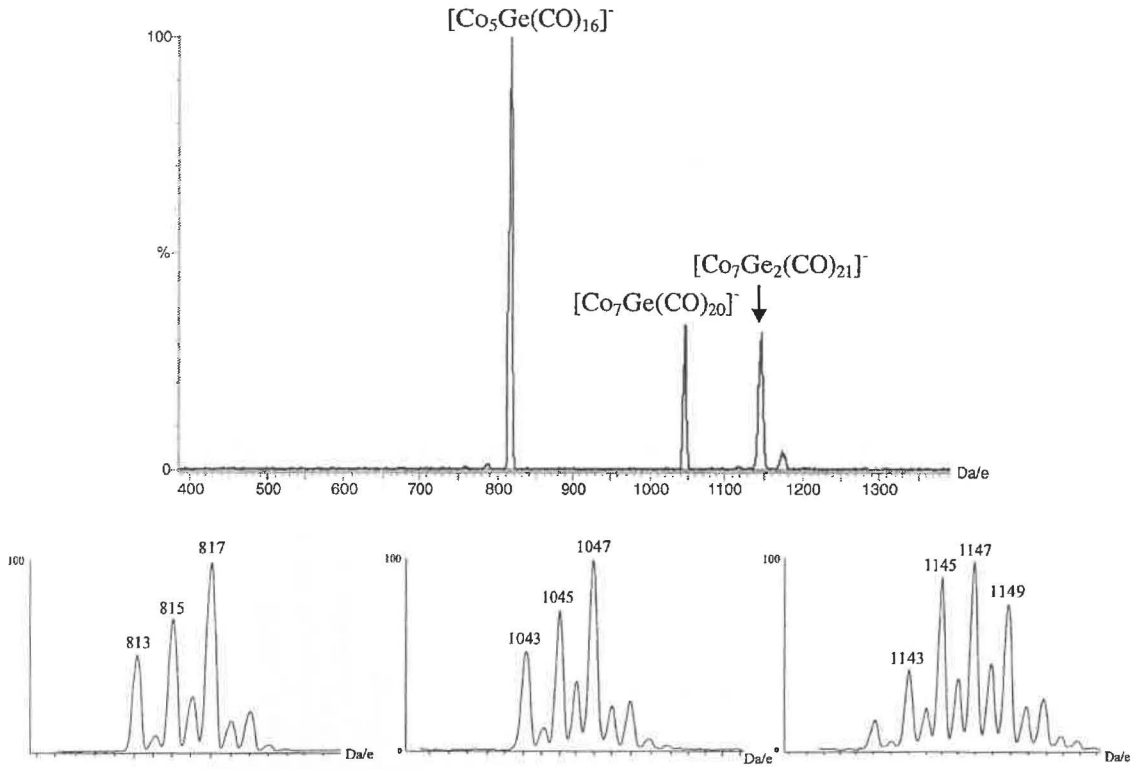

Figure 4.11 – The ES mass spectrum (-ve ion, 5 cV) of the reaction between μ_4-Ge[$Co_2(CO)_7$]$_2$ and [$Co(CO)_4$]$^-$ (Et_2O, 30 minutes), with isotope patterns (left to right) for [$Co_5Ge(CO)_{16}$]$^-$, [$Co_7Ge(CO)_{20}$]$^-$ and [$Co_7Ge_2(CO)_{21}$]$^-$.

The signals attributed to [$Co_7Ge(CO)_{20}$]$^-$ and [$Co_7Ge_2(CO)_{21}$]$^-$ were detected after 10-20 minutes, mimicking the reaction performed in Et_2O, with further reaction identifying a high-nuclearity di-anionic cluster signal at *m/z* 704 (Figure 4.12). The cluster charge was determined from high-resolution spectra (which also indicated the presence of two germanium atoms) and from induced CO loss (through systematically increased cone voltage) generating signals *m/z* 14 apart (Figure 4.13). An anion of this mass was calculated to correspond to the unheralded [$Co_{10}Ge_2(CO)_{24}$]$^{2-}$ cluster, with an additional signal noted at *m/z* 1408 corresponding to [$Co_{10}Ge_2(CO)_{24}$]$^-$, the oxidised form of the cluster. Initial suspicions that the latter signal corresponded to the protonated ion, [$HCo_{10}Ge_2(CO)_{24}$]$^-$ *m/z* 1409, proved unfounded.

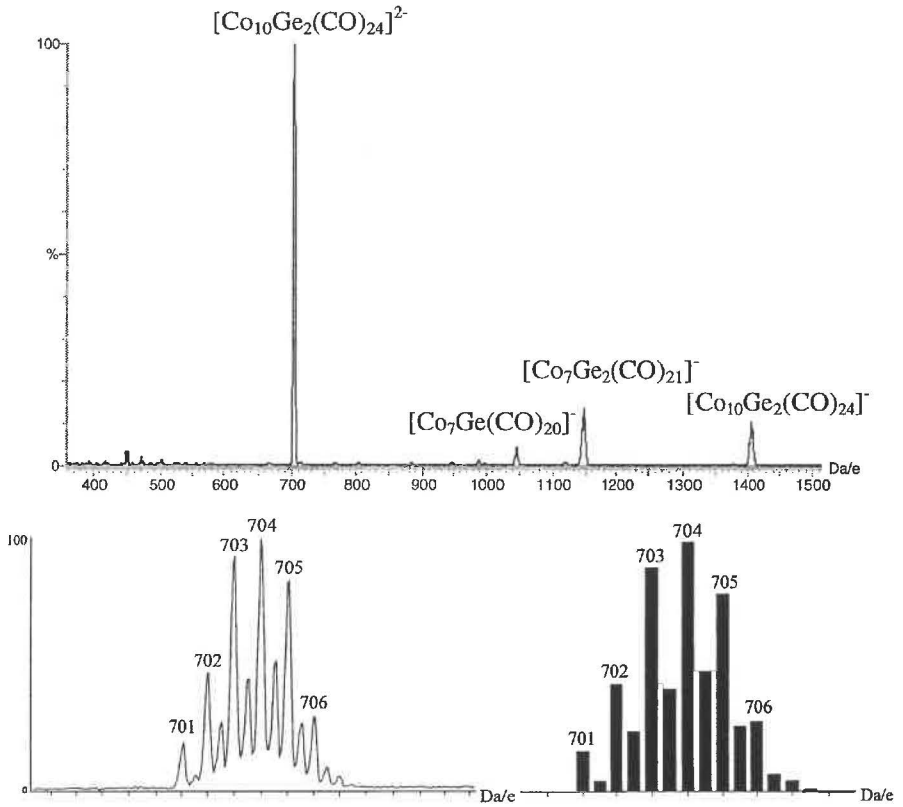

Figure 4.12 – The ES mass spectrum (-ve ion, 5 cV) of the reaction between μ_4-Ge[$Co_2(CO)_7$]$_2$ and [$Co(CO)_4$]$^-$ (CH_2Cl_2, 6 hours), with observed and calculated isotope patterns for [$Co_{10}Ge_2(CO)_{24}$]$^{2-}$.

Through repetition of the reaction numerous times on a small scale, the optimal conditions for production of the [$Co_{10}Ge_2(CO)_{24}$]$^{2-}$ cluster were determined as refluxing in CH_2Cl_2 for 5-6 hours using a 1:2 ratio of μ_4-Ge[$Co_2(CO)_7$]$_2$ to [$Co(CO)_4$]$^-$ (though the effect of the ratio of starting materials was fairly insignificant). The reaction was conducted on a larger scale under these conditions, allowing the isolation of [NEt_4]$_2$[$Co_{10}Ge_2(CO)_{24}$]. This is believed to be the first case where a novel cluster has been initially identified by ESMS with subsequent isolation and characterisation.

A range of stoichiometric ratios of μ_4-Ge[$Co_2(CO)_7$]$_2$:[$Co(CO)$]$_4^-$ were examined (1:1, 1:2, 1:4, 1:10) with no significant effect noted on the reaction rate or cluster products generated. The higher ratio experiments displayed more intense signals attributable to [$Co(CO)_4$]$^-$ (*m/z* 171) and associated aggregates {e.g. [NEt_4][$Co(CO)_4$]$_2^-$ (*m/z* 472), [Ag{$Co(CO)_4$}$_2$]$^-$ (*m/z* 449)} as expected. It was also apparent that [$Co(CO)_4$]$^-$ was generated during reaction, as determined by refluxing a CH_2Cl_2 solution of μ_4-Ge[$Co_2(CO)_7$]$_2$ in the absence of the anion. Under these conditions, the initial ES mass spectra lacked the *m/z* 171 signal but this ion became apparent within 10-20 minutes.

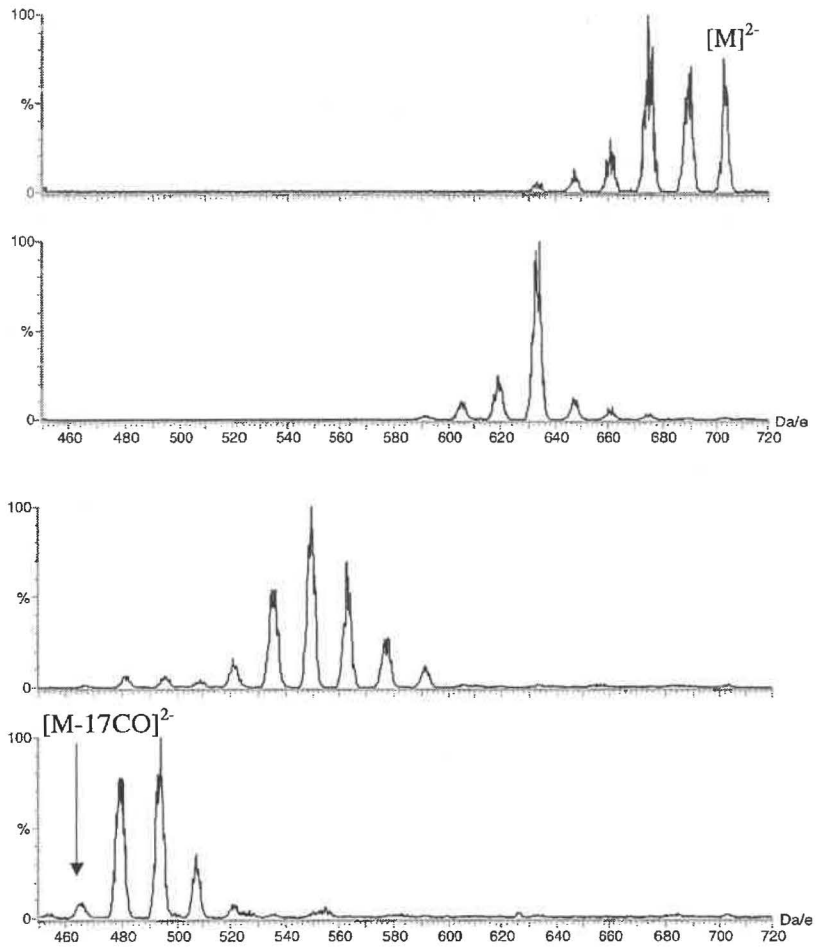

Figure 4.13 – The induced carbonyl loss from $[Co_{10}Ge_2(CO)_{24}]^{2-}$ at (top-bottom) 20, 30, 50 and 70 cV (-ve ion).

Various cations were employed in the examination of this reaction including $[NEt_4]^+$, $[NBu_4]^+$, $[PPN]^+$, $[PPh_4]^+$, $[PhCH_2NMe_3]^+$, $[AsPh_4]^+$ and Na^+. The reasons for this were two-fold; (i) the effect of changes in the cation upon the reaction rate and pathway were examinable, and (ii) it was considered that $[Co_{10}Ge_2(CO)_{24}]^{2-}$ may preferentially crystallise with one particular cation. There was no variation in the cluster products observed by ESMS between different cations and the differences in the time required to form the higher-nuclearity clusters were insignificant. In each case, the signal attributed to $[Co_{10}Ge_2(CO)_{24}]^{2-}$ dominated the ES mass spectrum after 5-7 hours in refluxing CH_2Cl_2 while extended reaction yielded no further cluster products.

4.4.2 Infra-red (IR) Analysis

The reaction was monitored using infra-red (IR) spectroscopy to correlate the ESMS results with previous reports. The reaction was monitored in CH_2Cl_2 through analysis of the carbonyl stretching-frequency region (2200-1600 cm^{-1}). A comparison of the reported IR spectra of various Ge/Co clusters is presented in Table 4.1.

Table 4.1 – A comparison of IR data (ν_{CO}, CH_2Cl_2) for Ge/Co clusters

$Ge[Co_2(CO)_7]_2$ [26]	$[Co_5Ge(CO)_{16}]^-$ [41]	$[Co_7Ge(CO)_{20}]^-$ [37]	$[Co_7Ge_2(CO)_{21}]^-$ [37]	$[Co_{10}Ge_2(CO)_{24}]^{2-}$
2079 (s)	2078 (w)			
2061 (vs)	2053 (m)	2054 (s)	2065 (m)	2066 (m,sh)
2040 (m)				
2032 (m)		2033 (s)		
2023 (w)	2025 (vs)	2028 (s)	2027 (vs)	2028 (vs)
2005 (w)	2004 (sh)		2004 (w)	2007 (m,sh)
	1970 (w)	1990 (w)		
1848 (w)	1825 (w)	1825 (m,br)		1730 (w,br)

Initial IR spectra of the reaction solution displayed signals corresponding to μ_4-$Ge[Co_2(CO)_7]_2$ [2081 (s), 2063 (s) cm^{-1}], with a 1888 cm^{-1} signal observed after addition of $[Co(CO)_4]^-$. The latter band was apparent throughout the reaction, in agreement with the detection of $[Co(CO)_4]^-$ throughout the experiment by ESMS. Signals associated with the μ_2-CO ligands were not often observed because of the weak absorbance of these bands and the strength of the $[Co(CO)_4]^-$ signal.

The carbonyl signals shifted to lower wavenumber during reaction, as expected for the formation of anionic cluster products. This was first noted approximately 20 minutes after addition with the decline of the parent signals and appearance of bands at 2043 and 2023 cm^{-1}. The first of these signals is indicative of $(CO)_4CoGeCo_3(CO)_9$ while the latter had previously been assigned to $[Co_5Ge(CO)_{16}]^-$. ESMS analysis of the solution did not indicate the presence of this anion, rather the spectra were dominated by the $[Co_7Ge(CO)_{20}]^-$ signal. This cluster has a very similar IR profile to $[Co_5Ge(CO)_{16}]^-$

(especially in regards to the strong signal around 2030 cm^{-1} used to monitor the reaction) and distinguishing between the two clusters by IR would be difficult.

After 2 hours, ES mass spectra indicated the predominant anion in solution was $[Co_7Ge_2(CO)_{21}]^-$, an assignment confirmed by IR spectra which were dominated by a signal at 2027 cm^{-1}, with weaker absorbances apparent at 2067 and 2006 cm^{-1}. The IR spectra of $[Co_7Ge(CO)_{20}]^-$ and $[Co_7Ge_2(CO)_{21}]^-$ were similar since the 2025 cm^{-1} signal was broad, and distinguishing between these clusters purely on IR evidence is difficult. In contrast, the ESMS signals of the two clusters were well separated and the clusters were readily distinguished.

After 6-7 hours at reflux, the signal attributed to $[Co_{10}Ge_2(CO)_{24}]^{2-}$ dominated the ES mass spectrum while IR spectra acquired at this time (Figure 4.14) were almost indistinguishable from those acquired for $[Co_7Ge_2(CO)_{21}]^-$. The dominant absorbance occurred at 2028 cm^{-1}, with a moderately intense shoulder at 2007 cm^{-1} and a broad absorbance at 1730 cm^{-1} (assigned to the bridging carbonyl ligands) was only apparent for concentrated solutions.

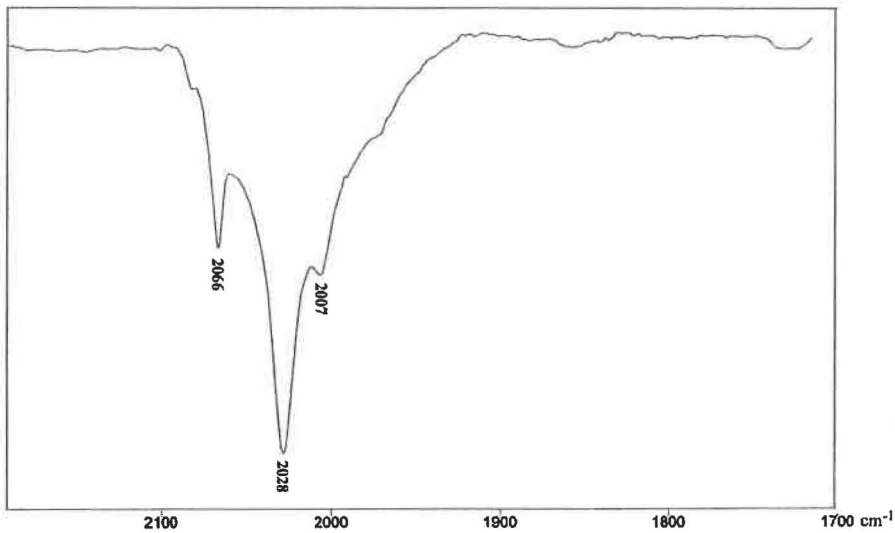

Figure 4.14 – The IR spectrum (ν_{CO}, CH_2Cl_2) of $[Co_{10}Ge_2(CO)_{24}]^{2-}$.

The high degree of similarity between the IR spectra of $[Co_7Ge_2(CO)_{21}]^-$ and $[Co_{10}Ge_2(CO)_{24}]^{2-}$ provides an explanation why the $[Co_{10}Ge_2(CO)_{24}]^{2-}$ cluster was not identified previously. As discussed above, cluster reactions were traditionally monitored by IR spectroscopy and refluxing the solution for 6 hours produced no significant changes in the IR spectra. This allows the assumption that no further compositional

changes were taking place, an assumption obviously incorrect from the ESMS results. The similarity between the IR spectra of different cluster species has been noted previously (discussed in Section 1.2.4.1) and the utility of IR spectroscopy in monitoring cluster reactions is questionable.

4.4.3 Crystal Structure Determination of $[NEt_4]_2[Co_{10}Ge_2(CO)_{24}]$

Crystals of the title compound were grown from a liquid/liquid diffusion of Et_2O into a CH_2Cl_2 solution at –20°C. The asymmetric unit contained one full cation and anion, two half cations, 1.5 molecules of CH_2Cl_2 and 0.5 molecules of Et_2O. The cations and solvent were disordered but the anion solved and refined without difficulty.

The full structure and core geometry of the $[Co_{10}Ge_2(CO)_{24}]^{2-}$ anion are displayed in Figures 4.15 and 4.16 respectively, with a stereo view of the core shown in Figure 4.17. Selected bond lengths are provided in Table 4.2 while full lists of atomic coordinates, temperature factors and bond parameters are supplied in Appendix A. Data relating to the structure solution are provided in the experimental section.

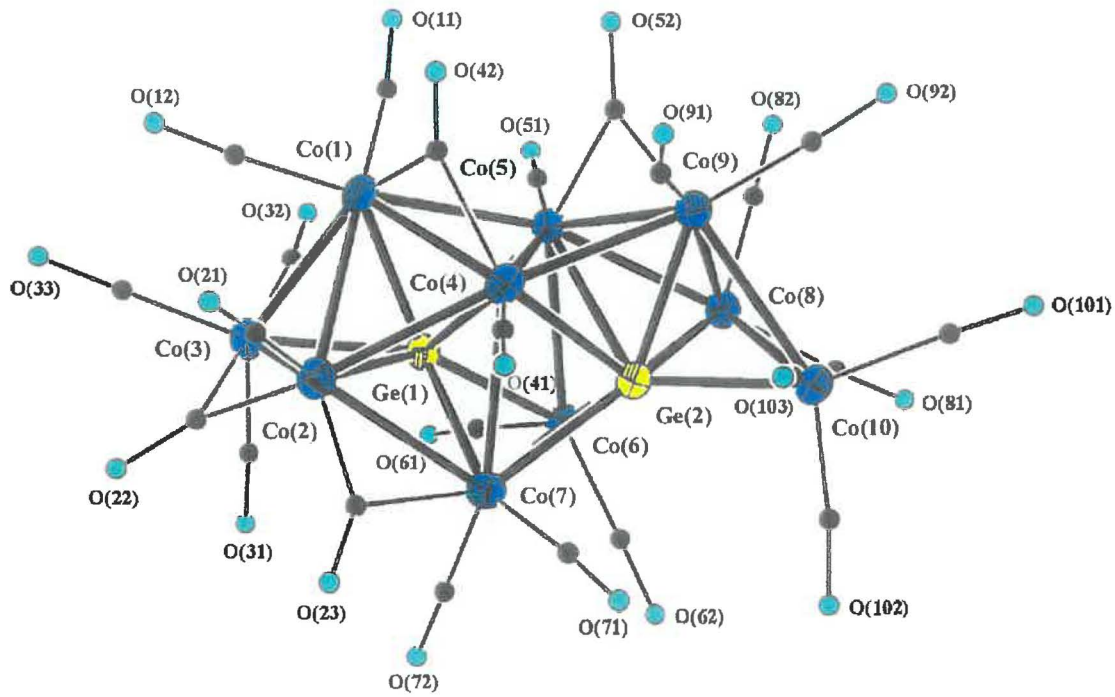

Figure 4.15 – A labelled diagram of the $[Co_{10}Ge_2(CO)_{24}]^{2-}$ anion. Ellipsoids of the cobalt and germanium atoms are drawn at the 50% probability level while the carbon and oxygen atoms are presented as arbitrary spheres to aid clarity.

Table 4.2 – Selected bond lengths (Å) for $[NEt_4]_2[Co_{10}Ge_2(CO)_{24}]$

Ge(1)-Co(1)	2.3940(12)	Ge(2)-Co(4)	2.4055(13)
Ge(1)-Co(2)	2.3662(13)	Ge(2)-Co(5)	2.6230(12)
Ge(1)-Co(3)	2.3890(12)	Ge(2)-Co(6)	2.4026(13)
Ge(1)-Co(4)	2.6107(13)	Ge(2)-Co(7)	2.3990(13)
Ge(1)-Co(5)	2.3643(12)	Ge(2)-Co(8)	2.3765(13)
Ge(1)-Co(6)	2.3951(12)	Ge(2)-Co(9)	2.3939(13)
Ge(1)-Co(7)	2.3971(13)	Ge(2)-Co(10)	2.3463(13)
Co-Co_{core}	2.6499-2.8526	Co-Co_{cap}	2.5477-2.8050
Co-$C_{terminal\ (av)}$	1.779	C-$O_{terminal\ (av)}$	1.137
Co-$C_{bridging\ (av)}$	1.918	C-$O_{bridging\ (av)}$	1.170
Co-$C_{semi\text{-}bridging\ (av)}$	1.767	C-$O_{semi\text{-}bridging\ (av)}$	1.162

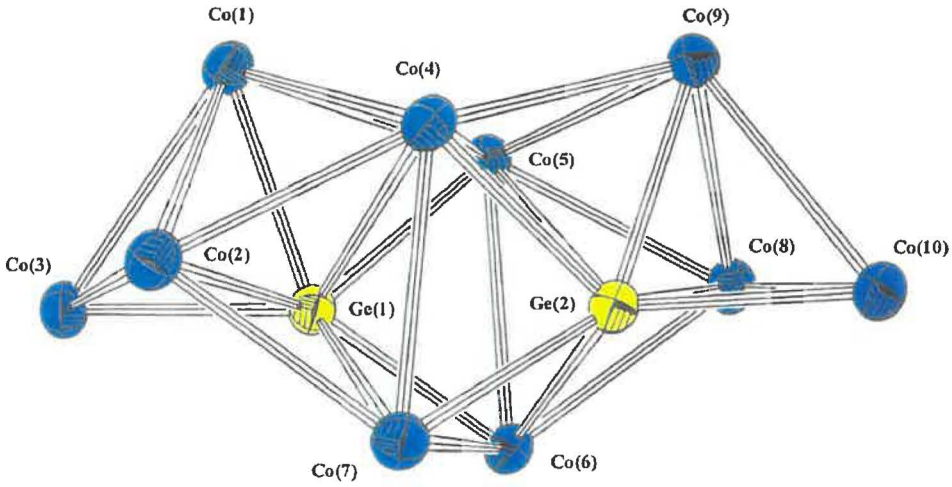

Figure 4.16 – The core geometry of the $[Co_{10}Ge_2(CO)_{24}]^{2-}$ anion.

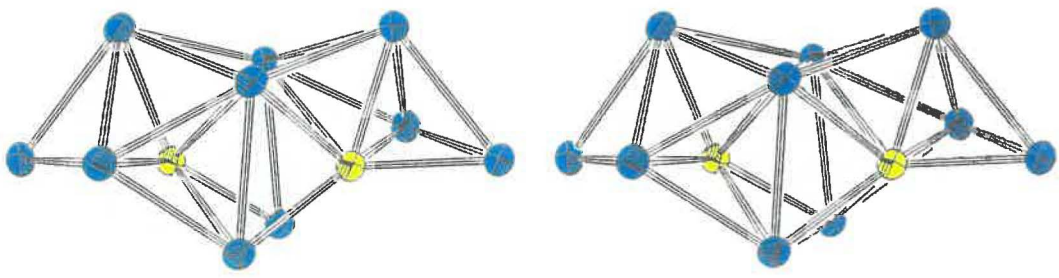

Figure 4.17 – A stereo view of the $[Co_{10}Ge_2(CO)_{24}]^{2-}$ core geometry.

The anion appears to contain C_2 symmetry through a central axis [the mid-points of the Co(4)-Co(5) and Co(6)-Co(7) bonds], though slight changes in ligand orientations and the arrangement of the cations and solvent associated with the structure break this symmetry. There are 18 Co-Co bonds present, ranging from 2.548-2.853 Å, which are of a similar magnitude to those reported for the other germanium/cobalt clusters (presented in Table 4.3).

There are three different ligand environments within the anion. A terminal orientation is displayed by sixteen carbonyl ligands, four adopt bridging positions, and four semi-bridging. The bridging ligands [CO(23), CO(42), CO(52) and CO(63)] are associated with the Co(2)-Co(7), Co(1)-Co(4), Co(5)-Co(9) and Co(6)-Co(8) bonds, all of which are involved in capping the core Ge_2Co_4 octahedron. The four semi-bridging ligands [CO(11), CO(22), CO(81), and CO(91)] are characterised by bond lengths and angles intermediate between the terminal and fully-bridging environments.

Of most interest with this structure is the arrangement of the cluster core. The two germanium atoms each form six short Ge-Co bonds (2.346-2.406 Å) and one longer contact [Ge(1)-Co(4) 2.611 Å, Ge(2)-Co(5) 2.623 Å]. The arrangement is such that one face on each germanium atom is remarkably open with the positions of the germanium atoms classified as semi-interstitial.

There are few reports of semi-encapsulated main group atoms in cluster compounds. The majority of mixed main group/transition metal clusters incorporate first row elements of small atomic size, which allows full encapsulation of the atoms. The use of larger atoms precludes encapsulation, forcing the main group atom to adopt a semi-interstitial position (though clusters containing encapsulated germanium and tin atoms are known, as discussed in Section 4.1.2). A semi-encapsulated main group element is reported for [$Co_6P(CO)_{16}$]$^-$ (Figure 4.18a), with the phosphorus atom enclosed within an irregular arrangement of cobalt atoms[50]. In comparison, the cobalt atoms in [$Co_{10}Ge_2(CO)_{24}$]$^{2-}$ (Figure 4.18b) appear arranged in a more regular "boat" formation about the germanium. The semi-encapsulated positions of the main group elements in

[50] P. Chini, G. Ciani, S. Martinengo and A. Sironi, *J. Chem. Soc., Chem. Commun.*, 1979, 188; G. Ciani and A. Sironi, *J. Organomet. Chem.*, 1983, **241**, 385.

$[Co_{10}Ge_2(CO)_{24}]^{2-}$ and $[Co_6P(CO)_{16}]^-$ indicate the clusters may display unusual reactivity (discussed in Section 4.5).

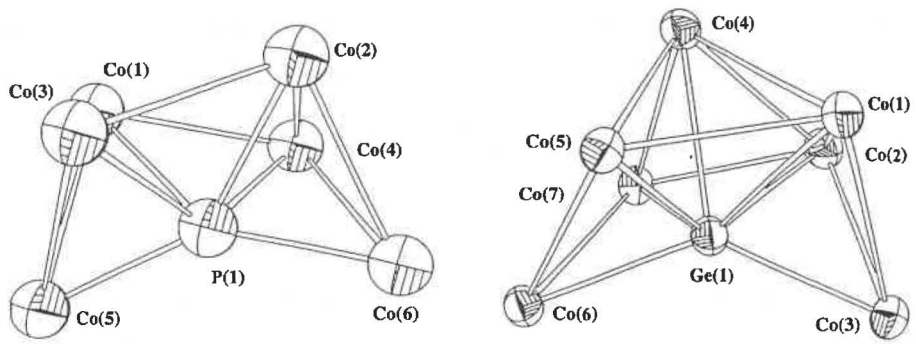

(a) (b)

Figure 4.18 – A comparison of the semi-encapsulated main group atoms in $[Co_6P(CO)_{16}]^-$ (a) and $[Co_{10}Ge_2(CO)_{24}]^{2-}$ (b). The Ge(2), Co(10), Co(9) and Co(8) atoms of the $[Co_{10}Ge_2(CO)_{24}]^{2-}$ core have been omitted to clarify the arrangement about Ge(1).

Table 4.3 – A comparison of selected bond lengths (Å) for Ge/Co clusters

	$[Co_5Ge(CO)_{16}]^-$ [41]	$[Co_7Ge(CO)_{20}]^-$ [37]	$[Co_7Ge_2(CO)_{21}]^-$ [37]	$[Co_{10}Ge_2(CO)_{24}]^{2-}$
Ge-Co	2.33-2.51 Ge-Co (Co_3) 2.43-2.48 Ge-Co (Co_2)	2.31-2.36 Ge-Co (Co_3) 2.27 Ge-Co (Co_4)	2.31-2.33 Ge-Co (Co_3) 2.28-2.29 Ge-Co_{bridge}	2.35–2.41 (short) 2.61-2.62 (long)
Co-Co	2.51-2.55	2.25-2.60	2.59-2.61	2.55-2.85
Co-C	1.54-2.03 (terminal) 1.63-2.04 (bridging)	Unavailable because of disorder	1.74-1.82 (terminal)	1.75-1.82 (terminal) 1.84-2.00 (bridging)

There are various possible descriptions of the core geometry of $[Co_{10}Ge_2(CO)_{24}]^{2-}$. The favoured view is based upon an octahedral Ge_2Co_4 core that is capped on four faces (in a symmetrical manner) with two of these new faces subsequently capped (effectively generating a bicapped-tetracapped-octahedron). From an electron-counting perspective, the cluster contains 148 valence-electrons (assuming 4 electrons per germanium atom despite their semi-interstitial appearance). This yields 12 SEP (assuming the germanium

atoms act as vertices) and a mono-capped 11 vertex structure is predicted from PSEP theory. A structure like this is clearly not evident. Alternatively, considering the germanium atoms purely as interstitial, the cluster possesses 14 SEP for a 10 vertex structure which predicts a *hypho*-icosahedron arrangement, a geometry not readily apparent. An alternate view of the cluster core arrangement (and one that fits well with the pathway outlined below) is that it is composed of two Co_3Ge units capping a central Co_4 plane.

The structure observed for $[Co_{10}Ge_2(CO)_{24}]^{2-}$ has no precedent among E_2M_{10} clusters. The majority of these clusters contain first row elements (C, N) of limited atomic size, allowing the main group atoms to adopt interstitial positions. Examples include the 138 electron $[Ru_{10}C_2(CO)_{24}]^{2-}$ cluster (composed of two C-centred octahedra linked through a common M-M bond[16]), the 142 electron $[Co_{10}N_2(CO)_{19}]^{4-}$ (with a linked trigonal prismatic arrangement[51] - refer to Figure 6.1a) and the 142 electron $[Ni_{10}C_2(CO)_{16}]^{2-}$ (two capped trigonal prisms linked through a common M_4 face[52]). The only $M_{10}E_2$ cluster reported with heavier main group elements is $Os_{10}S_2(CO)_{23}$ (134 valence-electrons), though in this structure the sulfur atoms are attached to the surface of the metal cluster rather than in encapsulated or semi-encapsulated positions.[53]

4.4.4 Predicted Reaction Pathway

Prior to this investigation, three anionic germanium cobalt clusters had been identified from the reaction between μ_4-Ge[$Co_2(CO)_7$]$_2$ and [$Co(CO)_4$]$^-$ but the relationship between these clusters was unknown. ESMS monitoring of the reaction allowed the sequence of products to be established, which allowed inference about the pathway of the reaction and key intermediate species.

The pathway presented (Scheme 4.1) accounts for the various clusters produced with regards both their composition and structure. The pathway is based around a

[51] A. Fumagalli, S. Martinengo, M. Tasselli, G. Ciani, P. Macchi and A. Sironi, *Inorg. Chem.*, 1998, **37**, 2826.

[52] A. Ceriotti, G. Longoni, M. Manassero, N. Masciocchi, L. Resconi and M. Sansoni, *J. Chem. Soc., Chem. Commun.*, 1985, 181.

[53] J.P. Attard, B.F.G. Johnson, J. Lewis, J.M. Mace, M. McPartlin and A. Sironi, *J. Chem. Soc., Chem. Commun.*, 1984, 595.

[$GeCo_3(CO)_9$]$^-$ intermediate which, though novel, is isoelectronic to the known $AsCo_3(CO)_9$ [54] and $BiCo_3(CO)_9$ [55] compounds. The [$GeCo_3(CO)_9$]$^-$ species was not directly detected in the ESMS investigation but through analogy to $AsCo_3(CO)_9$ is expected to be a reactive Lewis base, especially towards displacement of carbonyl ligands.

The initial step in the reaction sequence is the generation of [$Co_5Ge(CO)_{16}$]$^-$ from either μ_4-$Ge[Co_2(CO)_7]_2$ or $(CO)_4CoGeCo_3(CO)_9$ {produced thermally from μ_4-$Ge[Co_2(CO)_7]_2$}. Loss of "$Co_2(CO)_7$" from [$Co_5Ge(CO)_{16}$]$^-$ [presumably *via* formation of $Co_4(CO)_{12}$] provides a possible route to the [$GeCo_3(CO)_9$]$^-$ species, which can subsequently react with a range of clusters present. A simple ligand displacement reaction with $Co_4(CO)_{12}$ would produce the [$Co_7Ge(CO)_{20}$]$^-$ cluster and account for the odd structure reported. The arsenic analogue of this cluster, $Co_7As(CO)_{20}$, has been reported, though without direct evidence for reaction between $AsCo_3(CO)_9$ and $Co_4(CO)_{12}$ [56]. A similar ligand displacement reaction with $(CO)_4CoGeCo_3(CO)_9$ would produce the [$Co_7Ge_2(CO)_{21}$]$^-$ cluster, with two $GeCo_3$ tetrahedra linked through a common $Co(CO)_3$ unit. The [$Co_7Ge(CO)_{20}$]$^-$ cluster could undergo further addition by [$GeCo_3(CO)_9$]$^-$ which, with re-arrangement and CO loss, would produce the [$Co_{10}Ge_2(CO)_{24}$]$^{2-}$ cluster. Synthesis in this manner accounts for the 10:2 Co:Ge ratio and for the core geometry of the [$Co_{10}Ge_2(CO)_{24}$]$^{2-}$ cluster (with two $GeCo_3$ units capping a Co_4 plane).

---

[54] A. Vizi-Orosz, V. Galamb, G. Pályi, L. Markó, G. Bor and G. Natile, *J. Organomet. Chem.*, 1976, **107**, 235.

[55] K.H. Whitmire, J.S. Leigh and M.E. Gross, *J. Chem. Soc., Chem. Commun.*, 1987, 926.

[56] H. Lang, G. Huttner, B. Sigwarth, I. Jibril, L. Zsolnai and O. Orama, *J. Organomet. Chem.*, 1986, **304**, 137.

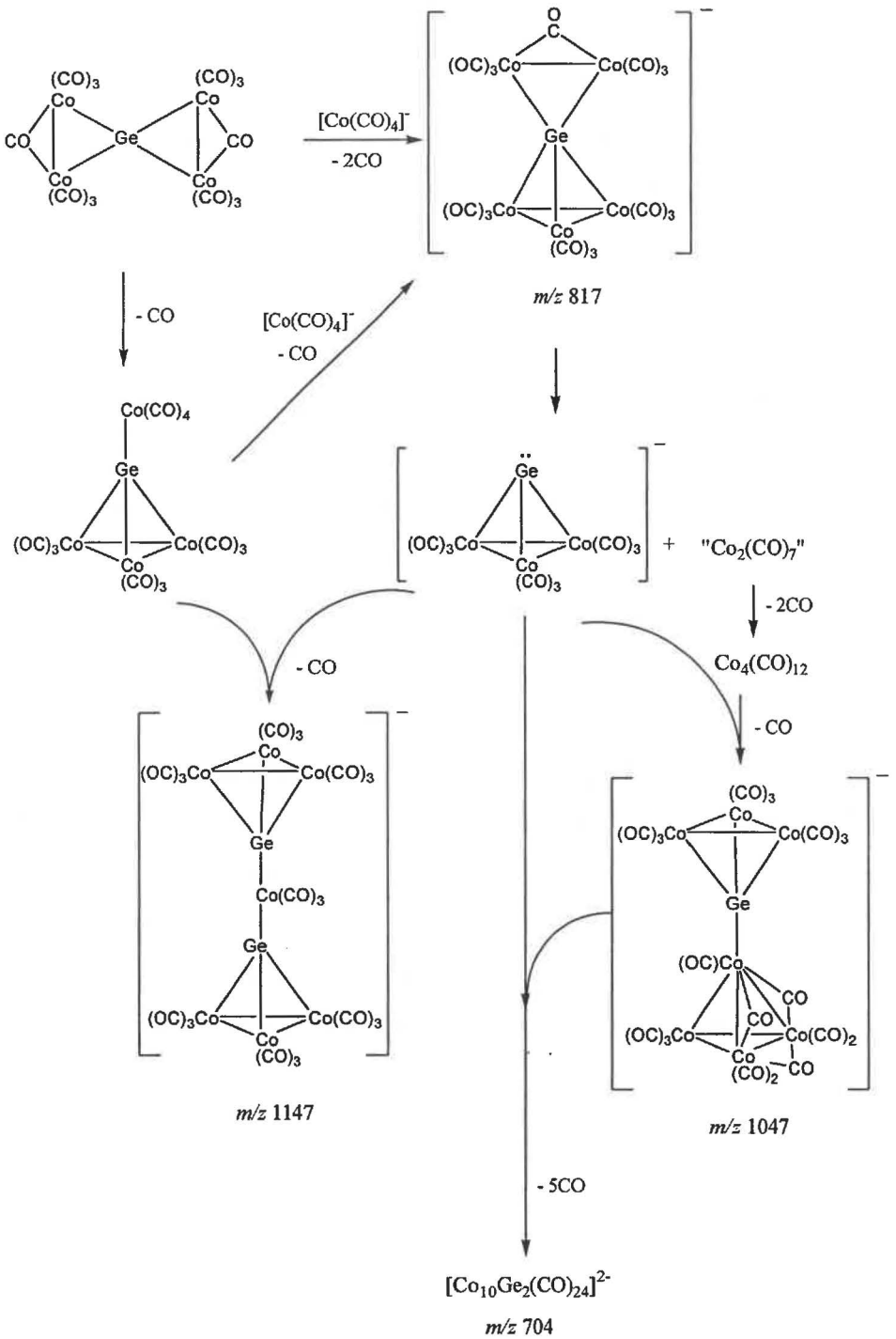

Scheme 4.1 – The predicted pathway for the reaction between μ_4-Ge[$Co_2(CO)_7$]$_2$ and [$Co(CO)_4$]$^-$ The species assigned *m/z* values were directly detected by ESMS.

4.4.5 Reaction of [$Co_7Ge(CO)_{20}$]$^-$/[$Co_7Ge_2(CO)_{21}$]$^-$ with Phosphines

Additional evidence for the pathway presented above was provided by the reaction of phosphines with an equimolar solution of [$Co_7Ge(CO)_{20}$]$^-$ and [$Co_7Ge_2(CO)_{21}$]$^-$ (as determined by approximately equally intense ESMS signals). When stirred at room

temperature, a reaction ensued generating the $[Co_{10}Ge_2(CO)_{24}]^{2-}$ cluster. This differed significantly from the 3-4 hours at reflux previously required to generate $[Co_{10}Ge_2(CO)_{24}]^{2-}$ from $[Co_7Ge(CO)_{20}]^-$ and $[Co_7Ge_2(CO)_{21}]^-$. The effect was initially noted with PPh_3 but equivalent use of 1,3,5-triaza-7-phosphaadamantane (PTA) or tris(2-carboxyethyl)phosphine (TCEP) produced similar results.

The production of $[Co_{10}Ge_2(CO)_{24}]^{2-}$ is presumably initiated by nucleophilic attack by the phosphine on the central cobalt of $[Co_7Ge_2(CO)_{21}]^-$, producing a $Ph_3P(CO)_3CoGeCo_3(CO)_9$ species and generating the $[GeCo_3(CO)_9]^-$ anion (Scheme 4.2). The anion could subsequently react with $[Co_7Ge(CO)_{20}]^-$ (in a similar manner to that discussed in the previous section) to generate $[Co_{10}Ge_2(CO)_{24}]^{2-}$.

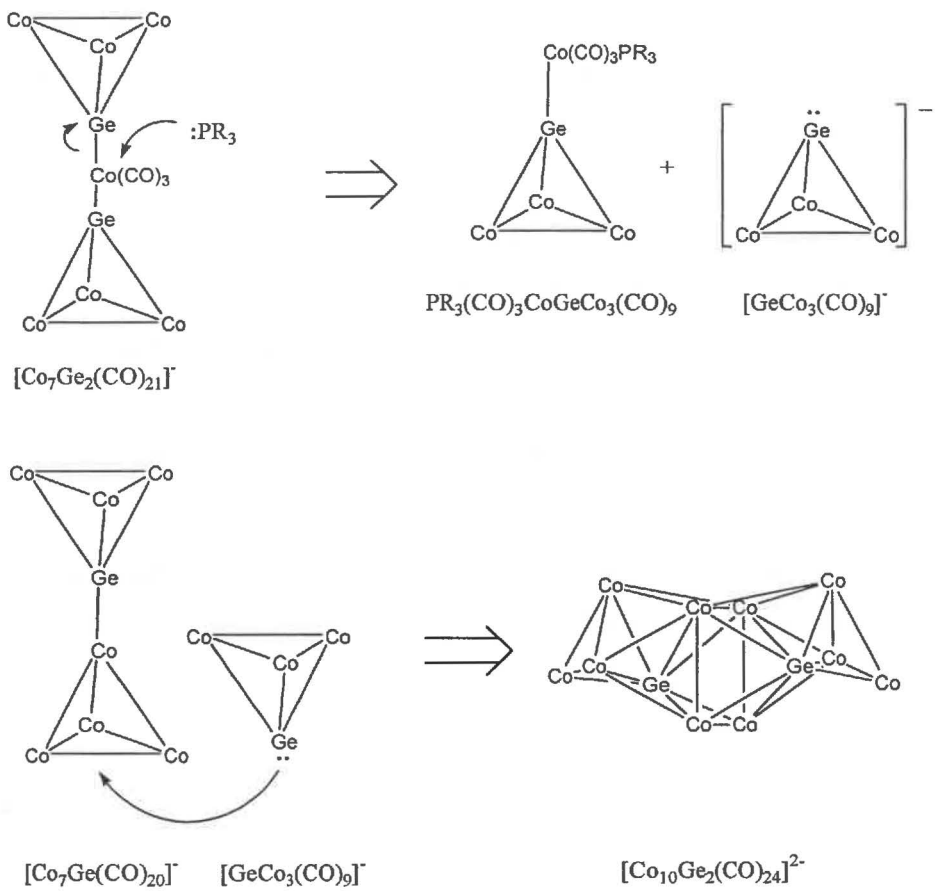

Scheme 4.2 – The effect of PR_3 on formation of $[Co_{10}Ge_2(CO)_{24}]^{2-}$.

Confirming the presence of $Ph_3P(CO)_3CoGeCo_3(CO)_9$ was difficult. The cluster is neutral and thus 'electrospray-invisible', though expected to be detectable by IR analysis. However, spectra acquired throughout the reaction were dominated by signals at 2030 and 2000 cm^{-1} (indicative of the anionic clusters) though a very weak signal was

detected at slightly higher wavenumber (2040 cm^{-1}), tentatively assigned to a $R(CO)_3CoGeCo_3(CO)_9$ species. In retrospect, use of an 'electrospray-friendly' phosphine [e.g. $P(C_6H_4OMe)_3$ as discussed in Section 1.3.5] may have provided more conclusive evidence for the $R_3P(CO)_3CoGeCo_3(CO)_9$ cluster.

4.5 Reactions of $[Co_{10}Ge_2(CO)_{24}]^{2-}$

4.5.1 Introduction

Following identification and isolation of the novel $[Co_{10}Ge_2(CO)_{24}]^{2-}$ cluster, reactions of this compound were of interest. The cluster displays a remarkably open geometry about the germanium atoms, making them likely targets for capping reagents. A number of Co_3 faces are also present in the structure that could potentially be capped. Ligand substitution reactions were also examined, though substitution appears rare for large anionic clusters[57].

The capping ability of cationic gold phosphine fragments is well reported[58]. In this study, the 'electrospray-friendly' reagent $MeOC_6H_4P(Ph)_2AuCl$ (henceforth referred to as P*AuCl) was employed since any neutral products would be identifiable by ESMS (through protonation of the basic methoxy substituent). The reaction was carried out both in the presence and absence of Tl[PF_6] as a halide-abstracting agent.

The ability of isonitrile compounds to substitute for carbonyl ligands in clusters has precedent in the literature, though reports appear limited to neutral compounds rather

[57] The majority of reports are associated with neutral $M_3(CO)_{12}$ compounds though one recent publication reports mono-substitution by phosphines on $[HIr_4(CO)_{11}]^-$ A. Fumagalli, M.C. Malatesta, A. Tentori, D. Monti, P. Macchi and A. Sironi, *Inorg. Chem.*, 2002, **41**, 76.

[58] Recent examples include M.I. Bruce, B.W. Skelton, A.H. White and N.N. Zaitseva, *J. Chem. Soc., Dalton Trans.*, 2000, 881; A.D. Hattersley, C.E. Housecroft and A.L. Rheingold, *J. Cluster Sci.*, 1997, **8**, 329; A.J. Amoroso, B.F.G. Johnson, J. Lewis, C-K. Li, C.A. Morewood, P.R. Raithby, M.D. Vargas and W-T. Wong, *J. Cluster Sci.*, 1995, **6**, 163.

than anionic clusters[59]. ESMS provides a unique method of monitoring these reactions since substitution should result in a series of signals of characteristic mass separation.

4.5.2 Results and Discussion

Treatment of $[Co_{10}Ge_2(CO)_{24}]^{2-}$ with P*AuCl failed to produce the capped cluster intended. ES mass spectra acquired in negative-ion mode were dominated by the *m/z* 704 signal attributable to the parent cluster while positive-ion spectra were dominated by a signal at *m/z* 781 corresponding to $[P^*_2Au]^+$. Although generation of a cationic gold fragment was noted, there was no evidence for the formation of any capped germanium/cobalt clusters.

The reaction of $[Co_{10}Ge_2(CO)_{24}]^{2-}$ with ^{t}BuNC was carried out in CH_2Cl_2 and monitored by ESMS over a 2 hour period. The intensity of the $[Co_{10}Ge_2(CO)_{24}]^{2-}$ signal decreased markedly, matched by an increase in the intensity of the *m/z* 171 signal corresponding to $[Co(CO)_4]^-$. The reaction solution also altered colour over this period from deep black to pale yellow, indicating decomposition of the parent cluster.

Literature examples of isonitrile ligand substitution reactions appear restricted to neutral clusters (discussed in detail in Chapter 7). Electrochemical studies of the substituted products indicate a higher susceptibility to oxidation, presumably a factor of the weaker π-acceptor character of isonitriles (compared to carbonyl). This character serves to increase the electron-density localised on the cluster, a situation unfavoured by anionic clusters providing an explanation for the absence of substitution products and the decomposition of the sample.

[59] Recent examples include S.M. Waterman, M.G. Humphrey and D.C.R. Hockless, *J. Organomet. Chem.*, 1999, **579**, 75; C.J. Adams, M.I. Bruce, B.W. Skelton and A.H. White, *J. Organomet. Chem.*, 1998, **561**, 97; D.M. Curtis and O.J. Curnow, *Organometallics*, 1994, **13**, 2489.

4.6 Reaction of μ_4-Si[$Co_2(CO)_7$]$_2$ with [$Co(CO)_4$]$^-$

4.6.1 Introduction

The reaction between μ_4-Si[$Co_2(CO)_7$]$_2$ and [$Co(CO)_4$]$^-$ has produced significantly fewer isolated clusters than the analogous germanium reaction. To date, the only clusters identified from this system are the starting compound {μ_4-Si[$Co_2(CO)_7$]$_2$}, the neutral $(CO)_4CoSiCo_3(CO)_9$ cluster (formed from thermal decarbonylation of the starting compound), and the unlikely [$Co_9Si(CO)_{21}$]$^{2-}$ cluster. The [$Co_9Si(CO)_{21}$]$^{2-}$ cluster is the most interesting of these, with the silicon adopting an interstitial position within a capped square anti-prism (the only example of an eight coordinate silicon atom)[39]. The absence of isolated clusters from this reaction indicated it was worthy of further examination, while the structure of [$Co_9Si(CO)_{21}$]$^{2-}$ implied that the system was likely to differ significantly from the analogous germanium reaction.

4.6.2 Results and Discussion

The reaction between μ_4-Si[$Co_2(CO)_7$]$_2$ and [$Co(CO)_4$]$^-$ was initially performed in CH_2Cl_2, though subsequent reactions in Et_2O indicated the same initial products without evidence for formation of the Co_9Si clusters.

Within 15-20 minutes of reflux in CH_2Cl_2, a signal attributed to [$Co_5Si(CO)_{16}$]$^-$ (*m/z* 771) was detected (Figure 4.19). This cluster, while novel, was not unexpected since the germanium analogue has been isolated and characterised. Further reaction (1-1.5 hours) led to detection of signal at *m/z* 1029, assignable as either [$Co_7Si(CO)_{21}$]$^-$ or [$Co_7Si_2(CO)_{20}$]$^-$, neither of which have been identified previously or possess a germanium analogue. ES mass spectra after extended reaction (3-4 hours) displayed signals at *m/z* 573.5 and 1175 corresponding to [$Co_9Si(CO)_{21}$]$^{2-}$ and [$Co_9Si(CO)_{22}$]$^-$ respectively, with [$Co_9Si(CO)_{21}$]$^{2-}$ becoming the dominant ion in the solution after 7-8 hours. An additional signal at *m/z* 1147 attributed to [$Co_9Si(CO)_{21}$]$^-$ (the oxidised form of the previously reported Co_9Si cluster) was detected but was never of significant intensity.

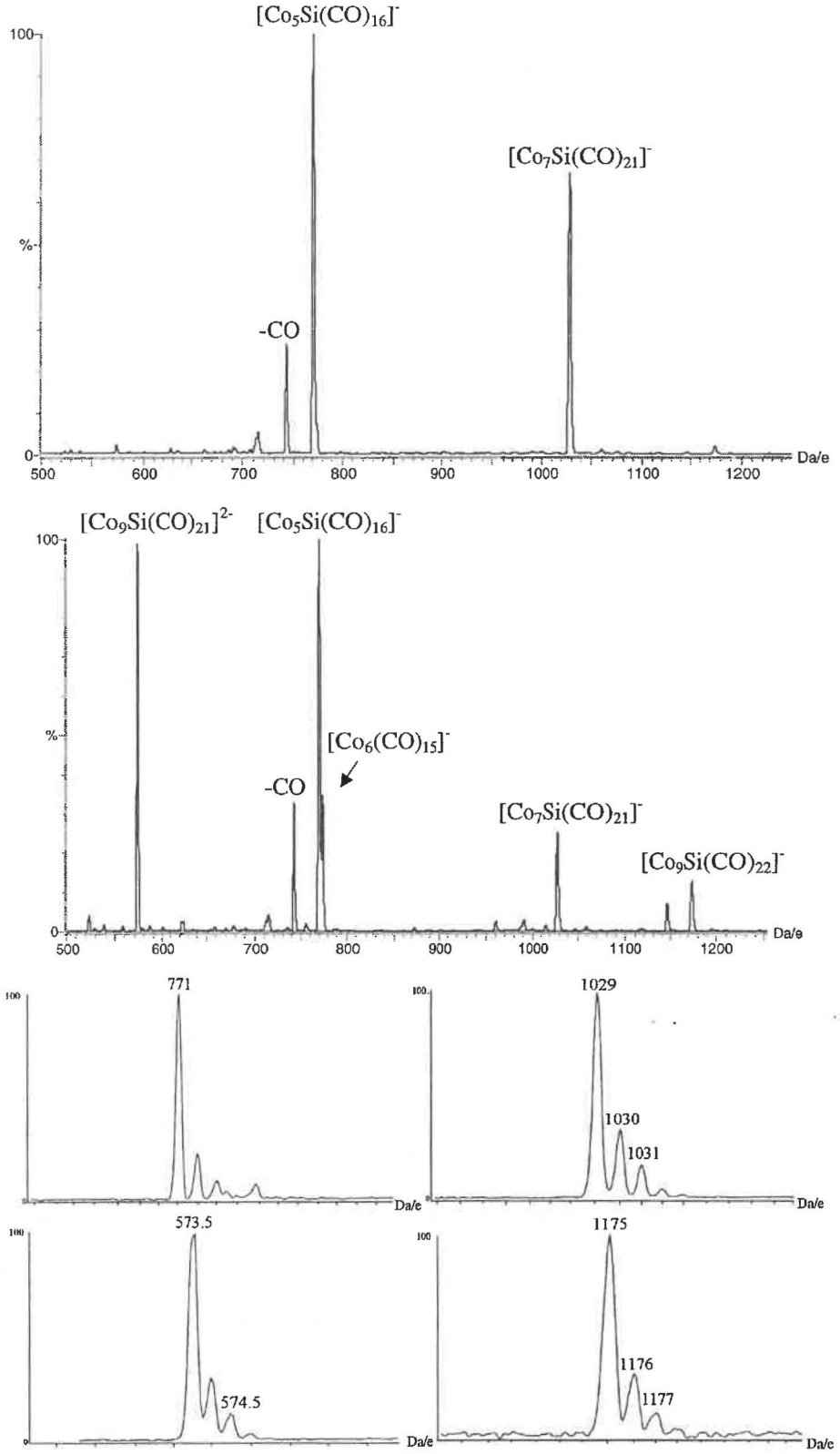

Figure 4.19 – The ES mass spectra (-ve ion, 5 cV) of the reaction between μ_4-Si[$Co_2(CO)_7$]$_2$ and [$Co(CO)_4$]$^-$ in CH_2Cl_2 after 2 hours (upper) and 6 hours (lower), with isotope patterns (clockwise from top left) for [$Co_5Si(CO)_{16}$]$^-$, [$Co_7Si(CO)_{21}$]$^-$, [$Co_9Si(CO)_{22}$]$^-$ and [$Co_9Si(CO)_{21}$]$^{2-}$

After 3-4 hours at reflux, an additional signal corresponding to $[Co_6(CO)_{15}]^-$ (*m/z* 774) was noted. The $[Co_6(CO)_{15}]^-$ signal was attributed to the presence of $[Co_6(CO)_{15}]^{2-}$ in the solution (a known by-product of the reaction, especially at elevated temperatures[60]), with the cluster undergoing oxidation within the spectrometer prior to detection. The assignment was confirmed by the detection of an identical signal (with an identical isotope pattern) in the synthesis of $[Co_6N(CO)_{15}]^-$ (presented in Chapter 6). Other reported by-products of this reaction {$[Co_8C(CO)_{18}]^{2-}$ (expected *m/z* 494, or 988 for $[M]^-$) and $[Co_7Si(CO)_{21}Cl_2]^-$ (*m/z* 1099)[61]} were not identified in this research. The absence of these anions indicates that the clusters produced are sensitive to reaction conditions, though throughout this ESMS investigation the series of products $[Co_5Si(CO)_{16}]^-$, $[Co_7Si(CO)_{21}]^-$, $[Co_9Si(CO)_{21}]^{2-}$, $[Co_9Si(CO)_{22}]^-$ and $[Co_6(CO)_{15}]^-$ were consistent across a series of reaction conditions.

The assignment of ions in this reaction was more difficult than for the analogous germanium reaction because of the mass (identical to that of CO) and isotopic uniformity of silicon. The assignment of $[Co_5Si(CO)_{16}]^-$ (*m/z* 771) was based on the previous detection and isolation of the germanium analogue. From a concentrated CH_2Cl_2 solution, crystals believed to be $[NEt_4][Co_5Si(CO)_{16}]$ were isolated but were of insufficient size or quality for structural analysis. The structure of $[Co_5Si(CO)_{16}]^-$ is presumably identical to that of $[Co_5Ge(CO)_{16}]^-$ but as the data for the germanium cluster were not of exceptional quality, a cleaner data set would have been useful.

The *m/z* 1029 ion can be assigned to either $[Co_7Si(CO)_{21}]^-$ or $[Co_7Si_2(CO)_{20}]^-$, neither of which have a germanium analogue. A comparison between expected and observed isotope patterns tentatively predicted the $[Co_7Si_2(CO)_{20}]^-$ assignment but a Co_5Si, Co_7Si_2, Co_9Si sequence of products is chemically unlikely. The assignment of this signal as $[Co_7Si(CO)_{21}]^-$ was based on a logical consideration of the underlying chemistry rather than purely on matching of isotope profiles. The structure of the $[Co_7Si(CO)_{21}]^-$ anion is unknown and attempts to grow crystals of suitable quality for crystallographic analysis were unsuccessful. The structure of the cluster cannot readily be predicted from electron-counting procedures as it possesses 110 valence electrons {intermediate between the 108 and 114 values calculated for $[Co_7Ge(CO)_{20}]^-$ and

[60] G.C. Barris, D.Phil. Thesis, University of Waikato, 1990.

[61] G.C. Barris, K.M. Mackay and B.K. Nicholson, *Acta Cryst. Sect. C*, 1992, **48**, 1204.

[$Co_7Ge_2(CO)_{21}$]$^-$ respectively}. The cluster is unlikely to contain an encapsulated silicon atom {as reported for [$Co_9Si(CO)_{21}$]$^{2-}$} and a more open geometry, less predictable from electron-counting rules, is expected. A range of possible structures for this anion were considered, often involving a Si-O-C arrangement {as observed in [$Co_7Si(CO)_{21}Cl_2$]$^-$ [61] and $Me_2NC_6H_4Si[OCCo_3(CO)_9]_2Co(CO)_4$ [62] - refer to Figure 7.21} but no sensible arrangement was uncovered.

The remaining two clusters identified in this reaction were the previously reported [$Co_9Si(CO)_{21}$]$^{2-}$ and the novel [$Co_9Si(CO)_{22}$]$^-$. The structures of these two clusters are more certain as the first has been structurally characterised and found as an electron-deficient capped square anti-prism. A number of attempts at reducing this cluster to generate the electron-precise [$Co_9Si(CO)_{21}$]$^{3-}$ cluster have been examined (discussed in Section 4.7.3). [$Co_9Si(CO)_{22}$]$^-$ corresponds to the electron-precise version of [$Co_9Si(CO)_{21}$]$^{2-}$, though the location of the additional carbonyl ligand within the structure is unknown. Crystals presumed to be [NEt_4][$Co_9Si(CO)_{22}$] were isolated but were of insufficient quality for a structure determination.

4.6.3 Infra–red Analysis

Infra-red examination of the reaction was performed in order to correlate this research with previous reports. Initial spectra were dominated by signals attributable to μ_4-Si[$Co_2(CO)_7$]$_2$, the most characteristic of which occurred at 2085 cm^{-1}. The intensity of this signal decreased with reaction, and the appearance of a broad absorbance at 2005 cm^{-1} was noted, with a shoulder around 1957 cm^{-1}. In addition, a strong signal at 1881 cm^{-1} corresponding to [$Co(CO)_4$]$^-$ was noted throughout. The spectra obtained during reaction were typically very broad, preventing discrimination between the different cluster species. The broad signals displayed and the similarity in spectra between different clusters are presumably why no other products have been identified from this reaction previously, and again demonstrates the advantages of ESMS over IR in analysis of cluster reactions.

[62] G.J. Harfoot, M.Sc. Thesis, University of Waikato, 2000.

4.7 Reactions of $[Co_9Si(CO)_{21}]^{2-}$

4.7.1 Introduction

The $[Co_9Si(CO)_{21}]^{2-}$ cluster is unusual in many respects. With regards to reactivity, the electron-deficient nature of the anion implies it should be susceptible to reduction. Electrochemical analysis by cyclic voltammetry indicated the cluster underwent a facile one-electron reduction but further oxidation or reduction resulted in decomposition of the sample[63]. The capped square anti-prism geometry also indicates that capping of the cluster should be possible, e.g. producing $[Co_{10}Si(CO)_{23}]^{2-}$, analogous to $[Co_{10}P(CO)_{22}]^{3-}$ (discussed in Section 6.3). Both reduction and capping reactions of the $[Co_9Si(CO)_{21}]^{2-}$ cluster were examined with various reagents.

4.7.2 Capping Reactions

Capping of the $[Co_9Si(CO)_{21}]^{2-}$ cluster was attempted using $(MeOC_6H_4)_3PAuCl$ (henceforth referred to as P***AuCl) and $Hg(OAc)_2$. The ability of cationic gold fragments to cap M_3 faces on clusters is well known[58] whereas Hg^{2+} usually inserts into M-M bonds, generating linear M-Hg-M units, though its bridging capability has been reported[64].

Treatment of $[Co_9Si(CO)_{21}]^{2-}$ with a 5 fold excess of P***AuCl in the presence of $Tl[PF_6]$ (as halide abstracting agent) was performed in CH_2Cl_2 and monitored by ESMS. Negative-ion spectra were dominated by the $[Co_9Si(CO)_{21}]^{2-}$ signal (*m/z* 573.5) with evidence for the presence of $[Co(CO)_4]^-$ (*m/z* 171), while positive-ion spectra were dominated by a signal from the cationic gold fragment, $[P^{***}{}_2Au]^+$ (*m/z* 901). The reaction was monitored over a 2 hour period without evidence for the formation of a capped cluster (predicted *m/z* 1696). Curiously, there was also no evidence for the formation of P***$AuCo(CO)_4$ (expected *m/z* 720) though such compounds are well known.

---

[63] G.C. Barris, M.Sc. Thesis, University of Waikato, 1986.

[64] e.g. R. Reina, O. Riba, O. Rossell, M. Seco, P. Gomez-Sal, A. Martin, D. de Montauzon and A. Mari, *Organometallics,* 1998, **17**, 4127.

The reaction between $[Co_9Si(CO)_{21}]^{2-}$ and $Hg(OAc)_2$ was performed in CH_2Cl_2 and monitored by ESMS. Upon dissolution of the mercury salt in the solution, the ES mass spectra changed substantially, with the appearance of an intense signal at *m/z* 715 corresponding to $[Hg\{Co(CO)_4\}_3]^-$ (Figure 4.20). Although $[Co(CO)_4]^-$ was initially present in the solution, the intensity observed for the mercury salt indicated decomposition of the $[Co_9Si(CO)_{21}]^{2-}$ cluster. The decomposition was also noted by a significant decrease in the intensity of the $[Co_9Si(CO)_{21}]^{2-}$ signal which was absent from the spectrum after 30 minutes.

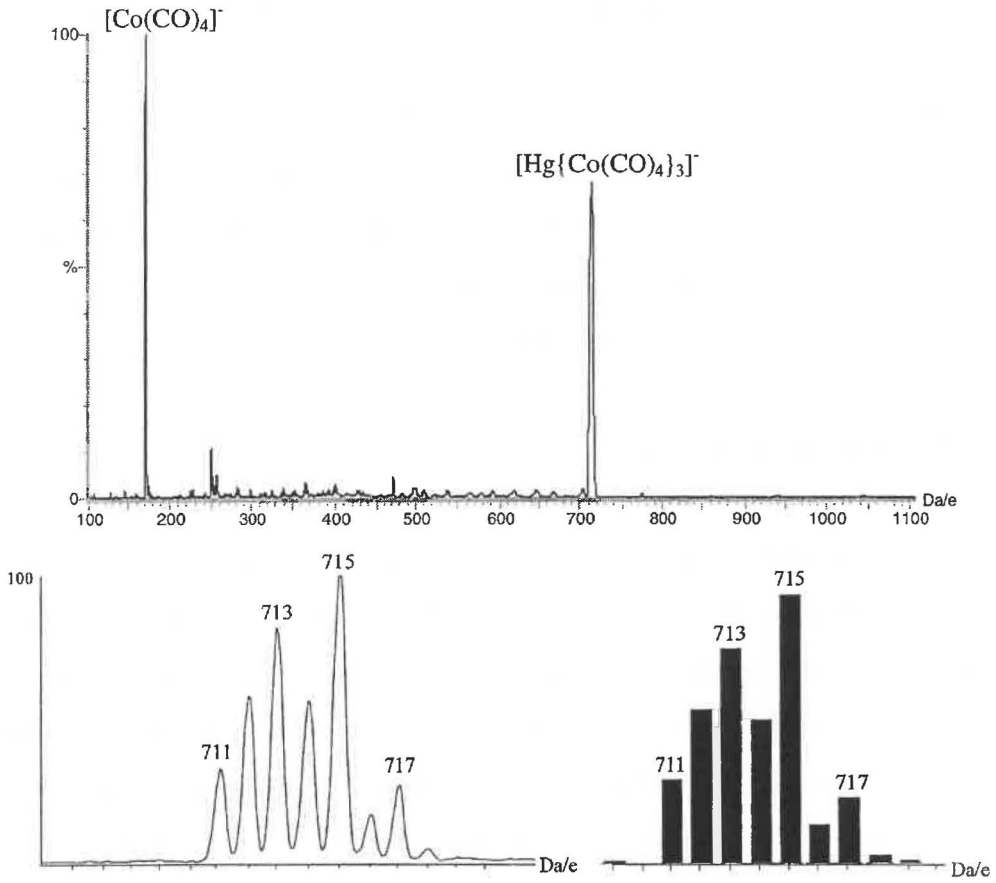

Figure 4.20 – The ES mass spectrum (-ve ion, 5 cV) of $[Hg\{Co(CO)_4\}_3]^-$ with observed and calculated isotope patterns.

4.7.3 Reduction Reactions

Reduction of $[Co_9Si(CO)_{21}]^{2-}$ was attempted by treatment of a CH_2Cl_2 solution of the cluster with zinc powder or $Co(\eta^5\text{-}C_5H_5)_2$, with changes in the composition of the solution monitored by ESMS. When an excess of zinc powder was added, a gradual decolourisation of the solution was apparent, matched by a decrease in the intensity of the $[Co_9Si(CO)_{21}]^{2-}$ signal and an increase in the $[Co(CO)_4]^-$ signal intensity. The

solution was monitored over a 2 hour period without evidence for the formation of a $[Co_9Si(CO)_{21}]^{3-}$ anion.

The reduction of $[Co_9Si(CO)_{21}]^{2-}$ was also attempted by addition of a stoichiometric amount of $Co(\eta^5\text{-}C_5H_5)_2$. Addition of 1 molar equivalent of $Co(\eta^5\text{-}C_5H_5)_2$ had little effect on the ES mass spectra, with the parent *m/z* 573.5 signal the only detectable ion. The solution was stirred for 20 minutes with no change noted. Excess $Co(\eta^5\text{-}C_5H_5)_2$ was added after this time, again with little effect though the intensity of the $[Co(CO)_4]^-$ signal increased over time. There was no evidence for formation of $[Co_9Si(CO)_{21}]^{3-}$.

The attempts at chemical reduction of $[Co_9Si(CO)_{21}]^{2-}$ were unsuccessful. In retrospect, ESMS was not the most appropriate technique for monitoring these reactions since electrochemical oxidation of highly-charged clusters during analysis has been noted. It is possible that the reduced species was formed in solution but oxidised to $[Co_9Si(CO)_{21}]^{2-}$ within the spectrometer prior to detection.

4.7.4 Effect of Carbon Monoxide

The identification of the electron-precise $[Co_9Si(CO)_{22}]^-$ cluster has implications for this research. The attempts at reduction of $[Co_9Si(CO)_{21}]^{2-}$ reported above were performed with the intention of forming an electron-precise $[Co_9Si(CO)_{21}]^{3-}$ species but there was no ESMS evidence for the generation of this cluster. The detection of $[SiCo_9(CO)_{22}]^-$ in the reaction between μ_4-$Si[Co_2(CO)_7]_2$ and $[Co(CO)_4]^-$ indicated that rather than reduction, a more effective route to an electron-precise cluster might be carbonyl addition. Thus it was that proposed that a solution of $[Co_9Si(CO)_{21}]^{2-}$ placed under a carbon monoxide atmosphere may generate an electron-precise cluster.

Stirring a CH_2Cl_2 solution of $[Co_9Si(CO)_{21}]^{2-}$ under a CO atmosphere for 3 hours had a significant effect on the composition of the solution. ES mass spectra acquired after exposure displayed a slight increase in the intensity of the $[Co_9Si(CO)_{22}]^-$ signal (*m/z* 1175), but a significant increase in the $[Co(CO)_4]^-$ signal intensity and a decline in the $[Co_9Si(CO)_{21}]^{2-}$ signal intensity were noted. The ESMS results indicate that though a CO atmosphere assisted formation of the $[Co_9Si(CO)_{22}]^-$ cluster, it also served to decompose the sample.

4.8 Reactions of μ_4-E[$Fe_2(CO)_8$]$_2$ (E = Si, Sn) with $[Co(CO)_4]^-$

4.8.1 Introduction

Following the success of the reactions of μ_4-E[$Co_2(CO)_7$]$_2$ (E = Si, Ge) with $[Co(CO)_4]^-$, the series was extended to include the iron 'spiro' clusters. Reactions of these compounds have not been examined to the same degree as the cobalt analogues and the identification of novel cluster compounds was anticipated.

4.8.2 Results and Discussion

The reaction between μ_4-Si[$Fe_2(CO)_8$]$_2$ and $[Co(CO)_4]^-$ was carried out in CH_2Cl_2 in a similar manner to the reactions described previously. The solution was refluxed over a 5 hour period without evidence for the formation of any mixed Si/Fe/Co clusters. Throughout reaction, ES mass spectra were dominated by signals attributable to $[Co(CO)_4]^-$ {*m/z* 171, $[NEt_4][Co(CO)_4]_2^-$ (*m/z* 472), $[Ag\{Co(CO)_4\}_2]^-$ (*m/z* 449)}. An aliquot of the reaction solution was removed after 5 hours, 'dosed' with a solution of Na[OMe] in methanol and analysed by ESMS with detection of a $[SiFe_4(CO)_{16}(OMe)]^-$ (*m/z* 731) signal. The absence of anionic cluster products and evidence for the unreacted parent compound indicated that no significant reaction occurred and the experiment was abandoned.

The equivalent reaction between μ_4-Sn[$Fe_2(CO)_8$]$_2$ and $[Co(CO)_4]^-$ was carried out in refluxing CH_2Cl_2 for 6 hours and monitored throughout by ESMS. There was no evidence over this period for formation of any mixed Sn/Co/Fe clusters. The *m/z* 171 signal corresponding to $[Co(CO)_4]^-$ was present throughout, as were signals attributable to $[HFe_3(CO)_{11}]^-$ (*m/z* 477) and $[CoFe_3(CO)_{13}]^-$ (*m/z* 591). After 6 hours at reflux, an aliquot of the reaction solution was removed and 'dosed' with a methanolic solution of Na[OMe]. ESMS analysis of the solution displayed a signal at *m/z* 823 corresponding to $[Fe_4Sn(CO)_{16}(OMe)]^-$ (Figure 4.21), indicating that no significant reaction occurred between the μ_4-Sn[$Fe_2(CO)_8$]$_2$ and $[Co(CO)_4]^-$ reagents.

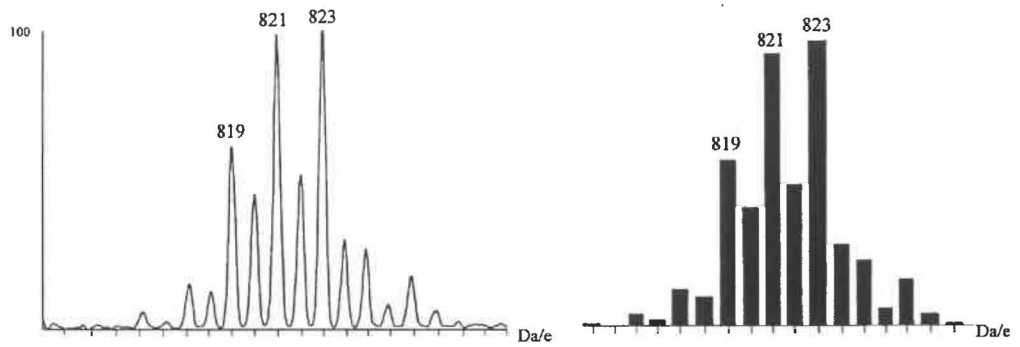

Figure 4.21 – The observed and calculated isotope patterns for [$Fe_4Sn(CO)_{16}(OMe)$]$^-$.

ESMS analysis of the reactions between μ_4-E[$Fe_2(CO)_8$]$_2$ and [$Co(CO)_4$]$^-$ in refluxing CH_2Cl_2 indicated that no cluster products were generated. The inert nature of the μ_4-E[$Fe_2(CO)_8$]$_2$ clusters is unusual, especially in comparison to their cobalt analogues. In retrospect, since the μ_4-E[$Fe_2(CO)_8$]$_2$ clusters are well known and the chemistry of the cobalt analogues so extensive, these reactions are likely to have been examined previously. The absence of any available literature on these reactions is probably indication that the lack of reactivity had been noted previously.

4.9 Conclusions

There are a number of conclusions and impressions that can be drawn from the research reported in this chapter.

Firstly, it is apparent that ESMS is a viable technique for monitoring cluster reactions. The intense spectra obtained allowed identification of all ionic reaction products, with the detected clusters parallelling those previously characterised structurally and spectroscopically. More importantly, different cluster products were easily distinguished by ESMS, avoiding the ambiguity associated with IR characterisation.

One of the more significant results from the research documented in this chapter was the isolation of the novel [NEt_4]$_2$[$Co_{10}Ge_2(CO)_{24}$] cluster, the highest-nuclearity germanium/cobalt cluster reported. The geometry of this cluster is highly unusual and one that cannot be explained from electron-counting procedures. This cluster was unheralded prior to this research though the synthetic route to this compound had been previously examined. The absence of this cluster in previous reports is attributed to

similarity between the IR spectra of $[Co_{10}Ge_2(CO)_{24}]^{2-}$ and $[Co_7Ge_2(CO)_{21}]^-$. This is believed to be the first instance where a cluster has been identified by ESMS, the conditions for optimal yield determined, and the cluster subsequently isolated and structurally characterised.

ESMS analysis established the sequence of clusters produced by reaction between μ_4-$Ge[Co_2(CO)_7]_2$ and $[Co(CO)_4]^-$, allowing formulation of a reaction pathway. The pathway provided (refer to Scheme 4.1), based around a proposed $[GeCo_3(CO)_9]^-$ species, accounts for the composition and structures of all the clusters observed. Confirmation of the proposed mechanism was provided by generation of $[Co_{10}Ge_2(CO)_{24}]^{2-}$ in the presence of phosphines.

The application of ESMS to the analogous silicon reaction identified a series of novel clusters. The detection of $[Co_5Si(CO)_{16}]^-$ indicates that the silicon and germanium reactions initially follow a similar pathway, though the two systems diverge after this point with evidence for the formation of a $[Co_7Si(CO)_{21}]^-$ cluster which has no germanium analogue. Two higher-nuclearity species were detected, $[Co_9Si(CO)_{21}]^{2-}$ and $[Co_9Si(CO)_{22}]^-$, with the latter cluster corresponding to the electron-precise version of the former. The encapsulated nature of the silicon atoms in these two clusters contrasts with the semi-encapsulated environment observed for germanium in the high-nuclearity $[Co_{10}Ge_2(CO)_{24}]^{2-}$ cluster, further indication of the difference between the two systems. Although several novel clusters were identified in this reaction, further study is necessary to establish the structures of these species.

The only disheartening aspect of this research was the inability to obtain crystals of the silicon clusters suitable for structural characterisation. In particular, the structure of the electron-precise $[Co_9Si(CO)_{22}]^-$ cluster is of interest as there is no obvious location on $[Co_9Si(CO)_{21}]^{2-}$ to bind another carbonyl ligand. The prediction that the structure of $[Co_7Si(CO)_{21}]^-$ is intermediate between the two Co_7Ge_x (x = 1, 2) clusters also cannot be confirmed without crystallographic evidence.

Finally, analogous reactions using μ_4-$E[Fe_2(CO)_8]_2$ (E = Si, Sn) were unsuccessful. No cluster products were identified from these reactions and ESMS analysis after extended reflux indicated the presence of the parent compounds. Examination of these reactions

at higher temperatures may yield high-nuclearity products, but in general the μ_4-E[$Fe_2(CO)_8$]$_2$ compounds appear significantly less reactive than their cobalt analogues.

4.10 Experimental

Reaction between μ_4-Ge[$Co_2(CO)_7$]$_2$ and [NEt_4][$Co(CO)_4$]

(i) To a CH_2Cl_2 solution (10 mL) of μ_4-Ge[$Co_2(CO)_7$]$_2$ (0.030 g, 0.043 mmol) was added [NEt_4][$Co(CO)_4$] (0.025 g, 0.086 mmol) and the mixture heated to reflux. Monitoring of the reaction by ESMS identified the previously reported [$Co_7Ge(CO)_{20}$]$^-$ (*m/z* 1047) and [$Co_7Ge_2(CO)_{21}$]$^-$ (*m/z* 1147) clusters after 15-20 minutes, along with a novel [$Co_{10}Ge_2(CO)_{24}$]$^{2-}$ cluster (*m/z* 704 and 1408 for the oxidised ion) after 2-3 hours. No additional cluster products were observed over 10-12 hours at reflux.

(ii) The effect of variation in the reactant ratio was examined. To a CH_2Cl_2 solution (10 mL) of μ_4-Ge[$Co_2(CO)_7$]$_2$ (0.030 g, 0.043 mmol) was added [NEt_4][$Co(CO)_4$] (either 0.015 g, 0.055 g, or 0.13 g giving ratios of 1:1, 1:4 and 1:10 respectively) and the mixture was refluxed for 6 hours. ES mass spectra indicated that the clusters produced and their relative rates of formation were similar to those found for the 1:2 ratio.

Reaction with other [$Co(CO)_4$]$^-$ salts

(i) To a CH_2Cl_2 solution (10 mL) of μ_4-Ge[$Co_2(CO)_7$]$_2$ (0.02 g, 0.03 mmol) was added a 1:2 ratio of the appropriate [$Co(CO)_4$]$^-$ salt {0.04 g [PPN][$Co(CO)_4$], 0.02 g [$PhCH_2NMe_3$][$Co(CO)_4$], 0.025 g [NBu_4][$Co(CO)_4$], 0.03 g [PPh_4][$Co(CO)_4$] or 0.03 g [$AsPh_4$][$Co(CO)_4$]} and the solution refluxed for 8 hours. In each case, ESMS analysis indicated that the products formed and their relative rate of formation were similar to those found for [NEt_4][$Co(CO)_4$].

(ii) To a CH_2Cl_2 solution (10 mL) of μ_4-Ge[$Co_2(CO)_7$]$_2$ (0.03 g, 0.043 mmol) was added 0.13 mmol (1 mL of a 0.129 mol L^{-1} CH_2Cl_2 solution) of Na[$Co(CO)_4$]. The mixture was refluxed for 8 hours and monitored by ESMS. A more intense signal than usual was detected for [$Hg\{Co(CO)_4\}_3$]$^-$ (*m/z* 715), as expected since the preparation of Na[$Co(CO)_4$] did not involve recrystallisation to remove this impurity. The only other

difference compared to the other salts was a higher than usual intensity for the $[Co_{10}Ge_2(CO)_{24}]^-$ (*m/z* 1408) oxidised ion.

Effect of solvent upon reaction between μ_4-$Ge[Co_2(CO)_7]_2$ and $[NEt_4][Co(CO)_4]$

To an Et_2O solution (10 mL) of μ_4-$Ge[Co_2(CO)_7]_2$ (0.035 g, 0.05 mmol) was added $[NEt_4][Co(CO)_4]$ (0.035 g, 0.12 mmol) and the solution was heated to reflux. ESMS analysis of the solution after 5 minutes indicated the presence of $[Co_5Ge(CO)_{16}]^-$ (*m/z* 817), with an increase in the intensity of this signal noted over a 20 minute period, after which signals attributable to $[Co_7Ge(CO)_{20}]^-$ (*m/z* 1047) and $[Co_7Ge_2(CO)_{21}]^-$ (*m/z* 1147) were observed. Further reaction resulted in a decrease in the $[Co_5Ge(CO)_{16}]^-$ signal intensity, with the ion absent after 3 hours. The $[Co_7Ge(CO)_{20}]^-$ and $[Co_7Ge_2(CO)_{21}]^-$ signals were present over the remaining course of the experiment. ES mass spectra of the solution after 10 hours at reflux were dominated by the $[Co_7Ge_2(CO)_{21}]^-$ signal, with no evidence for formation of the $[Co_{10}Ge_2(CO)_{24}]^{2-}$ cluster.

Synthesis of $[NEt_4]_2[Co_{10}Ge_2(CO)_{24}]$

The reaction was repeated on a larger scale to allow isolation of the $[Co_{10}Ge_2(CO)_{24}]^{2-}$ anion. To a CH_2Cl_2 solution (20 mL) containing μ_4-$Ge[Co_2(CO)_7]_2$ (0.210 g, 0.30 mmol) was added $[NEt_4][Co(CO)_4]$ (0.180 g, 0.6 mmol) and the solution was refluxed for 6 hours. ESMS analysis of the solution after reaction indicated that $[Co_{10}Ge_2(CO)_{24}]^{2-}$ (*m/z* 704) was the dominant ion present. The solution was concentrated to *ca.* 5 mL and Et_2O added to precipitate the product, $[NEt_4]_2[Co_{10}Ge_2(CO)_{24}]$ (0.199 g, 38%). Crystals of this compound were grown by slow diffusion of Et_2O into a CH_2Cl_2 solution of the compound at -20°C under nitrogen.

$[NEt_4]_2[Co_{10}Ge_2(CO)_{24}]$

M_r – 1661.3

IR – (ν_{CO}, CH_2Cl_2) 2066 (m,sh), 2028 (vs,br), 2007 (m,sh), 1730 (w,br) cm^{-1}

ESMS – ($C_2H_4Cl_2$, -ve ion, 5 cV) *m/z* 704 (100% - $[Co_{10}Ge_2(CO)_{24}]^{2-}$), *m/z* 1408 (10% - $[Co_{10}Ge_2(CO)_{24}]^-$)

X-Ray structure determination of $[NEt_4]_2[Co_{10}Ge_2(CO)_{24}].1.5CH_2Cl_2.0.5Et_2O$

Crystallographic data for $[NEt_4]_2[Co_{10}Ge_2(CO)_{24}].1.5CH_2Cl_2.0.5Et_2O$ are provided in Table 4.4. The anion refined cleanly but disorder was noted in both the cations and solvent. Placement of hydrogen atoms on these species was considered inappropriate because of the disorder.

Table 4.4 – Crystallographic data for $[NEt_4]_2[Co_{10}Ge_2(CO)_{24}].1.5CH_2Cl_2.0.5Et_2O$

Empirical Formula	$C_{40}H_{40}Co_{10}Ge_2N_2O_{24}.1.5CH_2Cl_2.0.5(C_2H_5)_2O$
M_r	1831.67
Temperature (K)	203
Crystal System	Orthorhombic
Space Group	Pcca
a(Å)	30.3922(6)
b(Å)	23.5597(5)
c(Å)	17.2684(3)
Volume (Å^3)	12364.7(4)
Z	8
Calculated Density (Mg m^{-3})	1.968
θ range collected	1.34 to 25.0
Reflections Collected	74629
Independent Reflections	10909 (R_{int} = 0.0398)
Goodness of Fit	1.096
R indices – I > 2σ(I)	R_1 = 0.0595, wR_2 = 0.1471
R indices – all data	R_1 = 0.0879, wR_2 = 0.1618
T_{max}/T_{min}	0.845/0.649

Reaction of $[Co_7Ge_x(CO)_y]^-$ anions with PR_3

To a CH_2Cl_2 solution (5 mL) containing an approximately 1:1 mixture (as determined by ESMS signals of equivalent intensity) of $[Co_7Ge(CO)_{20}]^-$ (*m/z* 1047) and $[Co_7Ge_2(CO)_{21}]^-$ (*m/z* 1147) (*ca.* 0.02 mmol) was added excess PPh_3 (0.015 g, 0.06 mmol). The reaction was stirred at room temperature for 4 hours and monitored by ESMS. A signal corresponding to $[Co_{10}Ge_2(CO)_{24}]^{2-}$ (*m/z* 704) was detected after 20 minutes, which increased in intensity over a 1-1.5 hour period, matched by a decrease in the intensity of the $[Co_7Ge(CO)_{20}]^-$ and $[Co_7Ge_2(CO)_{21}]^-$ signals. After 2 hours, the

[$GeCo_7(CO)_{20}$]$^-$ signal intensity was negligible and analysis over the remaining time displayed no further changes. IR spectra were dominated by signals attributable to the anionic clusters though a weak signal was noted at 2040 cm^{-1}, tentatively assigned to $Ph_3P(CO)_3CoGeCo_3(CO)_9$.

The reaction was repeated using TCEP and PTA instead of PPh_3 with similar results. A decrease in the intensity of the [$Co_7Ge(CO)_{20}$]$^-$ signal was noted in each case, along with detection of the [$Co_{10}Ge_2(CO)_{24}$]$^{2-}$ ion.

Reactions of [$Co_{10}Ge_2(CO)_{24}$]$^{2-}$

(i) P*AuCl (0.025 g, 0.05 mmol) and Tl[PF_6] (0.03 g, 0.09 mmol) were added to a CH_2Cl_2 solution of [NEt_4]$_2$[$Co_{10}Ge_2(CO)_{24}$] (0.025 g, 0.015 mmol). The solution was stirred at room temperature for 2 hours with little change noted in the ES mass spectra. Negative-ion spectra were dominated by the parent *m/z* 704 signal, while positive-ion spectra displayed an intense signal at *m/z* 781 attributed to [P*$_2$Au]$^+$. Equivalent results were obtained in the absence of Tl[PF_6].

(ii) ^{t}BuNC (12 μL, 0.009 g, 0.108 mmol) was added slowly to a CH_2Cl_2 solution (5 mL) of [NEt_4]$_2$[$Co_{10}Ge_2(CO)_{24}$] (0.03 g, 0.018 mmol) and the composition of the solution monitored by ESMS. The solution slowly decolourised over a 2 hour period indicating the decomposition of the parent cluster, confirmed by a decrease in the [$Co_{10}Ge_2(CO)_{24}$]$^{2-}$ signal intensity by ESMS. After 2 hours, the only recognisable ESMS signal was that attributed to [$Co(CO)_4$]$^-$ (*m/z* 171).

Reaction between μ_4-Si[$Co_2(CO)_7$]$_2$ and [NEt_4][$Co(CO)_4$]

To a CH_2Cl_2 solution (10 mL) containing μ_4-Si[$Co_2(CO)_7$]$_2$ (0.03 g, 0.046 mmol) was added [NEt_4][$Co(CO)_4$] (0.025 g, 0.08 mmol) and the solution was heated to reflux. ES mass spectra displayed signals corresponding to [$Co_5Si(CO)_{16}$]$^-$ (*m/z* 771), [$Co_7Si(CO)_{21}$]$^-$ (*m/z* 1029), [$Co_9Si(CO)_{21}$]$^{2-}$ (*m/z* 573.5) and [$Co_9Si(CO)_{22}$]$^-$ (*m/z* 1175) after 15 minutes, 60 minutes and 3-4 hours respectively. Further reaction resulted in an increase in the signal intensity of the last two ions, with the [$Co_9Si(CO)_{21}$]$^{2-}$ signal dominating the spectra after *ca.* 7-8 hours. After 3-4 hours of reaction, a signal at *m/z*

774 was detected, initially suspected to be a previously unknown cluster but later identified as $[Co_6(CO)_{15}]^-$.

The reaction was repeated several times and halted after production of the $[Co_5Si(CO)_{16}]^-$, $[Co_7Si(CO)_{21}]^-$ and $[Co_9Si(CO)_{22}]^-$ anions. The solution was reduced in volume to *ca.* 3-4 mL, layered with Et_2O and cooled to –20°C. Crystals were obtained in each case but were of insufficient quality to undertake crystal structure determination and of insufficient quantity for characterisation by alternative methods.

Reactions of $[Co_9Si(CO)_{21}]^{2-}$

Previous structural characterisation of the $[Co_9Si(CO)_{21}]^{2-}$ cluster indicated co-crystallisation of $[Co(CO)_4]^-$. The presence of $[Co(CO)_4]^-$ was also noted through ESMS and IR analyses.

(i) To a CH_2Cl_2 solution (5 mL) of $[NEt_4]_3[Co_9Si(CO)_{21}][Co(CO)_4]$ (0.01 g, 0.006 mmol) was added P***AuCl (0.015 g, 0.027 mmol) and Tl[PF_6] (0.018 g, 0.05 mmol). The solution was stirred under an inert atmosphere for 2 hours and monitored by ESMS. Negative-ion spectra were dominated by the parent cluster (*m/z* 573.5) while the signals detected in positive-ion spectra corresponded to $[P^{***}{}_2Au]^+$ (*m/z* 901) and $[NEt_4]^+$ (*m/z* 130). There was no ESMS evidence for the formation of a capped cluster product.

(ii) $Hg(OAc)_2$ (0.006 g, 0.018 mmol) was added to a CH_2Cl_2 solution (5 mL) of $[NEt_4]_3[Co_9Si(CO)_{21}][Co(CO)_4]$ (0.01 g, 0.006 mmol) and the solution stirred under an inert atmosphere. ESMS analysis indicated immediate formation of $[Hg\{Co(CO)_4\}_3]^-$ (*m/z* 715) and a decrease in the intensity of the $[Co_9Si(CO)_{21}]^{2-}$ signal (*m/z* 573.5) was noted over a 30 minute period.

(iii) Excess zinc powder was added to a CH_2Cl_2 solution (5 mL) of $[NEt_4]_3[Co_9Si(CO)_{21}][Co(CO)_4]$ (0.03 g, 0.018 mmol) and the solution monitored by ESMS over a 2 hour period. A decrease in the intensity of the $[Co_9Si(CO)_{21}]^{2-}$ signal (*m/z* 573.5) was noted, matched by an increase in the $[Co(CO)_4]^-$ signal intensity but there was no evidence by ESMS for the formation of a $[Co_9Si(CO)_{21}]^{3-}$ cluster.

(iv) To a CH_2Cl_2 solution (5 mL) of $[NEt_4]_3[Co_9Si(CO)_{21}][Co(CO)_4]$ (0.03 g, 0.018 mmol) was added 50 μL of a 0.360 mol L^{-1} solution of $Co(\eta^5\text{-}C_5H_5)_2$ [prepared by dissolution of 0.136 g of $Co(\eta^5\text{-}C_5H_5)_2$ in 2 mL of CH_2Cl_2]. The solution was stirred at room temperature for 20 minutes with no change noted in the ES mass spectra. A further 200 μL was added (5:1 excess) and the solution stirred for an additional hour without evidence by ESMS for the formation of a $[Co_9Si(CO)_{21}]^{3-}$ cluster.

(v) A CH_2Cl_2 solution (5 mL) of $[NEt_4]_3[Co_9Si(CO)_{21}][Co(CO)_4]$ (0.02 g, 0.012 mmol) was exposed to a CO atmosphere for 3 hours and the composition of the solution monitored by ESMS. The intensity of the $[Co_9Si(CO)_{22}]^-$ (*m/z* 1175) and $[Co(CO)_4]^-$ (*m/z* 171) signals increased over this time, while a decrease in the $[Co_9Si(CO)_{21}]^{2-}$ (*m/z* 573.5) signal intensity was noted. All three anionic species were still detectable after 3 hours and the reaction was abandoned.

Reaction between μ_4-E[$Fe_2(CO)_8$]$_2$ (E = Si, Sn) and $[NEt_4][Co(CO)_4]$

(i) $[NEt_4][Co(CO)_4]$ (0.035 g, 0.12 mmol) was added to a CH_2Cl_2 solution (10 mL) of μ_4-Si[$Fe_2(CO)_8$]$_2$ (0.04 g, 0.06 mmol) and the mixture was refluxed for 5 hours. Monitoring of the reaction by ESMS revealed no cluster products, with spectra dominated by signals corresponding to $[Co(CO)_4]^-$. After 5 hours, an aliquot of the solution was treated with Na[OMe] and a $[SiFe_4(CO)_{16}(OMe)]^-$ ion (*m/z* 731) was detected by ESMS.

(ii) $[NEt_4][Co(CO)_4]$ (0.03 g, 0.1 mmol) was added to a CH_2Cl_2 solution (10 mL) of μ_4-Sn[$Fe_2(CO)_8$]$_2$ (0.04 g, 0.05 mmol) and the mixture was refluxed for 6 hours. ESMS monitoring of reaction provided no indication for formation of any mixed Sn/Fe/Co clusters. Analysis of the cooled solution indicated unreacted $[Co(CO)_4]^-$, $[HFe_3(CO)_{11}]^-$ (*m/z* 477), $[CoFe_3(CO)_{13}]^-$ (*m/z* 591) and μ_4-Sn[$Fe_2(CO)_8$]$_2$ (detected as the methoxide adduct – *m/z* 823).

Chapter Five – Reactions of μ_4-E[$Co_2(CO)_7$]$_2$ (E = Si, Ge) with Transition Metal Carbonyl Anions

5.1 Introduction

The development of ESMS towards monitoring of cluster reactions was a key focus of the research reported in this thesis. Examination of the reaction between μ_4-Ge[$Co_2(CO)_7$]$_2$ and $[Co(CO)_4]^-$ was successful in identifying several cluster species, and was crucial in the identification and isolation of the novel $[Co_{10}Ge_2(CO)_{24}]^{2-}$ cluster. Research reported in this chapter involves equivalent reactions with various other anionic transition metal reagents. These reactions were examined in the expectation of identifying and isolating novel mixed-metal (heteronuclear) group 14 clusters.

5.1.1 Heteronuclear Transition Metal/Group 14 Clusters

As an introduction to this research, a brief discussion of the synthesis and structures of heteronuclear group 14 clusters is provided. In general, the synthetic routes and structures expressed are similar to the homonuclear clusters discussed in the previous chapter.

There are significantly fewer examples of heteronuclear 'spiro' clusters than the homonuclear analogues. The only structurally characterised examples are μ_4-Ge[$Fe_2(CO)_8$][$FeMn(CO)_6(\eta^5$-$C_5H_4CH_3)$] (Figure 5.1), formed from reaction between Ge[$Mn(CO)_2(\eta^5$-$C_5H_4CH_3)]_2$ and $Fe_2(CO)_9$ [1], and the extended 'spiro' compound $Fe_2[\mu_2$-$GeCo_2(CO)_7]_2(CO)_7$, a product of $[(CO)_4FeGeH_2]_2$ and $Co_2(CO)_8$ [2].

[1] D. Melzer and E. Weiss, *J. Organomet. Chem.*, 1983, **255**, 335.

[2] S.G. Anema, J.A. Audett, K.M. Mackay and B.K. Nicholson, *J. Chem. Soc., Dalton Trans.*, 1988, 2629.

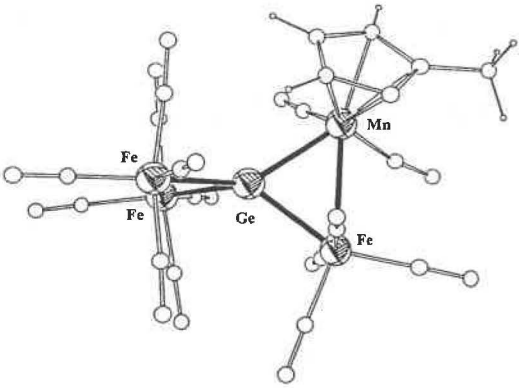

Figure 5.1 – The structure of μ_4-Ge[$Fe_2(CO)_8$][$FeMn(CO)_6(\eta^5$-$C_5H_4CH_3)$][1].

The MEM_3 arrangement is more common for heteronuclear group 14 clusters. The reported examples (listed in Table 5.1) are based around either the bi-capped $Fe_3(CO)_9$ or mono-capped $Co_3(CO)_9$ arrangements. The $Fe_3(\mu_3$-$EML)_2(CO)_9$ [E = Ge, ML = $Re(CO)_5$ [3]] cluster was produced by reaction of $MnRe(CO)_{10}$ with $GeCl_2$ and $Fe(CO)_5$, while [E = Si, Ge; ML = $Fe(CO)_2(\eta^5$-$C_5H_5)$ – Figure 5.2] were isolated from reaction between EH_4, $Fe(CO)_5$ and $[Fe(CO)_2(\eta^5$-$C_5H_5)]_2$ [4]. The most systematic route is reported for $Fe_3[\mu_3$-$GeCo(CO)_4]_2(CO)_9$, produced through decarbonylation and rearrangement of $Fe_2[\mu_2$-$GeCo_2(CO)_7]_2(CO)_7$ [5].

Table 5.1 – The reported heteronuclear MEM_3 group 14 clusters

$Fe_3[\mu_3$-$SiFe(CO)_2(\eta^5$-$C_5H_5)]_2(CO)_9$	[4]	$Fe_3[\mu_3$-$GeCo(CO)_4]_2(CO)_9$	[5]
$Fe_3[\mu_3$-$GeRe(CO)_5]_2(CO)_9$	[3]	$Fe_3[\mu_3$-$GeFe(CO)_2(\eta^5$-$C_5H_5)]_2(CO)_9$	[4]
$Fe_3[\mu_3$-$SnMn(CO)_5]_2(CO)_9$	[7]	$Fe_3[\mu_3$-$SnFe(CO)_2(\eta^5$-$C_5H_5)]_2(CO)_9$	[6]
$Fe_3[\mu_3$-$SnRe(CO)_5]_2(CO)_9$	[7]	$(CO)_2(\eta^5$-$C_5H_5)FeSiCo_3(CO)_9$	[11]
$(CO)_5MnSiCo_3(CO)_9$	[8]	$(CO)_2(\eta^5$-$C_5H_5)FeGeCo_3(CO)_9$	[12]
$(CO)_5MnGeCo_3(CO)_9$	[9]	$(CO)_3(\eta^5$-$C_5H_5)MoGeCo_3(CO)_9$	[10]
$(CO)_3(\eta^5$-$C_5H_5)CrGeCo_3(CO)_9$	[13]	$(CO)(\eta^5$-$C_5H_5)NiGeCo_3(CO)_9$	[12]
$(CO)_3(\eta^5$-$C_5H_5)WGeCo_3(CO)_9$	[13]	$(CO)_3(\eta^5$-$C_5H_5)WGeCo_2Mo(CO)_8(\eta^5$-$C_5H_5)$	[10]
$(CO)_3(\eta^5$-$C_5H_5)MoGeCo_2Mo(CO)_8(\eta^5$-$C_5H_5)$	[10]	$(CO)_2(\eta^5$-$C_5H_5)FeGeCo_2Mo(CO)_8(\eta^5$-$C_5H_5)$	[10]
$[(CO)_4FeGeCoFe_2(CO)_{10}]^-$	[14]	$[(CO)_3Co\{GeCo_3(CO)_9\}\{GeCoFe_2(CO)_{10}\}]^-$	[14]
referred to as $[CoFe_3Ge(CO)_{14}]^-$		referred to as $[Co_5Fe_2Ge_2(CO)_{22}]^-$	

[3] H-J. Haupt and H-J. Florke, *Acta Cryst. Sect. C*, 1988, **44**, 472.

[4] S.G. Anema, K.M. Mackay, B.K. Nicholson and M. Van Tiel, *Organometallics*, 1990, **9**, 2436.

[5] S.G. Anema, K.M. Mackay and B.K. Nicholson, *J. Chem. Soc., Dalton Trans.*, 1996, 3853.

[6] T.J. McNeese, S.S Wrenford, D.L. Tipton and R. Bau, *J. Chem. Soc., Chem Commun.*, 1977, 390.

[7] H.J. Haupt, U. Florke and A. Goetze, *Z. Anorg. Allg. Chem.*, 1988, **557**, 82.

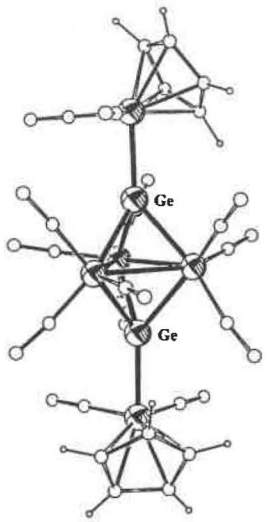

Figure 5.2 – The structure of $Fe_3[\mu_3\text{-}GeFe(CO)_2(\eta^5\text{-}C_5H_5)]_2(CO)_9$ [4].

The syntheses of $LMECo_3(CO)_9$ clusters are generally more systematic, with substitution of the apical "$Co(CO)_4$" unit from $(CO)_4CoECo_3(CO)_9$ effected by transition metal anions $[ML]^-$ [E = Si[8], Ge[9]; ML = $Mn(CO)_5$] and neutral dimeric metal carbonyls [E = Ge, ML = $Mo(CO)_3(\eta^5\text{-}C_5H_5)$ [10,12]]. Less systematic routes have been reported for $(CO)_2(\eta^5\text{-}C_5H_5)FeSiCo_3(CO)_9$ [reaction of $(CO)_2(\eta^5\text{-}C_5H_5)FeSiH_3$ and $Co_2(CO)_8$ [11]], $(CO)_2(\eta^5\text{-}C_5H_5)FeGeCo_3(CO)_9$ {salt elimination product of $[(CO)_2(\eta^5\text{-}C_5H_5)Fe]_2GeI_2$ and $K[Co(CO)_4]$ [12] - Figure 5.3} and $(CO)_3(\eta^5\text{-}C_5H_5)MGeCo_3(CO)_9$ [M = Cr, W – through thermolysis of $LMAsMe_2$ and $RGeCo_3(CO)_9$, R = Me, Ph[13]]. These clusters are all 66 electron species, isostructural and isoelectronic to $(CO)_4CoGeCo_3(CO)_9$.

[8] G.C. Barris, D.Phil. Thesis, University of Waikato, 1990.

[9] J.A. Christie, D.N. Duffy, K.M. Mackay and B.K. Nicholson, *J. Organomet. Chem.*, 1982, **226**, 165.

[10] P. Gusbeth and H. Vahrenkamp, *Chem. Ber.*, 1985, **118**, 1770.

[11] W. Malisch, H.U. Wekel, I. Grob, G.F.H. Kohler and M. Baudler, *Z. Naturforsch. B*, 1982, **37**, 601.

[12] P. Gusbeth and H. Vahrenkamp, *Chem. Ber.*, 1985, **118**, 1746.

[13] P. Gusbeth and H. Vahrenkamp, *Chem. Ber.*, 1985, **118**, 1758.

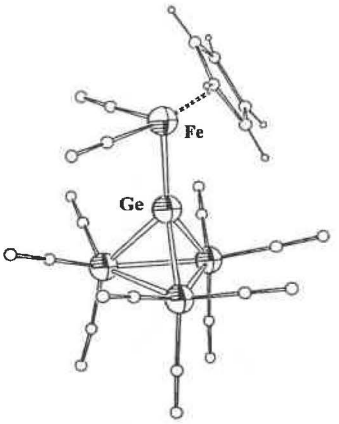

Figure 5.3 – The structure of $(CO)_2(\eta^5\text{-}C_5H_5)FeGeCo_3(CO)_9$ [12].

An alternative heteronuclear MEM_3 arrangement is displayed by $[CoFe_3Ge(CO)_{14}]^-$ {generated from reaction of $[Me_2GeFe(CO)_4]_2$ and $[Co(CO)_4]^-$ [14] - Figure 5.4a} where the unique cobalt atom is located within the M_3 triangle rather than the apical position. Similar mixed-metal M_3 triangles are reported for $LMGeCo_2Mo(CO)_8(\eta^5\text{-}C_5H_5)$ [ML = $Fe(CO)_2(\eta^5\text{-}C_5H_5)$, $Mo(CO)_3(\eta^5\text{-}C_5H_5)$, $W(CO)_3(\eta^5\text{-}C_5H_5)$ - Figure 5.4b], produced by reaction between $LMGeCo_3(CO)_9$ and $[Mo(CO)_3(\eta^5\text{-}C_5H_5)]_2$ [10].

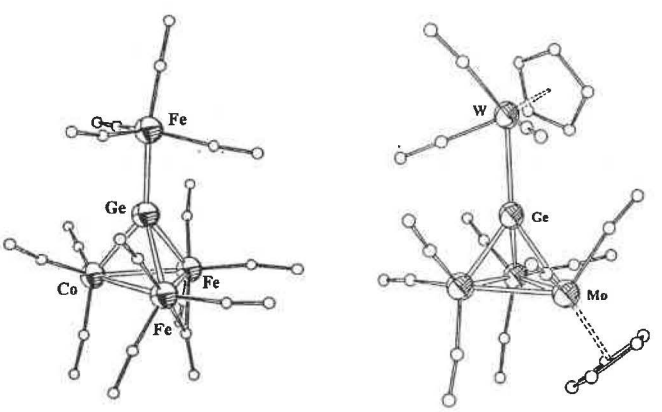

(a) (b)

Figure 5.4 – The structures of $[CoFe_3Ge(CO)_{14}]^-$ [14] (a) and $(CO)_3(\eta^5\text{-}C_5H_5)WGeCo_2Mo(CO)_8(\eta^5\text{-}C_5H_5)$ [10] (b – hydrogen atoms omitted).

Aside from the MEM_3 derivatives, there have been few reported examples of heteronuclear group 14 clusters. The only high-nuclearity example is $[Co_5Fe_2Ge_2(CO)_{22}]^-$ (Figure 5.5), produced by reaction between μ_4-$Ge[Co_2(CO)_7]_2$ and $[Fe_2(CO)_8]^{2-}$ [14]. This 114 valence-electron cluster is analogous to $[Co_7Ge_2(CO)_{21}]^-$

[14] S.G. Anema, G.C. Barris, K.M. Mackay and B.K. Nicholson, *J. Organomet. Chem.*, 1992, **441**, 35.

(discussed in the previous chapter), with replacement of two $Co(CO)_3$ units in one of the M_3 triangles by a $Fe_2(CO)_7$ moiety. Aside from the μ_2-CO ligand bridging the Fe-Fe bond, the structure is identical to that found for $[Co_7Ge_2(CO)_{21}]^-$.

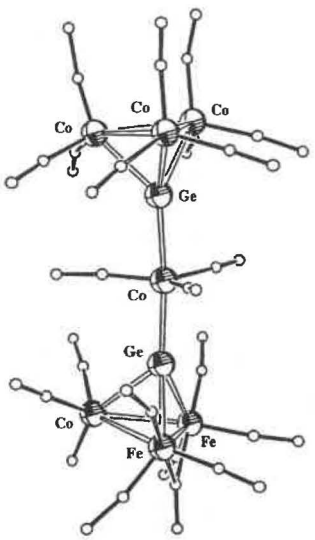

Figure 5.5 – The structure of $[Co_5Fe_2Ge_2(CO)_{22}]^-$ [14].

5.2 Reactions of μ_4-E[$Co_2(CO)_7$]$_2$ (E = Si, Ge) with Anionic Transition Metal Reagents

5.2.1 Reaction of μ_4-Ge[$Co_2(CO)_7$]$_2$ with [NEt_4]$_2$[$Fe_2(CO)_8$]

As discussed above, the reaction of μ_4-Ge[$Co_2(CO)_7$]$_2$ with $[Fe_2(CO)_8]^{2-}$ has been examined previously, with isolation of $[Co_5Fe_2Ge_2(CO)_{22}]^-$ though no indication of yield was provided[14]. The reaction was repeated with the expectation of identifying and isolating other high-nuclearity heteronuclear cluster products.

Results and Discussion

The reaction between μ_4-Ge[$Co_2(CO)_7$]$_2$ and $[Fe_2(CO)_8]^{2-}$ was performed initially in CH_2Cl_2 at room temperature. Analysis by ESMS over a 30-40 minute period (Figure 5.6) indicated generation of $[Co(CO)_4]^-$ (*m/z* 171), a series of GeM_5 anions: $[Co_3Fe_2Ge(CO)_{15}]^-$ (*m/z* 783), $[Co_3Fe_2Ge(CO)_{16}]^-$ (*m/z* 811), $[CoFe_4Ge(CO)_{17}]^-$ (*m/z* 833), and a trace of a signal corresponding to $[Co_3Fe_2Ge(CO)_{17}]^-$ (*m/z* 839). Over longer reaction times (1-1.5 hours), signals attributed to the higher-nuclearity clusters,

$[Co_7Ge_2(CO)_{21}]^-$ (*m/z* 1147) and $[Co_5Fe_2Ge_2(CO)_{22}]^-$ (*m/z* 1169), were detected along with $[Co_3FeGe(CO)_{13}]^-$ (*m/z* 671), $[CoFe_3Ge(CO)_{14}]^-$ (*m/z* 693) and $[Co_3Fe(CO)_{12}]^-$ (*m/z* 569). Extended reaction led to an increase in the intensity of these last three ions as well as an additional non-germanium species, $[CoFe_3(CO)_{13}]^-$ (*m/z* 591). The increased intensity of these signals was matched by a decrease in those associated with the higher-nuclearity (GeM_5, Ge_2M_7) clusters.

Monitoring of the reaction by IR spectroscopy was less effective. Prior to the addition of $[Fe_2(CO)_8]^{2-}$, spectra were dominated by signals attributable to μ_4-Ge[$Co_2(CO)_7$]$_2$ [2082 (s), 2063 (s), 2033 (br), 1840 (w,br) cm^{-1}]. ES mass spectra acquired 30 minutes after addition were dominated by signals attributable to several GeM_5 clusters while IR signals were less informative [2037 (m,sh), 2019 (s), 1995 (m,sh), 1958 (w), 1890 (s) cm^{-1}]. The first four signals are similar to other reported Ge/Fe/Co anions (discussed below) while the last corresponds to $[Co(CO)_4]^-$, the presence of which was also noted by ESMS. IR spectra acquired after 2 hours at room temperature were essentially identical [2032 (m,sh), 2017 (s), 1998 (m,sh), 1952 (w), 1889 (s) cm^{-1}] whereas ES mass spectra were dominated by signals corresponding to $[Co_3FeGe(CO)_{13}]^-$, $[CoFe_3Ge(CO)_{14}]^-$ and $[Co_3Fe(CO)_{12}]^-$. Aside from the strong band indicative of $[Co(CO)_4]^-$, the IR signals observed can be attributed to any of a variety of anionic mixed Ge/Fe/Co clusters, the IR spectra of which are indistinguishable {$[CoFe_3Ge(CO)_{14}]^-$ - 2070 (w), 2016 (vs), 1944 (mw), 1910 (ms), 1810 (w,br) cm^{-1} [14]; $[Co_5Fe_2Ge_2(CO)_{22}]^-$ - 2071 (w), 2016 (vs), 1949 (w), 1913 (m), 1810 (w,br) cm^{-1} [14]}. The similarity of IR spectra between the different cluster anions, in conjunction with the number of products generated, hampered the use of IR in monitoring the reaction.

The reaction was repeated at reflux with a similar series of clusters detected. Formation of several GeM_5 clusters (identical to those observed at room temperature) was noted but these signals rapidly decreased in intensity, yielding spectra dominated by the M_4 and $MGeM_3$ products; $[Co_3Fe(CO)_{12}]^-$, $[CoFe_3(CO)_{13}]^-$, $[Co_3FeGe(CO)_{13}]^-$ and $[CoFe_3Ge(CO)_{14}]^-$. The higher-nuclearity clusters, $[Co_7Ge_2(CO)_{21}]^-$ and $[Co_5Fe_2Ge_2(CO)_{22}]^-$, were detected along with an additional signal at *m/z* 923 attributed to $[Co_3Fe_3Ge(CO)_{18}]^-$. Throughout the reaction, the ES mass spectra of the solution were dominated by the M_4 and GeM_4 signals.

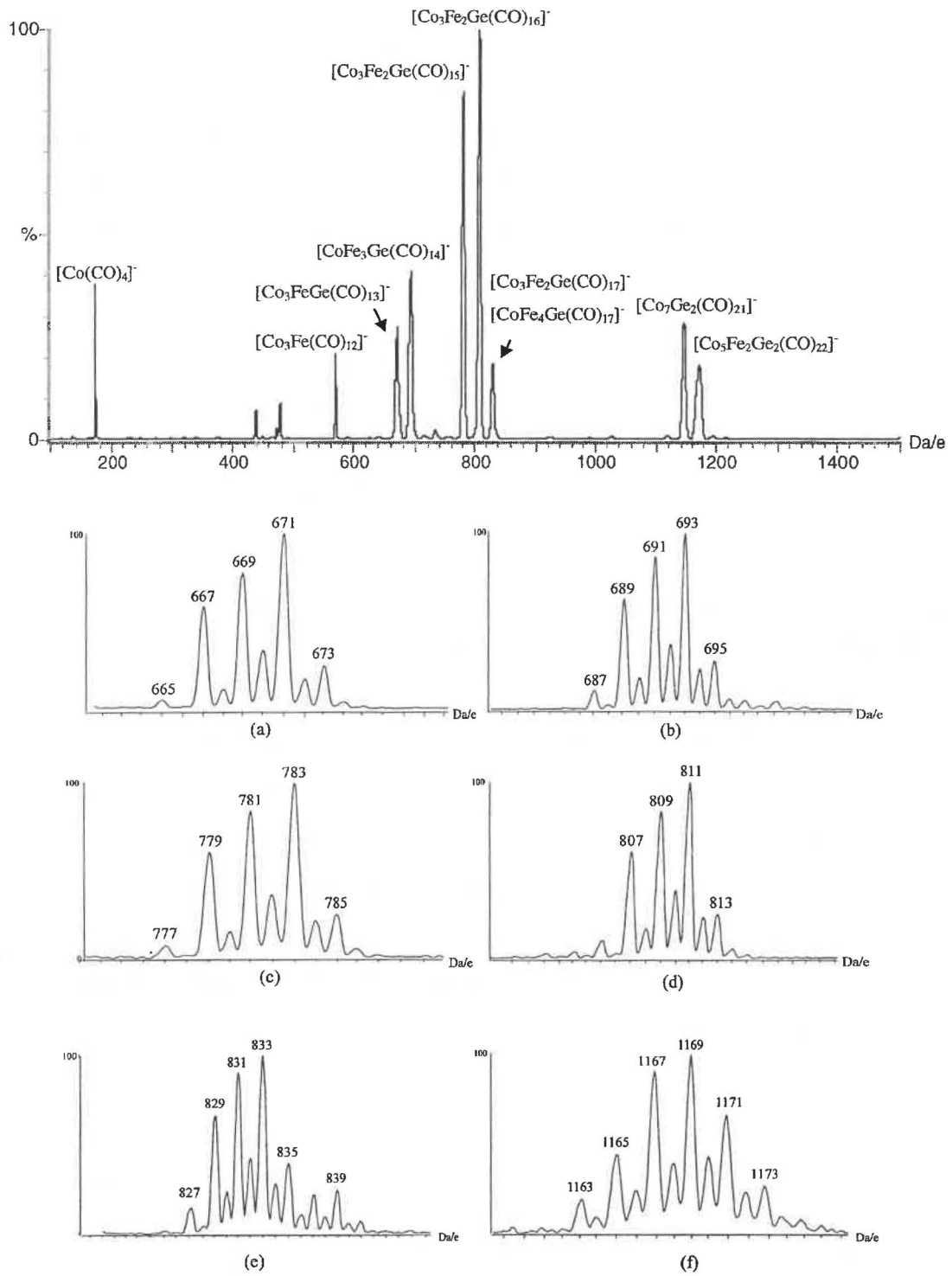

Figure 5.6 – The ES mass spectrum (-ve ion, 5 cV) of the reaction between μ_4-Ge[$Co_2(CO)_7$]$_2$ and $[Fe_2(CO)_8]^{2-}$ after stirring for 2 hours at room temperature. The isotope patterns for $[Co_3FeGe(CO)_{13}]^-$ (a), $[CoFe_3Ge(CO)_{14}]^-$ (b), $[Co_3Fe_2Ge(CO)_{15}]^-$ (c), $[Co_3Fe_2Ge(CO)_{16}]^-$ (d), $[CoFe_4Ge(CO)_{17}]^-$ and $[Co_3Fe_2Ge(CO)_{17}]^-$ (e) and $[Co_5Fe_2Ge_2(CO)_{22}]^-$ (f) are shown.

A number of the clusters observed require explanation. The 66 electron $[Co_3FeGe(CO)_{13}]^-$ and $[CoFe_3Ge(CO)_{14}]^-$ clusters are predicted to adopt a MEM_3 arrangement analogous to $(CO)_4CoGeCo_3(CO)_9$. Structural characterisation of

$[CoFe_3Ge(CO)_{14}]^-$ located the unique cobalt atom within the M_3 plane (Figure 5.7a)[14], whereas the unique iron atom in $[Co_3FeGe(CO)_{13}]^-$ would be expected in the apical position (Figure 5.7b). The detection of these clusters indicates that the MEM_3 arrangement has a significant role in these cluster reactions, an assumption made in the reactions discussed in the previous chapter but not confirmed by ESMS because the neutral $(CO)_4CoGeCo_3(CO)_9$ analogue failed to ionise under standard conditions.

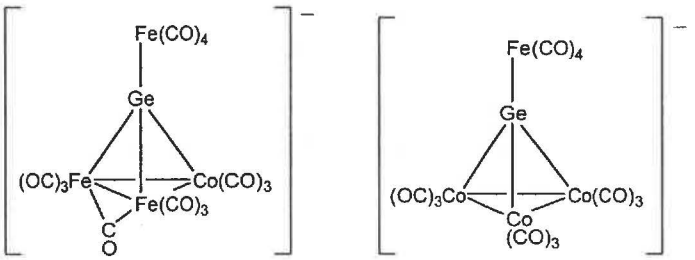

(a) (b)

Figure 5.7 – The structure of $[CoFe_3Ge(CO)_{14}]^-$ [14] (a) and predicted structure of $[Co_3FeGe(CO)_{13}]^-$ (b).

The two Ge_2M_7 clusters detected, $[Co_7Ge_2(CO)_{21}]^-$ and $[Co_5Fe_2Ge_2(CO)_{22}]^-$, are also readily explained. The synthesis of the former was discussed in the previous chapter and is attributable to reaction between μ_4-Ge[$Co_2(CO)_7$]$_2$ and $[Co(CO)_4]^-$ {$[Co(CO)_4]^-$ was detected by ESMS within minutes of $[Fe_2(CO)_8]^{2-}$ addition}. The other Ge_2M_7 cluster, $[Co_5Fe_2Ge_2(CO)_{22}]^-$, has been isolated from this reaction previously, with the ESMS results confirming earlier reports. The formation of $[Co_5Fe_2Ge_2(CO)_{22}]^-$ is attributed to reaction between $[CoFe_3Ge(CO)_{14}]^-$ and $(CO)_4CoGeCo_3(CO)_9$, accompanied by "$Fe(CO)_4$" loss (Scheme 5.1).

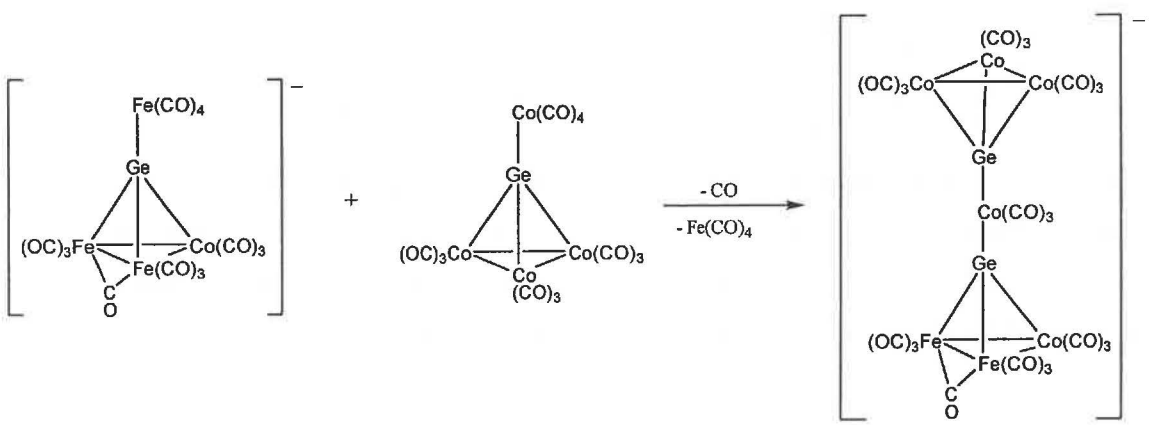

Scheme 5.1 – A suggested synthetic route to $[Co_5Fe_2Ge_2(CO)_{22}]^-$.

Of more interest are the series of GeM_5 clusters identified. The 82 electron $[Co_3Fe_2Ge(CO)_{17}]^-$ cluster is isoelectronic to $[Co_5Ge(CO)_{16}]^-$ and a similar atomic arrangement is predicted (Figure 5.8). The structures of the remaining GeM_5 clusters are less certain, with $[Co_3Fe_2Ge(CO)_{16}]^-$ and $[CoFe_4Ge(CO)_{17}]^-$ possessing 80 valence-electrons and $[Co_3Fe_2Ge(CO)_{15}]^-$ only 78 electrons. The $[Co_3Fe_2Ge(CO)_x]^-$ (x = 15, 16) ions are not related *via* CO loss during ESMS analysis, as lowering the applied voltage had no effect the relative intensities of the two signals. The atomic arrangements of these GeM_5 clusters are not readily apparent. A lower electron-count than that of $[Co_5Ge(CO)_{16}]^-$ indicates a more condensed structure, though not to the degree shown by square-pyramid or bridged-butterfly arrangements (74 and 76 valence-electrons respectively). One possible configuration is based around a 'spiked'-square $M_4(\mu_4$-GeM) arrangement (Figure 5.9), similar to that displayed by $Co_4(\mu_4$-ER)$_2$(CO)$_{11}$ clusters (discussed in Chapter 7). This requires $Co_3Fe(CO)_{12}$ and $CoFe_3(CO)_{13}$ M_4 units [assuming a $Fe(CO)_4$ capping group] for the $[Co_3Fe_2Ge(CO)_{16}]^-$ and $[CoFe_4Ge(CO)_{17}]^-$ clusters respectively. These M_4 arrangements have been isolated previously as tetrahedral anionic clusters but coordination to a GeM unit is unknown. The $[Co_3Fe_2Ge(CO)_{15}]^-$ cluster would require an even more condensed structure, one which is not obvious. This speculation would be settled by crystal structure determinations of these anions but, though the clusters were synthesised on numerous occasions, employing a variety of cations, attempts at isolation of these compounds as single crystals were unsuccessful. The cause is traced both to the inherent instability of these clusters and the complexity of the reaction preventing isolation of any single anionic cluster.

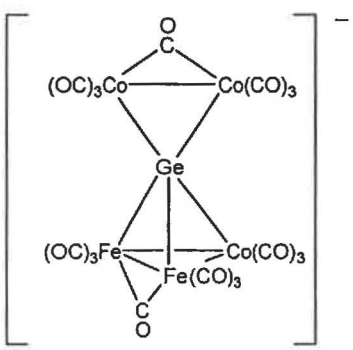

Figure 5.8 – The predicted structure of $[Co_3Fe_2Ge(CO)_{17}]^-$.

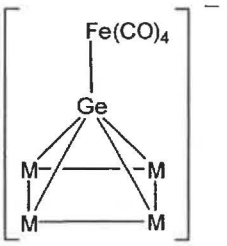

Figure 5.9 – A suggested structural arrangement for $[Co_3Fe_2Ge(CO)_{16}]^-$ and $[CoFe_4Ge(CO)_{17}]^-$.

The $[Co_3Fe_3Ge(CO)_{18}]^-$ species is unusual as it is the only group 14 EM_6 cluster detected in the course of this research. The cluster possesses 92 valence electrons, identical to $[Co_6P(CO)_{16}]^-$ (discussed in both Chapters 4 and 6) and it is possible that $[Co_3Fe_3Ge(CO)_{18}]^-$ possesses a similar atomic arrangement. This product was not formed in significant yield from this reaction and an alternative synthetic route was examined (Section 5.2.2).

One concerning aspect of this reaction was formation of mono-nuclear iron species though a di-nuclear reagent was employed. The generation of $[Fe(CO)_4]^{2-}$ from $[Fe_2(CO)_8]^{2-}$ has been reported[15], and a similar process may be occurring *in situ*. The initial products of this reaction all contained a Fe_2 unit, indicating that rearrangement of the iron reagent occurred after coordination to the germanium atom.

5.2.2 Reaction of μ_4-Ge[$Co_2(CO)_7$]$_2$ with $Fe_3(CO)_{12}$

One of the more unusual clusters identified in the reaction between μ_4-Ge[$Co_2(CO)_7$]$_2$ and $[Fe_2(CO)_8]^{2-}$ was $[Co_3Fe_3Ge(CO)_{18}]^-$. The limited yield of the cluster in the reaction precluded its isolation and based on the stoichiometry of this cluster, a more systematic synthesis involving $Fe_3(CO)_{12}$ was considered.

An equimolar CH_2Cl_2 solution of μ_4-Ge[$Co_2(CO)_7$]$_2$ and $Fe_3(CO)_{12}$ was stirred at room temperature for 2-3 hours without evidence of reaction between the two reagents. $[NEt_4][Co(CO)_4]$ was added and the solution heated to reflux for 1 hour, with subsequent ESMS analysis indicating formation of $[Co_3Fe(CO)_{12}]^-$ (*m/z* 569), $[CoFe_3(CO)_{13}]^-$ (*m/z* 591), $[Co_3FeGe(CO)_{13}]^-$ (*m/z* 671), $[Co_3Fe_3Ge(CO)_{18}]^-$ (*m/z* 923 –

[15] K. Farmery, M. Kilner, R. Greatrex and N.N. Greenwood, *J. Chem. Soc. A*, 1969, 2339.

Figure 5.10), [$Co_7Ge(CO)_{20}$]$^-$ (*m/z* 1047) and [$Co_7Ge_2(CO)_{21}$]$^-$ (*m/z* 1147). The [NEt_4][$Co(CO)_4$] was added to provide a cation source for subsequent isolation of anionic clusters and to provoke reaction between the neutral reagents. The dominant ESMS signals after reaction corresponded to the two M_4 clusters, with the intended cluster present at low intensity. The presence of [$Co_7Ge(CO)_{20}$]$^-$ and [$Co_7Ge_2(CO)_{21}$]$^-$ was attributed to reaction of μ_4-Ge[$Co_2(CO)_7$]$_2$ with [$Co(CO)_4$]$^-$ as reported in the previous chapter. The solution was reduced in volume and cooled to –20°C resulting in the formation of a deep red crystalline product. ES mass spectra of the crystals displayed signals from [$Co_3Fe(CO)_{12}$]$^-$, [$CoFe_3(CO)_{13}$]$^-$ and [$Co_3Fe_3Ge(CO)_{18}$]$^-$ though a X-ray crystal structure determination characterised the material as [NEt_4][$CoFe_3(CO)_{13}$] (presented in Chapter 8).

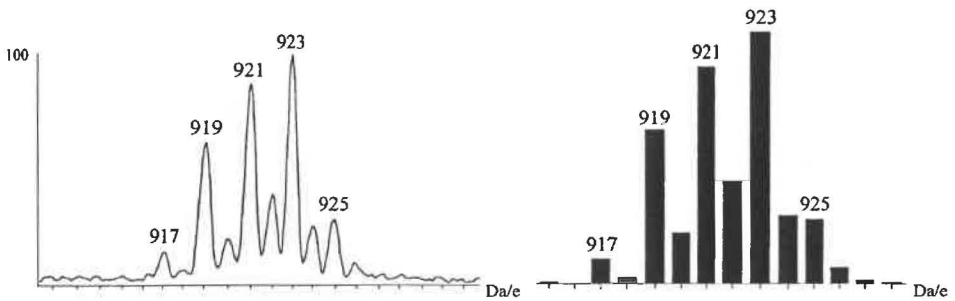

Figure 5.10 – The observed and calculated isotope patterns for [$Co_3Fe_3Ge(CO)_{18}$]$^-$.

The reaction between μ_4-Ge[$Co_2(CO)_7$]$_2$ and $Fe_3(CO)_{12}$ provided a more systematic synthesis of [$Co_3Fe_3Ge(CO)_{18}$]$^-$ {compared to the [$Fe_2(CO)_8$]$^{2-}$ route} though the hexa-nuclear cluster remained a minor product of the reaction. ESMS analysis indicated predominant formation of [$Co_3Fe(CO)_{12}$]$^-$ and [$CoFe_3(CO)_{13}$]$^-$, attributed to reaction between $Fe_3(CO)_{12}$ and [$Co(CO)_4$]$^-$.

5.2.3 Reaction of μ_4-Ge[$Co_2(CO)_7$]$_2$ with [PPN][$HFe(CO)_4$]

The reaction between μ_4-Ge[$Co_2(CO)_7$]$_2$ and [$HFe(CO)_4$]$^-$ was performed in a similar manner to that reported for [$Fe_2(CO)_8$]$^{2-}$. ESMS analysis of the CH_2Cl_2 solution immediately after [$HFe(CO)_4$]$^-$ addition indicated the presence of [$Co(CO)_4$]$^-$ (*m/z* 171), [$HFe_3(CO)_{11}$]$^-$ (*m/z* 477), [$Co_3FeGe(CO)_{13}$]$^-$ (*m/z* 671), [$CoFe_3Ge(CO)_{14}$]$^-$ (*m/z* 693), [$Co_3FeGe(CO)_{14}$]$^-$ (*m/z* 699), [$Co_3Fe_2Ge(CO)_{15}$]$^-$ (*m/z* 783) and [$Co_3Fe_2Ge(CO)_{16}$]$^-$ (*m/z* 811), though the GeM_5 signals were of limited intensity. The reaction mixture was stirred over a 4 hour period with no further change in the anionic species present (Figure

5.11). $[HFe_3(CO)_{11}]^-$ was noted as a by-product in the synthesis of $[HFe(CO)_4]^-$ (outlined in Chapter 2) and its presence does not imply formation during reaction.

The reaction was also followed by IR analysis, with the spectra altering from that indicative of μ_4-Ge[$Co_2(CO)_7$]$_2$ [2081 (s), 2063 (s), 2033 (m,br), 1840 (w,br) cm^{-1}] to a pattern similar to that observed in the $[Fe_2(CO)_8]^{2-}$ reaction [2049 (w), 2035 (m), 2016 (s), 1997 (m), 1965 (w), 1886 (s,br) cm^{-1}]. Only the $[Co(CO)_4]^-$ signal (1886 cm^{-1}) is readily assignable, with the remaining signals similar to those reported for other anionic heteronuclear germanium clusters (refer to Section 5.2.1).

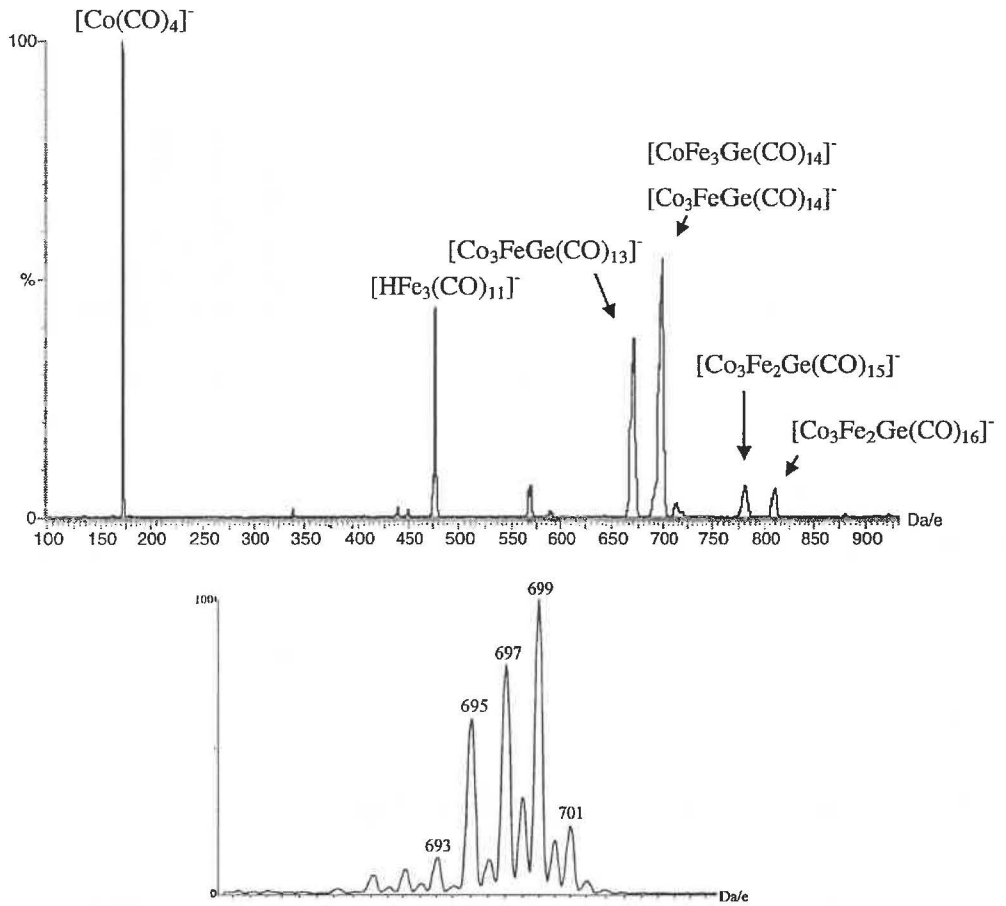

Figure 5.11 – The ES mass spectrum (-ve ion, 5 cV) of the reaction between μ_4-Ge[$Co_2(CO)_7$]$_2$ and $[HFe(CO)_4]^-$ (upper), and the isotope pattern for $[Co_3FeGe(CO)_{14}]^-$ (lower).

The generation of $[Co_3FeGe(CO)_{13}]^-$ in high yield was expected using the mononuclear anionic reagent. More curious are the $[CoFe_3Ge(CO)_{14}]^-$ and $[Co_3FeGe(CO)_{14}]^-$ anions. The former was identified in the reaction with $[Fe_2(CO)_8]^{2-}$ and, for this reaction, was attributed to generation of the di-nuclear iron reagent *in situ* {though synthesis of this

reagent from $[HFe(CO)_4]^-$ is unclear}. The 68 electron $[Co_3FeGe(CO)_{14}]^-$ species is more unusual, implying a 'spiro' configuration (Figure 5.12) rather than a MEM_3 arrangement {$[Co_3FeGe(CO)_{14}]^-$ is isoelectronic to μ_4-Ge[$Co_2(CO)_7$]$_2$}. The mechanism by which a heteronuclear 'spiro' cluster is produced from a homonuclear 'spiro' starting reagent is unknown. The formation of the $[Co_3Fe_2Ge(CO)_x]^-$ (x = 15, 16) ions in this reaction was also unexpected as they require the presence of a di-nuclear iron reagent. This reagent is presumably formed *in situ* during reaction, most likely from $[Fe(CO)_4]^{2-}$.

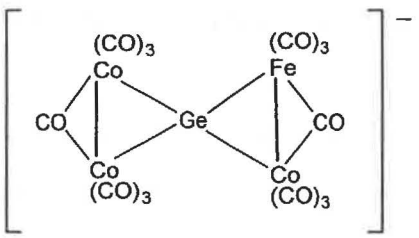

Figure 5.12 – A proposed arrangement for $[Co_3FeGe(CO)_{14}]^-$.

The reaction between μ_4-Ge[$Co_2(CO)_7$]$_2$ and $[HFe(CO)_4]^-$ resulted in formation of $[Co_3FeGe(CO)_{13}]^-$ and $[CoFe_3Ge(CO)_{14}]^-$, identical to those observed in extended reaction with $[Fe_2(CO)_8]^{2-}$. There was evidence for the formation of a $[Co_3FeGe(CO)_{14}]^-$ species {isoelectronic and presumably isostructural with μ_4-Ge[$Co_2(CO)_7$]$_2$}, and for the formation of two higher-nuclearity $[Co_3Fe_2Ge(CO)_x]^-$ (x = 15, 16) clusters, identical to those detected in the reaction with $[Fe_2(CO)_8]^{2-}$. The formation of anionic clusters containing di-nuclear iron units is attributed to a condensation reaction of the iron precursor *in situ*.

5.2.4 Reaction of μ_4-Ge[$Co_2(CO)_7$]$_2$ with $[NEt_4][HFe_3(CO)_{11}]$

The reaction between μ_4-Ge[$Co_2(CO)_7$]$_2$ and $[HFe_3(CO)_{11}]^-$ was examined in a similar manner to those discussed above. A CH_2Cl_2 solution of the two reagents was stirred at room temperature for 2 hours and monitored by ESMS. A signal corresponding to $[HFe_3(CO)_{11}]^-$ (*m/z* 477) was present throughout but there was no evidence for the formation of any heteronuclear clusters. The solution was heated to reflux to provoke reaction, leading to generation of $[Co(CO)_4]^-$ (*m/z* 171) and subsequent production of $[Co_7Ge(CO)_{20}]^-$ (*m/z* 1047) and $[Co_7Ge_2(CO)_{21}]^-$ (*m/z* 1147). These clusters were noted

in reaction of μ_4-Ge[$Co_2(CO)_7$]$_2$ with [$Co(CO)_4$]$^-$ and are unlikely to be an effect of [$HFe_3(CO)_{11}$]$^-$.

The absence of heteronuclear clusters from this reaction indicates the [$HFe_3(CO)_{11}$]$^-$ anion is unreactive towards μ_4-Ge[$Co_2(CO)_7$]$_2$ under these conditions. The generation of [$Co(CO)_4$]$^-$ is attributed to rearrangement of the germanium precursor, as are the two higher-nuclearity clusters.

5.2.5 Reaction of μ_4-Si[$Co_2(CO)_7$]$_2$ with [NEt_4]$_2$[$Fe_2(CO)_8$]

Following the identification of several heteronuclear germanium clusters from the reaction between μ_4-Ge[$Co_2(CO)_7$]$_2$ and [$Fe_2(CO)_8$]$^{2-}$, the equivalent reaction using the silicon analogue was examined.

Results and Discussion

ESMS analysis of a stirred CH_2Cl_2 solution of the two reagents indicated no reaction. A signal corresponding to [$Co(CO)_4$]$^-$ (*m/z* 171) was detected but this was present in the analysis of μ_4-Si[$Co_2(CO)_7$]$_2$ prior to [$Fe_2(CO)_8$]$^{2-}$ addition and attributed to partial decomposition of the starting reagent during storage. The solution was heated to reflux in an attempt to provoke reaction, producing signals corresponding to [$Co_3Fe(CO)_{12}$]$^-$ (*m/z* 569), [$Co_5Si(CO)_{16}$]$^-$ (*m/z* 771) and [$Co_7Si(CO)_{21}$]$^-$ (*m/z* 1029). The higher-nuclearity cluster anions were attributed to reaction between μ_4-Si[$Co_2(CO)_7$]$_2$ and [$Co(CO)_4$]$^-$ (as discussed in the previous chapter). The reaction was halted after 4 hours at reflux with no heteronuclear silicon clusters detected.

Examination by ESMS indicated no reaction between μ_4-Si[$Co_2(CO)_7$]$_2$ and [$Fe_2(CO)_8$]$^{2-}$, contrasting markedly with the analogous germanium reaction. The only high-nuclearity clusters observed were those associated with reaction between μ_4-Si[$Co_2(CO)_7$]$_2$ and [$Co(CO)_4$]$^-$.

5.2.6 Reaction of μ_4-Ge[$Co_2(CO)_7$]$_2$ with [PPN][$Mn(CO)_5$]

The reaction between μ_4-Ge[$Co_2(CO)_7$]$_2$ and $[Mn(CO)_5]^-$ has been reported, with spectroscopic identification of $(CO)_5MnGeCo_3(CO)_9$ [9]. The reaction was presumed to proceed through initial formation of $(CO)_4CoGeCo_3(CO)_9$, followed by substitution of the apical $Co(CO)_4$ group (displayed in Scheme 5.2).

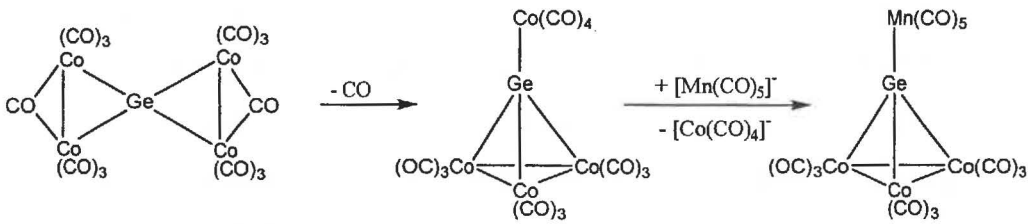

Scheme 5.2 – The synthesis of $(CO)_5MnGeCo_3(CO)_9$.

ESMS monitoring of the reaction in refluxing CH_2Cl_2 displayed a general deterioration in spectral quality over the course of 3 hours. Signals attributed to μ_4-Ge[$Co_2(CO)_7$] adducts (discussed in Section 4.3) were identified initially but decreased in intensity with time. Likewise, the $[Co(CO)_4]^-$ signal (*m/z* 171) was absent initially but came to dominate the spectra. There was no indication of high-nuclearity cluster formation over 5 hours at reflux.

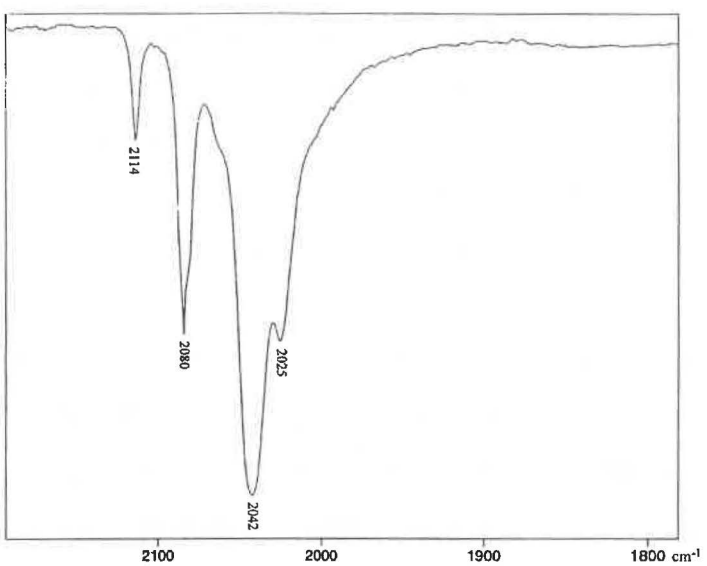

Figure 5.13 – The IR spectrum of $(CO)_5MnGeCo_3(CO)_9$ {ν_{CO}, CH_2Cl_2 – $[Co(CO)_4]^-$ signal subtracted}.

The lack of ESMS signals in this reaction was attributed to the formation of the 'electrospray-invisible' $(CO)_5MnGeCo_3(CO)_9$ cluster. This cluster, analogous to $(CO)_4CoGeCo_3(CO)_9$, is neutral and appeared resistant to ionisation under standard ESMS conditions. The formation of $(CO)_5MnGeCo_3(CO)_9$ was indicated by changes in the IR spectra from signals indicative of μ_4-Ge[$Co_2(CO)_7$]$_2$ [2081 (s), 2063 (s), 2033 (m,br), 1842 (w,br) cm^{-1}] to signals typical of a MEM_3 arrangement [2114 (w), 2080 (m), 2042 (s), 2025 (m,sh), 1891 (s) cm^{-1}], though these changes may indicate formation of either $(CO)_5MnGeCo_3(CO)_9$ [2115 (w), 2078 (m), 2041 (vs), 2022 (ms) cm^{-1} [9]] or $(CO)_4CoGeCo_3(CO)_9$ [2112 (vw), 2083 (s), 2045 (vs), 2029 (mw), 2008 (w), 1991 (vw) cm^{-1} [16]], both of which are 'electrospray-invisible' and difficult to distinguish spectroscopically. The assignment as the former cluster was based on the absence of the higher-nuclearity germanium cobalt species {$[Co_7Ge(CO)_{20}]^-$, $[Co_7Ge_2(CO)_{21}]^-$, $[Co_{10}Ge_2(CO)_{24}]^{2-}$} which result from reaction between $(CO)_4CoGeCo_3(CO)_9$ and $[Co(CO)_4]^-$.

5.2.7 Reaction of μ_4-Ge[$Co_2(CO)_7$]$_2$ with [NEt_4][$Fe(CO)_2(\eta^5$-$C_5H_5)$]

The reaction between μ_4-Ge[$Co_2(CO)_7$]$_2$ and $[Fe(CO)_2(\eta^5$-$C_5H_5)]^-$ was carried out in a similar manner to the those discussed above. Spectra acquired immediately after $[Fe(CO)_2(\eta^5$-$C_5H_5)]^-$ addition were composed of signals attributed to $[Co(CO)_4]^-$ (*m/z* 171) and μ_4-Ge[$Co_2(CO)_7$]$_2$ adducts, with a decrease in the intensity of the μ_4-Ge[$Co_2(CO)_7$]$_2$ signals being the only spectral change noted over 15-20 minutes. Heating the solution to reflux had little effect, though low intensity signals were observed for the higher-nuclearity clusters, $[Co_7Ge(CO)_{20}]^-$ (*m/z* 1047) and $[Co_7Ge_2(CO)_{21}]^-$ (*m/z* 1147). The reaction was halted after 2 hours at reflux without ESMS evidence for heteronuclear cluster formation.

Infra-red spectra acquired at the end of the reaction were dominated by a signal attributable to $[Co(CO)_4]^-$ at 1889 cm^{-1} (in agreement with ESMS detection), with a series of signals identified at higher wavenumber [2035 (s), 2029 (sh), 2005 (m), 1990 (s,br) cm^{-1}] similar to those reported for $(CO)_2(\eta^5$-$C_5H_5)FeGeCo_3(CO)_9$ [2081 (m), 2038 (s), 2031 (sh), 2008 (m), 1992 (s), 1983 (s) cm^{-1} [12]].

---

[16] G. Schmid and G. Etzrodt, *J. Organomet. Chem.*, 1977, **137**, 367.

The only identified product of the reaction between μ_4-Ge[$Co_2(CO)_7$]$_2$ and [$Fe(CO)_2(\eta^5$-$C_5H_5)$]$^-$ was a MEM_3 cluster, assigned as $(CO)_2(\eta^5$-$C_5H_5)FeGeCo_3(CO)_9$ on the basis of IR analysis. The anionic clusters detected were homonuclear germanium cobalt species produced by reaction between μ_4-Ge[$Co_2(CO)_7$]$_2$ and [$Co(CO)_4$]$^-$. The $(CO)_2(\eta^5$-$C_5H_5)FeGeCo_3(CO)_9$ cluster appeared immune to further reaction, contrasting markedly with the isoelectronic $(CO)_4CoGeCo_3(CO)_9$ cluster reported in the previous chapter.

5.2.8 Reaction of μ_4-Ge[$Co_2(CO)_7$]$_2$ with [NEt_4][$Fe(CO)_3(NO)$]

The success in monitoring the reactions involving simple iron carbonyl reagents led to analysis of the equivalent reaction involving [$Fe(CO)_3(NO)$]$^-$, a direct analogue of [$Co(CO)_4$]$^-$. The reaction was carried out in a similar manner to those discussed above, using ESMS to monitor the reaction. Spectra acquired of the stirred CH_2Cl_2 solution of the two reagents after 20 minutes were dominated by a signal attributable to [$Co_3FeGe(CO)_{13}$]$^-$ (*m/z* 671), with less intense ions observed at *m/z* 699 {corresponding to [$Co_3FeGe(CO)_{14}$]$^-$} and *m/z* 648 (Figure 5.14). The first two signals were identified in the equivalent reaction with [$HFe(CO)_4$]$^-$ (discussed in Section 5.2.3) whereas the *m/z* 648 signal was more unusual. From the mass and isotope profile (which indicated the presence of iron), the ion was assigned as [$Co_2Fe_2Ge(CO)_8(NO)_4$]$^-$. This composition initially appeared implausible but was the only composition identified which accounted for the mass and isotope pattern observed. [$Co_2Fe_2Ge(CO)_8(NO)_4$]$^-$ corresponds to a paramagnetic 67 electron species, highly unusual for EM_4 clusters. Generation of this cluster species requires exchange of nitrosyl ligands between metal centres, a phenomenon which has precedent in the formation of $Fe(CO)_2(NO)_2$ in reactions of [$Fe(CO)_3(NO)$]$^-$ [17]. Nitrosyl exchange would presumably also result in formation of [$Fe(CO)_4$]$^{2-}$ *in situ* (Scheme 5.3), whose reaction with μ_4-Ge[$Co_2(CO)_7$]$_2$ would generate the [$Co_3FeGe(CO)_x$]$^-$ (x = 13, 14) ions.

[17] K.H. Pannell, Y-J. Chen, K. Belknap, C.C. Wu, I. Bernal, M.W. Creswick and H.N. Huang, *Inorg. Chem.*, 1983, **22**, 418.

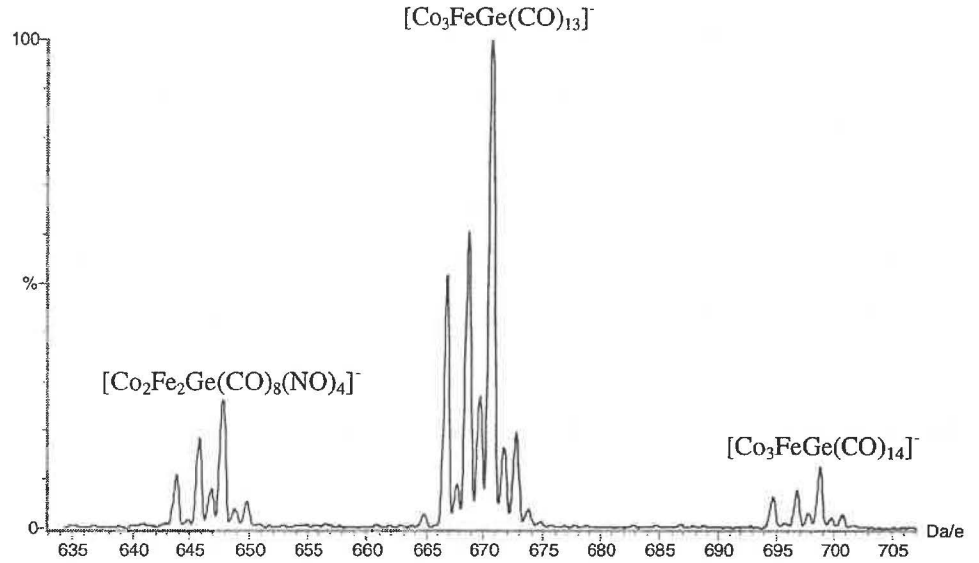

Figure 5.14 – The isotope patterns for $[Co_2Fe_2Ge(CO)_8(NO)_4]^-$, $[Co_3FeGe(CO)_{13}]^-$ and $[Co_3FeGe(CO)_{14}]^-$.

$$2\ [Fe(CO)_3(NO)]^- \longrightarrow [Fe(CO)_4]^{2-} + Fe(CO)_2(NO)_2$$

Scheme 5.3 – Nitrosyl exchange between metal centres.

Generation of $Fe(CO)_2(NO)_2$ *in situ* should be detectable spectroscopically, with signals reported for the carbonyl (2100-2040 cm^{-1}) and nitrosyl ligands (1810-1750 cm^{-1})[17]. However, IR spectra of the solution were dominated by signals identical to those found for the $[Fe_2(CO)_8]^{2-}$ and $[HFe(CO)_4]^-$ reactions [2032 (m,sh), 2018 (s), 1999 (m), 1889 (s,br) cm^{-1}], indicative of an anionic heteronuclear germanium cluster. The signals observed were attributed to $[Co_3FeGe(CO)_{13}]^-$, the dominant anionic reaction product observed by ESMS.

5.2.9 Reaction of μ_4-Ge[$Co_2(CO)_7$]$_2$ with [PPN][$Mo(CO)_3(\eta^5$-$C_5H_5)$]

Continuing the series of attempted redox condensation reactions, the reaction between μ_4-Ge[$Co_2(CO)_7$]$_2$ and $[Mo(CO)_3(\eta^5\text{-}C_5H_5)]^-$ was examined. Monitoring by ESMS indicated reaction of μ_4-Ge[$Co_2(CO)_7$]$_2$ and formation of $[Co(CO)_4]^-$ (*m/z* 171) without evidence for the formation of any heteronuclear group 14 clusters. The solution was heated to reflux to provoke cluster formation with similar results {i.e. reaction of μ_4-Ge[$Co_2(CO)_7$]$_2$ and formation of $[Co(CO)_4]^-$ without evidence for higher-nuclearity cluster formation}. In one instance, a higher-nuclearity cluster signal was detected at

m/z 1221 attributed to $[Co_6MoGe_2(CO)_{20}(\eta^5\text{-}C_5H_5)]^-$ (Figure 5.15), isoelectronic (114 valence-electrons) to $[Co_7Ge_2(CO)_{21}]^-$ and predicted to display a similar atomic arrangement [with $Mo(CO)_2(\eta^5\text{-}C_5H_5)$ replacing a $Co(CO)_3$ unit in either the unique bridging position or within the Co_3 plane – Figures 5.16a and b]. Substitution at both apical and basal locations has been identified previously[10]. Basal substitution is perhaps more likely as there are no known examples of a $Mo(CO)_2(\eta^5\text{-}C_5H_5)$ group bridging two cluster units.

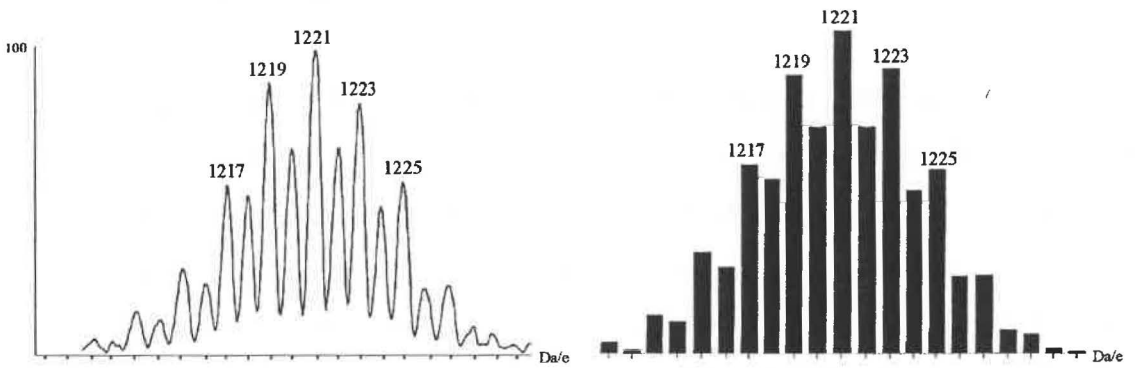

Figure 5.15 – The observed and calculated isotope patterns for $[Co_6MoGe_2(CO)_{20}(\eta^5\text{-}C_5H_5)]^-$.

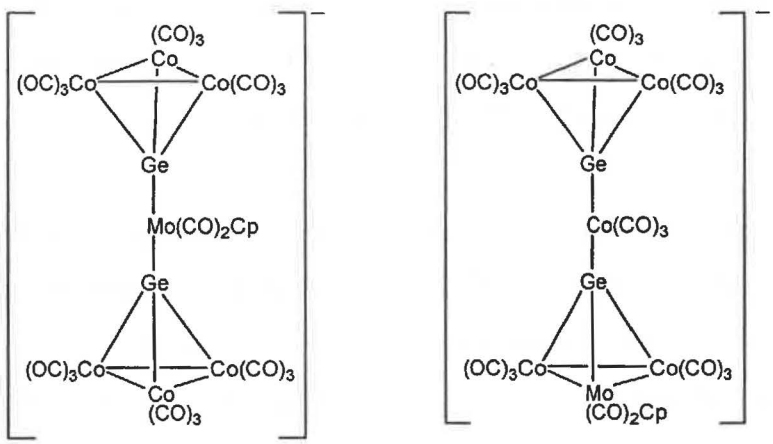

Figure 5.16 – Two possible structures of $[Co_6MoGe_2(CO)_{20}(\eta^5\text{-}C_5H_5)]^-$.

IR analysis of the solution after reaction indicated the presence of a neutral MEM_3 species [2042 (sh), 2031 (s), 2019 (s), 1980 (m), 1890 (s) cm^{-1}], a pattern similar in some respects to that reported for $(CO)_3(\eta^5\text{-}C_5H_5)MoGeCo_3(CO)_9$ [2082 (m), 2034 (vs), 2023 (sh), 2009 (s), 1993 (s), 1968 (m), 1944 (m) cm^{-1} [13]] and $(CO)_3(\eta^5\text{-}C_5H_5)MoGeCo_2Mo(CO)_8(\eta^5\text{-}C_5H_5)$ [2054 (m), 2022 (vs), 2006 (s), 1993 (m), 1980 (s), 1964 (s), 1956 (m), 1942 (m), 1933 (m), 1871 (m) cm^{-1} [13]] in addition to $[Co(CO)_4]^-$.

The dominant product of this reaction was a MEM_3 cluster, presumed to be $(CO)_3(\eta^5\text{-}C_5H_5)MoGeCo_3(CO)_9$. The inability of this cluster to ionise under standard ESMS conditions hampered unambiguous assignment, though facile production of $(CO)_3(\eta^5\text{-}C_5H_5)MoGeCo_3(CO)_9$ from $(CO)_4CoGeCo_3(CO)_9$ has been reported[10]. The presence of a higher-nuclearity $[Co_6MoGe_2(CO)_{20}(\eta^5\text{-}C_5H_5)]^-$ cluster was noted in one instance but synthesis was found to be irreproducible and the cluster was unable to be isolated.

5.2.10 Attempted Reaction of μ_4-Ge[$Co_2(CO)_7$]$_2$ with [PPN][$Ir(CO)_4$]

The reaction between μ_4-Ge[$Co_2(CO)_7$]$_2$ and $[Ir(CO)_4]^-$ has not been examined previously and there are no reported examples of Ge-Ir bond formation. The two reagents were stirred in CH_2Cl_2 at ambient temperature, using ESMS to monitor the formation of cluster products. Analysis of the solution immediately after addition indicated the presence of $[Ir(CO)_4]^-$ (*m/z* 305) and formation of $[HIr_4(CO)_{11}]^-$ (*m/z* 1079). Over a 2 hour period, complete conversion of $[Ir(CO)_4]^-$ to $[HIr_4(CO)_{11}]^-$ was noted, without evidence of reaction with μ_4-Ge[$Co_2(CO)_7$]$_2$. Heating the solution to reflux produced no mixed cobalt/iridium clusters but rather generated $[Co(CO)_4]^-$ (*m/z* 171), $[Co_7Ge(CO)_{20}]^-$ (*m/z* 1047) and $[Co_7Ge_2(CO)_{21}]^-$ (*m/z* 1147), the latter of which result from reaction of μ_4-Ge[$Co_2(CO)_7$]$_2$ and $[Co(CO)_4]^-$.

The ESMS results from this experiment indicate no reaction occurred between the germanium and iridium reagents. $[Ir(CO)_4]^-$ preferentially underwent condensation to $[HIr_4(CO)_{11}]^-$ rather than reaction with μ_4-Ge[$Co_2(CO)_7$]$_2$. The germanium/transition metal clusters identified all corresponded to reaction between μ_4-Ge[$Co_2(CO)_7$]$_2$ and $[Co(CO)_4]^-$ rather than involving the iridium reagent.

5.2.11 Attempted Reaction of μ_4-Ge[$Co_2(CO)_7$]$_2$ with [PPN][$Co_6N(CO)_{15}$]

The availability of $[PPN][Co_6N(CO)_{15}]$ (the synthesis and thermolysis of which are discussed in Chapter 6) allowed examination of the reaction between the nitrido cluster and μ_4-Ge[$Co_2(CO)_7$]$_2$.

An equimolar solution of the two metal carbonyl reagents was refluxed in CH_2Cl_2 for 4 hours and monitored by ESMS. Spectra were dominated throughout by a signal

corresponding to $[Co_6N(CO)_{15}]^-$ (*m/z* 788), with $[Co(CO)_4]^-$ (*m/z* 171) detected after 15-30 minutes, presumably a result of thermal treatment of μ_4-Ge[$Co_2(CO)_7$]$_2$. Higher-nuclearity anionic products were detected (after 1 hour) corresponding to $[Co_7Ge(CO)_{20}]^-$ and $[Co_7Ge_2(CO)_{21}]^-$ (*m/z* 1047 and 1147 respectively), their presence attributed to reaction between μ_4-Ge[$Co_2(CO)_7$]$_2$ and $[Co(CO)_4]^-$. The reaction was abandoned after 4 hours without evidence for reaction between μ_4-Ge[$Co_2(CO)_7$]$_2$ and $[Co_6N(CO)_{15}]^-$.

There was no evidence for reaction between the two reagents. The nitrido cluster was present throughout reaction (determined by ESMS analysis) and the cluster species produced corresponded to reaction between μ_4-Ge[$Co_2(CO)_7$]$_2$ and $[Co(CO)_4]^-$ rather than involving $[Co_6N(CO)_{15}]^-$.

5.3 Conclusions

An objective of the research reported in this chapter was the identification and isolation of novel heteronuclear group 14 clusters. Several novel GeM_5 anionic clusters were identified in the reaction between μ_4-Ge[$Co_2(CO)_7$]$_2$ and $[Fe_2(CO)_8]^{2-}$, though the complexity of the reaction hampered isolation of these species. One of these GeM_5 clusters, $[Co_3Fe_2Ge(CO)_{17}]^-$, is isoelectronic (and presumably isostructural) to $[Co_5Ge(CO)_{16}]^-$ while the structures of the remaining GeM_5 species are unknown. The previously isolated heteronuclear germanium clusters, $[Co_5Fe_2Ge_2(CO)_{22}]^-$ and $[CoFe_3Ge(CO)_{14}]^-$, were also identified by ESMS. A highly unusual $[Co_3Fe_3Ge(CO)_{18}]^-$ cluster was also detected, though more systematically produced by reaction between μ_4-Ge[$Co_2(CO)_7$]$_2$ and $Fe_3(CO)_{12}$ in the presence of $[Co(CO)_4]^-$. Attempted isolation of this cluster resulted in crystallisation and structural characterisation of $[NEt_4][CoFe_3(CO)_{13}]$ (refer to Chapter 8).

The analogous reaction with $[HFe(CO)_4]^-$ predominantly generated three heteronuclear species; $[Co_3FeGe(CO)_{13}]^-$, $[CoFe_3Ge(CO)_{14}]^-$ and $[Co_3FeGe(CO)_{14}]^-$. The higher-nuclearity $[Co_5Fe_2Ge(CO)_x]^-$ (x = 15, 16) clusters were also identified, attributed to formation of $[Fe_2(CO)_8]^{2-}$ *in situ*. The unusual $[Co_3FeGe(CO)_{14}]^-$ species is isoelectronic to μ_4-Ge[$Co_2(CO)_7$]$_2$.

Attempted reaction between μ_4-Si[$Co_2(CO)_7$]$_2$ and $[Fe_2(CO)_8]^{2-}$ produced the same series of cluster species as observed in reaction between μ_4-Si[$Co_2(CO)_7$]$_2$ and $[Co(CO)_4]^-$, indicating a significant difference in reactivity between the silicon and germanium reagents. Similarly, attempted reaction between μ_4-Ge[$Co_2(CO)_7$]$_2$ and $[HFe_3(CO)_{11}]^-$ yielded clusters identical to those observed in the reaction between μ_4-Ge[$Co_2(CO)_7$]$_2$ and $[Co(CO)_4]^-$, indicating the tri-nuclear iron reagent was significantly less reactive than the mono- and di-nuclear species.

Reaction between μ_4-Ge[$Co_2(CO)_7$]$_2$ and $[Fe(CO)_3(NO)]^-$ yielded similar clusters to those found for $[HFe(CO)_4]^-$, though an additional signal attributed to $[Co_2Fe_2Ge(CO)_8(NO)_4]^-$ was noted. The cluster was presumably generated from $Fe(CO)_2(NO)_2$ formed *in situ*.

For the remaining anionic transition metal reagents, reaction with μ_4-Ge[$Co_2(CO)_7$]$_2$ yielded $LMGeCo_3(CO)_9$ [ML = $Mn(CO)_5$, $Fe(CO)_2(\eta^5\text{-}C_5H_5)$, $Mo(CO)_3(\eta^5\text{-}C_5H_5)$] compounds, identified on the basis of IR analysis. The clusters are produced through replacement of $Co(CO)_4$ from $(CO)_4CoGeCo_3(CO)_9$. The cluster products are neutral and 'electrospray-invisible', hampering the analysis of these reactions. Unlike $(CO)_4CoGeCo_3(CO)_9$, the $LMGeCo_3(CO)_9$ compounds appear unreactive. The only high-nuclearity cluster identified from these reactions was $[Co_6MoGe_2(CO)_{20}(\eta^5\text{-}C_5H_5)]^-$, isoelectronic to $[Co_7Ge_2(CO)_{21}]^-$, though synthesis of this cluster was found to be irreproducible and all attempts at isolation were unsuccessful.

Finally, ESMS analysis of solutions of μ_4-Ge[$Co_2(CO)_7$]$_2$ with $[Ir(CO)_4]^-$ and $[Co_6N(CO)_{15}]^-$ provided no evidence for reaction between the reagents. The pair of high-nuclearity clusters, $[Co_7Ge(CO)_{20}]^-$ and $[Co_7Ge_2(CO)_{21}]^-$, were detected in each case, attributable to reaction between μ_4-Ge[$Co_2(CO)_7$]$_2$ and $[Co(CO)_4]^-$ rather than involving the iridium or nitrido anions.

5.4 Experimental

The syntheses of μ_4-E[$Co_2(CO)_7$]$_2$ and the anionic transition metal reagents were reported in Chapter 2.

Reaction between μ_4-Ge[$Co_2(CO)_7$]$_2$ and [NEt_4]$_2$[$Fe_2(CO)_8$]

To a CH_2Cl_2 solution (15 mL) of μ_4-Ge[$Co_2(CO)_7$]$_2$ (0.03 g, 0.04 mmol) was added [NEt_4]$_2$[$Fe_2(CO)_8$] (0.025 g, 0.04 mmol) and the mixture stirred at room temperature for 4 hours. Over this time, the generation of the following anionic species was noted: [$Co(CO)_4$]$^-$ (*m/z* 171), [$Co_3Fe(CO)_{12}$]$^-$ (*m/z* 569), [$CoFe_3(CO)_{13}$]$^-$ (*m/z* 591), [$Co_3FeGe(CO)_{13}$]$^-$ (*m/z* 671), [$CoFe_3Ge(CO)_{14}$]$^-$ (*m/z* 693), [$Co_3Fe_2Ge(CO)_{15}$]$^-$ (*m/z* 783), [$Co_3Fe_2Ge(CO)_{16}$]$^-$ (*m/z* 811), [$CoFe_4Ge(CO)_{17}$]$^-$ (*m/z* 833), [$Co_3Fe_2Ge(CO)_{17}$]$^-$ (*m/z* 839), [$Co_7Ge_2(CO)_{21}$]$^-$ (*m/z* 1147) and [$Co_5Fe_2Ge_2(CO)_{22}$]$^-$ (*m/z* 1169). The GeM_5 and Ge_2M_7 clusters were detected within 30-45 minutes of addition, with extended reaction times producing the M_4 and GeM_4 clusters.

Repetition of the reaction on a similar scale at reflux led to formation of the M_4 and GeM_4 clusters within a shorter period of time (20-30 minutes), along with evidence for the generation of [$Co_3Fe_3Ge(CO)_{18}$]$^-$ (*m/z* 923), [$Co_7Ge_2(CO)_{21}$]$^-$ and [$Co_5Fe_2Ge_2(CO)_{22}$]$^-$. The low signal intensity of the higher-nuclearity clusters precluded their isolation.

Reaction between μ_4-Ge[$Co_2(CO)_7$]$_2$ and $Fe_3(CO)_{12}$

A mixture of μ_4-Ge[$Co_2(CO)_7$]$_2$ (0.05 g, 0.07 mmol) and $Fe_3(CO)_{12}$ (0.04 g, 0.08 mmol) in CH_2Cl_2 (15 mL) was stirred at ambient temperature for 2 hours without indication of reaction. [NEt_4][$Co(CO)_4$] (0.025 g, 0.08 mmol) was added and the mixture was heated to reflux, with ESMS evidence for formation of [$Co_3Fe(CO)_{12}$]$^-$ (*m/z* 569), [$CoFe_3(CO)_{13}$]$^-$ (*m/z* 591), [$Co_3FeGe(CO)_{13}$]$^-$ (*m/z* 671), [$Co_3Fe_3Ge(CO)_{18}$]$^-$ (*m/z* 923), [$Co_7Ge(CO)_{20}$]$^-$ (*m/z* 1047) and [$Co_7Ge_2(CO)_{21}$]$^-$ (*m/z* 1147). The solution was reduced in volume to *ca.* 2-3 mL and cooled to –20°C, resulting in formation of deep red crystals characterised crystallographically as [NEt_4][$CoFe_3(CO)_{13}$] (refer to Chapter 8).

Reaction between μ_4-Ge[$Co_2(CO)_7$]$_2$ and [PPN][$HFe(CO)_4$]

[PPN][$HFe(CO)_4$] (0.035 g, 0.05 mmol) was added to a CH_2Cl_2 solution (10 mL) of μ_4-Ge[$Co_2(CO)_7$]$_2$ (0.025 g, 0.036 mmol) and stirred at ambient temperature for 3 hours. The presence of $[Co(CO)_4]^-$ (*m/z* 171), $[HFe_3(CO)_{11}]^-$ (*m/z* 477), $[Co_3FeGe(CO)_{13}]^-$ (*m/z* 671), $[CoFe_3Ge(CO)_{14}]^-$ (*m/z* 693), $[Co_3FeGe(CO)_{14}]^-$ (*m/z* 699), $[Co_3Fe_2Ge(CO)_{15}]^-$ (*m/z* 783) and $[Co_3Fe_2Ge(CO)_{16}]^-$ (*m/z* 811) were noted in ESMS analysis of the solution, with spectra dominated by the $[Co_3FeGe(CO)_{14}]^-$ signal.

Attempted reaction between μ_4-Ge[$Co_2(CO)_7$]$_2$ and [NEt_4][$HFe_3(CO)_{11}$]

A CH_2Cl_2 solution (10 mL) containing μ_4-Ge[$Co_2(CO)_7$]$_2$ (0.02 g, 0.029 mmol) and [NEt_4][$HFe_3(CO)_{11}$] (0.035 g, 0.06 mmol) was stirred at room temperature for 3 hours without evidence of reaction. The mixture was heated to reflux with generation of $[Co(CO)_4]^-$ (*m/z* 171), $[Co_7Ge(CO)_{20}]^-$ (*m/z* 1047) and $[Co_7Ge_2(CO)_{21}]^-$ (*m/z* 1147) noted by ESMS. The experiment was abandoned without evidence of reaction between the two starting reagents.

Attempted reaction between μ_4-Si[$Co_2(CO)_7$]$_2$ and [NEt_4]$_2$[$Fe_2(CO)_8$]

To a CH_2Cl_2 solution (10 mL) of μ_4-Si[$Co_2(CO)_7$]$_2$ (0.02 g, 0.030 mmol) was added [NEt_4]$_2$[$Fe_2(CO)_8$] (0.035 g, 0.06 mmol) and the mixture stirred at room temperature for 2 hours without indication of reaction. The mixture was refluxed for 2 hours with generation of $[Co(CO)_4]^-$ (*m/z* 171), $[Co_5Si(CO)_{16}]^-$ (*m/z* 771) and $[Co_7Si(CO)_{21}]^-$ (*m/z* 1029) noted by ESMS. The latter two products were attributed to reaction between μ_4-Si[$Co_2(CO)_7$]$_2$ and $[Co(CO)_4]^-$ rather than involving $[Fe_2(CO)_8]^{2-}$. The reaction was abandoned after 2 hours at reflux without evidence for reaction between μ_4-Si[$Co_2(CO)_7$]$_2$ and $[Fe_2(CO)_8]^{2-}$.

Reaction between μ_4-Ge[$Co_2(CO)_7$]$_2$ and [PPN][$Mn(CO)_5$]

A CH_2Cl_2 solution (10 mL) containing μ_4-Ge[$Co_2(CO)_7$]$_2$ (0.03 g, 0.043 mmol) and [PPN][$Mn(CO)_5$] (0.065 g, 0.089 mmol) was refluxed for 5 hours without evidence for formation of any high-nuclearity clusters. IR spectra acquired after reaction (discussed

in Section 5.2.6) indicate the presence of a MEM_3 compound presumed to be $(CO)_5MnGeCo_3(CO)_9$.

Reaction between μ_4-Ge[$Co_2(CO)_7$]$_2$ and [NEt_4][$Fe(CO)_2(\eta^5$-$C_5H_5)$]

[NEt_4][$Fe(CO)_2(\eta^5$-$C_5H_5)$] (0.02 g, 0.065 mmol) was added to a CH_2Cl_2 solution (10 mL) of μ_4-Ge[$Co_2(CO)_7$]$_2$ (0.02 g, 0.029 mmol) and stirred at room temperature for 1 hour with evidence (by ESMS) for generation of $[Co(CO)_4]^-$ (*m/z* 171). The solution was refluxed for 2 hours with production of $[Co_7Ge(CO)_{20}]^-$ (*m/z* 1047) and $[Co_7Ge_2(CO)_{21}]^-$ (*m/z* 1147) noted {indicative of reaction between of μ_4-Ge[$Co_2(CO)_7$]$_2$ and $[Co(CO)_4]^-$}. IR spectra acquired after reaction indicated the presence of a MEM_3 compound, presumed to be $(CO)_2(\eta^5$-$C_5H_5)FeGeCo_3(CO)_9$.

Reaction between μ_4-Ge[$Co_2(CO)_7$]$_2$ and [NEt_4][$Fe(CO)_3(NO)$]

A CH_2Cl_2 solution (15 mL) containing μ_4-Ge[$Co_2(CO)_7$]$_2$ (0.03 g, 0.043 mmol) and [NEt_4][$Fe(CO)_3(NO)$] (0.025 g, 0.083 mmol) was stirred at ambient temperature for 3 hours with ESMS detection of $[Co(CO)_4]^-$ (*m/z* 171), $[Co_2Fe_2Ge(CO)_8(NO)_4]^-$ (*m/z* 648), $[Co_3FeGe(CO)_{13}]^-$ (*m/z* 671) and $[Co_3FeGe(CO)_{14}]^-$ (*m/z* 699). The dominant signal after 3 hours corresponded to $[Co_3FeGe(CO)_{13}]^-$ and there was no evidence for the formation of higher-nuclearity clusters.

Reaction between μ_4-Ge[$Co_2(CO)_7$]$_2$ and [PPN][$Mo(CO)_3(\eta^5$-$C_5H_5)$]

[PPN][$Mo(CO)_3(\eta^5$-$C_5H_5)$] (0.065 g, 0.089 mmol) was added to a CH_2Cl_2 solution (10 mL) of μ_4-Ge[$Co_2(CO)_7$]$_2$ (0.03 g, 0.043 mmol) and the mixture stirred at room temperature for 2 hours with production of $[Co(CO)_4]^-$ (*m/z* 171) noted. The solution was heated to reflux without generation of high-nuclearity products, though in one case a signal attributed to $[Co_6MoGe_2(CO)_{20}(\eta^5$-$C_5H_5)]^-$ (*m/z* 1221) was detected. IR spectra acquired after reaction indicated the presence of a MEM_3 species, presumed to be $(CO)_3(\eta^5$-$C_5H_5)MoGeCo_3(CO)_9$.

Attempted reaction between μ_4-Ge[$Co_2(CO)_7$]$_2$ and [PPN][$Ir(CO)_4$]

To a CH_2Cl_2 solution (10 mL) of μ_4-Ge[$Co_2(CO)_7$]$_2$ (0.025 g, 0.036 mmol) was added [PPN][$Ir(CO)_4$] (0.030 g, 0.036 mmol) and the solution stirred at ambient temperature for 1 hour. Formation of [$HIr_4(CO)_{11}$]$^-$ (*m/z* 1079) from [$Ir(CO)_4$]$^-$ was noted but there was no evidence for reaction between the two starting reagents. Heating the solution to reflux generated [$Co(CO)_4$]$^-$ (*m/z* 171), [$Co_7Ge(CO)_{20}$]$^-$ (*m/z* 1047) and [$Co_7Ge_2(CO)_{21}$]$^-$ (*m/z* 1147), the latter two signals attributed to reaction between μ_4-Ge[$Co_2(CO)_7$]$_2$ and [$Co(CO)_4$]$^-$. No mixed germanium/iridium compounds were detected.

Attempted reaction between μ_4-Ge[$Co_2(CO)_7$]$_2$ and [PPN][$Co_6N(CO)_{15}$]

A CH_2Cl_2 solution (10 mL) of μ_4-Ge[$Co_2(CO)_7$]$_2$ (0.025 g, 0.036 mmol) and [PPN][$Co_6N(CO)_{15}$] (0.024 g, 0.018 mmol) was stirred at room temperature for 2 hours without evidence for reaction. The solution was refluxed for 2 hours with detection of [$Co(CO)_4$]$^-$ (*m/z* 171), [$Co_7Ge(CO)_{20}$]$^-$ (*m/z* 1047) and [$Co_7Ge_2(CO)_{21}$]$^-$ (*m/z* 1147), along with unreacted [$Co_6N(CO)_{15}$]$^-$ (*m/z* 788). The experiment was abandoned without evidence of reaction between the two starting reagents.

Chapter Six – Synthesis of Group 15/Transition Metal Clusters

6.1 Introduction

Following the successful application of ESMS to the group14/transition metal clusters reported in the preceding chapters, a series of reactions involving group 15 elements were examined. Some of these reactions have been previously reported and various anionic clusters isolated, though in all cases the presence of unidentified cluster products was possible. For this reason, the reactions were re-examined using ESMS to characterise the cluster products.

6.1.1 Group 15/Transition Metal Clusters

The range of transition metal clusters incorporating group 15 elements is extensive and has been reviewed in depth previously[1]. A brief mention of the synthesis and structures of these clusters is provided below, with emphasis on homoleptic carbonyl clusters as these are more relevant to the research documented in this chapter. The discussion is also restricted to higher-nuclearity (M > 4) clusters containing 'bare' group 15 elements (i.e. lacking any organic substituent).

The number and variety of nitrido clusters overshadows that of the remaining group 15 elements in the same manner that carbido clusters dominate group 14/transition metal examples. In all higher-nuclearity clusters, the nitrogen is encapsulated or semi-encapsulated by the transition metal elements. This is noted in the predominance of the square-pyramid structure for EM_5 compounds {e.g. $[M_5N(CO)_{14}]^-$ M = Ru[2,3], Fe[4]}, and the trigonal-prismatic {e.g. $[M_6N(CO)_{15}]^-$ M = Rh[5], Co[6]} and octahedral structures

[1] K.H. Whitmire, *J. Coord. Chem.*, 1988, **17**, 95; K.H. Whitmire, *Adv. Organomet. Chem.*, 1998, **42**, 1.

[2] M.L. Blohm, D.E. Fjare and W.L. Gladfelter, *Inorg. Chem.*, 1983, **22**, 1004.

[3] M.L. Blohm and W.L. Gladfelter, *Organometallics*, 1985, **4**, 45.

[4] M. Tachikawa, J. Stein, E.L. Muetterties, R.G. Teller, M.A. Beno, E. Gebert and J.M. Williams, *J. Am. Chem. Soc.*, 1980, **102**, 6648; A. Gourdon and Y. Jeannin, *J. Organomet. Chem.*, 1985, **290**, 199; R. Hourihane, T.R. Spalding, G. Ferguson, T. Deeny and P. Zanello, *J. Chem. Soc., Dalton Trans.*, 1993, 43.

[5] R. Bonfichi, G. Ciani, A. Sironi and S. Martinengo, *J. Chem. Soc., Dalton Trans.*, 1983, 253.

{$[Co_6N(CO)_{13}]^-$ [7], $[Fe_6N(CO)_{15}]^{3-}$ [8], $[Ru_6N(CO)_{16}]^-$ [2,3], $[Fe_5MN(CO)_{15}]^{2-}$ (M = Rh, Ir[9]), $[Fe_4Rh_2N(CO)_{15}]^-$ [9] and $[Fe_3Mo_3N(CO)_{18}]^{3-}$ [10]} adopted by EM_6 clusters. Capping of the trigonal-prism arrangement to generate the $[Rh_6MN(CO)_{15}]^{2-}$ (M = Co, Rh, Ir[11]) and $[Co_7N(CO)_{15}]^{2-}$ [12] clusters is also known.

Synthesis of higher-nuclearity nitrido clusters is usually performed through thermolysis of a smaller cluster precursor, often $[M_6N(CO)_{15}]^-$ (M = Co, Rh). This unsystematic synthetic method gives rise to various products with little resemblance to the parent cluster {e.g. $[Co_{14}N_3(CO)_{26}]^{3-}$ [13], $[HRh_{12}N_2(CO)_{23}]^{3-}$ [14], $[Rh_{14}N_2(CO)_{25}]^{2-}$ [15], $[Rh_{23}N_4(CO)_{38}]^{3-}$ [16] and $[H_xRh_{28}N_4(CO)_{41}]^{4-}$ [17]}. Treatment of a smaller precursor with basic reagents also generates higher-nuclearity clusters {e.g. $[Co_{10}N_2(CO)_{19}]^{4-}$ [18] was produced from $[Co_6N(CO)_{15}]^-$}. The structures of some higher-nuclearity nitrido clusters can be described with respect to condensed polyhedra {e.g. $[Co_{10}N_2(CO)_{19}]^{4-}$ is composed of two linked Co_6N trigonal prisms (Figure 6.1a) while $[Rh_{14}N_2(CO)_{25}]^{2-}$ adopts a capped cube-octahedron configuration (Figure 6.1b)} but the structures of many larger nitrido clusters are irregular {e.g. $[PtRh_{10}N(CO)_{21}]^{3-}$ [19]}, with the arrangement of metal atoms more comparable to that of the bulk metal than a polyhedral shape.

---

[6] S. Martinengo, G. Ciani, A. Sironi, B.T. Heaton and J. Mason, *J. Am. Chem. Soc.*, 1979, **101**, 7095.

[7] G. Ciani and S. Martinengo, *J. Organomet. Chem.*, 1986, **306**, C49.

[8] R.D. Pergola, C. Bandini, F. Demartin, E. Diana, L. Garlaschelli, P.L. Stanghellini and P. Zanello, *J. Chem. Soc., Dalton Trans.*, 1996, 747.

[9] R.D. Pergola, A. Cinquantini, E. Diana, L. Garlaschelli, F. Laschi, P. Luzzini, M. Manassero, A. Repossi, M. Sansoni, P.L. Stanghellini and P. Zanello, *Inorg. Chem.*, 1997, **36**, 3761.

[10] R.D. Pergola, M. Branchini, A. Fumagalli, L. Garlaschelli, M. Manassero and M. Sansoni, *Eur. J. Inorg. Chem.*, 2000, **39**, 1759.

[11] S. Martinengo, G. Ciani and A. Sironi, *J. Chem. Soc., Chem. Commun.*, 1984, 1577.

[12] G. Ciani, N. Masciocchi, A. Sironi, A. Fumagalli and S. Martinengo, *Inorg. Chem.*, 1992, **31**, 331.

[13] S. Martinengo, G. Ciani and A. Sironi, *J. Organomet. Chem.*, 1988, **358**, C23.

[14] S. Martinengo, G. Ciani and A. Sironi, *J. Chem. Soc., Chem. Commun.*, 1986, 1742.

[15] S. Martinengo, G. Ciani and A. Sironi, *J. Chem. Soc., Chem. Commun.*, 1991, 26.

[16] S. Martinengo, G. Ciani and A. Sironi, *J. Chem. Soc., Chem. Commun.*, 1992, 1405.

[17] A. Fumagalli, S. Martinengo, G. Bernasconi, G. Ciani, D.M. Proserpio and A. Sironi, *J. Am. Chem. Soc.*, 1997, **119**, 1450.

[18] A. Fumagalli, S. Martinengo, M. Tasselli, G. Ciani, P. Macchi and A. Sironi, *Inorg. Chem.*, 1998, **37**, 2826.

[19] S. Martinengo, G. Ciani and A. Sironi, *J. Am. Chem. Soc.*, 1982, **104**, 328.

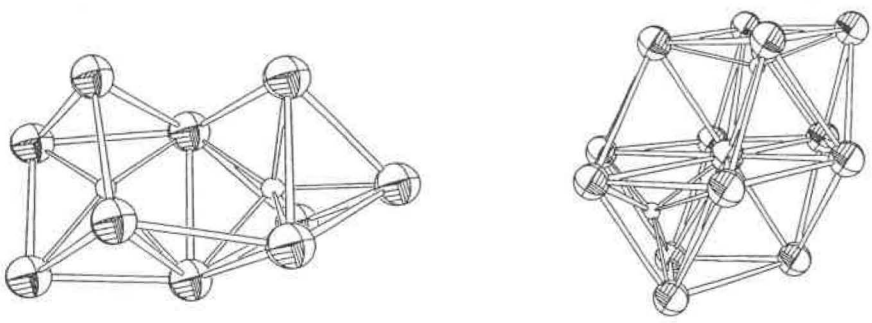

(a) (b)

Figure 6.1 – The core structures of $[Co_{10}N_2(CO)_{19}]^{4-}$ [18] (a) and $[Rh_{14}N_2(CO)_{25}]^{2-}$ [15] (b).

The interstitial locations favoured by nitrogen are less common for the heavier group 15 elements since the increased atomic size precludes encapsulation. This is apparent in the structure of $[Co_6P(CO)_{16}]^-$ [20] (refer to Figure 4.18), where the phosphorus atom is surrounded by an irregular "boat" type arrangement of cobalt atoms [a similar arrangement was also reported for $Co_6P(CO)_{12}(SMe)_3$ [21]]. Parallels between the semi-encapsulated environment for phosphorus and that observed for germanium in $[Co_{10}Ge_2(CO)_{24}]^{2-}$ were discussed in Chapter 4.

The only lower-nuclearity cluster to contain a fully encapsulated phosphorus atom is $[Os_6P(CO)_{18}]^-$ [22]. The encapsulated structure is facilitated by the larger central cavity within a trigonal prism of osmium atoms (as compared to cobalt). The $[Os_6P(CO)_{18}]^-$ cluster is also rare with regards to group 15/transition metal clusters since a rational multi-step synthetic method to the cluster from $Os_3(CO)_{11}(MeCN)$ and PH_3 was reported, rather than the random thermolytic processes usually adopted.

For higher-nuclearity phosphido clusters, an increase in cavity size allows full encapsulation of the main group atom. A preference for structures based around the

[20] P. Chini, G. Ciani, S. Martinengo and A. Sironi, *J. Chem. Soc., Chem. Commun.*, 1979, 188; G. Ciani and A. Sironi, *J. Organomet. Chem.*, 1983, **241**, 385.

[21] X. Hu, Q-W. Li, S-T. Liu, L-P. Zhang and B-S. Wu, *J. Chem. Soc., Chem. Commun.*, 1994, 139.

[22] S.B. Colbran, C.M. Hay, B.F.G. Johnson, F.J. Lahoz, J. Lewis and P.R. Raithby, *J. Chem. Soc., Chem. Commun.*, 1986, 1766; S.B. Colbran, F.J. Lahoz, P.R. Raithby, J. Lewis, B.F.G. Johnson and C.J. Cardin, *J. Chem. Soc., Dalton Trans.*, 1988, 173.

square anti-prism is noted, as observed for $[Ru_8P(CO)_{22}]^-$ [23], $[M_9P(CO)_{21}]^{2-}$ (M = Co[24], Rh[25]) and $[M_{10}P(CO)_{22}]^{3-}$ (M = Co[24], Rh[26]) (Figures 6.2a, b and c).

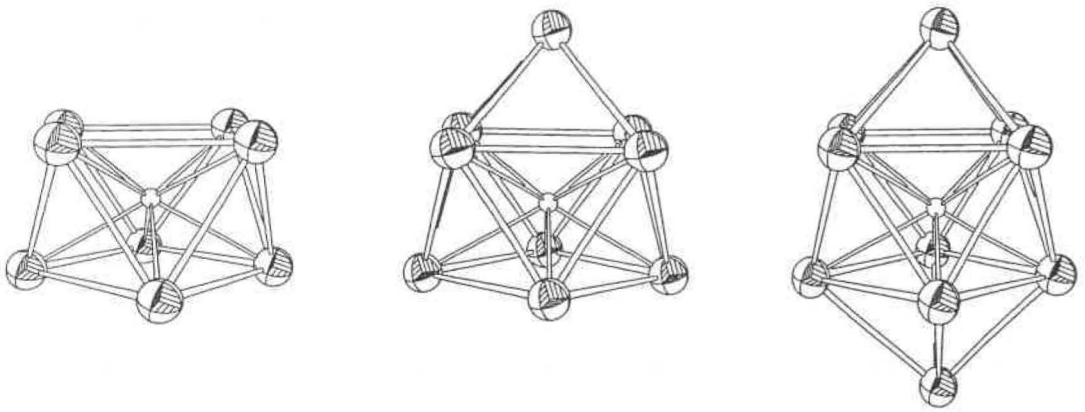

(a) (b) (c)

Figure 6.2 – The core structures of $[Ru_8P(CO)_{22}]^-$ [23] (a), $[Rh_9P(CO)_{21}]^{2-}$ [25] (b) and $[Rh_{10}P(CO)_{22}]^{3-}$ [26] (c).

The larger size of the heavier group 15 elements (As, Sb, Bi) precludes encapsulation in the majority of clusters reported. Rare examples include $[Rh_9As(CO)_{21}]^{2-}$ and $[Rh_{10}As(CO)_{22}]^{3-}$ [27] {isoelectronic and isostructural with the $[M_9P(CO)_{21}]^{2-}$ and $[M_{10}P(CO)_{22}]^{3-}$ (M = Co, Rh) clusters discussed above}, the ESMS analysis of which was reported in Chapter 3. Encapsulation of antimony is known for $[Rh_{12}Sb(CO)_{27}]^{3-}$ [28] (Figure 6.3) and $[Ni_{15}Sb(CO)_{24}]^{2-}$ [29], with the main group atom located within an icosahedron of metal atoms (which is subsequently capped on three adjacent faces in the nickel cluster). There are no known examples of clusters with encapsulated bismuth atoms.

---

[23] M.P. Cifuentes, S.M. Waterman, M.G. Humphrey, G.A. Heath, B.W. Skelton, A.H. White, M.P.S. Perera and M.L. Williams, *J. Organomet. Chem.*, 1998, **565**, 193.

[24] G. Ciani, A. Sironi, S. Martinengo, L. Garlaschelli, R.D. Pergola, P. Zanello, F. Laschi and N. Masciocchi, *Inorg. Chem.*, 2001, **40**, 3905.

[25] J.L. Vidal, W.E. Walker, R.L. Pruett and R.C. Schoening, *Inorg. Chem.*, 1979, **18**, 129.

[26] J.L. Vidal, W.E. Walker and R.C. Schoening, *Inorg. Chem.*, 1981, **20**, 238.

[27] J.L. Vidal, *Inorg. Chem.*, 1981, **20**, 243.

[28] J.L. Vidal and J.M. Troup, *J. Organomet. Chem.*, 1981, **213**, 351; B.T. Heaton, L. Strona, R.D. Pergola, J.L. Vidal and R.C. Schoening, *J. Chem. Soc., Dalton Trans.*, 1983, 1941.

[29] V.G. Albano, F. Demartin, C. Femoni, M.C. Iapalucci, G. Longoni, M. Monari and P. Zanello, *J. Organomet. Chem.*, 2000, **593-594**, 325.

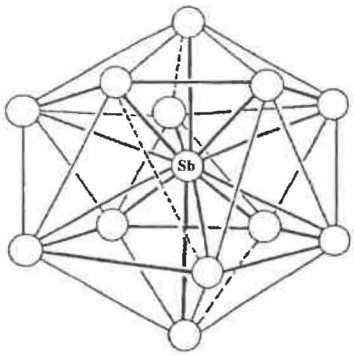

Figure 6.3 – The core structure of $[Rh_{12}Sb(CO)_{27}]^{3-}$ [28].

The heavier main group atoms more commonly adopt positions on the surface of the cluster, effectively vertices of the polyhedra rather than interstices. There are many examples of the heavier elements forming tetrahedral EM_3, 'spiked'-tetrahedral EM_4, trigonal bi-pyramidal E_2M_3, and octahedral E_2M_4 clusters, though being of limited nuclearity these clusters are beyond the scope of this discussion. The higher-nuclearity examples are mainly restricted to icosahedral structures formed with nickel {e.g. $[Ni_{11}Bi_2(CO)_{18}]^{n-}$ [30]}. The $[Ni_{10}(ER)_2(CO)_{18}]^{2-}$ (E = P[31], As[32], Sb[33]) clusters adopt a similar icosahedral geometry, with the ER fragments in vertex positions. The icosahedral clusters are known in both non-centred and nickel-centred forms.

Although of low-nuclearity, mention is made of the $[Co_4E_2(CO)_{11}]^{n-}$ (E = Sb[34], Bi[35]; n = 1, 2) clusters (Figure 6.4a), the structures of which can be considered as bi-capped tetrahedra (or mono-capped trigonal bi-pyramids), but are more often referred to as *nido*-pentagonal bi-pyramids, or *arachno*-dodecahedra. None of the descriptions account for the arrangement observed with respect to electron-counting procedures and

---

[30] V.G. Albano, F. Demartin, M.C. Iapalucci, G. Longoni, M. Monari and P. Zanello, *J. Chem. Soc., Dalton Trans.*, 1992, 497.

[31] D.F. Rieck, J.A. Gavney, R.L. Norman, R.K. Hayashi and L.F. Dahl, *J. Am. Chem. Soc.*, 1992, **114**, 10369.

[32] D.F. Rieck, R.A. Montag, T.S. McKechnie and L.F. Dahl, *J. Am. Chem. Soc.*, 1986, **108**, 1330.

[33] R.E. DesEnfants, J.A. Gavney, R.K. Hayashi, A.D. Rae, L.F. Dahl and A. Bjarnason, *J. Organomet. Chem.*, 1990, **383**, 543.

[34] J.S. Leigh, K.H. Whitmire, K.A. Yee and T.A. Albright, *J. Am. Chem. Soc.*, 1989, **111**, 2726; T.A. Albright, K.A. Yee, J-Y. Saillard, S. Kahlal, J-F. Halet, J.S. Leigh and K.H. Whitmire, *Inorg. Chem.*, 1991, **30**, 1179.

[35] S. Martinengo and G. Ciani, *J. Chem. Soc., Chem. Commun.*, 1987, 1589.

the latter descriptions also fail to account for the significant E-E interaction observed. These structures are a simple example of numerous clusters that contain E_x fragments with strong E-E character. Mild oxidation of $[Co_4Bi_2(CO)_{11}]^-$ caused Bi-Bi bond cleavage, producing $[Co_9Bi_4(CO)_{16}]^{2-}$ (Figure 6.4b) and $[Co_{14}Bi_8(CO)_{20}]^{2-}$, whose structures possess alternate Co_4 and Bi_4Co planes[36].

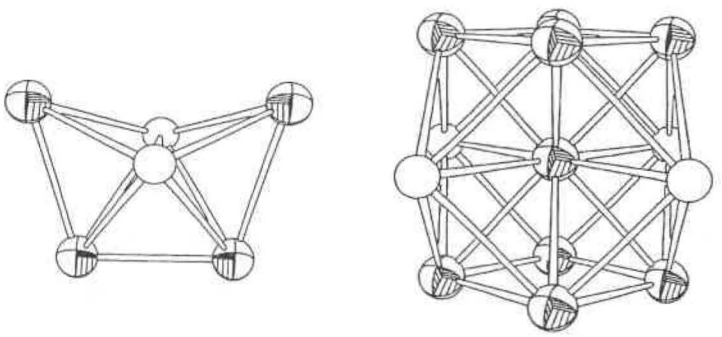

(a) (b)

Figure 6.4 – The core structures of $[Co_4Sb_2(CO)_{11}]^-$ [34] and $[Co_9Bi_4(CO)_{16}]^{2-}$ [36].

6.2 Synthesis of Cobalt Nitrido Clusters

6.2.1 Introduction

The synthesis of high-nuclearity clusters through thermolysis of smaller nitrido reagents is well known, especially with respect to rhodium clusters. The thermolysis of $[Rh_6N(CO)_{15}]^-$ has resulted in several high-nuclearity nitrido clusters (as discussed above) whereas equivalent treatment of $[Co_6N(CO)_{15}]^-$ has yielded only $[Co_{14}N_3(CO)_{26}]^{3-}$ [13]. $[Co_6N(CO)_{15}]^-$ has proven a useful precursor in the synthesis of other cobalt nitrido clusters (Scheme 6.1) but there is an apparent dearth of thermolysis products.

[36] K.H. Whitmire and J.R. Eveland, *J. Chem. Soc., Chem. Commun.*, 1994, 1335; B. Zouchoune, F. Oligaro, J-F. Halet, J-Y. Saillard, J.R. Eveland and K.H. Whitmire, *Inorg. Chem.*, 1998, **37**, 865.

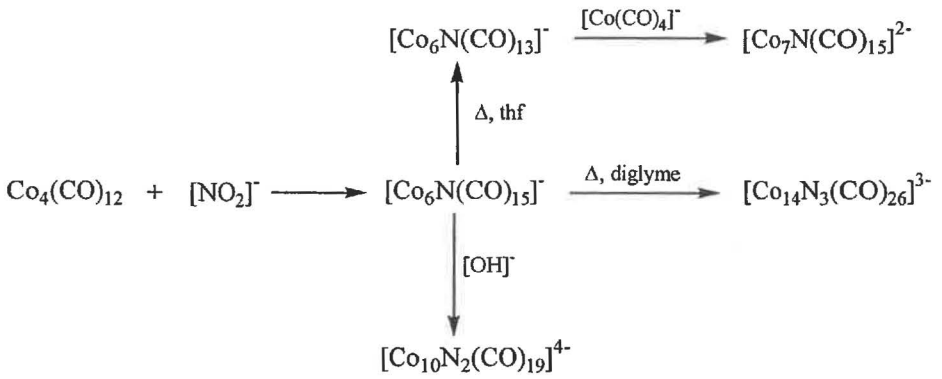

Scheme 6.1 – Different synthetic routes to cobalt nitrido clusters.

The core structure of $[Co_{14}N_3(CO)_{26}]^{3-}$ (Figure 6.5) consists of a pair of folded centred hexagons of cobalt atoms arranged in an eclipsed manner[13]. The structure was unprecedented, though it can effectively be considered as composed of three N-centred trigonal prisms linked through common vertices. The synthesis of $[Co_{14}N_3(CO)_{26}]^{3-}$ was also unusual as this was the only high-nuclearity product isolated and no indication of yield was provided. It appeared likely that other unidentified clusters were produced and the thermolysis reaction was re-examined using ESMS to identify all anionic products.

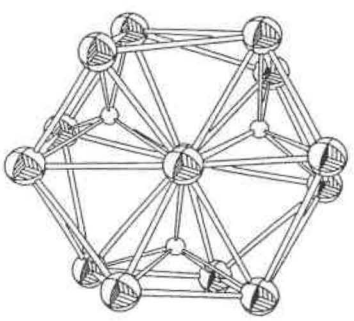

Figure 6.5 – The core structure of $[Co_{14}N_3(CO)_{26}]^{3-}$ [13].

6.2.2 Results and Discussion

The parent nitrido cluster, $[Co_6N(CO)_{15}]^-$, can be synthesised from treatment of $[Co_6(CO)_{15}]^{2-}$ with $[NO][BF_4]$[6] or by reaction of $Co_4(CO)_{12}$ with $[PPN][NO_2]$[37]. The latter method was adopted because of its simplicity and the low reported yield (13%) possibly indicating the presence of other nitrido species. Synthesis according to that reported yielded an orange powder composed primarily (as determined by ESMS) of

[37] R.E. Stevens, P.C.C. Liu and W.L. Gladfelter, *J. Organomet. Chem.*, 1985, **287**, 133.

$[Co_6N(CO)_{15}]^-$ (*m/z* 788) with a trace amount of $[Co_6(CO)_{15}]^{2-}$ {detected by ESMS as the oxidised ion, $[Co_6(CO)_{15}]^-$ (*m/z* 774)}. No other anionic species were detected.

Thermolysis of $[Co_6N(CO)_{15}]^-$ was performed in diglyme at 110°C under an inert atmosphere. Under these conditions, a signal attributed to $[Co_{14}N_3(CO)_{26}]^{2-}$ (*m/z* 798) was detected after 2 hours (Figure 6.6). The detected cluster corresponded to the oxidised form of the reported $[Co_{14}N_3(CO)_{26}]^{3-}$ cluster, with the charge determined both from high-resolution spectra and induced CO loss (generating signals *m/z* 14 apart). High-resolution spectra also confirmed that the signal corresponded to the oxidised form of the $[Co_{14}N_3(CO)_{26}]^{3-}$ cluster rather than the protonated ion, though unambiguous assignment of nitrido clusters is difficult since the mass of CO matches that of N_2 with no appreciable difference in the isotope patterns. The detection of the oxidised ion of $[Co_{14}N_3(CO)_{26}]^{3-}$ is understandable in light of reports indicating that the cluster has an extensive redox chemistry, with the isolation of all ions in the series $[Co_{14}N_3(CO)_{26}]^{2-/3-/4-}$ [38].

The only other nitrido clusters detected during thermolysis (though in significantly lower yield) were $[Co_6(CO)_{15}]^{2-}$ {a by-product of the synthesis of $[Co_6N(CO)_{15}]^-$} and the octahedral $[Co_6N(CO)_{13}]^-$ (*m/z* 732) cluster generated by decarbonylation of $[Co_6N(CO)_{15}]^-$. Decomposition of the sample was noted after 4-5 hours at 110°C (both from decolourisation of the solution and marked decrease in ESMS signal intensity) and the reaction was abandoned.

[38] A. Fumagalli and R.D. Pegola, *Synthesis and Properties of Metal Carbonyl Clusters Containing Nitrido Ligands*, Metal Clusters in Chemistry, Ed. P. Braunstein, L.A. Oro and P.R. Raithby, Wiley-VCH (Weinheim, Germany), 1999, 323 and references therein.

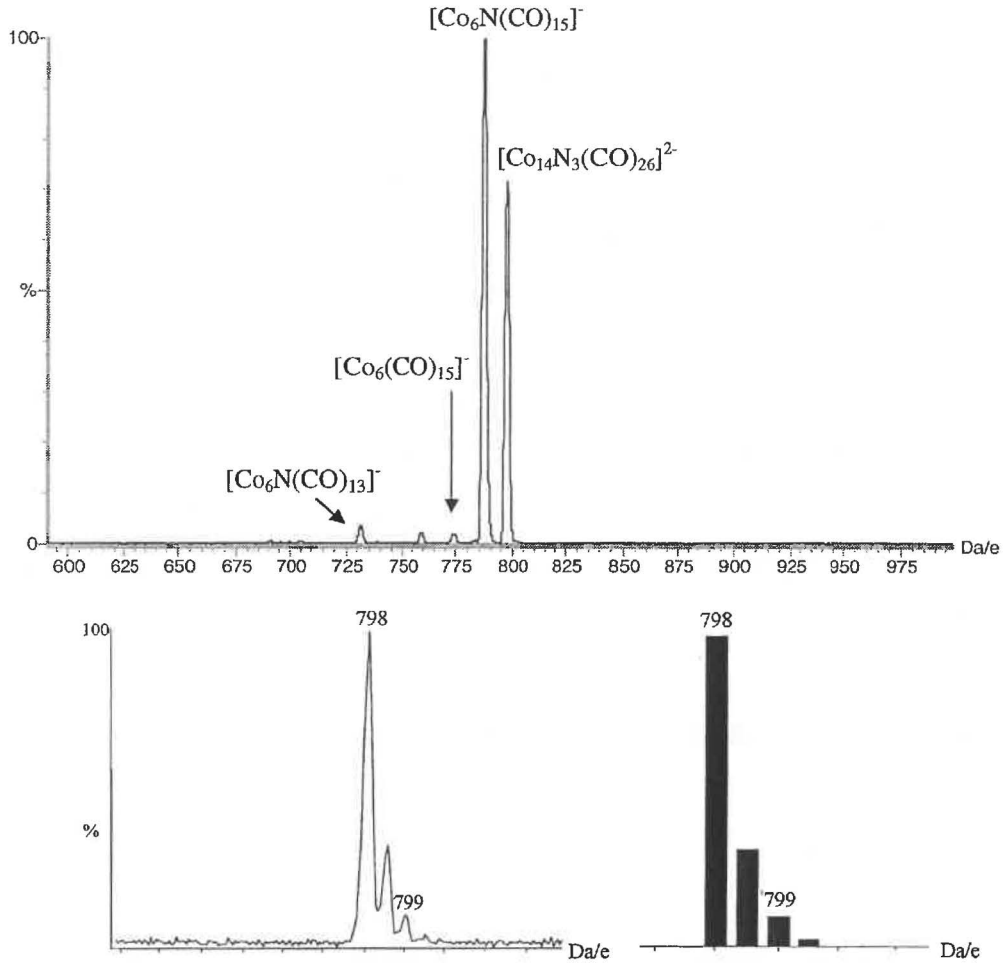

Figure 6.6 – The ES mass spectrum (-ve ion, 5 cV) of the thermolysis of $[Co_6N(CO)_{15}]^-$ after 2 hours, with the observed and calculated isotope patterns for $[Co_{14}N_3(CO)_{26}]^{2-}$.

The thermolysis of $[Co_6N(CO)_{15}]^-$ was also examined at lower temperatures in both diglyme and isopropylalcohol. There was no evidence under these conditions for the formation of any high-nuclearity cluster products, though decomposition of the reactant cluster was noted. The only species detected by ESMS in these reactions were the parent $[Co_6N(CO)_{15}]^-$ ion, $[Co_6(CO)_{15}]^-$, and $[Co_6N(CO)_{13}]^-$. In each case, decomposition of the parent cluster over time resulted in decolourisation of the reaction solution and yielded cobalt metal as a by-product.

ESMS examination of the thermolysis of $[Co_6N(CO)_{15}]^-$ confirmed the reported formation of $[Co_{14}N_3(CO)_{26}]^{3-}$. Of more importance is the fact that the $Co_{14}N_3$ cluster was the only high-nuclearity cluster formed, indicating a high degree of specificity for this product despite the significant atomic reorganisation required. The specificity can only be established from ESMS analysis since IR spectra of the various nitrido products

are similar and the $[Co_{14}N_3(CO)_{26}]^{3-}$ cluster may have been only a minor product of the thermolysis (one that fortuitously crystallised).

The capping of $[Co_6N(CO)_{15}]^-$ was also examined by ESMS. According to literature reports, $[Co_6N(CO)_{15}]^-$ initially undergoes decarbonylation to generate the octahedral $[Co_6N(CO)_{13}]^-$ cluster, which is subsequently capped by $[Co(CO)_4]^-$ to form $[Co_7N(CO)_{15}]^{2-}$ (though the structure of the hepta-nuclear cluster is a capped trigonal-prism rather than a capped octahedron[12]). The reaction was undertaken in refluxing thf and monitored by ESMS over 9 hours. Analysis over this period indicated conversion of $[Co_6N(CO)_{15}]^-$ to $[Co_6N(CO)_{13}]^-$ was complete after 6-7 hours but there was no evidence for the $[Co_7N(CO)_{15}]^{2-}$ product (expected *m/z* 423.5 or 847 depending on the extent of oxidation).

6.3 Synthesis of Cobalt Phosphido Clusters

6.3.1 Introduction

The salt elimination reaction between PCl_3 and $Na[Co(CO)_4]$ is reported to produce a range of cluster products including $PCo_3(CO)_9$, $P_2Co_2(CO)_6$, $[PCo_3(CO)_8]_3$ [39] and $[Co_6P(CO)_{16}]^-$ [20]. The anionic product is the most interesting with respect to formation of higher-nuclearity clusters and the structure of this cluster was discussed previously (Section 6.1.1). An alternative synthesis of this anion from PCl_5 and $Na[Co(CO)_4]$ was reported recently, with subsequent thermolysis producing $[Co_9P(CO)_{21}]^{2-}$ and a neutral by-product of unknown composition[24]. The capping of $[Co_9P(CO)_{21}]^{2-}$ by $[Co(CO)_4]^-$ to produce $[Co_{10}P(CO)_{22}]^{3-}$ was also reported.

The $[Co_9P(CO)_{21}]^{2-}$ and $[Co_{10}P(CO)_{22}]^{3-}$ clusters adopt capped and bi-capped square anti-prism structures, with the phosphorus atom fully encapsulated within the central cavity (refer to Figures 6.2b and c). The $[Co_9P(CO)_{21}]^{2-}$ cluster is of particular interest as it corresponds to the electron-precise analogue of $[Co_9Si(CO)_{21}]^{2-}$, the synthesis and reactions of which were described in Chapter 4. The capping of $[Co_9P(CO)_{21}]^{2-}$ is interesting as all attempts to cap the analogous silicon cluster were unsuccessful. The

[39] A. Vizi-Orosz, *J. Organomet. Chem.*, 1976, **111**, 61.

examination of these reactions by ESMS was of interest, both in order to confirm the specificity of the reaction and to provide a contrast to the silicon system.

6.3.2 Results and Discussion

The reactions were monitored throughout by ESMS. Monitoring of the reactions using ^{31}P NMR was also intended but no signals were detected from any of the clusters at room temperature (closer examination of the literature revealed that these clusters fail to give ^{31}P NMR signals at temperatures > -35°C [20]).

Upon warming a mixture of $Na[Co(CO)_4]$ and PCl_5 to room temperature, ES mass spectra of the reaction solution were dominated by a signal attributable to $[Co_6P(CO)_{16}]^-$ (*m/z* 833). After the solution was brought to reflux, signals corresponding to $[Co_9P(CO)_{21}]^{2-}$ (*m/z* 575) and the oxidised form of this cluster, $[Co_9P(CO)_{21}]^-$ (*m/z* 1150), were observed. The signals associated with the high-nuclearity cluster increased in intensity in the 6 hours over which the reaction was examined, with no other cluster anions formed in any significant quantity (Figure 6.7). After reflux, the reaction solution was placed under a carbon monoxide atmosphere for 3 hours without any detectable change in the composition of the solution {contradicting literature reports that claim conversion of all anionic products to $[Co_9P(CO)_{21}]^{2-}$ [24]}. A by-product was detected at *m/z* 1035, attributed to $[Co_8P(CO)_{19}]^-$, but this cluster was never a dominant product of the reaction and isolation was not attempted. With 10 SEP, the structure of this cluster would not be based around the 11 SEP square anti-prism geometry reported for $[Co_9P(CO)_{21}]^{2-}$ and $[Co_{10}P(CO)_{22}]^{3-}$.

A neutral by-product was also isolated in low yield in the synthesis of $[Co_9P(CO)_{21}]^{2-}$. The colour (orange/red) and IR signals [2039 (vs), 2028 (sh), 2006 (s), 1880 (m) cm^{-1}] of this by-product are remarkably similar to those displayed by $Co_4(\mu_4\text{-}ER)_2(CO)_{11}$ clusters (discussed in Chapter 7). From this similarity, the product was postulated to be $Co_4[\mu_4\text{-}PCo(CO)_4]_2(CO)_{10}$ (Figure 6.8), a structure that has precedent both in $Co_4(\mu_4\text{-}PR)_2(CO)_{10}$ (R = Ph, Bu, Pr[40]) and $Co_4[\mu_4\text{-}ECo(CO)_4]_2(CO)_{11}$ (E = Si, Ge) clusters[41].

---

[40] R.C. Ryan and L.F. Dahl, *J. Am. Chem. Soc.*, 1975, **97**, 6904; R.C. Ryan, C.U. Pittman, J.P. O'Connor and L.F. Dahl, *J. Organomet. Chem.*, 1980, **193**, 247; J. Queisser and D. Fenske, *Z. Anorg. Allg. Chem.*, 1994, **620**, 58; D. Fenske, J. Queisser and H. Schottmuller, *Z. Anorg. Allg. Chem.*, 1996, **622**, 1731.

Attempts to ionise the cluster to allow ESMS detection by treatment with $[OMe]^-$ and N_3^- (a methodology outlined in Section 1.3.5) were unsuccessful. Similarly, attempts to substitute the carbonyl ligands using isonitrile reagents to produce a more easily oxidised derivative (discussed in Section 7.2.2) were also unsuccessful, presumably because the terminal $Co(CO)_4$ units complicate the substitution reaction. Crystals were produced by cooling a heptane solution of the neutral product to –20°C but were of insufficient size for structural characterisation.

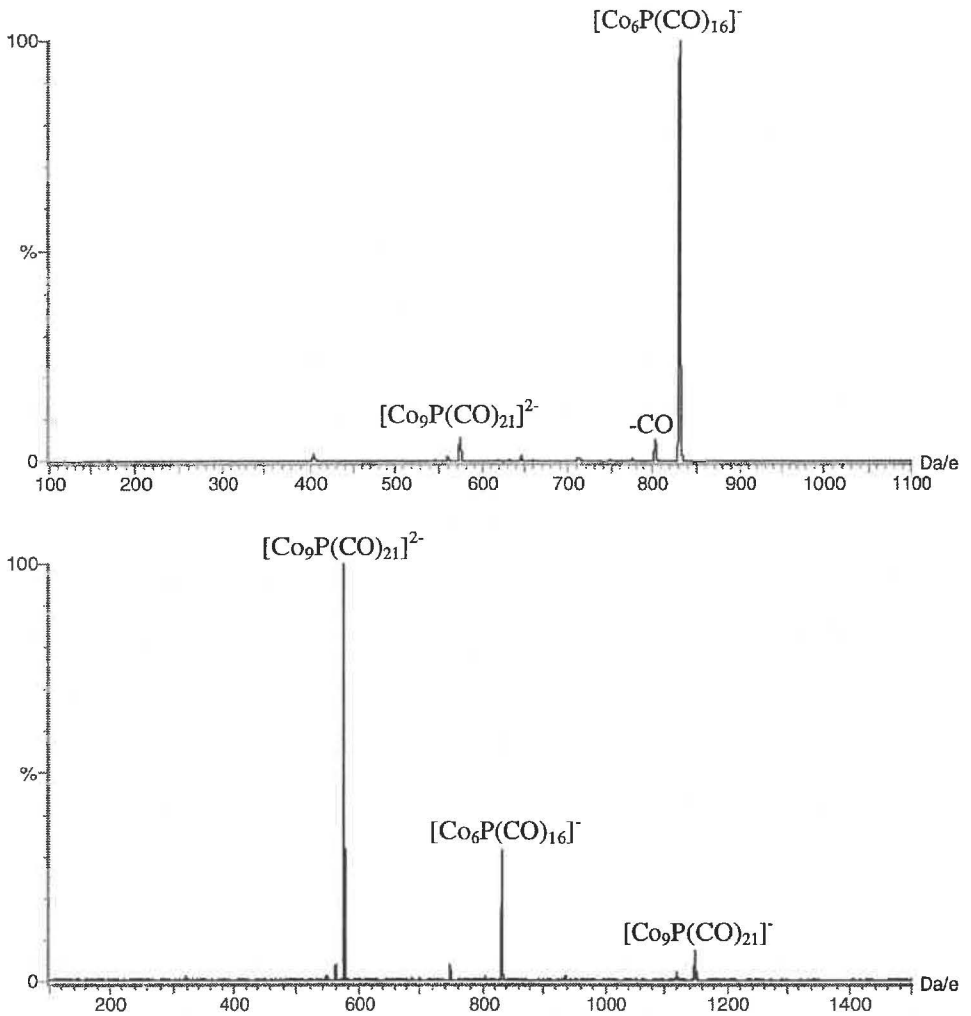

Figure 6.7 – The ES mass spectra (-ve ion, 5 cV) of the reaction between PCl_5 and $[Co(CO)_4]^-$ prior to reflux (upper), and after reflux for 6 hours (lower).

[41] S.P. Foster, K.M. Mackay and B.K. Nicholson, *Inorg. Chem.*, 1985, **24**, 909; M. Van Tiel, K.M. Mackay and B.K. Nicholson, *J. Organomet. Chem.*, 1987, **326**, C101.

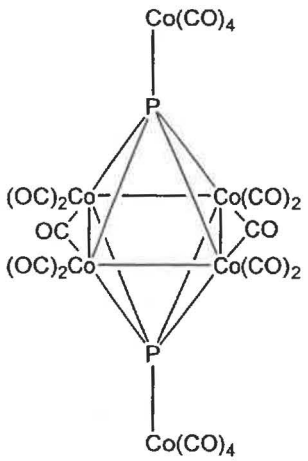

Figure 6.8 – $Co_4[\mu_4\text{-}PCo(CO)_4]_2(CO)_{10}$ - The postulated structure of the neutral by-product.

The capping of the $[Co_9P(CO)_{21}]^{2-}$ cluster was attempted through thermolysis of the parent cluster (in thf) with $[NEt_4][Co(CO)_4]$ and $Na[Co(CO)_4]$. A black deposit was formed in each case, which ESMS analysis (after dissolution in CH_2Cl_2) indicated was composed primarily of $[Co_9P(CO)_{21}]^{2-}$ with a small amount of $[Co_6P(CO)_{16}]^-$, rather than the $[Co_{10}P(CO)_{22}]^{3-}$ product (expected *m/z* 412.3, 618.5 or 1237 depending on the extent of oxidation). Equivalent reaction with $[NEt_4][HFe(CO)_4]$ instead of $[Co(CO)_4]^-$ was also examined without any indication of capping of the $[Co_9P(CO)_{21}]^{2-}$ cluster, though production of $[HFe_3(CO)_{11}]^-$ (*m/z* 477) as a by-product was noted.

The successful synthesis of the $[Co_9P(CO)_{21}]^{2-}$ cluster indicated that it might be possible to generate large heteronuclear phosphido clusters by the addition of $Fe_3(CO)_{12}$ to $[Co_6P(CO)_{16}]^-$. Although the resultant clusters would be difficult to characterise by IR spectroscopy and X-ray crystallography (since the scattering factors of cobalt and iron atoms are similar), the differences in mass and isotope distribution between cobalt and iron should allow unambiguous characterisation by ESMS. The reaction was carried out in a similar manner to those discussed above but analysis only indicated the presence of $[Co_9P(CO)_{21}]^{2-}$ (*m/z* 575 and 1150 for the oxidised ion), $[Co_3Fe(CO)_{12}]^-$ (*m/z* 569) and trace amounts of $[CoFe_3(CO)_{13}]^-$ (*m/z* 591). There was no evidence for the formation of any mixed cobalt/iron phosphido clusters. Although a disappointing outcome, the failure to produce heteronuclear clusters indicates a high degree of affinity of phosphorus for cobalt, mimicked to a degree by that observed for silicon (as reported in preceding chapters).

Another variation attempted was the use of $Na[Fe(CO)_3(NO)]$ rather than $Na[Co(CO)_4]$. For this experiment, ESMS analysis did not indicate the formation of any identifiable anionic cluster products and the reaction solution remained pale in colour (which contrasted with the deeply coloured solutions observed for the analogous cobalt reaction). The reason why $[Fe(CO)_3(NO)]^-$ fails to react in a similar manner to the isoelectronic $[Co(CO)_4]^-$ anion is not fully understood.

6.4 Synthesis of Cobalt Arsenido Clusters

6.4.1 Introduction

As with the phosphorus system reported above, several neutral products have been identified in the salt elimination reaction between $AsCl_3$ and $Na[Co(CO)_4]$[42], the most interesting of which was the trimeric $[AsCo_3(CO)_8]_3$ species (Figure 6.9). This cluster was also synthesised directly from AsH_3 and $Co_2(CO)_8$ [43]. Although several neutral compounds have been isolated, no anionic cobalt arsenido clusters have been identified from this reaction. Following the success of ESMS in monitoring the phosphido cluster synthesis, an extension to arsenido clusters was considered appropriate, with the expectation of identifying novel cluster products.

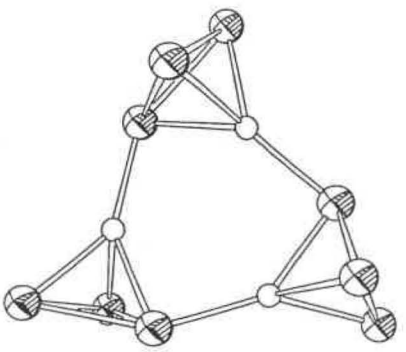

Figure 6.9 – The core structure of $[AsCo_3(CO)_8]_3$ [43].

[42] A. Vizi-Orosz, V. Galamb, G. Palyi, L. Marko, G. Bor and G. Natile, *J. Organomet. Chem.*, 1976, **107**, 235.

[43] L.J. Arnold, K.M. Mackay and B.K. Nicholson, *J. Organomet. Chem.*, 1990, **387**, 197.

6.4.2 Results and Discussion

The reaction between $AsCl_3$ and $Na[Co(CO)_4]$ was carried out in an identical manner to that outlined for the phosphorus system reported above. The use of $AsCl_3$ compared to PCl_5 was considered to have little effect on the reaction pathway since the synthesis of $[Co_9P(CO)_{21}]^{2-}$ proceeds through thermolysis of $[Co_6P(CO_{16}]^-$, generated by the reaction of $Na[Co(CO)_4]$ with either PCl_3 or PCl_5 [24].

Upon heating of the reaction solution, ESMS analysis indicated the formation of $[Co_6As(CO)_{16}]^-$ (*m/z* 877), the arsenic analogue of $[Co_6P(CO)_{16}]^-$. The reaction solution was refluxed for 8 hours in an attempt to generate higher-nuclearity clusters. Monitoring of the reaction over this time indicated the formation of two larger clusters, $[Co_7As_2(CO)_{17}]^-$ (*m/z* 1039) and $[Co_9As_2(CO)_{21}]^-$ (*m/z* 1269), but the spectra remained dominated by the $[Co_6As(CO)_{16}]^-$ signal (Figure 6.10). Continuing the reaction for longer periods of time (12 hours) failed to produce any further anionic cluster products.

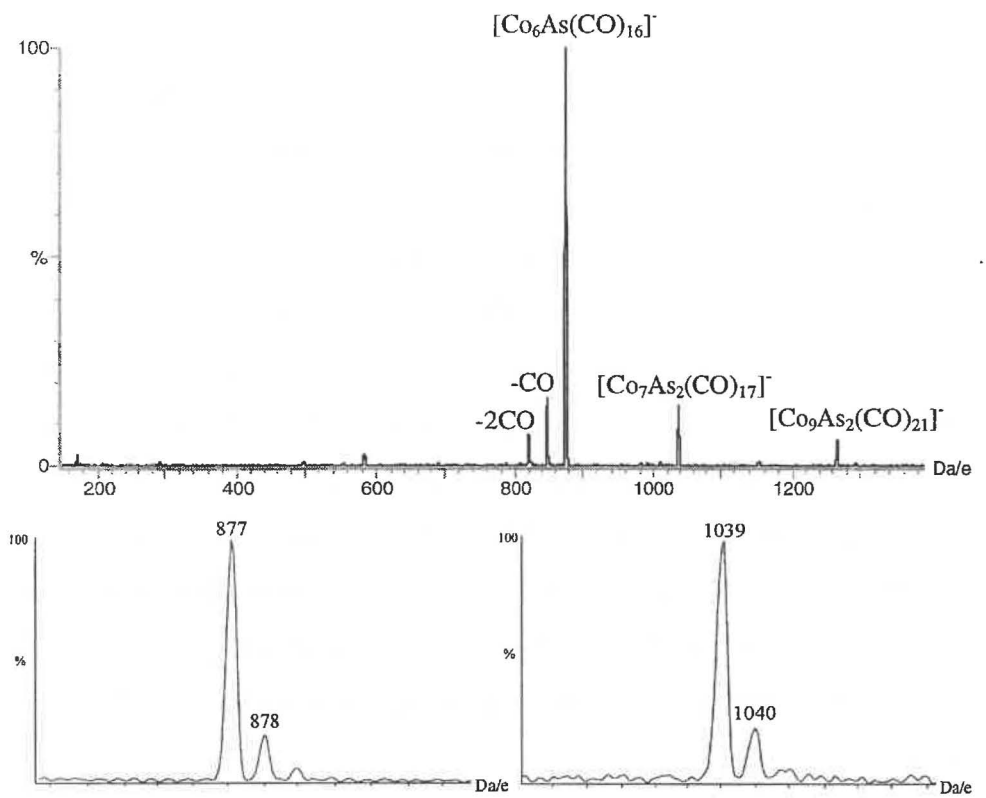

Figure 6.10 – The ES mass spectrum (-ve ion, 5 cV) of the reaction between $AsCl_3$ and $[Co(CO)_4]^-$ after 2 hours (above), with the isotope patterns for $[Co_6As(CO)_{16}]^-$ and $[Co_7As_2(CO)_{17}]^-$.

The detection of the novel $[Co_6As(CO)_{16}]^-$ cluster was an important result from this experiment. The structure is likely to be similar to that found for $[Co_6P(CO)_{16}]^-$ (refer to Figure 4.18), with the arsenic atom occupying a semi-encapsulated position, though the larger size of the arsenic would presumably result in a more open arrangement of cobalt atoms. The isostructural relationship between $[Co_6As(CO)_{16}]^-$ and $[Co_6P(CO)_{16}]^-$ was also indicated by similarity in the IR spectra [2027 (vs), 2011 (sh), 1881 (w), 1807 (m) cm^{-1} for the arsenido cluster compared to 2070 (w), 2020 (s), 2010 (sh), 1975 (w), 1965 (sh), 1800 (m) cm^{-1} reported for the phosphorus analogue[20]].

The structures of the $[Co_7As_2(CO)_{17}]^-$ and $[Co_9As_2(CO)_{21}]^-$ clusters are less predictable. The presence of two arsenic atoms compared to the single atom in the phosphorus case is presumably a factor of the larger size of the arsenic atom precluding encapsulation. In this aspect, parallels can be drawn to the structure of $[Co_{10}Ge_2(CO)_{24}]^{2-}$ reported earlier. The partial encapsulation of the arsenic atoms would prevent the clusters adopting simple polyhedral structures and thus the application of electron-counting rules to these clusters is inappropriate.

Attempts at crystallisation of $[Co_6As(CO)_{16}]^-$ were hampered by the presence of free $[Co(CO)_4]^-$. In each case, formation of pale yellow crystals of [Cat.][$Co(CO)_4$] (Cat. = PPh_4, PPN, NEt_4) was observed, along with precipitation of a crude black solid. It was noted that in the analogous phosphorus reaction, the formation of $[Co_9P(CO)_{21}]^{2-}$ served to remove all traces of $[Co(CO)_4]^-$ from the solution whereas in the arsenic case, the formation of $[Co_7As_2(CO)_{17}]^-$ and $[Co_9As_2(CO)_{21}]^-$ would effectively *increase* the amount of $[Co(CO)_4]^-$ available, hampering isolation of the high-nuclearity clusters. For this reason the reaction was repeated using a 1:3 ratio of $AsCl_3$:Na[$Co(CO)_4$] and stopped after generation of $[Co_6As(CO)_{16}]^-$. Under these conditions, the yield of $[Co_7As_2(CO)_{17}]^-$ was slightly increased but more importantly, there was no indication (by ESMS) for the presence of $[Co(CO)_4]^-$. However, pure samples of $[Co_6As(CO)_{16}]^-$ are not yet available and all attempts at obtaining single crystals of the cluster were unsuccessful.

6.5 Synthesis of Cobalt Antimonido and Bismuthido Clusters

6.5.1 Introduction

The success in monitoring the arsenic and phosphorus reactions allowed extension of the synthetic method to antimony and bismuth analogues. The salt elimination reaction between $BiCl_3$ and excess $Na[Co(CO)_4]$ is reported to produce $[Bi\{Co(CO)_4\}_4]^-$ and $BiCo_3(CO)_9$, with subsequent pyrolysis of $[Bi\{Co(CO)_4\}_4]^-$ yielding the paramagnetic $[Co_4Bi_2(CO)_{11}]^-$ cluster[35]. Attempts at capping $[Co_4Bi_2(CO)_{11}]^-$ using $Mo(CO)_3$(toluene) resulted in the formation of $[Co_9Bi_4(CO)_{16}]^{2-}$ and $[Co_{14}Bi_8(CO)_{20}]^{2-}$ [36] (the structures of which were discussed in Section 6.1.1). The equivalent reaction between $SbCl_3$ and $Na[Co(CO)_4]$ produced the unstable $Sb[Co(CO)_4]_3$ compound which decomposed to form $[Co_4Sb_2(CO)_{11}]^{2-/-}$ [34].

6.5.2 Results and Discussion

The reaction between $SbCl_3$ and $Na[Co(CO)_4]$ at a ratio of 1:6 was performed in a similar manner to the phosphorus and arsenic reactions reported above. ESMS analysis of the reaction solution within 30 minutes of warming to ambient temperature (Figure 6.11) indicated the presence of the previously reported $[Sb_2Co_4(CO)_{11}]^-$ ion (*m/z* 788) and a previously unidentified $[Sb_2Co_5(CO)_{14}]^-$ cluster (*m/z* 931), along with signals associated with $[Co(CO_4]^-$ {$[Co(CO)_4]^-$ (*m/z* 171) and $[Hg\{Co(CO)_4\}_3]^-$ (*m/z* 715)}. The reaction was heated to reflux and monitored by ESMS over a 4 hour period but, while the cluster products appeared soluble in the heated solvent, cooling to room temperature prior to analysis resulted in the formation of an insoluble black precipitate, leaving the supernatant only slightly coloured. IR analysis of the black precipitate (KBr disc) displayed two broad signals at 1981 and 1806 cm^{-1}, roughly similar to those reported for $[Co_4Sb_2(CO)_{11}]^-$ [2010 (s), 1995 (ms), 1975 (m), 1802 (w) cm^{-1} [34]].

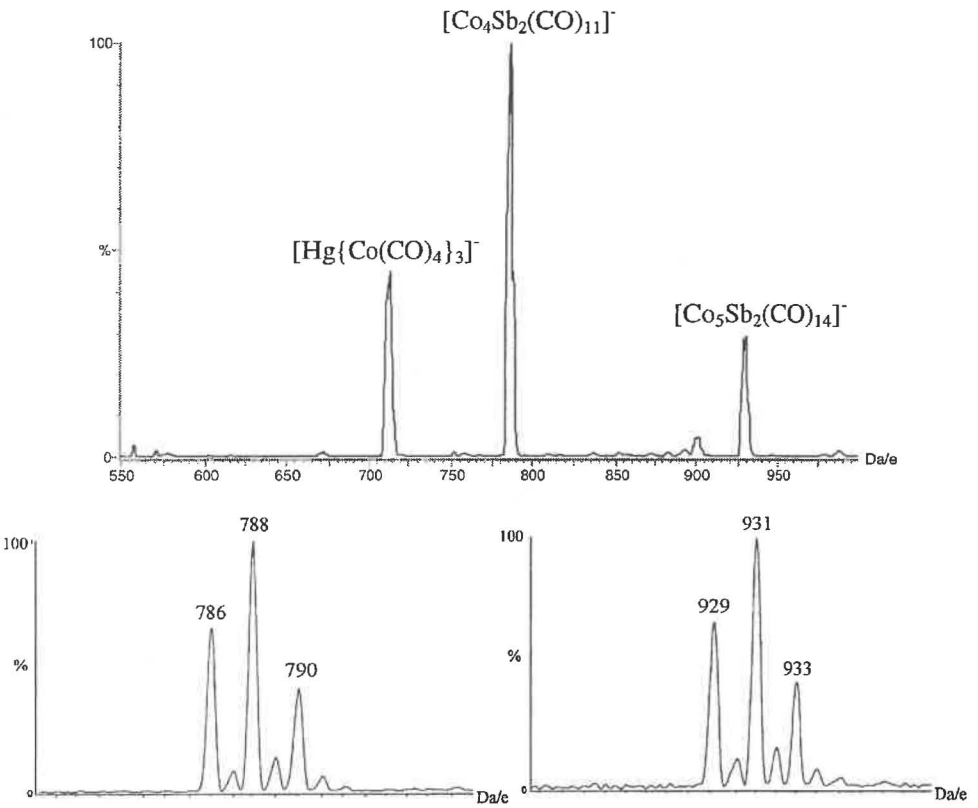

Figure 6.11 – The ES mass spectrum (-ve ion, 5 cV) of the reaction between $SbCl_3$ and $[Co(CO)_4]^-$ after 1 hour (above), with the isotope patterns for $[Co_4Sb_2(CO)_{11}]^-$ (left) and $[Co_5Sb_2(CO)_{14}]^-$ (right).

Although the absence of larger anionic clusters in this system (or the inability to detect their presence) was disappointing, the identification of the previously unknown $[Co_5Sb_2(CO)_{14}]^-$ cluster was significant. The structure of $[Co_5Sb_2(CO)_{14}]^-$ was initially presumed to be the capped form of $[Co_4Sb_2(CO)_{11}]^-$ (i.e. a pentagonal bi-pyramid - Figure 6.12). From electron-counting procedures, such a structure is unlikely since the $[Co_5Sb_2(CO)_{14}]^-$ cluster possesses 10 skeletal electron pairs (SEP) whereas the capped structure should possess 9 SEP (the same as the $[Co_4Sb_2(CO)_{11}]^{2-}$ cluster). Similarly, if both the $[Co_4Sb_2(CO)_{11}]^-$ and $[Co_5Sb_2(CO)_{14}]^-$ clusters were based around a dodecahedral structure (the *arachno* and *nido* forms respectively as has been speculated previously[34]), they should both possess the same number of SEP. The difference in the number of SEP indicates that the two structures are not based around the same parent polyhedron and the structure of $[Co_5Sb_2(CO)_{14}]^-$ is therefore uncertain. It should be noted that the electron-count for $[Co_4Sb_2(CO)_{11}]^{2-/-}$ is inconsistent with the structure observed and a similar inconsistency is likely for the $[Co_5Sb_2(CO)_{14}]^-$ cluster.

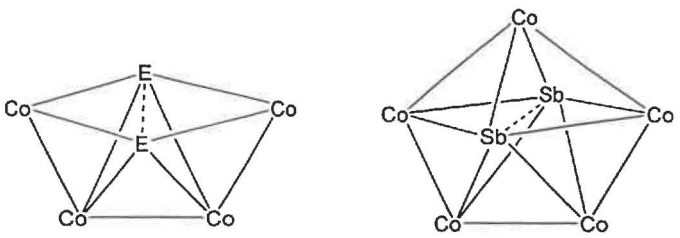

Figure 6.12 – The structure of $[Co_4E_2(CO)_{11}]^{2-/-}$ (E = Bi, Sb) and a postulated structure of $[Co_5Sb_2(CO)_{14}]^-$.

The equivalent reaction between $BiBr_3$ and $Na[Co(CO)_4]$ resulted in immediate formation of $[Bi\{Co(CO)_4\}_4]^-$ (*m/z* 893) as determined by ESMS analysis, while heating to reflux caused a darkening of the solution from intense red to black. ESMS analysis of the solution displayed a decrease in the $[Bi\{Co(CO)_4\}_4]^-$ signal intensity over time, replaced by a number of unidentified anionic species. Some of these ions appeared to contain bromine or silver (based on the isotope patterns observed) though analogous ions were not detected in any of the previous reactions. A few signals displaying limited isotopic variation (as expected from mixed bismuth/cobalt clusters) were detected, the most interesting at *m/z* 1481 and 1579. Both were singly charged carbonyl species (as determined from high-resolution spectra and induced decarbonylation) but no appropriate assignment of these signals was identified. As with the analogous antimony reaction, ESMS analysis was hampered by precipitation of the sample within minutes of removal from the reaction solution. There was no ESMS evidence for the formation of $[Co_4Bi_2(CO)_{11}]^-$ (expected *m/z* 962), $[Co_9Bi_4(CO)_{16}]^{2-}$ (*m/z* 907.5) or $[Co_{14}Bi_8(CO)_{20}]^{2-}$ (*m/z* 1529) at any stage during reaction. After 9 hours at reflux the reaction was abandoned without any mixed bismuth/cobalt clusters identified {besides $[Bi\{Co(CO)_4\}_4]^-$}.

6.6 Reactions of $M_3(CO)_{12}$ (M = Ru, Os) with $[PPN]N_3$

6.6.1 Introduction

The activation of the normally inert $M_3(CO)_{12}$ (M = Ru, Os) clusters through the use of nucleophiles is of catalytic interest (e.g. in the water/gas shift reaction[44]) and the use of

[44] D.C. Gross and P.C. Ford, *J. Am. Chem. Soc.*, 1985, **107**, 585; T. Chin-Choy, W.T.A. Harrison, G.D. Stucky, N. Keder and P.C. Ford, *Inorg. Chem.*, 1989, **28**, 2028.

the azide ion (facilitating production of isocyanate ligands) is one commonly applied method of activating the cluster towards ligand substitution reactions[45]. In particular, the products of the reaction between $Ru_3(CO)_{12}$ and N_3^- have shown catalytic properties in the hydrogenation of olefins[46].

The reported products from the reaction of $Ru_3(CO)_{12}$ with N_3^- are outlined in Scheme 6.2. Mild thermolysis produced the octahedral $[Ru_6N(CO)_{16}]^-$ [2] cluster, from which $[Ru_{10}N(CO)_{24}]^-$ [47] and $[Ru_5N(CO)_{14}]^-$ [3] have been generated. The $[Ru_{10}N(CO)_{24}]^-$ cluster was also produced directly from $Ru_3(CO)_{12}$ and N_3^- using more forcing conditions[48]. At room temperature, the formation of $[Ru_4(CO)_{13}(NCO)]^-$ {through $[Ru_3(CO)_{11}(NCO)]^-$ and $[Ru_3(CO)_{10}(NCO)]^-$ intermediate species} has been reported[49], from which $[Ru_4N(CO)_{12}]^-$ was generated[3]. The two trinuclear ruthenium clusters have been characterised spectroscopically[45] and also detected by ESMS[50].

The analogous reaction with $Os_3(CO)_{12}$ has been examined but reports appear contradictory. Initial reports stipulated that there was no reaction between the two species at room temperature, though in the presence of R_3PAuCl compounds, capped osmium isocyanato clusters were isolated[51]. Subsequent publications report quantitative production of $[Os_3(CO)_{11}(NCO)]^-$, with subsequent thermolysis yielding $[Os_3(CO)_{10}(NCO)]^-$ [52]. No osmium nitrido clusters have been isolated from this reaction to date.

---

[45] L.A.P. Kane-Maguire, M. Manthey and B. Robinson, *J. Chem. Soc., Dalton Trans.*, 1995, 905 and references therein.

[46] J.L. Zuffa, M.L. Blohm and W.L. Gladfelter, *J. Am. Chem. Soc,* 1986, **108**, 552.

[47] P.J. Bailey, G. Conole, B.F.G. Johnson, J. Lewis, M. McPartlin, A. Moule, H.R. Powell and D.A. Wilkinson, *J. Chem. Soc., Dalton Trans.*, 1995, 741.

[48] P.J. Bailey, G. Conole, B.F.G. Johnson, J. Lewis, M. McPartlin, A. Moule and D.A. Wilkinson, *Angew. Chem. Int. Ed. Engl.*, 1991, **30**, 1706.

[49] D.E. Fjare, J.A. Jensen and W.L. Gladfelter, *Inorg. Chem.*, 1983, **22**, 1774.

[50] J.S. McIndoe and B.K. Nicholson, *J. Organomet. Chem.*, 1999, **573**, 232; J.S. McIndoe, D.Phil. Thesis, University of Waikato, 1998.

[51] K. Burgess, B.F.G. Johnson and J. Lewis, *J. Chem. Soc., Dalton Trans.*, 1983, 1179; K. Burgess, B.F.G. Johnson and J. Lewis, *J. Organomet. Chem.*, 1983, **247**, C42.

[52] J.L. Zuffa and W.L. Gladfelter, *J. Am. Chem. Soc.*, 1986, **108**, 4669.

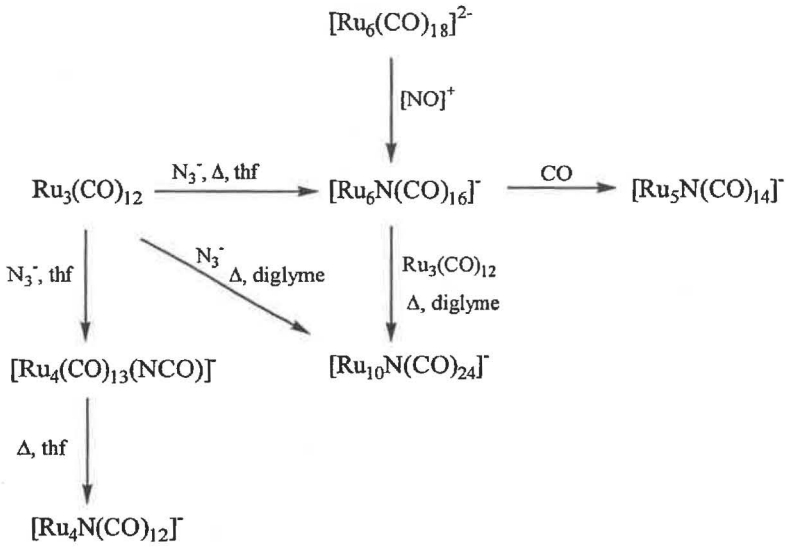

Scheme 6.2 – Different synthetic routes to ruthenium nitrido clusters.

The application of ESMS to the complex reaction between $Ru_3(CO)_{12}$ and N_3^- was expected to assist characterisation of the cluster products formed. More importantly, the identification of novel osmium nitrido clusters was anticipated from examination of the analogous reaction with $Os_3(CO)_{12}$.

6.6.2 Results and Discussion

The reaction between $Ru_3(CO)_{12}$ and N_3^- was examined in thf and diglyme to compare ESMS findings with previous reports. The equivalent reaction with $Os_3(CO)_{12}$ was carried out in diglyme at various temperatures. The reactions were monitored by ESMS analysis of aliquots removed from the reaction solution after suitable time intervals.

The reaction between $Ru_3(CO)_{12}$ and N_3^- was initially performed in thf, with immediate formation of $[Ru_4(CO)_{13}(NCO)]^-$ (*m/z* 812) noted. ES mass spectra obtained for this reaction were typically of poor quality (i.e. low intensity) though the reasons for this are unknown. The two trinuclear clusters reported to be intermediates *en route* to the Ru_4 cluster {$[Ru_3(CO)_{11}(NCO)]^-$ and $[Ru_3(CO)_{10}(NCO)]^-$ at expected *m/z* 655 and 627 respectively} were not detected (though this may be a solvent effect as both clusters have been identified previously by ESMS in MeCN[50]). The solution was refluxed for 8 hours with little change noted in the spectra. After cooling to 60°C for 16 hours, ES mass spectra indicated that the $[Ru_4(CO)_{13}(NCO)]^-$ signal had been replaced by new signals at *m/z* 912, 456 and 536.5. The first of these corresponds to the previously

reported $[Ru_5N(CO)_{14}]^-$ cluster[2], while the latter two signals were di-anions (determined from induced decarbonylation) of unknown composition. The assignment of these ions is uncertain since the complexity of the ruthenium isotope pattern and the poor quality of the ES mass spectra hamper unambiguous assignment.

The reaction was repeated in diglyme at 135°C in the expectation of generating the $[Ru_{10}N(CO)_{24}]^-$ cluster. The spectra obtained under these conditions were more intense than those obtained previously and the detected clusters more closely matched expectation. Within minutes of azide addition, a signal corresponding to $[Ru_4(CO)_{13}(NCO)]^-$ (*m/z* 812) was observed (paralleling that observed in thf), with the absence of the $[Ru_3(CO)_x(NCO)]^-$ (x = 10, 11) clusters noted. Within 30 minutes, ESMS analysis of the solution indicated three dominant cluster species; $[Ru_4(CO)_{13}(NCO)]^-$, $[Ru_5N(CO)_{14}]^-$ (*m/z* 912) and $[Ru_6N(CO)_{16}]^-$ (*m/z* 1070), with the $[Ru_6N(CO)_{16}]^-$ signal becoming more intense with time (Figure 6.13). Three other clusters were observed after extended reaction (4-5 hours), the previously reported $[HRu_6(CO)_{18}]^-$ (*m/z* 1110) ion[53], the novel $[Ru_7N(CO)_{18}]^-$ cluster (*m/z* 1227), and the high-nuclearity $[Ru_{10}N(CO)_{24}]^-$ cluster (*m/z* 1699). Additional signals were observed at *m/z* 853.5 and 771 corresponding to di-anions but no sensible assignment of these signals was uncovered.

[53] C.R. Eady, B.F.G. Johnson, J. Lewis, M.C. Malatesta, P. Machin and M. McPartlin, *J. Chem. Soc., Chem. Commun.*, 1976, 945; P.F. Jackson, B.F.G. Johnson, J. Lewis, P.R. Raithby, M. McPartlin, W.J.H. Nelson, K.D. Rouse, J. Allibon and S.A. Mason, *J. Chem. Soc., Chem. Commun.*, 1980, 295.

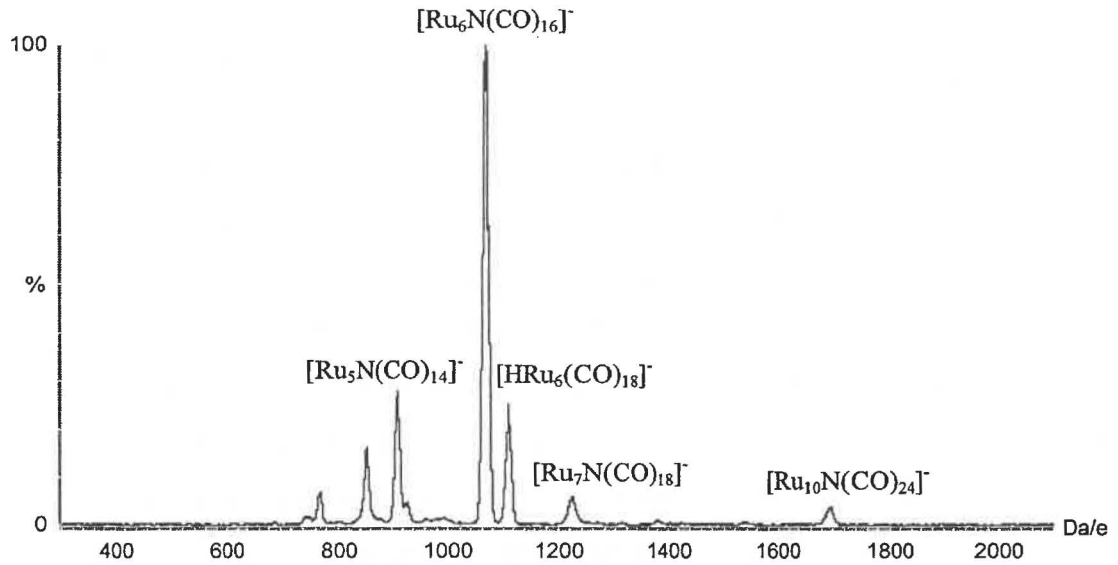

Figure 6.13 – The ES mass spectrum (-ve ion, 5 cV) of the thermolysis of $Ru_3(CO)_{12}$ and $[PPN]N_3$ after 4 hours in diglyme.

The only anion of interest identified in the reaction was the novel $[Ru_7N(CO)_{18}]^-$ cluster. The structure is predicted from electron-counting procedures to be a mono-capped octahedron (98 valence-electrons, 7 SEP), with the nitrogen atom located in the central cavity (Figure 6.14). This structure is consistent with other ruthenium nitrido clusters since the structures of $[Ru_5N(CO)_{14}]^-$, $[Ru_6N(CO)_{16}]^-$ and $[Ru_{10}N(CO)_{24}]^-$ are all based around a parent Ru_6N octahedron.

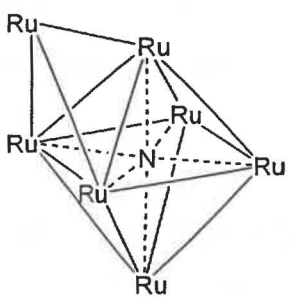

Figure 6.14 – The predicted core structure of $[Ru_7N(CO)_{18}]^-$.

During the experiment, a number of smaller cluster anions were detected of unknown assignment. The low intensity of these signals and the complexity of the ruthenium isotope pattern (spread over a 20 amu range for a Ru_4 or larger cluster) hindered assignment of these species, and as none of there clusters were dominant species in the solution, unambiguous identification was not considered crucial.

In contrast to the ruthenium system discussed above, the reaction between $Os_3(CO)_{12}$ and N_3^- resulted in immediate formation of $[Os_3(CO)_{11}(NCO)]^-$ (*m/z* 922). This cluster is a known product of the reaction[52] and has also been identified by ESMS[50]. Thermolysis in diglyme resulted in the formation of various cluster species. Within 30 minutes at 135°C, ES mass spectra indicated the presence of a range of Os_3 species {the only assignable signal being attributable to $[Os_3(CO)_{11}(NCO)]^-$}. Also identified were two Os_4 clusters, $[Os_4(CO)_{13}(NCO)]^-$ (*m/z* 1168) and $[H_3Os_4(CO)_{12}]^-$ (*m/z* 1101). The first of these is novel but presumably isostructural with $[Ru_4(CO)_{13}(NCO)]^-$. The $[H_3Os_4(CO)_{12}]^-$ cluster has been isolated previously[54], though its presence was unusual both because of the lack of nitrogen in the cluster and the presence of hydride ligands. Traces of water in the solvent may have been acting as a hydrogen source, though the solvent was dried prior to use and analogous ruthenium hydrido clusters were absent in the previous reaction {aside from $[HRu_6(CO)_{18}]^-$}. Also detectable in small quantities were the previously characterised $[HOs_5(CO)_{15}]^-$ cluster[55] (*m/z* 1373) and a series of signals *ca. m/z* 1720-1780 corresponding to Os_6 or Os_7 clusters of unknown composition.

With extended reaction, the intensity of the larger cluster signals increased (Figure 6.15). Tri-nuclear osmium clusters were observed throughout the reaction but assignment became more difficult. After 20 hours, the parent $[Os_3(CO)_{11}(NCO)]^-$ cluster was still detectable but the dominant tri-nuclear signal corresponded to an ion of empirical formula $H_1Os_3C_{10}O_9N_1$ (*m/z* 851), with the arrangement of ligands for such a cluster unknown. The larger clusters were more easily identified, with the previously characterised tetra-nuclear $[H_3Os_4(CO)_{12}]^-$ (*m/z* 1101) and $[HOs_4(CO)_{13}]^-$ (*m/z* 1127)[56] clusters readily apparent. The $[HOs_5(CO)_{15}]^-$ signal remained, along with higher-nuclearity cluster signals at *m/z* 1616, 1647 and 1862. The *m/z* 1647 signal was attributed to $[HOs_6(CO)_{18}]^-$ but the assignment of the other two signals was unknown. ES mass spectra acquired after 72 hours indicated the dominant species was $[H_3Os_4(CO)_{12}]^-$ and the reaction was halted at this point.

---

[54] M. McPartlin and W.J.H. Nelson, *J. Chem. Soc., Dalton Trans.*, 1986, 1557; S. Chan, S-M. Lee, Z. Lin and W-T. Wong, *J. Organomet. Chem.*, 1996, **510**, 219.

[55] J.J. Guy and G.M. Sheldrick, *Acta Cryst. Sect. B*, 1978, **34**, 1722.

[56] P.A. Dawson, B.F.G. Johnson, J. Lewis, D.A. Kaner and P.R. Raithby, *J. Chem. Soc., Chem. Commun.*, 1980, 961.

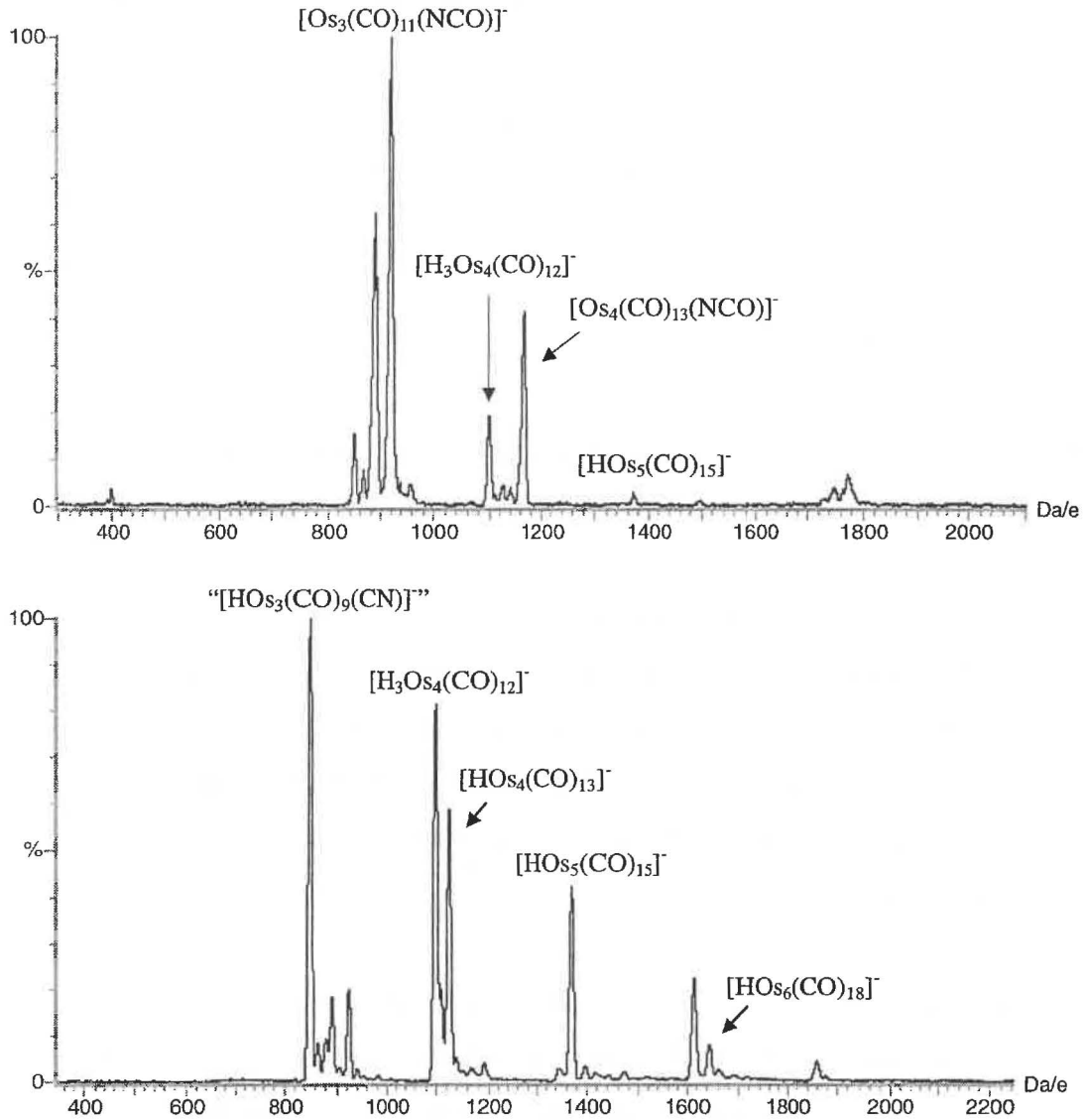

Figure 6.15 – The ES mass spectra (-ve ion, 5 cV) of the thermolysis of $Os_3(CO)_{12}$ and $[PPN]N_3$ after 30 minutes (upper), and 20 hours (lower) in diglyme.

The reaction between $Os_3(CO)_{12}$ and N_3^- was repeated at various temperatures (50, 80 and 100°C) with similar results. The presence of hydrido clusters was noted in each case and no signals attributable to osmium nitrido clusters were detected. The reaction at 135°C produced the highest yield of higher-nuclearity clusters (based on ESMS signal intensity) but examination of the reaction at higher temperatures than this was not considered.

The absence of high-nuclearity osmium nitrido clusters was a disappointing result of this experiment, though it indicates that the reactivity of ruthenium and osmium are

significantly different. Although a variety of ruthenium nitrido clusters were identified, analysis of the osmium system after 24 hours indicated the absence of any nitrogen-containing clusters. The detection of the hydrido clusters was curious and indicates the presence of a hydrogen source (either H^+ or H_2O) in the reaction. The absence of analogous ruthenium hydrido clusters indicates that osmium is significantly more sensitive to reaction conditions.

6.7 Conclusions and Future Work

ESMS analysis of group 15/transition metal clusters has proven successful. The technique was effective in monitoring the reactions and identifying all cluster products.

The synthesis, thermolysis and capping reactions of $[Co_6N(CO)_{15}]^-$ were examined. ESMS results indicated that $[Co_{14}N_3(CO)_{26}]^{3-}$ was the only high-nuclearity thermolysis product of $[Co_6N(CO)_{15}]^-$, in agreement with previous reports. The specificity of the reaction can only be established from ESMS analysis, which allows identification of all anionic cluster species present. Attempts to generate the capped $[Co_7N(CO)_{15}]^{2-}$ cluster were unsuccessful.

The synthesis of $[Co_6P(CO)_{16}]^-$ from PCl_5 and $Na[Co(CO)_4]$, and its subsequent thermolysis to form $[Co_9P(CO)_{21}]^{2-}$ were successfully monitored by ESMS. In contrast to previous reports, treatment of the reaction solution with CO was found unnecessary. Attempts to generate the capped $[Co_{10}P(CO)_{22}]^{3-}$ cluster and heteronuclear phosphido clusters were unsuccessful.

Extending the salt elimination reaction to the heavier group 15 elements led to the identification of $[Co_6As(CO)_{16}]^-$, the arsenic analogue of $[Co_6P(CO)_{16}]^-$. Thermolysis of the reaction mixture generated two novel cobalt arsenido clusters, $[Co_7As_2(CO)_{17}]^-$ and $[Co_9As_2(CO)_{21}]^-$, the structures of which are unknown. Repetition of the reaction using a 1:3 ratio of $AsCl_3$:$Na[Co(CO)_4]$ produced a higher yield of $[Co_7As_2(CO)_{17}]^-$ (determined by ESMS) and removed free $[Co(CO)_4]^-$. Further experimentation with the reactant ratios and reaction conditions may lead to isolation of these clusters.

Analysis of the reaction between $SbCl_3$ and $Na[Co(CO)_4]$ identified the known $[Co_4Sb_2(CO)_{11}]^-$ and the novel $[Co_5Sb_2(CO)_{14}]^-$ clusters. From electron-counting

procedures, the latter cluster is unlikely to be the capped version of the former. Further examination of this reaction, especially with respect to the $SbCl_3$:$Na[Co(CO)_4]$ ratio and reaction conditions may allow isolation of this cluster. $[Bi\{Co(CO)_4\}_4]^-$ was the only identified product in the analogous reaction between $BiBr_3$ and $Na[Co(CO)_4]$. Extended reaction led to several unidentified reaction products rather than the $[Co_4Bi_2(CO)_{11}]^-$, $[Co_9Bi_4(CO)_{16}]^{2-}$ and $[Co_{14}Bi_8(CO)_{20}]^{2-}$ clusters reported.

Finally, ESMS analysis of the reaction between $Ru_3(CO)_{12}$ and N_3^- confirmed the presence of previously identified ruthenium nitrido clusters. A novel $[Ru_7N(CO)_{18}]^-$ cluster was identified, though the low yield prevented isolation. The analogous reaction with $Os_3(CO)_{12}$ yielded the isocyanato clusters, $[Os_3(CO)_{11}(NCO)]^-$ and $[Os_4(CO)_{13}(NCO)]^-$, along with a raft of osmium hydrido clusters. There was no evidence for the formation of any osmium nitrido clusters.

6.8 Experimental

Synthesis of $[PPN][Co_6N(CO)_{15}]$[37]

To a thf (20 mL) solution of $Co_4(CO)_{12}$ (0.3 g, 0.524 mmol) was added $[PPN][NO_2]$ (0.18 g, 0.308 mmol) and the solution refluxed for 3 hours {until ESMS analysis indicated that $[Co_6N(CO)_{15}]^-$ was the dominant anion present}. The solution was cooled to room temperature, solvent and $Co(CO)_3(NO)$ removed under vacuum, unreacted $Co_4(CO)_{12}$ extracted with petroleum spirits, and the product extracted with Et_2O. Layering the Et_2O extract with petroleum spirits produced a red/orange powder composed primarily of $[PPN][Co_6N(CO)_{15}]$ (0.0584 g, 14%) with a trace amount of $[Co_6(CO)_5]^{2-}$. The crude product was used without further purification.

$[PPN][Co_6N(CO)_{15}]$

M_r – 1326.3

ESMS – (MeOH, -ve ion, 5 cV) *m/z* 788 (100% - $[Co_6N(CO)_{15}]^-$), *m/z* 774 (10% - $[Co_6(CO)_{15}]^-$)

IR – (ν_{CO}, CH_2Cl_2) 2061 (w), 2025 (sh), 2014 (vs), 1973 (m), 1855 (s) cm^{-1} [Lit. 2060 (vw), 2010 (vs), 1895 (vw), 1860 (vs) cm^{-1} [37]]

Thermolysis of $[Co_6N(CO)_{15}]^-$

A diglyme solution (10 mL) of $[PPN][Co_6N(CO)_{15}]$ (0.02 g, 0.015 mmol) was heated to 110°C and the thermolysis monitored by ESMS. Spectra of the reaction solution after 2 hours displayed signals attributable to $[Co_{14}N_3(CO)_{26}]^{2-}$ (*m/z* 798), $[Co_6N(CO)_{15}]^-$ (*m/z* 788), $[Co_6(CO)_{15}]^-$ (*m/z* 774) and $[Co_6N(CO)_{13}]^-$ (*m/z* 732). $[Co_{14}N_3(CO)_{26}]^{2-}$ became the dominant anionic species present in subsequent spectra. After thermolysis for 4-5 hours, the intensity of the ES mass spectra decreased significantly, the solution decolourised and the thermolysis reaction was abandoned.

Thermolysis of $[Co_6N(CO)_{15}]^-$ was repeated at 80°C in diglyme and at 50°C in ^{i}PrOH on a similar scale to that reported above. The only detected anionic species in each case were $[Co_6N(CO)_{15}]^-$, $[Co_6(CO)_{15}]^-$ and $[Co_6N(CO)_{13}]^-$. The solutions decolourised during thermolysis over the course of 10-12 hours and the formation of cobalt metal was noted.

Attempted synthesis of $[Co_7N(CO)_{15}]^{2-}$ [12]

$[NEt_4][Co(CO)_4]$ (0.005 g, 0.016 mmol) was added to a thf (5 mL) solution of $[PPN][Co_6N(CO)_{15}]$ (0.02 g, 0.016 mmol) and the mixture refluxed for 6 hours. The solution darkened rapidly upon heating, though ESMS analysis indicated that the parent $[Co_6N(CO)_{15}]^-$ cluster remained the dominant anionic species present. The generation of $[Co_6N(CO)_{13}]^-$ (*m/z* 732) was noted, though at no time was a signal corresponding to $[Co_7N(CO)_{15}]^{2-}$ (*m/z* 423.5 or 847 for the oxidised ion) detected.

Synthesis of $[Co_9P(CO)_{21}]^{2-}$ [24]

A thf solution (10 mL) of resublimed PCl_5 (0.106 g, 0.51 mmol) was added slowly to a thf solution (20 mL) of $Na[Co(CO)_4]$ (0.6 g, 3.1 mmol – prepared as outlined in Chapter 2) at –60°C ($CHCl_3$ slush bath). This solution was warmed to ambient temperature and ESMS analysis indicated the presence of $[Co_6P(CO)_{16}]^-$ (*m/z* 833), $[Co(CO)_4]^-$ (*m/z* 171) and a small amount of $[Hg\{Co(CO)_4\}_3]^-$ (*m/z* 715). The solution was refluxed for 6 hours and monitored by ESMS. Analysis indicated conversion of $[Co_6P(CO)_{16}]^-$ to $[Co_9P(CO)_{21}]^{2-}$ (*m/z* 575) over this time {though the high-nuclearity cluster was also detected as the oxidised anion, $[Co_9P(CO)_{21}]^-$ *m/z* 1150}. The reaction was maintained

at 50°C overnight with no change noted in the composition of the solution. The cooled solution was placed under a carbon monoxide atmosphere for 3 hours, though ESMS analysis indicated no change in the composition of the solution during this time. Solvent was removed under vacuum and a neutral by-product {postulated to be $Co_4[\mu_4\text{-}PCo(CO)_4]_2(CO)_{10}$} was extracted with petroleum spirits (0.012 g). Further extraction using CH_2Cl_2 yielded a crude black product (after solvent removal), characterised as $Na_2[Co_9P(CO)_{21}]$ (0.099 g, 23%). The crude product was used without further purification {though ESMS analysis indicated the presence of a small amount of $[Co_6P(CO)_{16}]^-$}.

$Na_2[Co_9P(CO)_{21}]$

M_r – 1196.0

IR – (ν_{CO}, thf) 2006 (vs), 1976 (sh), 1809 (m) cm^{-1} [Lit. 2001 (vs), 1980 (sh), 1808 (m) cm^{-1} [24]]

ESMS – (MeOH, -ve ion, 5 cV) *m/z* 575 (100% - $[Co_9P(CO)_{21}]^{2-}$), *m/z* 833 (15% - $[Co_6P(CO)_{16}]^-$), *m/z* 1150 (15% - $[Co_9P(CO)_{21}]^-$)

"$Co_4[\mu_4\text{-}PCo(CO)_4]_2(CO)_{10}$"

M_r – 919.7

IR – (ν_{CO}, pet. spirits) 2039 (vs), 2028 (sh), 2006 (s), 1880 (m) cm^{-1} [Lit. 2037 (vs), 2028 (s), 2007 (s), 1880 (m) cm^{-1} [24]]

ESMS – No signals were obtained under standard conditions.

Attempted capping reactions of $[Co_9P(CO)_{21}]^{2-}$ [24]

To a thf solution (10 mL) of $Na_2[Co_9P(CO)_{21}]$ (0.02 g, 0.02 mmol) was added $[NEt_4][Co(CO)_4]$ (0.035 g, 0.12 mmol) and the mixture refluxed for 4 hours. After cooling to ambient temperature the solution was filtered, yielding a black precipitate. ESMS analysis of this precipitate (and of the thf supernatant) indicated the presence of $[Co_9P(CO)_{21}]^{2-}$ (*m/z* 575) and unreacted $[Co(CO)_4]^-$ (*m/z* 171) without evidence for the formation of the reported $[Co_{10}P(CO)_{22}]^{3-}$ cluster. The reaction was repeated using $Na[Co(CO)_4]$ with identical results.

To a thf solution (10 mL) containing $Na_2[Co_9P(CO)_{21}]$ (0.02 g, 0.02 mmol) was added $[PPN][HFe(CO)_4]$ (0.08 g, 0.11 mmol) and the mixture refluxed for 4 hours. ESMS analysis after reflux indicated only the presence of $[Co_9P(CO)_{21}]^{2-}$ (*m/z* 575) and $[HFe_3(CO)_{11}]^-$ (*m/z* 477).

Reaction of $[Co_6P(CO)_{16}]^-$ with $Fe_3(CO)_{12}$

A thf solution (5 mL) of PCl_5 (0.05 g, 0.24 mmol) was added slowly to a cooled (-60°C) thf solution (15 mL) of $Na[Co(CO)_4]$ (0.28 g, 1.44 mmol). The solution was warmed to room temperature and ESMS analysis indicated the formation of $[Co_6P(CO)_{16}]^-$ (*m/z* 833). $Fe_3(CO)_{12}$ (0.1 g, 0.2 mmol) was added and the solution was refluxed for 4 hours. ES mass spectra after reflux were dominated by signals corresponding to $[Co_3Fe(CO)_{12}]^-$ (*m/z* 569) and $[Co_9P(CO)_{21}]^{2-}$ (*m/z* 575), with less intense signals detected for $[CoFe_3(CO)_{13}]^-$ (*m/z* 591) and $[Co_9P(CO)_{21}]^-$ (*m/z* 1150).

Reaction of PCl_5 with $Na[Fe(CO)_3(NO)]$

A thf solution (10 mL) of PCl_5 (0.05 g, 0.24 mmol) was added slowly to a cooled (-60°C) thf solution (20 mL) of $Na[Fe(CO)_3(NO)]$ {0.25 g, 1.3 mmol – produced from reduction of $Hg[Fe(CO)_3(NO)]_2$}. The mixed solution was warmed to ambient temperature and refluxed for 6 hours. ESMS analysis of the solution over this period failed to indicate the formation of any anionic cluster products.

Reaction of $AsCl_3$ with $Na[Co(CO)_4]$

To a cooled (-60°C) thf solution (20 mL) of $Na[Co(CO)_4]$ (0.681 g, 3.5 mmol) was slowly added a thf solution (5 mL) of $AsCl_3$ (50 μL, 0.11 g, 0.61 mmol). The reaction solution was warmed to ambient temperature and refluxed for 2 hours {until ES mass spectra of the solution were dominated by the $[Co_6As(CO)_{16}]^-$ signal – *m/z* 877}. The solution was reduced in volume (*ca.* 5 mL) and layered with petroleum spirits (20 mL). The solution was stored at -20°C for 48 hours with formation of a black precipitate {assumed to be $Na[Co_6As(CO)_{16}]$ (0.102 g, 19%)} noted. Preparation of the $[PPh_4]^+$ salt was achieved by addition of a thf solution of $[PPh_4]Br$ to a solution of $Na[Co_6As(CO)_{16}]$, with no attempt made to remove the NaBr produced.

The reaction was repeated using a 1:3 ratio of $AsCl_3$:$Na[Co(CO)_4]$ with the intention of reducing the amount of unreacted $[Co(CO)_4]^-$. This approach appeared successful, with ES mass spectra acquired after refluxing for 1 hour indicating the presence of $[Co_6As(CO)_{16}]^-$ (*m/z* 877) and $[Co_7As_2(CO)_{17}]^-$ (*m/z* 1039), and the absence of any free

$[Co(CO)_4]^-$. Isolation of $[Co_6As(CO)_{16}]^-$ was carried out in a similar manner to that reported above. It should be noted that though ESMS analysis indicated the absence of $[Co(CO)_4]^-$, the IR signal at 1881 cm^{-1} is characteristic of the anion.

$[Ph_4P][Co_6As(CO)_{16}]$
M_r – 1216.4
IR – (ν_{CO}, thf) 2027 (vs), 2011 (sh), 1881 (w), 1807 (w) cm^{-1}
ESMS – (MeOH, -ve ion, 5 cV) *m/z* 877 (100% - $[Co_6As(CO)_{16}]^-$), *m/z* 1039 (20% - $[Co_7As_2(CO)_{17}]^-$)

The synthesis of larger cobalt arsenic clusters was attempted by extending the reaction of $AsCl_3$ and $Na[Co(CO)_4]$ after identification of $[Co_6As(CO)_{16}]^-$ (*m/z* 877). The thf solution was refluxed for 12 hours, with the formation of $[Co_7As_2(CO)_{17}]^-$ (*m/z* 1039) and $[Co_9As_2(CO)_{21}]^-$ (*m/z* 1269) noted by ESMS but these species were of significantly lower intensity than the $[Co_6As(CO)_{16}]^-$ signal.

Reaction of $SbCl_3$ with $Na[Co(CO)_4]$

A thf solution (10 mL) of $SbCl_3$ (0.133 g, 0.59 mmol) was added slowly to a cooled (-60°C) thf solution of $Na[Co(CO)_4]$ (0.68 g, 3.51 mmol). The solution was warmed to ambient temperature, refluxed for 8 hours, and the composition monitored by ESMS. Signals corresponding to $[Sb_2Co_4(CO)_{11}]^-$ (*m/z* 788) and $[Sb_2Co_5(CO)_{14}]^-$ (*m/z* 931) were detected after 30 minutes at reflux and no further cluster species were observed over the course of the reaction (though attempts to analyse the reaction solution using ESMS were hampered by precipitation of the sample).

Reaction of $BiBr_3$ with $Na[Co(CO)_4]$

A thf solution (5 mL) of $BiBr_3$ (0.2 g, 0.45 mmol) was added slowly to a cooled thf solution (20 mL) of $Na[Co(CO)_4]$ (0.34 g, 1.76 mmol). The mixed solution was warmed to ambient temperature at which point ESMS analysis indicated the presence of $[Bi\{Co(CO)_4\}_4]^-$ (*m/z* 893). The reaction solution was refluxed for 9 hours with a decrease noted in the intensity of the $[Bi\{Co(CO)_4\}_4]^-$ ion and detection of a series of unidentified signals, some (based on high-resolution spectra) containing Br^- or Ag^+ (e.g. *m/z* 1487) while others displayed little isotopic variation (e.g. *m/z* 1481, 1579).

Reaction of $Ru_3(CO)_{12}$ with $[PPN]N_3$

To a thf solution (10 mL) containing $Ru_3(CO)_{12}$ (0.02 g, 0.03 mmol) was added $[PPN]N_3$ (0.018 g, 0.03 mmol) and the mixture was heated to reflux. Immediate gas evolution (presumably N_2 and CO) was noted and the colour of the solution deepened from pale orange to deep red/brown over 8 hours. ESMS monitoring of the reaction indicated immediate formation of $[Ru_4(CO)_{13}(NCO)]^-$ (*m/z* 812), which remained the dominant anion throughout the reaction. The solution was maintained at 60°C overnight (16 hours) with subsequent ESMS analysis indicating the presence of three anionic species; $[Ru_5N(CO)_{14}]^-$ (*m/z* 912) and two unidentified di-anions, *m/z* 456 and *m/z* 536.5.

The reaction was repeated in diglyme (10 mL) using an excess of $Ru_3(CO)_{12}$ {0.03 mmol *cf.* 0.016 mmol of $[PPN]N_3$}. The solution was heated to 135°C for 72 hours and monitored at suitable time intervals by ESMS. The following nitrido clusters were identified; $[Ru_5N(CO)_{14}]^-$ (*m/z* 912), $[Ru_6N(CO)_{16}]^-$ (*m/z* 1070), $[Ru_7N(CO)_{18}]^-$ (*m/z* 1227) and $[Ru_{10}N(CO)_{24}]^-$ (*m/z* 1699), along with unassigned signals at *m/z* 853.5 and 771.

Reaction of $Os_3(CO)_{12}$ with $[PPN]N_3$

To a diglyme solution (10 mL) containing $Os_3(CO)_{12}$ (0.02 g, 0.022 mmol) was added $[PPN]N_3$ (0.006 g, 0.011 mmol) and the solution was heated to 135°C for 72 hours. Immediate gas evolution was noted upon heating and ESMS analysis indicated formation of $[Os_3(CO)_{11}(NCO)]^-$ (*m/z* 922). The solution was analysed at suitable time intervals and the following osmium clusters identified; $[Os_4(CO)_{13}(NCO)]^-$ (*m/z* 1168), $[HOs_4(CO)_{13}]^-$ (*m/z* 1127), $[H_3Os_4(CO)_{12}]^-$ (*m/z* 1101), $[HOs_5(CO)_{15}]^-$ (*m/z* 1373) and $[HOs_6(CO)_{18}]^-$ (*m/z* 1647), along with unassigned signals of low intensity. An intense signal at *m/z* 851 was tentatively assigned to $[HOs_3(CO)_9(CN)]^-$. ESMS analysis after 72 hours indicated the dominant anion was $[H_3Os_4(CO)_{12}]^-$ and the reaction was halted at this point.

Thermolysis was repeated at 50, 80 and 100°C on a similar scale with similar results. Only limited formation of the higher-nuclearity clusters was observed at the lower temperatures and the presence of hydrido clusters was always noted.

Chapter Seven – Synthesis, Characterisation and Reactivity of $Co_4(\mu_4\text{-}ER)_2(CO)_{11}$ (E = Si, Ge) Clusters

7.1 Introduction

7.1.1 Preface to Chapter

The research reported within this chapter relates to the synthesis and characterisation of a range of neutral $Co_4(\mu_4\text{-}ER)_2(CO)_{11}$ (E = Si, Ge) clusters (henceforth referred to as E_2Co_4 clusters). There were three main interconnected goals of this project; (i) to establish ESMS methods for the characterisation of these neutral clusters, (ii) to examine their reactivity with regards ligand exchange and (iii) to establish new examples of linked Si_2Co_4 clusters. A review of the literature concerning these materials is provided.

7.1.2 Synthesis and Structures of Octahedral E_2M_4 Clusters

Since initial reports of $Co_4(\mu_4\text{-}PPh)_2(CO)_{10}$ (Figure 7.1a)[1], the synthesis and chemistry of compounds containing E_2M_4 cores has attracted considerable interest. The structures of these compounds are based around a M_4 plane, capped above and below by a μ_4-E unit. E_2M_4 clusters are known for group 14, 15 and 16 elements, with the group 14 (Si, Ge) and most group 15 elements (N[2], P, As[3], Sb[4]) five coordinate (with an additional organic or metallic substituent perpendicular to the M_4 plane) while bismuth[5] and the group 16 elements (S[6], Se[7], Te[8]) are only four coordinate [e.g. $Ru_4Te_2(CO)_{11}$ [9] - Figure

[1] R.C. Ryan and L.F. Dahl, *J. Am. Chem. Soc.*, 1975, **97**, 6904.

[2] e.g. $Fe_4(\mu_4\text{-}NEt)_2(CO)_{11}$ – B. Hanset, A.K. Powell and H. Vahrenkamp, *Chem. Ber.*, 1991, **124**, 2697.

[3] e.g. $Co_4(\mu_4\text{-}AsPh)_2(CO)_{10}$ – R.M. De Silva, M.J. Mays, J.E. Davies, P.R. Raithby, M.A. Rennie and G.P. Shields, *J. Chem. Soc., Dalton Trans.*, 1998, 439.

[4] e.g. $[Fe_4\{\mu_4\text{-}SbFe(CO)_4\}_2(CO)_{12}]^{2-}$ – S. Luo and K.H. Whitmire, *J. Organomet. Chem.*, 1989, **376**, 297.

[5] e.g. $Ru_4Bi_2(CO)_{12}$ – C.M. Hay, B.F.G. Johnson, J. Lewis, P.R. Raithby and A.J. Whitton, *J. Chem. Soc., Dalton Trans.*, 1988, 2091.

[6] e.g. $Fe_4S_2(CO)_{11}$ – R.D. Adams, J.E. Babin, J. Estrada, J-G. Wang, M.B. Hall and A.A. Low, *Polyhedron*, 1989, **8**, 1885.

[7] e.g. $Fe_4Se_2(CO)_{11}$ – P. Mathur, M.M. Hossain and R.S. Rashid, *J. Organomet. Chem.*, 1994, **467**, 245.

7.1b]. Octahedral E_2M_4 clusters containing a mixture of group 15 and 16 elements have also been reported [e.g. $Fe_4(\mu_4\text{-}PPh)(\mu_4\text{-}S)(CO)_{11}$ [10] and $Ru_4(\mu_4\text{-}PPh)(\mu_4\text{-}Se)(CO)_{10}(PEt_3)$ [11]].

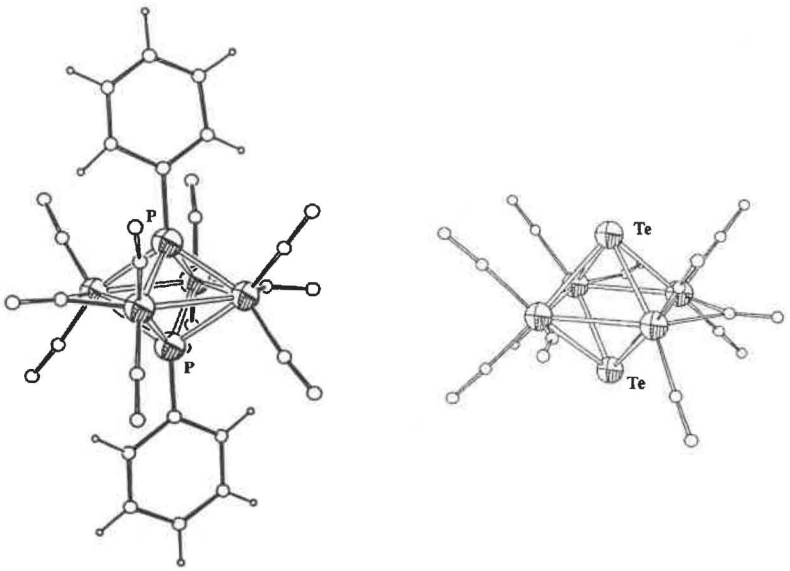

(a) (b)

Figure 7.1 – The structures of $Co_4(\mu_4\text{-}PPh)_2(CO)_{10}$ [1] (a) and $Ru_4Te_2(CO)_{11}$ [9] (b).

The E_2M_4 arrangement is known for various metallic elements (Co, Fe, Ru, Mn, Re), though the majority of reports concern Fe, Ru and Co. The group 14 examples (listed in Table 7.1) are predominantly restricted to cobalt, the exceptions being $Co_3M(\mu_4\text{-}Ge^tBu)_2(CO)_x(\eta^5\text{-}C_5H_5)$ [M = Mo (x = 10), Ni (x = 8)[12]] and $Fe_2Co_2[\mu_4\text{-}GeCo(CO)_4]_2(CO)_{12}$ [13].

[8] e.g. $[Mn_4Te_2(CO)_{12}]^{2-}$ - M. Shieh, H-S. Chen, H-Y. Yang and C-H. Ueng, *Angew. Chem. Int. Ed. Engl.*, 1999, **38**, 1252.

[9] P. Marthur, B.H.S. Thimmappa and A.L. Rheingold, *Inorg. Chem.*, 1990, **29**, 4658.

[10] E. Eber, G. Huttner, D. Gunauer, W. Imhof and L. Zsolnai, *J. Organomet. Chem.*, 1991, **414**, 361.

[11] F. Van Gastel, L. Agocs, A.A. Cherkas, J.F. Corrigan, S. Doherty, R. Ramachandran, N.J. Taylor and A.J. Carty, *J. Cluster Sci.*, 1991, **2**, 131.

[12] P. Gusbeth and H. Vahrenkamp, *Chem. Ber.*, 1985, **118**, 1746.

[13] S.G. Anema, K.M. Mackay and B.K. Nicholson, *J. Chem. Soc., Dalton Trans.*, 1996, 3853.

Table 7.1 – The reported group 14 E_2M_4 clusters

$Co_4(\mu_4\text{-}GeMe)_2(CO)_{11}$	[14]	$Co_4(\mu_4\text{-}SiMe)_2(CO)_{11}$	[19]
$Co_4(\mu_4\text{-}GePh)_2(CO)_{11}$	[12]	$Co_4(\mu_4\text{-}SiPh)_2(CO)_{11}$	[23]
$Co_4[\mu_4\text{-}GeCo(CO)_4]_2(CO)_{11}$	[21]	$Co_4[\mu_4\text{-}SiCo(CO)_4]_2(CO)_{11}$	[20]
$Co_4(\mu_4\text{-}Ge^tBu)_2(CO)_{11}$	[12]	$Co_4(\mu_4\text{-}SiBr)_2(CO)_{11}$	[23]
$Co_4(\mu_4\text{-}GeMe)[\mu_4\text{-}GeCo(CO)_4](CO)_{11}$	[22]	$Co_4(\mu_4\text{-}SiMe)[\mu_4\text{-}SiCo(CO)_4](CO)_{11}$	[15]
$Co_4(\mu_4\text{-}GeEt)[\mu_4\text{-}GeCo(CO)_4](CO)_{11}$	[22]	$Co_4(\mu_4\text{-}SiC_6H_4OMe)_2(CO)_{11}$	[24]
$Co_4(\mu_4\text{-}GePh)[\mu_4\text{-}GeCo(CO)_4](CO)_{11}$	[15]	$Co_4(\mu_4\text{-}SiC_6H_4NMe_2)_2(CO)_{11}$	[24]
$Co_4[\mu_4\text{-}GeMn(CO)_5][\mu_4\text{-}GeCo(CO)_4](CO)_{11}$	[22]	$Co_4(\mu_4\text{-}SiMe)_2(CO)_{10}(\mu_2\text{-}GeMe_2)$	[19]
$Co_4(\mu_4\text{-}GeEt)_2(CO)_{10}[\mu_2\text{-}GeCo_2(CO)_7]$	[16]	$Co_4(\mu_4\text{-}SiMe)_2(CO)_{10}[\mu_2\text{-}Si(Me)Co(CO)_4]$	[15]
$Co_4(\mu_4\text{-}GeMe)_2(CO)_{10}[\mu_2\text{-}Ge(Me)Co(CO)_4]$	[17]	$Co_4[\mu_4\text{-}SiCo(CO)_4](\mu_4\text{-}GeMe)(CO)_{11}$	[15]
$Co_3Mo(\mu_4\text{-}Ge^tBu)_2(CO)_{10}(\eta^5\text{-}C_5H_5)$	[12]	$Co_4[\mu_4\text{-}SiCo(CO)_4](\mu_4\text{-}GeEt)(CO)_{11}$	[15]
$Fe_2Co_2[\mu_4\text{-}GeCo(CO)_4]_2(CO)_{12}$	[13]	$Co_3Ni(\mu_4\text{-}Ge^tBu)_2(CO)_8(\eta^5\text{-}C_5H_5)$	[12]

Group 14 E_2M_4 clusters are accessible through various synthetic routes. The salt elimination reaction between $RGeCl_3$ (R = Ph, ^{t}Bu) and $K[Co(CO)_4]$ provided $Co_4(\mu_4\text{-}GeR)_2(CO)_{11}$ clusters in moderate yield (10-47%)[12,18], whereas $Co_4(\mu_4\text{-}SiMe)_2(CO)_{11}$ (Figure 7.2a) was first isolated as an unlikely product of the reaction between $Co_2(CO)_8$ and $Fe[Si(Me)H_2]_2(CO)_4$ [19] (though a more systematic synthesis involving $MeSiH_3$ is known[19]). An alternative method involved reaction of E_2H_6 reagents with $Co_2(CO)_8$, yielding $Co_4[\mu_4\text{-}ECo(CO)_4]_2(CO)_{11}$ (E = Si[20], Ge[21]) clusters {*via* an isolated extended 'spiro' intermediate, $Co_2[\mu_4\text{-}GeCo_2(CO)_7]_2(CO)_6$ for the germanium cluster}. The inherent difficulties associated with synthesis and handling of the E_2H_6 reagents detract from the general application of this synthetic method.

[14] S.P. Foster, K.M. Mackay and B.K. Nicholson, *J. Chem. Soc., Chem. Commun.*, 1982, 1156.

[15] S.K. Lee, D.Phil. Thesis, University of Waikato, 1988.

[16] S.K. Lee, K.M. Mackay and B.K. Nicholson, *J. Chem. Soc., Dalton Trans.*, 1993, 715.

[17] S.G. Anema, S.K. Lee, K.M. Mackay, B.K. Nicholson and M. Service, *J. Chem. Soc., Dalton Trans.*, 1991, 1201.

[18] P. Gusbeth and H. Vahrenkamp, *J. Organomet. Chem.*, 1983, **247**, C53.

[19] S.G. Anema, S.K. Lee, K.M. Mackay and B.K. Nicholson, *J. Organomet. Chem.*, 1993, **444**, 211.

[20] M.L. Van Tiel, K.M. Mackay and B.K. Nicholson, *J. Organomet. Chem.*, 1987, **326**, C101.

[21] S.P. Foster, K.M. Mackay and B.K. Nicholson, *Inorg. Chem.*, 1985, **24**, 909.

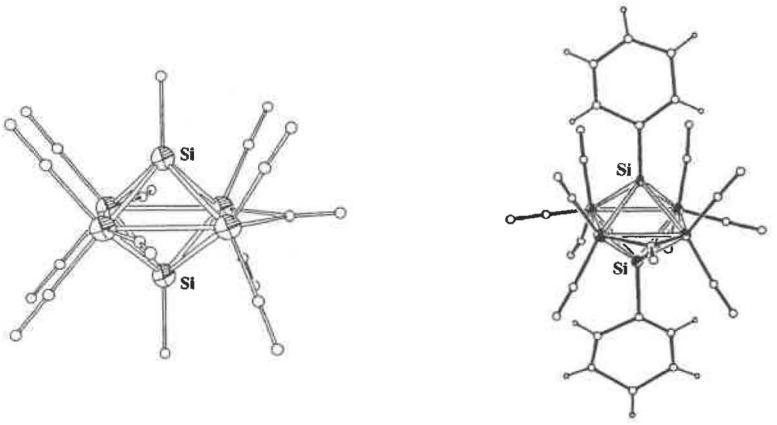

(a) (b)

Figure 7.2 – The structures of $Co_4(\mu_4\text{-}SiMe)_2(CO)_{11}$ [19] (a - hydrogen atoms omitted) and $Co_4(\mu_4\text{-}SiPh)_2(CO)_{11}$ [23] (b).

A preference for the E_2M_4 structure is apparent, as displayed by $Co_4(\mu_4\text{-}GeMe)_2(CO)_{11}$ which is produced from thermal rearrangement of $Co_2[\mu_2\text{-}Ge(Me)Co(CO)_4](CO)_7$ or $Co_2[\mu_2\text{-}Ge(Me)Co(CO)_4]_2(CO)_6$, from reaction between $H_2Ge(Me)Ge(Me)H_2$ and $Co_2(CO)_8$, and from reaction between $MeGeH_3$ and $Co_4(CO)_{12}$ [22]. This last synthesis is the most systematic, utilising a preformed Co_4 core to direct reaction towards the E_2M_4 product. Similar syntheses involving primary silanes have been reported, with yields of Si_2Co_4 clusters [e.g. $Co_4(\mu_4\text{-}SiPh)_2(CO)_{11}$ – Figure 7.2b] varying between quantitative[23] and mediocre (24%)[24]. Equivalent reaction between $PhPH_2$ and $Co_2(CO)_8$ produced $Co_4(\mu_4\text{-}PPh)_2(CO)_{10}$ in greater yield than the traditional salt elimination route[25].

7.1.3 Metal Substitution Reactions

The substitution of units within the metal plane has been reported, producing mixed metal E_2M_4 clusters but leaving the M_4 plane intact. Examples include $Co_3Mo(\mu_4\text{-}Ge^tBu)_2(CO)_{10}(\eta^5\text{-}C_5H_5)$ and $Co_3Ni(\mu_4\text{-}Ge^tBu)_2(CO)_8(\eta^5\text{-}C_5H_5)$ (Figure 7.3), which are produced from reaction between $Co_4(\mu_4\text{-}Ge^tBu)_2(CO)_{11}$ and $[M(CO)_x(\eta^5\text{-}C_5H_5)]_2$ [M =

[22] S.G. Anema, S.K. Lee, K.M. Mackay, L.C. McLeod, B.K. Nicholson and M. Service, *J. Chem. Soc., Dalton Trans*, 1991, 1209.

[23] M.L. Van Tiel, D.Phil. Thesis, University of Waikato, 1991.

[24] G.J. Harfoot, M.Sc. Thesis, University of Waikato, 2000.

[25] B-H. Chang, *Inorg. Chim. Acta*, 1982, **65**, L189.

Mo (x = 3); Ni (x = 1)][12]. The mechanism by which the $M(CO)_x(\eta^5\text{-}C_5H_5)$ moiety can substitute for a $Co(CO)_3$ unit is unknown.

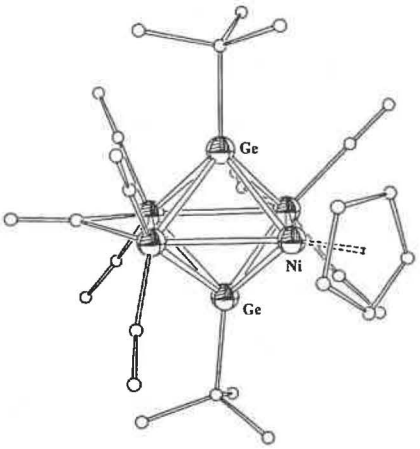

Figure 7.3 – The structure of $Co_3Ni(\mu_4\text{-}Ge^tBu)_2(CO)_8(\eta^5\text{-}C_5H_5)$ (hydrogen atoms omitted)[12].

7.1.4 Ligand Substitution Reactions

An area of considerable research for E_2M_4 clusters is ligand substitution by phosphines, phosphites or isonitriles. To date, these substitution reactions have been limited to the $Co_4(\mu_4\text{-}PPh)_2(CO)_{10}$ and $Fe_4(\mu_4\text{-}PR)_2(CO)_x$ (R = Ph, $C_6H_4CH_3$; x = 11, 12) clusters.

Phosphine substitution was initially identified for $Co_4(\mu_4\text{-}PPh)_2(CO)_{10}$, with enhanced catalytic activity (towards hydroformylation) observed in the presence of PPh_3 [26]. There have been numerous subsequent reports of phosphine substitution[27] including the use of bridging (e.g. $\mu_2\text{-}PPh_2$ [28]) and chelating [e.g. $Ph_2P(CH_2)_xPPh_2$] di-phosphines[29].

---

[26] C.U. Pittman, G.M. Wileman, W.D. Wilson and R.C. Ryan, *Angew. Chem. Int. Ed. Engl.*, 1980, **19**, 478; R.C. Ryan, C.U. Pittman and J.P. O'Connor, *J. Am. Chem. Soc.*, 1977, **99**, 1986.

[27] R.C. Ryan, C.U. Pittman, J.P. O'Connor and L.F. Dahl, *J. Organomet. Chem.*, 1980, **193**, 247; M-J. Don, M.G. Richmond, W.H. Watson and A. Nagl, *Acta Cryst. Sect. C.*, 1991, **47**, 93.

[28] P. Frediani, C. Faggi, S. Papaleo, A. Salvini, M. Bianchi, F. Piacenti, S. Ianelli and M. Nardelli, *J. Organomet. Chem.*, 1997, **536**, 123; U. Florke and H-J. Haupt, *Z. Krystallogr.*, 1990, **192**, 278.

[29] C.L. Schulman, M.G. Richmond, W.H. Waton and A. Nagl, *J. Organomet. Chem.*, 1989, **368**, 367; M.G. Richmond and J.K. Kochi, *Inorg. Chem.*, 1987, **26**, 541; M.G. Richmond and J.K. Kochi, *Organometallics*, 1987, **6**, 254.

Phosphite substitution has been examined in depth for $Co_4(\mu_4\text{-}PPh)_2(CO)_{10}$, with systematic replacement of up to four ligands observed[30,32]. Similar substitution by isonitriles has been reported for $Fe_4(\mu_4\text{-}PR)_2(CO)_{11}$, with maximum substitution of three ligands observed (though the tri-substituted product was unable to be isolated in a pure form[31]). No isonitrile-substituted E_2M_4 clusters have been structurally characterised.

The mechanism for ligand substitution on $Fe_4(\mu_4\text{-}PPh)_2(CO)_{11}$ has been established as ligand addition with subsequent decarbonylation. This was determined through isolation of the series of products; $Fe_4(\mu_4\text{-}PPh)_2(CO)_{11}$, $Fe_4(\mu_4\text{-}PPh)_2L(CO)_{11}$ and $Fe_4(\mu_4\text{-}PPh)_2L(CO)_{10}$ [L = $P(OMe)_3$, ^tBuNC], though only the unsaturated (eleven ligand) di- and tri-substituted products have been isolated[31]. The $Fe_4(\mu_4\text{-}PR)_2(CO)_x$ (x = 11, 12) system is rare as both the saturated and unsaturated E_2M_4 clusters are stable.

A substitution mechanism for $Co_4(\mu_4\text{-}PPh)_2(CO)_{10}$ has been reported[32], though in this case phosphite addition causes cleavage of a Co-Co bond, with the M_4 plane regenerated through decarbonylation. An alternative electron-transfer catalytic (ETC) mechanism (Scheme 7.1) has been reported for phosphine substitution[33]. Evidence for this mechanism was provided by enhanced substitution in the presence of a reducing agent (e.g. Na/benzophenone) or through application of a cathodic current to the reaction solution.

The electrochemistry of the phosphite-substituted clusters (the di-substituted product is shown in Figure 7.4) has been examined in depth, with a shift to more negative reduction potential observed with increasing substitution[33]. The increasing ease of oxidation is presumably a factor of the weaker π-acceptor character of the phosphite ligand (compared to carbonyl) localising electron density on the cluster core and promoting oxidation. Equivalent electrochemistry has been reported for the phosphite- and isonitrile-substituted $Fe_4(\mu_4\text{-}PPh)_2(CO)_{11}$ clusters[34].

---

[30] M.G. Richmond and J.K. Kochi, *Inorg. Chim. Acta*, 1987, **126**, 83.

[31] J.T. Jaeger, S. Aime and H. Vahrenkamp, *Organometallics*, 1986, **5**, 245.

[32] M.G. Richmond and J.K. Kochi, *Inorg. Chem.*, 1986, **25**, 1334.

[33] M.G. Richmond and J.K. Kochi, *Inorg. Chem.*, 1986, **25**, 656.

[34] J.T. Jeager, J.S. Field, D. Collison, G.P. Speck, B.M. Peake, J. Hähnle and H. Vahrenkamp, *Organometallics*, 1988, **7**, 1753.

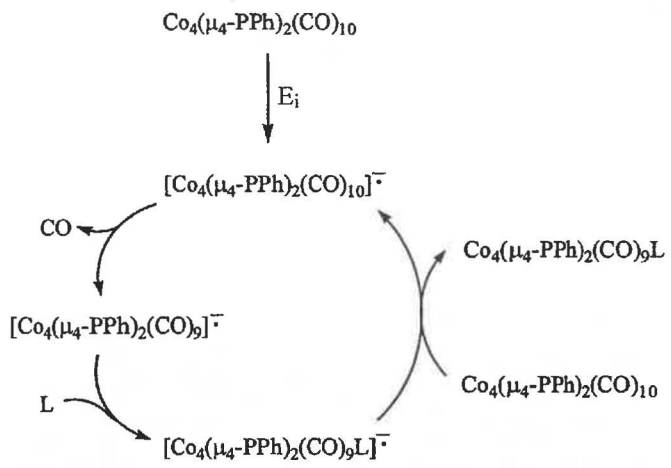

Scheme 7.1 – Electrocatalytic ligand substitution for $Co_4(\mu_4\text{-}PPh)_2(CO)_{10}$ [33].

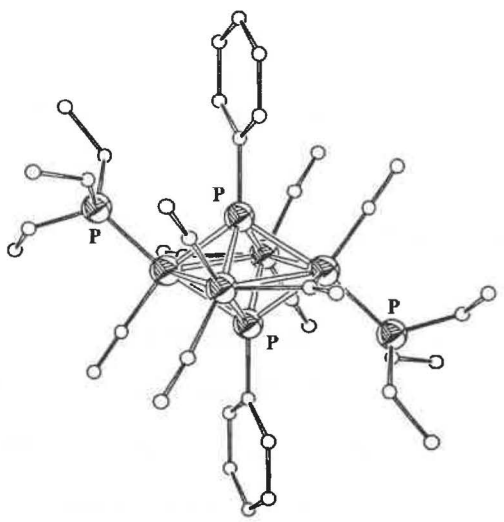

Figure 7.4 – The structure of $Co_4(\mu_4\text{-}PPh)_2(CO)_8[P(OMe)_3]_2$ (hydrogen atoms omitted) [32].

7.1.5 Linked Clusters

An interesting aspect of the chemistry of E_2M_4 clusters is the ability to link the octahedral centres through bridging moieties. The use of di-fuctionalised ligand substitution reagents {e.g. *p*-$[(CH_3O)_2P]_2C_6H_4$, $(CH_3O)_2PCH_2CH_2P(OCH_3)_2$, *p*-$(CN)_2C_6H_4$} allowed isolation of compounds containing two and three linked P_2Fe_4 cluster cores[35] (Figure 7.5). Curiously, though use of the alkyl diphosphite produced the linked cluster, this product decomposed prior to isolation. Electrochemical studies of the linked clusters indicate electronic communication between the P_2Fe_4 centres for the

[35] J.T. Jaeger and H. Vahrenkamp, *Organometallics*, 1988, **7**, 1746.

isonitrile-linked pair but not for the phosphite analogue[34]. An alternative approach using a di-functionalised capping agent [e.g. *p*-$(H_3Si)_2C_6H_4$] has produced the linked cluster *p*-$[Co_4(\mu_4\text{-}SiPh)(CO)_{11}Si]_2C_6H_4$[24].

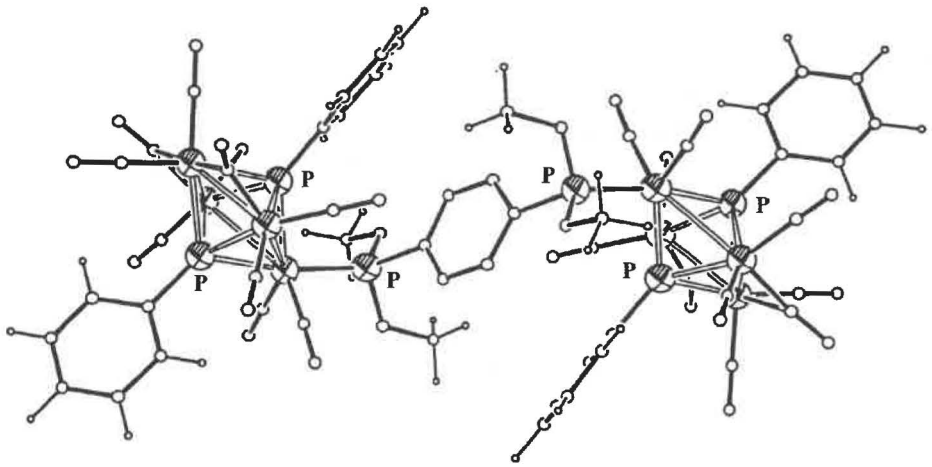

Figure 7.5 – The structure of *p*-$[Fe_4(\mu_4\text{-}PPh)_2(CO)_{10}P(OCH_3)_2]_2C_6H_4$[35].

7.1.6 Theoretical Considerations

There exists some ambiguity in the literature regarding the application of electron-counting procedures to E_2M_4 clusters[36]. The ambiguity arises from the role of the main group element, whether it is considered as a ligand or as part of the cluster core. The different roles produce different cluster electron-counts. For example, $Co_4(\mu_4\text{-}GeMe)_2(CO)_{11}$ is *formally* considered a 68 electron cluster (with 4 electrons provided by the germanium atom, 1 by the methyl substituent) but is more accurately described as a 64 electron species, with each μ_4-GeMe group acting as a 3 electron ligand. Equivalent ambiguity has been reported for other mixed transition metal/main group clusters, the most recent example being $Ru_4(\mu_2\text{-}PF_2)(\mu_4\text{-}P)(CO)_{12}$, where the 'naked' phosphorus atom can be considered as either a 3 or 5 electron-donor[37].

Although ambiguity exists with respect to the role of the main group elements in E_2M_4 clusters, there is agreement that the clusters possess 8 skeletal electron pairs (SEP),

---

[36] Compare W. Wang, J.F. Corrigan, G.D. Enright, N.J. Taylor and A.J. Carty, *Organometallics*, 1998, **17**, 427 to J-F. Halet, *Coord. Chem. Reviews*, 1995, **635**, 637.

[37] S. Kahlal, W. Wang, L. Scoles, K.A. Udachin, J-Y. Saillard and A.J. Carty, *Organometallics*, 2001, **20**, 4469.

higher than the 7 SEP predicted for a *closo*-E_2M_4 octahedron. The electron-rich E_2M_4 clusters are more common than the electron-precise analogues [e.g. $Fe_4(\mu_4\text{-}PR)_2(CO)_{11}$ [31]], provoking theoretical examination to account for the discrepancy. Molecular orbital (MO) calculations (shown diagrammatically in Figure 7.6) indicate a M-M anti-bonding orbital (b_{1u}) is positioned at slightly higher energy than the 7 occupied MO's[39]. Occupation of this MO (leading to the 8 SEP clusters) results in increased M-M bond distances accompanied by a slight E--E attraction. Stabilisation of the 8 SEP species is considered a factor of electronegativity of the transition element (8 SEP clusters are common for cobalt whereas both 7 and 8 SEP E_2Fe_4 clusters are known). Further addition of skeletal electrons results in cleavage of the M-M bond, allowing greater interaction between the main group elements {as noted in the 9 SEP $[Co_4Sb_2(CO)_{11}]^{2-}$ cluster discussed in Section 6.5, which contains a formal Sb-Sb bond[38]}.

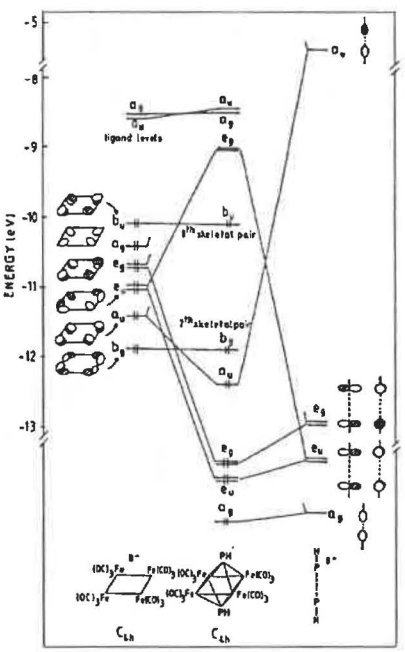

Figure 7.6 – The molecular orbital diagram for $Fe_4(\mu_4\text{-}PH)_2(CO)_{12}$ [39].

The existence of the two stable electron-counts for the $Fe_4(\mu_4\text{-}PR)_2(CO)_x$ (x = 11, 12) clusters has been demonstrated chemically, with the unsaturated (x = 11) clusters undergoing facile addition of 2 electron ligands (phosphines, phosphites, isonitriles) as discussed in Section 7.1.4. With respect to the research documented in this chapter, the

[38] J.S. Leigh, K.H. Whitmire, K.A. Yee and T.A. Albright, *J. Am. Chem. Soc.*, 1989, **111**, 2726.

[39] J-F. Halet, R. Hoffman and J-Y. Saillard, *Inorg. Chem.*, 1985, **24**, 1695.

electron-rich nature of the $Co_4(\mu_4\text{-}ER)_2(CO)_{11}$ (E = Si, Ge) clusters should assist protonation and/or oxidation, allowing ESMS detection of these compounds.

7.2 Synthesis and Characterisation of $Co_4(\mu_4\text{-}ER)_2(CO)_{11}$ [E = Si, R = Ph, C_6H_4OMe, $C_6H_4NMe_2$, $(CH_2)_3OMe$; E = Ge, R = $C_6H_4NMe_2$]

7.2.1 Synthesis

Various synthetic routes to group 14 E_2M_4 clusters have been reported (discussed in Section 7.1.2). The most systematic synthesis involves condensation of a primary silane or germane with $Co_4(CO)_{12}$, releasing H_2 and CO (Scheme 7.2). The synthesis of $Co_4(\mu_4\text{-}SiR)_2(CO)_{11}$ (R = Ph[23], C_6H_4OMe [24], $C_6H_4NMe_2$ [24]) have been reported using this procedure. A crystal structure determination of $Co_4(\mu_4\text{-}SiPh)_2(CO)_{11}$ has been performed though not widely published[23]. Synthesis of these compounds was traditionally performed in sealed ampoules, with reported reaction times ranging from weeks to months.

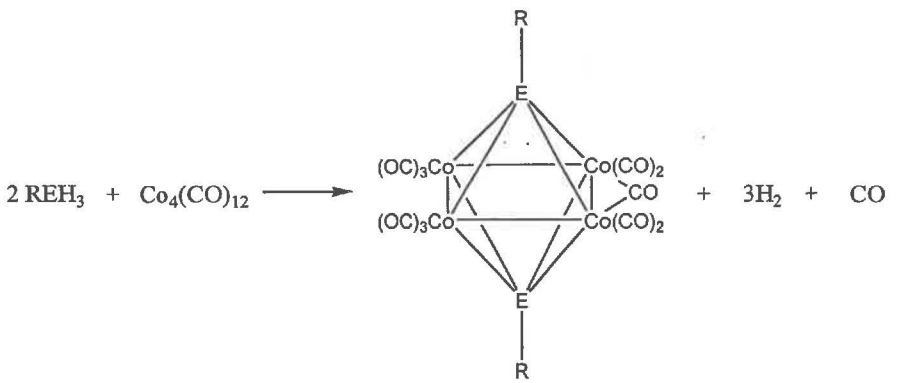

Scheme 7.2 – The synthesis of $Co_4(\mu_4\text{-}ER)_2(CO)_{11}$ clusters.

In this research, the series of $Co_4(\mu_4\text{-}ER)_2(CO)_{11}$ [E = Si, R = Ph, C_6H_4OMe, $C_6H_4NMe_2$, $(CH_2)_3OMe$; E = Ge, R = $C_6H_4NMe_2$] clusters have been prepared, with isolation and subsequent characterisation by ESMS, IR, NMR and elemental analyses. The cluster products were separated from unreacted $Co_4(CO)_{12}$ by column chromatography using an appropriate solvent mixture.

Experimentation with regards reaction conditions indicated that $Co_4(\mu_4\text{-}ER)_2(CO)_{11}$ synthesis using standard Schlenk techniques provided similar yields to reactions performed in sealed ampoules. The previous use of these ampoules is attributed to the highly volatile and pyrophoric silane reagents employed (e.g. $MeSiH_3$, Si_2H_6) which made Schlenk techniques inappropriate. Similarly, suitable yields of the $Co_4(\mu_4\text{-}ER)_2(CO)_{11}$ compounds were isolated after reaction for 24-48 hours at 50°C rather than the extended reaction times previously reported.

A large quantity of unreacted $Co_4(CO)_{12}$ was noted in all syntheses. This was easily separated from the intended $Co_4(\mu_4\text{-}ER)_2(CO)_{11}$ cluster using standard chromatographic procedures but its presence was of concern. Synthesis of the $Co_4(\mu_4\text{-}EC_6H_4NMe_2)_2(CO)_{11}$ (E = Si, Ge) clusters produced both a purple by-product (of unknown origin, though ESMS and NMR indicate the absence of the NMe_2 functionality) and an intractable black solid, which may account for the unreacted $Co_4(CO)_{12}$ and low yield of the E_2Co_4 clusters. These by-products were absent in the remaining syntheses and the large amount of unreacted $Co_4(CO)_{12}$ less easily explained. The clusters all displayed a degree of air-sensitivity, most pronounced for $Co_4[\mu_4\text{-}Si(CH_2)_3OMe]_2(CO)_{11}$ which decomposed within 15-20 minutes at room temperature upon exposure to oxygen.

7.2.2 ESMS Characterisation

The $Co_4(\mu_4\text{-}ER)_2(CO)_{11}$ [E = Si, R = Ph, C_6H_4OMe, $C_6H_4NMe_2$, $(CH_2)_3OMe$; E = Ge, R = $C_6H_4NMe_2$] clusters were characterised in the first instance by ESMS. The dimethylamino-functionalised clusters were detected as their protonated ions {$[M+H]^+$, *m/z* 841 and 931 for E = Si, Ge respectively}. Induced carbonyl loss (by increasing the applied cone voltage) resulted in the removal of 7 ligands before spectral quality deteriorated (Figure 7.7).

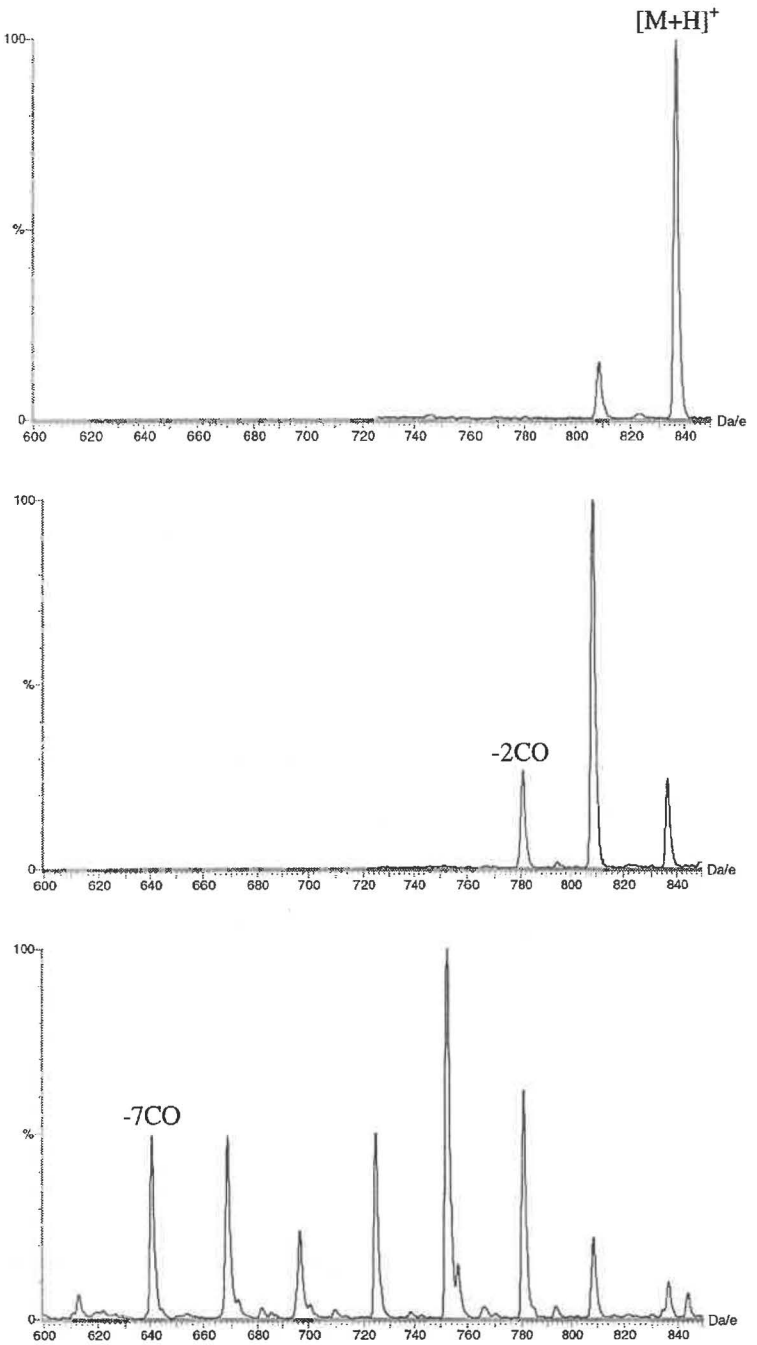

Figure 7.7 – The induced CO loss from $Co_4(\mu_4\text{-}SiC_6H_4NMe_2)_2(CO)_{11}$ at 20, 40 and 60 cV (+ve ion).

The remaining $Co_4(\mu_4\text{-}SiR)_2(CO)_{11}$ [R = Ph, C_6H_4OMe, $(CH_2)_3OMe$] clusters failed to ionise under standard conditions. The lack of a suitable basic site for protonation on $Co_4(\mu_4\text{-}SiPh)_2(CO)_{11}$ accounts for its inability to ionise but the methoxy functionality present on the remaining clusters should promote protonation. The functionalised silanes were specifically synthesised to allow ESMS detection of these clusters in a

similar manner to the use of methoxy-functionalised phosphines and arsines[40]. Contrary to previous reports[24], the $Co_4(\mu_4\text{-}SiR)_2(CO)_{11}$ (R = Ph, C_6H_4OMe) clusters failed to undergo oxidation during ESMS analysis despite their electron-rich character.

Various techniques were employed in attempts to ionise the clusters to allow ESMS detection. Attempts to enhance oxidation of the clusters through the addition of oxidising agents {e.g. Ag^+, $[NO]^+$, $[Fe(\eta^5\text{-}C_5H_5)_2]^+$ (plus mono- and di-acetyl substituted ferricenium salts)} were unsuccessful. Other cluster ionisation agents including Na^+, $[OMe]^-$ and N_3^- (the use of which were discussed in Chapter 1) were also unsuccessful in ionising the Si_2Co_4 clusters.

Attempts to systematically ionise the clusters using $Na[BH_4]$ were also unsuccessful. The quantitative production of $[Co_4(\mu_4\text{-}PPh)_2(CO)_9H]^-$ from $Co_4(\mu_4\text{-}PPh)_2(CO)_{10}$ is known[41] and equivalent generation of $[Co_4(\mu_4\text{-}ER)_2(CO)_{10}H]^-$ was considered viable. However, ESMS analysis of the solution after hydride addition showed no evidence for formation of the ionised cluster.

Finally, a method for the systematic derivatisation of $Co_4(\mu_4\text{-}SiR)_2(CO)_{11}$ clusters for ESMS detection was discovered in isonitrile substitution (discussed in detail in Section 7.3.2). Under standard conditions, a preference for the substitution of six ligands was observed (Figure 7.8), with the substituted products significantly more prone to oxidation than the parent cluster. Therefore, the $Co_4(\mu_4\text{-}SiR)_2(CO)_{11}$ [R = Ph, C_6H_4OMe, $(CH_2)_3OMe$] clusters were characterised by ESMS as their $[Co_4(\mu_4\text{-}SiR)_2(CO)_5(RNC)_6]^+$ ions.

[40] C. Decker, W. Henderson and B.K. Nicholson, *J. Chem. Soc., Dalton Trans.*, 1999, 3501; C. Decker, unpublished results.

[41] M.G. Richmond and J.K. Kochi, *Organometallics*, 1987, **6**, 777.

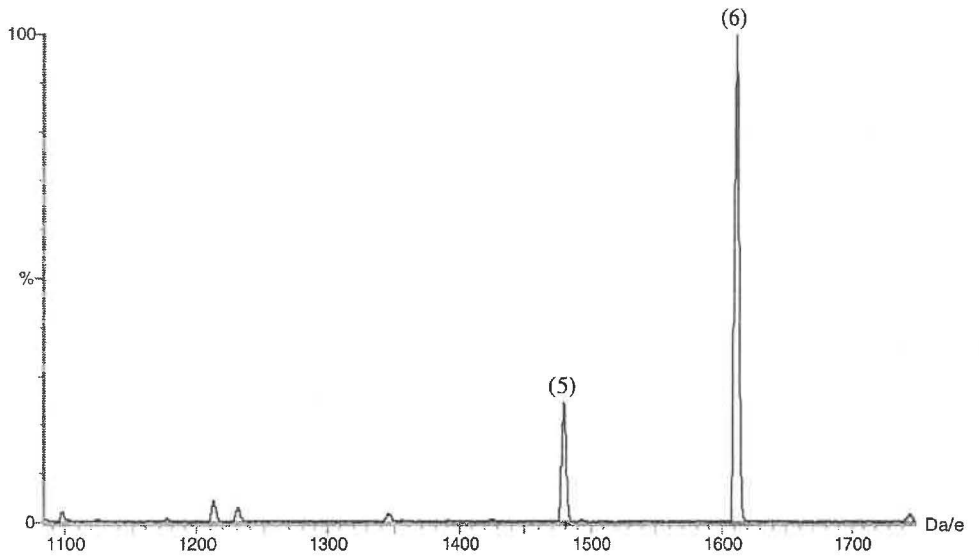

Figure 7.8 – The ES mass spectrum (+ve ion, 10 cV) of $Co_4(\mu_4\text{-}SiC_6H_4OMe)_2(CO)_{11}$ after treatment with AdNC. Signals are labelled with respect to the degree of substitution i.e. (6) = $[Co_4(\mu_4\text{-}SiC_6H_4OMe)_2(CO)_5(AdNC)_6]^+$.

7.2.3 Infra-red (IR) Characterisation

The predominant characterisation method reported for $Co_4(\mu_4\text{-}ER)_2(CO)_{11}$ clusters has been IR spectroscopy. The spectra of these clusters are distinctive, with a strong signal in the region 2050-2030 cm^{-1} and shoulder signals apparent between 2030-2000 cm^{-1}. A weak signal around 1800-1870 cm^{-1}, attributed to the bridging carbonyl, is also characteristic of these compounds. IR data for the clusters produced in this research are presented in Table 7.2 with the spectrum of $Co_4(\mu_4\text{-}GeC_6H_4NMe_2)_2(CO)_{11}$ displayed in Figure 7.9.

Table 7.2 – IR data (ν_{CO}, CH_2Cl_2) for the $Co_4(\mu_4\text{-}ER)_2(CO)_{11}$ clusters

SiPh	SiC_6H_4OMe	$SiC_6H_4NMe_2$	$Si(CH_2)_3OMe$	$GeC_6H_4NMe_2$
2085 (w)	2082 (w)	2073 (w)	2083 (w)	2073 (w)
2045 (vs)	2044 (vs)	2040 (vs)	2039 (vs)	2034 (s)
2028 (s,sh)	2027 (m,sh)	2027 (m,sh)	2019 (m,sh)	2016 (m,sh)
2014 (m,sh)	2013 (m,sh)	2011 (m,sh)	2006 (m,sh)	2001 (m,sh)
		1976 (w)	1979 (m,sh)	
1852 (w,br)	1849 (w,br)	1848 (w,br)	1851 (w,br)	1846 (w,br)

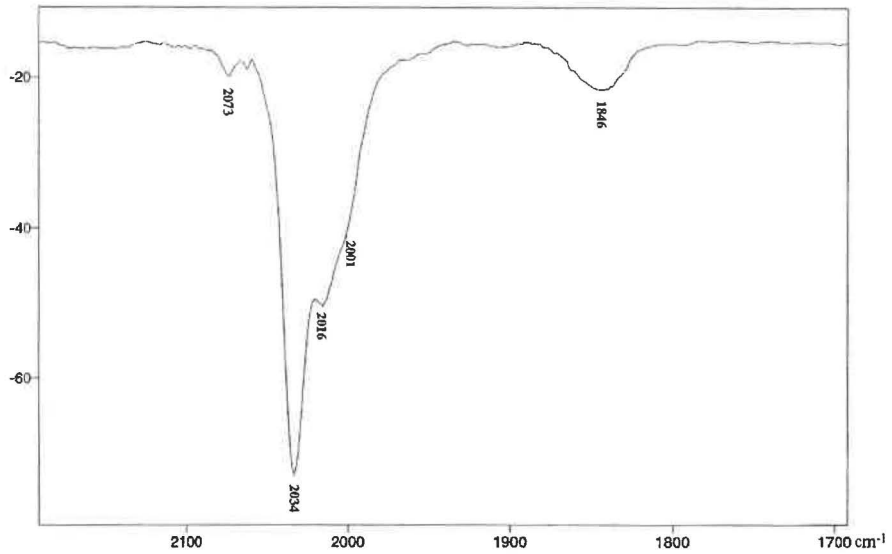

Figure 7.9 – The IR spectrum (ν_{CO}, CH_2Cl_2) of $Co_4(\mu_4\text{-}GeC_6H_4NMe_2)_2(CO)_{11}$.

The distinctive $Co_4(\mu_4\text{-}ER)_2(CO)_{11}$ IR pattern is easily distinguished from $Co_4(CO)_{12}$, allowing spectroscopic monitoring of the synthesis. Obviously, reaction monitoring was unavailable using sealed ampoules but the analysis of $Co_4(\mu_4\text{-}ER)_2(CO)_{11}$ formation using Schlenk techniques indicated completion of reaction within 48-72 hours, though a large quantity of unreacted $Co_4(CO)_{12}$ was still detectable.

7.2.4 Nuclear Magnetic Resonance (NMR) Characterisation

The $Co_4(\mu_4\text{-}ER)_2(CO)_{11}$ clusters were also characterised by NMR spectroscopy. The signals detected were typically broad (caused by the quadrupolar ^{59}Co nuclei) and evaluation of the fine structure associated with the signals was not possible. The spectra obtained mimicked that of the starting silane and signals were not shifted significantly through reaction. Loss of the signals associated with the EH_3 functionality and the presence of a carbonyl signal in the ^{13}C spectra were the only points of interest. Although both bridging and terminal ligands are present on the clusters, only a single carbonyl signal was detected with a chemical shift (203-206 ppm) indicative of a terminal orientation [more similar to the 203.9 ppm for terminal CO ligands than 238.6 ppm for μ_2-CO reported for $Co_4(\mu_4\text{-}PPh)_2(CO)_{10}$ [32]]. The absence of a bridging signal was attributed to ligand fluxionality in solution at standard temperatures [the μ_2-CO signal for $Co_4(\mu_4\text{-}PPh)_2(CO)_{10}$ was identified at $-75^{\circ}C$[32]]. Spectra were assigned using a variety of NMR experiments (discussed in Chapter 2), an example being the ^1H-^{13}C

correlation spectrum (HSQC – Heteronuclear Single Quantum Coherence) of $Co_4[\mu_4\text{-}Si(CH_2)_3OMe]_2(CO)_{11}$ (Figure 7.10).

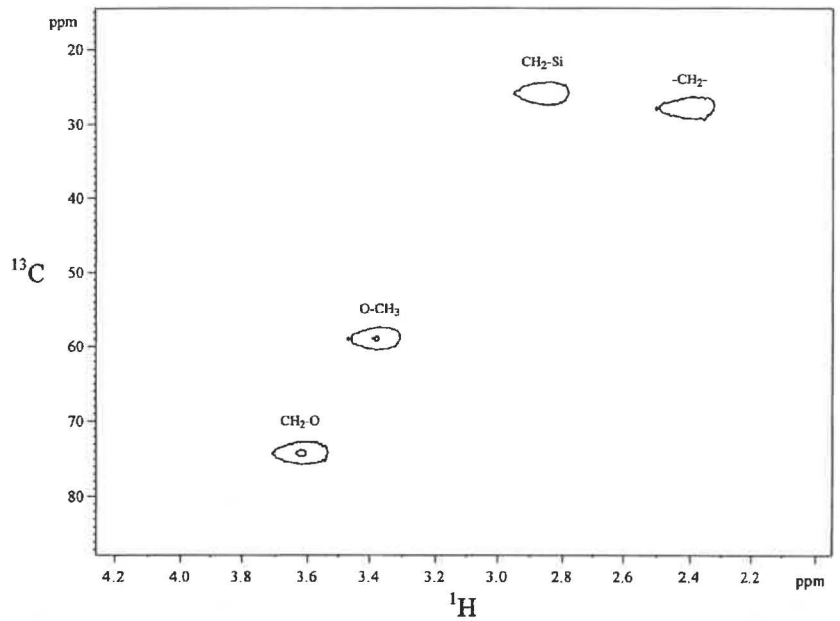

Figure 7.10 – The ^1H-^{13}C correlation spectrum of $Co_4[\mu_4\text{-}Si(CH_2)_3OMe]_2(CO)_{11}$.

7.2.5 Attempted ^{29}Si NMR Analysis

^{29}Si NMR analysis of transition metal silyl complexes is relatively rare. The majority of data available relate to simple R_3SiML [ML = $Co(CO)_4$, $Mn(CO)_5$, $Re(CO)_5$ [42], $Fe(CO)_2(\eta^5\text{-}C_5H_5)$ [42,43]] complexes, though bridging examples [e.g. $Fe_2(\mu_2\text{-}SiMe_2)(CO)_8$ [44]] have been reported. ^{29}Si data for the all-metal substituted $(CO)_2(\eta^5\text{-}C_5H_5)FeSiCo_3(CO)_9$ cluster have also been reported[45].

Although $Co_4(\mu_4\text{-}SiR)_2(CO)_{11}$ clusters are well known, ^{29}Si NMR analysis of these compounds has been elusive. This failure has been attributed to the low sensitivity of the ^{29}Si nuclei (a factor of low natural abundance, a relatively small gyromagnetic ratio and long spin-lattice relaxation times) and to the quadrupolar ^{59}Co nuclei causing broadening of the signal.

---

[42] S. Li, D.L. Johnson, J.A. Gladysz and K.L. Servis, *J. Organomet. Chem.*, 1979, **166**, 317.

[43] K.H. Pannell and A.R. Bassindale, *J. Organomet. Chem.*, 1982, **229**, 1.

[44] A.L. Bikovetz, O.V. Kuzmin, V.M. Vdovin and A.M. Krapivin, *J. Organomet. Chem.*, 1980, **194**, C33.

[45] W. Malisch, H.U. Wekel, I. Grob and F.H. Koehler, *Z. Naturforsch. B*, 1982, **37**, 601.

The synthesis of $Co_4[\mu_4\text{-}Si(CH_2)_3OMe]_2(CO)_{11}$ allowed an alternative approach to ^{29}Si NMR analysis through use of an insensitive nuclei enhancement by polarisation transfer (INEPT) experiment. The intensity of a NMR signal is an effect of the population difference between excited and ground spin states. In a spin-coupled system it is possible to enhance the signal of insensitive nuclei through a transfer of energy from sensitive coupled nuclei (usually ^1H). This approach is used extensively to enhance ^{13}C signals (the DEPT experiments) and has also been applied to ^{29}Si spectra of both organic[46] and organometallic compounds[42].

The INEPT method was applied to ^{29}Si NMR analysis of $Co_4[\mu_4\text{-}Si(CH_2)_3OMe]_2(CO)_{11}$ without success. A difficulty with this approach is that enhancement of the ^{29}Si signal is dependent upon $^2J_{Si\text{-}H}$, a value that was unable to be directly measured because of line broadening in the ^1H spectrum. Comparison to other Si-M systems indicated a value *ca.* 6-7 Hz was appropriate [e.g. $Me_3SiCo(CO)_4$, $^2J_{Si\text{-}H}$ = 6.7 Hz; $Me_3SiFe(CO)_2(\eta^5\text{-}C_5H_5)$, $^2J_{Si\text{-}H}$ = 6.5 Hz[42]] but extended irradiation for $^2J_{Si\text{-}H}$ at 5, 6, 7 and 10 Hz failed to enhance the ^{29}Si signal to allow detection.

To ensure that the technique had been appropriately applied, a ^{29}Si NMR spectrum of $H_3Si(CH_2)_8SiH_3$ was acquired, with enhancement using a $^2J_{Si\text{-}H}$ value of 10 Hz. This produced a strong quartet signal (attributable to $^1J_{Si\text{-}H}$ coupling) centred at -56.95 ppm with respect to TMS. The inability to observe equivalent enhancement in the cluster sample was frustrating and ^{29}Si NMR analysis of these clusters remains unavailable.

The absence of the ^{29}Si signal may be an effect of the cobalt nuclei. ^{31}P is a significantly more sensitive nucleus than ^{29}Si yet ^{31}P NMR analysis of $[Co_6P(CO)_{16}]^-$ provides no signal at standard temperatures, with cooling to –35°C required for detection[47]. The difficulties associated with ^{31}P NMR analysis of cluster species indicate that ^{29}Si NMR analysis may be an unattainable goal.

---

[46] B.J. Helmer and R. West, *Organometallics*, 1982, **1**, 877.

[47] P. Chini, G. Ciani, S. Martinengo and A. Sironi, *J. Chem. Soc., Chem. Commun.*, 1979, 188.

7.2.6 Electrochemistry of $Co_4(\mu_4\text{-}SiR)_2(CO)_{11}$ Clusters

A preliminary electrochemical analysis of the $Co_4(\mu_4\text{-}SiC_6H_4R)_2(CO)_{11}$ (R = H, OMe, NMe_2) clusters was performed using an Optically Transparent Thin Layer Electrochemical (OTTLE) cell[48]. The OTTLE cell combines rapid electrolysis of a small sample volume with *in situ* spectroscopic characterisation techniques (FTIR, UV-Vis). Although the electrochemical products are seldom able to be isolated, information about their composition can be inferred from the spectroscopic analysis.

Electrochemical analysis of the $Co_4(\mu_4\text{-}SiC_6H_4R)_2(CO)_{11}$ clusters was performed in CH_2Cl_2 and monitored by FTIR. The electrochemical characteristics of the three compounds were similar, though the features were broad and a more rigorous examination is required if significant importance is to be placed on these results.

In each case, a broad reduction wave was detected at –0.5 V, with a second reduction noted at *ca.* –1.2 V. IR analysis of the R = NMe_2 cluster during the initial reduction (Figure 7.11) displayed a decrease in the intensity of the signals attributed to the parent cluster (2079, 2039, 2023, 2008 and 1849 cm^{-1}), with new signals detected at 1943, 1923, 1909 and 1751 cm^{-1}. In essence, the spectrum of the reduced species is similar to that of the parent cluster but shifted to lower wavenumber, the shift attributed to the formation of a radical anionic species, possibly $[Co_4(\mu_4\text{-}SiR)_2(CO)_{11}]^{\bullet-}$ {the group 14 analogue of $[Co_4(\mu_4\text{-}PPh)_2(CO)_{10}]^{\bullet-}$}. The formation of this radical anion accounts for the observed signals, especially the 1751 cm^{-1} absorbance attributed to μ_2-CO in an anionic cluster [a similar pattern was reported for the radical anion of $Fe_4(\mu_4\text{-}PPh)_2(CO)_{11}$ [34]]. The second reduction process resulted in a decrease in the intensity of these signals matched by detection of signals associated with CO_2, attributed to decomposition of the sample.

[48] Prof. B.H. Robinson, University of Otago is thanked for performing these analyses.

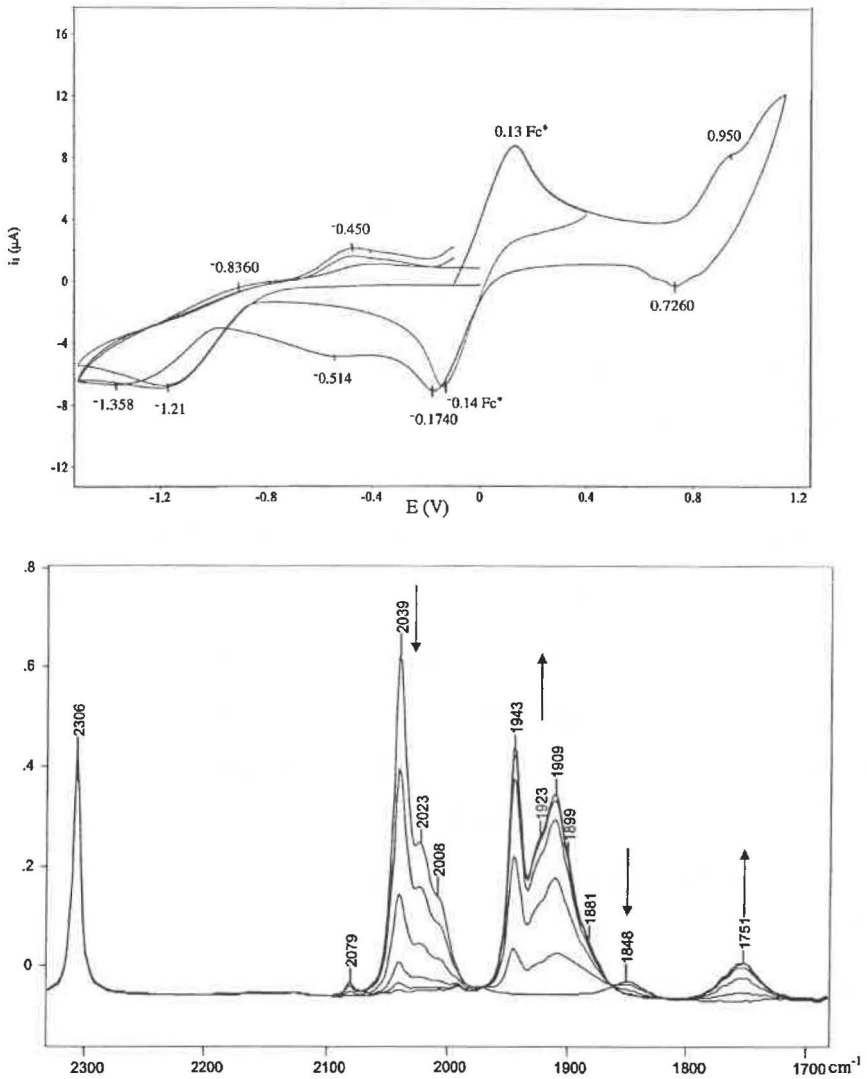

Figure 7.11 – The cyclic voltametric scan of $Co_4(\mu_4\text{-}SiC_6H_4NMe_2)_2(CO)_{11}$ (upper) and FTIR spectrum of the first reduction process (lower).

The formation of a chemically irreversible oxidation product was noted electrochemically at *ca.* 0.95 V. IR analysis of the dimethylamino cluster during oxidation displayed a decrease in the signals associated with the parent cluster (2079, 2039, 2023, 2008 cm^{-1}) accompanied by appearance of new signals at 2063, 2055 and 2035 cm^{-1}. These signals were attributed to $Co_4(CO)_{12}$, produced during decomposition of the cluster material. Reduction of the solution failed to regenerate the parent cluster.

In summary, oxidation of the $Co_4(\mu_4\text{-}SiC_6H_4R)_2(CO)_{11}$ clusters was possible but appeared irreversible. Reduction generated an anionic cluster species, possibly $[Co_4(\mu_4\text{-}SiR)_2(CO)_{11}]^-$, though further reduction of the solution caused decomposition of this cluster.

7.3 Reactions of $Co_4(\mu_4\text{-}ER)_2(CO)_{11}$ Clusters

7.3.1 Introduction

The reactions of $Co_4(\mu_4\text{-}SiR)_2(CO)_{11}$ clusters with various ligand and metal reagents have been briefly examined previously with very limited results[49]. Attempted characterisation of the reaction products by IR and NMR met with limited success since the spectra of different substitution products were similar and all attempts at crystallographic structure determination were unsuccessful.

The presence of the 'electrospray-friendly' dimethylamino functionality on $Co_4(\mu_4\text{-}SiC_6H_4NMe_2)_2(CO)_{11}$ allows detection of this cluster under standard conditions {as the $[M+H]^+$ ion, *m/z* 841} making it ideal for examining substitution reactions of $Co_4(\mu_4\text{-}ER)_2(CO)_{11}$ clusters. As both the starting cluster and substituted products were 'electrospray-friendly', the extent of substitution was monitored by ESMS analysis of the reaction solution. Both ligand (phosphines, phosphites and isonitriles) and metal $\{[Mo(CO)_3(\eta^5\text{-}C_5H_5)]_2\}$ substitution reactions were examined.

7.3.2 Isonitrile Substitution Reactions

Results and Discussion

The reactions between $Co_4(\mu_4\text{-}ER)_2(CO)_{11}$ and various isonitrile reagents [*tert*-butylisonitrile (^{t}BuNC), xylylisonitrile (XyNC) and adamantylisonitrile (AdNC)] were performed in various solvents (heptane, toluene and CH_2Cl_2). Substitution was noted in all solvents and monitored by ESMS (though CH_2Cl_2 was used in preference as the starting materials were more soluble in this solvent and the ES mass spectra typically more intense). The reactions were initially examined using the 'electrospray-friendly' $Co_4(\mu_4\text{-}SiC_6H_4NMe_2)_2(CO)_{11}$ cluster but were later applied to the full series of $Co_4(\mu_4\text{-}ER)_2(CO)_{11}$ compounds.

ESMS analysis of the reaction between an excess of XyNC (10:1) and $Co_4(\mu_4\text{-}SiC_6H_4NMe_2)_2(CO)_{11}$ in CH_2Cl_2 indicated formation of the mono-substituted product

[49] R. Gilkison, M.Sc. Thesis, University of Waikato, 1993.

$\{Co_4(\mu_4\text{-}SiC_6H_4NMe_2)_2(CO)_{10}(XyNC)$, $[M+H]^+$ - *m/z* 944$\}$ within 5-10 minutes. Further substitution was noted over the course of 3-4 hours, with the detection of all products in the range $Co_4(\mu_4\text{-}SiC_6H_4NMe_2)_2(CO)_{11-x}(XyNC)_x$ (x = 0-8 - Figure 7.12), the dominant product after extended reaction times (2-4 hours) corresponding to the hexa-substituted product $\{Co_4(\mu_4\text{-}SiC_6H_4NMe_2)_2(CO)_5(XyNC)_6$, $[M+H]^+$ - *m/z* 1459$\}$. The rate of substitution was increased by heating the solution to 35°C in an oil bath, with facile substitution of six ligands observed within 60 minutes.

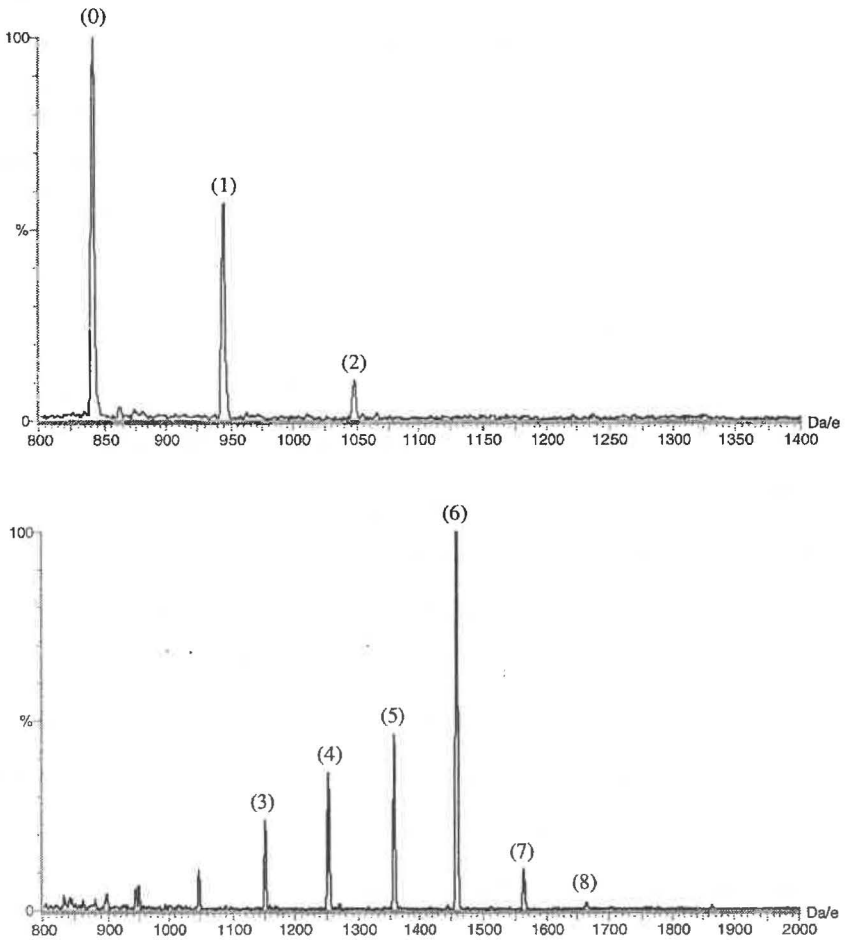

Figure 7.12 – The ES mass spectrum (+ve ion, 15 cV) of XyNC substitution on $Co_4(\mu_4\text{-}SiC_6H_4NMe_2)_2(CO)_{11}$, 5 minutes (upper) and 20 minutes (lower) after isonitrile addition. Signals are labelled with respect to the degree of substitution i.e. (6) = $[Co_4(\mu_4\text{-}SiC_6H_4NMe_2)_2(CO)_5(XyNC)_6+H]^+$.

The use of ^{t}BuNC or AdNC rather than XyNC resulted in a similar pattern of substitution on a similar time scale. In each case, spectra acquired after 45-60 minutes at 30-35°C were dominated by the $Co_4(\mu_4\text{-}SiC_6H_4NMe_2)_2(CO)_5(RNC)_6$ product $\{[M+H]^+$, *m/z* 1171 and 1640 for R = ^{t}Bu, Ad respectively$\}$.

Examination of these reactions revealed an increase in the ES mass spectral intensity with substitution. An explanation for this is the difference in electronic character between carbonyl and isonitrile ligands. Isonitriles are stronger σ-donors but weaker π-acceptor ligands with respect to carbonyls, indicating that isonitrile substitution would increase the electron density localised on the metal core of the cluster and thereby activate the cluster towards protonation.

The substitution of carbonyl ligands by isonitriles also had implications for the 'electrospray-invisible' $Co_4(\mu_4\text{-}SiR)_2(CO)_{11}$ (R = Ph, C_6H_4OMe) clusters. These clusters are electron-rich (8 SEP) and isonitrile substitution should promote oxidation of these clusters, allowing ESMS detection. An equivalent effect has been reported for the $Fe_4(\mu_4\text{-}PPh)_2(CO)_{11-x}L_x$ (x = 1, 2; L = ^{t}BuNC) clusters, with the isonitrile-substituted products more easily oxidised electrochemically than the parent cluster[31].

The reactions of $Co_4(\mu_4\text{-}SiC_6H_4R)_2(CO)_{11}$ (R = H, OMe) with R'NC (R' = ^{t}Bu, Xy) were performed in an identical manner to that discussed above, though initial spectra lacked signals associated with the parent cluster. Within 15-20 minutes of heating, $[M]^+$ signals attributable to the substituted products $Co_4(\mu_4\text{-}SiC_6H_4R)_2(CO)_{11-x}(R'NC)_x$ (x = 3-6) were detected, with spectra after extended reaction (Figure 7.13) dominated by the signals corresponding to hexa-substituted products [$Co_4(\mu_4\text{-}SiC_6H_4R)_2(CO)_5(R'NC)_6$; R = H, R' = ^{t}Bu (*m/z* 1084), Xy (*m/z* = 1372); R = OMe, R' = ^{t}Bu (*m/z* 1144), Xy (*m/z* 1432)]. The signals observed corresponded to oxidation of the substituted cluster rather than the protonation observed for the dimethylamino analogues. The simplicity and selectivity of substitution provided an ideal method for the characterisation of the 'electrospray-invisible' $Co_4(\mu_4\text{-}SiR)_2(CO)_{11}$ clusters.

As with the dimethylamino analogue, the dominant signals after extended reaction time corresponded to the hexa-substituted products. The maximum degree of substitution detected were the $Co_4(\mu_4\text{-}SiC_6H_4R)_2(CO)_2(XyNC)_9$ clusters {R = NMe_2, $[M+H]^+$ - *m/z* 1769; R = OMe, H, $[M]^+$ *m/z* 1742 and 1682 respectively - Figure 7.14}, with the substitution of all bar two carbonyl ligands. In equivalent reactions involving ^{t}BuNC and AdNC, the $Co_4(\mu_4\text{-}SiR)_2(CO)_4(R'NC)_7$ clusters were the most highly-substituted products identified.

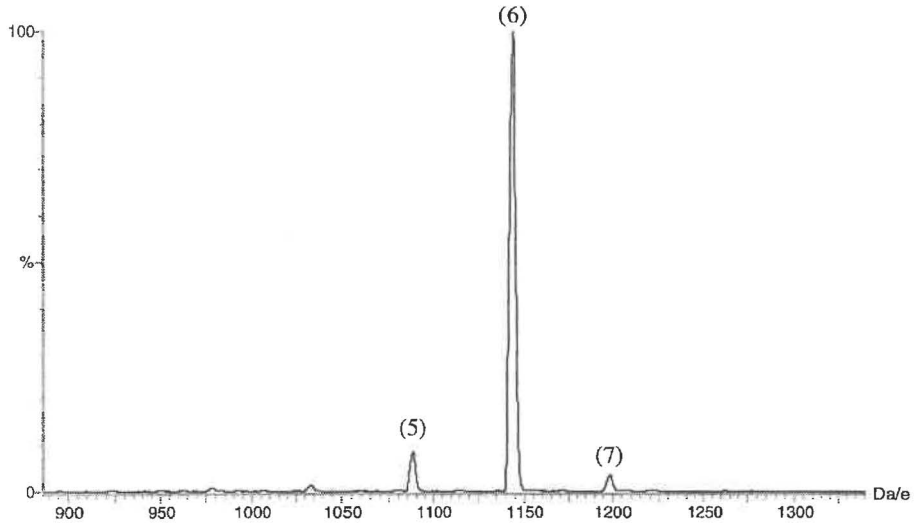

Figure 7.13 – The ES mass spectrum (+ve ion, 10 cV) of ^{t}BuNC substitution on $Co_4(\mu_4\text{-}SiC_6H_4OMe)_2(CO)_{11}$. Signals are labelled with respect to the degree of substitution i.e. (6) = $[Co_4(\mu_4\text{-}SiC_6H_4OMe)_2(CO)_5(^t\text{BuNC})_6]^+$.

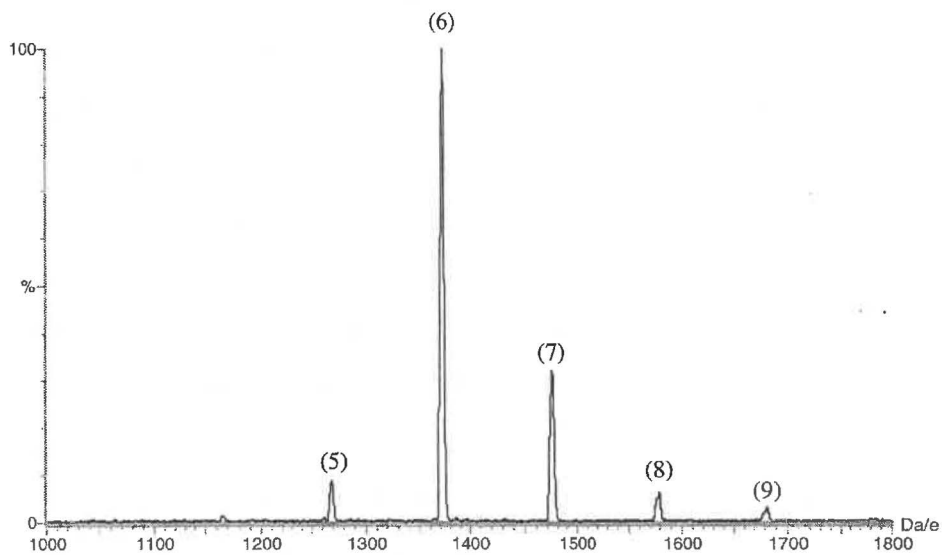

Figure 7.14 – The ES mass spectrum (+ve ion, 10 cV) of XyNC substitution on $Co_4(\mu_4\text{-}SiPh)_2(CO)_{11}$. Signals are labelled with respect to the degree of substitution i.e. (6) = $[Co_4(\mu_4\text{-}SiPh)_2(CO)_5(XyNC)_6]^+$.

The degree of substitution reported here exceeds any previous reports of ligand substitution reactions. The most highly-substituted E_2M_4 cluster reported is $Co_4(\mu_4\text{-}PPh)_2(CO)_7[P(OMe)_3]_4$, with one phosphite per cobalt atom[32]. $Fe_4(\mu_4\text{-}PPh)_2(CO)_{10}(^t\text{BuNC})$ and $Fe_4(\mu_4\text{-}PPh)_2(CO)_9(^t\text{BuNC})_2$ are the only isonitrile-substituted E_2M_4 clusters isolated, with the tri-substituted product unable to be purified[31]. The

extent of substitution noted in formation of the $Co_4(\mu_4\text{-}SiR)_2(CO)_2(RNC)_9$ clusters (82%) is unprecedented in transition metal carbonyl cluster chemistry.

ESMS provided a simple and effective method of monitoring the substitution of carbonyl ligands by isonitriles. The more highly-substituted clusters were readily detected but these signals were likely to be exaggerated at the expense of the less substituted variants. This was of particular importance for the $Co_4(\mu_4\text{-}SiC_6H_4R)_2(CO)_{11}$ (R = H, OMe) clusters since the parent and less substituted clusters were not detected by ESMS.

Examination of the reactions by IR and TLC displayed subtle differences from the ESMS results. The IR pattern of the substituted products were similar to the parent cluster but shifted to lower wavenumber [an equivalent effect was noted for $Fe_4(\mu_4\text{-}PPh)_2(CO)_{11-x}(^tBuNC)_x$ (x = 1, 2)[31]]. The tendency for ESMS to exaggerate the presence of the more highly-substituted products was noted by IR analysis. For example, ESMS analysis of the reaction between $Co_4(\mu_4\text{-}SiC_6H_4NMe_2)_2(CO)_{11}$ and XyNC indicated formation of the mono-, di- and hexa-substituted products within 15-20 minutes. IR analysis confirmed the absence of the parent cluster [2075 (w), 2039 (vs), 2022 (sh), 2007 (m,sh) and 1848 (w,br) cm^{-1}] though the signals detected [2149 (s,NC), 2128 (s,NC), 2028 (s), 2013 (m,sh), 2000 (m,sh) 1836 (w,br) cm^{-1}] were indicative of mono- and di-substituted products rather than the hexa-substituted variant. ES mass spectra after extended reaction times were dominated by signals attributable to the penta-, hexa- and hepta-substituted products, with IR spectra [2126 (s,NC), 1999 (m,sh), 1970 (s), 1794 (w,br) cm^{-1}] also indicative of highly-substituted products. Monitoring of the reaction by TLC was also possible, with the more substituted products less mobile. Unfortunately, the more highly-substituted products tended to decompose and bind to the silica support, hampering the isolation of these products.

In one instance, a 4:1 petroleum spirits:toluene solution containing a mixture of $Co_4(\mu_4\text{-}SiC_6H_4OMe)_2(CO)_5(XyNC)_6$ and $Co_4(\mu_4\text{-}SiC_6H_4OMe)_2(CO)_6(XyNC)_5$ (determined by ESMS) was cooled to –20°C producing a deep red/brown crystalline product, characterised crystallographically as $Co_4(\mu_4\text{-}SiC_6H_4OMe)_2(CO)_7(XyNC)_4$ (Section 7.3.2.1). The crystallisation of the tetra-substituted product may be a result of several factors; (i) crystal packing preference (the tetra-substituted product is highly symmetric

and likely to provide a more ordered lattice than the penta- or hexa-substituted variants), (ii) decomposition of the highly-substituted products in solution (producing CO which may displace the isonitrile ligands) or (iii) ESMS exaggeration of the more highly-substituted products (implying that the tetra-substituted cluster was the dominant reaction product but undetected).

ESMS analysis of a single isolated crystal of $Co_4(\mu_4\text{-}SiC_6H_4OMe)_2(CO)_7(XyNC)_4$ indicated the presence of $Co_4(\mu_4\text{-}SiC_6H_4OMe)_2(CO)_{11-x}(XyNC)_x$ (x = 3-6), though the spectrum was dominated by equally intense signals corresponding to the tetra- and penta-substituted products. This indicates that either the crystalline product was a mixture of various products (only one structurally characterised) or that ligand exchange was occurring in solution. To determine whether the presence of CO can reverse isonitrile substitution, a CH_2Cl_2 solution composed primarily of $Co_4(\mu_4\text{-}SiC_6H_4OMe)_2(CO)_5(^tBuNC)_6$ was placed under a CO atmosphere, with no change in the composition of the solution noted over a 2 hour period. There appears to be a discrepancy between ESMS and crystallographic analyses of the reaction products, with ESMS indicating a higher degree of substitution than that crystallographically determined. Although there is discrepancy between the different characterisation methods, there is no doubt that the $Co_4(\mu_4\text{-}SiR)_2(CO)_{11}$ clusters undergo facile substitution of carbonyl ligands by isonitriles to an unprecedented degree.

7.3.2.1 Crystal Structure Determination of $Co_4(\mu_4\text{-}SiC_6H_4OMe)_2(CO)_7(XyNC)_4$

A mixed petroleum spirits:toluene solution composed primarily (from ESMS analysis) of $Co_4(\mu_4\text{-}SiC_6H_4OMe)_2(CO)_{11-x}(XyNC)_x$ (x = 5, 6) was cooled to –20°C resulting in formation of deep red/brown crystals, structurally characterised as $Co_4(\mu_4\text{-}SiC_6H_4OMe)_2(CO)_7(XyNC)_4$. The $Co_4(\mu_4\text{-}SiC_6H_4OMe)_2(CO)_7(XyNC)_4$ cluster crystallised in the monoclinic space group C2/c on a 2-fold rotation axis [coincident with the C(2)-O(2) bond] with one half of the molecule unique. A labelled diagram of the structure (Figure 7.15) and a stereo view (Figure 7.16) are displayed. Selected bond lengths and angles are provided in Table 7.3 while details relating to the structure solution are presented in the experimental section of this chapter. Full tables of crystallographic data are provided in Appendix B.

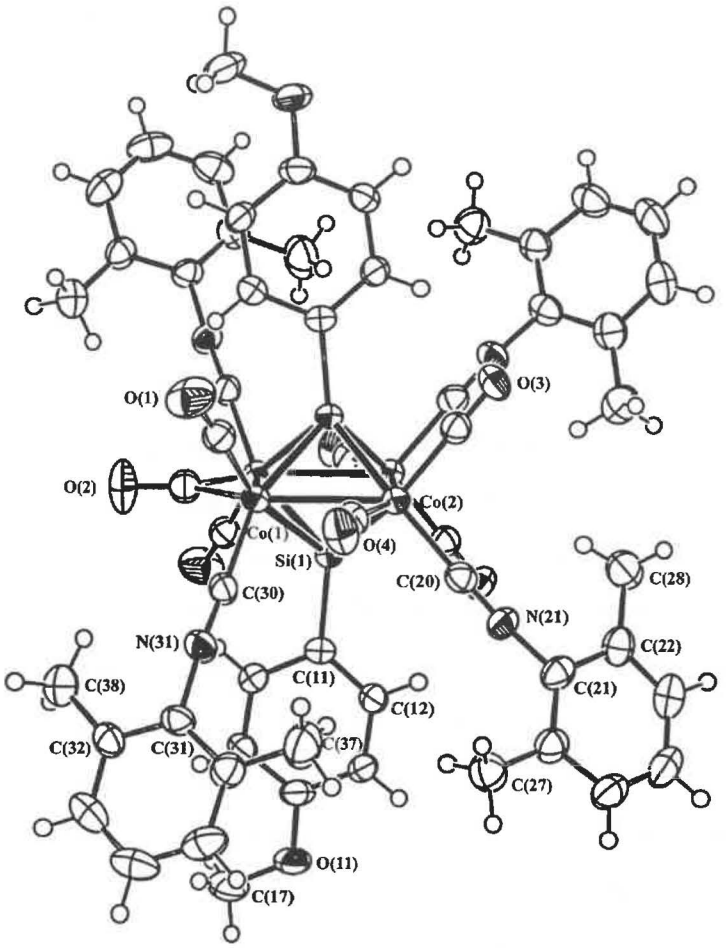

Figure 7.15 – A labelled perspective view of $Co_4(\mu_4\text{-}SiC_6H_4OMe)_2(CO)_7(XyNC)_4$. Ellipsoids are drawn at the 50% probability level.

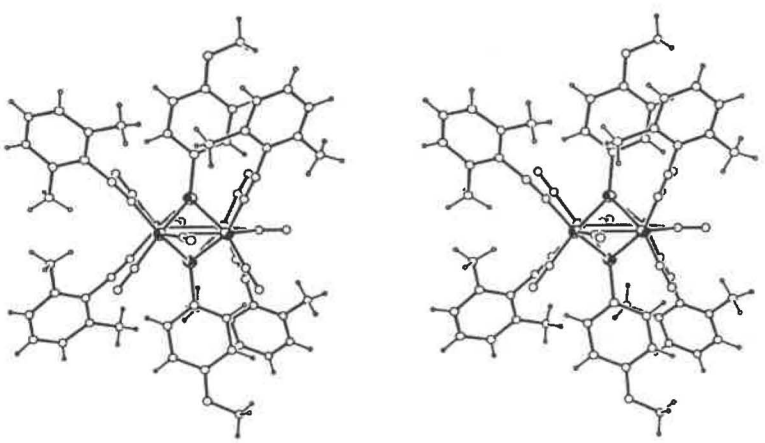

Figure 7.16 – A stereo view of $Co_4(\mu_4\text{-}SiC_6H_4OMe)_2(CO)_7(XyNC)_4$.

Table 7.3 – Selected bond lengths (Å) and angles (°) for $Co_4(\mu_4\text{-}SiC_6H_4OMe)_2(CO)_7(XyNC)_4$

Co(1)-Co(2)	2.6624(5)	Co(1)-Co(1)$^{\#}$	2.5594(6)
Co(2)-Co(2)$^{\#}$	2.7468(7)	Si(1)-Co(1)	2.3039(7)
Si(1)-Co(1)$^{\#}$	2.3284(7)	Si(1)-Co(2)	2.3087(7)
Si(1)-Co(2)$^{\#}$	2.3208(7)	Co(1)-C(2)	1.905(3)
C(2)-O(2)	1.178(5)	Co(2)-C(4)	1.783(3)
C(4)-O(4)	1.150(3)	Co-C_{CO}	1.790-1.792
C-O	1.139-1.143	Co-C_{XyNC}	1.858-1.865
N-C	1.167-1.168		
Co(1)-C(2)-O(2)	137.79(8)	Co(1)-C(2)-Co(1)$^{\#}$	84.41(16)
Co(2)-C(4)-O(4)	163.1(3)	Co-C-O	176.1-177.9

$^{\#}$ indicates the symmetry related equivalent of the unique atom.

The Co_4 square is distorted by the presence of the bridging [CO(2)] and semi-bridging [CO(4)] ligands which lie within the Co_4 plane (Figure 7.17). A similar distortion is noted in all $Co_4(\mu_4\text{-}ER)_2(CO)_{11}$ structures, and the Co-Co bond distances [2.5594(6), 2.6624(5) and 2.7468(7) Å for the bridged, semi-bridged and non-bridged bonds respectively] are similar to those reported for $Co_4(\mu_4\text{-}SiPh)_2(CO)_{11}$ [2.565, 2.647, 2.685 and 2.726 Å respectively][23]. The non-bonded Si(1)--Si(1)$^{\#}$ distance [2.7036(13) Å] is comparable with that found for $Co_4(\mu_4\text{-}SiPh)_2(CO)_{11}$ [2.705(2) Å]. The semi-bridging character of the CO(4) ligand is apparent from the C-O bond distance and Co-C-O angle, which are intermediate between those found for the fully-bridged and terminal ligands.

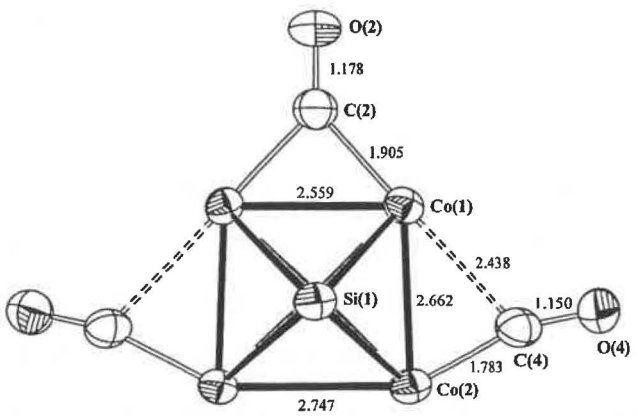

Figure 7.17 – The bond distances within the Co_4 plane for $Co_4(\mu_4\text{-}SiC_6H_4OMe)_2(CO)_7(XyNC)_4$.

The dihedral angle of 88.64(4)° between the Co_4 plane [defined by Co(1), Co(2), C(2) and O(2)] and $SiC_6H_4OCH_3$ [defined by Si(1), C(11), C(12) and C(16)] is slightly distorted from the 90° expected if perpendicular (indicated in Figure 7.18). The XyNC planes bisect the Co_4 plane at angles of 61.89(6)° and 62.13(7)° for the ligands containing N(21) and N(31) respectively.

The XyNC ligands are arranged in a *cis-trans-cis* configuration rather than the all *trans* arrangement that might be expected. The ligands are *cis* about the semi-bridged Co(1)-Co(2) bond while *trans* across both the bridged Co(1)-Co(1)$^{\#}$ and unbridged Co(2)-Co(2)$^{\#}$ bonds. A similar ligand arrangement was noted for the tetra-substituted trimethylphosphite compound, $Co_4(\mu_4\text{-}PPh)_2(CO)_6[P(OMe)_3]_4$, though in this case the ligand configuration was *cis* across the bridged Co-Co bonds[32].

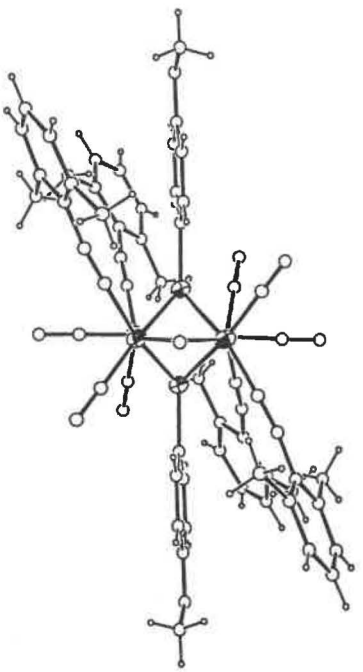

Figure 7.18 – A view of $Co_4(\mu_4\text{-}SiC_6H_4OMe)_2(CO)_7(XyNC)_4$ parallel to the SiC_6H_4OMe plane.

Although $Co_4(\mu_4\text{-}SiC_6H_4OMe)_2(CO)_7(XyNC)_4$ is a crowded molecule, the bond parameters associated with the isonitrile ligands are similar to those found for other substituted clusters. The C-N-C-Co arrangements are approximately linear (171-178°) while the N≡C bond distances [1.168(3) Å and 1.167(3) Å for N(21)-C(20) and N(31)-C(30) respectively] are typical of a coordinated isonitrile. There are no obvious analogues to this structure reported, with the closest potential examples being the $Fe_4(\mu_4\text{-}PPh)_2(CO)_{11-x}(^tBuNC)_x$ (x = 1, 2) clusters, neither of which were structurally

characterised, while the more highly-substituted $Fe_4(\mu_4\text{-}PPh)_2(CO)_8(^tBuNC)_3$ cluster was unable to be isolated in a pure form[31]. The $Co_4(\mu_4\text{-}SiC_6H_4OMe)_2(CO)_7(XyNC)_4$ cluster is the most highly isonitrile-substituted E_2M_4 compound reported.

7.3.3 Competitive Isonitrile Substitution Reactions

The ease of identification of the isonitrile-substituted derivatives of $Co_4(\mu_4\text{-}SiC_6H_4NMe_2)_2(CO)_{11}$ makes this cluster ideal for the examination of competitive substitution reactions. The affinity of the different reagents for substitution can be evaluated from these reactions and the extent of substitution possible determined. In particular, competitive reaction between different isonitrile reagents allows the influence of steric factors to be gauged.

Results and Discussion

The competitive reactions were performed using an equimolar solution of the appropriate isonitrile reagents in CH_2Cl_2. In analysis of the substituted products formed, the nomenclature (x,y) has been used to describe the cluster $Co_4(\mu_4\text{-}SiC_6H_4NMe_2)_2(CO)_{11\text{-}(x+y)}(R'NC)_x(R''NC)_y$. In each case, the signals observed corresponded to the $[M+H]^+$ ion of the neutral cluster. Ligand substitution rather than addition was observed, with cluster products always containing a total of eleven ligands.

For the competitive reaction between ^{t}BuNC and XyNC, ESMS analysis indicated formation of substituted products within 10-15 minutes of heating. The mono- and di-substituted clusters [R' = ^{t}BuNC, R" = XyNC; (1,0) *m/z* 896, (0,1) *m/z* 944, (2,0) *m/z* 951, (1,1) *m/z* 999 and (0,2) *m/z* 1047] were formed within minutes of isonitrile addition, with extended reaction producing a range of penta-, hexa- and hepta-substituted products (Figure 7.19 and summarised in Table 7.4).

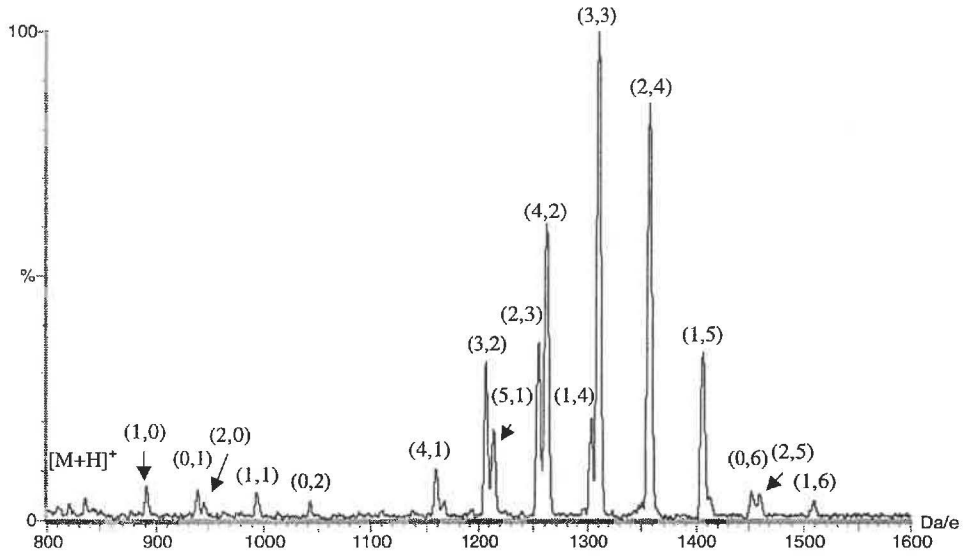

Figure 7.19 – The ES mass spectrum (+ve ion, 10 cV) of the competitive reaction between ^{t}BuNC and XyNC on $Co_4(\mu_4\text{-}SiC_6H_4NMe_2)_2(CO)_{11}$ after 40 minutes at 30°C. The label (x,y) indicates the $[M+H]^+$ signal of the $Co_4(\mu_4\text{-}SiC_6H_4NMe_2)_2(CO)_{11\text{-}(x+y)}(^t\text{BuNC})_x(\text{XyNC})_y$ cluster.

Table 7.4 – The $Co_4(\mu_4\text{-}SiC_6H_4NMe_2)_2(CO)_{11\text{-}(x+y)}(^t\text{BuNC})_x(\text{XyNC})_y$ clusters observed after extended reaction

Penta-substituted	Hexa-substituted	Hepta-substituted
(4,1) *m/z* 1164	(5,1) *m/z* 1219	(3,4) *m/z* 1418
(3,2) *m/z* 1212	(4,2) *m/z* 1267	(2,5) *m/z* 1466
(2,3) *m/z* 1260	(3,3) *m/z* 1315	(1,6) *m/z* 1515
(1,4) *m/z* 1308	(2,4) *m/z* 1363	
	(1,5) *m/z* 1411	
	(0,6) *m/z* 1459	

Competitive reactions using AdNC (with both ^{t}BuNC and XyNC) showed a similar pattern of mixed ligand substitution, though clusters with a higher degree of ^{t}BuNC or XyNC substitution were typically more intense. The reason for the enhanced reactivity of these reagents over AdNC is unknown.

The competitive substitution reactions were also applied to the 'electrospray-invisible' $Co_4(\mu_4\text{-}SiC_6H_4R)_2(CO)_{11}$ (R = H, OMe) clusters with similar success. For these reactions, the mono- and di-substituted products were seldom observed but signals attributable to more highly substituted products $[Co_4(\mu_4\text{-}SiC_6H_4R)_2(CO)_{11}$-

$_{(x+y)}(RNC)_x(R'NC)_y$, x+y = 3-7] were readily detected. As with the dimethylamino analogues, a preference for substitution by XyNC or ^{t}BuNC over AdNC was noted.

From ESMS analysis of the competitive substitution reactions, the following conclusions can be drawn. Firstly, the reactions can be analysed effectively by ESMS whereas the complexity of the reaction prevents the use of other techniques (IR, NMR). Secondly, a preference for the hexa-substituted products was apparent (from signal intensity), though both lesser and greater degrees of substitution were noted. Finally, there appeared little distinction between ^{t}BuNC and XyNC with regard to substitution, with the dominant signals from these reactions corresponding to clusters containing equal quantities of the two reagents. In comparison, AdNC tentatively appeared less active towards ligand substitution.

7.3.4 Phosphite Substitution Reactions

As discussed above (Section 7.1.3), the replacement of carbonyl ligands by phosphites has been extensively reported, particularly for $Co_4(\mu_4\text{-}PPh)_2(CO)_{10}$. A maximum substitution of four ligands was reported, with electrochemical studies indicating the substituted products were more susceptible to oxidation than the parent cluster[33].

Results and Discussion

The replacement of carbonyl ligands by $P(OMe)_3$ on $Co_4(\mu_4\text{-}SiC_6H_4NMe_2)_2(CO)_{11}$ was performed in a similar manner to the isonitrile substitution reactions. Ligand substitution was initially examined in toluene at 50°C (no reaction was observed at room temperature) though further study indicated similar substitution in CH_2Cl_2 at 35°C.

ESMS analysis of the toluene reaction solution over 2-4 hours indicated formation of the series of substituted products, $Co_4(\mu_4\text{-}SiC_6H_4NMe_2)_2(CO)_{11-x}[P(OMe)_3]_x$ (x = 0-4). The mono-substituted product {$[M+H]^+$, *m/z* 937} was apparent after 5 minutes, the di-substituted {$[M+H]^+$, *m/z* 1033} after 15-20 minutes, and the tri- and tetra-substituted clusters {$[M+H]^+$, *m/z* 1129 and 1225 respectively} were observed after 45-60 minutes (Figure 7.20). There was no evidence for further substitution [confirming the reports for

$Co_4(\mu_4\text{-}PPh)_2(CO)_{10}$ which limited substitution to one phosphite per cobalt atom[32], with spectra acquired after extended reaction indicating a mixture of the tri- and tetra-substituted products. The lack of selectivity for one product may be a factor of the 'soft' reaction conditions {the analogous $Co_4(\mu_4\text{-}PPh)_2(CO)_6[P(OMe)_3]_4$ cluster was produced after 24 hours at reflux in toluene[32]}. Unlike the isonitrile reactions, a series of unidentified by-products were detected at low intensity (*m/z* 951, 967, 982, 1021 and 1270).

As with the isonitrile reactions, an increase in spectral intensity was observed upon substitution allowing an extension to include the 'electrospray-invisible' $Co_4(\mu_4\text{-}SiC_6H_4R)_2(CO)_{11}$ (R = H, OMe) clusters. Treatment of these clusters with $P(OMe)_3$ resulted in the maximum substitution of four carbonyl ligands though signals associated with the mono- and di-substituted products were not detected. There was less evidence for reaction by-products for these clusters but this was likely a factor of the inability of these products to ionise rather than the absence of such products.

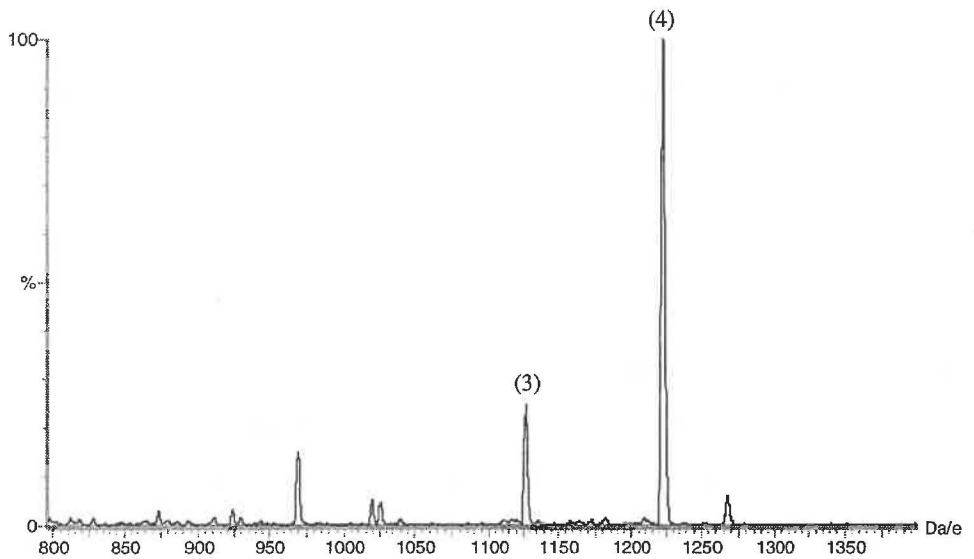

Figure 7.20 – The ES mass spectrum (+ve ion, 10 cV) of $P(OMe)_3$ substitution on $Co_4(\mu_4\text{-}SiC_6H_4NMe_2)_2(CO)_{11}$ after 4 hours. Signals are labelled with respect to the degree of substitution i.e. (4) = $[Co_4(\mu_4\text{-}SiC_6H_4NMe_2)_2(CO)_7\{P(OMe)_3\}_4+H]^+$.

The reactions were repeated in CH_2Cl_2 at 35°C with ESMS analysis indicating formation of the tri-substituted clusters though further substitution was limited. It is presumed that the forcing reaction conditions required for high yields of the tetra-substituted cluster are unavailable in CH_2Cl_2.

The presence of the NMR-active ^{31}P nuclei should allow monitoring of the reaction through NMR spectroscopy. This was possible to a limited degree, with a decrease in the intensity of the signal associated with the free phosphite (141.9 ppm) noted as the reaction progressed, replaced by a broad signal (151-156 ppm) attributed to the substituted reaction products {the chemical shift is comparable to that reported for the $Fe_4(\mu_4\text{-}PPh)_2(CO)_{11-x}[P(OMe)_3]_x$ (x = 1-4) clusters (159-163 ppm)[31]}. The low intensity and width of this signal precluded its use in distinguishing between the various substitution products.

Separation and isolation of the phosphite-substituted products was possible using chromatographic methods. From a larger scale reaction between $Co_4(\mu_4\text{-}SiC_6H_4OMe)_2(CO)_{11}$ and $P(OMe)_3$, $Co_4(\mu_4\text{-}C_6H_4OMe)_2(CO)_8[P(OMe)_3]_3$ was isolated in acceptable yield. ES mass spectra of the single chromatographic fraction were dominated by the $[Co_4(\mu_4\text{-}SiC_6H_4OMe)_2(CO)_8\{P(OMe)_3\}_3]^+$ signal (*m/z* 1102), though less intense signals were detected for the di- and tetra-substituted variants {$[M]^+$, *m/z* 1006 and 1198 respectively}. The IR spectrum of the tri-substituted cluster [2047 (w), 2015 (m,sh), 1990 (s), 1817 (w,br) cm^{-1}] was similar to the parent cluster but shifted to lower wavenumber [a similar effect was reported for $Co_4(\mu_4\text{-}PPh)_2(CO)_{10-x}\{P(OMe)_3\}_x$, x = 1-4 [32]], while ^1H NMR spectra displayed an approximately 4.5:1 integration ratio between the $P(OC\underline{H}_3)_3$ and $C_6H_4OC\underline{H}_3$ signals (though accurate integration was hampered by the overlap and width of the signals). Crystals were grown from a 6:1 petroleum spirits:toluene solution at –20°C but found to be of insufficient size for crystallographic analysis.

7.3.5 Phosphine Substitution Reactions

Phosphine substitution was also examined for the $Co_4(\mu_4\text{-}SiR)_2(CO)_{11}$ clusters. As discussed above (Section 7.1.4), phosphine substitution is well documented and of catalytic interest. In this series of experiments, tri-*n*-butylphosphine was employed as it is fairly easily handled (compared to the methyl or ethyl analogues) and has less steric influence than triphenylphosphine (with regard to cone angle).

Results and Discussion

The phosphine substitution reactions were examined in a similar manner to the isonitrile and phosphite examples reported above. Initial reactions were performed in toluene though further examination indicated that a heated CH_2Cl_2 solution provided similar results.

Phosphine substitution was examined for the series of clusters $Co_4(\mu_4\text{-}SiC_6H_4R)_2(CO)_{11}$ (R = H, OMe, NMe_2) with little success. In each case, a gradual colour change from deep red/orange to pale green was noted, accompanied in the R = NMe_2 case by a decrease in the intensity of the $[M+H]^+$ signal of the parent cluster. ESMS analysis of the reaction with $Co_4(\mu_4\text{-}SiC_6H_4OMe)_2(CO)_{11}$ displayed signals at *m/z* 1336 and 1510 that may correspond to the tri- and tetra-substituted clusters, but these signals were of limited intensity and emphasis upon these signals is unwarranted. In general, there was no conclusive evidence by ESMS for the formation of any tri-*n*-butylphosphine-substituted clusters.

7.3.6 Attempted Metal Substitution using $[Mo(CO)_3(\eta^5\text{-}C_5H_5)]_2$

The substitution of "$Mo(CO)_2(\eta^5\text{-}C_5H_5)$" and "$Ni(\eta^5\text{-}C_5H_5)$" moieties for "$Co(CO)_3$" within the core of $Co_4(\mu_4\text{-}Ge^tBu)_2(CO)_{11}$ has been reported[12]. These substituted clusters are produced through thermal reaction between $[M(CO)_x(\eta^5\text{-}C_5H_5)]_2$ [M = Mo (x = 3), Ni (x = 1)] and the parent $Co_4(\mu_4\text{-}Ge^tBu)_2(CO)_{11}$ cluster, presumably *via* a reduced intermediate. The availability of the 'electrospray-friendly' $Co_4(\mu_4\text{-}SiC_6H_4NMe_2)_2(CO)_{11}$ cluster allowed examination of the substitution reaction, with the characteristic molybdenum isotope pattern expected to assist identification of any substituted products.

Results and Discussion

A toluene solution of $Co_4(\mu_4\text{-}SiC_6H_4NMe_2)_2(CO)_{11}$ and $[Mo(CO)_3(\eta^5\text{-}C_5H_5)]_2$ was refluxed for 4 hours and monitored throughout by ESMS. Analysis of the cooled solution after reflux displayed a signal attributed to the parent $Co_4(\mu_4\text{-}$

$SiC_6H_4NMe_2)_2(CO)_{11}$ cluster {$[M+H]^+$, *m/z* 841 - though at significantly lower intensity than prior to reflux} without any evidence for formation of $Co_3Mo(\mu_4\text{-}SiC_6H_4NMe_2)_2(CO)_{10}(\eta^5\text{-}C_5H_5)$.

The reaction was repeated with addition of a trace amount of sodium benzophenone ketyl, with the radical initiator expected to assist metal substitution in a similar manner to that reported in ligand substitution reactions[33]. The solution was stirred for 24 hours following addition of the radical initiator without evidence (by ESMS) for the formation of any substituted clusters. Treatment with an excess of the radical initiator also failed to result in substitution.

7.4 Reaction of $Me_2NC_6H_4SiH_3$ with $Co_2(CO)_8$

7.4.1 Introduction

The reaction of primary silanes with $Co_2(CO)_8$ typically results in the formation of a $RSi[Co(CO)_4]Co_2(CO)_7$ cluster, with subsequent decarbonylation yielding $RSiCo_3(CO)_9$ [50]. However, the reaction between $Me_2NC_6H_4SiH_3$ and $Co_2(CO)_8$ was reported to produce $Co_4(\mu_4\text{-}SiC_6H_4NMe_2)_2(CO)_{11}$ [presumably *via* $Co_4(CO)_{12}$] and *p*-$Me_2NC_6H_4Si[OCCo_3(CO)_9]_2Co(CO)_4$ (characterised crystallographically - Figure 7.21 [24]). Previous ESMS analysis indicated that an additional high-nuclearity product (*m/z* 1367) of unknown composition was produced and re-examination of this reaction was considered appropriate.

[50] R. Ball, M.J. Bennett, E.H. Brooks, W.A.G. Graham, J. Hoyano and S.M. Illingsworth, *J. Chem. Soc., Chem. Commun.*, 1970, 592.

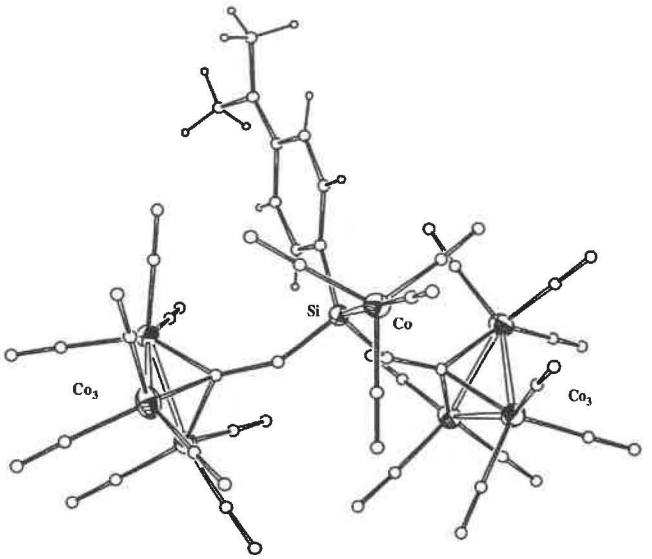

Figure 7.21 – The structure of *p*-$Me_2NC_6H_4Si[OCCo_3(CO)_9]_2Co(CO)_4$ [24].

7.4.2 Results and Discussion

The reaction between $Me_2NC_6H_4SiH_3$ and $Co_2(CO)_8$ was performed in toluene at 50°C using standard Schlenk techniques. All attempts to monitor the reaction using ESMS were unsuccessful, presumably a factor of the complexity of the reaction.

After four hours at 50°C, the reaction was cooled to room temperature and solvent removed under vacuum. Spot TLC indicated the presence of four products; (i) a purple oil identical to that found in the $Co_4(CO)_{12}$ reaction, (ii) a mixture of unreacted $Co_2(CO)_8$ and $Co_4(CO)_{12}$ [produced by thermal treatment of $Co_2(CO)_8$], (iii) a purple oil composed primarily of *p*-$Me_2NC_6H_4Si[OCCo_3(CO)_9]_2Co(CO)_4$, and (iv) $Co_4(SiC_6H_4NMe_2)_2(CO)_{11}$. ESMS analysis of the second purple fraction (Figure 7.22) indicated the presence of *p*-$Me_2NC_6H_4Si[OCCo_3(CO)_9]_2Co(CO)_4$ {$[M+H]^+$, *m/z* 1234} with a trace signal at *m/z* 1367 (< 10% the intensity of the *m/z* 1234 signal). The latter signal lacks the intensity previously reported and attempts at isolation of the compound were abandoned. This fraction was also analysed by ^1H NMR and noted to contain a high concentration of various contaminants (CH_2Cl_2, petroleum spirits), with the signals associated with the $C_6H_4NMe_2$ functionality observed at very low intensity.

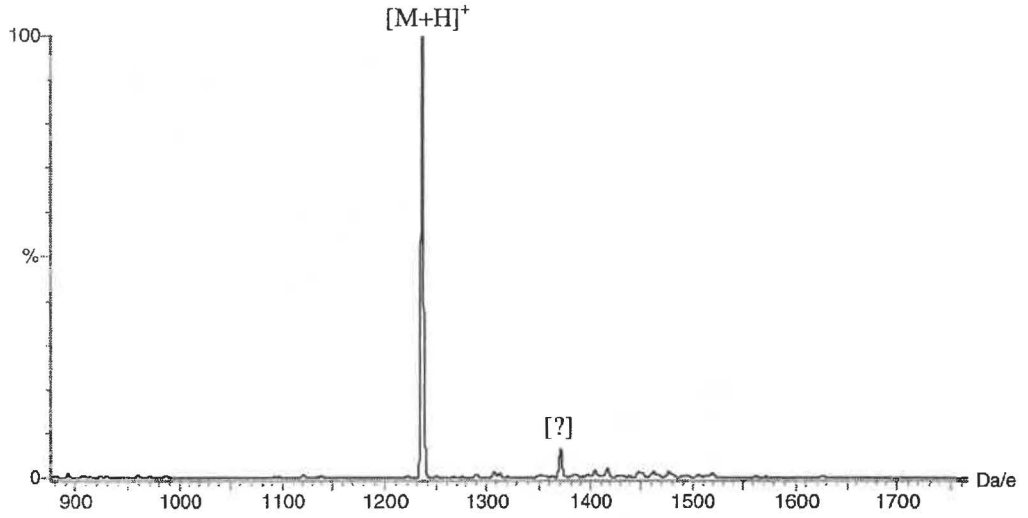

Figure 7.22 – The ES mass spectrum (+ve ion, 5 cV) of *p*-$Me_2NC_6H_4Si[OCCo_3(CO)_9]_2Co(CO)_4$.

7.5 Synthesis of Linked Si_2Co_4 Clusters

7.5.1 Introduction

As discussed in the introduction to this chapter (Section 7.1.5), the linking of E_2M_4 clusters through phosphite or isonitrile ligands has been reported. Electrochemical studies of *p*-$[Fe_4(\mu_4\text{-}PPh)_2(CO)_{10}(CN)]_2C_6H_4$ indicate that the two cluster cores were in electronic communication (i.e. four separate one-electron reductions were observed rather than the two two-electron reduction waves apparent for the phosphite linked clusters)[34].

An alternative approach is to use a disilane or digermane reagent and link the clusters through their E vertices. This approach has been successfully demonstrated using *p*-$(H_3Si)_2C_6H_4$ to generate the *p*-$[Co_4(\mu_4\text{-}SiC_6H_4R)(CO)_{11}Si]_2C_6H_4$ (R = H, OMe, NMe_2) clusters, with the phenyl capped cluster structurally characterised (Figure 7.23[24]). The linking of the E_2M_4 clusters through a conjugated spacer unit should allow electronic communication between the octahedral cores, though this has yet to be proven for these systems.

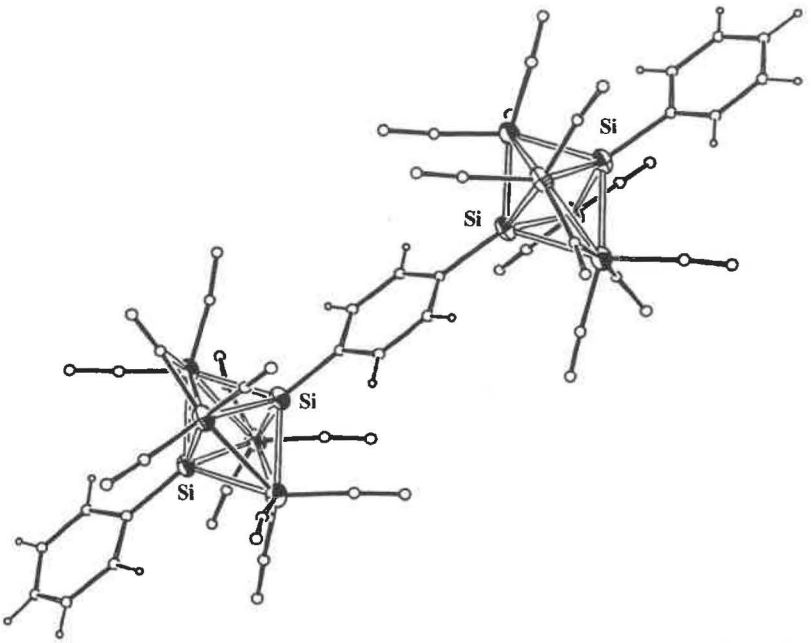

Figure 7.23 – The structure of *p*-$[Co_4(\mu_4\text{-}SiPh)(CO)_{11}Si]_2C_6H_4$ [24].

7.5.2 Synthesis and Characterisation of $[Co_4(\mu_4\text{-}SiC_6H_4R)(CO)_{11}Si]_2X$ [R = H, OMe; X = $(CH_2)_8$, C_6H_4]

A series of reactions were performed in attempts to generate oligomeric Si_2Co_4 materials using three linking disilanes; *p*-$(H_3Si)_2C_6H_4$, $H_3Si(CH_2)_8SiH_3$ and $Fe(\eta^5\text{-}C_5H_4SiH_3)_2$. In particular, the ferrocenyl clusters were expected to display unique electrochemical properties as both the ferrocenyl and Si_2Co_4 units are redox active. The synthesis of the three linking agents was reported in Chapter 2.

Results and Discussion

Synthesis of the linked clusters was undertaken in a similar manner to the monomeric species (refer to Section 7.2) using the appropriate reactant ratios (Scheme 7.3). Under these conditions, $[Co_4(\mu_4\text{-}SiC_6H_4R)(CO)_{11}Si]_2(CH_2)_8$ [R = H, OMe; X = $(CH_2)_8$, C_6H_4] were produced, albeit in very low yield. The clusters were characterised by both IR and NMR spectroscopy, with detection by ESMS as their isonitrile-substituted derivatives. Previous synthesis and characterisation of the di-silylbenzene-linked clusters indicated that oxidation was readily observed under ESMS conditions[24], an effect not apparent in this investigation.

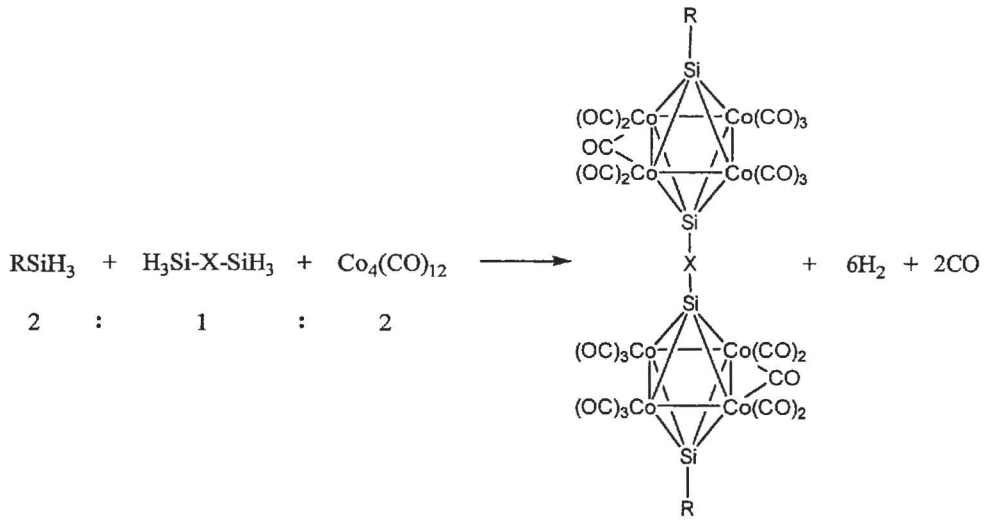

Scheme 7.3 – The synthesis of linked Si_2Co_4 clusters [X = $(CH_2)_8$, C_6H_4].

IR and NMR analyses of the linked cluster products yielded little information. NMR analysis of the $[Co_4(\mu_4\text{-}SiC_6H_4R)(CO)_{11}Si]_2(CH_2)_8$ clusters indicated the presence of the aromatic and alkyl units expected, though the signals were typically broad. Similarly, NMR analysis of the *p*-$[\mu_4\text{-}Co_4(SiC_6H_4R)(CO)_{11}Si]_2C_6H_4$ clusters displayed a broad series of aromatic signals attributed to both capping and bridging phenyl groups. Signals corresponding to traces of petroleum spirits and toluene were noted for all clusters, their presence attributed to the low yield of the linked clusters preventing recrystallisation. IR analysis was of limited use in characterising the linked clusters as the spectra were typically very similar to the monomeric species, a similarity noted previously both in linked $Co_4(\mu_4\text{-}SiR)_2(CO)_{11}$ [24] and $Fe_4(\mu_4\text{-}PR)_2(CO)_{11}$ [35] clusters.

An electrochemical analysis of *p*-$[Co_4(\mu_4\text{-}SiC_6H_4R)(CO)_{11}Si]_2C_6H_4$ was performed using the OTTLE technique (discussed in Section 7.2.6). The linked cluster displayed a similar electrochemical profile to that discussed for the monomeric species, without evidence for electronic communication between the two Si_2Co_4 units (indicated by separate oxidation and reduction waves rather than the overlap observed). However, the electrochemical features were broad and only a preliminary investigation was performed. Further study would be required to confirm the independent electrochemical properties of the two Si_2Co_4 units.

The only conclusive characterisation method found for the linked clusters was ESMS analysis. Previous studies of the *p*-$[Co_4(\mu_4\text{-}SiC_6H_4R)(CO)_{11}Si]_2C_6H_4$ clusters reported

that oxidation {forming $[M]^+$ ions} readily occurred under ESMS conditions[24] but this was not apparent in this investigation. The most reliable method for ESMS characterisation of the clusters was through isonitrile substitution. As discussed in Section 7.2.2, $Co_4(\mu_4\text{-}ER)_2(CO)_{11}$ clusters undergo facile ligand substitution, with the substituted products more susceptible to oxidation than the parent compound. ESMS analysis of the product mixture displayed a series of signals with characteristic mass separation (Figure 7.24), the interpretation of which allowed the mass of the parent cluster to be determined.

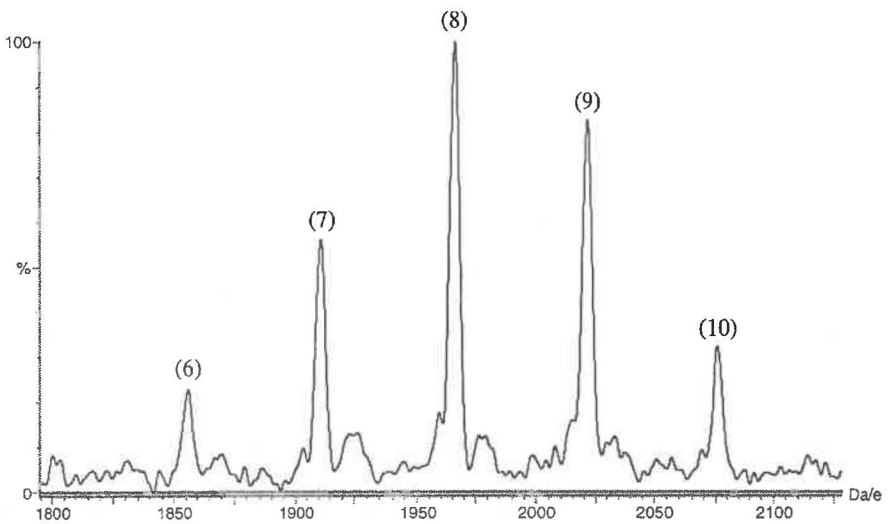

Figure 7.24 – The ES mass spectrum (+ve ion, 10 cV) of ^{t}BuNC substitution on $[Co_4(\mu_4\text{-}SiC_6H_4OMe)(CO)_{11}Si]_2(CH_2)_8$. Signals are labelled with respect to the degree of substitution i.e. (10) = $[\{Co_4(\mu_4\text{-}SiC_6H_4OMe)(CO)_6(^tBuNC)_5Si\}_2(CH_2)_8]^+$.

Synthesis of the dimethylamino-functionalised clusters, *p*-$[Co_4(\mu_4\text{-}SiC_6H_4NMe_2)(CO)_{11}Si]_2C_6H_4$ and $[Co_4(\mu_4\text{-}SiC_6H_4NMe_2)(CO)_{11}Si]_2(CH_2)_8$, was attempted using a similar synthetic method. These clusters were considered of significant interest to this project since their 'electrospray-friendly' character would assist detection and provide a useful handle for the study of higher oligomers. Unfortunately, no substantial evidence for the formation of these clusters was obtained. In one instance, an ESMS analysis of the crude product mixture displayed a signal at *m/z* 1573, possibly attributable to the $[M+H]^+$ ion of $[Co_4(\mu_4\text{-}SiC_6H_4NMe_2)(CO)_{11}Si]_2(CH_2)_8$, but the signal was of exceedingly low intensity and the cluster was not identified by spot TLC of the reaction mixture. Experiments using an excess of the linking silane were trialed in an attempt to synthesise the clusters without

success. The inability to produce the *p*-$[Co_4(\mu_4\text{-}SiC_6H_4NMe_2)(CO)_{11}Si]_2C_6H_4$ compound is in conflict with earlier reports of its isolation, albeit in very low yield (0.5%)[24].

The use of $Fe(\eta^5\text{-}C_5H_4SiH_3)_2$ as a linking agent was also unsuccessful in this research. Using identical procedures to the alkyl and aryl disilanes there was no evidence for the formation of any ferrocenyl-linked clusters. In the presence of capping silanes, the monomeric $Co_4(\mu_4\text{-}SiC_6H_4R)_2(CO)_{11}$ clusters were identified, without evidence for the formation of either a linked cluster or an oligomeric material. In the absence of capping agents, the only isolated fraction of the crude mixture corresponded to unreacted $Co_4(CO)_{12}$.

7.5.3 Attempted Synthesis of Higher Oligomers

Following the successful synthesis of the dimeric $[Co_4(\mu_4\text{-}SiC_6H_4R)(CO)_{11}Si]_2X$ [R = H, OMe; X = $(CH_2)_8$, C_6H_4] clusters, attempts were made to synthesise higher oligomers. Using an appropriate stoichiometric ratio of capping silane to linking disilane, the formation of higher oligomers was considered feasible, with an added advantage that a higher ratio of the linking agent may produce higher yields of the dimeric species. However, using similar reaction conditions to those described for the monomeric and dimeric clusters, synthesis of higher oligomers proved unsuccessful. In some cases, TLC analysis identified a reaction product of suitable R_f for a trimeric species but the yield of this cluster was exceedingly low and all attempts at isolation were unsuccessful. An increase in the ratio of the linking agent failed to increase the yield of oligomeric clusters, but rather resulted in the formation of an intractable solid (suspected to be a cyclic Si_2Co_4 oligomer – discussed below). In general, higher oligomers consisting of linked Si_2Co_4 octahedra are unavailable using these methods.

During attempted synthesis of linked Si_2Co_4 clusters, an additional product (suspected to be a cyclic Si_2Co_4 oligomer) was identified. This product was slightly soluble in CH_2Cl_2 but all attempts at chromatographic isolation resulted in the material binding irreversibly to the silica support. The product was most noticeable in the attempted synthesis of higher oligomers using the $H_3Si(CH_2)_8SiH_3$ linking reagent, with equivalent

products noted in the synthesis of dimeric $[Co_4(\mu_4\text{-}SiC_6H_4R)(CO)_{11}Si]_2X$ [R = H, OMe; X = $(CH_2)_8$, C_6H_4] clusters and reactions involving *p*-$(H_3Si)_2C_6H_4$ to a lesser degree.

The material was also synthesised directly from reaction between the disilane reagents and $Co_4(CO)_{12}$. Gaseous release from the mixture upon heating was taken as evidence of reaction, with formation of an insoluble product noted within 24-48 hours. Extraction of unreacted $Co_4(CO)_{12}$ yielded an orange/brown solid found to be insoluble in a variety of solvents (CH_2Cl_2, acetone, thf, ethylacetate). The product is presumed to be a cyclic Si_2Co_4 oligomer on the basis of colour and IR analysis (as a KBr disc – Figure 7.25). IR spectra displayed significant similarity to those found for the monomeric and dimeric Si_2Co_4 clusters (refer to Section 7.2.3 and the experimental section). The material was significantly more sensitive to oxygen than the isolated monomeric and dimeric clusters, which hampered characterisation.

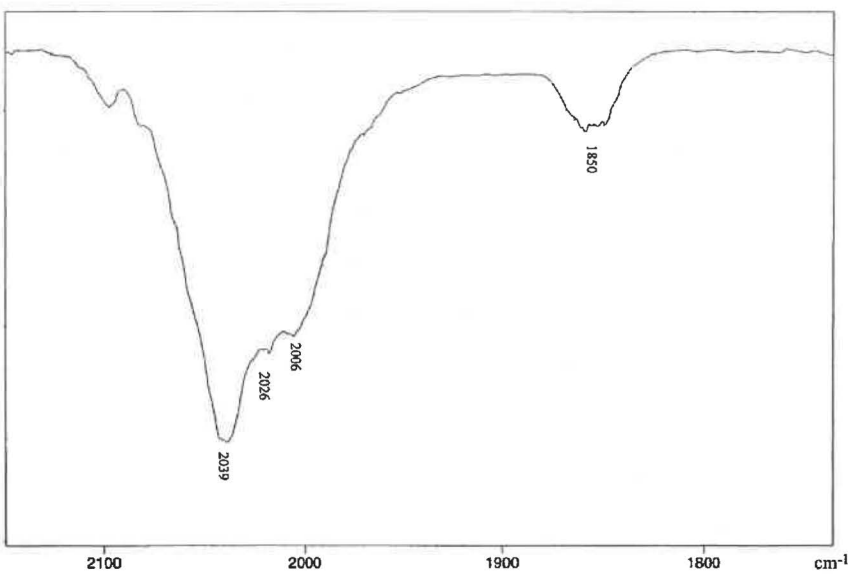

Figure 7.25 – The IR spectrum (KBr disc) of the "cyclic Si_2Co_4 oligomer".

The structure of this material can only be speculated upon. The use of the alkyl disilane reagent provides a degree of flexibility to the system and the formation of a cyclic oligomer (Figure 7.26) is plausible. Formation of an equivalent material from the inflexible aromatic disilane is less obvious and no ready explanation is provided for this analogue.

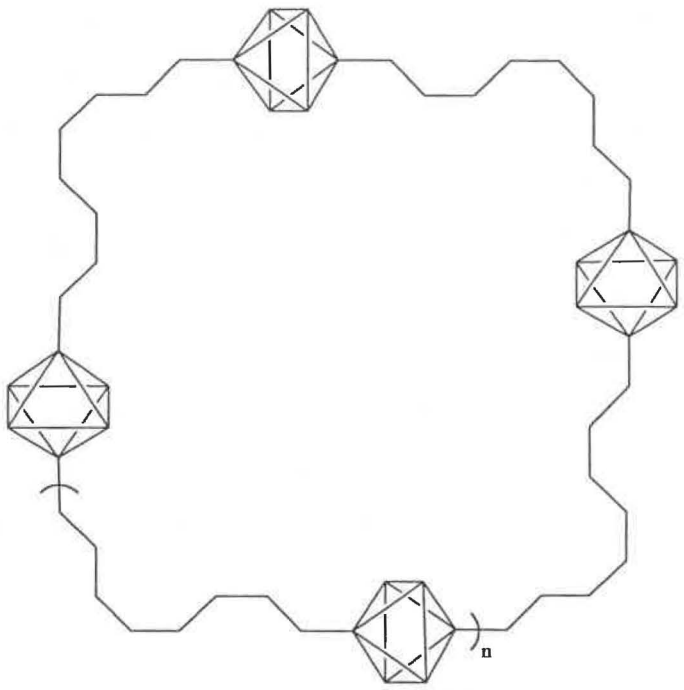

Figure 7.26 – A possible structure of the "cyclic Si_2Co_4 oligomer".

7.6 Conclusions and Future Research

The research presented in this chapter outlined the synthesis and reactivity of a series of $Co_4(\mu_4\text{-}ER)_2(CO)_{11}$ [E = Si, R = Ph, C_6H_4OMe, $C_6H_4NMe_2$, $(CH_2)_3OMe$; E = Ge, R = $C_6H_4NMe_2$] clusters. These clusters were prepared in satisfactory yield using significantly shorter reaction times than previously reported, and synthesis using standard Schlenk techniques provided similar yields of the E_2Co_4 clusters to previous methods.

The $Co_4(\mu_4\text{-}ER)_2(CO)_{11}$ clusters were characterised by IR, NMR, ESMS and elemental analyses. The dimethylamino-functionalised clusters were detected by ESMS as their protonated ions, $[M+H]^+$, whereas the remaining clusters were characterised as their isonitrile-substituted derivatives. Electrochemical studies on the clusters using the OTTLE technique indicated the formation of an irreversible oxidation product, while reduction produced a cluster with an IR profile similar to the parent material, postulated to be $[Co_4(\mu_4\text{-}SiR)_2(CO)_{11}]^-$.

A variety of ligand substitution reactions (involving isonitriles, phosphites and phosphines) were examined using ESMS. The isonitrile-substituted products displayed

intense ESMS signals, attributed to the weaker π-acceptor character of the ligand (compared to carbonyl) activating the clusters towards protonation and/or oxidation. A preference for the hexa-substituted isonitrile product was observed by ESMS, though attempts at isolating this material were unsuccessful. The tetra-substituted $Co_4(\mu_4\text{-}SiC_6H_4OMe)_2(CO)_7(XyNC)_4$ cluster was isolated and structurally characterised. This cluster displays a higher degree of isonitrile substitution than any previously reported examples and is the only isonitrile-substituted E_2M_4 cluster structurally characterised. Equivalent substitution using $P(OMe)_3$ led to a mixture of tri- and tetra-substituted products while there was no conclusive evidence for phosphine-substituted products. Attempted substitution of a cobalt atoms within the Si_2Co_4 core using $[Mo(CO)_2(\eta^5\text{-}C_5H_5)]_2$ was unsuccessful.

The synthesis and characterisation of the linked dimeric clusters $[Co_4(\mu_4\text{-}SiC_6H_4R)(CO)_{11}Si]_2X$ [R = H, OMe; X = $(CH_2)_8$, C_6H_4] are reported, though equivalent reactions involving R = NMe_2 and X = $Fe(\eta^5\text{-}C_5H_4)_2$ were unsuccessful. Contrary to previous reports, these clusters failed to oxidise under ESMS conditions and derivatisation using isonitrile reagents was required for characterisation. Electrochemical analysis using the OTTLE technique indicated no communication between the Si_2Co_4 octahedra for $[Co_4(\mu_4\text{-}SiPh)(CO)_{11}Si]_2C_6H_4$, though this was a preliminary investigation and requires further examination. Use of higher ratios of the linking disilanes to capping silanes resulted in formation of a polymeric (or cyclic oligomeric) material rather than the tri- and tetra-meric clusters intended.

There are many aspects of this research that deserve further examination. The study of linked clusters using an extensive range of disilanes should yield a host of new clusters, though the very low yield of these products is a major deterrent. Although synthesis of $Fe(\eta^5\text{-}C_5H_4SiH_3)_2$ was successful, no clusters containing this bridging unit were detected in this research. Similarly, a systematic synthesis of $Fe(\eta^5\text{-}C_5H_5)(\eta^5\text{-}C_5H_4SiH_3)$ (henceforth referred to as $FcSiH_3$) may yield $Co_4(\mu_4\text{-}SiFc)_2(CO)_{11}$, the electrochemistry of which would be fascinating. Unfortunately, the lack of success in producing the ferrocenyl clusters is a deterrent to further study in this area. A more productive approach may be the synthesis of $M_4(\mu_4\text{-}PFc)_2(CO)_{11}$ (M = Fe, Ru) clusters through use of primary ferrocenyl-phosphines. The synthesis of $Ru_4(\mu_4\text{-}PCH_2Fc)_2(CO)_{11}$

[51] in this manner has been reported, and the use of $FcPH_2$ [52] should allow electronic communication between the ferrocenyl units and the cluster core. In particular, use of the recently reported diphosphine, $Fe(\eta^5\text{-}C_5H_4PH_2)_2$ [54], as a cluster linking agent would provide an electrochemically active spacer unit for the formation of oligomeric materials. The lower degree of air-sensitivity of the ruthenium clusters should assist isolation and manipulation of these materials.

7.7 Experimental

Synthesis of $Co_4(\mu_4\text{-}ER)_2(CO)_{11}$ clusters

$Co_4(\mu_4\text{-}SiPh)_2(CO)_{11}$ [23]

A toluene solution (20 mL) of $PhSiH_3$ (175 μL, 0.15 g, 1.40 mmol) and $Co_4(CO)_{12}$ (0.2 g, 0.35 mmol) was sealed under vacuum in a glass ampoule and heated to 50°C for 2 weeks (though later syntheses displayed similar yields when heated in a Schlenk flask for 72 hours). After opening, solvent was removed under vacuum and the desired compound separated from unreacted $Co_4(CO)_{12}$ by column chromatography using a 4:1 petroleum spirits:CH_2Cl_2 solvent mix. Solvent was removed from the orange band to yield $Co_4(\mu_4\text{-}SiPh)_2(CO)_{11}$ (0.071 g, 0.094 mmol, 27%). Deep red cubes of the product suitable for elemental analysis were obtained by cooling a saturated solution of the product in toluene to –4°C.

$Co_4(\mu_4\text{-}SiPh)_2(CO)_{11}$
M_r – 754.2
m.p. 106-110°C (decomposed)
IR – (ν_{CO}, CH_2Cl_2) 2085 (w), 2045 (s), 2028 (m,sh), 2014 (m,sh), 1852 (w) cm^{-1}
NMR – ^1H – 8.20-7.70 (m, 10H, C_6H_5) ppm
^{13}C – 203.0 (CO), 139.3 (C_1), 134.4 (C_2), 132.0 (C_4), 129.0 (C_3) ppm
ESMS – (MeOH, +ve ion, 10 cV) *m/z* 1029 (25% - $[M\text{-}5CO\text{+}5^tBuNC]^+$), *m/z* 1084 (100% - $[M\text{-}6CO\text{+}6^tBuNC]^+$) after treatment with ^tBuNC
Elemental analysis – $C_{23}H_{10}Co_4O_{11}Si_2$ requires C 36.63, H 1.34%; found C 35.95, H 1.90%

[51] N.J. Goodwin, W. Henderson, B.K. Nicholson, J. Fawcett and D.R. Russell, *J. Chem. Soc., Dalton Trans.*, 1999, 1785.

[52] S.R. Alley, D.Phil. Thesis, University of Waikato, 2001.

$Co_4(\mu_4\text{-}SiC_6H_4OMe)_2(CO)_{11}$ [24]

A toluene solution (20 mL) of *p*-$CH_3OC_6H_4SiH_3$ (170 µl, 0.166 g, 1.12 mmol) and $Co_4(CO)_{12}$ (0.212 g, 0.37 mmol) was sealed in a glass ampoule under vacuum and heated to 50°C for 2 weeks (though, as discussed below, similar yields of the product were obtained when heated for 48 hours in an ampoule or in a Schlenk flask). After cooling to ambient temperature, the ampoule was broken into a Schlenk flask, solvent removed and the product isolated by column chromatography using a 3:1 petroleum spirits:CH_2Cl_2 solvent mixture. An orange crystalline material was isolated and identified as $Co_4(\mu_4\text{-}SiC_6H_4OMe)_2(CO)_{11}$ (0.157 g, 0.19 mmol, 52%). Recrystallisation from a 1:1 petroleum spirits:toluene solution at –20°C produced a mixture of deep red rectangular crystals and intense orange needles which TLC analysis indicated were the same compound.

$Co_4(\mu_4\text{-}SiC_6H_4OMe)_2(CO)_{11}$

M_r – 814.3

m.p. 98-104°C (decomposed)

IR – (ν_{CO}, CH_2Cl_2) 2082 (w), 2044 (s), 2027 (m,sh), 2013 (m,sh), 1849 (w) cm^{-1}

NMR – ^1H – 8.11, 7.24 (m, 8H, C_6H_4), 3.97 (s, 6H, CH_3) ppm

^{13}C – 203.3 (CO), 164.5 (C_4), 136.3 (C_2), 130.9 (C_1), 114.6 (C_3), 55.4 (CH_3) ppm

ESMS – (MeOH, +ve ion, 10 cV) *m/z* 1089 (30% - $[M\text{-}5CO\text{+}5^tBuNC]^+$), *m/z* 1144 (100% - $[M\text{-}6CO\text{+}6^tBuNC]^+$), *m/z* 1199 (10% - $[M\text{-}7CO\text{+}7^tBuNC]^+$) after treatment with ^tBuNC

Elemental analysis – $C_{25}H_{14}Co_4O_{13}Si_2.C_7H_8$ [53] requires C 42.40, H 2.45%; found C 42.24, H 2.38%

$Co_4(\mu_4\text{-}SiC_6H_4NMe_2)_2(CO)_{11}$ [24]

$Me_2NC_6H_4SiH_3$ (0.18 g, 1.2 mmol) was added to a toluene solution (20 mL) of $Co_4(CO)_{12}$ (0.3 g, 0.52 mmol), sealed in a glass ampoule under vacuum and heated to 50°C for 3 weeks. Once cooled to room temperature, the ampoule was opened and the contents transferred to a Schlenk flask. Solvent was removed under vacuum and the sample extracted into CH_2Cl_2. TLC of the solution showed the presence of 3 species; a purple band of unknown origin, unreacted $Co_4(CO)_{12}$, and an intense orange band of the desired product. A black precipitate was also produced in the reaction and found to be

[53] The presence of toluene was detected in NMR analysis of the crystals.

insoluble in a variety of solvents (CH_2Cl_2, Et_2O, THF, acetone). The desired product was isolated by column chromatography using a 3:1 petroleum spirits:CH_2Cl_2 solvent mixture. Solvent was removed from the orange fraction to yield $Co_4(\mu_4\text{-}SiC_6H_4NMe_2)_2(CO)_{11}$ (0.056 g, 0.07 mmol, 13%). Crystals of the compound suitable for elemental analysis were grown from a 1:1 petroleum spirits:toluene solution at –20°C.

ESMS and NMR analyses of the purple fraction yielded no recognisable signals (indicating the absence of the NMe_2 functionality), while IR analysis [2050 (s), 2040 (m) cm^{-1}] indicated the compound was based on a $RCo_3(CO)_9$ arrangement. IR analysis of the black deposit (by KBr disc) displayed similar signals to the purple compound, though the nature of this solid is unknown.

$Co_4(\mu_4\text{-}SiC_6H_4NMe_2)_2(CO)_{11}$

M_r – 840.4

m.p. 108-112°C (decomposed)

IR – (ν_{CO}, CH_2Cl_2) 2073 (w), 2040 (s), 2027 (m,sh), 2011 (m,sh), 1976 (w), 1848 (w,br) cm^{-1}

NMR – ^1H – 8.00, 6.92 (m, 8H, C_6H_4), 3.10 (s, 12H, CH_3) ppm

^{13}C – 204.0 (CO), 152.3 (C_4), 136.0 (C_2), 126.0 (C_1), 111.5 (C_3), 40.0 (CH_3) ppm

ESMS – (MeOH, +ve ion, 10 cV) *m/z* 841 (100% - $[M+H]^+$)

Elemental Analysis – $C_{27}H_{20}Co_4N_2O_{11}Si_2$ requires C 38.59, H 2.40, N 3.33%; found C 38.23, H 2.58, N 2.97%.

$Co_4[\mu_4\text{-}Si(CH_2)_3OMe]_2(CO)_{11}$

"$MeO(CH_2)_3SiH_3$" (250 µL, *ca.* 0.135 g, 1.3 mmol)[54] was added to a toluene solution (10 mL) of $Co_4(CO)_{12}$ (0.28 g, 0.5 mmol), sealed in a glass ampoule under vacuum and heated to 50°C for 4 days. After cooling to room temperature, the ampoule was opened and the contents transferred under argon to a Schlenk flask. Solvent was removed under vacuum and the sample extracted into CH_2Cl_2. Spot TLC indicated the presence of 3 species; unreacted $Co_4(CO)_{12}$, a green fraction in low yield (lost in chromatographic separation) and an intense orange band of the desired product. An intractable black solid was also produced in the reaction. The desired cluster was isolated by column chromatography using a 1:1 petroleum spirits:CH_2Cl_2 solvent mixture. Removal of

[54] The sample of $MeO(CH_2)_3SiH_3$ contained a significant amount of Et_2O (*ca.* 50% identified by NMR analysis) and an excess of the solution was used to compensate for this.

solvent from the orange fraction yielded $Co_4[\mu_4\text{-}Si(CH_2)_3OMe]_2(CO)_{11}$ (0.067 g, 0.09 mmol, 18%). The compound was significantly less stable than other clusters in this series, with decomposition noted at –20°C over the course of 1-2 months. Because of this sensitivity, no attempt was made to recrystallise the sample.

$Co_4[\mu_4\text{-}Si(CH_2)_3OMe]_2(CO)_{11}$

M_r – 746.2

IR – (ν_{CO}, CH_2Cl_2) 2083 (w), 2039 (s), 2019 (m,sh), 2006 (m,sh), 1979 (m,sh), 1851 (w) cm^{-1}

NMR – ^1H – 3.69 (m, 4H, $-CH_2O$), 3.45 (m, 6H, CH_3), 2.92 (m, 4H, CH_2-Si), 2.45 (m, 4H, $-CH_2-$) ppm

^{13}C – 203.3 (CO), 74.4 (CH_2O), 58.9 (CH_3), 28.3 ($-CH_2-$), 26.0 (CH_2Si) ppm

ESMS – (MeOH, +ve ion, 10 cV) *m/z* 1021 (80% - $[M\text{-}5CO\text{+}5^tBuNC]^+$), *m/z* 1076 (100% - $[M\text{-}6CO\text{+}6^tBuNC]^+$) after treatment with ^tBuNC

$Co_4(\mu_4\text{-}GeC_6H_4NMe_2)_2(CO)_{11}$

The synthesis of "$Me_2NC_6H_4GeH_3$" was presented in Chapter 2. As mentioned, the synthesis resulted in the formation of R_2GeH_2 and R_3GeH by-products (as determined by ESMS and NMR analyses). Since $Me_2NC_6H_4GeH_3$ was the dominant species present, removal of the by-products was not considered essential and the mixture was used without isolation of $Me_2NC_6H_4GeH_3$.

"$Me_2NC_6H_4GeH_3$" (380 µL, *ca.* 0.275 g, 1.4 mmol) was added to a toluene (10 mL) solution of $Co_4(CO)_{12}$ (0.34 g, 0.6 mmol), sealed in a glass ampoule under vacuum and heated to 50°C for 5 days. After cooling to room temperature overnight, the ampoule was opened and solvent removed under vacuum. TLC indicated the presence of a purple by-product (with an identical IR spectrum to that reported in the analogous silane reaction), unreacted $Co_4(CO)_{12}$, the desired $Co_4(\mu_4\text{-}GeC_6H_4NMe_2)_2(CO)_{11}$ compound and an intractable black solid. The purple by-product and $Co_4(CO)_{12}$ were removed from the intended product by column chromatography (using a 2:1 petroleum spirits:CH_2Cl_2 solvent mixture) to yield $Co_4(\mu_4\text{-}GeC_6H_4NMe_2)_2(CO)_{11}$ (0.044 g, 0.048 mmol, 8%). The compound was recrystallised from a 1:1 petroleum spirits:toluene solution at –20°C.

$Co_4(\mu_4\text{-}GeC_6H_4NMe_2)_2(CO)_{11}$

m.p. 118-124°C (decomposed)

M_r – 929.41

IR – (ν_{CO}, CH_2Cl_2) 2073 (w), 2034 (s), 2016 (m,sh), 2001 (m,sh), 1846 (w,br) cm^{-1}

NMR – ^1H – 8.05, 6.99 (m, C_6H_4, 8H), 3.14 (s, 6H, CH_3) ppm

^{13}C – 203.8 (CO), 153.0 (C_1), 134.0 (C_2), 126.7 (C_4), 111.6 (C_3), 40.6 (CH_3) ppm

ESMS – (MeOH, +ve ion, 10 cV) *m/z* 931 (100% - $[M+H]^+$)

Evaluation of reaction conditions

Four separate reaction mixtures were prepared simultaneously, each containing a toluene solution (5 mL) of $Co_4(CO)_{12}$ (0.15 g, 0.25 mmol) and $MeOC_6H_4SiH_3$ (72 μL, 0.070 g, 0.50 mmol). The ampoules were sealed under vacuum and heated to 50°C in an oil bath. The first ampoule was removed after 48 hours, with the remaining ampoules removed after 4 days, 1 week and 2 weeks respectively. In each case, the samples were cooled to room temperature overnight before isolation of the reaction products by column chromatography using a 3:1 petroleum spirits:CH_2Cl_2 solvent mixture. Yields of unreacted $Co_4(CO)_{12}$ and $Co_4(\mu_4\text{-}SiC_6H_4OMe)_2(CO)_{11}$ are presented in Table 7.5. $Co_4(CO)_{12}$ was identified by its characteristic IR pattern (2065, 2055, 1867 cm^{-1}) while $Co_4(\mu_4\text{-}SiC_6H_4OMe)_2(CO)_{11}$ was identified on the basis of IR and NMR analyses.

Table 7.5 – Yields of $Co_4(\mu_4\text{-}SiC_6H_4OMe)_2(CO)_{11}$

Time at 50°C	Unreacted $Co_4(CO)_{12}$	Yield of $Co_4(\mu_4\text{-}SiC_6H_4OMe)_2(CO)_{11}$
2 days	0.053 g (35%)	0.122 g (57%)
4 days	0.049 g (33%)	0.121 g (57%)
1 week	0.051 g (34%)	0.107 g (51%)
2 weeks	0.048 g (32%)	0.101 g (45%)

The reaction between $MeOC_6H_4SiH_3$ and $Co_4(CO)_{12}$ was repeated using standard Schlenk techniques. A toluene solution (10 mL) of $Co_4(CO)_{12}$ (0.20 g, 0.35 mmol) and $MeOC_6H_4SiH_3$ (100 μL, 0.097 g, 0.70 mmol) was heated to 50°C for 3 days, at which time IR analysis indicated the presence of $Co_4(\mu_4\text{-}SiC_6H_4OMe)_2(CO)_{11}$ and unreacted $Co_4(CO)_{12}$. The reaction mixture was cooled to room temperature and solvent removed under vacuum. Column chromatography separated unreacted $Co_4(CO)_{12}$ (0.062 g, 33%)

from $Co_4(\mu_4\text{-}SiC_6H_4OMe)_2(CO)_{11}$ (0.115 g, 40%). A similar synthesis of $Co_4(\mu_4\text{-}SiPh)_2(CO)_{11}$ using standard Schlenk conditions was also successful.

Reactions of $Co_4(\mu_4\text{-}ER)_2(CO)_{11}$ clusters

The $Co_4(\mu_4\text{-}ER)_2(CO)_{11}$ clusters were prepared as set out above. Adamantylisonitrile (AdNC) was provided by Corry Decker and xylylisonitrile (XyNC) by Dr Trevor Mathieson. *tert*-Butylisonitrile (^{t}BuNC) was provided by Wade Mace and distilled prior to use (fraction collected between 88-92°C). Trimethylphosphite (BDH) and tri–*n*-butylphosphine (BDH) were fractionally distilled under vacuum prior to use.

Isonitrile substitution

To a CH_2Cl_2 solution (5 mL) of $Co_4(\mu_4\text{-}SiC_6H_4NMe_2)_2(CO)_{11}$ (0.01 g, 0.012 mmol) was added RNC [0.12 mmol; 13 μL ^{t}BuNC (0.01 g), 0.016 g XyNC, or 0.019 g AdNC[55]] and the solution was heated in either a water or oil bath to *ca.* 30-35°C. ESMS analysis of the solution indicated facile substitution of 6 ligands over a 3-4 hour period. The reactions were repeated on a similar scale using the $Co_4(\mu_4\text{-}SiC_6H_4R)_2(CO)_{11}$ (R = H, OMe) clusters.

The reaction between $Co_4(\mu_4\text{-}SiC_6H_4OMe)_2(CO)_{11}$ and ^{t}BuNC was repeated on a larger scale to attempt isolation of the highly-substituted clusters. To a CH_2Cl_2 solution (20 mL) of $Co_4(\mu_4\text{-}SiC_6H_4OMe)_2(CO)_{11}$ (0.05 g, 0.06 mmol) was added ^{t}BuNC (45 μL, 0.036 g, 0.43 mmol) and the mixture heated to 35°C for 4 hours. ES mass spectra indicated exclusive formation of $Co_4(\mu_4\text{-}SiC_6H_4OMe)_2(CO)_5(^t\text{BuNC})_6$ {$[M]^+$, *m/z* 1144} while spot TLC displayed two red products along with extensive decomposition (which remained on the baseline). The isolated fractions were separated from the decomposition material by column chromatography in low yield (0.01 g recovered), with ESMS analysis indicating an equal mixture of the penta- and hexa-substituted clusters.

[55] The XyNC and AdNC reagents were added in appropriate quantity from a prepared standard CH_2Cl_2 solution of the isonitrile.

Competitive substitution reactions were performed by addition of a stoichiometric excess (10:1) of a mixed isonitrile solution (containing equimolar amounts of the two isonitrile reagents in CH_2Cl_2) to a CH_2Cl_2 solution of $Co_4(\mu_4\text{-}SiC_6H_4NMe_2)_2(CO)_{11}$ (0.01 g, 0.012 mmol). The solution was heated to 40°C for 3 hours and monitored by ESMS. In each case, the dominant signals after reaction corresponded to a series of penta- and hexa-substituted clusters. The dominant signals in the competition between XyNC and ^{t}BuNC corresponded to clusters containing approximately equal quantities of the two reagents while the equivalent reactions with AdNC indicated a lower affinity for substitution. Competitive isonitrile substitution reactions were also examined for the $Co_4(\mu_4\text{-}SiC_6H_4R)_2(CO)_{11}$ (R = H, OMe) clusters on a similar scale with similar results.

X-ray structure determination of $Co_4(\mu_4\text{-}SiC_6H_4OMe)_2(CO)_7(XyNC)_4$

Crystals of the title compound were obtained by cooling a 4:1 petroleum spirits:toluene solution composed primarily of $Co_4(\mu_4\text{-}SiC_6H_4OMe)_2(CO)_{11-x}(XyNC)_x$ (x = 5, 6 as determined by ESMS) to –20°C. The structure refined cleanly without disorder or solvation. Refinement information is provided in Table 7.6.

Table 7.6 – Crystallographic data for $Co_4(\mu_4\text{-}SiC_6H_4OMe)_2(CO)_7(XyNC)_4$

Empirical Formula	$C_{57}H_{50}Co_4N_4O_9Si_2$
M_r	1226.91
Temperature (K)	203
Crystal System	Monoclinic
Space Group	C2/c
a(Å)	21.5814(4)
b(Å)	15.3852(3)
c(Å)	17.4610(2)
β(°)	110.106(1)
Volume (Å^3)	5444.33(16)
Z	4
Calculated Density (Mg m^{-3})	1.497
θ range collected	1.66 to 25.38
Reflections Collected	14736
Independent Reflections	4939 (R_{int} = 0.0225)
Goodness of Fit	1.052
R Indices – I > 2σ(I)	R_1 = 0.0336; wR_2 = 0.0848
R Indices – all data	R_1 = 0.0423, wR_2 = 0.0912
T_{max}/T_{min}	0.9152/0.8075

Phosphite substitution

To a toluene solution (5 mL) of $Co_4(\mu_4\text{-}SiC_6H_4NMe_2)_2(CO)_{11}$ (0.02 g, 0.024 mmol) was added $P(OMe)_3$ (28 μL, 0.030 g, 0.25 mmol) and the solution was heated to 45°C. ESMS analysis of the solution over a 3-4 hour period indicated substitution of three or four ligands, generating the $Co_4(\mu_4\text{-}SiC_6H_4NMe_2)_2(CO)_{11-x}[P(OMe)_3]_x$ (x = 3, 4) clusters {$[M+H]^+$, *m/z* = 1129 and 1225 respectively}. The reaction was extended to the $Co_4(\mu_4\text{-}SiC_6H_4R)_2(CO)_{11}$ (R = H, OMe) clusters on a similar scale, with formation of the tri- and tetra-substituted clusters noted in each case {$[M]^+$ - *m/z* 1042, 1138 for R = H; *m/z* 1102, 1198 for R = OMe}.

Equivalent reactions on a similar scale in CH_2Cl_2 indicated formation of the tri-substituted products, $Co_4(\mu_4\text{-}SiC_6H_4R)_2(CO)_8[P(OMe)_3]_3$. In each case, signals attributable to the tetra-substituted clusters were detected by ESMS but failed to

dominate the spectra. Similarly, spot TLC indicated a preference for the tri-substituted species.

Synthesis of $Co_4(\mu_4\text{-}SiC_6H_4OMe)_2(CO)_8[P(OMe)_3]_3$

To a CH_2Cl_2 solution (5 mL) of $Co_4(\mu_4\text{-}SiC_6H_4OMe)_2(CO)_{11}$ (0.04 g, 0.05 mmol) was added $P(OMe)_3$ (28 μL, 0.03 g, 0.25 mmol) and the mixture was heated to 35°C for 4 hours. ES mass spectra at this time were dominated by a signal corresponding to the tri-substituted product {$[M]^+$, *m/z* 1102}. The solvent was reduced in volume to *ca.* 0.5 mL and separated on a silica preparative plate to yield $Co_4(\mu_4\text{-}SiC_6H_4OMe)_2(CO)_8[P(OMe)_3]_3$ (0.0372 g, 69%). Crystals of the cluster were grown from a 5:1 petroleum spirits:toluene solution at –20°C but were of insufficient size for structural characterisation.

$Co_4(\mu_4\text{-}SiC_6H_4OMe)_2(CO)_8[P(OMe)_3]_3$

M_r – 1102.4

IR – (ν_{CO}, CH_2Cl_2) 2047 (w), 2015 (m,sh), 1990 (s), 1817 (w,br) cm^{-1}

NMR – ^1H – 8.30, 7.08 (m, 8H, C_6H_4), 3.90 (s, 6H, C-OCH_3), 3.49 (s, 27H, P-OCH_3) ppm

^{13}C – 210.0 (CO), 137.8 (C_2), 112.6 (C_3), 52.7 (C-OCH_3), 52.4 (P-OCH_3) ppm

^{31}P – 151-159 (P-OCH_3) ppm

ESMS – (MeOH, +ve ion, 10 cV) *m/z* 1006 (5% - $[Co_4(\mu_4\text{-}SiC_6H_4OMe)_2(CO)_9\{P(OMe)_3\}_2]^+$), *m/z* 1102 (100% - $[Co_4(\mu_4\text{-}SiC_6H_4OMe)_2(CO)_8\{P(OMe)_3\}_3]^+$), *m/z* 1198 (10% - $[Co_4(\mu_4\text{-}SiC_6H_4OMe)_2(CO)_7\{P(OMe)_3\}_4]^+$)

Attempted phosphine substitution

To a CH_2Cl_2 solution (5 mL) of $Co_4(\mu_4\text{-}SiC_6H_4NMe_2)_2(CO)_{11}$ (0.01 g, 0.012 mmol) was added PBu_3 (30 μL, 0.024 g, 0.12 mmol) and the mixture heated to 35°C. The solution was analysed by ESMS over a 4 hour period without evidence for ligand substitution. The solution changed colour from deep orange/red to pale green over this period and a decrease in the intensity of the parent signal {$[M+H]^+$, *m/z* 841} was noted. Equivalent reaction with $Co_4(\mu_4\text{-}SiC_6H_4OMe)_2(CO)_{11}$ indicated formation of the tri- and tetra-substituted products {$[M]^+$ - *m/z* 1336 and 1510}, but these signals were of limited intensity and further examination of this system was abandoned.

Attempted substitution using $[Mo(CO)_3(\eta^5\text{-}C_5H_5)]_2$

To a toluene solution (10 mL) of $Co_4(\mu_4\text{-}SiC_6H_4NMe_2)_2(CO)_{11}$ (0.010 g, 0.012 mmol) was added $[Mo(CO)_3(\eta^5\text{-}C_5H_5)]_2$ (0.015 g, 0.031 mmol) and the mixture was refluxed for 4 hours. ESMS monitoring over this time provided no evidence for mixed-metal cluster formation. The signal attributable to $Co_4(\mu_4\text{-}SiC_6H_4NMe_2)_2(CO)_{11}$ {$[M+H]^+$, *m/z* 841} was present after reflux but at significantly lower intensity than prior to reaction.

The reaction was repeated on a similar scale but initiated by addition of 1 mL of a 0.0082 mol L^{-1} solution of $Na[Ph_2CO]$ [produced by stirring sodium metal in a toluene solution (20 mL) of Ph_2CO (0.03 g)]. The solution was stirred under an argon atmosphere for 24 hours with ESMS analysis after this time providing no indication for substituted products. An additional 2 mL of the initiating agent was added (giving a cluster:initiator ratio of 1:2) with no effect. The synthesis was abandoned at this point.

Reaction of $Co_2(CO)_8$ and $Me_2NC_6H_4SiH_3$

$Me_2NC_6H_4SiH_3$ (0.22 g, 1.5 mmol) was added to a toluene solution (20 mL) of $Co_2(CO)_8$ (1.0 g, 2.9 mmol) and the resultant mixture was heated to 50°C for 4 hours. The solution was analysed by ESMS over this time but spectra were found to be of low intensity and irreproducible. Following reaction, the solvent was removed under vacuum and the mixture extracted into CH_2Cl_2. TLC of this solution showed the presence of 4 distinct products which were subsequently isolated through column chromatography using a 4:1 petroleum spirits:CH_2Cl_2 mobile phase. The 4 reaction components were; (i) a purple fraction [of composition identical to that found in the reaction of $NMe_2C_6H_4SiH_3$ with $Co_4(CO)_{12}$], (ii) a mixture of unreacted $Co_2(CO)_8$ and $Co_4(CO)_{12}$, (iii) a second purple fraction in agreement with previous reports (0.030 g), and (iv) an orange band of $Co_4(\mu_4\text{-}SiC_6H_4NMe_2)_2(CO)_{11}$ (0.015 g, 1%).

All products were identified on the basis of IR spectra, with ESMS evidence for the last two products. The initial purple fraction failed to provide an ESMS signal, indicating loss of the NMe_2 functionality. ES mass spectra of the second purple fraction were dominated by a signal at *m/z* 1234 corresponding to the $[M+H]^+$ adduct of the

previously characterised $Me_2NC_6H_4Si[OCCo_3(CO)_9]_2Co(CO)_4$ compound. An additional signal at *m/z* 1367 was detected but at very low (< 10%) intensity.

(i) – IR – (ν_{CO}, CH_2Cl_2) 2052(s), 2038 (m) cm^{-1}

(ii) – IR – (ν_{CO}, CH_2Cl_2) 2064 (s), 2055 (s), 1867 (s), 1858 (s) cm^{-1}

(iii) – ESMS – (MeOH, +ve ion, 10 cV) *m/z* 1234 (100% - $[M+H]^+$), *m/z* 1367 (8% - $[?]^+$)

– IR – (ν_{CO}, CH_2Cl_2) 2110 (w), 2101 (w), 2061 (s), 2053 (s), 2034 (s), 2005 (m) cm^{-1}

– ^1H NMR – 7.66, 6.75 (m, 4H, C_6H_4), 4.13 (s, 6H, CH_3) ppm

(iv) – ESMS – (MeOH, +ve ion, 10 cV) *m/z* 841 (100% - $[M+H]^+$)

– IR – (ν_{CO}, CH_2Cl_2) 2053 (m), 2043 (s), 2022 (m), 2007 (m,sh), 1971 (w), 1850 (w) cm^{-1}

Synthesis of Linked Si_2Co_4 Octahedra

$[Co_4(\mu_4\text{-}SiPh)(CO)_{11}Si]_2(CH_2)_8$

To a toluene solution (20 mL) of $Co_4(CO)_{12}$ (0.38 g, 0.67 mmol) was added $PhSiH_3$ (60 µl, 0.051 g, 0.47 mmol) and $H_3Si(CH_2)_8SiH_3$ (96 µL, 0.083 g, 0.47 mmol), and the mixture sealed in an ampoule under vacuum. The mixture was heated to 50°C for 2 weeks after which the ampoule was opened, the contents transferred to a Schlenk flask and solvent removed under vacuum. TLC indicated the presence of unreacted $Co_4(CO)_{12}$, $Co_4(\mu_4\text{-}SiPh)_2(CO)_{11}$, $[Co_4(\mu_4\text{-}SiPh)(CO)_{11}Si]_2(CH_2)_8$ and an immobile orange product. Column chromatography using a 5:1 petroleum spirits:CH_2Cl_2 solvent mixture allowed isolation of the first three products, affording an orange microcrystalline solid of $[Co_4(\mu_4\text{-}SiPh)(CO)_{11}Si]_2(CH_2)_8$ (0.012 g, 0.008 mmol, 2%).

$[Co_4(\mu_4\text{-}SiPh)(CO)_{11}Si]_2(CH_2)_8$

M_r – 1466.5

IR – (ν_{CO}, CH_2Cl_2) 2083 (w), 2065 (w), 2043 (s), 2026 (m,sh), 1835 (w,br) cm^{-1}

NMR – ^1H – 8.55-7.70 (m, 10H, C_6H_5), 0.8-1.9 (m, 16H, CH_2) ppm

^{13}C – 204.5 (CO), 134.6 (C_2), 132.0 (C_4), 129.1 (C_3), 35.4 (C_γ), 31.0 (C_δ), 30.8 (C_β), 10.1 (C_α) ppm[56]

ESMS – (MeOH, +ve ion, 10 cV) *m/z* 1852 (40% - $[M\text{-}7CO+7^tBuNC]^+$), *m/z* 1907 (100% - $[M\text{-}8CO+8^tBuNC]^+$), *m/z* 1962 (30% - $[M\text{-}9CO+9^tBuNC]^+$) after treatment with ^{t}BuNC

[56] The C_1 signal was not detected because of the low yield of the cluster and poor spectral intensity.

$[Co_4(\mu_4\text{-}SiC_6H_4OMe)(CO)_{11}Si]_2(CH_2)_8$

To a toluene solution (20 mL) of $Co_4(CO)_{12}$ (0.35 g, 0.61 mmol) was added $MeOC_6H_4SiH_3$ (86 µl, 0.084 g, 0.61 mmol) and $H_3Si(CH_2)_8SiH_3$ (65 µL, 0.053 g, 0.31 mmol). The resultant mixture was sealed in an ampoule under vacuum and heated to 50°C for 2 weeks after which the ampoule was opened, the contents transferred to a Schlenk flask and solvent removed under vacuum. TLC indicated the presence of unreacted $Co_4(CO)_{12}$, $Co_4(\mu_4\text{-}SiC_6H_4OMe)_2(CO)_{11}$, $[Co_4(\mu_4\text{-}SiC_6H_4OMe)(CO)_{11}Si]_2(CH_2)_8$ and an immobile orange product. Column chromatography using a 3:1 petroleum spirits:CH_2Cl_2 solvent mixture allowed isolation of the unreacted $Co_4(CO)_{12}$ and the monomeric and dimeric clusters. Solvent was removed from the second orange fraction to afford $[Co_4(\mu_4\text{-}SiC_6H_4OMe)(CO)_{11}Si]_2(CH_2)_8$ (0.018 g, 0.012 mmol, 4%).

$[Co_4(\mu_4\text{-}SiC_6H_4OMe)(CO)_{11}Si]_2(CH_2)_8$

M_r – 1526.5

IR – (ν_{CO}, CH_2Cl_2) 2045 (s), 2025 (m,sh), 2010 (m, sh), 1840 (w,br) cm^{-1}

NMR – ^1H – 8.50, 7.55 (m, 8H, C_6H_4), 3.95 (s, 6H, CH_3), 0.7-2.0 (m, 16H) ppm

^{13}C – 205.3 (CO), 136.3 (C_2), 114.8 (C_3), 54.7 (CH_3), 36.0 (C_γ), 28.8 (C_δ), 28.6 (C_β), 9.3 (C_α) ppm[57]

ESMS – (MeOH, +ve ion, 10 cV) *m/z* 1857 (20% - $[M\text{-}6CO\text{+}6^tBuNC]^+$), *m/z* 1912 (55% - $M\text{-}7CO\text{+}7^tBuNC]^+$), *m/z* 1967 (100% - $[M\text{-}8CO\text{+}8^tBuNC]^+$), *m/z* 2022 (80% - $[M\text{-}9CO\text{+}9^tBuNC]^+$), *m/z* 2077 (30% - $[M\text{-}10CO\text{+}10^tBuNC]^+$) after treatment with ^tBuNC

p-$[Co_4(\mu_4\text{-}SiPh)(CO)_{11}Si]_2C_6H_4$ [24]

To a toluene solution (10 mL) of $Co_4(CO)_{12}$ (0.28 g, 0.49 mmol) was added $PhSiH_3$ (60 µL, 0.051 g, 0.47 mmol) and *p*-$(H_3Si)_2C_6H_4$ (40 µl, 0.35 g, 0.25 mmol). The mixture was sealed in an ampoule under vacuum and heated to 50°C for 3 weeks, after which the ampoule was opened, the contents transferred to a Schlenk flask, and solvent removed under vacuum. TLC indicated the presence of unreacted $Co_4(CO)_{12}$, $Co_4(\mu_4\text{-}SiPh)_2(CO)_{11}$, *p*-$[Co_4(\mu_4\text{-}SiPh)(CO)_{11}Si]_2C_6H_4$ and a green compound (of low yield and lost during chromatographic separation). The compounds were separated by column

[57] The C_1 and C_4 signals were not detected because of the low yield of the cluster and poor spectral intensity.

chromatography using a 5:1 petroleum spirits:CH_2Cl_2 solvent mixture, with solvent removal from the second orange band yielding *p*-$[Co_4(\mu_4\text{-}SiPh)(CO)_{11}Si]_2C_6H_4$ (0.007 g, 0.005 mmol, 2%).

p-$[Co_4(\mu_4\text{-}SiPh)(CO)_{11}Si]_2C_6H_4$

M_r – 1430.3

IR – (ν_{CO}, CH_2Cl_2) 2048 (s), 2028 (m), 2014 (m), 1854 (w) cm^{-1}

NMR – ^1H – 8.51-7.68 (m, 14H, C_6H_5 and C_6H_4) ppm

ESMS – (MeOH, +ve ion, 10 cV) *m/z* 1816 (35% - $[M\text{-}7CO\text{+}7^tBuNC]^+$), *m/z* 1871 (100% - $[M\text{-}8CO\text{+}8^tBuNC]^+$), *m/z* 1926 (30% - $[M\text{-}9CO\text{+}9^tBuNC]^+$) after treatment with ^{t}BuNC

p-$[Co_4(\mu_4\text{-}SiC_6H_4OMe)(CO)_{11}Si]_2C_6H_4$ [24]

To a toluene solution (10 mL) of $Co_4(CO)_{12}$ (0.4 g, 0.7 mmol) was added $MeOC_6H_4SiH_3$ (100 μL, 0.097 g, 0.7 mmol) and *p*-$(H_3Si)_2C_6H_4$ (55 μl, 0.48 g, 0.35 mmol). The mixture was sealed in an ampoule under vacuum and heated to 50°C for 2 weeks, after which the ampoule was opened, contents transferred to a Schlenk flask, and solvent removed under vacuum. TLC indicated the presence of unreacted $Co_4(CO)_{12}$, $Co_4(\mu_4\text{-}SiC_6H_4OMe)_2(CO)_{11}$, *p*-$[Co_4(\mu_4\text{-}SiC_6H_4OMe)(CO)_{11}Si]_2C_6H_4$ and a green compound (of low yield and lost during chromatographic separation). The compounds were separated by column chromatography using a 3:1 petroleum spirits:CH_2Cl_2 solvent mixture, with solvent removal from the second orange band yielding *p*-$[Co_4(\mu_4\text{-}SiC_6H_4OMe)(CO)_{11}Si]_2C_6H_4$ (0.005 g, 0.003 mmol, 1%).

p-$[Co_4(\mu_4\text{-}SiC_6H_4OMe)(CO)_{11}Si]_2C_6H_4$

M_r – 1490.4

IR – (ν_{CO}, CH_2Cl_2) 2046 (s), 2028 (m), 2012 (m), 1854 (w) cm^{-1}

NMR – ^1H – 8.50-7.25 (m, 12H, C_6H_4), 4.0 (s, 6H, CH_3) ppm

ESMS – (MeOH, +ve ion, 10 cV) *m/z* 1820 (40% - $[M\text{-}6CO\text{+}6^tBuNC]^+$), *m/z* 1876 (100% - $[M\text{-}7CO\text{+}7^tBuNC]^+$), *m/z* 1931 (55% - $[M\text{-}8CO\text{+}8^tBuNC]^+$) after treatment with ^{t}BuNC

Attempted synthesis of $[Co_4(\mu_4\text{-}SiC_6H_4NMe_2)(CO)_{11}Si]_2X$ [X = $(CH_2)_8$, C_6H_4]

To a toluene solution (10 mL) of $Co_4(CO)_{12}$ (0.35 g, 0.6 mmol) was added $Me_2NC_6H_4SiH_3$ (0.1 g, 0.66 mmol) and $H_3Si(CH_2)_8SiH_3$ (50 μL, 0.42 g, 0.3 mmol), the mixture was sealed in an ampoule under vacuum and heated to 50°C for 2 weeks. After

cooling to room temperature, the ampoule was opened and the contents transferred under argon into a Schlenk flask. Solvent was removed under vacuum and the solid extracted with CH_2Cl_2. Spot TLC indicated the presence of unreacted $Co_4(CO)_{12}$, $Co_4(\mu_4\text{-}SiC_6H_4NMe_2)_2(CO)_{11}$ and an orange/red product which irreversibly bound to the silica support. Column chromatography allowed isolation of the first two components, though the irreversible binding of the third product hampered visualisation of the different chromophores. TLC analysis of the sample after pre-treatment with a silica column (using neat CH_2Cl_2 as the solvent) indicated only the presence of $Co_4(CO)_{12}$ and $Co_4(\mu_4\text{-}SiC_6H_4NMe_2)_2(CO)_{11}$.

Reactions on a similar scale using the aromatic disilane *p*-$(H_3Si)_2C_6H_4$ were also unsuccessful. The only isolated fractions after chromatography corresponded to $Co_4(CO)_{12}$ and $Co_4(\mu_4\text{-}SiC_6H_4NMe_2)_2(CO)_{11}$, with an additional product binding irreversibly to the silica support.

Attempted Synthesis of $[Co_4(\mu_4\text{-}SiC_6H_4R)(CO)_{11}Si]_2Fe(\eta^5\text{-}C_5H_4)_2$ (R = H, OMe)

To a toluene solution (10 mL) of $Co_4(CO)_{12}$ (0.20 g, 0.35 mmol) was added $PhSiH_3$ (40 μL, 0.034 g, 0.31 mmol) and "$Fe(\eta^5\text{-}C_5H_4SiH_3)_2$" (*ca.* 0.1 g, 0.41 mmol)[58], the mixture was sealed in an ampoule under vacuum and heated to 50°C for 3 weeks. After cooling to room temperature, the ampoule was opened and the contents transferred under argon into a Schlenk flask. Solvent was removed under vacuum and the crude mixture extracted with CH_2Cl_2. Spot TLC indicated the presence of unreacted $Co_4(CO)_{12}$ and the $Co_4(\mu_4\text{-}SiPh)_2(CO)_{11}$ product. There was no evidence for either a dimeric or oligomeric material.

Equivalent syntheses involving $MeOC_6H_4SiH_3$ as a capping silane were also unsuccessful in producing dimeric or oligomeric clusters. In the absence of capping silanes, the only species detected by TLC corresponded to unreacted $Co_4(CO)_{12}$.

[58] The $Fe(\eta^5\text{-}C_5H_4SiH_3)_2$ material contained detectable amounts of $Fe(\eta^5\text{-}C_5H_5)(\eta^5\text{-}C_5H_4SiH_3)$ and $Fe(\eta^5\text{-}C_5H_5)_2$, as reported in Chapter 2.

Attempted Synthesis of Higher Oligomers

Attempts at synthesis of trimeric and tetrameric clusters were attempted using appropriate ratios of the capping and linking silanes [$H_3Si(CH_2)_8SiH_3$ and *p*-$(SiH_3)_2C_6H_4$] in a similar manner to that reported for the dimeric clusters. The sealed ampoules were heated to 50°C for 2-4 weeks before opening and attempted isolation of the cluster products. Unreacted $Co_4(CO)_{12}$ and the appropriate monomeric cluster were noted in each case, as were traces of the dimeric clusters (by TLC). An additional orange product was detected but all attempts at isolation by chromatography resulted in irreversible binding of the product to the support.

The suspected cyclic Si_2Co_4 oligomer was synthesised directly by addition of $H_3Si(CH_2)SiH_3$ (100 μL, 0.086 g, 0.5 mmol) to a toluene solution (10 mL) of $Co_4(CO)_{12}$ (0.3 g, 0.5 mmol). The solution was heated to 50°C for 5 days under an inert atmosphere[59] with gas evolution (presumably CO and H_2) noted. Removal of the solvent followed by extraction of unreacted $Co_4(CO)_{12}$ into petroleum spirits yielded an insoluble orange/brown product. The product proved significantly more air-sensitive than either the monomeric or dimeric clusters, with decomposition noted within 10-20 minutes on exposure to air. A similar product of similar sensitivity was noted with *p*-$(H_3Si)_2C_6H_4$ though at lower yield.

"Cyclic $\{Co_4[\mu_4\text{-}Si(CH_2)_4]_2(CO)_{11}\}_n$ oligomer"

IR – (ν_{CO}, KBr disc) 2039 (s), 2026 (m,sh), 2005 (m,sh), 1850 (w,br) cm^{-1}

[59] A similar reaction was noted when the mixture was sealed in an ampoule under vacuum and heated to 50°C for 1-2 weeks.

Chapter Eight – Structure Solutions of Anionic Metal Carbonyls

8.1 A New Structural Isomer of $[CoFe_3(CO)_{13}]^-$

8.1.1 Introduction

There is no uniquely obvious way of arranging thirteen ligands about a metal tetrahedron. The most common arrangement (Figure 8.1a) involves three bridging ligands from an apical metal atom to each other metal, with all remaining ligands terminal (one associated with the apical atom and three for each metal in the basal plane). This arrangement is displayed by the $[PPN]^+$ salts of $[CoFe_3(CO)_{13}]^-$ [1], $[CoRu_3(CO)_{13}]^-$ [2] and $[RhRu_3(CO)_{13}]^-$ [3]. A variation of this structure is reported for $[CoRu_3(CO)_{13}H]$, with the hydride ligand bridging a Ru-Ru bond[4].

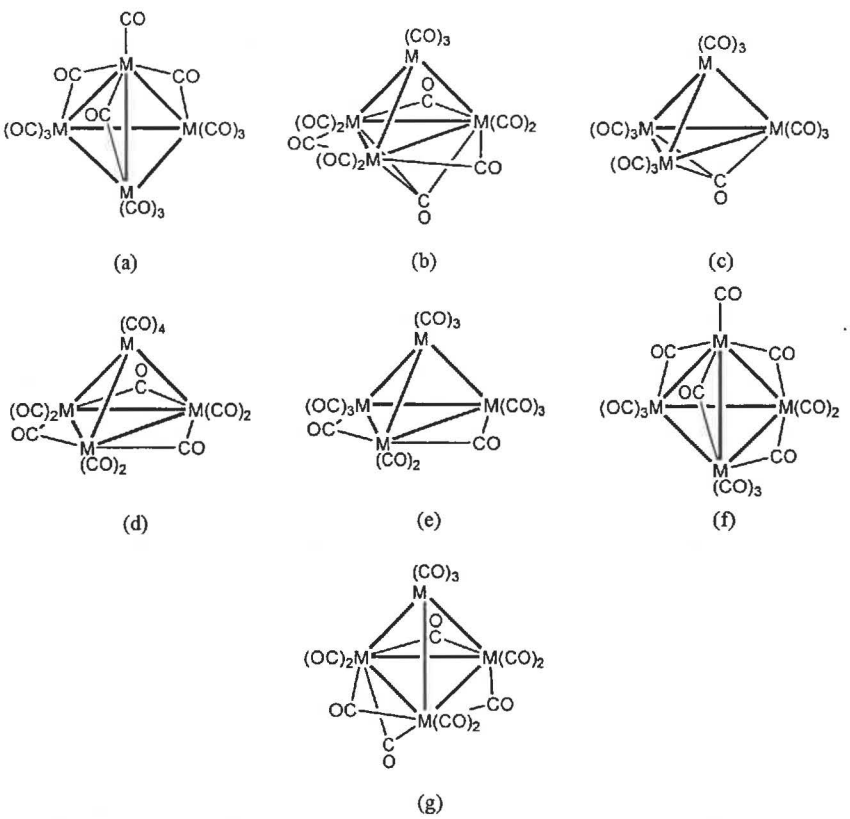

Figure 8.1 – The known $M_4(CO)_{13}$ arrangements.

[1] C.P. Horwitz, E.M. Holt and D.F. Shriver, *Organometallics*, 1985, **4**, 1117.
[2] P.C. Steinhardt, W.L. Gladfelter, A.D. Harley, J.R. Fox and G.L. Geoffroy, *Inorg. Chem.*, 1980, **19**, 332.
[3] A. Fumagalli, M. Bianchi, M.C. Malatesta, G. Ciani, M. Moret and A. Sironi, *Inorg. Chem.*, 1998, **37**, 1324.
[4] L.J. Farrugia, *Acta. Cryst. Sect. C*, 1988, **44**, 219.

An alternative arrangement is displayed by $[Fe(py)_6][Fe_4(CO)_{13}]$ (Figure 8.1b)[5]. In this structure there are three μ_2-CO ligands in the same plane as the Fe_3 triangle, with one μ_3-CO beneath the plane. The remaining ligands are terminal, two on each basal Fe and three on the unique apical Fe. Structural isomerism is reported for this anion, with the $[PPN]^+$ salt adopting a different ligand arrangement[6]. In this case, the CO ligands in the basal plane have lost their bridging character, with the μ_3-CO beneath the plane the only bridging ligand observed (Figure 8.1c). This arrangement is related to that of the $[Fe(py)_6]^{2+}$ salt by a rotation of the M_4 tetrahedron within the same ligand arrangement. In contrast, the structure of $[Ru_4(CO)_{13}]^{2-}$ has four terminal CO on the unique apical metal atom (though two could be considered semi-bridging), with three μ_2-CO in the basal plane (Figure 8.1d)[7].

Two other arrangements are displayed by $[PPN][IrRu_3(CO)_{13}]$[8], which crystallised with three independent anions in the unit cell. Two of these possess the same ligand arrangement (with two bridging ligands, both in the basal plane – Figure 8.1e) while the third adopts an alternative arrangement (with four bridging ligands, three associated with bonds to an apical ruthenium atom and one bridging a Ru-Ir bond - Figure 8.1f). The latter arrangement is also adopted by $Co_2Ru_2(CO)_{13}$[9].

The structural variation reported for $M_4(CO)_{13}$ compounds indicates there is little energy difference between the various arrangements. This is confirmed by the structural isomerism reported for $[Fe_4(CO)_{13}]^{2-}$ and $[IrRu_3(CO)_{13}]^-$. In attempts to isolate $[Co_3Fe_3Ge(CO)_{18}]^-$ (discussed in Chapter 5), $[NEt_4][CoFe_3(CO)_{13}]$ was inadvertently crystallised and structurally characterised. The anion adopts a different arrangement (Figure 8.1g) from that observed for the $[PPN]^+$ salt and is another example of structural isomerism.

8.1.2 Crystal Structure Determination of $[NEt_4][CoFe_3(CO)_{13}]$

The structure of the anion in $[NEt_4][CoFe_3(CO)_{13}]$ is displayed in Figures 8.2 and 8.3. Selected bond lengths and angles are provided in Table 8.1 while full details of the

[5] R.J. Doedens and L.F. Dahl, *J. Am. Chem. Soc.*, 1966, **88**, 4827.
[6] G. Van Buskirk, C.B. Knobler and H.D. Kaesz, *Organometallics*, 1985, **4**, 149.
[7] R. Suter, A.A. Bhattacharyya, L-Y. Hsu, J.A. Krause Bauer and S.G. Shore, *Polyhedron*, 1998, **17**, 2889.
[8] G. Süss-Fink, S. Haak, V. Ferrand and H. Stoeckli-Evans, *J. Chem. Soc., Dalton Trans.*, 1997, 3861.
[9] E. Roland and H. Vahrenkamp, *Chem. Ber.*, 1985, **118**, 1133.

structure are listed in Appendix C. Details relating to the structure solution are provided in the experimental section (Section 8.1.5).

The structure of $[NEt_4][CoFe_3(CO)_{13}]$ is based around a M_4 tetrahedron (as expected for a 60 valence-electron cluster) within a ligand sphere. There are nine terminal CO [2 per basal M and three for the unique apical Fe(2)] and four μ_2-CO ligands. Three of the μ_2 ligands [CO(2), CO(3), CO(4)] are located in the same plane as the M_3 triangle, while the fourth [CO(1)] is positioned below the plane and associated with the Fe(1)-Fe(3) bond. The Co(1)-C(1) distance [2.396(7) Å] indicates little bonding interaction between the two atoms [compared to 1.959(8) and 1.993(8) Å between Fe(1)-C(1) and Fe(3)-C(1) respectively]. The position of the CO(1) ligand breaks the C_{3v} symmetry displayed by the rest of the anion and provides support for the assignment of Co(1) (since a μ_3-CO ligand would be expected if all basal atoms were identical).

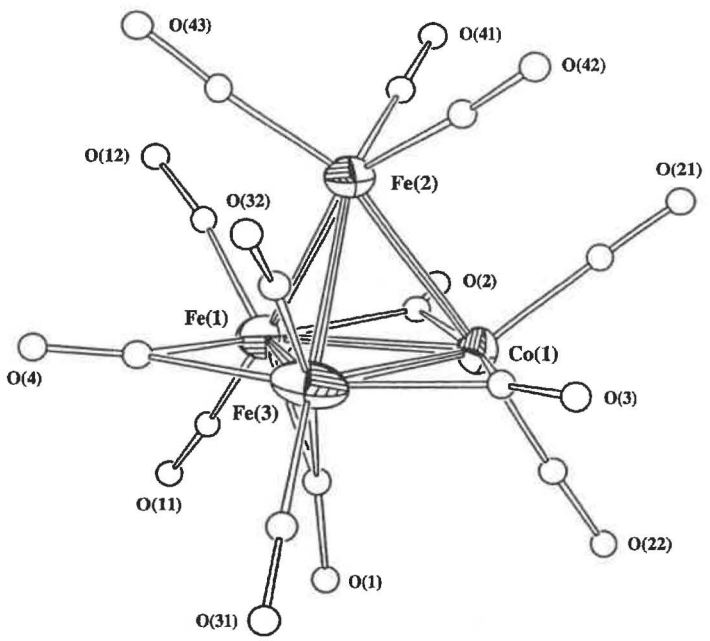

Figure 8.2 – A labelled view of the $[CoFe_3(CO)_{13}]^-$ anion. Ellipsoids of the metal atoms are drawn at the 50% probability level while the carbon and oxygen atoms are presented as arbitrary spheres to aid clarity.

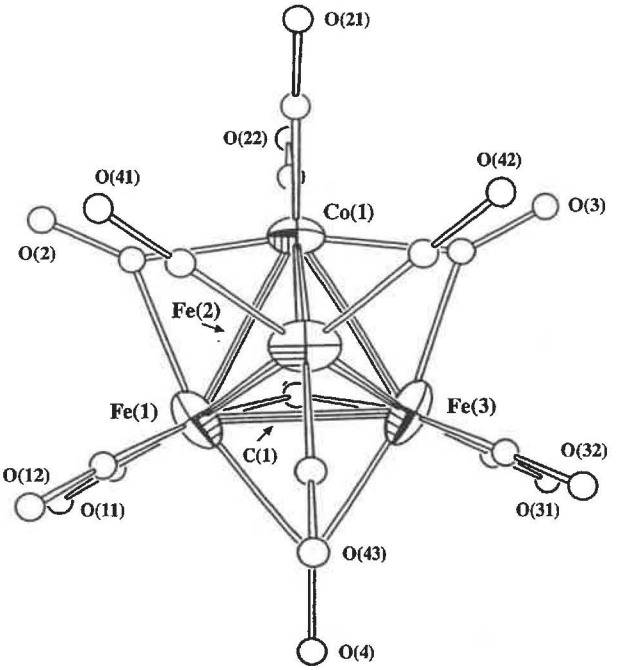

Figure 8.3 – A view of $[CoFe_3(CO)_{13}]^-$ perpendicular to the basal plane.

Table 8.1 – Selected bond lengths (Å) and angles (°) for $[NEt_4][CoFe_3(CO)_{13}]$

Co(1)–Fe(1)	2.5260(10)	Co(1)–Fe(2)	2.5879(9)
Co(1)–Fe(3)	2.5229(10)	Fe(1)–Fe(2)	2.5749(11)
Fe(2)–Fe(3)	2.5688(11)	Fe(1)– Fe(3)	2.4979(11)
Fe(1)–C(1)	1.959(8)	Fe(3)–C(1)	1.993(8)
C(1)–O(1)	1.216(8)	Co(1)–C(1)	2.396(7)
Co(1)–C(2)	1.938(5)	Co(1)–C(3)	1.950(5)
Fe(1)–C(2)	2.078(5)	Fe(3)–C(3)	2.058(5)
Fe(1)–C(4)	2.126(8)	Fe(3)–C(4)	2.088(8)
Co(1)-Fe(1)-Fe(3)	60.28(3)	Co(1)-Fe(3)-Fe(1)	60.41(3)
Fe(1)-Co(1)-Fe(3)	59.31(3)	Co(1)-C(2)-Fe(1)	77.85(18)
Co(1)-C(3)-Fe(3)	77.95(17)	Fe(1)-C(4)-Fe(3)	72.7(2)
Fe(1)-C(1)-Fe(3)	78.4(2)		

The structure of $[NEt_4][CoFe_3(CO)_{13}]$ differs significantly from that reported for $[PPN][CoFe_3(CO)_{13}]$[1], showing more resemblance to that displayed by $[Fe(py)_6][Fe_4(CO)_{13}]$[5] (though in the latter case the unique CO is μ_3 rather than μ_2). Interestingly, the bridging ligands in the basal plane are more symmetric in $[NEt_4][CoFe_3(CO)_{13}]$ than for $[Fe(py)_6][Fe_4(CO)_{13}]$. With regard to localised electron-

counting procedures, the $[NEt_4][CoFe_3(CO)_{13}]$ structure associates the free electron with Fe(2) whereas in the $[PPN]^+$ salt it is assigned to the cobalt atom.

8.1.3 Theoretical Models

The possible arrangements of thirteen ligands about a M_4 tetrahedral have been examined from a theoretical perspective previously. In particular, the Ligand Polyhedral Model (LPM) developed by Johnson and colleagues[10] has recently been applied to rationalising $M_4(CO)_{13}$ structures[11]. This model differs from many other cluster theories as it focuses on the arrangement of the ligands rather than the metal atoms. The metal core can adopt various orientations within a ligand envelope, with little energy difference between such orientations.

The LPM approach has been applied to the different arrangements observed for $M_4(CO)_{12}$ (Co, Rh, Ir) compounds[10]. The structures of $Co_4(CO)_{12}$ and $Rh_4(CO)_{12}$ display C_{3v} symmetry (with three μ_2-CO ligands associated with a basal M_3 plane) while $Ir_4(CO)_{12}$ expresses T_d symmetry (with all ligands terminal). There is no obvious reason based on the M_4 geometry (tetrahedral in each case) to account for the difference but with respect to the LPM model, the carbonyls of the cobalt and rhodium clusters map out icosahedra whereas the iridium analogue displays a cube-octahedron ligand arrangement. The icosahedron is the lowest-energy arrangement for 12 points on a sphere (the model applied) while the cube-octahedron has a larger central cavity, more suitable to the larger elements (though the size difference between rhodium and iridium atoms is insignificant). An alternative icosahedral $M_4(CO)_{12}$ arrangement expressing T symmetry (with all ligands terminal[12]) has been proposed but this geometry has not been identified experimentally.

The addition of a thirteenth vertex produces a range of possible capped icosahedra and cube-octahedra. The capped cube-octahedra are more appropriate to the larger elements {observed in the structures of $[IrOs_3(CO)_{13}]^-$ [13] and one isomer of $[IrRu_3(CO)_{13}]^-$ [8]}

[10] B.F.G. Johnson, *J. Chem. Soc., Chem. Commun.*, 1976, 211; R.E. Benfield and B.F.G. Johnson, *J. Chem. Soc., Dalton Trans.*, 1980, 1743; B.F.G. Johnson and R.E. Benfield, *Topics in Stereochemistry*, 1981, **12**, 253.
[11] B.F.G. Johnson, E.A. Quadrelli, V. Ferrand and A.W. Bott, *J. Chem. Soc., Dalton Trans.*, 2001, 1063.
[12] T symmetry differs from T_d by a rotation of the M_4 tetrahedron breaking the dihedral mirror component of T_d symmetry.
[13] G. Süss-Fink, S. Haak, V. Ferrand and H. Stoeckli-Evans, *J. Mol. Catal.*, 1999, **143**, 163.

while structures based around capped C_{3v} and T icosahedra are more common for the smaller transition metal elements.

In M_4 centred icosahedra displaying T symmetry, four icosahedral faces lie above M vertices, four lie directly above a M_3 face, and the remaining twelve are associated with M_3 faces but are offset. Capping of the first of these faces results in an apical M atom having an additional terminal ligand, forcing the remaining three ligands to adopt bridging positions {as observed for $[PPN][CoFe_3(CO)_{13}]$, $[CoRu_3(CO)_{13}]^-$ and $[RhRu_3(CO)_{13}]^-$}. Capping of one of the second types of icosahedral face (lying above a M_3 plane) leads to a structure with twelve terminal ligands and a single μ_3 ligand {as observed for $[PPN]_2[Fe_4(CO)_{13}]$}. Finally, capping of the third face type would give a structure similar to that mentioned above but with the unique CO bridging an edge rather than a face.

In comparison, in C_{3v} icosahedra the M_4 tetrahedron is oriented so there are three μ_2-CO ligands associated with the basal plane. In this case, capping of the icosahedral face above the apical metal produces a structure with four terminal ligands on the apical atom and three μ_2-CO within the basal plane {as displayed by $[Ru_4(CO)_{13}]^{2-}$}. Capping of the icosahedral face beneath the basal plane leads to a structure with a μ_3-CO associated with the plane {as observed for $[Fe(py)_6][Fe_4(CO)_{13}]$} while capping an offset face results in a structure with three μ_2-CO's within the M_3 plane and one μ_2-CO beneath the plane. Johnson and colleagues noted that such an arrangement had not been reported to date but the structure of $[NEt_4][CoFe_3(CO)_{13}]$ falls into this category.

The capped icosahedra observed for the $[NEt_4]^+$ and $[PPN]^+$ salts of $[CoFe_3(CO)_{13}]^-$ are displayed in Figure 8.4 (with the capping ligand indicated). Although the two appear dissimilar, this is an effect of the different nature of the capping ligand (μ_2 compared to terminal) rather than a different ligand polyhedral arrangement. The two icosahedra are related by an inversion of the M_4 tetrahedron within the ligand polygon, with the cobalt atoms occupying different vertices in the two tetrahedra. The different locations of the capping ligand (terminally attached to the apical atom compared to μ_2 beneath the Fe_2Co plane) are clearly observed.

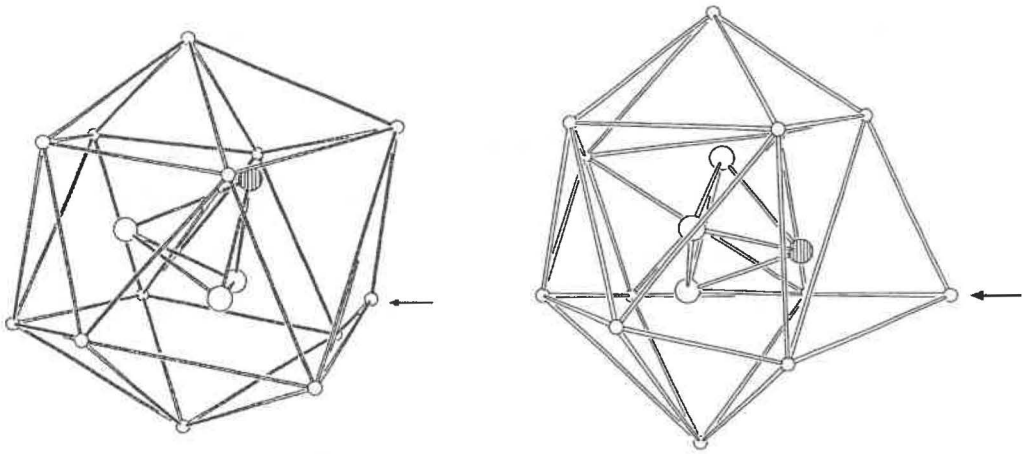

(a) (b)

Figure 8.4 – The ligand icosahedra for the $[NEt_4]^+$ (a) and $[PPN]^+$ (b) salts of $[CoFe_3(CO)_{13}]^-$.

An alternative model developed by J.W. Lauher involving a force-field or molecular mechanics approach (similar to that applied to organic molecules) has also been applied to metal carbonyl structures[14]. The surface of lowest energy around a metal core is modeled, with ligands adopting positions upon this surface (as compared to the purely spherical model used in LPM). For a $M_4(CO)_{12}$ structure, the lowest-energy arrangement corresponds to the idealised T isomer discussed above.

The structures of $[PPN][CoFe_3(CO)_{13}]$ and both salts of $[Fe_4(CO)_{13}]^{2-}$ were compared through use of this model[14]. The difference between the two $[Fe_4(CO)_{13}]^{2-}$ isomers was attributed to rotation of the Fe_4 core within the ligand shell, while the difference between $[CoFe_3(CO)_{13}]^-$ and $[Fe_4(CO)_{13}]^{2-}$ was considered a factor of the thirteenth CO binding to the apical cobalt rather than to the Fe_3 face. The different positions adopted by the thirteenth ligand were attributed to the asymmetry introduced to the system by the cobalt atom. This argument is flawed since two different ligand arrangements are displayed by $[CoFe_3(CO)_{13}]^-$, with the energy difference between the two forms sufficiently small that altering the cation can induce such a change.

8.1.4 Crystal Structure Determination of $[NEt_4][CoRu_3(CO)_{13}]$

Following identification of the novel geometry of $[NEt_4][CoFe_3(CO)_{13}]$, it was proposed that $[NEt_4][CoRu_3(CO)_{13}]$ might display similar structural isomerism. The compound

was synthesised from $Ru_3(CO)_{12}$ and $[NEt_4][Co(CO)_4]$, and crystallised from an Et_2O/CH_2Cl_2 diffusion at –20°C. The structure of $[NEt_4][CoRu_3(CO)_{13}]$ (Figure 8.5) contains three μ_2-CO, all bridging Co-Ru bonds. This arrangement is identical to that previously reported for the $[PPN]^+$ salt. The different ligand arrangements displayed by $[NEt_4][CoFe_3(CO)_{13}]$ and $[NEt_4][CoRu_3(CO)_{13}]$ are presumably caused by the longer Ru-Ru distance hampering bridging ligands (whereas the similarity in Co-Fe and Fe-Fe distances allows variation in the ligand arrangement, resulting in the structural isomerism observed).

The bond lengths and angles observed for $[NEt_4][CoRu_3(CO)_{13}]$ (a selection are presented in Table 8.2, with full tables provided in Appendix D) are of similar magnitude to those reported for $[PPN][CoRu_3(CO)_{13}]$[2].

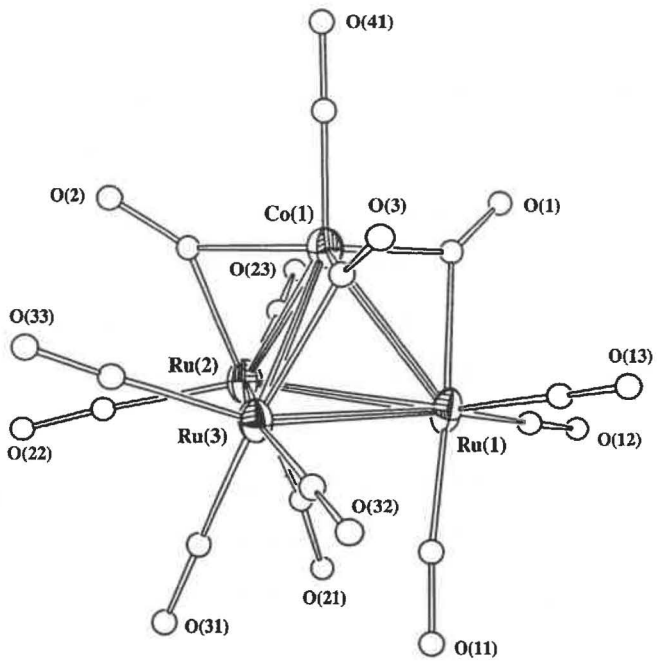

Figure 8.5 – A labelled view of the $[CoRu_3(CO)_{13}]^-$ anion. Ellipsoids of the metal atoms are drawn at the 50% probability level while the carbon and oxygen atoms are presented as arbitrary spheres to aid clarity

[14] J.W. Lauher, *J. Am. Chem. Soc.*, 1986, **108**, 1521.

Table 8.2 – Selected bond lengths (Å) and angles (°) for $[NEt_4][CoRu_3(CO)_{13}]$

Co(1)–Ru(1)	2.6495(15)	Co(1)–Ru(2)	2.6473(16)
Co(1)–Ru(3)	2.6654(15)	Ru(1)–Ru(2)	2.8869(11)
Ru(2)–Ru(3)	2.8707(13)	Ru(1)–Ru(3)	2.8431(13)
Co(1)–C(1)	1.891(9)	Co(1)–C(2)	1.906(10)
Co(1)–C(3)	1.888(11)	Ru(1)–C(1)	2.212(10)
Ru(2)–C(2)	2.159(10)	Ru(3)–C(3)	2.219(10)
Co(1)-C(1)-O(1)	142.6(8)	Ru(1)-C(1)-O(1)	137.3(8)
Co(1)-C(2)-O(2)	139.3(8)	Ru(2)-C(2)-O(2)	139.7(8)
Co(1)-C(3)-O(3)	143.0(8)	Ru(3)-C(3)-O(3)	136.5(8)

8.1.5 Experimental

Synthesis of $[NEt_4][CoFe_3(CO)_{13}]$

A CH_2Cl_2 solution containing μ_4-$Ge[Co_2(CO)_7]_2$, $Fe_3(CO)_{12}$ and $[NEt_4][Co(CO)_4]$ was refluxed for 3-4 hours. ESMS analysis of the solution revealed the presence of $[Co_3Fe_3Ge(CO)_{18}]^-$ (*m/z* 923), along with $[CoFe_3(CO)_{13}]^-$ (*m/z* 591) and $[Co_3Fe(CO)_{12}]^-$ (*m/z* 569). The solution was reduced in volume to *ca.* 2-3 mL and cooled to –20°C. A deep red crystalline product was isolated and characterised by X-ray structure determination as $[NEt_4][CoFe_3(CO)_{13}]$.

The synthesis of $[Co_3Fe_3Ge(CO)_{18}]^-$ and related anionic clusters were presented in Chapter 5. The $[CoFe_3(CO)_{13}]^-$ anion was prepared more systematically from refluxing an equimolar CH_2Cl_2 solution of $Fe_3(CO)_{12}$ and $[Co(CO)_4]^-$ [2].

$[NEt_4][CoFe_3(CO)_{13}]$

M_r – 720.9

IR – (ν_{CO}, CH_2Cl_2) 2000 (vs), 1965 (m), 1810 (m,br) cm^{-1} [Lit. 2074 (w), 2004 (vs), 1971 (m), 1930 (m,sh), 1816 (m,br) cm^{-1} [2]]

ESMS – ($C_2H_4Cl_2$, -ve ion, 5 cV) *m/z* 591 (100% - $[CoFe_3(CO)_{13}]^-$)

Synthesis of $[NEt_4][CoRu_3(CO)_{13}]$[2]

A thf solution (10 mL) of $Ru_3(CO)_{12}$ (0.10 g, 0.16 mmol) and $[NEt_4][Co(CO)_4]$ (0.05 g, 0.17 mmol) was refluxed until IR and ESMS analyses indicated conversion to $[CoRu_3(CO)_{13}]^-$ (*ca.* 2 hours). Solvent was removed under vacuum and $[NEt_4][CoRu_3(CO)_{13}]$ (0.07 g, 52%) recrystallised from CH_2Cl_2/Et_2O. Crystals suitable for structure determination were grown by diffusion of Et_2O into a CH_2Cl_2 solution of the compound at –20°C.

$[NEt_4][CoRu_3(CO)_{13}]$

M_r – 856.5

IR – (ν_{CO}, thf) 2017 (vs), 1997 (sh), 1792 (m) cm^{-1} [Lit. 2072 (w), 2024 (vs), 1992 (m), 1823 (w), 1794 (m,br) cm^{-1} [2]]

ESMS – ($C_2H_4Cl_2$, -ve ion, 5 cV) *m/z* 728 (100% - $[CoRu_3(CO)_{13}]^-$)

X-ray structure determinations of $[NEt_4][CoM_3(CO)_{13}]$ (M = Fe, Ru)

Both structures were solved using direct methods to locate the metal atoms, with the remaining atoms found through difference maps. The $[NEt_4][CoFe_3(CO)_{13}]$ structure refined cleanly and the hydrogen atoms associated with the cation were placed in calculated positions (U_{iso} 1.2 times that of the carbon atoms to which they were attached) using a riding model. The anionic metal carbonyl in $[NEt_4][CoRu_3(CO)_{13}]$ refined cleanly but the two ½ cations were positioned on symmetry sites, with the carbon atoms disordered over two locations. Assignment of hydrogen atoms to the cations was inappropriate because of the extent of disorder.

The similarity in the scattering factors of cobalt and iron atoms hampers discrimination between the elements. Analysis of bond parameters in the structure of $[NEt_4][CoFe_3(CO)_{13}]$ also provided no clear distinction between the two elements. The assignment provided is based on analysis of the U_{iso} values of the metal atoms and on consideration of the unique CO(1). The solution presented provides U_{iso} values of 0.0319 for Co(1) and 0.0391, 0.0400, 0.0430 for Fe(1), Fe(2) and Fe(3) respectively. The alternative arrangement in which the Fe(2) and Co(1) atoms are interchanged provides U_{iso} values of 0.0440 for Co(1), 0.0290 [Fe(2)], 0.0392 [Fe(1)] and 0.0432 [Fe(3)]. Locating the cobalt in the basal plane also provides an explanation for the μ_2 nature of CO(1) whereas a μ_3 bonding mode would be expected for a Fe_3 plane.

The high symmetry of the anion resulted in the compound initially being solved in the higher symmetry Pnma space group [where Co(1) and Fe(2) lie on a symmetry plane and only one of Fe(1) and Fe(3) is unique]. The structure solution refined cleanly for the anion but caused considerable disorder in the $[NEt_4]^+$ cation. Solving the structure in the lower symmetry $P2_12_12_1$ space group eliminated this disorder.

Table 8.3 – Crystallographic data for $[NEt_4][CoM_3(CO)_{13}]$ (M = Fe, Ru)

	$[NEt_4][CoFe_3(CO)_{13}]$	$[NEt_4][CoRu_3(CO)_{13}]$
Empirical Formula	$C_{21}H_{20}CoFe_3NO_{13}$	$C_{21}H_{20}CoRu_3NO_{13}$
M_r	720.86	856.52
Temperature (K)	163	168
Crystal System	Orthorhombic	Monoclinic
Space Group	$P2_12_12_1$	$P2_1/n$
a(Å)	12.138(3)	12.787(4)
b(Å)	12.717(3)	12.397(4)
c(Å)	17.462(5)	18.232(6)
β(°)	90	94.520(4)
Volume (Å^3)	2695.4(12)	2881.2(16)
Z	4	4
Calculated Density (Mg m^{-3})	1.776	1.975
θ range collected	2.04 to 27.72	1.88 to 26.40
Reflections Collected	35463	20501
Independent Reflections	5900 (R_{int} = 0.0267)	5658 (R_{int} = 0.0459)
Goodness of Fit	1.070	1.103
R Indices – I > 2σ(I)	R_1 = 0.0406, wR_2 = 0.1174	R_1 = 0.0566, wR_2 = 0.1279
R Indices – all Data	R_1 = 0.0502, wR_2 = 0.1215	R_1 = 0.0886, wR_2 = 0.1342
T_{max}/T_{min}	1.0000/0.8943	1.0000/0.7395

8.2 Crystal Structure Determination of $[PPN][Mo(CO)_3(\eta^5\text{-}C_5H_5)]$

8.2.1 Introduction

During the course of this research, bis(triphenylphosphine)iminium cyclopentadienyltricarbonylmolybdate, $[PPN][Mo(CO)_3(\eta^5\text{-}C_5H_5)]$, was prepared and crystallised. The structure was unknown in the literature and a crystallographic structure determination was performed.

The anion has been previously structurally characterised as the $[NBu_4]^+$ salt[15] and has co-crystallised in a series of molybdenum compounds[16].

8.2.2 Structure of $[PPN][Mo(CO)_3(\eta^5\text{-}C_5H_5)]$

The structure of $[PPN][Mo(CO)_3(\eta^5\text{-}C_5H_5)]$ is displayed in Figure 8.6. Selected bond lengths and angles are provided in Table 8.4 while full details are listed in Appendix E.

The anion adopts the 'piano stool' arrangement common for $CpML_3$ compounds. The average $M\text{-}C_{CO}$ bond length [1.930(3) Å] is longer than that previously reported [1.909(9) Å] while the average $C_{CO}\text{-}Mo\text{-}C_{CO}$ angle [87(2)°] and $Mo\text{-}C_{Cp}$ distance [2.37(2) Å] are similar to previous reports [88.1(3)° and 2.37(1) Å respectively[15]].

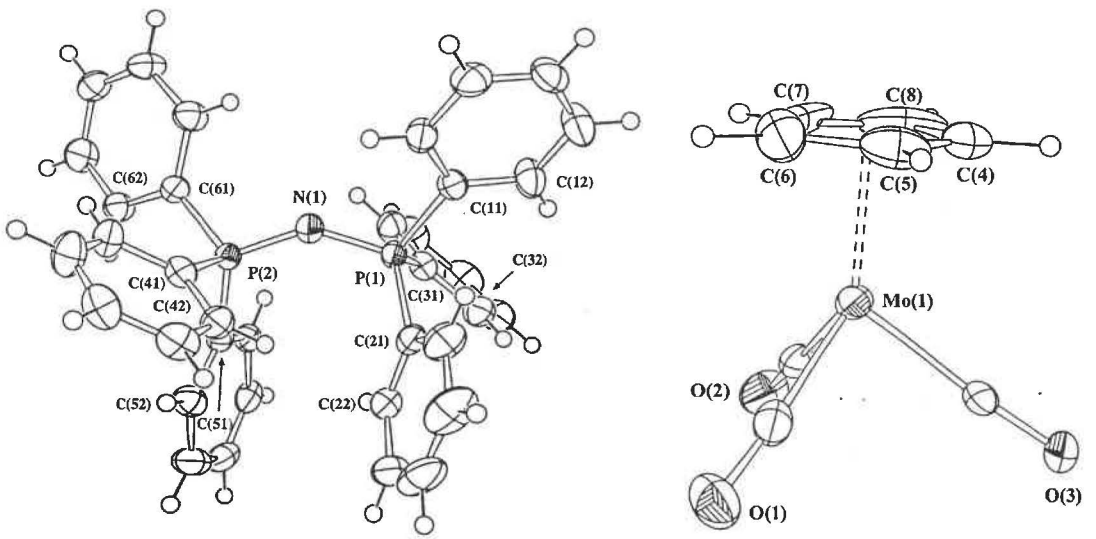

Figure 8.6 – A labelled view of $[PPN][Mo(CO)_3(\eta^5\text{-}C_5H_5)]$. Ellipsoids are drawn at the 50% probability level.

The structure of the $[PPN]^+$ cation is unremarkable with bond lengths and angles similar to those previously reported. The cation adopts a bent configuration about the P-N-P bond [142.62(14)°] with an angle typical of $[PPN]^+$ salts (which vary between 130-180°

[15] D.E. Crotty, E.R. Corey, T.J. Anderson, M.D. Glick and J.P. Oliver, *Inorg. Chem.*, 1977, **16**, 920.
[16] R. Janta, W. Albert, H. Rossner, W. Malisch, H-J. Langenbach, E. Rottinger and H. Vahrenkamp, *Chem. Ber.*, 1980, **113**, 2729; U. Schubert, K. Ackermann, R. Janta, S. Voran and W. Malisch, *Chem. Ber.*, 1982, **115**, 2003; M.A. Adams, K. Folting, J.C. Huffman and K.G. Caulton, *Inorg. Chem.*, 1979, **18**, 3020; M.D. Curtis and W.M. Butler, *J. Chem. Soc., Chem. Commun.*, 1980, 998; S.E. Nefedov, A.A. Pasynskii, I.L. Eremenko, B. Orazsakhatov, O.G. Ellert, V.M. Novotortsev, Y.T. Struchkov and A.I. Yanovsky, *J. Organomet. Chem.*, 1990, **385**, 277.

[17]). The phenyl rings are not arranged in an eclipsed manner as has been observed for some $[PPN]^+$ salts[18].

Table 8.4 – Selected bond lengths (Å) and angles (°) for $[PPN][Mo(CO)_3(\eta^5\text{-}C_5H_5)]$

Mo(1)–C(1)	1.930(3)	Mo(1)–C(2)	1.928(3)
Mo(1)–C(3)	1.933(3)	Mo(1)–$Cp_{centroid}$	2.062
C(1)–O(1)	1.175(4)	C(2)–O(2)	1.175(3)
C(3)–O(3)	1.173(3)	C(1)-Mo(1)-C(2)	84.49(12)
C(2)-Mo(1)-C(3)	88.43(11)	C(1)-Mo(1)-C(3)	88.93 (11)
P(1)–N(1)	1.579(2)	P(2)–N(1)	1.584(2)
P(1)-N(1)-P(2)	142.62(14)		

8.2.3 Crystal Packing of $[PPN][Mo(CO)_3(\eta^5\text{-}C_5H_5)]$

Of more interest is the supramolecular packing of $[PPN][Mo(CO)_3(\eta^5\text{-}C_5H_5)]$. The 'sextuple phenyl embrace' crystal packing motif was first noted in the structures of compounds containing the PPh_3 moiety[19]. These embraces correspond to a set of edge-edge and edge-face attractions between inter-molecular phenyl groups that direct the crystal packing of the compound. Variations on this packing motif have been observed in structures containing $[PPh_4]^+$ [20], $[P(Me)Ph_3]^+$ [21], $[AsPh_4]^+$ [22] and $[PPN]^+$ [17] cations, along with compounds containing PPh_3 [23] and substituted triphenylphosphine [24] ligands.

[17] G.R. Lewis and I. Dance, *J. Chem. Soc., Dalton Trans.*, 2000, 299.
[18] A.L. Rheingold, C.B. White, P.D. Macklin and G.L. Geoffroy, *Acta Cryst. Sect. C*, 1992, **49**, 80; D. Braga, K. Henrick, B.F.G. Johnson, J. Lewis, M. McPartlin, W.J.H. Nelson and M.D. Vagas, *J. Chem. Soc., Chem. Commun.*, 1982, 419; D. Braga, K. Henrick, B.F.G. Johnson, J. Lewis, M. McPartlin, W.J.H. Nelson and J. Puga, *J. Chem. Soc., Chem. Commun.*, 1982, 1083.
[19] I. Dance and M. Scudder, *J. Chem. Soc., Chem. Commun.*, 1995, 1039.
[20] I. Dance and M. Scudder, *Eur. J. Chem.*, 1996, **2**, 481; I. Dance and M. Scudder, *J. Chem. Soc., Dalton Trans.*, 1996, 3755; M. Scudder and I. Dance, *J. Chem. Soc., Dalton Trans.*, 1998, 3155; M. Scudder and I. Dance, *J. Chem. Soc., Dalton Trans.*, 1998, 3167; G.R. Lewis and I. Dance, *J. Chem. Soc., Dalton Trans.*, 2000, 3176.
[21] C. Hasselgren, P.A. Dean, M. Scudder, D.C. Craig and I. Dance, *J. Chem. Soc., Dalton Trans.*, 1997, 2019; S. Lorenzo, C. Horn, D. Craig, M. Scudder and I. Dance, *Inorg. Chem.*, 2000, **39**, 401.
[22] G.R. Lewis and I. Dance, *Inorg. Chim. Acta.*, 2000, **306**, 160.
[23] I. Dance and M. Scudder, *J. Chem. Soc., Dalton Trans.*, 2000, 1579; I. Dance and M. Scudder, *J. Chem. Soc., Dalton Trans.*, 2000, 1587.
[24] M. Scudder and I. Dance, *J. Chem. Soc., Dalton Trans.*, 2000, 2909.

Various 'phenyl embrace' arrangements have been observed for structures containing $[PPN]^+$. These different arrangements are distinguished by the inter-molecular P--P distance and N–P--P angle[17].

The simplest form of 'phenyl embrace' in $[PPN]^+$ structures involves a sextuple arrangement (so named because of the six edge-face attractions that characterise the embrace). The sextuple phenyl embrace (SPE) motif requires the arrangement of two PPh_3 moieties in a co-linear fashion (as indicated by a N-P--P angle of approximately 180°) and is common in compounds with PPh_3 ligands (especially *trans* oriented) but less prevalent in structures containing $[PPN]^+$.

More common are 'expanded phenyl embraces' (EPE's) in which the two interacting cations are either orthogonal or parallel (but not co-linear) to one another (OEPE and PEPE respectively). These EPE's are characterised by both the inter-molecular N–P--P angle (40-120°) and P--P distance (6.0-7.2 Å). EPE's differ from SPE's in that they involve more than two PPh_3 groups (3 in the case of OEPE's and 4 for PEPE's - Figure 8.7), with the different EPE forms most easily distinguished from the magnitude of the P--P distances. For OEPE's, there are typically two short inter-molecular non-bonded P--P interactions (both from the same P atom) and two considerably longer interactions, whereas PEPE's are characterised by three short P--P distances and one longer distance. For an offset PEPE arrangement, there is typically one short P--P interaction, two of medium magnitude, and one significantly longer.

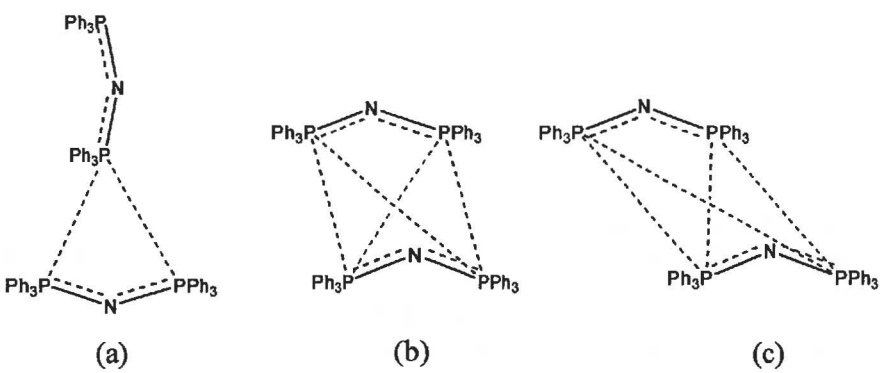

Figure 8.7 – The various EPE arrangements – (a) orthogonal, (b) parallel, and (c) offset parallel.

In the structure of $[PPN][Mo(CO)_3(\eta^5\text{-}C_5H_5)]$, the shortest P--P distance is 6.8606(8) Å (between P_1 and the equivalent atom generated by the symmetry operation 1-x, 1-y, z)

with a N-P--P angle of 72.41(7)°. These parameters indicate an EPE motif, with analysis of the P--P distances (Figure 8.8) favouring an offset PEPE arrangement.

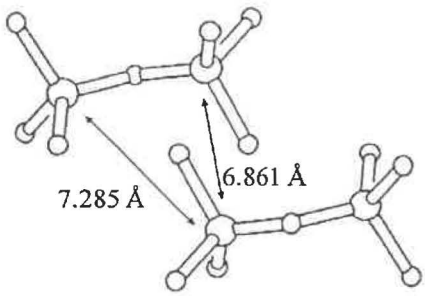

Figure 8.8 – The PEPE arrangement displayed by the $[PPN]^+$ cation of $[PPN][Mo(CO)_3(\eta^5\text{-}C_5H_5)]$. The phenyl rings of the cation have been omitted to aid clarity.

The $[PPN]^+$ structures which display phenyl embraces often possess both SPE and EPE motifs[17]. The mixture of the two packing conformations results in the formation of chains of cations (arranged in columns or layers), with the structure adopted independent of the size or properties of the anion involved. The structure of $[PPN][Mo(CO)_3(\eta^5\text{-}C_5H_5)]$ displays a layered arrangement (Figure 8.9), with alternating cation and anion layers separated by a minimum distance of 9.3 Å (of similar magnitude to other layered arrangements[17]).

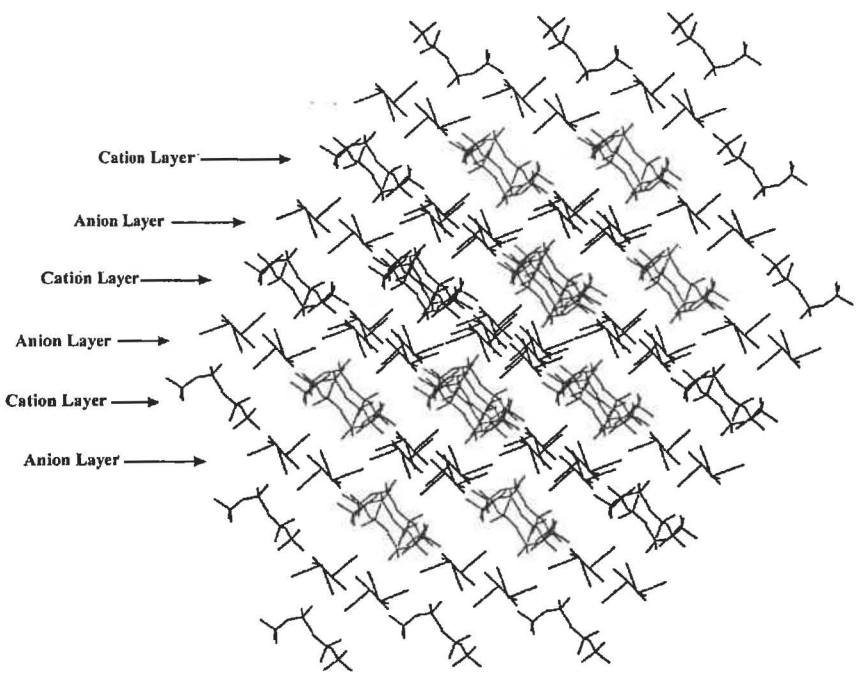

Figure 8.9 – The layered arrangement displayed by $[PPN][Mo(CO)_3(\eta^5\text{-}C_5H_5)]$. The phenyl rings have been removed from the $[PPN]^+$ cations and both the $(\eta^5\text{-}C_5H_5)$ ring and oxygen atoms from $[Mo(CO)_3(\eta^5\text{-}C_5H_5)]^-$ to aid clarity.

8.2.4 Experimental

The preparation of $[PPN][Mo(CO)_3(\eta^5\text{-}C_5H_5)]$ was presented in Chapter 2, as were general details relating to X-ray structure determinations. Crystals were grown by slow diffusion of Et_2O and petroleum spirits into a CH_2Cl_2 solution of the compound. Diffusion was carried out in a modified Schlenk flask (narrowed to 5 mm diameter) under a nitrogen atmosphere at –20°C.

Table 8.5 – Crystallographic data for $[PPN][Mo(CO)_3(\eta^5\text{-}C_5H_5)]$

Empirical Formula	$C_{44}H_{35}N_1Mo_1O_3P_2$
M_r	783.61
Temperature (K)	203
Crystal System	Monoclinic
Space Group	$P2_1/c$
a(Å)	14.0385(2)
b(Å)	19.1269(2)
c(Å)	13.8322 (1)
β(°)	90.7280
Volume (Å^3)	3713.83(7)
Z	4
Calculated Density (Mg m^{-3})	1.401
θ range collected	1.45 to 27.46
Reflections Collected	22556
Independent Reflections	8177 (R_{int} = 0.0245)
Goodness of Fit	1.075
R Indices – I > 2σ(I)	R_1 = 0.0374, wR_2 = 0.0822
R Indices – all data	R_1 = 0.0515, wR_2 = 0.0898
T_{max}/T_{min}	0.9100/0.8852

Appendix A – Crystallographic Data for $[NEt_4]_2[Co_{10}Ge_2(CO)_{24}].1.5CH_2Cl_2.0.5O(CH_2CH_3)_2$

Table A1.

Atomic coordinates ($x10^4$) and equivalent isotropic displacement parameters ($Å^2 \times 10^3$) for $[NEt_4]_2[Co_{10}Ge_2(CO)_{24}].1.5CH_2Cl_2.0.5O(CH_2CH_3)_2$. U(eq) is defined as one third of the trace of the orthogonalized U_{ij} tensor.

	x	y	z	U(eq)
Ge(1)	1616(1)	2485(1)	8963(1)	24(1)
Ge(2)	1197(1)	2319(1)	10465(1)	26(1)
Co(1)	1105(1)	3004(1)	8181(1)	28(1)
Co(2)	1202(1)	1878(1)	8150(1)	29(1)
Co(3)	1885(1)	2494(1)	7663(1)	30(1)
Co(4)	779(1)	2413(1)	9288(1)	27(1)
Co(5)	1317(1)	3254(1)	9667(1)	25(1)
Co(6)	1962(1)	2492(1)	10209(1)	26(1)
Co(7)	1438(1)	1601(1)	9576(1)	27(1)
Co(8)	1475(1)	3112(1)	11159(1)	29(1)
Co(9)	658(1)	3058(1)	10540(1)	29(1)
Co(10)	899(1)	2335(1)	11718(1)	33(1)
O(11)	1175(2)	4237(3)	8168(4)	55(2)
O(12)	834(2)	2906(3)	6568(4)	51(2)
O(21)	442(2)	1646(4)	7188(5)	71(2)
O(22)	1680(2)	1369(3)	6915(4)	60(2)
O(23)	1158(3)	701(3)	8535(4)	61(2)
O(31)	2687(2)	1854(3)	8027(4)	52(2)
O(32)	2212(2)	3637(3)	7970(4)	56(2)
O(33)	1804(2)	2617(3)	5975(3)	53(2)
O(41)	156(2)	1479(3)	9241(4)	52(2)
O(42)	172(2)	3098(3)	8388(4)	48(2)
O(51)	1918(2)	4209(3)	9567(4)	49(2)
O(52)	644(2)	4118(3)	9704(4)	46(2)
O(61)	2771(2)	2760(4)	9372(4)	67(2)
O(62)	2312(2)	1630(3)	11256(4)	51(2)
O(63)	2390(2)	3404(3)	11070(4)	54(2)
O(71)	933(2)	815(3)	10528(4)	60(2)
O(72)	2283(2)	1031(3)	9482(4)	57(2)
O(81)	1661(3)	2932(3)	12775(4)	59(2)
O(82)	1351(2)	4322(3)	11330(4)	56(2)
O(91)	-201(2)	2755(3)	9949(4)	54(2)
O(92)	271(3)	3779(3)	11719(4)	61(2)
O(101)	512(3)	2850(3)	13112(4)	71(2)
O(102)	1412(3)	1366(3)	12257(4)	66(2)
O(103)	110(2)	1754(3)	11174(4)	60(2)
C(11)	1156(3)	3751(4)	8229(5)	40(2)
C(12)	946(3)	2932(4)	7197(5)	36(2)
C(22)	1575(3)	1695(4)	7395(5)	41(2)
C(21)	734(3)	1740(4)	7577(5)	39(2)
C(23)	1218(3)	1186(4)	8646(5)	39(2)
C(31)	2377(3)	2099(4)	7888(5)	37(2)
C(32)	2061(3)	3201(4)	7871(5)	37(2)
C(33)	1835(3)	2574(4)	6627(5)	35(2)
C(41)	397(3)	1848(4)	9246(5)	37(2)
C(42)	511(3)	2920(4)	8564(4)	32(2)
C(51)	1687(3)	3834(3)	9599(4)	30(2)
C(52)	800(3)	3675(4)	9873(5)	34(2)
C(61)	2451(3)	2654(4)	9676(5)	42(2)

C(62)	2173(3)	1968(4)	10854(5)	35(2)
C(63)	2071(3)	3146(4)	10920(5)	36(2)
C(71)	1135(3)	1136(4)	10174(5)	42(2)
C(72)	1961(3)	1275(4)	9523(5)	37(2)
C(81)	1536(3)	2940(4)	12142(5)	43(2)
C(82)	1394(3)	3846(4)	11260(5)	36(2)
C(91)	169(3)	2827(4)	10088(5)	46(2)
C(92)	433(3)	3489(4)	11277(5)	38(2)
C(101)	664(3)	2670(4)	12571(5)	42(2)
C(102)	1219(3)	1761(4)	12060(5)	42(2)
C(103)	418(3)	2001(4)	11352(5)	45(2)
N(1)	1206(2)	4194(3)	4669(4)	37(2)
C(1C)	1313(6)	4569(8)	5365(11)	44(4)
C(1C1)	1296(6)	3769(8)	5311(11)	44(4)
C(1D)	1591(6)	4573(8)	4512(11)	47(5)
C(1D1)	1589(7)	3769(10)	4456(13)	62(6)
C(1E)	1140(7)	4620(10)	4011(13)	63(6)
C(1E1)	1080(7)	3826(9)	3970(12)	54(5)
C(1F)	830(6)	4596(8)	4887(11)	49(5)
C(1F1)	804(7)	3834(9)	4805(13)	60(6)
C(2C)	1436(4)	4124(5)	6098(7)	74(3)
C(2D)	2019(5)	4157(7)	4297(9)	102(5)
C(2E)	989(4)	4238(6)	3238(8)	83(4)
C(2F)	391(5)	4235(6)	4979(9)	91(4)
N(2)	2500	0	7218(7)	46(3)
C(1A)	2345(3)	-493(4)	7699(7)	57(3)
C(1B)	2120(4)	237(5)	6712(7)	62(3)
C(2A)	1986(4)	-341(5)	8316(7)	66(3)
C(2B)	1944(4)	-202(5)	6127(8)	78(4)
N(3)	0	88(5)	2500	61(3)
C(1G1)	-363(8)	-315(10)	2699(14)	70
C(1G2)	391(8)	495(10)	2397(14)	70
C(1H1)	-133(8)	-147(11)	890(15)	70
C(1H2)	77(8)	496(10)	3191(14)	70
C(2G)	-797(4)	143(5)	2838(7)	70
C(2H)	-186(4)	157(6)	1112(7)	70
O(110)	2500	5000	984(6)	34(2)
C(1I)	2411(5)	4825(6)	1154(8)	78(4)
C(2I)	2155(3)	5004(4)	2575(6)	47(2)
Cl(1)	331(2)	4759(3)	6945(4)	166(2)
C(99)	0	4304(11)	7500	117(8)
Cl(2)	982(3)	919(4)	5219(5)	208(3)
Cl(3)	1236(3)	1910(4)	4298(5)	219(3)
C(98)	938(7)	1656(9)	5095(12)	135(7)

Table A2.

Bond lengths [Å] and angles [°] for $[NEt_4]_2[Co_{10}Ge_2(CO)_{24}].1.5CH_2Cl_2.0.5O(CH_2CH_3)_2$.

Ge(1)-Co(5)	2.3643(12)	Ge(1)-Co(2)	2.3662(13)
Ge(1)-Co(3)	2.3890(12)	Ge(1)-Co(1)	2.3940(12)
Ge(1)-Co(6)	2.3951(12)	Ge(1)-Co(7)	2.3971(13)
Ge(1)-Co(4)	2.6107(13)	Ge(1)-Ge(2)	2.9155(11)
Ge(2)-Co(10)	2.3463(13)	Ge(2)-Co(8)	2.3765(13)
Ge(2)-Co(9)	2.3939(13)	Ge(2)-Co(7)	2.3990(13)
Ge(2)-Co(6)	2.4026(13)	Ge(2)-Co(4)	2.4055(13)
Ge(2)-Co(5)	2.6230(12)	Co(1)-C(11)	1.770(10)
Co(1)-C(12)	1.775(8)	Co(1)-C(42)	1.934(8)
Co(1)-Co(4)	2.5645(14)	Co(1)-Co(2)	2.6701(15)
Co(1)-Co(5)	2.7106(14)	Co(1)-Co(3)	2.8050(15)
Co(2)-C(21)	1.764(9)	Co(2)-C(22)	1.779(9)
Co(2)-C(23)	1.842(9)	Co(2)-Co(7)	2.6454(14)

Co(2)-Co(4)	2.6663(15)	Co(2)-Co(3)	2.6688(15)
Co(3)-C(32)	1.787(10)	Co(3)-C(31)	1.800(10)
Co(3)-C(33)	1.806(9)	Co(3)-C(22)	2.154(9)
Co(4)-C(41)	1.769(9)	Co(4)-C(42)	1.913(8)
Co(4)-C(91)	2.509(10)	Co(4)-Co(5)	2.6499(14)
Co(4)-Co(9)	2.6677(14)	Co(4)-Co(7)	2.8137(14)
Co(5)-C(51)	1.774(9)	Co(5)-C(52)	1.892(8)
Co(5)-Co(9)	2.5477(14)	Co(5)-Co(8)	2.6412(14)
Co(5)-Co(6)	2.8194(14)	Co(6)-C(62)	1.781(9)
Co(6)-C(61)	1.789(10)	Co(6)-C(63)	1.999(8)
Co(6)-Co(8)	2.6507(14)	Co(6)-Co(7)	2.8526(14)
Co(7)-C(71)	1.766(10)	Co(7)-C(72)	1.767(9)
Co(7)-C(23)	1.995(8)	Co(8)-C(82)	1.753(9)
Co(8)-C(81)	1.754(10)	Co(8)-C(63)	1.861(9)
Co(8)-Co(9)	2.7052(15)	Co(8)-Co(10)	2.7104(15)
Co(9)-C(92)	1.765(9)	Co(9)-C(91)	1.765(10)
Co(9)-C(52)	1.905(8)	Co(9)-Co(10)	2.7514(14)
Co(10)-C(102)	1.768(9)	Co(10)-C(103)	1.777(11)
Co(10)-C(101)	1.817(10)	Co(10)-C(81)	2.514(10)
O(11)-C(11)	1.151(11)	O(12)-C(12)	1.141(10)
O(21)-C(21)	1.134(10)	O(22)-C(22)	1.174(10)
O(23)-C(23)	1.173(10)	O(31)-C(31)	1.133(10)
O(32)-C(32)	1.137(10)	O(33)-C(33)	1.135(10)
O(41)-C(41)	1.137(10)	O(42)-C(42)	1.152(9)
O(51)-C(51)	1.129(9)	O(52)-C(52)	1.182(10)
O(61)-C(61)	1.133(11)	O(62)-C(62)	1.137(10)
O(63)-C(63)	1.171(10)	O(71)-C(71)	1.150(11)
O(72)-C(72)	1.137(10)	O(81)-C(81)	1.159(11)
O(82)-C(82)	1.136(10)	O(91)-C(91)	1.163(10)
O(92)-C(92)	1.138(10)	O(101)-C(101)	1.126(11)
O(102)-C(102)	1.151(10)	O(103)-C(103)	1.144(11)
N(1)-C(1D)	1.50(2)	N(1)-C(1F1)	1.51(2)
N(1)-C(1C1)	1.517(19)	N(1)-C(1C)	1.526(19)
N(1)-C(1E)	1.53(2)	N(1)-C(1F)	1.53(2)
N(1)-C(1E1)	1.53(2)	N(1)-C(1D1)	1.58(2)
C(1C)-C(1F)	1.68(3)	C(1C)-C(2C)	1.68(2)
C(1C)-C(1D)	1.70(3)	C(1C)-C(1C1)	1.89(3)
C(1C1)-C(2C)	1.65(2)	C(1C1)-C(1D1)	1.72(3)
C(1C1)-C(1F1)	1.74(3)	C(1D)-C(1E)	1.63(3)
C(1D)-C(2D)	1.67(2)	C(1D)-C(1D1)	1.90(3)
C(1D1)-C(2D)	1.62(3)	C(1D1)-C(1E1)	1.76(3)
C(1E)-C(2E)	1.67(3)	C(1E)-C(1F)	1.78(3)
C(1E)-C(1E1)	1.88(3)	C(1E1)-C(2E)	1.62(2)
C(1E1)-C(1F1)	1.67(3)	C(1F)-C(2F)	1.59(2)
C(1F)-C(1F1)	1.80(3)	C(1F1)-C(2F)	1.60(3)
N(2)-C(1A)#1	1.505(11)	N(2)-C(1A)	1.505(11)
N(2)-C(1B)	1.553(12)	N(2)-C(1B)#1	1.553(12)
C(1A)-C(2A)	1.567(15)	C(1B)-C(2B)	1.541(15)
N(3)-C(1G1)#2	1.49(2)	N(3)-C(1G1)	1.49(2)
N(3)-C(1G2)	1.54(2)	N(3)-C(1G2)#2	1.54(2)
N(3)-C(1H2)	1.55(3)	N(3)-C(1H2)#2	1.55(3)
C(1G1)-C(2G)	1.72(3)	C(1G1)-C(1G2)#2	1.92(3)
C(1G2)-C(2G)#2	1.54(3)	C(1G2)-C(1H2)	1.67(3)
C(1G2)-C(1H2)#2	1.75(3)	C(1G2)-C(1G1)#2	1.92(3)
C(1H1)-C(2H)	0.83(2)	C(1H2)-C(2H)#2	1.48(3)
C(1H2)-C(1G2)#2	1.75(3)	C(2G)-C(1G2)#2	1.54(3)
C(2H)-C(1H2)#2	1.48(3)	O(110)-C(1I)#3	0.574(15)
O(110)-C(1I)	0.574(15)	C(1I)-C(1I)#3	0.99(3)
Cl(1)-C(99)	1.756(16)	C(99)-Cl(1)#4	1.756(16)
Cl(2)-C(98)	1.75(2)	Cl(3)-C(98)	1.75(2)

Co(5)-Ge(1)-Co(2)	124.32(5)	Co(5)-Ge(1)-Co(3)	127.47(5)
Co(2)-Ge(1)-Co(3)	68.28(4)	Co(5)-Ge(1)-Co(1)	69.45(4)

Co(2)-Ge(1)-Co(1)	68.24(4)	Co(3)-Ge(1)-Co(1)	71.81(4)
Co(5)-Ge(1)-Co(6)	72.65(4)	Co(2)-Ge(1)-Co(6)	140.41(5)
Co(3)-Ge(1)-Co(6)	133.90(5)	Co(1)-Ge(1)-Co(6)	142.02(5)
Co(5)-Ge(1)-Co(7)	110.60(5)	Co(2)-Ge(1)-Co(7)	67.47(4)
Co(3)-Ge(1)-Co(7)	119.96(5)	Co(1)-Ge(1)-Co(7)	123.11(5)
Co(6)-Ge(1)-Co(7)	73.06(4)	Co(5)-Ge(1)-Co(4)	64.14(4)
Co(2)-Ge(1)-Co(4)	64.57(4)	Co(3)-Ge(1)-Co(4)	122.45(5)
Co(1)-Ge(1)-Co(4)	61.47(4)	Co(6)-Ge(1)-Co(4)	103.60(4)
Co(7)-Ge(1)-Co(4)	68.22(4)	Co(5)-Ge(1)-Ge(2)	58.47(3)
Co(2)-Ge(1)-Ge(2)	102.38(4)	Co(3)-Ge(1)-Ge(2)	170.55(4)
Co(1)-Ge(1)-Ge(2)	106.66(4)	Co(6)-Ge(1)-Ge(2)	52.69(3)
Co(7)-Ge(1)-Ge(2)	52.59(3)	Co(4)-Ge(1)-Ge(2)	51.24(3)
Co(10)-Ge(2)-Co(8)	70.04(4)	Co(10)-Ge(2)-Co(9)	70.95(4)
Co(8)-Ge(2)-Co(9)	69.09(4)	Co(10)-Ge(2)-Co(7)	136.06(5)
Co(8)-Ge(2)-Co(7)	140.26(5)	Co(9)-Ge(2)-Co(7)	139.18(5)
Co(10)-Ge(2)-Co(6)	122.70(5)	Co(8)-Ge(2)-Co(6)	67.37(4)
Co(9)-Ge(2)-Co(6)	123.30(5)	Co(7)-Ge(2)-Co(6)	72.90(4)
Co(10)-Ge(2)-Co(4)	125.00(5)	Co(8)-Ge(2)-Co(4)	122.75(5)
Co(9)-Ge(2)-Co(4)	67.54(4)	Co(7)-Ge(2)-Co(4)	71.70(4)
Co(6)-Ge(2)-Co(4)	109.90(5)	Co(10)-Ge(2)-Co(5)	121.58(5)
Co(8)-Ge(2)-Co(5)	63.56(4)	Co(9)-Ge(2)-Co(5)	60.83(4)
Co(7)-Ge(2)-Co(5)	102.33(4)	Co(6)-Ge(2)-Co(5)	68.09(4)
Co(4)-Ge(2)-Co(5)	63.43(4)	Co(10)-Ge(2)-Ge(1)	170.67(5)
Co(8)-Ge(2)-Ge(1)	100.83(4)	Co(9)-Ge(2)-Ge(1)	104.47(4)
Co(7)-Ge(2)-Ge(1)	52.53(3)	Co(6)-Ge(2)-Ge(1)	52.46(3)
Co(4)-Ge(2)-Ge(1)	57.82(3)	Co(5)-Ge(2)-Ge(1)	50.20(3)
C(11)-Co(1)-C(12)	99.4(4)	C(11)-Co(1)-C(42)	99.6(4)
C(12)-Co(1)-C(42)	93.6(4)	C(11)-Co(1)-Ge(1)	115.2(3)
C(12)-Co(1)-Ge(1)	131.9(3)	C(42)-Co(1)-Ge(1)	111.2(2)
C(11)-Co(1)-Co(4)	122.6(3)	C(12)-Co(1)-Co(4)	123.8(3)
C(42)-Co(1)-Co(4)	47.8(2)	Ge(1)-Co(1)-Co(4)	63.43(4)
C(11)-Co(1)-Co(2)	168.6(3)	C(12)-Co(1)-Co(2)	85.2(3)
C(42)-Co(1)-Co(2)	90.5(2)	Ge(1)-Co(1)-Co(2)	55.39(4)
Co(4)-Co(1)-Co(2)	61.20(4)	C(11)-Co(1)-Co(5)	73.7(3)
C(12)-Co(1)-Co(5)	172.7(3)	C(42)-Co(1)-Co(5)	85.4(2)
Ge(1)-Co(1)-Co(5)	54.76(3)	Co(4)-Co(1)-Co(5)	60.23(4)
Co(2)-Co(1)-Co(5)	102.04(4)	C(11)-Co(1)-Co(3)	111.6(3)
C(12)-Co(1)-Co(3)	83.4(3)	C(42)-Co(1)-Co(3)	148.7(3)
Ge(1)-Co(1)-Co(3)	54.01(3)	Co(4)-Co(1)-Co(3)	109.37(5)
Co(2)-Co(1)-Co(3)	58.28(4)	Co(5)-Co(1)-Co(3)	101.20(4)
C(21)-Co(2)-C(22)	93.4(4)	C(21)-Co(2)-C(23)	96.8(4)
C(22)-Co(2)-C(23)	96.4(4)	C(21)-Co(2)-Ge(1)	150.8(3)
C(22)-Co(2)-Ge(1)	104.0(3)	C(23)-Co(2)-Ge(1)	104.2(3)
C(21)-Co(2)-Co(7)	134.0(3)	C(22)-Co(2)-Co(7)	116.7(3)
C(23)-Co(2)-Co(7)	48.9(2)	Ge(1)-Co(2)-Co(7)	56.82(4)
C(21)-Co(2)-Co(4)	96.4(3)	C(22)-Co(2)-Co(4)	164.0(3)
C(23)-Co(2)-Co(4)	95.1(3)	Ge(1)-Co(2)-Co(4)	62.16(4)
Co(7)-Co(2)-Co(4)	63.97(4)	C(21)-Co(2)-Co(3)	123.5(3)
C(22)-Co(2)-Co(3)	53.5(3)	C(23)-Co(2)-Co(3)	127.4(3)
Ge(1)-Co(2)-Co(3)	56.26(4)	Co(7)-Co(2)-Co(3)	102.48(5)
Co(4)-Co(2)-Co(3)	110.50(5)	C(21)-Co(2)-Co(1)	96.0(3)
C(22)-Co(2)-Co(1)	109.0(3)	C(23)-Co(2)-Co(1)	150.8(3)
Ge(1)-Co(2)-Co(1)	56.38(4)	Co(7)-Co(2)-Co(1)	104.84(5)
Co(4)-Co(2)-Co(1)	57.45(4)	Co(3)-Co(2)-Co(1)	63.39(4)
C(32)-Co(3)-C(31)	101.0(4)	C(32)-Co(3)-C(33)	97.3(4)
C(31)-Co(3)-C(33)	109.8(4)	C(32)-Co(3)-C(22)	171.3(4)
C(31)-Co(3)-C(22)	87.6(4)	C(33)-Co(3)-C(22)	80.9(4)
C(32)-Co(3)-Ge(1)	85.5(3)	C(31)-Co(3)-Ge(1)	94.4(3)
C(33)-Co(3)-Ge(1)	154.5(3)	C(22)-Co(3)-Ge(1)	92.5(2)
C(32)-Co(3)-Co(2)	132.6(3)	C(31)-Co(3)-Co(2)	107.2(3)
C(33)-Co(3)-Co(2)	107.6(3)	C(22)-Co(3)-Co(2)	41.6(2)
Ge(1)-Co(3)-Co(2)	55.45(4)	C(32)-Co(3)-Co(1)	77.8(3)
C(31)-Co(3)-Co(1)	148.6(3)	C(33)-Co(3)-Co(1)	101.4(3)

C(22)-Co(3)-Co(1)	94.1(2)	Ge(1)-Co(3)-Co(1)	54.18(3)
Co(2)-Co(3)-Co(1)	58.33(4)	C(41)-Co(4)-C(42)	99.4(4)
C(41)-Co(4)-Ge(2)	108.2(3)	C(42)-Co(4)-Ge(2)	146.6(3)
C(41)-Co(4)-C(91)	80.2(4)	C(42)-Co(4)-C(91)	78.6(3)
Ge(2)-Co(4)-C(91)	87.8(2)	C(41)-Co(4)-Co(1)	129.2(3)
C(42)-Co(4)-Co(1)	48.5(2)	Ge(2)-Co(4)-Co(1)	118.41(5)
C(91)-Co(4)-Co(1)	119.0(2)	C(41)-Co(4)-Ge(1)	132.9(3)
C(42)-Co(4)-Ge(1)	103.6(2)	Ge(2)-Co(4)-Ge(1)	70.94(4)
C(91)-Co(4)-Ge(1)	144.4(2)	Co(1)-Co(4)-Ge(1)	55.10(3)
C(41)-Co(4)-Co(5)	167.9(3)	C(42)-Co(4)-Co(5)	87.6(2)
Ge(2)-Co(4)-Co(5)	62.29(4)	C(91)-Co(4)-Co(5)	91.7(2)
Co(1)-Co(4)-Co(5)	62.62(4)	Ge(1)-Co(4)-Co(5)	53.41(3)
C(41)-Co(4)-Co(2)	86.0(3)	C(42)-Co(4)-Co(2)	91.1(2)
Ge(2)-Co(4)-Co(2)	108.93(5)	C(91)-Co(4)-Co(2)	161.1(2)
Co(1)-Co(4)-Co(2)	61.35(4)	Ge(1)-Co(4)-Co(2)	53.27(3)
Co(5)-Co(4)-Co(2)	103.78(5)	C(41)-Co(4)-Co(9)	111.8(3)
C(42)-Co(4)-Co(9)	96.6(2)	Ge(2)-Co(4)-Co(9)	56.03(4)
C(91)-Co(4)-Co(9)	39.7(2)	Co(1)-Co(4)-Co(9)	110.37(5)
Ge(1)-Co(4)-Co(9)	105.77(4)	Co(5)-Co(4)-Co(9)	57.25(4)
Co(2)-Co(4)-Co(9)	158.96(5)	C(41)-Co(4)-Co(7)	87.9(3)
C(42)-Co(4)-Co(7)	147.5(2)	Ge(2)-Co(4)-Co(7)	54.05(3)
C(91)-Co(4)-Co(7)	133.9(2)	Co(1)-Co(4)-Co(7)	103.02(5)
Ge(1)-Co(4)-Co(7)	52.29(3)	Co(5)-Co(4)-Co(7)	91.48(4)
Co(2)-Co(4)-Co(7)	57.65(4)	Co(9)-Co(4)-Co(7)	110.04(5)
C(51)-Co(5)-C(52)	97.7(4)	C(51)-Co(5)-Ge(1)	108.2(2)
C(52)-Co(5)-Ge(1)	144.9(3)	C(51)-Co(5)-Co(9)	132.6(2)
C(52)-Co(5)-Co(9)	48.1(2)	Ge(1)-Co(5)-Co(9)	117.91(5)
C(51)-Co(5)-Ge(2)	140.3(2)	C(52)-Co(5)-Ge(2)	103.1(3)
Ge(1)-Co(5)-Ge(2)	71.33(4)	Co(9)-Co(5)-Ge(2)	55.14(3)
C(51)-Co(5)-Co(8)	92.7(2)	C(52)-Co(5)-Co(8)	91.9(3)
Ge(1)-Co(5)-Co(8)	109.58(5)	Co(9)-Co(5)-Co(8)	62.82(4)
Ge(2)-Co(5)-Co(8)	53.67(3)	C(51)-Co(5)-Co(4)	161.9(2)
C(52)-Co(5)-Co(4)	85.8(3)	Ge(1)-Co(5)-Co(4)	62.45(4)
Co(9)-Co(5)-Co(4)	61.73(4)	Ge(2)-Co(5)-Co(4)	54.28(3)
Co(8)-Co(5)-Co(4)	104.99(5)	C(51)-Co(5)-Co(1)	104.8(2)
C(52)-Co(5)-Co(1)	95.5(3)	Ge(1)-Co(5)-Co(1)	55.79(3)
Co(9)-Co(5)-Co(1)	109.54(5)	Ge(2)-Co(5)-Co(1)	106.36(4)
Co(8)-Co(5)-Co(1)	159.91(5)	Co(4)-Co(5)-Co(1)	57.15(4)
C(51)-Co(5)-Co(6)	94.1(2)	C(52)-Co(5)-Co(6)	148.2(3)
Ge(1)-Co(5)-Co(6)	54.18(3)	Co(9)-Co(5)-Co(6)	103.60(4)
Ge(2)-Co(5)-Co(6)	52.24(3)	Co(8)-Co(5)-Co(6)	57.97(4)
Co(4)-Co(5)-Co(6)	92.00(4)	Co(1)-Co(5)-Co(6)	109.93(4)
C(62)-Co(6)-C(61)	99.9(4)	C(62)-Co(6)-C(63)	95.2(4)
C(61)-Co(6)-C(63)	90.8(4)	C(62)-Co(6)-Ge(1)	135.7(3)
C(61)-Co(6)-Ge(1)	84.5(3)	C(63)-Co(6)-Ge(1)	129.0(2)
C(62)-Co(6)-Ge(2)	96.6(3)	C(61)-Co(6)-Ge(2)	159.2(3)
C(63)-Co(6)-Ge(2)	100.3(3)	Ge(1)-Co(6)-Ge(2)	74.84(4)
C(62)-Co(6)-Co(8)	101.3(3)	C(61)-Co(6)-Co(8)	131.7(3)
C(63)-Co(6)-Co(8)	44.5(3)	Ge(1)-Co(6)-Co(8)	108.31(5)
Ge(2)-Co(6)-Co(8)	55.85(4)	C(62)-Co(6)-Co(5)	154.0(3)
C(61)-Co(6)-Co(5)	105.7(3)	C(63)-Co(6)-Co(5)	80.1(2)
Ge(1)-Co(6)-Co(5)	53.17(3)	Ge(2)-Co(6)-Co(5)	59.67(3)
Co(8)-Co(6)-Co(5)	57.64(4)	C(62)-Co(6)-Co(7)	86.1(3)
C(61)-Co(6)-Co(7)	115.1(3)	C(63)-Co(6)-Co(7)	153.6(3)
Ge(1)-Co(6)-Co(7)	53.50(3)	Ge(2)-Co(6)-Co(7)	53.49(3)
Co(8)-Co(6)-Co(7)	109.34(5)	Co(5)-Co(6)-Co(7)	87.28(4)
C(71)-Co(7)-C(72)	103.3(4)	C(71)-Co(7)-C(23)	89.5(4)
C(72)-Co(7)-C(23)	92.7(4)	C(71)-Co(7)-Ge(1)	156.2(3)
C(72)-Co(7)-Ge(1)	98.7(3)	C(23)-Co(7)-Ge(1)	98.4(3)
C(71)-Co(7)-Ge(2)	84.4(3)	C(72)-Co(7)-Ge(2)	127.9(3)
C(23)-Co(7)-Ge(2)	139.3(3)	Ge(1)-Co(7)-Ge(2)	74.87(4)
C(71)-Co(7)-Co(2)	123.8(3)	C(72)-Co(7)-Co(2)	107.6(3)
C(23)-Co(7)-Co(2)	44.1(3)	Ge(1)-Co(7)-Co(2)	55.71(4)

Ge(2)-Co(7)-Co(2)	109.81(5)	C(71)-Co(7)-Co(4)	98.8(3)
C(72)-Co(7)-Co(4)	157.9(3)	C(23)-Co(7)-Co(4)	87.3(3)
Ge(1)-Co(7)-Co(4)	59.50(3)	Ge(2)-Co(7)-Co(4)	54.26(3)
Co(2)-Co(7)-Co(4)	58.37(4)	C(71)-Co(7)-Co(6)	121.6(3)
C(72)-Co(7)-Co(6)	80.6(3)	C(23)-Co(7)-Co(6)	148.9(3)
Ge(1)-Co(7)-Co(6)	53.44(3)	Ge(2)-Co(7)-Co(6)	53.61(3)
Co(2)-Co(7)-Co(6)	109.08(5)	Co(4)-Co(7)-Co(6)	88.00(4)
C(82)-Co(8)-C(81)	98.4(4)	C(82)-Co(8)-C(63)	96.6(4)
C(81)-Co(8)-C(63)	96.9(4)	C(82)-Co(8)-Ge(2)	140.9(3)
C(81)-Co(8)-Ge(2)	110.1(3)	C(63)-Co(8)-Ge(2)	105.6(3)
C(82)-Co(8)-Co(5)	87.0(3)	C(81)-Co(8)-Co(5)	172.6(3)
C(63)-Co(8)-Co(5)	87.5(3)	Ge(2)-Co(8)-Co(5)	62.77(4)
C(82)-Co(8)-Co(6)	133.1(3)	C(81)-Co(8)-Co(6)	114.3(3)
C(63)-Co(8)-Co(6)	48.8(3)	Ge(2)-Co(8)-Co(6)	56.78(4)
Co(5)-Co(8)-Co(6)	64.39(4)	C(82)-Co(8)-Co(9)	87.6(3)
C(81)-Co(8)-Co(9)	117.9(3)	C(63)-Co(8)-Co(9)	143.9(3)
Ge(2)-Co(8)-Co(9)	55.76(4)	Co(5)-Co(8)-Co(9)	56.90(4)
Co(6)-Co(8)-Co(9)	104.02(5)	C(82)-Co(8)-Co(10)	122.7(3)
C(81)-Co(8)-Co(10)	64.4(3)	C(63)-Co(8)-Co(10)	137.5(3)
Ge(2)-Co(8)-Co(10)	54.46(4)	Co(5)-Co(8)-Co(10)	108.36(5)
Co(6)-Co(8)-Co(10)	102.04(5)	Co(9)-Co(8)-Co(10)	61.07(4)
C(92)-Co(9)-C(91)	99.8(4)	C(92)-Co(9)-C(52)	94.9(4)
C(91)-Co(9)-C(52)	99.2(4)	C(92)-Co(9)-Ge(2)	136.2(3)
C(91)-Co(9)-Ge(2)	109.1(3)	C(52)-Co(9)-Ge(2)	111.6(2)
C(92)-Co(9)-Co(5)	128.8(3)	C(91)-Co(9)-Co(5)	117.1(3)
C(52)-Co(9)-Co(5)	47.6(2)	Ge(2)-Co(9)-Co(5)	64.03(4)
C(92)-Co(9)-Co(4)	164.8(3)	C(91)-Co(9)-Co(4)	65.3(3)
C(52)-Co(9)-Co(4)	85.1(3)	Ge(2)-Co(9)-Co(4)	56.44(4)
Co(5)-Co(9)-Co(4)	61.02(4)	C(92)-Co(9)-Co(8)	92.5(3)
C(91)-Co(9)-Co(8)	164.1(3)	C(52)-Co(9)-Co(8)	89.7(2)
Ge(2)-Co(9)-Co(8)	55.15(4)	Co(5)-Co(9)-Co(8)	60.28(4)
Co(4)-Co(9)-Co(8)	102.75(5)	C(92)-Co(9)-Co(10)	85.7(3)
C(91)-Co(9)-Co(10)	111.1(3)	C(52)-Co(9)-Co(10)	149.2(2)
Ge(2)-Co(9)-Co(10)	53.72(4)	Co(5)-Co(9)-Co(10)	109.90(5)
Co(4)-Co(9)-Co(10)	102.11(5)	Co(8)-Co(9)-Co(10)	59.56(4)
C(102)-Co(10)-C(103)	103.4(4)	C(102)-Co(10)-C(101)	106.1(4)
C(103)-Co(10)-C(101)	99.1(4)	C(102)-Co(10)-Ge(2)	94.8(3)
C(103)-Co(10)-Ge(2)	89.0(3)	C(101)-Co(10)-Ge(2)	155.1(3)
C(102)-Co(10)-C(81)	85.1(4)	C(103)-Co(10)-C(81)	171.4(4)
C(101)-Co(10)-C(81)	79.6(4)	Ge(2)-Co(10)-C(81)	88.9(2)
C(102)-Co(10)-Co(8)	106.3(3)	C(103)-Co(10)-Co(8)	134.7(3)
C(101)-Co(10)-Co(8)	104.4(3)	Ge(2)-Co(10)-Co(8)	55.50(4)
C(81)-Co(10)-Co(8)	39.0(2)	C(102)-Co(10)-Co(9)	150.1(3)
C(103)-Co(10)-Co(9)	78.0(3)	C(101)-Co(10)-Co(9)	103.1(3)
Ge(2)-Co(10)-Co(9)	55.33(4)	C(81)-Co(10)-Co(9)	94.0(2)
Co(8)-Co(10)-Co(9)	59.37(4)	O(11)-C(11)-Co(1)	171.7(8)
O(12)-C(12)-Co(1)	177.1(8)	O(22)-C(22)-Co(2)	148.0(8)
O(22)-C(22)-Co(3)	127.1(7)	Co(2)-C(22)-Co(3)	84.9(4)
O(21)-C(21)-Co(2)	177.6(9)	O(23)-C(23)-Co(2)	141.4(7)
O(23)-C(23)-Co(7)	131.4(7)	Co(2)-C(23)-Co(7)	87.1(4)
O(31)-C(31)-Co(3)	179.5(9)	O(32)-C(32)-Co(3)	173.2(8)
O(33)-C(33)-Co(3)	179.0(9)	O(41)-C(41)-Co(4)	177.9(8)
O(42)-C(42)-Co(4)	141.3(7)	O(42)-C(42)-Co(1)	135.0(6)
Co(4)-C(42)-Co(1)	83.6(3)	O(51)-C(51)-Co(5)	178.5(8)
O(52)-C(52)-Co(5)	138.6(7)	O(52)-C(52)-Co(9)	137.0(7)
Co(5)-C(52)-Co(9)	84.3(3)	O(61)-C(61)-Co(6)	176.7(8)
O(62)-C(62)-Co(6)	178.8(8)	O(63)-C(63)-Co(8)	141.1(7)
O(63)-C(63)-Co(6)	132.2(7)	Co(8)-C(63)-Co(6)	86.6(4)
O(71)-C(71)-Co(7)	176.2(9)	O(72)-C(72)-Co(7)	175.4(8)
O(81)-C(81)-Co(8)	162.2(9)	O(81)-C(81)-Co(10)	121.2(7)
Co(8)-C(81)-Co(10)	76.6(3)	O(82)-C(82)-Co(8)	178.6(9)
O(91)-C(91)-Co(9)	162.0(9)	O(91)-C(91)-Co(4)	123.0(7)
Co(9)-C(91)-Co(4)	75.0(4)	O(92)-C(92)-Co(9)	175.8(8)

O(101)-C(101)-Co(10)	176.4(9)	O(102)-C(102)-Co(10)	176.1(9)
O(103)-C(103)-Co(10)	173.7(8)	C(1D)-N(1)-C(1F1)	177.0(13)
C(1D)-N(1)-C(1C1)	112.7(11)	C(1F1)-N(1)-C(1C1)	70.2(11)
C(1D)-N(1)-C(1C)	68.4(10)	C(1F1)-N(1)-C(1C)	112.0(12)
C(1C1)-N(1)-C(1C)	76.6(10)	C(1D)-N(1)-C(1E)	64.9(11)
C(1F1)-N(1)-C(1E)	112.3(13)	C(1C1)-N(1)-C(1E)	177.1(12)
C(1C)-N(1)-C(1E)	103.4(12)	C(1D)-N(1)-C(1F)	105.0(11)
C(1F1)-N(1)-C(1F)	72.8(11)	C(1C1)-N(1)-C(1F)	111.3(11)
C(1C)-N(1)-C(1F)	66.8(10)	C(1E)-N(1)-C(1F)	71.2(11)
C(1D)-N(1)-C(1E1)	112.9(12)	C(1F1)-N(1)-C(1E1)	66.5(12)
C(1C1)-N(1)-C(1E1)	104.4(11)	C(1C)-N(1)-C(1E1)	177.6(12)
C(1E)-N(1)-C(1E1)	75.7(12)	C(1F)-N(1)-C(1E1)	110.8(12)
C(1D)-N(1)-C(1D1)	76.1(11)	C(1F1)-N(1)-C(1D1)	106.1(13)
C(1C1)-N(1)-C(1D1)	67.7(11)	C(1C)-N(1)-C(1D1)	113.3(12)
C(1E)-N(1)-C(1D1)	109.8(13)	C(1F)-N(1)-C(1D1)	178.8(13)
C(1E1)-N(1)-C(1D1)	69.1(11)	N(1)-C(1C)-C(1F)	56.8(9)
N(1)-C(1C)-C(2C)	106.1(12)	C(1F)-C(1C)-C(2C)	125.8(14)
N(1)-C(1C)-C(1D)	55.0(9)	C(1F)-C(1C)-C(1D)	90.5(13)
C(2C)-C(1C)-C(1D)	122.9(13)	N(1)-C(1C)-C(1C1)	51.5(8)
C(1F)-C(1C)-C(1C1)	89.5(12)	C(2C)-C(1C)-C(1C1)	54.7(9)
C(1D)-C(1C)-C(1C1)	88.6(12)	N(1)-C(1C1)-C(2C)	108.3(12)
N(1)-C(1C1)-C(1D1)	57.8(10)	C(2C)-C(1C1)-C(1D1)	124.9(14)
N(1)-C(1C1)-C(1F1)	54.6(10)	C(2C)-C(1C1)-C(1F1)	126.2(14)
C(1D1)-C(1C1)-C(1F1)	90.8(14)	N(1)-C(1C1)-C(1C)	51.9(8)
C(2C)-C(1C1)-C(1C)	56.4(9)	C(1D1)-C(1C1)-C(1C)	91.7(13)
C(1F1)-C(1C1)-C(1C)	87.8(12)	N(1)-C(1D)-C(1E)	58.6(11)
N(1)-C(1D)-C(2D)	107.4(13)	C(1E)-C(1D)-C(2D)	125.4(15)
N(1)-C(1D)-C(1C)	56.6(9)	C(1E)-C(1D)-C(1C)	92.4(14)
C(2D)-C(1D)-C(1C)	125.3(14)	N(1)-C(1D)-C(1D1)	53.9(9)
C(1E)-C(1D)-C(1D1)	92.2(14)	C(2D)-C(1D)-C(1D1)	53.6(10)
C(1C)-C(1D)-C(1D1)	92.1(13)	N(1)-C(1D1)-C(2D)	106.0(14)
N(1)-C(1D1)-C(1C1)	54.5(10)	C(2D)-C(1D1)-C(1C1)	124.1(16)
N(1)-C(1D1)-C(1E1)	54.3(10)	C(2D)-C(1D1)-C(1E1)	125.8(16)
C(1C1)-C(1D1)-C(1E1)	87.4(14)	N(1)-C(1D1)-C(1D)	50.0(9)
C(2D)-C(1D1)-C(1D)	56.0(11)	C(1C1)-C(1D1)-C(1D)	87.6(13)
C(1E1)-C(1D1)-C(1D)	87.2(13)	N(1)-C(1E)-C(1D)	56.5(11)
N(1)-C(1E)-C(2E)	105.9(14)	C(1D)-C(1E)-C(2E)	128.2(17)
N(1)-C(1E)-C(1F)	54.4(10)	C(1D)-C(1E)-C(1F)	89.5(14)
C(2E)-C(1E)-C(1F)	120.9(15)	N(1)-C(1E)-C(1E1)	52.2(10)
C(1D)-C(1E)-C(1E1)	91.9(14)	C(2E)-C(1E)-C(1E1)	53.7(10)
C(1F)-C(1E)-C(1E1)	87.0(13)	N(1)-C(1E1)-C(2E)	108.6(14)
N(1)-C(1E1)-C(1F1)	55.9(11)	C(2E)-C(1E1)-C(1F1)	125.7(16)
N(1)-C(1E1)-C(1D1)	56.6(10)	C(2E)-C(1E1)-C(1D1)	124.5(15)
C(1F1)-C(1E1)-C(1D1)	91.8(15)	N(1)-C(1E1)-C(1E)	52.1(10)
C(2E)-C(1E1)-C(1E)	56.6(11)	C(1F1)-C(1E1)-C(1E)	90.4(14)
C(1D1)-C(1E1)-C(1E)	88.4(14)	N(1)-C(1F)-C(2F)	108.6(13)
N(1)-C(1F)-C(1C)	56.4(9)	C(2F)-C(1F)-C(1C)	131.4(15)
N(1)-C(1F)-C(1E)	54.4(10)	C(2F)-C(1F)-C(1E)	123.0(15)
C(1C)-C(1F)-C(1E)	87.5(13)	N(1)-C(1F)-C(1F1)	52.9(10)
C(2F)-C(1F)-C(1F1)	55.8(10)	C(1C)-C(1F)-C(1F1)	92.2(13)
C(1E)-C(1F)-C(1F1)	89.3(14)	N(1)-C(1F1)-C(2F)	109.5(15)
N(1)-C(1F1)-C(1E1)	57.5(11)	C(2F)-C(1F1)-C(1E1)	124.3(17)
N(1)-C(1F1)-C(1C1)	55.2(10)	C(2F)-C(1F1)-C(1C1)	129.2(16)
C(1E1)-C(1F1)-C(1C1)	90.1(14)	N(1)-C(1F1)-C(1F)	54.3(10)
C(2F)-C(1F1)-C(1F)	55.3(11)	C(1E1)-C(1F1)-C(1F)	93.2(14)
C(1C1)-C(1F1)-C(1F)	90.5(14)	C(1C1)-C(2C)-C(1C)	68.9(10)
C(1D1)-C(2D)-C(1D)	70.4(12)	C(1E1)-C(2E)-C(1E)	69.7(12)
C(1F)-C(2F)-C(1F1)	68.9(12)	C(1A)#1-N(2)-C(1A)	113.0(11)
C(1A)#1-N(2)-C(1B)	105.5(6)	C(1A)-N(2)-C(1B)	110.8(6)
C(1A)#1-N(2)-C(1B)#1	110.8(6)	C(1A)-N(2)-C(1B)#1	105.5(6)
C(1B)-N(2)-C(1B)#1	111.5(11)	N(2)-C(1A)-C(2A)	114.6(8)
C(2B)-C(1B)-N(2)	112.6(8)	C(1G1)#2-N(3)-C(1G1)	101(2)
C(1G1)#2-N(3)-C(1G2)	78.4(12)	C(1G1)-N(3)-C(1G2)	173.1(14)

C(1G1)#2-N(3)-C(1G2)#2	173.1(14)	C(1G1)-N(3)-C(1G2)#2	78.4(12)
C(1G2)-N(3)-C(1G2)#2	103(2)	C(1G1)#2-N(3)-C(1H2)	117.4(13)
C(1G1)-N(3)-C(1H2)	109.2(13)	C(1G2)-N(3)-C(1H2)	65.5(13)
C(1G2)#2-N(3)-C(1H2)	68.9(13)	C(1G1)#2-N(3)-C(1H2)#2	109.2(13)
C(1G1)-N(3)-C(1H2)#2	117.4(13)	C(1G2)-N(3)-C(1H2)#2	68.9(13)
C(1G2)#2-N(3)-C(1H2)#2	65.5(13)	C(1H2)-N(3)-C(1H2)#2	103(2)
N(3)-C(1G1)-C(2G)	101.5(14)	N(3)-C(1G1)-C(1G2)#2	51.8(11)
C(2G)-C(1G1)-C(1G2)#2	49.8(10)	C(2G)#2-C(1G2)-N(3)	108.3(16)
C(2G)#2-C(1G2)-C(1H2)	132.4(19)	N(3)-C(1G2)-C(1H2)	57.6(12)
C(2G)#2-C(1G2)-C(1H2)#2	120.0(18)	N(3)-C(1G2)-C(1H2)#2	55.9(12)
C(1H2)-C(1G2)-C(1H2)#2	90.7(17)	C(2G)#2-C(1G2)-C(1G1)#2	58.5(12)
N(3)-C(1G2)-C(1G1)#2	49.8(11)	C(1H2)-C(1G2)-C(1G1)#2	92.7(16)
C(1H2)#2-C(1G2)-C(1G1)#2	85.1(15)	C(2H)#2-C(1H2)-N(3)	109.0(16)
C(2H)#2-C(1H2)-C(1G2)	122.5(19)	N(3)-C(1H2)-C(1G2)	56.9(12)
C(2H)#2-C(1H2)-C(1G2)#2	130.8(19)	N(3)-C(1H2)-C(1G2)#2	55.2(11)
C(1G2)-C(1H2)-C(1G2)#2	89.3(17)	C(1G2)#2-C(2G)-C(1G1)	71.7(13)
C(1H1)-C(2H)-C(1H2)#2	143(3)	C(1I)#3-O(110)-C(1I)	118(4)
O(110)-C(1I)-C(1I)#3	31(2)	Cl(1)-C(99)-Cl(1)#4	104.6(14)
Cl(2)-C(98)-Cl(3)	113.2(12)		

Symmetry transformations used to generate equivalent atoms:

#1 -x+1/2,-y,z #2 -x,y,-z+1/2 #3 -x+1/2,-y+1,z #4 -x,y,-z+3/2

Table A3.

Anisotropic displacement parameters ($Å^2$ x 10^3) for $[NEt_4]_2[Co_{10}Ge_2(CO)_{24}].1.5CH_2Cl_2.0.5O(CH_2CH_3)_2$. The anisotropic displacement factor exponent takes the form: $-2\pi^2[h^2a^{*2}U^{11} + \ldots + 2hka^*b^*U^{12}]$.

	U^{11}	U^{22}	U^{33}	U^{23}	U^{13}	U^{12}
Ge(1)	25(1)	25(1)	21(1)	-1(1)	-1(1)	0(1)
Ge(2)	29(1)	26(1)	22(1)	1(1)	0(1)	1(1)
Co(1)	29(1)	30(1)	23(1)	3(1)	-1(1)	0(1)
Co(2)	32(1)	29(1)	25(1)	-2(1)	-3(1)	-3(1)
Co(3)	31(1)	34(1)	23(1)	-2(1)	3(1)	0(1)
Co(4)	27(1)	29(1)	24(1)	3(1)	-2(1)	-2(1)
Co(5)	27(1)	25(1)	24(1)	0(1)	1(1)	1(1)
Co(6)	27(1)	29(1)	23(1)	-1(1)	-2(1)	2(1)
Co(7)	32(1)	23(1)	26(1)	1(1)	-1(1)	0(1)
Co(8)	36(1)	29(1)	23(1)	-3(1)	-1(1)	1(1)
Co(9)	30(1)	30(1)	26(1)	3(1)	4(1)	4(1)
Co(10)	41(1)	34(1)	25(1)	6(1)	5(1)	5(1)
O(11)	82(5)	31(4)	54(4)	5(3)	-3(4)	-3(3)
O(12)	45(4)	76(5)	33(4)	6(3)	-6(3)	0(3)
O(21)	56(5)	93(6)	65(5)	-6(4)	-26(4)	-19(4)
O(22)	61(4)	48(4)	72(5)	-24(4)	25(4)	-5(3)
O(23)	94(6)	28(3)	61(4)	-3(3)	-29(4)	-12(3)
O(31)	42(4)	60(4)	56(4)	-10(3)	-3(3)	13(3)
O(32)	68(5)	40(4)	61(5)	-3(3)	14(4)	-15(3)
O(33)	63(5)	73(5)	23(3)	2(3)	0(3)	-3(4)
O(41)	49(4)	50(4)	56(4)	-1(3)	-6(3)	-19(3)
O(42)	31(3)	71(5)	44(4)	26(3)	2(3)	9(3)
O(51)	49(4)	42(4)	55(4)	-8(3)	6(3)	-18(3)
O(52)	44(4)	38(3)	57(4)	15(3)	12(3)	11(3)
O(61)	39(4)	123(7)	38(4)	-2(4)	5(3)	-24(4)
O(62)	69(5)	41(4)	44(4)	6(3)	-21(3)	4(3)

O(63)	41(4)	47(4)	74(5)	-24(3)	-7(3)	-4(3)
O(71)	68(5)	41(4)	72(5)	19(4)	11(4)	-11(3)
O(72)	48(4)	61(4)	62(4)	-15(4)	0(3)	20(4)
O(81)	81(5)	71(5)	25(4)	1(3)	-6(3)	-4(4)
O(82)	70(5)	36(4)	61(4)	-5(3)	5(4)	9(3)
O(91)	46(4)	65(4)	49(4)	6(3)	0(3)	-9(3)
O(92)	81(5)	59(4)	43(4)	-8(3)	25(4)	21(4)
O(101)	87(6)	79(5)	46(4)	-13(4)	24(4)	14(5)
O(102)	81(5)	50(4)	68(5)	12(4)	-7(4)	25(4)
O(103)	55(5)	58(4)	66(5)	13(4)	2(4)	-14(4)
C(11)	33(5)	49(6)	37(5)	5(4)	-1(4)	2(4)
C(12)	34(5)	44(5)	30(5)	2(4)	-3(4)	-2(4)
C(22)	40(5)	41(5)	41(5)	-4(4)	6(4)	3(4)
C(21)	44(5)	43(5)	30(5)	2(4)	1(4)	-6(4)
C(23)	47(5)	39(5)	30(4)	-4(4)	-14(4)	-1(4)
C(31)	35(5)	39(5)	35(5)	-5(4)	8(4)	-7(4)
C(32)	41(5)	46(5)	25(4)	3(4)	7(4)	1(4)
C(33)	33(5)	39(5)	34(5)	-5(4)	5(4)	-6(4)
C(41)	33(5)	50(5)	28(4)	4(4)	-4(4)	-6(4)
C(42)	34(5)	41(5)	20(4)	3(3)	1(3)	1(4)
C(51)	35(4)	32(4)	25(4)	-2(3)	-2(3)	6(4)
C(52)	29(4)	40(5)	33(5)	5(4)	0(3)	3(4)
C(61)	38(5)	58(6)	29(5)	0(4)	-13(4)	-2(4)
C(62)	39(5)	39(5)	28(4)	-5(4)	-2(4)	-3(4)
C(63)	37(5)	35(5)	36(5)	-5(4)	-7(4)	8(4)
C(71)	47(5)	36(5)	44(5)	0(4)	-7(4)	2(4)
C(72)	47(5)	32(4)	31(5)	-1(4)	0(4)	0(4)
C(81)	49(6)	39(5)	42(6)	-8(4)	6(4)	5(4)
C(82)	44(5)	36(5)	30(4)	0(4)	2(4)	4(4)
C(91)	48(6)	48(6)	41(5)	10(4)	-7(4)	-7(4)
C(92)	37(5)	43(5)	35(5)	7(4)	3(4)	0(4)
C(101)	43(5)	43(5)	40(5)	11(4)	0(4)	1(4)
C(102)	50(6)	42(5)	34(5)	7(4)	6(4)	11(4)
C(103)	53(6)	44(5)	36(5)	10(4)	10(4)	1(5)
N(2)	47(6)	25(5)	65(7)	0	0	3(5)
C(1A)	61(7)	32(5)	78(8)	8(5)	4(6)	-3(5)
C(1B)	63(7)	51(6)	71(7)	0(5)	-20(6)	5(5)
C(2A)	54(7)	67(7)	77(8)	18(6)	13(6)	-6(5)
C(2B)	78(8)	73(8)	83(9)	-13(7)	-20(7)	-13(7)

Appendix B – Crystallographic Data for $Co_4(\mu_4\text{-}SiC_6H_4OMe)_2(CO)_7(XyNC)_4$

Table B1.

Atomic coordinates (x 10^4) and equivalent isotropic displacement parameters ($Å^2$ x 10^3) for $Co_4(\mu_4\text{-}SiC_6H_4OMe)_2(CO)_7(XyNC)_4$. U(eq) is defined as one third of the trace of the orthogonalized U_{ij} tensor.

	x	y	z	U(eq)
Co(1)	4389(1)	6806(1)	2054(1)	30(1)
Co(2)	4343(1)	8536(1)	2027(1)	30(1)
Si(1)	5159(1)	7702(1)	1816(1)	29(1)
N(21)	3822(1)	9831(2)	2966(1)	39(1)
N(31)	3416(1)	6127(2)	2809(1)	38(1)
C(1)	4102(1)	6360(2)	1046(2)	41(1)
C(2)	5000	5889(2)	2500	40(1)
C(3)	4404(1)	9230(2)	1232(2)	35(1)
C(4)	3596(1)	7972(2)	1502(2)	40(1)
C(10)	6014(3)	6412(3)	-1456(3)	93(2)
C(11)	5402(1)	7597(2)	886(2)	31(1)
C(12)	5581(1)	8291(2)	488(2)	34(1)
C(13)	5786(1)	8152(2)	-175(2)	38(1)
C(14)	5815(1)	7314(2)	-458(2)	39(1)
C(15)	5634(1)	6612(2)	-83(2)	39(1)
C(16)	5434(1)	6760(2)	582(2)	36(1)
C(20)	4027(1)	9310(2)	2628(2)	36(1)
C(21)	3671(1)	10529(2)	3397(2)	40(1)
C(22)	4031(1)	11304(2)	3462(2)	46(1)
C(23)	3900(2)	11966(2)	3930(2)	54(1)
C(24)	3422(2)	11876(2)	4279(2)	57(1)
C(25)	3056(2)	11126(2)	4176(2)	50(1)
C(26)	3180(1)	10423(2)	3745(2)	43(1)
C(27)	2798(2)	9597(2)	3644(2)	53(1)
C(28)	4511(2)	11410(2)	3025(2)	57(1)
C(30)	3784(1)	6403(2)	2512(2)	35(1)
C(31)	3018(1)	5863(2)	3254(2)	36(1)
C(32)	3080(1)	5018(2)	3556(2)	40(1)
C(33)	2669(2)	4781(2)	3986(2)	53(1)
C(34)	2228(2)	5363(2)	4109(2)	56(1)
C(35)	2189(2)	6196(2)	3815(2)	57(1)
C(36)	2578(1)	6472(2)	3372(2)	45(1)
C(37)	2544(2)	7372(2)	3037(3)	69(1)
C(38)	3577(2)	4397(2)	3440(2)	56(1)
O(1)	3912(1)	6033(2)	423(1)	69(1)
O(2)	5000	5124(2)	2500	65(1)
O(3)	4440(1)	9694(1)	738(1)	48(1)
O(4)	3059(1)	7813(1)	1112(2)	54(1)
O(11)	6016(1)	7249(1)	-1122(1)	55(1)

Table B2.

Bond lengths [Å] and angles [°] for $Co_4(\mu_4\text{-}SiC_6H_4OMe)_2(CO)_7(XyNC)_4$.

Co(1)-Co(1)#1	2.5594(6)	Co(1)-Co(2)	2.6624(5)

Co(2)-Co(2)#1	2.7468(7)	Co(2)-Si(1)	2.3087(7)
Co(1)-Si(1)	2.3039(7)	Co(2)-Si(1)#1	2.3208(7)
Co(1)-Si(1)#1	2.3284(7)	Si(1)-Co(1)#1	2.3284(7)
Si(1)-Co(2)#1	2.3208(7)	Si(1)-C(11)	1.877(2)
Si(1)-Si(1)#1	2.7036(13)	Co(1)-C(2)	1.905(3)
Co(1)-C(1)	1.790(3)	Co(2)-C(4)	1.783(3)
Co(1)-C(4)	2.438(3)	C(2)-Co(1)#1	1.905(3)
Co(2)-C(3)	1.792(3)	Co(2)-C(20)	1.865(3)
Co(1)-C(30)	1.858(3)	N(21)-C(21)	1.413(3)
N(21)-C(20)	1.168(3)	N(31)-C(31)	1.402(3)
N(31)-C(30)	1.167(3)	C(2)-O(2)	1.178(5)
C(1)-O(1)	1.139(3)	C(4)-O(4)	1.150(3)
C(3)-O(3)	1.143(3)	C(11)-C(12)	1.399(3)
C(10)-O(11)	1.413(4)	C(12)-C(13)	1.390(3)
C(11)-C(16)	1.403(4)	C(14)-O(11)	1.375(3)
C(13)-C(14)	1.390(4)	C(15)-C(16)	1.389(3)
C(14)-C(15)	1.388(4)	C(21)-C(22)	1.407(4)
C(21)-C(26)	1.399(4)	C(22)-C(28)	1.491(4)
C(22)-C(23)	1.396(4)	C(24)-C(25)	1.374(5)
C(23)-C(24)	1.374(5)	C(26)-C(27)	1.493(4)
C(25)-C(26)	1.395(4)	C(31)-C(36)	1.399(4)
C(31)-C(32)	1.393(4)	C(32)-C(38)	1.501(4)
C(32)-C(33)	1.393(4)	C(34)-C(35)	1.372(5)
C(33)-C(34)	1.375(5)	C(35)-C(36)	1.389(4)
C(36)-C(37)	1.495(4)		

C(1)-Co(1)-C(30)	103.77(12)	C(1)-Co(1)-C(2)	94.28(11)
C(30)-Co(1)-C(2)	93.80(9)	C(1)-Co(1)-Si(1)	94.58(9)
C(30)-Co(1)-Si(1)	159.26(8)	C(2)-Co(1)-Si(1)	94.39(7)
C(1)-Co(1)-Si(1)#1	164.41(9)	C(30)-Co(1)-Si(1)#1	89.08(8)
C(2)-Co(1)-Si(1)#1	93.60(7)	Si(1)-Co(1)-Si(1)#1	71.41(3)
C(1)-Co(1)-C(4)	86.29(11)	C(30)-Co(1)-C(4)	85.02(10)
C(2)-Co(1)-C(4)	178.79(7)	Si(1)-Co(1)-C(4)	86.63(7)
Si(1)#1-Co(1)-C(4)	86.09(7)	C(1)-Co(1)-Co(1)#1	122.32(9)
C(30)-Co(1)-Co(1)#1	117.86(8)	C(2)-Co(1)-Co(1)#1	47.79(8)
Si(1)-Co(1)-Co(1)#1	56.92(2)	Si(1)#1-Co(1)-Co(1)#1	56.005(19)
C(4)-Co(1)-Co(1)#1	132.63(7)	C(1)-Co(1)-Co(2)	111.62(9)
C(30)-Co(1)-Co(2)	108.29(8)	C(2)-Co(1)-Co(2)	139.81(8)
Si(1)-Co(1)-Co(2)	54.830(19)	Si(1)#1-Co(1)-Co(2)	54.931(19)
C(4)-Co(1)-Co(2)	40.63(7)	Co(1)#1-Co(1)-Co(2)	92.016(10)
C(4)-Co(2)-C(3)	100.70(12)	C(4)-Co(2)-C(20)	99.12(12)
C(3)-Co(2)-C(20)	101.19(11)	C(4)-Co(2)-Si(1)	104.64(9)
C(3)-Co(2)-Si(1)	86.79(8)	C(20)-Co(2)-Si(1)	153.07(8)
C(4)-Co(2)-Si(1)#1	104.16(9)	C(3)-Co(2)-Si(1)#1	150.30(8)
C(20)-Co(2)-Si(1)#1	90.71(8)	Si(1)-Co(2)-Si(1)#1	71.46(3)
C(4)-Co(2)-Co(1)	62.90(9)	C(3)-Co(2)-Co(1)	126.63(8)
C(20)-Co(2)-Co(1)	130.33(8)	Si(1)-Co(2)-Co(1)	54.663(19)
Si(1)#1-Co(2)-Co(1)	55.200(19)	C(4)-Co(2)-Co(2)#1	150.87(9)
C(3)-Co(2)-Co(2)#1	97.51(8)	C(20)-Co(2)-Co(2)#1	99.41(8)
Si(1)-Co(2)-Co(2)#1	53.811(19)	Si(1)#1-Co(2)-Co(2)#1	53.403(19)
Co(1)-Co(2)-Co(2)#1	87.982(10)	C(11)-Si(1)-Co(1)	122.48(8)
C(11)-Si(1)-Co(2)	129.87(8)	Co(1)-Si(1)-Co(2)	70.51(2)
C(11)-Si(1)-Co(2)#1	128.17(8)	Co(1)-Si(1)-Co(2)#1	108.67(3)
Co(2)-Si(1)-Co(2)#1	72.79(2)	C(11)-Si(1)-Co(1)#1	121.52(8)
Co(1)-Si(1)-Co(1)#1	67.07(2)	Co(2)-Si(1)-Co(1)#1	108.25(3)
Co(2)#1-Si(1)-Co(1)#1	69.87(2)	C(11)-Si(1)-Si(1)#1	174.86(8)
Co(1)-Si(1)-Si(1)#1	54.72(2)	Co(2)-Si(1)-Si(1)#1	54.48(2)
Co(2)#1-Si(1)-Si(1)#1	54.06(2)	Co(1)#1-Si(1)-Si(1)#1	53.87(2)
C(20)-N(21)-C(21)	170.9(3)	C(30)-N(31)-C(31)	172.5(3)
O(1)-C(1)-Co(1)	176.1(3)	O(2)-C(2)-Co(1)#1	137.79(8)
O(2)-C(2)-Co(1)	137.79(8)	Co(1)#1-C(2)-Co(1)	84.41(16)
O(3)-C(3)-Co(2)	177.9(2)	O(4)-C(4)-Co(2)	163.1(3)
O(4)-C(4)-Co(1)	120.4(2)	Co(2)-C(4)-Co(1)	76.46(10)

C(12)-C(11)-C(16)	117.0(2)	C(12)-C(11)-Si(1)	124.81(19)
C(16)-C(11)-Si(1)	118.12(18)	C(13)-C(12)-C(11)	121.1(2)
C(14)-C(13)-C(12)	120.4(2)	O(11)-C(14)-C(15)	124.4(2)
O(11)-C(14)-C(13)	115.7(2)	C(15)-C(14)-C(13)	119.9(2)
C(14)-C(15)-C(16)	119.0(2)	C(15)-C(16)-C(11)	122.5(2)
N(21)-C(20)-Co(2)	175.8(2)	C(26)-C(21)-C(22)	123.0(3)
C(26)-C(21)-N(21)	119.4(3)	C(22)-C(21)-N(21)	117.6(2)
C(23)-C(22)-C(21)	116.6(3)	C(23)-C(22)-C(28)	122.4(3)
C(21)-C(22)-C(28)	121.0(3)	C(24)-C(23)-C(22)	121.3(3)
C(25)-C(24)-C(23)	120.8(3)	C(24)-C(25)-C(26)	120.9(3)
C(25)-C(26)-C(21)	117.2(3)	C(25)-C(26)-C(27)	121.6(3)
C(21)-C(26)-C(27)	121.2(3)	N(31)-C(30)-Co(1)	177.9(2)
C(32)-C(31)-C(36)	123.4(2)	C(32)-C(31)-N(31)	118.9(2)
C(36)-C(31)-N(31)	117.7(2)	C(31)-C(32)-C(33)	116.9(3)
C(31)-C(32)-C(38)	121.5(2)	C(33)-C(32)-C(38)	121.6(3)
C(34)-C(33)-C(32)	121.2(3)	C(35)-C(34)-C(33)	120.4(3)
C(34)-C(35)-C(36)	121.5(3)	C(35)-C(36)-C(31)	116.6(3)
C(35)-C(36)-C(37)	122.9(3)	C(31)-C(36)-C(37)	120.5(3)
C(14)-O(11)-C(10)	117.1(2)		

Symmetry transformations used to generate equivalent atoms: #1 -x+1,y,-z+1/2

Table B3.

Anisotropic displacement parameters ($Å^2$ x 10^3) for $Co_4(\mu_4\text{-}SiC_6H_4OMe)_2(CO)_7(XyNC)_4$. The anisotropic displacement factor exponent takes the form: $-2\pi^2[h^2a^{*2}U^{11} + \ldots + 2hka^*b^*U^{12}]$.

	U^{11}	U^{22}	U^{33}	U^{23}	U^{13}	U^{12}
Co(1)	30(1)	30(1)	33(1)	-1(1)	16(1)	-3(1)
Co(2)	34(1)	28(1)	33(1)	2(1)	17(1)	2(1)
Si(1)	32(1)	29(1)	31(1)	-1(1)	17(1)	-1(1)
N(21)	43(1)	42(1)	35(1)	1(1)	15(1)	11(1)
N(31)	35(1)	38(1)	45(1)	2(1)	18(1)	-4(1)
C(1)	39(1)	42(2)	45(2)	-3(1)	18(1)	-5(1)
C(2)	38(2)	35(2)	50(2)	0	18(2)	0
C(3)	33(1)	31(1)	42(1)	-1(1)	14(1)	1(1)
C(4)	43(2)	35(2)	47(2)	2(1)	22(1)	-3(1)
C(10)	149(4)	73(3)	103(3)	-44(2)	102(3)	-38(3)
C(11)	32(1)	37(1)	29(1)	-1(1)	14(1)	0(1)
C(12)	35(1)	33(1)	38(1)	-3(1)	16(1)	-3(1)
C(13)	43(2)	38(2)	38(1)	-1(1)	21(1)	-7(1)
C(14)	39(1)	48(2)	37(1)	-7(1)	22(1)	-8(1)
C(15)	44(2)	36(1)	42(2)	-8(1)	22(1)	-1(1)
C(16)	39(1)	34(1)	39(1)	0(1)	19(1)	-4(1)
C(20)	35(1)	38(1)	34(1)	6(1)	12(1)	3(1)
C(21)	39(1)	42(2)	36(1)	2(1)	11(1)	14(1)
C(22)	43(2)	40(2)	51(2)	4(1)	12(1)	9(1)
C(23)	58(2)	36(2)	64(2)	-2(1)	14(2)	7(1)
C(24)	66(2)	46(2)	61(2)	-8(2)	24(2)	17(2)
C(25)	52(2)	53(2)	48(2)	0(1)	22(1)	16(2)
C(26)	42(2)	43(2)	43(2)	3(1)	14(1)	9(1)
C(27)	51(2)	53(2)	57(2)	3(2)	19(2)	0(2)
C(28)	54(2)	56(2)	64(2)	9(2)	23(2)	3(2)
C(30)	35(1)	31(1)	40(1)	1(1)	14(1)	-1(1)
C(31)	32(1)	39(2)	39(1)	-2(1)	16(1)	-8(1)
C(32)	41(1)	38(2)	39(1)	-1(1)	13(1)	-9(1)
C(33)	51(2)	55(2)	50(2)	9(1)	15(1)	-17(2)
C(34)	42(2)	85(3)	48(2)	3(2)	23(1)	-14(2)
C(35)	40(2)	76(2)	61(2)	-13(2)	26(2)	-3(2)

C(36)	38(2)	47(2)	53(2)	-7(1)	19(1)	-4(1)
C(37)	66(2)	46(2)	103(3)	0(2)	39(2)	9(2)
C(38)	66(2)	41(2)	64(2)	5(2)	27(2)	7(2)
O(1)	67(2)	87(2)	52(1)	-28(1)	20(1)	-20(1)
O(2)	60(2)	28(2)	94(3)	0	9(2)	0
O(3)	55(1)	41(1)	51(1)	12(1)	25(1)	-1(1)
O(4)	37(1)	45(1)	73(2)	9(1)	12(1)	-1(1)
O(11)	75(2)	54(1)	56(1)	-18(1)	47(1)	-18(1)

Table B4.

Hydrogen coordinates (x 10^4) and isotropic displacement parameters ($Å^2$x 10^3) for $Co_4(\mu_4\text{-}SiC_6H_4OMe)_2(CO)_7(XyNC)_4$.

	x	y	z	U(eq)
H(10A)	6162	6449	-1914	139
H(10B)	5574	6180	-1631	139
H(10C)	6303	6037	-1049	139
H(12)	5562	8855	669	41
H(13)	5905	8621	-430	45
H(15)	5645	6050	-274	46
H(16)	5318	6287	836	43
H(23)	4142	12480	4008	65
H(24)	3345	12328	4588	69
H(25)	2722	11087	4397	59
H(27A)	2485	9643	3922	80
H(27B)	3094	9124	3872	80
H(27C)	2568	9491	3075	80
H(28A)	4530	10883	2740	86
H(28B)	4940	11536	3413	86
H(28C)	4372	11880	2642	86
H(33)	2692	4221	4193	63
H(34)	1954	5190	4392	67
H(35)	1896	6584	3915	68
H(37A)	2218	7701	3172	104
H(37B)	2425	7344	2455	104
H(37C)	2966	7648	3268	104
H(38A)	3813	4676	3131	84
H(38B)	3355	3892	3153	84
H(38C)	3883	4228	3963	84

Appendix C – Crystallographic Data for $[NEt_4][CoFe_3(CO)_{13}]$

Table C1.
Atomic coordinates (x 10^4) and equivalent isotropic displacement parameters ($Å^2$ x 10^3) for $[NEt_4][CoFe_3(CO)_{13}]$. U(eq) is defined as one third of the trace of the orthogonalized U_{ij} tensor.

	x	y	z	U(eq)
Co(1)	3937(1)	5858(1)	9990(1)	32(1)
Fe(1)	2329(1)	5096(1)	10722(1)	39(1)
Fe(2)	3565(1)	3856(1)	9935(1)	40(1)
Fe(3)	2261(1)	5180(1)	9293(1)	43(1)
C(1)	2024(6)	6311(5)	10066(6)	90(2)
C(2)	3857(4)	5637(4)	11087(3)	34(1)
C(3)	3714(4)	5798(4)	8885(3)	35(1)
C(4)	1085(6)	4469(5)	9996(6)	79(2)
C(11)	1503(6)	5822(6)	11363(5)	79(3)
C(12)	2393(5)	3958(5)	11280(3)	48(1)
C(21)	5378(3)	5574(3)	9930(3)	34(1)
C(22)	4096(4)	7256(3)	10031(3)	40(1)
C(31)	1387(5)	5972(5)	8727(4)	59(2)
C(32)	2280(5)	4070(4)	8698(3)	47(1)
C(41)	4570(4)	3519(4)	10655(3)	41(1)
C(42)	4524(5)	3582(4)	9156(3)	43(1)
C(43)	2851(3)	2616(3)	9923(3)	38(1)
O(1)	1678(5)	7207(4)	10108(5)	107(2)
O(2)	4303(3)	5695(3)	11672(2)	51(1)
O(3)	4092(4)	5943(4)	8292(2)	60(1)
O(4)	279(3)	3993(3)	10029(3)	61(1)
O(11)	959(5)	6253(6)	11805(4)	140(3)
O(12)	2312(5)	3293(4)	11708(3)	93(2)
O(21)	6298(2)	5424(3)	9873(2)	48(1)
O(22)	4237(3)	8137(2)	10047(3)	61(1)
O(31)	847(4)	6449(5)	8314(4)	112(2)
O(32)	2190(5)	3446(4)	8224(3)	79(2)
O(41)	5215(3)	3285(4)	11104(2)	56(1)
O(42)	5144(4)	3378(4)	8686(2)	57(1)
O(43)	2451(3)	1803(3)	9922(3)	58(1)
N(1)	2481(4)	10032(4)	7520(2)	26(1)
C(111)	2248(4)	9347(4)	6827(3)	36(1)
C(112)	1057(5)	8961(5)	6761(3)	50(1)
C(121)	1741(4)	11004(4)	7509(3)	46(1)
C(122)	1924(7)	11693(5)	6804(4)	82(3)
C(131)	2188(4)	9459(4)	8266(3)	45(1)
C(132)	2834(7)	8456(5)	8392(4)	78(2)
C(141)	3688(4)	10318(4)	7495(3)	41(1)
C(142)	4090(5)	11038(5)	8137(3)	52(2)

Table C2.
Bond lengths [Å] and angles [°] for $[NEt_4][CoFe_3(CO)_{13}]$.

Co(1)-C(21)	1.789(4)	Co(1)-C(22)	1.789(4)
Co(1)-C(2)	1.938(5)	Co(1)-C(3)	1.950(5)
Co(1)-C(1)	2.396(7)	Co(1)-Fe(3)	2.5229(10)
Co(1)-Fe(1)	2.5260(10)	Co(1)-Fe(2)	2.5879(9)
Fe(1)-C(12)	1.747(5)	Fe(1)-C(11)	1.763(6)
Fe(1)-C(1)	1.959(8)	Fe(1)-C(2)	2.078(5)
Fe(1)-C(4)	2.126(8)	Fe(1)-Fe(3)	2.4979(11)
Fe(1)-Fe(2)	2.5749(11)	Fe(2)-C(43)	1.799(4)

Fe(2)-C(41)	1.804(6)	Fe(2)-C(42)	1.823(6)
Fe(2)-Fe(3)	2.5688(11)	Fe(3)-C(32)	1.753(6)
Fe(3)-C(31)	1.766(6)	Fe(3)-C(1)	1.993(8)
Fe(3)-C(3)	2.058(5)	Fe(3)-C(4)	2.088(8)
C(1)-O(1)	1.216(8)	C(2)-O(2)	1.160(6)
C(3)-O(3)	1.148(6)	C(4)-O(4)	1.152(7)
C(11)-O(11)	1.154(7)	C(12)-O(12)	1.133(7)
C(21)-O(21)	1.137(5)	C(22)-O(22)	1.133(5)
C(31)-O(31)	1.147(7)	C(32)-O(32)	1.151(7)
C(41)-O(41)	1.147(7)	C(42)-O(42)	1.144(7)
C(43)-O(43)	1.143(5)	N(1)-C(141)	1.511(7)
N(1)-C(111)	1.518(6)	N(1)-C(121)	1.529(6)
N(1)-C(131)	1.534(6)	C(111)-C(112)	1.531(7)
C(121)-C(122)	1.526(8)	C(131)-C(132)	1.513(9)
C(141)-C(142)	1.528(7)		

C(21)-Co(1)-C(22)	95.57(19)	C(21)-Co(1)-C(2)	94.4(2)
C(22)-Co(1)-C(2)	96.3(2)	C(21)-Co(1)-C(3)	94.0(2)
C(22)-Co(1)-C(3)	95.4(2)	C(2)-Co(1)-C(3)	164.82(18)
C(21)-Co(1)-C(1)	177.7(2)	C(22)-Co(1)-C(1)	82.2(2)
C(2)-Co(1)-C(1)	86.1(3)	C(3)-Co(1)-C(1)	85.9(3)
C(21)-Co(1)-Fe(3)	133.74(15)	C(22)-Co(1)-Fe(3)	116.50(16)
C(2)-Co(1)-Fe(3)	112.74(16)	C(3)-Co(1)-Fe(3)	52.93(16)
C(1)-Co(1)-Fe(3)	47.7(2)	C(21)-Co(1)-Fe(1)	135.03(16)
C(22)-Co(1)-Fe(1)	116.38(17)	C(2)-Co(1)-Fe(1)	53.54(16)
C(3)-Co(1)-Fe(1)	112.21(16)	C(1)-Co(1)-Fe(1)	46.8(2)
Fe(3)-Co(1)-Fe(1)	59.31(3)	C(21)-Co(1)-Fe(2)	88.25(13)
C(22)-Co(1)-Fe(2)	176.18(14)	C(2)-Co(1)-Fe(2)	83.43(15)
C(3)-Co(1)-Fe(2)	84.26(15)	C(1)-Co(1)-Fe(2)	94.00(17)
Fe(3)-Co(1)-Fe(2)	60.33(3)	Fe(1)-Co(1)-Fe(2)	60.45(3)
C(12)-Fe(1)-C(11)	96.0(4)	C(12)-Fe(1)-C(1)	171.3(3)
C(11)-Fe(1)-C(1)	81.5(4)	C(12)-Fe(1)-C(2)	93.6(2)
C(11)-Fe(1)-C(2)	98.0(3)	C(1)-Fe(1)-C(2)	95.0(3)
C(12)-Fe(1)-C(4)	93.1(3)	C(11)-Fe(1)-C(4)	99.8(3)
C(1)-Fe(1)-C(4)	79.2(3)	C(2)-Fe(1)-C(4)	160.2(3)
C(12)-Fe(1)-Fe(3)	126.5(2)	C(11)-Fe(1)-Fe(3)	126.4(3)
C(1)-Fe(1)-Fe(3)	51.4(3)	C(2)-Fe(1)-Fe(3)	108.78(14)
C(4)-Fe(1)-Fe(3)	52.9(2)	C(12)-Fe(1)-Co(1)	124.4(2)
C(11)-Fe(1)-Co(1)	124.0(2)	C(1)-Fe(1)-Co(1)	63.1(2)
C(2)-Fe(1)-Co(1)	48.60(14)	C(4)-Fe(1)-Co(1)	113.0(2)
Fe(3)-Fe(1)-Co(1)	60.28(3)	C(12)-Fe(1)-Fe(2)	76.4(2)
C(11)-Fe(1)-Fe(2)	172.2(3)	C(1)-Fe(1)-Fe(2)	106.3(3)
C(2)-Fe(1)-Fe(2)	81.17(14)	C(4)-Fe(1)-Fe(2)	82.30(18)
Fe(3)-Fe(1)-Fe(2)	60.82(3)	Co(1)-Fe(1)-Fe(2)	60.97(3)
C(43)-Fe(2)-C(41)	97.2(2)	C(43)-Fe(2)-C(42)	97.6(2)
C(41)-Fe(2)-C(42)	92.5(2)	C(43)-Fe(2)-Fe(3)	105.81(15)
C(41)-Fe(2)-Fe(3)	151.21(16)	C(42)-Fe(2)-Fe(3)	101.18(17)
C(43)-Fe(2)-Fe(1)	105.16(15)	C(41)-Fe(2)-Fe(1)	99.59(17)
C(42)-Fe(2)-Fe(1)	152.52(16)	Fe(3)-Fe(2)-Fe(1)	58.11(3)
C(43)-Fe(2)-Co(1)	161.16(13)	C(41)-Fe(2)-Co(1)	95.13(17)
C(42)-Fe(2)-Co(1)	96.01(16)	Fe(3)-Fe(2)-Co(1)	58.58(3)
Fe(1)-Fe(2)-Co(1)	58.58(3)	C(32)-Fe(3)-C(31)	97.7(3)
C(32)-Fe(3)-C(1)	169.9(3)	C(31)-Fe(3)-C(1)	83.2(3)
C(32)-Fe(3)-C(3)	95.2(2)	C(31)-Fe(3)-C(3)	95.9(2)
C(1)-Fe(3)-C(3)	94.7(3)	C(32)-Fe(3)-C(4)	90.5(3)
C(31)-Fe(3)-C(4)	99.6(3)	C(1)-Fe(3)-C(4)	79.4(3)
C(3)-Fe(3)-C(4)	162.6(3)	C(32)-Fe(3)-Fe(1)	123.9(2)
C(31)-Fe(3)-Fe(1)	127.1(2)	C(1)-Fe(3)-Fe(1)	50.2(3)
C(3)-Fe(3)-Fe(1)	109.50(14)	C(4)-Fe(3)-Fe(1)	54.3(3)
C(32)-Fe(3)-Co(1)	123.4(2)	C(31)-Fe(3)-Co(1)	124.0(2)
C(1)-Fe(3)-Co(1)	62.8(2)	C(3)-Fe(3)-Co(1)	49.12(14)
C(4)-Fe(3)-Co(1)	114.5(3)	Fe(1)-Fe(3)-Co(1)	60.41(3)
C(32)-Fe(3)-Fe(2)	73.9(2)	C(31)-Fe(3)-Fe(2)	171.3(2)

C(1)-Fe(3)-Fe(2)	105.5(2)	C(3)-Fe(3)-Fe(2)	82.70(14)
C(4)-Fe(3)-Fe(2)	83.2(2)	Fe(1)-Fe(3)-Fe(2)	61.07(3)
Co(1)-Fe(3)-Fe(2)	61.09(3)	O(1)-C(1)-Fe(1)	140.2(9)
O(1)-C(1)-Fe(3)	140.1(9)	Fe(1)-C(1)-Fe(3)	78.4(2)
O(1)-C(1)-Co(1)	124.3(6)	Fe(1)-C(1)-Co(1)	70.1(2)
Fe(3)-C(1)-Co(1)	69.5(2)	O(2)-C(2)-Co(1)	147.0(4)
O(2)-C(2)-Fe(1)	135.1(4)	Co(1)-C(2)-Fe(1)	77.85(18)
O(3)-C(3)-Co(1)	146.2(5)	O(3)-C(3)-Fe(3)	135.8(5)
Co(1)-C(3)-Fe(3)	77.95(17)	O(4)-C(4)-Fe(3)	146.9(8)
O(4)-C(4)-Fe(1)	140.4(8)	Fe(3)-C(4)-Fe(1)	72.7(2)
O(11)-C(11)-Fe(1)	176.7(9)	O(12)-C(12)-Fe(1)	169.3(6)
O(21)-C(21)-Co(1)	177.4(5)	O(22)-C(22)-Co(1)	177.4(5)
O(31)-C(31)-Fe(3)	175.2(8)	O(32)-C(32)-Fe(3)	168.4(6)
O(41)-C(41)-Fe(2)	178.4(5)	O(42)-C(42)-Fe(2)	177.2(5)
O(43)-C(43)-Fe(2)	176.3(4)	C(141)-N(1)-C(111)	107.2(4)
C(141)-N(1)-C(121)	112.0(4)	C(111)-N(1)-C(121)	110.1(4)
C(141)-N(1)-C(131)	111.4(4)	C(111)-N(1)-C(131)	111.2(4)
C(121)-N(1)-C(131)	105.0(4)	N(1)-C(111)-C(112)	114.9(4)
C(122)-C(121)-N(1)	112.9(5)	C(132)-C(131)-N(1)	113.8(5)
N(1)-C(141)-C(142)	115.6(4)		

Table C3.

Anisotropic displacement parameters ($Å^2$ x 10^3) for $[NEt_4][CoFe_3(CO)_{13}]$. The anisotropic displacement factor exponent takes the form: $-2\pi_2[h_2a^{*2}U^{11} + \ldots + 2hka^*b^*U^{12}]$.

	U^{11}	U^{22}	U^{33}	U^{23}	U^{13}	U^{12}
Co(1)	25(1)	27(1)	44(1)	-1(1)	1(1)	-4(1)
Fe(1)	46(1)	37(1)	34(1)	10(1)	17(1)	13(1)
Fe(2)	34(1)	24(1)	62(1)	-2(1)	2(1)	4(1)
Fe(3)	52(1)	42(1)	35(1)	-10(1)	-23(1)	17(1)
C(1)	85(5)	60(4)	125(6)	-20(5)	-22(6)	20(3)
C(2)	38(3)	30(2)	35(2)	-2(2)	3(2)	3(2)
C(3)	37(3)	33(2)	34(2)	6(2)	2(2)	9(2)
C(4)	87(4)	43(3)	107(5)	-13(5)	15(6)	5(3)
C(11)	54(4)	61(4)	123(6)	-51(4)	37(4)	-20(3)
C(12)	36(3)	42(3)	66(3)	16(3)	-3(3)	0(3)
C(21)	32(2)	31(2)	37(2)	-6(2)	-1(2)	-2(2)
C(22)	50(2)	33(2)	38(2)	-2(3)	4(3)	-2(2)
C(31)	34(3)	54(4)	90(5)	21(3)	-8(3)	2(3)
C(32)	42(3)	37(3)	63(3)	-10(2)	7(3)	-1(3)
C(41)	36(3)	37(3)	51(3)	-13(2)	9(2)	-8(2)
C(42)	36(3)	31(3)	61(3)	11(2)	-13(3)	-12(2)
C(43)	36(2)	40(2)	37(3)	-4(2)	3(2)	3(2)
O(1)	105(4)	62(3)	153(6)	7(4)	1(5)	19(3)
O(2)	57(2)	51(2)	46(2)	-10(2)	-20(2)	0(2)
O(3)	70(3)	68(3)	41(2)	14(2)	22(2)	16(2)
O(4)	66(2)	76(2)	41(2)	-5(2)	2(2)	-28(2)
O(11)	77(4)	135(6)	207(7)	-125(6)	78(5)	-39(4)
O(12)	126(5)	51(3)	101(4)	34(3)	52(4)	14(3)
O(21)	27(2)	53(2)	65(3)	0(2)	2(2)	4(1)
O(22)	91(3)	30(2)	63(2)	-6(2)	-1(3)	-6(2)
O(31)	51(3)	105(5)	179(6)	85(4)	-29(3)	-2(3)
O(32)	103(4)	52(3)	81(3)	-21(2)	-24(3)	11(3)
O(41)	39(2)	67(3)	62(2)	-5(2)	-13(2)	-6(2)
O(42)	55(3)	58(3)	59(2)	-1(2)	15(2)	-13(2)
O(43)	54(2)	42(2)	77(3)	-2(2)	0(3)	-17(2)
N(1)	27(2)	26(1)	25(1)	-2(1)	1(1)	0(1)
C(111)	34(2)	35(2)	39(2)	-10(2)	1(2)	-5(2)
C(112)	36(3)	60(3)	54(3)	-26(3)	-8(2)	-7(3)

C(121)	43(3)	34(3)	61(3)	-10(2)	-10(2)	13(2)
C(122)	124(7)	36(3)	86(5)	16(3)	-49(5)	10(4)
C(131)	48(3)	54(3)	33(2)	10(2)	-2(2)	-12(2)
C(132)	105(6)	52(4)	78(5)	33(3)	-25(4)	-8(4)
C(141)	30(2)	50(3)	42(3)	-10(2)	5(2)	-5(2)
C(142)	37(3)	61(4)	57(3)	-17(3)	-3(3)	-10(3)

Table C4.

Hydrogen coordinates (x 10^4) and isotropic displacement parameters ($Å^2$ x 10^3) for $[NEt_4][CoFe_3(CO)_{13}]$.

	x	y	z	U(eq)
H(11A)	2731	8740	6845	43
H(11B)	2430	9742	6369	43
H(11C)	967	8582	6290	75
H(11D)	566	9553	6768	75
H(11E)	891	8506	7184	75
H(12A)	976	10782	7522	56
H(12B)	1880	11418	7965	56
H(12C)	1490	12321	6848	123
H(12D)	1707	11314	6353	123
H(12E)	2689	11876	6768	123
H(13A)	2321	9929	8694	54
H(13B)	1409	9292	8261	54
H(13C)	2488	8048	8787	117
H(13D)	3573	8626	8543	117
H(13E)	2849	8057	7925	117
H(14A)	3838	10659	7009	49
H(14B)	4116	9675	7510	49
H(14C)	4863	11172	8074	78
H(14D)	3966	10704	8623	78
H(14E)	3693	11691	8119	78

Appendix D – Crystallographic Data for $[NEt_4][CoRu_3(CO)_{13}]$

Table D1.

Atomic coordinates (x 10^4) and equivalent isotropic displacement parameters ($Å^2$ x 10^3) for $[NEt_4][CoRu_3(CO)_{13}]$. U(eq) is defined as one third of the trace of the orthogonalized U_{ij} tensor.

	x	y	z	U(eq)
Ru(1)	1211(1)	5788(1)	2340(1)	28(1)
Ru(2)	-223(1)	4255(1)	2904(1)	27(1)
Ru(3)	-910(1)	6387(1)	2483(1)	24(1)
Co(1)	-367(1)	4912(1)	1518(1)	25(1)
C(1)	1064(7)	4575(7)	1448(5)	32(2)
C(2)	-1370(8)	4061(8)	1979(6)	36(2)
C(3)	-751(7)	6348(8)	1280(5)	32(2)
C(11)	1249(7)	6795(8)	3141(6)	36(3)
C(12)	2575(8)	5083(7)	2545(6)	37(2)
C(13)	1657(8)	6898(8)	1700(6)	40(3)
C(21)	817(8)	4595(8)	3704(6)	40(3)
C(22)	-1352(8)	3808(8)	3494(6)	39(3)
C(23)	378(8)	2896(8)	2700(6)	41(3)
C(31)	-857(7)	6360(9)	3544(7)	44(3)
C(32)	-811(7)	7920(8)	2368(6)	38(2)
C(33)	-2416(7)	6292(8)	2373(5)	31(2)
C(41)	-776(8)	4350(8)	650(6)	38(2)
O(1)	1628(6)	4015(6)	1135(5)	58(2)
O(2)	-2202(5)	3651(6)	1833(4)	49(2)
O(3)	-866(6)	6958(6)	788(4)	50(2)
O(11)	1385(5)	7414(6)	3637(5)	53(2)
O(12)	3366(6)	4676(6)	2654(5)	58(2)
O(13)	1887(7)	7587(6)	1310(5)	62(2)
O(21)	1374(6)	4699(7)	4231(4)	62(2)
O(22)	-2019(6)	3597(7)	3856(4)	59(2)
O(23)	730(6)	2044(6)	2575(5)	64(2)
O(31)	-876(6)	6443(7)	4185(4)	62(2)
O(32)	-745(6)	8857(6)	2303(5)	63(2)
O(33)	-3312(5)	6242(6)	2286(4)	49(2)
O(41)	-1046(7)	3962(7)	91(4)	58(2)
N(1)	5000	5000	0	40(3)
C(95A)	4184(16)	4193(19)	299(12)	48(6)
C(95B)	5710(20)	5350(20)	631(15)	79(10)
C(96)	3327(10)	3819(11)	-295(8)	73(4)
C(97A)	4613(17)	5351(18)	746(11)	44(5)
C(97B)	5800(18)	3910(16)	314(12)	47(6)
C(98)	3821(14)	6499(14)	487(11)	122(7)
N(2)	0	0	0	33(3)
C(91A)	682(14)	254(14)	722(12)	37(5)
C(91B)	-597(15)	-1051(14)	110(11)	38(5)
C(92)	-1307(9)	-1367(8)	-640(7)	58(4)
C(93A)	-544(16)	-120(17)	723(11)	38(5)
C(93B)	921(15)	-1010(13)	94(11)	32(5)
C(94)	1447(11)	-976(13)	-676(8)	86(5)

Table D2.
Bond lengths [Å] and angles [°] for $[NEt_4][CoRu_3(CO)_{13}]$.

Ru(1)-C(11)	1.919(11)	Ru(1)-C(13)	1.919(11)
Ru(1)-C(12)	1.960(10)	Ru(1)-C(1)	2.212(10)
Ru(1)-Co(1)	2.6495(15)	Ru(1)-Ru(3)	2.8431(13)
Ru(1)-Ru(2)	2.8869(11)	Ru(2)-C(23)	1.901(10)
Ru(2)-C(21)	1.942(10)	Ru(2)-C(22)	1.946(10)
Ru(2)-C(2)	2.159(10)	Ru(2)-Co(1)	2.6473(16)
Ru(2)-Ru(3)	2.8707(13)	Ru(3)-C(32)	1.918(10)
Ru(3)-C(33)	1.925(9)	Ru(3)-C(31)	1.931(12)
Ru(3)-C(3)	2.219(10)	Ru(3)-Co(1)	2.6654(15)
Co(1)-C(41)	1.771(11)	Co(1)-C(3)	1.888(11)
Co(1)-C(1)	1.891(9)	Co(1)-C(2)	1.906(10)
C(1)-O(1)	1.181(11)	C(2)-O(2)	1.191(11)
C(3)-O(3)	1.173(11)	C(11)-O(11)	1.188(11)
C(12)-O(12)	1.134(11)	C(13)-O(13)	1.165(12)
C(21)-O(21)	1.157(11)	C(22)-O(22)	1.149(11)
C(23)-O(23)	1.177(11)	C(31)-O(31)	1.176(12)
C(32)-O(32)	1.171(11)	C(33)-O(33)	1.146(10)
C(41)-O(41)	1.155(11)	N(1)-C(95B)	1.47(2)
N(1)-C(95B)#1	1.47(2)	N(1)-C(97A)#1	1.55(2)
N(1)-C(97A)	1.55(2)	N(1)-C(95A)	1.574(19)
N(1)-C(95A)#1	1.574(19)	N(1)-C(97B)#1	1.763(19)
N(1)-C(97B)	1.763(19)	C(95A)-C(96)	1.55(2)
C(95A)-C(97A)	1.72(3)	C(95A)-C(95B)#1	1.80(3)
C(95B)-C(97A)	1.43(3)	C(95B)-C(96)#1	1.75(3)
C(95B)-C(95A)#1	1.80(3)	C(95B)-C(97B)	1.88(3)
C(96)-C(95B)#1	1.75(3)	C(97A)-C(98)	1.79(3)
C(97B)-C(98)#1	1.65(3)	C(98)-C(97B)#1	1.65(3)
N(2)-C(91B)	1.532(15)	N(2)-C(91B)#2	1.532(15)
N(2)-C(93A)	1.545(19)	N(2)-C(93A)#2	1.545(19)
N(2)-C(91A)#2	1.553(18)	N(2)-C(91A)	1.553(18)
N(2)-C(93B)#2	1.718(18)	N(2)-C(93B)	1.718(18)
C(91A)-C(92)#2	1.607(19)	C(91A)-C(93A)	1.64(3)
C(91A)-C(91B)#2	1.81(3)	C(91A)-C(93B)	1.98(3)
C(91B)-C(93A)	1.60(3)	C(91B)-C(92)	1.63(2)
C(91B)-C(91A)#2	1.81(3)	C(91B)-C(93B)	1.94(3)
C(92)-C(91A)#2	1.607(19)	C(93A)-C(94)#2	1.78(2)
C(93B)-C(94)	1.60(2)	C(94)-C(93A)#2	1.78(2)

C(11)-Ru(1)-C(13)	90.3(4)	C(11)-Ru(1)-C(12)	100.2(4)
C(13)-Ru(1)-C(12)	97.7(4)	C(11)-Ru(1)-C(1)	175.8(4)
C(13)-Ru(1)-C(1)	93.0(4)	C(12)-Ru(1)-C(1)	81.9(4)
C(11)-Ru(1)-Co(1)	132.0(3)	C(13)-Ru(1)-Co(1)	101.5(3)
C(12)-Ru(1)-Co(1)	123.5(3)	C(1)-Ru(1)-Co(1)	44.7(2)
C(11)-Ru(1)-Ru(3)	74.2(3)	C(13)-Ru(1)-Ru(3)	101.5(3)
C(12)-Ru(1)-Ru(3)	160.0(3)	C(1)-Ru(1)-Ru(3)	102.6(2)
Co(1)-Ru(1)-Ru(3)	57.93(4)	C(11)-Ru(1)-Ru(2)	97.8(3)
C(13)-Ru(1)-Ru(2)	156.4(3)	C(12)-Ru(1)-Ru(2)	102.7(3)
C(1)-Ru(1)-Ru(2)	78.1(2)	Co(1)-Ru(1)-Ru(2)	56.94(4)
Ru(3)-Ru(1)-Ru(2)	60.12(3)	C(23)-Ru(2)-C(21)	94.4(5)
C(23)-Ru(2)-C(22)	100.6(4)	C(21)-Ru(2)-C(22)	98.1(4)
C(23)-Ru(2)-C(2)	90.5(4)	C(21)-Ru(2)-C(2)	173.7(4)
C(22)-Ru(2)-C(2)	85.0(4)	C(23)-Ru(2)-Co(1)	94.9(3)
C(21)-Ru(2)-Co(1)	129.9(3)	C(22)-Ru(2)-Co(1)	128.0(3)
C(2)-Ru(2)-Co(1)	45.3(3)	C(23)-Ru(2)-Ru(3)	152.1(3)
C(21)-Ru(2)-Ru(3)	100.2(3)	C(22)-Ru(2)-Ru(3)	100.7(3)
C(2)-Ru(2)-Ru(3)	73.7(3)	Co(1)-Ru(2)-Ru(3)	57.60(3)
C(23)-Ru(2)-Ru(1)	103.6(3)	C(21)-Ru(2)-Ru(1)	73.0(3)
C(22)-Ru(2)-Ru(1)	154.6(3)	C(2)-Ru(2)-Ru(1)	101.9(3)

Co(1)-Ru(2)-Ru(1)	57.01(3)	Ru(3)-Ru(2)-Ru(1)	59.18(3)
C(32)-Ru(3)-C(33)	97.1(4)	C(32)-Ru(3)-C(31)	97.4(5)
C(33)-Ru(3)-C(31)	93.4(4)	C(32)-Ru(3)-C(3)	84.4(4)
C(33)-Ru(3)-C(3)	93.7(4)	C(31)-Ru(3)-C(3)	172.4(4)
C(32)-Ru(3)-Co(1)	125.8(3)	C(33)-Ru(3)-Co(1)	101.5(3)
C(31)-Ru(3)-Co(1)	131.2(3)	C(3)-Ru(3)-Co(1)	44.3(3)
C(32)-Ru(3)-Ru(1)	100.2(3)	C(33)-Ru(3)-Ru(1)	158.2(3)
C(31)-Ru(3)-Ru(1)	97.4(3)	C(3)-Ru(3)-Ru(1)	75.0(2)
Co(1)-Ru(3)-Ru(1)	57.39(3)	C(32)-Ru(3)-Ru(2)	157.0(3)
C(33)-Ru(3)-Ru(2)	104.7(3)	C(31)-Ru(3)-Ru(2)	74.3(3)
C(3)-Ru(3)-Ru(2)	101.2(3)	Co(1)-Ru(3)-Ru(2)	56.99(4)
Ru(1)-Ru(3)-Ru(2)	60.69(2)	C(41)-Co(1)-C(3)	96.4(4)
C(41)-Co(1)-C(1)	94.1(4)	C(3)-Co(1)-C(1)	115.3(4)
C(41)-Co(1)-C(2)	90.8(5)	C(3)-Co(1)-C(2)	116.9(4)
C(1)-Co(1)-C(2)	126.5(4)	C(41)-Co(1)-Ru(2)	136.5(3)
C(3)-Co(1)-Ru(2)	120.5(3)	C(1)-Co(1)-Ru(2)	90.1(3)
C(2)-Co(1)-Ru(2)	53.7(3)	C(41)-Co(1)-Ru(1)	145.6(3)
C(3)-Co(1)-Ru(1)	85.2(3)	C(1)-Co(1)-Ru(1)	55.3(3)
C(2)-Co(1)-Ru(1)	119.1(3)	Ru(2)-Co(1)-Ru(1)	66.05(4)
C(41)-Co(1)-Ru(3)	141.8(3)	C(3)-Co(1)-Ru(3)	55.2(3)
C(1)-Co(1)-Ru(3)	120.0(3)	C(2)-Co(1)-Ru(3)	82.6(3)
Ru(2)-Co(1)-Ru(3)	65.41(4)	Ru(1)-Co(1)-Ru(3)	64.68(4)
O(1)-C(1)-Co(1)	142.6(8)	O(1)-C(1)-Ru(1)	137.3(8)
Co(1)-C(1)-Ru(1)	80.0(3)	O(2)-C(2)-Co(1)	139.3(8)
O(2)-C(2)-Ru(2)	139.7(8)	Co(1)-C(2)-Ru(2)	81.0(4)
O(3)-C(3)-Co(1)	143.0(8)	O(3)-C(3)-Ru(3)	136.5(8)
Co(1)-C(3)-Ru(3)	80.5(4)	O(11)-C(11)-Ru(1)	173.1(8)
O(12)-C(12)-Ru(1)	179.1(10)	O(13)-C(13)-Ru(1)	177.3(9)
O(21)-C(21)-Ru(2)	171.2(9)	O(22)-C(22)-Ru(2)	176.5(9)
O(23)-C(23)-Ru(2)	178.6(9)	O(31)-C(31)-Ru(3)	173.2(10)
O(32)-C(32)-Ru(3)	179.4(11)	O(33)-C(33)-Ru(3)	178.0(9)
O(41)-C(41)-Co(1)	178.6(10)	C(95B)-N(1)-C(95B)#1	180(2)
C(95B)-N(1)-C(97A)#1	123.3(15)	C(95B)#1-N(1)-C(97A)#1	56.7(15)
C(95B)-N(1)-C(97A)	56.7(15)	C(95B)#1-N(1)-C(97A)	123.3(15)
C(97A)#1-N(1)-C(97A)	180.0(16)	C(95B)-N(1)-C(95A)	107.5(13)
C(95B)#1-N(1)-C(95A)	72.5(13)	C(97A)#1-N(1)-C(95A)	113.1(12)
C(97A)-N(1)-C(95A)	66.9(12)	C(95B)-N(1)-C(95A)#1	72.5(13)
C(95B)#1-N(1)-C(95A)#1	107.5(13)	C(97A)#1-N(1)-C(95A)#1	66.9(12)
C(97A)-N(1)-C(95A)#1	113.1(12)	C(95A)-N(1)-C(95A)#1	180.0(19)
C(95B)-N(1)-C(97B)#1	109.6(14)	C(95B)#1-N(1)-C(97B)#1	70.4(14)
C(97A)#1-N(1)-C(97B)#1	98.5(11)	C(97A)-N(1)-C(97B)#1	81.5(11)
C(95A)-N(1)-C(97B)#1	102.5(11)	C(95A)#1-N(1)-C(97B)#1	77.5(11)
C(95B)-N(1)-C(97B)	70.4(14)	C(95B)#1-N(1)-C(97B)	109.6(14)
C(97A)#1-N(1)-C(97B)	81.5(11)	C(97A)-N(1)-C(97B)	98.5(11)
C(95A)-N(1)-C(97B)	77.5(11)	C(95A)#1-N(1)-C(97B)	102.5(11)
C(97B)#1-N(1)-C(97B)	180.0(14)	C(96)-C(95A)-N(1)	113.6(14)
C(96)-C(95A)-C(97A)	139.7(18)	N(1)-C(95A)-C(97A)	55.8(10)
C(96)-C(95A)-C(95B)#1	62.5(11)	N(1)-C(95A)-C(95B)#1	51.2(9)
C(97A)-C(95A)-C(95B)#1	97.9(15)	C(97A)-C(95B)-N(1)	64.2(12)
C(97A)-C(95B)-C(96)#1	140(2)	N(1)-C(95B)-C(96)#1	107.8(17)
C(97A)-C(95B)-C(95A)#1	106.4(17)	N(1)-C(95B)-C(95A)#1	56.3(11)
C(96)#1-C(95B)-C(95A)#1	51.6(11)	C(97A)-C(95B)-C(97B)	97.5(16)
N(1)-C(95B)-C(97B)	62.0(12)	C(96)#1-C(95B)-C(97B)	113(2)
C(95A)#1-C(95B)-C(97B)	89.9(17)	C(95A)-C(96)-C(95B)#1	65.9(11)
C(95B)-C(97A)-N(1)	59.2(13)	C(95B)-C(97A)-C(95A)	102.1(18)
N(1)-C(97A)-C(95A)	57.3(10)	C(95B)-C(97A)-C(98)	120.2(19)
N(1)-C(97A)-C(98)	101.9(13)	C(95A)-C(97A)-C(98)	112.7(15)
C(98)#1-C(97B)-N(1)	98.7(13)	C(98)#1-C(97B)-C(95B)	126.3(16)
N(1)-C(97B)-C(95B)	47.6(8)	C(97B)#1-C(98)-C(97A)	77.8(11)
C(91B)-N(2)-C(91B)#2	180(2)	C(91B)-N(2)-C(93A)	62.8(11)
C(91B)#2-N(2)-C(93A)	117.2(11)	C(91B)-N(2)-C(93A)#2	117.2(11)
C(91B)#2-N(2)-C(93A)#2	62.8(11)	C(93A)-N(2)-C(93A)#2	180.0(13)
C(91B)-N(2)-C(91A)#2	71.7(10)	C(91B)#2-N(2)-C(91A)#2	108.3(10)

C(93A)-N(2)-C(91A)#2	116.3(11)	C(93A)#2-N(2)-C(91A)#2	63.7(11)
C(91B)-N(2)-C(91A)	108.3(10)	C(91B)#2-N(2)-C(91A)	71.7(10)
C(93A)-N(2)-C(91A)	63.7(11)	C(93A)#2-N(2)-C(91A)	116.3(11)
C(91A)#2-N(2)-C(91A)	180.0(14)	C(91B)-N(2)-C(93B)#2	106.7(10)
C(91B)#2-N(2)-C(93B)#2	73.3(10)	C(93A)-N(2)-C(93B)#2	78.7(10)
C(93A)#2-N(2)-C(93B)#2	101.3(10)	C(91A)#2-N(2)-C(93B)#2	74.2(10)
C(91A)-N(2)-C(93B)#2	105.8(10)	C(91B)-N(2)-C(93B)	73.3(10)
C(91B)#2-N(2)-C(93B)	106.7(10)	C(93A)-N(2)-C(93B)	101.3(10)
C(93A)#2-N(2)-C(93B)	78.7(10)	C(91A)#2-N(2)-C(93B)	105.8(10)
C(91A)-N(2)-C(93B)	74.2(10)	C(93B)#2-N(2)-C(93B)	180.0(9)
N(2)-C(91A)-C(92)#2	110.2(12)	N(2)-C(91A)-C(93A)	57.9(9)
C(92)#2-C(91A)-C(93A)	136.6(15)	N(2)-C(91A)-C(91B)#2	53.6(8)
C(92)#2-C(91A)-C(91B)#2	56.6(9)	C(93A)-C(91A)-C(91B)#2	99.3(12)
N(2)-C(91A)-C(93B)	56.7(9)	C(92)#2-C(91A)-C(93B)	121.7(15)
C(93A)-C(91A)-C(93B)	88.2(12)	C(91B)#2-C(91A)-C(93B)	87.1(12)
N(2)-C(91B)-C(93A)	59.0(9)	N(2)-C(91B)-C(92)	110.2(12)
C(93A)-C(91B)-C(92)	138.4(16)	N(2)-C(91B)-C(91A)#2	54.7(8)
C(93A)-C(91B)-C(91A)#2	100.8(13)	C(92)-C(91B)-C(91A)#2	55.5(9)
N(2)-C(91B)-C(93B)	57.8(8)	C(93A)-C(91B)-C(93B)	90.2(12)
C(92)-C(91B)-C(93B)	119.0(14)	C(91A)#2-C(91B)-C(93B)	88.1(11)
C(91A)#2-C(92)-C(91B)	67.9(10)	N(2)-C(93A)-C(91B)	58.2(9)
N(2)-C(93A)-C(91A)	58.3(10)	C(91B)-C(93A)-C(91A)	101.0(14)
N(2)-C(93A)-C(94)#2	102.6(11)	C(91B)-C(93A)-C(94)#2	121.6(15)
C(91A)-C(93A)-C(94)#2	113.7(14)	C(94)-C(93B)-N(2)	103.0(12)
C(94)-C(93B)-C(91B)	120.1(14)	N(2)-C(93B)-C(91B)	49.0(7)
C(94)-C(93B)-C(91A)	125.5(13)	N(2)-C(93B)-C(91A)	49.1(7)
C(91B)-C(93B)-C(91A)	79.2(10)	C(93B)-C(94)-C(93A)#2	75.4(10)

Symmetry transformations used to generate equivalent atoms:
#1 -x+1,-y+1,-z #2 -x,-y,-z

Table D3.
Anisotropic displacement parameters ($Å^2$ x 10^3) for $[NEt_4][CoRu_3(CO)_{13}]$. The anisotropic displacement factor exponent takes the form: $-2\pi^2[h^2a^{*2}U^{11} + \ldots + h^2a^{*2}b^{*2}U^{12}]$.

	U^{11}	U^{22}	U^{33}	U^{23}	U^{13}	U^{12}
Ru(1)	17(1)	23(1)	44(1)	-1(1)	8(1)	-1(1)
Ru(2)	23(1)	24(1)	34(1)	7(1)	6(1)	1(1)
Ru(3)	18(1)	22(1)	33(1)	1(1)	8(1)	2(1)
Co(1)	24(1)	23(1)	28(1)	1(1)	5(1)	2(1)
C(1)	29(6)	21(5)	47(6)	1(4)	7(4)	0(4)
C(2)	27(6)	39(6)	42(6)	4(5)	6(4)	6(4)
C(3)	27(5)	39(6)	30(6)	-7(5)	5(4)	-2(4)
C(11)	15(5)	26(5)	68(8)	-5(5)	1(4)	-1(4)
C(12)	26(6)	24(5)	62(7)	-1(5)	12(5)	0(4)
C(13)	32(6)	26(6)	63(8)	-7(5)	17(5)	-1(4)
C(21)	36(6)	44(7)	40(7)	7(5)	-3(5)	-6(5)
C(22)	41(7)	36(6)	42(7)	12(5)	14(5)	7(5)
C(23)	33(6)	36(6)	54(7)	-3(5)	6(5)	0(5)
C(31)	23(6)	50(7)	61(8)	-12(6)	6(5)	3(5)
C(32)	26(6)	27(6)	62(8)	0(5)	14(5)	3(4)
C(33)	17(5)	35(5)	42(6)	-2(5)	10(4)	2(4)
C(41)	34(6)	40(6)	40(7)	-9(5)	3(4)	2(4)
O(1)	39(5)	60(5)	76(6)	-25(4)	9(4)	23(4)
O(2)	29(4)	53(5)	62(5)	4(4)	-9(3)	-19(3)
O(3)	64(5)	39(4)	48(5)	20(4)	21(4)	16(4)
O(11)	33(4)	52(5)	74(6)	-23(5)	-2(4)	0(3)
O(12)	22(4)	43(5)	105(7)	2(4)	-5(4)	8(3)
O(13)	79(6)	36(5)	77(6)	1(4)	37(5)	-10(4)
O(21)	56(6)	77(6)	51(5)	17(5)	-14(4)	-7(4)

O(22)	46(5)	65(5)	68(6)	21(5)	23(4)	-8(4)
O(23)	53(6)	42(5)	99(7)	1(5)	17(5)	18(4)
O(31)	68(6)	89(7)	32(5)	-3(5)	12(4)	27(5)
O(32)	35(5)	27(4)	130(8)	1(4)	21(4)	0(3)
O(33)	20(4)	51(5)	74(6)	-12(4)	0(3)	0(3)
O(41)	70(6)	65(6)	39(5)	-9(4)	4(4)	-8(4)
N(1)	54(8)	41(7)	27(7)	-3(6)	13(5)	-17(6)
C(95A)	35(13)	59(14)	50(14)	9(12)	3(9)	-23(11)
C(95B)	64(19)	73(18)	90(20)	12(16)	-50(15)	-50(14)
C(96)	53(9)	81(10)	82(10)	-5(8)	-17(7)	-37(7)
C(97A)	50(15)	55(14)	27(12)	-3(10)	11(9)	8(11)
C(97B)	53(15)	32(12)	58(15)	25(11)	18(11)	15(9)
C(98)	109(15)	94(13)	174(19)	-66(13)	77(13)	-7(11)
N(2)	29(7)	27(6)	41(7)	-1(5)	4(5)	-17(5)
C(91A)	27(11)	19(10)	59(14)	12(9)	-23(9)	-10(8)
C(91B)	37(12)	20(10)	53(14)	8(9)	-9(9)	-27(8)
C(92)	49(7)	28(6)	90(10)	4(6)	-36(6)	-17(5)
C(93A)	42(13)	44(13)	30(12)	10(10)	14(9)	13(10)
C(93B)	34(11)	14(9)	48(13)	4(8)	9(9)	0(7)
C(94)	67(10)	103(12)	95(12)	-29(9)	50(8)	-14(8)

Appendix E – Crystallographic Data for [PPN][Mo(CO)$_3$(η^5-C$_5$H$_5$)]

Table E1.

Atomic coordinates (x 10^4) and equivalent isotropic displacement parameters (Å^2 x 10^3) for [PPN][Mo(CO)$_3$(η_5-C$_5$H$_5$)]. U(eq) is defined as one third of the trace of the orthogonalized U_{ij} tensor.

	x	y	z	U(eq)
Mo(1)	7828(1)	1336(1)	9650(1)	34(1)
C(1)	7895(2)	1998(2)	8601(2)	45(1)
C(2)	7354(2)	703(2)	8672(2)	42(1)
C(3)	6529(2)	1629(1)	9866(2)	34(1)
C(4)	8258(2)	1278(2)	11316(2)	63(1)
C(5)	8875(3)	1730(2)	10911(3)	65(1)
C(6)	9412(3)	1359(4)	10253(3)	117(2)
C(7)	9091(5)	665(4)	10280(5)	134(3)
C(8)	8396(4)	633(2)	10935(4)	102(2)
O(1)	7951(2)	2397(1)	7958(2)	67(1)
O(2)	7075(2)	317(1)	8071(2)	67(1)
O(3)	5746(1)	1795(1)	10038(1)	49(1)
P(2)	2955(1)	1691(1)	4434(1)	25(1)
P(1)	2889(1)	569(1)	5944(1)	26(1)
N(1)	3274(1)	1165(1)	5261(2)	32(1)
C(11)	3711(2)	486(1)	6945(2)	30(1)
C(12)	3777(2)	-135(1)	7472(2)	44(1)
C(13)	4365(2)	-170(2)	8284(2)	49(1)
C(14)	4899(2)	404(2)	8557(2)	44(1)
C(15)	4852(2)	1014(2)	8030(2)	42(1)
C(16)	4256(2)	1059(1)	7226(2)	35(1)
C(21)	1731(2)	762(1)	6438(2)	32(1)
C(22)	921(2)	719(1)	5848(2)	40(1)
C(23)	50(2)	956(2)	6191(3)	56(1)
C(24)	-18(2)	1227(2)	7111(3)	66(1)
C(25)	777(3)	1259(2)	7702(3)	64(1)
C(26)	1653(2)	1030(2)	7370(2)	47(1)
C(31)	2815(2)	-267(1)	5342(2)	29(1)
C(32)	2169(2)	-779(1)	5630(2)	36(1)
C(33)	2147(2)	-1418(1)	5152(2)	44(1)
C(34)	2748(2)	-1550(2)	4398(2)	48(1)
C(35)	3389(2)	-1043(2)	4111(2)	49(1)
C(36)	3433(2)	-403(1)	4587(2)	40(1)
C(41)	2685(2)	2545(1)	4912(2)	28(1)
C(42)	1994(2)	2602(1)	5633(2)	34(1)
C(43)	1739(2)	3251(1)	5979(2)	40(1)
C(44)	2170(2)	3846(1)	5632(2)	45(1)
C(45)	2864(2)	3796(1)	4941(2)	48(1)
C(46)	3121(2)	3144(1)	4569(2)	38(1)
C(51)	1908(2)	1415(1)	3754(2)	28(1)
C(52)	1066(2)	1804(1)	3721(2)	36(1)
C(53)	261(2)	1538(2)	3254(2)	44(1)
C(54)	293(2)	886(2)	2822(2)	43(1)
C(55)	1126(2)	504(1)	2838(2)	37(1)
C(56)	1938(2)	765(1)	3295(2)	31(1)
C(61)	3933(2)	1790(1)	3620(2)	26(1)
C(62)	3785(2)	1902(1)	2633(2)	36(1)
C(63)	4557(2)	2015(2)	2036(2)	42(1)
C(64)	5469(2)	2030(1)	2421(2)	39(1)

C(65)	5619(2)	1924(2)	3400(2)	40(1)
C(66)	4859(2)	1798(1)	4001(2)	35(1)

Table E2.
Bond lengths [Å] and angles [°] for [PPN][Mo(CO)$_3$(η^5-C$_5$H$_5$)].

Mo(1)-C(2)	1.928(3)	Mo(1)-C(1)	1.930(3)
Mo(1)-C(3)	1.933(3)	Mo(1)-C(7)	2.347(4)
Mo(1)-C(8)	2.359(4)	Mo(1)-C(6)	2.366(4)
Mo(1)-C(4)	2.377(3)	Mo(1)-C(5)	2.390(3)
C(1)-O(1)	1.175(4)	C(2)-O(2)	1.175(3)
C(3)-O(3)	1.173(3)	C(4)-C(5)	1.351(5)
C(4)-C(8)	1.356(6)	C(5)-C(6)	1.385(7)
C(6)-C(7)	1.403(8)	C(7)-C(8)	1.341(8)
P(2)-N(1)	1.584(2)	P(2)-C(61)	1.796(2)
P(2)-C(41)	1.804(2)	P(2)-C(51)	1.813(2)
P(1)-N(1)	1.579(2)	P(1)-C(11)	1.797(2)
P(1)-C(31)	1.806(2)	P(1)-C(21)	1.810(2)
C(11)-C(16)	1.391(3)	C(11)-C(12)	1.396(3)
C(12)-C(13)	1.388(4)	C(13)-C(14)	1.378(4)
C(14)-C(15)	1.377(4)	C(15)-C(16)	1.386(4)
C(21)-C(26)	1.392(4)	C(21)-C(22)	1.394(4)
C(22)-C(23)	1.393(4)	C(23)-C(24)	1.378(5)
C(24)-C(25)	1.377(6)	C(25)-C(26)	1.389(4)
C(31)-C(36)	1.390(3)	C(31)-C(32)	1.396(3)
C(32)-C(33)	1.390(4)	C(33)-C(34)	1.373(4)
C(34)-C(35)	1.385(4)	C(35)-C(36)	1.392(4)
C(41)-C(46)	1.385(3)	C(41)-C(42)	1.404(3)
C(42)-C(43)	1.379(4)	C(43)-C(44)	1.378(4)
C(44)-C(45)	1.376(4)	C(45)-C(46)	1.398(4)
C(51)-C(56)	1.397(3)	C(51)-C(52)	1.398(3)
C(52)-C(53)	1.391(4)	C(53)-C(54)	1.384(4)
C(54)-C(55)	1.379(4)	C(55)-C(56)	1.389(3)
C(61)-C(62)	1.394(3)	C(61)-C(66)	1.397(3)
C(62)-C(63)	1.388(4)	C(63)-C(64)	1.382(4)
C(64)-C(65)	1.382(4)	C(65)-C(66)	1.383(3)

C(2)-Mo(1)-C(1)	84.49(12)	C(2)-Mo(1)-C(3)	88.43(11)
C(1)-Mo(1)-C(3)	88.93(11)	C(2)-Mo(1)-C(7)	99.75(15)
C(1)-Mo(1)-C(7)	126.4(3)	C(3)-Mo(1)-C(7)	144.1(2)
C(2)-Mo(1)-C(8)	106.34(14)	C(1)-Mo(1)-C(8)	157.13(17)
C(3)-Mo(1)-C(8)	111.04(19)	C(7)-Mo(1)-C(8)	33.1(2)
C(2)-Mo(1)-C(6)	124.99(19)	C(1)-Mo(1)-C(6)	101.43(17)
C(3)-Mo(1)-C(6)	145.50(17)	C(7)-Mo(1)-C(6)	34.6(2)
C(8)-Mo(1)-C(6)	55.79(19)	C(2)-Mo(1)-C(4)	137.09(13)
C(1)-Mo(1)-C(4)	138.18(14)	C(3)-Mo(1)-C(4)	95.29(11)
C(7)-Mo(1)-C(4)	55.50(16)	C(8)-Mo(1)-C(4)	33.29(15)
C(6)-Mo(1)-C(4)	55.47(14)	C(2)-Mo(1)-C(5)	156.10(12)
C(1)-Mo(1)-C(5)	107.84(13)	C(3)-Mo(1)-C(5)	111.64(13)
C(7)-Mo(1)-C(5)	56.40(16)	C(8)-Mo(1)-C(5)	55.30(13)
C(6)-Mo(1)-C(5)	33.86(17)	C(4)-Mo(1)-C(5)	32.92(12)
O(1)-C(1)-Mo(1)	178.8(3)	O(2)-C(2)-Mo(1)	179.3(3)
O(3)-C(3)-Mo(1)	177.0(2)	C(5)-C(4)-C(8)	109.0(4)
C(5)-C(4)-Mo(1)	74.05(19)	C(8)-C(4)-Mo(1)	72.6(2)
C(4)-C(5)-C(6)	107.6(4)	C(4)-C(5)-Mo(1)	73.03(19)
C(6)-C(5)-Mo(1)	72.1(2)	C(5)-C(6)-C(7)	106.8(4)
C(5)-C(6)-Mo(1)	74.0(2)	C(7)-C(6)-Mo(1)	72.0(2)
C(8)-C(7)-C(6)	107.3(4)	C(8)-C(7)-Mo(1)	73.9(2)
C(6)-C(7)-Mo(1)	73.4(3)	C(7)-C(8)-C(4)	109.3(5)
C(7)-C(8)-Mo(1)	73.0(3)	C(4)-C(8)-Mo(1)	74.1(2)

N(1)-P(2)-C(61)	107.97(11)	N(1)-P(2)-C(41)	111.66(11)
C(61)-P(2)-C(41)	107.49(11)	N(1)-P(2)-C(51)	114.13(11)
C(61)-P(2)-C(51)	109.04(10)	C(41)-P(2)-C(51)	106.34(11)
N(1)-P(1)-C(11)	107.69(11)	N(1)-P(1)-C(31)	112.45(11)
C(11)-P(1)-C(31)	108.00(11)	N(1)-P(1)-C(21)	113.27(11)
C(11)-P(1)-C(21)	107.31(11)	C(31)-P(1)-C(21)	107.88(11)
P(1)-N(1)-P(2)	142.62(14)	C(16)-C(11)-C(12)	119.4(2)
C(16)-C(11)-P(1)	119.42(18)	C(12)-C(11)-P(1)	121.07(19)
C(13)-C(12)-C(11)	120.0(3)	C(14)-C(13)-C(12)	119.9(3)
C(15)-C(14)-C(13)	120.6(3)	C(14)-C(15)-C(16)	120.1(3)
C(15)-C(16)-C(11)	120.0(2)	C(26)-C(21)-C(22)	119.4(2)
C(26)-C(21)-P(1)	120.4(2)	C(22)-C(21)-P(1)	119.8(2)
C(23)-C(22)-C(21)	119.6(3)	C(24)-C(23)-C(22)	120.6(3)
C(25)-C(24)-C(23)	120.0(3)	C(24)-C(25)-C(26)	120.3(3)
C(25)-C(26)-C(21)	120.2(3)	C(36)-C(31)-C(32)	119.9(2)
C(36)-C(31)-P(1)	118.54(19)	C(32)-C(31)-P(1)	121.58(19)
C(33)-C(32)-C(31)	119.4(3)	C(34)-C(33)-C(32)	120.9(3)
C(33)-C(34)-C(35)	119.8(3)	C(34)-C(35)-C(36)	120.3(3)
C(31)-C(36)-C(35)	119.7(3)	C(46)-C(41)-C(42)	119.4(2)
C(46)-C(41)-P(2)	121.80(19)	C(42)-C(41)-P(2)	118.80(18)
C(43)-C(42)-C(41)	120.2(2)	C(44)-C(43)-C(42)	120.3(2)
C(45)-C(44)-C(43)	120.2(2)	C(44)-C(45)-C(46)	120.4(3)
C(41)-C(46)-C(45)	119.6(2)	C(56)-C(51)-C(52)	119.3(2)
C(56)-C(51)-P(2)	117.80(18)	C(52)-C(51)-P(2)	122.80(19)
C(53)-C(52)-C(51)	120.2(3)	C(54)-C(53)-C(52)	119.9(3)
C(55)-C(54)-C(53)	120.2(2)	C(54)-C(55)-C(56)	120.6(3)
C(55)-C(56)-C(51)	119.8(2)	C(62)-C(61)-C(66)	119.6(2)
C(62)-C(61)-P(2)	121.64(18)	C(66)-C(61)-P(2)	118.62(18)
C(63)-C(62)-C(61)	119.9(2)	C(64)-C(63)-C(62)	120.0(2)
C(63)-C(64)-C(65)	120.3(2)	C(64)-C(65)-C(66)	120.3(2)
C(65)-C(66)-C(61)	119.8(2)		

Table E3.

Anisotropic displacement parameters ($Å^2$ x 10^3) for [PPN][$Mo(CO)_3(\eta^5\text{-}C_5H_5)$]. The anisotropic displacement factor exponent takes the form: $-2\pi^2[h^2a^{*2}U^{11} + \ldots + 2hka^*b^*U^{12}]$.

	U^{11}	U^{22}	U^{33}	U^{23}	U^{13}	U^{12}
Mo(1)	31(1)	37(1)	33(1)	-4(1)	-1(1)	4(1)
C(1)	39(2)	51(2)	45(2)	-4(1)	7(1)	2(1)
C(2)	41(2)	46(2)	39(2)	-8(1)	-2(1)	16(1)
C(3)	39(1)	38(1)	23(1)	-2(1)	-1(1)	3(1)
C(4)	47(2)	98(3)	43(2)	10(2)	-11(1)	9(2)
C(5)	76(2)	55(2)	63(2)	0(2)	-35(2)	-8(2)
C(6)	28(2)	268(8)	54(2)	4(4)	-8(2)	-17(3)
C(7)	113(4)	169(6)	119(5)	-96(4)	-83(4)	112(5)
C(8)	131(4)	46(2)	127(4)	26(3)	-91(4)	-12(2)
O(1)	78(2)	68(2)	56(1)	17(1)	20(1)	0(1)
O(2)	68(2)	68(2)	63(2)	-33(1)	-14(1)	19(1)
O(3)	41(1)	68(1)	40(1)	-1(1)	7(1)	13(1)
P(2)	25(1)	26(1)	24(1)	1(1)	1(1)	0(1)
P(1)	28(1)	26(1)	26(1)	2(1)	1(1)	-2(1)
N(1)	32(1)	33(1)	31(1)	8(1)	-2(1)	-4(1)
C(11)	31(1)	32(1)	25(1)	1(1)	-1(1)	0(1)
C(12)	57(2)	34(1)	40(2)	4(1)	-11(1)	-6(1)
C(13)	67(2)	42(2)	39(2)	10(1)	-13(1)	3(1)
C(14)	43(2)	57(2)	33(1)	2(1)	-10(1)	4(1)

C(15)	40(1)	50(2)	37(1)	-5(1)	-4(1)	-9(1)
C(16)	40(1)	34(1)	33(1)	3(1)	-2(1)	-5(1)
C(21)	32(1)	27(1)	38(1)	2(1)	7(1)	-1(1)
C(22)	34(1)	39(1)	47(2)	8(1)	3(1)	-1(1)
C(23)	31(1)	53(2)	85(2)	16(2)	7(2)	3(1)
C(24)	46(2)	48(2)	104(3)	-1(2)	38(2)	5(1)
C(25)	68(2)	54(2)	71(2)	-18(2)	34(2)	-3(2)
C(26)	48(2)	49(2)	43(2)	-7(1)	12(1)	-7(1)
C(31)	32(1)	29(1)	28(1)	1(1)	-2(1)	2(1)
C(32)	36(1)	33(1)	38(1)	0(1)	0(1)	-2(1)
C(33)	45(2)	32(1)	55(2)	-2(1)	-10(1)	-3(1)
C(34)	58(2)	34(1)	50(2)	-12(1)	-10(1)	9(1)
C(35)	59(2)	51(2)	38(2)	-6(1)	8(1)	17(2)
C(36)	41(1)	40(2)	39(1)	3(1)	5(1)	4(1)
C(41)	33(1)	25(1)	27(1)	-2(1)	-3(1)	3(1)
C(42)	35(1)	35(1)	32(1)	-1(1)	4(1)	-1(1)
C(43)	42(1)	46(2)	31(1)	-7(1)	3(1)	8(1)
C(44)	61(2)	32(1)	41(2)	-10(1)	-1(1)	11(1)
C(45)	63(2)	29(1)	51(2)	1(1)	7(2)	-4(1)
C(46)	46(2)	31(1)	37(1)	1(1)	9(1)	0(1)
C(51)	27(1)	32(1)	24(1)	2(1)	2(1)	-2(1)
C(52)	34(1)	40(1)	33(1)	-1(1)	0(1)	4(1)
C(53)	28(1)	66(2)	39(2)	3(1)	1(1)	4(1)
C(54)	32(1)	62(2)	33(1)	5(1)	-1(1)	-17(1)
C(55)	44(2)	38(1)	30(1)	2(1)	-1(1)	-13(1)
C(56)	31(1)	32(1)	30(1)	1(1)	0(1)	-2(1)
C(61)	27(1)	26(1)	27(1)	0(1)	1(1)	0(1)
C(62)	31(1)	47(2)	29(1)	1(1)	0(1)	0(1)
C(63)	43(2)	57(2)	27(1)	1(1)	6(1)	2(1)
C(64)	32(1)	44(2)	42(2)	-4(1)	13(1)	1(1)
C(65)	25(1)	51(2)	44(2)	-3(1)	1(1)	0(1)
C(66)	32(1)	46(2)	28(1)	-1(1)	0(1)	2(1)

Table E4.

Hydrogen coordinates (x 10^4) and isotropic displacement parameters ($Å^2$ x 10^3) for [PPN][$Mo(CO)_3(\eta^5$-$C_5H_5)$].

	x	y	z	U(eq)
H(4)	7805	1392	11786	75
H(5)	8931	2210	11051	78
H(6)	9898	1538	9863	140
H(7)	9320	292	9908	161
H(8)	8058	228	11103	122
H(12)	3422	-528	7278	52
H(13)	4400	-585	8648	59
H(14)	5298	378	9106	53
H(15)	5225	1400	8217	51
H(16)	4221	1478	6871	43
H(22)	962	532	5222	48
H(23)	-496	930	5793	67
H(24)	-607	1391	7334	79
H(25)	727	1437	8333	77
H(26)	2195	1056	7775	56
H(32)	1752	-692	6143	43
H(33)	1715	-1764	5348	53
H(34)	2724	-1984	4078	57
H(35)	3797	-1132	3591	59

H(36)	3878	-63	4400	47
H(42)	1705	2198	5880	41
H(43)	1268	3288	6454	48
H(44)	1990	4287	5867	54
H(45)	3166	4202	4717	57
H(46)	3587	3112	4090	45
H(52)	1043	2246	4016	43
H(53)	-305	1801	3232	53
H(54)	-255	702	2517	51
H(55)	1145	64	2537	45
H(56)	2507	505	3294	38
H(62)	3163	1901	2373	43
H(63)	4458	2082	1369	51
H(64)	5990	2112	2016	47
H(65)	6242	1939	3658	48
H(66)	4964	1717	4664	43

Appendix F – List of Publications

The material reported within this thesis has been presented in the following publications.

Cameron Evans, Kenneth M. Mackay and Brian K. Nicholson; The Formation of Mixed Germanium-Cobalt Carbonyl Clusters: An Electrospray Mass Spectrometric Study, and the Structure of a High-Nuclearity $[Ge_2Co_{10}(CO)_{24}]^{2-}$ anion, *J. Chem. Soc., Dalton Trans.*, 2001, 1645.

Cameron Evans, Brian. K. Nicholson and Allan G. Oliver, Bis(triphenylphosphine)iminium tricarbonylcyclopentadienylmolybdate, *Acta Cryst. Sect. E,* 2001, **57**, m504.

Cameron Evans and Brian K. Nicholson, A New Structural Isomer of the $[CoFe_3(CO)_{13}]^-$ Anion, *J. Organomet. Chem.*, 2002, **645**, 281.

Cameron Evans, *Analysis of Transition Metal Cluster Reactions by Electrospray Mass Spectrometry*, Oral Presentation at Molecules for Life, Napier, December 2001.

Brian K. Nicholson, J. Scott McIndoe, Cameron Evans; *Investigation of Metal Carbonyl Cluster Chemistry using Electrospray Mass Spectrometry*, Poster Presentation at XXXIIIrd ICCC Conference, Florence, Italy, August 1998.

Cameron Evans, Brian K. Nicholson, Kenneth M. Mackay, *Analysis of High-Nuclearity Air-Sensitive Metal Carbonyl Clusters by Electrospray Mass Spectrometry*, Poster Presentation at RACI/NZIC Conference, Wellington, February 1999.

Cameron Evans, Brian K. Nicholson, Kenneth M. Mackay, *The Application of Electrospray Mass Spectrometry to Metal Carbonyl Cluster Characterisation*, Poster Presentation at NZIC Conference, Wellington, November 1999.

Cameron Evans, Brian K. Nicholson and Kenneth M. Mackay, *Electrospray Mass Spectrometry Applied to the Analysis of Air-Sensitive Systems*, Poster Presentation at 11RACIC, Canberra (Australia), February 2000.

Cameron Evans, Brian K. Nicholson and Kenneth M. Mackay, *The Study of Mixed Group14/Transition Metal Clusters by Electrospray Mass Spectrometry*, Poster Presentation at ICCOC-GTL-10, Bordeaux (France), July 2001.

Brian K. Nicholson and Cameron Evans, *A Structural Isomer of the* $[CoFe_3(CO)_{13}]^-$ *Anion*, Poster Presentation at Molecules for Life, Napier, December 2001.